



The
University
Of
Sheffield.

Synthesis of oxidation responsive drug delivery systems

By:
Emma Owens

A thesis submitted in partial fulfilment of the requirements for the degree of
Doctor of Philosophy

The University of Sheffield
Faculty of Science
Department of Chemistry

Submission Date

25th September 2019

Declaration

The work described in this Thesis was undertaken at the University of Sheffield under the supervision of Dr Sebastian Spain between October 2015 and September 2019 and has not been submitted, either wholly or in part, for this or any other degree. All the work is the original work of the author, except where acknowledged.

Signature: _____

Emma Louise Owens

September 2019

Acknowledgements

"You're braver than you believe, and stronger than you seem, and smarter than you think." - Winnie the Pooh

There are a lot of people I am grateful to for their support over the last 4 years. First of all, my parents, as well as the rest of my close family. They are always there for me no matter what I decide to do and support me 100%.

My partner, David, has probably dealt with the brunt of my PhD, whether it be getting excited about a new idea or piece of research or just listening to me complain about things not going to plan. He's always there with a cup of tea ready to listen. Without him this would definitely have been a lot harder.

The Spain group, old and new, are the most supportive research group I could ask for and are always there to lend a hand when needed, whether this is to run an idea past them or to provide cake and beer after a particularly trying week.

I also feel like a lot of thanks needs to be given to my friends outside of science who still to this day have no idea what I have been working on for the last 4 years. The life outside science has been my saviour when PhD life became a little bit stressful.

Without these fantastic people in my life, and those I have met along the way, I don't believe my PhD would have been half as exciting and fulfilling.

From the bottom of my heart, thanks to each and every one of you.

Abstract

Oxidation-responsive polymers are useful in the field of drug delivery as they allow the targeted release of drugs in areas where there is a high concentration of reactive oxygen species, i.e. from autoimmune diseases. In this thesis a variety of dual temperature- and oxidation-responsive materials were synthesised.

In chapter 2, a series of polymers of *N*-isopropylacrylamide (NIPAM) were synthesised by Reversible Addition–Fragmentation chain-Transfer (RAFT) polymerisation with varying degrees of polymerisation from 10 – 100 using different chain transfer agents (CTA). These polymers were oxidised to determine the applicability of the RAFT CTA end group as oxidative triggers for morphological change. Full polymer characterisation was performed before and after oxidation via ¹H NMR, GPC, IR spectra and mass spectra and their cloud points were determined. A difference was seen in the colour of the polymer samples, from yellow to white on oxidation which indicated cleavage of the RAFT chain end group. This was confirmed by mass spectrometry showing cleavage of the Z group of the RAFT agent converting the trithiocarbonate to a sulfonic acid group as the major product. This changed the hydrophobicity of the polymer as can be seen with an increase in the cloud point. This effect was greater for shorter chain polymers as the ratio of polymer to RAFT chain transfer agent is lower. When the RAFT agent was changed to one which was dodecyl based and therefore more hydrophobic, there was no change in cloud point and the mass spectra were complex showing multiple species present after oxidation.

To determine whether the cleavage of the RAFT chain end group could cause disassembly of self-assembled polymers, a series of short pNIPAM block diblock copolymers were synthesised using three different RAFT agents and *N*-(2-Hydroxyethyl)acrylamide (HEA) as the water-soluble macro chain transfer agent (mCTA). These were analysed by DLS to assess any self-assembly above the LCST. DLS showed that self-assembly did not occur above the LCST.

Using MPP and PPA as the RAFT agents, a series of pHEA-*b*-pNIPAM_n copolymers were synthesised with varying lengths of the pNIPAM block from a targeted length of 100 – 300. Also, diblock copolymer were synthesised with 2 mol% of BAPE, an oxidation responsive monomer incorporated into the pNIPAM block, pHEA-*b*-p(NIPAM-*stat*-BAPE)_n, with the targeted DP of these blocks the same as above. The samples with a temperature responsive block length of over 150 units showed self-assembly above the LCST and their effective diameter, as determined by DLS was less than 100 nm. On oxidation of the polymer with a pNIPAM based hydrophobic block, no change in size is seen, however when BAPE is incorporated into the hydrophobic block of the polymer there is an increase in size of the particles as seen by DLS. The change in the LCST on oxidation of BAPE does not cause the polymer chains to become soluble at 37 °C and self-assembly is still observed.

Complementary nanogels (NG) were synthesised of pHEA-*b*-pNIPAM and pHEA-*b*-p(NIPAM-*stat*-BAPE) with the core crosslinked with varying ratios of *N,N'*-Methylenebis(acrylamide) during synthesis of the second block. This was to ensure more stable assembly of the particles than the micelles formed above. The targeted lengths of the second block were the same as with the above diblock copolymers. The conversion was determined via moisture analysis and the particle size was determine by DLS and TEM. There was a difference seen in the trend of size and morphology between the NG with and without oxidation responsive groups, yet both shrunk in size on heating to temperatures above the LCST.

The oxidation responsive behaviour of the nanogels with H₂O₂ was determined in detail using DLS to analyse the particle size and by TEM to assess the morphological difference between the native and oxidised particles. The particles swell on oxidation when the nanogels contain BAPE with the amount of swelling being dependant on the crosslinker concentration in the core. The higher the concentration of H₂O₂, the faster the response, however the nanogels are sensitive to concentrations as low as 0.1 mM. The sensitivity to reactive oxygen species other than H₂O₂; SIN-1

and hydroxy radicals, and a common reducing agent, glutathione, was also determined using in situ DLS studies, which showed that these nanogels are specifically sensitive to H₂O₂.

In-depth analysis of the morphology of numerous samples was performed. The combination of DLS, SAXS, TEM and AF4 combined with DLS and MALS allowed for successful determination of the size and shape of some of the NGs. This showed that these nanogels were composed of two different particle morphologies, and therefore particle sizes, usually with one more elongated, although the length of these varied. The NGs with BAPE in the core had more well-defined morphologies than those with pNIPAM alone. Overall, a more accurate view of these particles was achieved by minimising the limitations of individual techniques.

Conferences attended during PhD

5th – 6th April 2016 – *Attended* Macro group Young researchers meeting at the University of Liverpool

11th – 14th June 2016 – *Attended* Warwick international polymer conference

15th June 2016 – *Attended* Molecular Imaging 2016

10th April 2017 – *Attended* Colloids Young researchers meeting

16th May 2017 – *Poster presentation* at Nanomaterials at the University of Manchester

19th – 20th June 2017 – *Oral presentation* at Macro group Young researchers meeting University of Edinburgh

10th – 11th January 2018 – *Poster presentation* at RSC biomaterials in Bradford

16th-17th July 2018 - *Poster presentation* at Macro group Young researchers meeting University of Dublin

9th – 11th January 2019 - *Oral presentation* at RSC biomaterials University of Liverpool

Contents

1.	Introduction to oxidation-responsive polymeric drug delivery systems	1
1.	Introduction	2
1.1.	The need for drug delivery systems.....	2
1.2.	Autoimmune diseases and oxidative stress	3
1.3.	Diseases affected by oxidative stress	5
1.3.1	Cancer.....	5
1.3.2.	Rheumatoid arthritis.....	7
1.3.5.	Multiple sclerosis	11
1.4.	General polymer drug delivery.....	13
1.4.1	Criteria for a suitable polymer therapeutic.....	13
1.5.	Types of potential polymeric drug delivery systems	16
1.6.	Historical clinical trials of polymer therapeutics	19
1.7.	Redox responsive polymers.....	29
1.7.1.	Reduction responsive systems	29
1.7.2.	Oxidation responsive systems	31
1.7.3.	Summary of responsive systems	50
1.8.	Temperature Responsive Polymers	51
1.8.1.	Poly(N-isopropylacrylamide)	54
1.9.	Synthesis of polymers	55
1.9.1.	Free radical polymerisation.....	55
1.9.2.	Controlled/Living radical polymerisation.....	56
1.10.	Thesis Outline.....	62
1.11.	References	64
2.	Experimental	71
2.1.	General materials	72
2.2.	Instrumentation	73
2.2.1.	NMR Spectroscopy.....	73
2.2.2.	Gel Permeation Chromatography (GPC).....	73
2.2.3.	Infrared (IR) Spectroscopy	73
2.2.4.	Cloud point determination.....	73

2.2.5. Mass spectrometry.....	74
2.2.6. Elemental analysis.....	74
2.2.7. Gravimetric Analysis.....	74
2.2.8. Dynamic Light Scattering (DLS).....	74
2.2.9. Transmission Electron Microscopy (TEM).....	75
2.2.10. Small-Angle X-ray Scattering (SAXS) measurements.....	75
2.2.11. Asymmetric Flow Field-Flow Fractionation (AF4).....	75
2.3. Synthetic methods.....	77
2.3.1. General synthesis of RAFT chain transfer agents.....	77
2.3.2. Synthesis of methyl (2-dodecanethiocarbonothioylthio) propanoate (MDDP) RAFT chain transfer agent.....	78
2.3.3. General synthesis of pNIPAM by RAFT polymerisation.....	79
2.3.4. Oxidation of pNIPAM using hydrogen peroxide.....	80
2.3.5. Synthesis of 2-(propylthiocarbonothioylthio)propanoic acid (PPA) RAFT agent.....	80
2.3.6. Synthesis of pHEA-mCTA by RAFT polymerisation.....	81
2.3.7. Synthesis of pHEA- <i>b</i> -pNIPAM diblock copolymers.....	82
2.3.8. Synthesis of pNIPAM- <i>b</i> -pHEA diblock copolymers.....	82
2.3.9. Synthesis of 4-(acryloyloxymethyl) phenylboronic acid pinacol ester (BAPE).....	83
2.3.10. Synthesis of pHEA- <i>b</i> -pNIPAM diblock copolymers in cononsolvents.....	84
2.3.11. Synthesis of linear statistical copolymers of p(NIPAM- <i>stat</i> -BAPE).....	84
2.3.12. Synthesis of pHEA- <i>b</i> -p(NIPAM- <i>stat</i> -BAPE) diblock copolymers in cononsolvents.....	85
2.3.15. Calculation of theoretical BAPE content in NGs	87
3. Utilisation of the RAFT chain end group as an oxidation sensitive trigger.....	89
3.1. Introduction.....	90
3.2. Results and Discussion.....	93
3.2.1. Synthesis of pNIPAM via RAFT solution polymerisation.....	93
3.2.2. Analysis of the effect of oxidation on the cloud point.....	97
3.2.3. Synthesis of pNIPAM via RAFT solution polymerisation using non-ionisable RAFT agents.....	100
3.2.4. Effects of oxidation on the RAFT chain end group.....	104
3.2.5. Determination of the chemical change in the end group of pNIPAM ₈ by chemical analysis.....	106
3.2.6. The effect of oxidation of polymers with different RAFT chain transfer agents	111
3.2.7. Oxidation using different concentrations of hydrogen peroxide.....	114

3.2.8. Synthesis of pNIPAM via RAFT solution polymerisation using a more hydrophobic non-ionisable RAFT agent	118
3.3. Conclusion	125
3.4. References	127
Appendix A.....	129
4 Oxidation-responsive block copolymer micelles of poly(<i>N</i> -(2-hydroxyethyl)acrylamide)- <i>b</i> -poly(<i>N</i> -isopropylacrylamide)	141
4.1. Introduction	142
4.2. Results and Discussion	145
4.2.1. Forming diblock copolymers with a short pNIPAM block to induce a change in cloud point large enough to disrupt self-assembly.....	145
4.2.1.1. Diblock copolymers using polymers of <i>N</i> -(2-hydroxyethyl)acrylamide as macro-chain transfer agents.....	146
4.2.1.2. Diblock copolymers using polymers of <i>N</i> -isopropylacrylamide as macro-chain transfer agents	153
4.2.1.3. Determination of the particle size of the self-assembled structures	157
4.2.2. Synthesis of pHEA- <i>b</i> -pNIPAM diblock copolymers with longer pNIPAM block lengths in consolvents via RAFT dispersion polymerisation.....	159
4.2.2.1. Forming diblock copolymers which self-assemble in an aqueous environment at body temperature	159
4.2.2.2. Determination of the particle size of the self-assembled structures	162
4.2.2.3. Using a more hydrophilic RAFT agent (PPA) to promote self-assembly	166
4.2.2.4. Determination of the particle size of the self-assembled structures	169
4.2.3. Synthesis of an oxidation responsive monomer and analysis of its impact on size and LCST of pNIPAM polymers.....	171
4.2.4. Synthesis of oxidation responsive diblock copolymers of pHEA- <i>b</i> -p(NIPAM- <i>stat</i> -BAPE) in consolvents via RAFT dispersion polymerisation	177
4.2.4.1. Determination of the particle size of the self-assembled structures	180
4.3. Conclusions.....	186
4.4. References	188
Appendix B.....	191
5. Synthesis and characterisation of oxidation responsive nanogels	217
5.1. Introduction	218
5.2. Results and Discussion	221
5.2.1. Synthesis of pHEA- <i>b</i> -p(NIPAM- <i>stat</i> -BAPE) nanogels	221

5.2.2.	The effect of the length of the core-forming block on particle size.....	222
5.2.3.	The temperature responsive behaviour of core-crosslinked nanogels.....	231
5.2.4.	Effect of crosslinker concentration on nanogel swelling.....	233
5.2.5.	The effect of BAPE concentration on particle size, morphology and oxidation response.....	237
5.2.6.	The effect of increasing the amount of BAPE in the core forming block	245
5.2.7.	In depth analysis on the morphology and oxidation properties of the nanogels	250
5.3.	Conclusions.....	278
5.4.	References	280
Appendix C.....		287
6	Conclusions and Future work	304
6.1.	Conclusions.....	305
6.2.	Future work	307
6.3.	References	311

Abbreviations

ACVA	4,4'-Azobis(4-cyanovaleric acid)
AIBN	Azobisisobutyronitrile
ATRP	Atom transfer radical polymerisation
BAPE	4-(4,4,5,5-tetramethyl-1,3,2-dioxaborolan-2-yl) benzyl acrylate – oxidation responsive monomer
BIS	Methylene bisacrylamide
CMC	Critical micelle concentration
CNS	Central nervous system
CTA	Chain transfer agent
CPT	Camptothecin
α -CD	α -cyclodextrin
DCM	Dichloromethane
DDS	Drug delivery system
DLS	Dynamic light scattering
DMARDS	Disease-modifying antirheumatic drugs
DMF	Dimethyl formamide
DMSO	Dimethyl sulfoxide
DNA	Deoxyribonucleic acid
DOX	Doxorubicin
DP	Degree of polymerisation
DPBS	Dulbecco's phosphate buffer solution
DTT	Dithiothreitol
EMEM	methyl 2-(ethylthiocarbonothioylthio)propanoate
EMP	2-(ethylsulfanylthiocarbonylsulfanyl)-2-methylpropionic acid
ES	Electrospray
GPC	Gel permeation chromatography
GSH	Glutathione
HEA	Hydroxyethyl acrylamide

HeLa	Human cervical cell line
HepG2	Human hepatoma cell line
HIFU	High intensity focused ultrasound
IFN- γ	Interferon-gamma
Ig	Immunoglobulin
IL-1	Interleukin-1
IR	Infrared
LCST	Lower critical solution temperature
MALDI-ToF MS	Matrix-assisted laser desorption time of flight mass spectroscopy
MBP	methyl 2-(butylthiocarbonothioylthio)propanoate
MDDP	methyl 2-(dodecylthiocarbonothioylthio)propanoate
MMA	Methyl methacrylate
M_n	Number average molecular weight
MPP	methyl 2-(propylthiocarbonothioylthio)propanoate
PPA	2-(propylthiocarbonothioylthio)propanoic acid
NADPH	Nicotinamide adenine dinucleotide phosphate
NIPAM	N-isopropylacrylamide
NG	Nanogel
NMR	Nuclear magnetic resonance
TMBQ	Trimethyl-locked benzoquinone
TNF	Tumour necrosis factor
PDI	Polydispersity index - Weight average molecular weight/Number average molecular weight
PEG	Polyethylene glycol
PF1	Fluorescein peroxyfluor-1
PFS	Polyferrocenylsilane
PISA	Polymerisation induced self-assembly
PPS	Polypropylene sulphide
PRX	Polyrotaxanes
RAFT	Reversible addition fragmentation chain transfer
RNA	Ribonucleic acid

RNS	Reactive nitrogen species
ROP	Ring opening polymerisation
ROS	Reactive oxygen species
TEA	Triethylamine
TEM	Transmission electron microscopy
UCST	Upper critical solution temperature
-ss-	Disulfide linkage

Glossary

Angiogenesis	The development of new blood vessels
Apoptosis	Cell death
Biocompatible	Compatible with living tissue i.e. non-toxic and non-injurious effects on the body
Biodistribution	A method of tracking where compounds travel in the body
Cononsolvency	Where a mixture of two good solvents for a polymer is a bad solvent for the same polymer
Cytokines	Small proteins involved in cell signalling
Dendritic cells	Antigen-presenting cells of the immune system
Hypoxia	A condition where there is insufficient oxygen reaching the lungs
IFN-γ	A soluble cytokine, type II interferon which activates macrophages. It is associated mainly with autoimmune disease
Immunoglobulin	Antibody
Leukocyte	A white blood cell
Lipophilicity	The ability of a compound to dissolve in fats, oils, lipids, and non-polar solvents
Lymphocytes	A form of white blood cell
Macrophages	A type of white blood cell that engulfs and digests substances which the cell deems as a foreign object
Metastasis	The spread of disease from one part of the body to another
Monocytes	Large phagocytic white blood cells
Neutrophils	A neutrophilic white blood cell
Oligodendrocytes	Non-neuronal cells which support and insulate the axons of the central nervous system
Oncogenes	A gene which has the potential to cause cancer to another gene
Oxidative responsive	Where a species undergoes a change due to the presence of an oxidising species
P53 proteins	Proteins which regulate the cell cycle
Pharmacokinetics	The movement of drugs within the body
Proliferate	Reproduce rapidly
Topoisomerase	An enzyme that participates in the overwinding or underwinding of DNA

List of Figures

Figure 1.1 - Schematic of possible pharmacokinetic routes of drug within the body. Reproduced with permission. ³ Copyright © 2017 Elsevier Inc. All rights reserved.	3
Figure 1.2 - Examples commonly used chemotherapeutics for the treatment of cancer.....	7
Figure 1.3- Comparison of a healthy joint to one affected by rheumatoid arthritis.....	8
Figure 1.4- A comparison of a healthy nerve cell compared to one which has been damaged by the action of multiple sclerosis.....	11
Figure 1.5 - Schematic of the common polymer-based drug delivery systems.....	17
Figure 1.6 - A summary of the main oxidation-responsive functional groups and the products of oxidation (reproduced) ⁹⁵	32
Figure 1.7 - A representation of the three types of self-assembled structures; linear, star and comb, and graphs comparing the lag time to oxidation dependant on the number of arms. Reproduced with permission from ref. 99. © 2016 WILEY-VCH Verlag GmbH & Co. KGaA, Weinheim. ⁹⁹	34
Figure 1.8 - A) Schematic illustration of the formation of PPS-PNIPAm micellar aggregation. B) DLS measurement of PPS ₁₀ -PNIPAm ₄₀ particles in water. Polymer concentration: 1 mg/mL. C) SEM image of PPS ₁₀ -PNIPAm ₄₀ particles. Polymer concentration: 0.5 mg/mL. Magnification: 30.0 kx. Reproduced with permission from ref.100. Copyright © 2016 Elsevier Ltd. ¹⁰⁰	35
Figure 1.9 - A schematic of the oxidation and disassembly of selenium-containing block copolymer micelles with 0.1% v/v H ₂ O ₂ , causing the release of DOX. ¹⁰⁶ Reproduced by permission of The Royal Society of Chemistry	37
Figure 1.10 - TEM (a) and cryo-TEM (b) images of PEG-PUSe-PEG copolymer micelles; TEM images of the aggregates after 2 h (c) and 5 h (d) oxidation in 0.1% H ₂ O ₂ solution; cryo-TEM image of the oxidized aggregates after 5 h (e). Reproduced from Ref. ¹⁰⁶ with permission from The Royal Society of Chemistry. ¹⁰⁶	37
Figure 1.11 – The disassembly and reassembly of spherical PEG-b-PAA structures in the presence of H ₂ O ₂ and vitamin C. Reproduced by permission of The Royal Society of Chemistry. ¹⁰⁸	38
Figure 1.12 – Synthesis of the 6 different oxalates with their half-life on oxidation and the degradation of AOE1 Δ, AOE2 ○, AOE3 ▴, AOE4 –, AOE5x, AOE6 ◆. (0.5 mg/mL oxalates, 50 mmol/L H ₂ O ₂), showing that the degradation rate depends on the position and nature of the substituents. Reproduced with permission from ref. ¹¹⁰ . Copyright © 2011 Elsevier Ltd.	40
Figure 1.13 - Multifunctional H ₂ O ₂ -activatable nanoparticles as a novel strategy for bioimaging and therapy. HPOX nanoparticles can serve as H ₂ O ₂ imaging agents, therapeutics and site-directed drug delivery systems. Reprinted from ref. ¹¹¹ , Copyright (2013), with permission from Elsevier Ltd.	41
Figure 1.14 - The general structure of an oxalate-ester containing ferulic acid-based poly(anhydride ester). ¹¹²	41
Figure 1.15 - Schematics for the Fabrication of Oxidation-Responsive Multifunctional Polymersomes Exhibiting Intracellular Milieu-Triggered Vesicle Bilayer Cross-Linking, Permeability Switching, and Enhanced Imaging/Drug Release Features. Reprinted with permission from Ref. ¹¹⁵ Copyright 2019 American Chemical Society.....	43
Figure 1.16 – Oxidation-promoted degradation of aliphatic Poly(carbonate)s via sequential 1,6-elimination and intramolecular cyclisation. Reprinted with permission from ref. ¹¹⁶ . Copyright 2015 American Chemical Society. ¹¹⁶	44
Figure 1.17 -TEM images of nanoparticles. (a, c) After 72 h of incubation in PBS; (b, d) after 72 h in PBS containing 1 mM H ₂ O ₂ . Reprinted with permission from reference ¹¹⁸ . Copyright 2012 American Chemical Society. ¹¹⁸	45
Figure 1.18 - Synthesis of oxidation responsive amphiphilic poly(amino ester)s which can be completely degraded in aqueous media via H ₂ O ₂ oxidation. Reprinted with permission from reference ¹²¹ . Copyright 2013 American Chemical Society. ¹²¹	46
Figure 1.19 - Schematic Illustration of (a) ONOO ⁻ -induced oxidation-elimination reaction, (b) ONOO ⁻ signalling molecule responsive block copolymer (PEO-b-PMATFK), and their controllable self-assembly and disassembly. Reprinted with permission from Ref. ¹³⁰ Copyright 2019 American Chemical Society.....	49

Figure 1.20 - Illustration of the assembly and disassembly of thermo- and oxidation-responsive supramolecular polymeric vesicles from PNIPAM-P[6] \cap mPEG-Fc. Reproduced from Ref. ¹³² with permission from The Royal Society of Chemistry. ¹³²	50
Figure 1.21 - An example figure showing polymer phase transitions including LCST and UCST.....	51
Figure 1.22 - The effect of temperature on pNIPAM showing the coil to globule transition when heated to temperatures above the LCST.	55
Figure 1.23 - The equilibrium steps of the three common types of RDRP. ¹⁵⁸⁻¹⁶⁰	58
Figure 1.24 - A schematic of a RAFT polymerisation denoting many of the species present during a polymerisation of this kind. It must be noted however, that the concentration of initiator fragments is ideally not this high, and that the proportion of dormant chains is much higher than shown. Reprinted with permission from Ref. ¹⁵⁸ . Copyright 2006 American Chemical Society.	59
Figure 1.25 - The mechanism of RAFT polymerisation. ^{157,163}	60
Figure 1.26 - Typical types of RAFT chain transfer agents: a) xanthates, b) trithiocarbonates, c) dithioesters and d) dithiocarbamates. ^{164,165,167,168}	62
Figure 1.27- The general structure of a chain transfer agent. ¹⁶³	62
Figure 2.1 - Optimised method for fractionation conditions of the nanogels looking at the cross-flow over time...	76
Figure 3.1 - The general structure of a RAFT agent indicating R and Z groups	93
Figure 3.2 - ¹ H NMR spectrum of pNIPAM ₅₀ synthesised with EMP as the CTA in CDCl ₃ before purification to determine the monomer to polymer conversion.	95
Figure 3.3 - GPC chromatograms (DMF 0.1% LiBr) of pNIPAM polymers with nominal targeted DP of 50, 75 and 100, where M _n refers to the number-average molecular weight and M _w /M _n refers to the dispersity calculated. ...	96
Figure 3.4 - ¹ H NMR spectrum of pNIPAM synthesised with EMP as the CTA in CDCl ₃ to determine the degree of polymerisation	97
Figure 3.5 - UV/vis spectra monitoring change in absorbance over temperature at 550 nm of various pNIPAM-EMP samples before and after oxidation in water	99
Figure 3.6 - UV/vis spectra monitoring change in absorbance over temperature at 550 nm of various pNIPAM-EMP samples before and after oxidation in DPBS	99
Figure 3.7 - Monomer conversion and pseudo-first order kinetic plot determined by ¹ H NMR spectroscopy for the polymerisation of NIPAM (DP 22 as determined ¹ H NMR spectroscopy) using MPP as the RAFT agent.	101
Figure 3.8 - a) GPC chromatograms (DMF 0.1% LiBr) of samples removed during the polymerisation of NIPAM (DP 22) using MPP as the RAFT agent. M _n and M _w /M _n were determined relative to pMMA standards and b) Evolution of M _n and M _w /M _n with monomer conversion.....	102
Figure 3.9 - GPC chromatograms (DMF 0.1% LiBr) of polymers of NIPAM synthesised using MPP RAFT agent with a DP of 8, 19, 37, 69 and 78, as determined by NMR spectroscopy.....	104
Figure 3.10 - Cloud point measurements of pNIPAM polymers synthesised using MPP before and after oxidation. Cloud point curves were recorded by monitoring the absorbance at 550 nm with increasing temperatures. The DP of the polymers refers to those calculated by ¹ H NMR spectroscopy. The solid lines indicate polymers before oxidation and the dashed lines represent the polymers after oxidation.	106
Figure 3.11 - GPC chromatograms (DMF 0.1% LiBr) of pNIPAM synthesised using MPP before and after oxidation with H ₂ O ₂ . The solid lines indicate polymers before oxidation and the dashed lines represent the polymers after oxidation with 15 mM H ₂ O ₂	107
Figure 3.12 - A comparison of the IR spectra before and after oxidation of pNIPAM-MPP with a DP of 8. The green ovals highlight the main differences.	109
Figure 3.13 - Comparison of mass spectra data of pNIPAM8-MPP before and after oxidation in ES+ and ES- respectively.	110
Figure 3.14 - GPC traces of pNIPAM with a DP of 25, synthesised using the RAFT agents EMEM, MPP and MBP.	112
Figure 3.15 - Cloud point analysis at 550 nm of DP 25 pNIPAM synthesised using EMEM, MPP and MBP RAFT agents, before and after oxidation. The solid lines indicate polymers before oxidation and the dashed lines represent the polymers after oxidation.	113
Figure 3.16 - A comparison of the IR spectra before and after oxidation with 15 mM H ₂ O ₂ , of pNIPAM-MPP with a DP of 25. No obvious differences can be observed.	114

Figure 3.17 - Cloud point analysis at 550 nm of DP 25 pNIPAM-MPP before oxidation and after oxidation at a polymer concentration of 1 mg mL ⁻¹ , where the concentration of H ₂ O ₂ has been varied.	115
Figure 3.18 - Mass spectra of pNIPAM ₂₅ -MPP before and after oxidation with two different concentrations of H ₂ O ₂ , 0.1 and 15 mM. The double-headed arrow indicates NIPAM units and the single-headed arrow indicates the change from trithiocarbonate to a sulfonic acid end group.	116
Figure 3.19 - Comparison of negative mode mass spectra of pNIPAM ₂₅ -MPP before and after oxidation with different concentrations of H ₂ O ₂	116
Figure 3.20 - a) GPC chromatograms (DMF 0.1% LiBr) of samples removed during the polymerisation of NIPAM (DP 21) using MDDP as the RAFT agent. M _n and M _w /M _n were determined relative to pMMA standards and b) Evolution of M _n and M _w /M _n with monomer conversion.	119
Figure 3.21 - GPC chromatograms (DMF 0.1% LiBr) for pNIPAM DP 21, 48 and 97 polymerised using MDDP as the RAFT agent.	120
Figure 3.22 - Graphs showing the difference in cloud point between native pNIPAM and polymer oxidised with a) 15 mM H ₂ O ₂ and b) 100 mM H ₂ O ₂	121
Figure 3.23 - DLS chromatograms (DMF 0.1% LiBr) of pNIPAM ₂₅ -MDDP at a concentration of 0.1 wt% in water at 15 °C. All 3 traces are different measurements at the same temperature of the same polymer to determine where self-assembly occurs. No stable self-assembly of these pseudo-amphiphilic polymers is observed with no overlap between traces.	122
Figure 3.24 - A comparison of the IR spectra before and after oxidation of pNIPAM-MDDP with a DP of 21.	123
Figure 3.25 - Mass spectra of pNIPAM ₂₁ -MDDP before and after oxidation with 15 mM H ₂ O ₂ . The single-headed arrows indicate potential known products. ^{5-7,32}	124
Figure A.1 - ¹ H NMR spectrum of EMEM RAFT agent recorded in CDCl ₃	129
Figure A.2 - ¹³ C NMR spectrum of EMEM RAFT agent recorded in CDCl ₃	129
Figure A.3 - ¹ H NMR spectrum of MPP RAFT agent recorded in CDCl ₃	130
Figure A.4 - ¹³ C NMR spectrum of MPP RAFT agent recorded in CDCl ₃	130
Figure A.5 - ¹ H NMR spectrum of MBP RAFT agent recorded in CDCl ₃	131
Figure A.6 - ¹³ C NMR spectrum of MBP RAFT agent recorded in CDCl ₃	131
Figure A.7 - GPC trace of DP 10, 27, 48 and 100 pNIPAM synthesised using EMEM as the RAFT agent.	132
Figure A.8 - GPC trace of DP 27, 42 and 90 pNIPAM synthesised using MBP as the RAFT agent.	132
Figure A.9 - UV/vis traces giving the cloud point of pNIPAM polymers synthesised using the EMEM chain transfer agent before and after oxidation. The cloud point was determined with a polymer concentration of 1 mg mL ⁻¹ in water at a wavelength of 550 nm. The solid lines indicate polymers before oxidation and the dashed lines represent the polymers after oxidation.	133
Figure A.10 - UV/vis traces giving the cloud point of pNIPAM polymers synthesised using the MBP chain transfer agent before and after oxidation. The cloud point was determined with a polymer concentration of 1 mg mL ⁻¹ in water at a wavelength of 550 nm. The solid lines indicate polymers before oxidation and the dashed lines represent the polymers after oxidation.	133
Figure A.11 - Comparison of the GPC traces before and after oxidation of pNIPAM-EMEM. The solid lines indicate polymers before oxidation and the dashed lines represent the polymers after oxidation.	134
Figure A.12 - Comparison of the GPC traces before and after oxidation of pNIPAM-MBP. The solid lines indicate polymers before oxidation and the dashed lines represent the polymers after oxidation.	134
Figure A.13 - A comparison of the IR spectra before and after oxidation of pNIPAM-EMEM with a DP of 22.	135
Figure A.14 - A comparison of the IR spectra before and after oxidation of pNIPAM-MBP with a DP of 26.	135
Figure A.15 - Comparison of mass spectra data of pNIPAM ₂₃ -EMEM before and after oxidation in ES+ and ES- respectively.	136
Figure A.16 - Comparison of mass spectra data of pNIPAM ₂₄ -MBP before and after oxidation in ES+ and ES- respectively.	136
Figure A.17 - ¹ H NMR spectrum of MDDP RAFT agent recorded in CDCl ₃	137
Figure A.18 - ¹³ C NMR spectrum of MDDP RAFT agent recorded in CDCl ₃	138
Figure A.19 - ¹ H NMR spectrum of MDDP acid RAFT agent recorded in CDCl ₃	139
Figure A.20 - ¹³ C NMR spectrum of MDDP acid RAFT agent recorded in CDCl ₃	140

Figure 4.1 - a) The synthesis of pHEA-b-pNIPAM using the RAFT agent MPP as an example, defining where the RAFT chain end groups are bound to the polymer chains, b) The expected result on oxidation of the self-assembled polymer showing disassembly due to the chain in the RAFT chain end group bound to the pNIPAM block	146
Figure 4.2 - A ^1H NMR spectrum of pHEA-MPP (target DP 50) in D_2O 90 minutes into the reaction to determine the monomer to polymer conversion. The ratio of total protons seen in both monomer and polymer (d and e) and those in the monomer only (a,b and c) can be used to determine the actual DP.	147
Figure 4.3 - Monomer conversion and pseudo-first order kinetic plot for the polymerisation of HEA (targeted DP 50) using MPP as the RAFT agent. Monomer conversion was determined by ^1H NMR spectroscopy.....	148
Figure 4.4 – a) GPC chromatograms (DMF 0.1% LiBr) of samples removed during the polymerisation of HEA (DP 50) using MPP as the RAFT agent. M_n and M_w/M_n were determined relative to pMMA standards and b) Comparison of the monomer conversion with M_n and M_w/M_n	149
Figure 4.5 - GPC chromatograms (DMF 0.1% LiBr) of pHEA-mCTAs synthesised using 3 different RAFT agents....	151
Figure 4.6 - GPC chromatograms (DMF 0.1% LiBr) of pHEA-mCTA and pHEA-b-pNIPAM, synthesised using 3 different RAFT agents: a) EMEM, b) MPP, c) MBP, and d) a comparison of the GPC chromatograms of the 3 diblock copolymers.	153
Figure 4.7 - a) The synthesis of pNIPAM-b-pHEA using the RAFT agent MPP as an example, defining where the RAFT chain end groups are bound to the polymer chains, b) The expected result on oxidation of the self-assembled polymer showing no disassembly as the resulting sulfonic acid group is not bound to the temperature responsive pNIPAM block	154
Figure 4.9 - The GPC chromatograms (DMF 0.1% LiBr) of three pNIPAM-mCTA synthesised using 3 different RAFT agents; EMEM, MPP and MBP, where M_n refers to the number average molecular weight and M_w/M_n refers to the dispersity.	155
Figure 4.10 - GPC chromatograms (DMF 0.1% LiBr) of pNIPAM-mCTA and the chain extension of this with HEA, synthesised using 3 different RAFT agents: a) EMEM, b) MPP, c) MBP and d) a comparison of the GPC chromatograms of the 3 diblock copolymers.	156
Figure 4.11 - DLS particle size distributions of a) pHEA-b-pNIPAM and b) pNIPAM-b-pHEA at a concentration of 1 mg/ml. These were recorded in water at 35 °C in water where the RAFT agent used initially to synthesise the macro-CTA is i) EMEM, ii) MPP and iii) MBP	158
Figure 4.12 – Particle size distributions of pHEA ₄₆ -b-pNIPAM ₂₀ MPP at 0.1 wt% in water at varying temperatures, 25, 35 and 45 °C.....	159
Figure 4.13 - GPC chromatograms (DMF 0.1% LiBr) of pHEA ₄₅ -mCTA compared with the chain extended diblock copolymers of pHEA ₄₅ -b-p(NIPAM-stat-BAPE) _n , where n=132, 194, 250, 292 and 370	162
Figure 4.14 – Photograph above the LCST of diblock polymer samples of pHEA ₄₅ -b-pNIPAM _n , with n being 132, 194, 250, 292 and 370 from left to right.....	163
Figure 4.15 - DLS chromatograms and corresponding correlation curves (DMF 0.1% LiBr) of diblock copolymers of pHEA ₄₅ -b-pNIPAM _n , at a concentration of 1 mg/ml. These were recorded in water held at 37 °C, before and after oxidation where a) n=132, b) n=194, c) n=250, d) n=292 and e) n=370.	165
Figure 4.16 - A comparison of DLS of pHEA ₄₅ -b-pNIPAM ₂₉₂ at a concentration of 1 mg/ml. These were recorded in water at temperatures above and below the LCST of the polymer to determine self-whether self-assembly occurs as the pNIPAM block becomes hydrophobic	166
Figure 4.17 - GPC chromatograms (DMF 0.1% LiBr) of pHEA ₃₇ -mCTA compared with the chain extended diblock copolymers of pHEA ₃₇ -b-pNIPAM _n , where n=89, 146, 202, 199, 274.....	168
Figure 4.18 - DLS particle size distributions and the corresponding correlation curves of diblock copolymers of pHEA ₃₇ -b-pNIPAM _n , at a concentration of 1 mg/ml. These were recorded in water held at 37 °C, before and after oxidation where a) n=89, b) n=146, c) n=202, d) n=199 and e) n=274.	170
Figure 4.19 – A comparison of DLS of pHEA ₃₇ -b-pNIPAM ₁₉₉ at a concentration of 1 mg/ml. These were recorded in water at temperatures above and below the LCST of the polymer to determine self-whether self-assembly occurs as the pNIPAM block becomes hydrophobic	171
Figure 4.20 - GPC chromatograms (DMF 0.1% LiBr) for linear statistical polymers of pNIPAM-stat-BAPE with 2, 3, 5 and 10 mol% BAPE.....	175

Figure 4.21 - UV-vis traces of the absorbance of $p(\text{NIPAM-stat-BAPE})_{100}$ at a concentration of 0.1 wt%, with a range of different mole percent of BAPE. This occurred over a range of temperatures, giving cloud point values before and after oxidation. Solid lines indicate native polymers and dashed lines indicate the oxidised polymer.	177
Figure 4.22 - GPC chromatograms (DMF 0.1% LiBr) of $p\text{HEA}_{37}\text{-mCTA}$ compared with the chain extended diblock copolymers of $p\text{HEA}_{45}\text{-b-}p(\text{NIPAM-stat-BAPE})_n$, where $n=127, 193, 244, 301$ and 330 .	179
Figure 4.23 - GPC chromatograms (DMF 0.1% LiBr) of $p\text{HEA}_{37}\text{-mCTA}$ compared with the chain extended diblock copolymers of $p\text{HEA}_{37}\text{-b-}p(\text{NIPAM-stat-BAPE})_n$, where $n=101, 147, 193, 262, 318$.	180
Figure 4.24 - A comparison of DLS of $p\text{HEA}_{45/37}\text{-b-}p(\text{NIPAM-stat-BAPE})_{301/262}$, where a) MPP RAFT agent and b) PPA RAFT agent, at temperatures above and below the LCST of the polymer to determine whether self-assembly occurs as the $p(\text{NIPAM-stat-BAPE})$ block becomes hydrophobic.	181
Figure 4.25 - DLS size comparison of two similar diblock copolymers, one with a pNIPAM hydrophobic core at temperatures above the LCST and the other with a NIPAM and BAPE core, at a concentration of 1 mg/ml. These were recorded in water and show that when BAPE is incorporated into the core the self-assembled structure is smaller at 35 °C.	183
Figure 4.26 - DLS particle size distributions and corresponding correlation curves of diblock copolymers of $p\text{HEA}_{45}\text{-b-}p(\text{NIPAM-stat-BAPE})_n$, with MPP as the RAFT agent and 2 mol% BAPE, at a concentration of 1 mg/ml. These were recorded in water and held at 37 °C, before and after oxidation where a) $n=127$, b) $n=193$, c) $n=244$, d) $n=301$ and e) $n=330$.	184
Figure 4.27 - DLS particle size distributions and corresponding correlation curves (DMF 0.1% LiBr) of diblock copolymers of $p\text{HEA}_{37}\text{-b-}p(\text{NIPAM-stat-BAPE})_n$, with PPA as the RAFT agent and 2 mol% BAPE, at a concentration of 1 mg/ml. These were recorded in water and held at 37 °C, before and after oxidation where a) $n=101$, b) $n=147$, c) $n=193$, d) $n=262$ and e) $n=318$.	185
Figure B.1 - ^1H NMR spectrum of $p\text{HEA}_{19}\text{-EMEM}$ in D_2O . Degree of polymerisation was determined from the ratio of the integrals for methyl group of RAFT end group (1.20 ppm) and side chains on HEA (3.00-3.65 ppm).	192
Figure B.2 - ^1H NMR spectrum of $p\text{HEA}_{20}\text{-MPP}$ in D_2O . Degree of polymerisation was determined from the ratio of the integrals for methyl group of RAFT end group (0.85 ppm) and side chains on HEA (3.00-3.65 ppm).	193
Figure B.3 - ^1H NMR spectrum of $p\text{HEA}_{20}\text{-MBP}$ in D_2O . Degree of polymerisation was determined from the ratio of the integrals for methyl group of RAFT end group (0.75 ppm) and side chains on HEA (3.00-3.65 ppm).	194
Figure B.4 - ^1H NMR spectrum of $p\text{NIPAM}_{24}\text{-EMEM}$ in CDCl_3 . Degree of polymerisation was determined from the ratio of the integrals for methylene group of RAFT end group (3.35 ppm) and the CH_3CH group on NIPAM (4.05 ppm).	195
Figure B.5 - ^1H NMR spectrum of $p\text{NIPAM}_{22}\text{-MPP}$ in CDCl_3 . Degree of polymerisation was determined from the ratio of the integrals for methylene group of RAFT end group (3.35 ppm) and the CH_3CH group on NIPAM (4.05 ppm).	196
Figure B.6 - ^1H NMR spectrum of $p\text{NIPAM}_{23}\text{-MBP}$ in CDCl_3 . Degree of polymerisation was determined from the ratio of the integrals for methylene group of RAFT end group (3.35 ppm) and the CH_3CH group on NIPAM (4.05 ppm).	197
Figure B.7 - ^1H NMR spectrum of $p\text{HEA}_{42}\text{-b-}p\text{NIPAM}_{19}\text{-EMEM}$ in D_2O . Degree of polymerisation was determined from the ratio of the integrals for the CH_3CH group on NIPAM (3.75 ppm) and the side chains on HEA (3.00-3.65 ppm), knowing the DP of the $p\text{HEA-mCTA}$.	198
Figure B.8 - ^1H NMR spectrum of $p\text{HEA}_{47}\text{-b-}p\text{NIPAM}_{20}\text{-MPP}$ in D_2O . Degree of polymerisation was determined from the ratio of the integrals for the CH_3CH group on NIPAM (3.75 ppm) and the side chains on HEA (3.00-3.65 ppm), knowing the DP of the $p\text{HEA-mCTA}$.	199
Figure B.9 - ^1H NMR spectrum of $p\text{HEA}_{50}\text{-b-}p\text{NIPAM}_{20}\text{-MBP}$ in D_2O . Degree of polymerisation was determined from the ratio of the integrals of the CH_3CH group on NIPAM (3.75 ppm) and the side chains on HEA (3.00-3.65 ppm), knowing the DP of the $p\text{HEA-mCTA}$.	200
Figure B.10 - ^1H NMR spectrum of $p\text{NIPAM}_{24}\text{-b-}p\text{HEA}_{43}\text{-EMEM}$ in D_2O . Degree of polymerisation was determined from the ratio of the integrals of the CH_3CH group on NIPAM (3.75 ppm) and the side chains on HEA (3.00-3.65 ppm), knowing the DP of the $p\text{NIPAM-mCTA}$.	201
Figure B.11 - ^1H NMR spectrum of $p\text{NIPAM}_{22}\text{-b-}p\text{HEA}_{38}\text{-MPP}$ in D_2O . Degree of polymerisation was determined from the ratio of the integrals of the CH_3CH group on NIPAM (3.75 ppm) and the side chains on HEA (3.00-3.65 ppm), knowing the DP of the $p\text{NIPAM-mCTA}$.	202
Figure B.12 - ^1H NMR spectrum of $p\text{NIPAM}_{23}\text{-b-}p\text{HEA}_{31}\text{-MBP}$ in D_2O . Degree of polymerisation was determined from the ratio of the for the CH_3CH group on NIPAM (3.75 ppm) and the side chains on HEA (3.00-3.65 ppm), knowing the DP of the $p\text{NIPAM-mCTA}$.	203

Figure B.13 - DLS correlation curves for all short chain pHEA-b-pNIPAM and pNIPAM-b-pHEA with EMEM, MPP and MBP RAFT agents at temperatures above and below the LCST, showing lack of self-assembly for these polymers as expected from the corresponding DLS chromatograms.	204
Figure B.14 - ^1H NMR spectrum of pHEA ₄₅ -MPP in D ₂ O. Degree of polymerisation was determined from the ratio of the integrals for methyl group of RAFT end group (0.85 ppm) and side chains on HEA (3.00-3.65 ppm).	205
Figure B.15 - ^1H NMR spectrum of pHEA ₃₇ -PPA in D ₂ O. Degree of polymerisation was determined from the ratio of the integrals for methyl group of RAFT end group (0.85 ppm) and side chains on HEA (3.00-3.65 ppm).	206
Figure B.16 - ^1H NMR spectrum of PPA recorded in CDCl ₃	207
Figure B.17 - ^{13}C NMR spectrum of PPA recorded in CDCl ₃	208
Figure B.18 - ^1H NMR spectrum of pHEA ₄₅ -b-pNIPAM ₂₉₂ -MPP in D ₂ O. Degree of polymerisation was determined from the ratio of the integrals for the CH ₃ CH group on NIPAM (3.75 ppm) and the side chains on HEA (3.00-3.65 ppm), knowing the DP of the pHEA-mCTA.	209
Figure B.19 - ^1H NMR spectrum of BAPE recorded in CDCl ₃	210
Figure B.20 - ^{13}C NMR spectrum of BAPE recorded in CDCl ₃	211
Figure B.21 - ^1H NMR spectrum of pHEA ₄₅ -b-p(NIPAM-stat-BAPE) ₃₀₁ -MPP in D ₂ O. Degree of polymerisation was determined from the ratio of the integrals for the CH ₃ CH group on NIPAM (3.75 ppm) and the aromatic ring in BAPE (7.35 and 7.75 ppm) with the side chains on HEA (3.00-3.65 ppm), knowing the DP of the pHEA-mCTA.....	212
Figure B.22 - A comparison of DLS of pHEA ₄₅ -b-pNIPAM _n , where MPP is the RAFT agent, at temperatures above and below the LCST of the polymer to determine whether self-assembly occurs as the pNIPAM block becomes hydrophobic.....	213
Figure B.23 - A comparison of DLS of pHEA ₄₅ -b-p(NIPAM-stat-BAPE) _n , where MPP is the RAFT agent, at temperatures above and below the LCST of the polymer to determine whether self-assembly occurs as the p(NIPAM-stat-BAPE) block becomes hydrophobic.....	214
Figure B.24 - A comparison of DLS of pHEA ₃₇ -b-pNIPAM _n , where PPA is the RAFT agent, at temperatures above and below the LCST of the polymer to determine whether self-assembly occurs as the pNIPAM block becomes hydrophobic.....	215
Figure B.25 - A comparison of DLS of pHEA ₃₇ -b-p(NIPAM-stat-BAPE) _n , where PPA is the RAFT agent, at temperatures above and below the LCST of the polymer to determine whether self-assembly occurs as the p(NIPAM-stat-BAPE) block becomes hydrophobic.....	216
Figure 5.1 - DLS analysis at 37 °C showing particle size with increasing core block length of H ₄₅ -N _n with a crosslinker to mCTA ratio of 5:1, at a NG concentration of 0.1wt%.The wavelength of the laser used is 640 nm and the backscattering was measured.	223
Figure 5.2 - TEM of particles of H ₄₅ -N _n , where n varies between 100 and 321, prepared at room temperature at a concentration of 0.05 wt% and stained with pH 7 phosphotungstic acid. The scale bars all represent 200 nm.	225
Figure 5.3 – A diagrammatical representation of BAPE incorporated into a crosslinked pNIPAM core, showing how BAPE is changed after dialysis and then the product of oxidation of the BAPE units.	227
Figure 5.4 – DLS showing particle size with increasing core block length of pHEA ₄₅ -b-p(NIPAM-stat-BAPE) _n with a crosslinker to mCTA ratio of 5:1 at 37 °C, with a NG concentration of 0.1 wt%. The wavelength of the laser used is 640 nm and the backscattering was measured.	228
Figure 5.5 - TEM of particles of pHEA ₄₅ -b-p(NIPAM-stat-BAPE) _n , where n varies between 88 and 315, prepared at room temperature at a concentration of 0.05 wt% and stained with pH 7 phosphotungstic acid. The scale bars are all equal to 200 nm.	229
Figure 5.6 - TEM of particles of H ₄₅ -N ₂₆₉ and H ₄₅ -NB ₂₄₅ prepared at room temperature at a concentration of 0.05 wt% and stained with pH 7 phosphotungstic acid.....	230
Figure 5.7 – A diagrammatical representation of the collapse of the crosslinked pNIPAM core on heating a nanogel solution to temperatures above it's LCST. The hydrophilic chains remain the same but the core of the nanogel shrinks as the chains collapse from the coil form to a globule formation.....	231
Figure 5.8 - The observable shrinking behaviour by DLS analysis of a) H ₄₅ -N ₂₆₉ BIS and b) H ₄₅ -NB ₂₄₅ with crosslinker to mCTA ratios of 5:1, on heating to temperatures above the LCST of pNIPAM, with a NG concentration of 0.1 wt%. The wavelength of the laser used is 640 nm and the backscattering was measured. ...	232
Figure 5.9 – Effective diameter of H ₄₅ -NB ₂₉₁ 3:1 from DLS with increasing (purple) and decreasing (black) temperature, at a concentration of 0.1wt%. The wavelength of the laser used is 633 nm and the backscattering was measured.	233
Figure 5.10 - DLS comparison of H ₄₅ -N _{269/269} and H ₄₅ -NB _{245/228} with crosslinker to mCTA ratio of 5:1 and 3:1 after polymerisation to observe the extent of shrinkage on heating the nanogels to temperatures above the LCST,	

with a NG concentration of 0.1wt%,. The wavelength of the laser used is 640 nm and the backscattering was measured.	235
Figure 5.11 - TEM of particles of $H_{45}\text{-}N_{269/269}$ with a crosslinker to mCTA ratio of 5:1 and 3:1 respectively, prepared at room temperature at a concentration of 0.05 wt% and stained with pH 7 phosphotungstic acid.	236
Figure 5.12 - TEM of particles of $H_{45}\text{-}NB_{245/228}$ with a crosslinker to mCTA ratio of 5:1 and 3:1 respectively, prepared at room temperature at a concentration of 0.05 wt% and stained with pH 7 phosphotungstic acid.	237
Figure 5.13 – Comparison DLS analysis at increasing temperatures of two samples with similar core forming block lengths to determine the effect of BAPE incorporation on LCST. The wavelength of the laser used is 640 nm and the backscattering was measured. Some very high eff. diam. Results were removed as anomalous values as these are continuous measurements therefore the large particles would be there at every measurement if they were real, and to make the data clearer. See zoomed out DLS in appendix (figure C.15).	238
Figure 5.14 - DLS particle size distributions at 37 °C of a) $H_{45}\text{-}N_{269}$ and b) $H_{45}\text{-}NB_{245}$, both with a crosslinker to mCTA ratio of 5:1, before and after oxidation with 15 mM H_2O_2 , at a NG concentration of 0.1wt%,. The wavelength of the laser used is 640 nm and the backscattering was measured.	239
Figure 5.15 DLS analysis at 15°C and 37 °C before oxidation and 37 °C after oxidation of $H_{45}\text{-}NB_{245}$, 5:1, to show the extent of swelling, at a NG concentration of 0.1wt%,. The wavelength of the laser used is 640 nm and the backscattering was measured.	240
Figure 5.16 – Comparison of particle diameter by DLS analysis at increasing temperatures of $H_{45}\text{-}NB_{245}$ 5:1 to determine the effect of BAPE incorporation on LCST before and after oxidation, using a NG concentration of 0.1 wt%. The wavelength of the laser used is 640 nm and the backscattering was measured.	241
Figure 5.17 - DLS analysis at 37 °C of native $H_{45}\text{-}NB_{291}$ with a crosslinker to mCTA ratio of 3:1 and the oxidised nanogel using H_2O_2 at concentrations of 0.01, 0.1, 1, 5 and 15 mM, at a NG concentration of 0.1wt%,. The wavelength of the laser used is 640 nm and the backscattering was measured.	242
Figure 5.18 - DLS particle size distributions at 37 °C of native $H_{45}\text{-}NB_{291}$ with a crosslinker to mCTA ratio of 3:1 and the oxidised nanogel at 2 different time periods using H_2O_2 at concentrations of 0.1 and 5 mM, at a NG concentration of 0.1wt%. The wavelength of the laser used is 640 nm and the backscattering was measured.	243
Figure 5.19 - Monitoring in situ oxidation by DLS at 37 °C at a NG concentration of 0.1wt%,. $H_{45}\text{-}NB_{291}$ with a crosslinker to mCTA ratio of 3:1 was oxidised with concentrations of H_2O_2 of 0.1 mM and 5 mM over 48 h. The labelled size distributions relate to the labelled points on the kinetics plot. The wavelength of the laser used is 640 nm and the backscattering was measured.	245
Figure 5.20 - LCST measurements using DLS to measure shrinking behaviour on increasing temperature of $H_{45}\text{-}NB_{291/304}$ 3:1 with 2 and 5 mol% BAPE respectively at a concentration of 0.1wt%. The wavelength of the laser used is 640 nm and the backscattering was measured. Some very high eff. diam. Results were removed as anomalous values as these are continuous measurements therefore the large particles would be there at every measurement if they were real, and to make the data clearer. See zoomed out DLS in appendix (figure C.16).	246
Figure 5.21 – Swelling behaviour of $H_{45}\text{-}NB_{291/304}$ 3:1 with 2 and 5 mol% BAPE respectively, at a concentration of 0.1wt%, when oxidised with 15 mM H_2O_2 . The solid lines represent the native polymers and the dashed lines represent the polymers after oxidation. The wavelength of the laser used is 640 nm and the backscattering was measured.	247
Figure 5.22 - In situ oxidation by DLS at 37 °C. $H_{45}\text{-}NB_{291/304}$ with a crosslinker to mCTA ratio of 3:1 and 2 and 5 mol% BAPE respectively, at a concentration of 0.1wt%, oxidised with a H_2O_2 concentration of 5 mM over 48 h. The wavelength of the laser used is 640 nm and the backscattering was measured. Some very high eff. diam. Results were removed as anomalous values as these are continuous measurements therefore the large particles would be there at every measurement if they were real, and to make the data clearer. See zoomed out DLS in appendix (figure C.17).	248
Figure 5.23 – TEM images of particles of $H_{45}\text{-}NB_{291/304}$ with BAPE concentrations of 2 and 5 mol% respectively, prepared at room temperature at a concentration of 0.05 wt% and stained with pH 7 phosphotungstic acid.	249
Figure 5.24 – Effective diameter measurements of four NGs, H-N and H-NB with crosslinker to mCTA ratios of 3:1 and 5:1, by DLS at a concentration of 0.1wt%, over a range of temperatures. The wavelength of the laser used is 640 nm and the backscattering was measured. Some very high eff. diam. Results were removed as anomalous values as these are continuous measurements therefore the large particles would be there at every measurement if they were real, and to make the data clearer. See zoomed out DLS in appendix (figure C.18).	252
Figure 5.25 - DLS analysis at 37 °C of $H_{45}\text{-}N_n$ and $H_{45}\text{-}NB_n$ with 3:1 and 5:1 crosslinker to mCTA ratio, before and after oxidation with 15 mM H_2O_2 at a concentration of 0.1wt%. The wavelength of the laser used is 640 nm and the backscattering was measured.	253

Figure 5.26 - Monitoring <i>in situ</i> oxidation by DLS at 37 °C of H ₄₅ -N _n and H ₄₅ -NB _n with crosslinker to mCTA ratio of 5:1 and 3:1, at a concentration of 0.1wt%, oxidised with a H ₂ O ₂ concentration of 1 mM over 48 h. The wavelength of the laser used is 640 nm and the backscattering was measured. Some very high eff. diam. Results were removed as anomalous values as these are continuous measurements therefore the large particles would be there at every measurement if they were real, and to make the data clearer. See zoomed out DLS in appendix (figure C.19).	254
Figure 5.27 – Comparison of the <i>in situ</i> oxidation data from the two H-NB samples; H ₄₅ -NB ₂₁₅ 5:1 and H ₄₅ -NB ₂₅₃ 3:1, with different crosslinker to mCTA ratios, at a concentration of 0.1wt%. The wavelength of the laser used is 640 nm and the backscattering was measured. Some very high eff. diam. Results were removed as anomalous values as these are continuous measurements therefore the large particles would be there at every measurement if they were real, and to make the data clearer. See zoomed out DLS in appendix (figure C.20). ...	255
Figure 5.28 - TEM images of particles of H ₄₅ -NB ₂₅₃ with a 3:1 ratio of crosslinker to mCTA before and after oxidation prepared at room temperature at a concentration of 0.05 wt% and stained with pH 7 phosphotungstic acid. The scale bars all represent 200 nm.	256
Figure 5.29 - TEM of particles of H ₄₅ -NB ₂₁₅ with a 5:1 ratio of crosslinker to mCTA before and after oxidation prepared at room temperature at a concentration of 0.05 wt% and stained with pH 7 phosphotungstic acid. The scale bars all represent 200 nm.	257
Figure 5.30 – <i>In situ</i> oxidation studies monitored by DLS of pH ₄₅ -pNB ₂₅₃ with a crosslinker to mCTA ratio of 3:1 at a concentration of 0.1wt%, to determine the sensitivity of BAPE to other oxidants and reductants; H ₂ O ₂ , hydroxyl radical, SIN-1 and glutathione. The wavelength of the laser used is 640 nm and the backscattering was measured. Some very high eff. diam. Results were removed as anomalous values as these are continuous measurements therefore the large particles would be there at every measurement if they were real, and to make the data clearer. See zoomed out DLS in appendix (figure C.21).	259
Figure 5.31 - DLS analysis at 25 °C of H ₄₅ -N _n and H ₄₅ -NB _n with 3:1 and 5:1 crosslinker to mCTA ratio. The wavelength of the laser used is 640 nm and the backscattering was measured.	260
Figure 5.32 - TEM of particles of H ₄₅ -N _n with crosslinker to mCTA ratios of 3:1 and 5:1 prepared at room temperature at a concentration of 0.05 wt% and stained with pH 7 phosphotungstic acid. The scale bars all represent 200 nm.	262
Figure 5.33 - TEM of particles of H ₄₅ -NB _n with crosslinker to mCTA ratios of 3:1 and 5:1 prepared at room temperature at a concentration of 0.05 wt% and stained with pH 7 phosphotungstic acid. The scale bars all represent 200 nm.	263
Figure 5.34 – An example SAXS pattern defining the Guinier region and the Porod region. Reproduced from Ref. ⁶⁸ with permission from The Royal Society of Chemistry. ⁶⁸	265
Figure 5.35 – SAXS patterns of pHEA ₄₅ -b-pNIPAM _{230/259} NGs synthesised with a crosslinker to mCTA ratios of 5:1 and 3:1. Patterns were recorded at 0.1 wt% in water.	266
Figure 5.36 - Comparison of SAXS pattern recorded for 1.0 wt % nanogels in water where the NGs are pHEA ₄₅ -b-p(NIPAM-stat-BAPE) _{215/253} with a crosslinker to mCTA ratio of 5:1 and 3:1 respectively.	267
Figure 5.37 - Schematic representation of the AF4 principle. The eluent is pumped from the inlet to the outlet, and the cross-flow is applied perpendicular to the flow direction. The different steps are (A) the focusing process (stopped flow) and (B) the elution process under normal mode; part C shows elution under steric conditions. Reprinted with permission from reference. ⁶¹ Copyright 2014 American Chemical Society.	269
Figure 5.38 – AF4 data showing the concentration, R _g and R _h over time of 4 NGs with and without BAPE and at different crosslinker concentrations, as specified by the titles on each graph, showing the difference in size of the particles by DLS and MALS. The wavelength of the lasers used is 633 nm and 532 nm for DLS and MALS respectively.	271
Figure 5.39 – Determination of the shape factor, R _g /R _h of 4 NGs with and without BAPE and at different crosslinker concentrations, as specified by the titles on each graph, showing the different morphologies observed by separation.	273
Figure C.1 – Correlation curves related to DLS analysis of H ₄₅ -N _n 3:1 for the native and the oxidised polymer, at a NG concentration of 0.1wt%.	288
Figure C.2 - Correlation curves related to DLS analysis of H ₄₅ -N _n 5:1 for the native and the oxidised polymer, at a NG concentration of 0.1wt%.	289
Figure C.3 - Correlation curves related to DLS analysis of H ₄₅ -NB _n 3:1 for the native and the oxidised polymer, at a NG concentration of 0.1wt%.	290
Figure C.4 - Correlation curves related to DLS analysis of H ₄₅ -NB _n 5:1 for the native and the oxidised polymer, at a NG concentration of 0.1wt%.	291

Figure C.5 - DLS analysis at 37 °C of $H_{45}\text{-}N_n$ with a crosslinker to mCTA ratio of 3:1 at a NG concentration of 0.1wt%, before and after oxidation with 15 mM H_2O_2 .	292
Figure C.6 - DLS analysis at 37 °C of $H_{45}\text{-}NB_n$ with a crosslinker to mCTA ratio of 3:1 at a NG concentration of 0.1wt%, before and after oxidation with 15 mM H_2O_2 .	293
Figure C.7 - The observable shrinking behaviour by DLS analysis of $H_{45}\text{-}N_n$ with crosslinker to mCTA ratios of 3:1 at a NG concentration of 0.1wt%, on heating to temperatures above the LCST of pNIPAM.	294
Figure C.8 - The observable shrinking behaviour by DLS analysis of $H_{45}\text{-}N_n$ with crosslinker to mCTA ratios of 5:1 at a NG concentration of 0.1wt%, on heating to temperatures above the LCST of pNIPAM.	295
Figure C.9 - The observable shrinking behaviour by DLS analysis of $H_{45}\text{-}NB_n$ with crosslinker to mCTA ratios of 5:1 at a NG concentration of 0.1wt%, on heating to temperatures above the LCST of pNIPAM.	296
Figure C.10 - The observable shrinking behaviour by DLS analysis of $H_{45}\text{-}NB_n$ with crosslinker to mCTA ratios of 3:1 at a NG concentration of 0.1wt%, on heating to temperatures above the LCST of pNIPAM.	297
Figure C.11 - The observable shrinking behaviour by DLS analysis of $H_{45}\text{-}NB_{304}$ with crosslinker to mCTA ratios of 3:1 and 5 mol% BAPE incorporated into the core, at a NG concentration of 0.1wt%, on heating to temperatures above the LCST of pNIPAM.	298
Figure C.12 - Correlation curves related to DLS analysis of $H_{45}\text{-}NB_{304}$ with a mCTA to crosslinker concentration of 3:1 and 5 mol% BAPE incorporated into the core, for the native and the oxidised polymer, at a NG concentration of 0.1wt%.	298
Figure C.13 - Correlation curves related to DLS analysis of $H_{45}\text{-}N_n$ and $H_{45}\text{-}NB_n$ at 37 °C with a mCTA to crosslinker concentration of 3:1 and 5:1, for the native and the oxidised polymer, at a NG concentration of 0.1wt%.	299
Figure C.14 - The observable shrinking behaviour by DLS analysis $H_{45}\text{-}N_n$ and $H_{45}\text{-}NB_n$ on heating to temperatures above the LCST of pNIPAM at a NG concentration of 0.1wt%.	299
Figure C.15 - Comparison DLS analysis at increasing temperatures of two samples with similar core forming block lengths to determine the effect of BAPE incorporation on LCST. The wavelength of the laser used is 640 nm and the backscattering was measured.	300
Figure C.16 - LCST measurements using DLS to measure shrinking behaviour on increasing temperature of $H_{45}\text{-}NB_{291/304}$ 3:1 with 2 and 5 mol% BAPE respectively at a concentration of 0.1wt%. The wavelength of the laser used is 640 nm and the backscattering was measured.	300
Figure C.17 - In situ oxidation by DLS at 37 °C. $H_{45}\text{-}NB_{291/304}$ with a crosslinker to mCTA ratio of 3:1 and 2 and 5 mol% BAPE respectively, at a concentration of 0.1wt%, oxidised with a H_2O_2 concentration of 5 mM over 48 h. The wavelength of the laser used is 640 nm and the backscattering was measured.	301
Figure C.18 - Effective diameter measurements of four NGs, H-N and H-NB with crosslinker to mCTA ratios of 3:1 and 5:1, by DLS at a concentration of 0.1wt%, over a range of temperatures. The wavelength of the laser used is 640 nm and the backscattering was measured. Some very high eff. diam.	301
Figure C.19 - Monitoring in situ oxidation by DLS at 37 °C of $H_{45}\text{-}N_n$ and $H_{45}\text{-}NB_n$ with crosslinker to mCTA ratio of 5:1 and 3:1, at a concentration of 0.1wt%, oxidised with a H_2O_2 concentration of 1 mM over 48 h. The wavelength of the laser used is 640 nm and the backscattering was measured.	302
Figure C.20 - Comparison of the in situ oxidation data from the two H-NB samples; $H_{45}\text{-}NB_{215}$ 5:1 and $H_{45}\text{-}NB_{253}$ 3:1, with different crosslinker to mCTA ratios, at a concentration of 0.1wt%. The wavelength of the laser used is 640 nm and the backscattering was measured.	303
Figure C.21 - In situ oxidation studies monitored by DLS of $pH_{45}\text{-}pNB_{253}$ with a crosslinker to mCTA ratio of 3:1 at a concentration of 0.1wt%, to determine the sensitivity of BAPE to other oxidants and reductants; H_2O_2 , hydroxyl radical, SIN-1 and glutathione. The wavelength of the laser used is 640 nm and the backscattering was measured.	303
Figure 6.1 - Two oxidation responsive crosslinkers which were synthesised, with preliminary studies carried out testing their crosslinking ability in the nanogel system above.	309

List of Schemes

<i>Scheme 1.1 - The general structure of the PEG-polysulfide arms</i>	34
<i>Scheme 1.2 - Syntheses and H₂O₂-induced decomposition of the dual responsive copolymers. (i) MCP, CuCl, Me6TREN, DMF, 60 °C, 24 h; (ii) dialysis against H₂O, 4 °C; (iii) H₂O₂, phosphate buffer solution (pH 7.4). Reproduced from Ref. 114 with permission from The Royal Society of Chemistry.114</i>	42
<i>Scheme 1.3 - The oxidation of ferrocene to ferrocenium</i>	49
<i>Scheme 3.1 – The oxidation of a dithioester RAFT agent with tert-butyl hydroperoxide to give a thioester⁶</i>	91
<i>Scheme 3.2 - The reaction of a RAFT chain end group with H₂O₂ at 60 °C to transform the dithioester group to a hydroxyl group⁵</i>	91
<i>Scheme 3.3 - A reaction scheme for the polymerisation of NIPAM using the RAFT agent [2-ethyl sulfonyl thiocarbonyl] 2-methyl propionic acid (EMP)</i>	93
<i>Scheme 3.4 - Synthesis of non-ionisable trithiocarbonate RAFT agents.</i>	100
<i>Scheme 3.5 - The major and minor oxidation products observed by mass spectrometry of pNIPAM₈-MPP when oxidised with 15 mM H₂O₂</i>	110
<i>Scheme 4.1 - Synthesis of pHEA-mCTA via RAFT dispersion polymerisation</i>	150
<i>Scheme 4.2 - Chain extension of pHEA-mCTA with NIPAM via aqueous RAFT dispersion polymerisation</i>	151
<i>Scheme 4.3 - Synthesis of pNIPAM-mCTA via non-aqueous RAFT dispersion polymerisation using 3 different RAFT agents; EMEM, MPP and MBP.</i>	153
<i>Scheme 4.4 - Synthesis of pHEA-b-pNIPAM via RAFT solution polymerisation using a pHEA-mCTA synthesised with MPP as the RAFT agent</i>	159
<i>Scheme 4.5 - Synthesis of pHEA-b-pNIPAM via RAFT solution polymerisation using a pHEA-mCTA synthesised with PPA as the RAFT agent</i>	167
<i>Scheme 4.6 - Oxidation of a boronic acid pinacol esters using hydrogen peroxide</i>	172
<i>Scheme 4.7 - Synthesis of the oxidisable monomer 4-(acryloyloxymethyl)phenylboronic acid pinacol ester (BAPE)</i>	173
<i>Scheme 4.8 - Synthesis of statistical copolymers of NIPAM and BAPE via RAFT polymerisation</i>	173
<i>Scheme 4.9 - Synthesis of pHEA-b-p(NIPAM-stat-BAPE) diblock copolymers using pHEA-PPA and pHEA-MPP as the macro-CTAs</i>	178
<i>Scheme 5.1 - A general synthetic scheme for the polymerisation of pHEA-b-pNIPAM crosslinked nanogels both with a without the incorporated of the oxidation responsive monomer BAPE into the core forming block.</i>	221

List of Tables

Table 1.1 - Common drugs used currently to treat rheumatoid arthritis, their function and common side effects. ^{35,36,37,38,39}	10
Table 1.2 - A table of commonly used drugs to treat MS and their side effects ^{44,45,46,47,48,49}	12
Table 1.3 - A summary of polymeric drug delivery systems currently on the market (FDA/EMA approved), the type of system and their intended use. ^{23,59,62,72}	20
Table 1.4 - A summary of polymeric drug delivery systems currently in clinical trials and their intended use. ⁷³	24
Table 1.5 - A table to compare bond dissociation energies of sulfur and selenium bonds. ⁹¹	30
Table 1.6 - A list of temperature responsive polymers alongside their LCST values in water. ¹³⁴	52
Table 3.1 - Analytical data for pNIPAM synthesised by RAFT polymerisation using EMP as the CTA.	96
Table 3.2 - Cloud point analysis of the three polymers synthesised using EMP RAFT agent	98
Table 3.3 - Polymers synthesised using the RAFT agents EMEM, MPP and MBP giving their conversion, DP by NMR and GPC data	103
Table 3.4 - A table of the cloud point analysis before and after oxidation of the polymers synthesised using the RAFT agents EMEM, MPP and MBP . Analysis of cloud point was repeated twice for each sample.	105
Table 3.5 - A table giving conversion, DP by NMR and GPC data of DP25 pNIPAM synthesised using the RAFT agents EMEM, MPP and MBP	111
Table 3.6 - A table giving the cloud point data for DP 25 pNIPAM synthesised using the RAFT agents EMEM, MPP and MBP. Analysis of cloud point was repeated twice for each sample.	112
Table 3.7 - A table giving the cloud point data for pNIPAM ₂₅ -MPP before and after oxidation with various concentrations of H ₂ O ₂ . Analysis was repeated twice for each sample.	114
Table 3.8 - Conversion, DP and GPC data from the polymerisation of NIPAM using MDDP as the RAFT agent.....	120
Table 3.9 - Cloud point data from before and after the oxidation of pNIPAM with 15 mM and 100 mM H ₂ O ₂ . Analysis was repeated twice for each sample.	121
Table 3.10 -Detailed summary of expected mass spectrum peaks from oxidation of the RAFT chain end group of pNIPAM ₂₁ -MDDP and annotation with those seen in figure 2.25.....	125
Table 4.1 – Analytical data for pHEA-mCTAs synthesised using EMEM, MPP and MBP RAFT agents	150
Table 4.2 - Analytical data for the 3 diblock copolymers: pHEA-b-pNIPAM with EMEM, MPP and MBP RAFT agents.....	151
Table 4.3 - A table giving NMR and GPC data from all three pNIPAM-mCTAs synthesised using EMEM, MPP and MBP RAFT agents	155
Table 4.4 – Analytical data for pNIPAM-b-pHEA diblock copolymers synthesised with EMEM, MPP and MBP RAFT agents	156
Table 4.5 - A table showing the conversion of monomer to polymer by gravimetric analysis and the actual DP of pHEA ₄₅ -b-pNIPAM _n	162
Table 4.6 – Characterisation data for the synthesis of pHEA ₃₇ -b-pNIPAM _n diblock copolymers synthesised with PPA as the RAFT agent.....	167
Table 4.7 - Analytical data for p(NIPAM-stat-BAPE) ₁₀₀ statistical copolymers with 3, 5 and 10 mol% BAPE	174
Table 4.8 - Cloud point analysis of the three statistical copolymers p(NIPAM-stat-BAPE) synthesised using various mol% of BAPE. Analysis was repeated twice for each sample.....	176
Table 4.9 - A table showing the conversion of monomer to polymer by gravimetric analysis and the actual DP of pHEA _{45/37} -b-p(NIPAM-stat-BAPE) _n	178
Table 5.1 – Analytical data for nanogels synthesised with the same crosslinker to mCTA ratio but different concentrations of BAPE in the core forming block. 245	
Table 5.2 – Analytical data for H ₄₅ -N and H ₄₅ -NB _n with a crosslinker:mCTA ratio of 5/3:1 after conversion.	251
Table 5.3 – Approximate LCST of NGs with 3 mol% BAPE determined by DLS, comparing the effective diameter over a temperature range.....	251

Table 5.4 – Effective diameter and PDI at 25 °C of all four nanogels with 3 mol% determined by DLS analysis at a concentration of 0.1wt% and averaged over three runs..... 260

Table 5.5 – Particle size and morphological information from DLS, SAXS, TEM and AF4 combined with DLS and MALS..... 274

Table C.1 - A table showing the conversion of monomer to polymer by moisture analysis and the actual DP of nanogels synthesised. 287

Chapter One

1. Introduction to oxidation-responsive polymeric drug delivery systems

1. Introduction

1.1. The need for drug delivery systems.

In order to have more effective and efficient treatment of diseases within a body, targeted drug delivery is needed whereby the drug is carried through the body using a drug delivery system (DDS). Without a delivery system, drugs circulate the body until they either reach the intended site of action or are excreted, meaning a lot of the administered drug does not reach the site where it is needed.¹ This leads to larger and more frequent dosing of patients, which can be harmful and increases the risk of negative side effects, and increases the cost of treatment. This is the reason why pharmacokinetics and biodistribution can be problematic when designing a new drug or determining whether a drug delivery system is suitable. Pharmacokinetics is the term used to describe the movement of the drug throughout the body and biodistribution describes the accumulation and distribution of the drug (Figure 1.1).² The most important stages in drug administration are absorption, distribution, metabolism and excretion.² Therefore, the important aspects for a drug to have are a good bioavailability and a desirable half-life, whereby is eventually excreted but remains in the body long enough to provide the desired therapeutic effects.

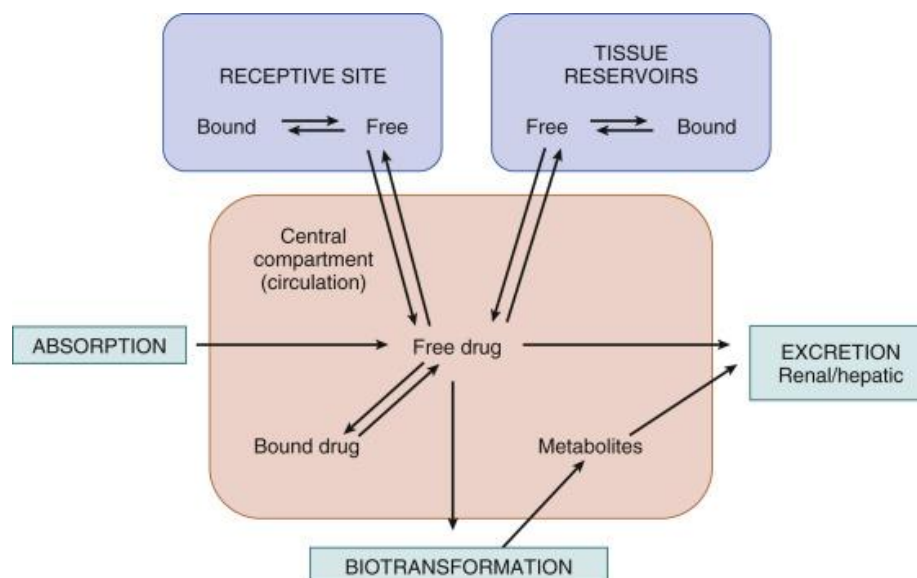


Figure 1.1 - Schematic of possible pharmacokinetic routes of drug within the body. Reproduced with permission.³ Copyright © 2017 Elsevier Inc. All rights reserved.

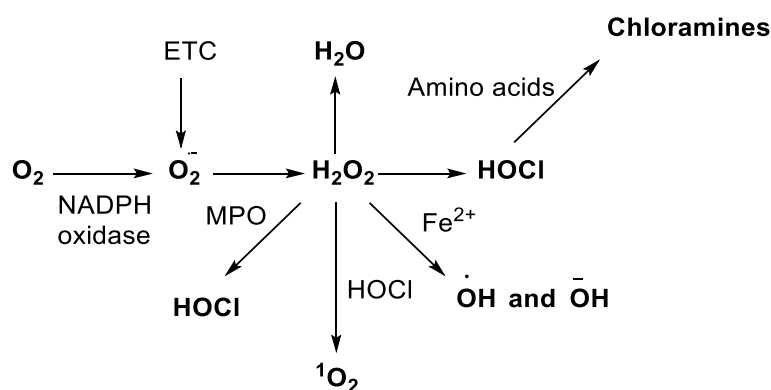
The absorption of a drug is dependent on both the lipophilicity and aqueous solubility of a drug. This means that drug delivery systems are also subject to these parameters. Lipophilicity also affects the distribution and binding of the drug. The size of the drug is especially important too when crossing the blood brain barrier (BBB). The blood capillaries are approximately 5-10 μm however, in between the capillary and the neural cells, there are very tightly packed endothelial cells which only let water, nutrients and small hydrophobic molecules through, using active transport across protein channels.⁴ Therefore, the size must be very small to pass across the disrupted BBB caused by disease.⁵ Excretion may occur before the drug reaches the target site in the body as the blood supply of the upper gastrointestinal tract only reaches system circulation after it has passed through the liver. This means that the drug could be metabolised in the liver or gut wall before having any effect, which is known as the first pass effect. These are initially determined using *in vitro* techniques before applying to *in vivo* animal studies.

1.2. Autoimmune diseases and oxidative stress

At the sites of certain diseases; such as cancer, rheumatoid arthritis, multiple sclerosis and other autoimmune disease, reactive oxygen species (ROS) are produced due to the

inflammation. Therefore, creating materials which respond to ROS may be useful in drug delivery. Many of the reactive species found within the body are synthesised for defence against invading foreign bodies. Immune cells such as macrophages and neutrophils produce O_2^- , which in turn forms hydrogen peroxide (H_2O_2), either spontaneously or via the enzyme superoxide dismutase (Figure 1.1).⁶ This process regulates inflammatory and immune response by allowing cell signalling and is able to control cell apoptosis.^{7,8}

However, oxidation reactions do occur within the body, causing formation of ROS continuously. Production of these species occurs in the phagocyte nicotinamide adenine dinucleotide phosphate (NADPH) oxidase complex, alongside a large increase in oxygen consumption.⁷ These species are also released as by products in some biochemical processes, such as aerobic metabolism.⁹



NADPH oxidase - nicotinamide adenine dinucleotide phosphate oxidase
MPO - myeloperoxidase
ETC - electron transport chain

Scheme 1.1 – A scheme showing the formation route of ROS within the body.

Oxygen radicals are used in the body for cell signalling and gene translation.¹⁰ However, they can cause problems when the ROS cannot be neutralised, i.e. when more ROS are produced compared to the amount of antioxidants present. Antioxidants neutralise ROS, inhibit their formation and bind to the metal ions which catalyse their formation.⁹ The ROS produced initially are free radicals, where the unpaired electrons increase their reactivity. Although they are usually used to fight off invading microorganisms via an inflammatory

response, they can also destroy healthy tissue when in excess.¹¹ This occurs as radicals primarily react with non-radicals due to the increased concentration of the latter. This causes the formation of radical chains when they attack DNA, proteins and lipids, which become radicals themselves and cause extensive damage to the body.

At sites where ROS are present, inflammation occurs. This gives an indication that the immune system is fighting off 'foreign bodies' and is a possible target for drug delivery. There are many diseases which cause, or are caused by, inflammation including Parkinson's disease, Alzheimer's disease, heart disorders, diabetes and cancer.¹²⁻¹⁷ Targeting a molecule which is involved in oxidative stress, such as H₂O₂, is a strategy which may enable drugs to be specifically delivered.

1.3. Diseases affected by oxidative stress

Although there are many diseases which are affected by oxidative stress as stated above, in this review the main conditions discussed are cancer, rheumatoid arthritis and multiple sclerosis.

1.3.1 Cancer

Cancer is the disease which has been studied the most with regards to the use of drug delivery systems for treatment.¹⁸⁻²³ In particular, redox-responsive drug delivery systems, which are described in more detail in section 3.1.

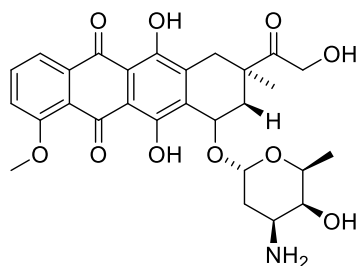
Cancer is defined as the uncontrolled growth of cells within the body due to a malfunction in the genes which control cell proliferation. This malfunction occurs due to gene mutations.²⁴ In order to minimise damage, these mutations are usually discovered and fixed or, if they cannot be fixed, programmed cell death (apoptosis) occurs. Once a mutation has occurred, the cell containing this mutation replicates as the cell undergoes mitosis, creating exact copies of the mutated DNA and eventually a tumour. There are many things which people come across in life which are carcinogenic, i.e. cancer causing,

such as radiation. However, mutations can be caused by hypoxia, a lack of oxygen supply, and repeated injuries, amongst many other things.²⁵

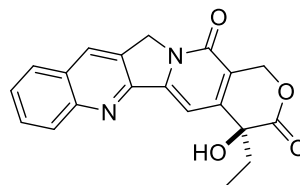
Cancer is notoriously difficult to treat due to the accumulation of mutations throughout the body. Also, as the mutations occur in our cells, many current treatments cannot differentiate between healthy and cancerous cells and therefore kill healthy cells surrounding the cancerous tumour. Tumour cells can also metastasize, forming secondary tumours which spread throughout the body.²⁶

As with many diseases, including autoimmune disease, cancer causes inflammation to occur in tissue surrounding the cancerous tumours. Cancer and inflammation are strongly linked, however in some cases, inflammation occurs before the presence of cancer, which increases the chance of cancer formation, and others where it occurs after, inflammation is due to genetic alterations.²⁷ Inflammation is able to promote angiogenesis and metastasis, aiding the proliferation of the cancerous cells, as well as disrupting the immune response.²⁶

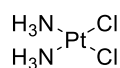
Cancer has numerous different treatment routes including surgery, radiation therapy and hyperthermia to name a few. However, the most commonly used treatments involve drugs e.g. immunotherapy, a biological therapy that boosts the body's immune system function, so it can fight off the cancer naturally, and chemotherapy, which uses drugs to slow the growth of cancer cells. Chemotherapy kills cancerous cells in the body, however, it also damages living tissue and causes various side effects including hair loss, sickness and feeling tired and weak.²⁸ The majority of people undergoing treatment will experience the side effects above, therefore specific drug targeting treatment which minimises side effects is beneficial. There are over 400 chemotherapeutic agents including cisplatin, anthracyclines, inhibitors of topoisomerase and many more (Figure 1.2).^{29,30}



Anthracyclines - derived from streptomycetes e.g. Doxorubicin (DOX)



Inhibitors of topoisomerase interfere with the action of these enzymes which control changes in DNA structure e.g. Topotecan (Hycamtin)



Cisplatin

Figure 1.2 - Examples commonly used chemotherapeutics for the treatment of cancer

Overall, although there are positive results seen when cancer patients are treated via chemotherapy and other drug-based methods, there are still numerous negative side effects. By only targeting the cancerous cells, the dosage of drug can be lowered, the therapy will be more efficient, cost effective and will reduce systemic toxicity. This will reduce the need for new drugs as the current chemotherapeutic agents can be conjugated to or encapsulated within a polymer system which is responsive to particular stimuli.

1.3.2. Rheumatoid arthritis

Rheumatoid arthritis is a disease which causes synovitis, the thickening and inflammation of the synovial membrane (Figure 1.3).³¹

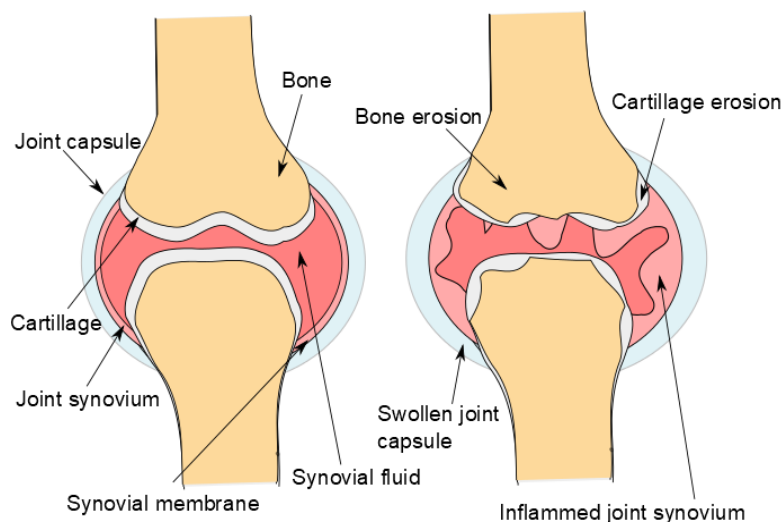


Figure 1.3- Comparison of a healthy joint to one affected by rheumatoid arthritis

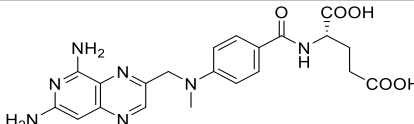
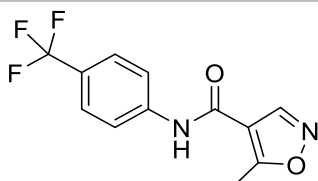
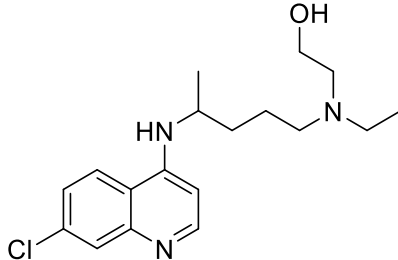
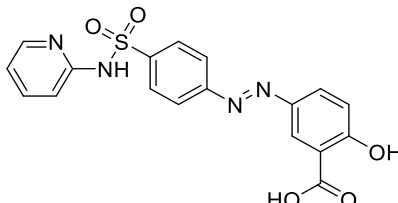
The cause of this disease is unknown, but it is believed to occur due to a mixture of both genetic and environmental factors. The onset of inflammation is caused by macrophages.³² It has been suggested however, that when cells die, proteins and enzymes can leak into the extracellular fluid. Many of these molecules are not usually found outside of cells and therefore trigger an immune response when they come into contact with an immune system cell.³¹ The synovial membrane becomes flooded with inflammatory mediators, which ultimately causes damage to the joint (Figure 1.3). The cells which enter the membrane include neutrophils, lymphocytes (T and B cells), dendritic cells, macrophages and monocytes.³³ Due to this response, the mast cells surrounding the joint release cytokines including interferon ($\text{IFN-}\gamma$), tumour necrosis factor (TNF), interleukin-1 (IL-1) and growth factors.³³ Immunoglobulin (Ig) is released due to the triggering of the immune system which increases the inflammatory response and consequently activates the macrophages.³¹

Although the joint will ultimately be destroyed without treatment, there are a series of stages of damage leading to this. The synovial membrane becomes thicker in patients with Rheumatoid arthritis, which physically restricts movement of the joint.³¹ The joints become swollen and tender, and over time, cartilage and bone damage occur due to decreased

lubrication.³¹ Phagocytes which produce reactive oxygen species are attracted to the inflammation. The pro-inflammatory mediators at the site of inflammation are able to activate the phagocytes so ROS are produced.³⁴ A drug delivery system which targets higher than average concentrations of ROS, such as H₂O₂, may be beneficial for the treatment of rheumatoid arthritis and the other diseases mentioned in this review.

There are two types of drugs used for the treatment of rheumatoid arthritis; disease-modifying antirheumatic drugs (DMARDs) and biological drugs. DMARDs reduce the immune response from the autoimmune disease, and therefore prevent further damage.³⁵ The four most commonly prescribed DMARDs are methotrexate, leflunomide, hydroxychloroquine and sulfasalazine. More information for these can be found below (Table 1.1).

Table 1.1 - Common drugs used currently to treat rheumatoid arthritis, their function and common side effects.^{35,36,37,38,39}

Drug	Structure	Function	Side effects
Methotrexate		Interferes with the metabolism of folate - reduction in the proliferation of cells. Depletes the body of folic acid	Nausea Sore mouth Diarrhoea Headache Hair loss Increase in liver enzymes
Leflunomide		Stops overactive lymphocytes	Diarrhoea High blood pressure
Hydroxychloroquine		Dampens down the effects of the immune system. Non-specific	Accumulates behind the eye
Sulfasalazine		Suppress the immune system Antibiotic and anti-inflammatory agent	Affects blood cell count Negative effect on the liver

In cases where DMARDs have not been successful, biological treatments can be employed.

These are anti-TNF- α antibodies which are able to block TNF from activating inflammation.³⁸ These cannot be taken orally so must be injected or administered via intravenous infusion. Common side effects of biological treatments include high temperature, nausea, rash and headaches.⁴⁰ However, intravenous injections can cause irritation occurs at the injection site or infection due to the bodies weaken immune system.

As can be seen from the above information, many of these treatments have side effects. These are mainly due to the high dosage of the treatments needed. This is because they are not targeting a specific region of the body, so the entire drug does not reach the site where treatment is required. With more specific targeting, less drug needs to be administered, and therefore the treatment will be more successful and the side effects less frequent.

1.3.5. Multiple sclerosis

Multiple sclerosis, like rheumatoid arthritis, is an autoimmune disease. It is a disease without any known cause but it is presumed that genetic and environmental factors both play a role.¹ In this disease, the immune system destroys the myelin sheaths present in the white matter, i.e. the brain stem, nerves and spinal cord, that enable electrical signals to be transmitted through the nerve cells (Figure 1.4). These electrical signals allow a connection between areas of grey matter.¹ The target of this disease is the myelin protein which insulates and protects the axons. Lesions where the myelin sheath has been destroyed are called 'plaques'. The places in which these plaques form determine the type of symptoms and disability, however these generally affect sensory input and ultimately causing paralysis.⁴¹



Figure 1.4- A comparison of a healthy nerve cell compared to one which has been damaged by the action of multiple sclerosis

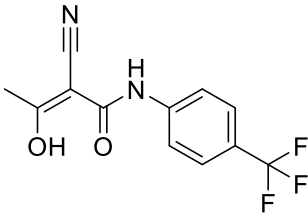
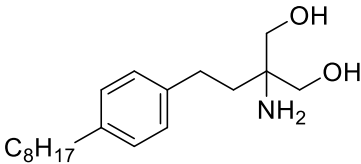
This autoimmune response is initiated by self-reactive T-cells. These cause inflammation as they recognise the protein antigens and cause the secretion of cytokines and consequently, cause macrophages to respond.⁴² As above, the inflammation causes the production of reaction oxygen species. T-cells which are activated are able to cross the blood brain barrier due to disruptions within it, causing myelin to be recognised as a foreign body and triggers an immune response.⁴² It has been correlated that an increase in permeability of

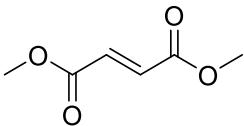
the blood brain barrier to blood or plasma proteins links with demyelination.⁴³ Remyelination occurs in around 20% of cases, however cycles of demyelination and remyelination can cause tissue repair to cease due to the loss of oligodendrocytes, which enable the production of myelin.⁴²

Multiple sclerosis is known to be a relapsing-remitting disease where patients suffer from periods of worsening, relapses or attacks, followed by remission.⁴² Therefore, correctly determining the dosage of treatment is complex. It would be beneficial for a treatment to be used where the drug is already in the body and can respond as soon as a relapse occurs.

Treatments are available to patients who suffer with relapsing-remitting multiple sclerosis to control the pain. As with rheumatoid arthritis, these are defined as disease-modifying drugs which reduce the damage to the CNS, which is what causes the relapses of symptoms. There are several commonly used drugs to treat this (Table 1.2).

Table 1.2 - A table of commonly used drugs to treat MS and their side effects^{44,45,46,47,48,49}

Drug	Structure	Side effects
Interferon beta-1a and 1b	Protein	Flu-like symptoms for up to 48 hours after the injection
Glatiramer acetate (Copaxone ®)	Random polymer of L-alanine, L-glutamic acid, L-lysine and L-tyrosine. This structurally resembles myelin basic protein.	Relatively rare – tightness in the chest.
Teriflunomide		Nausea Headaches Hair loss Diarrhoea Liver problems
Fingolimod		Liver problems Macular oedema, slowing of the heart rate Increased risk of infections.

Dimethyl fumarate		Nausea Headaches Hair loss Diarrhoea Liver problems Hot flushes Stomach pains
Natalizumab	Monoclonal anti-body against the cell adhesion molecule α 4-integrin	Headaches Nausea Itchy rashes Vomiting
Alemtuzumab	Monoclonal anti-body that binds to CD52, a protein present on the surface of mature lymphocytes.	Headaches Nausea Itchy rashes Vomiting Overactive/underactive thyroid Clotting disorders.

Many of these side effects can be prevented by using a targeting delivery system. This means that the dosage given to a patient is lower, and that it can be administered less frequently. It will also mean that the drug is a more effective treatment for the symptoms of multiple sclerosis if it is present in the body for longer, as it can treat the symptoms of a relapse quicker.

1.4. General polymer drug delivery

1.4.1 *Criteria for a suitable polymer therapeutic*

Polymers are becoming more widely used in the medical industry due to their advantages over the administration of free drugs, which are generally hydrophobic and are not targeted. Although they must conform to stringent testing, they are able to target areas of the body more specifically. They can do this in many ways including response to both internal and external stimuli, and through response to cell signalling via conjugation of the

polymer to antibodies and DNA.⁵⁰ The presence of functional groups allow targeting to occur as they can respond to either internal stimuli; such as redox potential, temperature, pH, or to external stimuli; electric or magnetic fields or ultrasound, to release encapsulated or conjugated drugs from the polymer delivery system. Specific targeting means that drugs do not need to be administered in such a high dose or as frequently as unlike non-targeted delivery methods, most of the drug reaches the desired target site.

Before using any drug inside the human body, the potential effects must be considered. This is generally discussed in terms of biocompatibility and toxicity. Toxicity is a measure of unwanted harm that a chemical has once placed inside the body on cells, organs and the patient as a whole, such as metabolism of the chemical and the harmful nature of those products. The biocompatibility is 'the ability of a material to perform with an appropriate host response in a specific application',⁵¹ which implies that biocompatibility of a material depends on both the characteristics of the material and the host in which it is placed, as different hosts may respond differently to the same material.⁵² It is also of importance to determine how the molecules may change once inside the body, as differences in pH, concentration, temperature can drastically alter their structure, with the formation of crosslinks, micelles, aggregates etc.⁵³

The molecular weight of polymers used for drug delivery can determine whether they are able to pass through areas of the body into the target site, therefore both the drugs and drug delivery systems must be small enough to freely circulate around the body.⁵⁴ High molecular weight polymers may be unable to pass through the semi-permeable blood brain barrier as it is formed of epithelial cells which are packed tightly together. This protects the brain from potentially harmful substances, such as toxins, but increases the difficulty in administering drugs which are required to pass this barrier.^{4,43} For transport around the circulatory system, the target dimensions of drug carriers should be $<1 \mu\text{m}$, therefore in the

nanometre range. These dimensions avoid arterial clots and stop issues regarding diffusion into the tissues where the drug is required.⁵⁵⁻⁵⁷ Size is important to get a balance between avoiding rapid renal excretion and the accumulation of high molecular weight particles in tissues.

The molecular weight can also influence the pharmacokinetics of the DDS, i.e. how long the polymers carrier is present in the body. Ideally, they should be removed via renal excretion which requires the polymer to have a low molecular weight, the threshold for renal excretion is a molecular weight of <45 kDa,⁵⁰ and be water-soluble.⁵⁸ Polymers with a molecular weight over the threshold cause a size-dependent accumulation in organs as they are slowly removed from circulation by extravasation into tissues.⁵⁰ This could become problematic as the polymer could react and release any drug still encapsulated at unwanted sites, destroying healthy tissue.⁵⁹

If the polymer does not biodegrade, and cannot be excreted renally, it may need to be removed through surgery, depending on the amount present in the body and the type of polymer. This is a risk to the patient and is time consuming and expensive.⁶⁰ It should be noted however, that although the polymer should not remain in the body indefinitely, it must have a prolonged circulation time in order to reach the target site and release the drug in response to stimuli. If the circulation time is short, excretion may occur before the drug has been delivered to the target area. For the circulation time to be increased, larger drug delivery systems are needed. Therefore, it is important to balance the size and therefore molecular weight of the polymer to maximise circulation time but still allow renal excretion. To be excreted safely from the body, it is beneficial to use polymer drug delivery systems with a degradable backbone where the degradation products are non-toxic. Degradation of polymers occurs mainly via hydrolysis and oxidation therefore the more crystalline and more hydrophobic a polymer, the longer degradation time.⁶¹

The safety of a drug can be affected by the way in which it is administered. This can alter the time taken to reach the target site, and therefore the need for control of degradation. It can also determine the frequency and dose of the drug needed. The three main types of administration are oral, intravenous and subcutaneous. Intravenous refers to administration straight into a vein and subcutaneous injections are administered into the fatty tissue under the skin.⁵⁹ As well as the size of the polymer, the overall biocompatibility is important. This includes the polymers, all degradation products and all forms of the polymer which may be present in different conditions within the body. Inert polymers are not wanted in most cases as this may mean that it is unable to respond to stimuli and release the drug at the target site.⁵⁹ Polymers are therefore referred to as bioinert if they do not respond or react with anything other than the target site. The polymer must avoid absorption of proteins, lipids and other molecules within the body which may cause recognition and then trigger an immune response. However, it must interact strongly with the target site in order to release the drug.⁵⁹ In conjunction with this, they must bind to the drug strongly, without conjugation degrading or drug leaching before reaching the target site.⁵⁰ This is of particular importance if the drug is only bound via non-covalent interactions. For example, the highly dilute nature in which the system will be administered into the blood may cause the drug to diffuse out of the carrier.⁶²

It can there be seen that using polymeric formulations as drug delivery vehicles requires careful planning as the specific needs of these systems are very complex.

1.5. Types of potential polymeric drug delivery systems

Polymer synthesis is a large area of research for targeted drug delivery due to the wide range of polymerisation techniques, monomers available, different structures of polymers and the ability to functionalise them after polymerisation, making the scope of research available to form appropriate DDS is very large. The main types of polymeric structures that

show promise as drug delivery systems are described below. The structure of these depends on the method of targeting and how the drug is bound, as well as the target location. The main examples are illustrated in Figure 1.5.

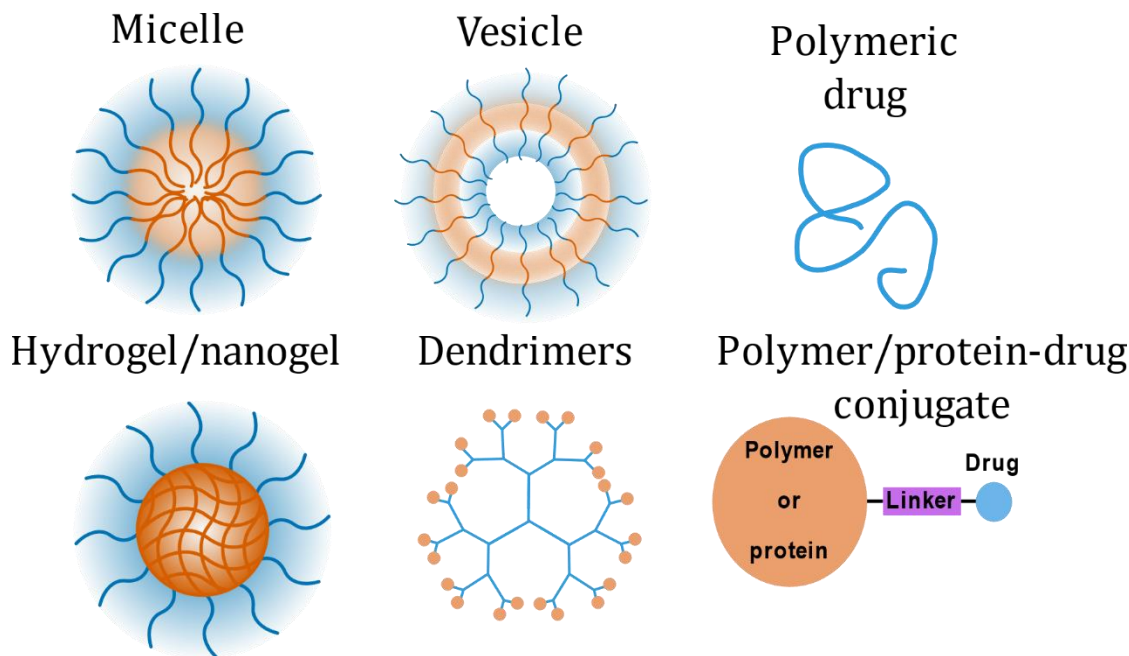


Figure 1.5 - Schematic of the common polymer-based drug delivery systems.

Polymer-drug conjugates feature heavily in the literature.⁶³ The drug is bound to the carrier via a cleavable linker meaning that it is only released in response to certain stimuli at the target site. Although these are discussed as a different class of materials, these can self-assemble into many of the other structures here, with the main difference being that the drug is covalently bound, rather than just encapsulated. These have been reviewed extensively.^{23,64,65} Polymer-protein conjugates have also been widely studied as therapeutics, linking in a similar way to above.⁶³

Micelles are another form of a DDS that has been researched extensively. Micelles are formed from amphiphilic di- and tri-block copolymers that self-assemble in aqueous environments forming a particle with a hydrophobic core and a hydrophilic shell. As mentioned previously, polymer-drug conjugates can self-assemble and may form micelles where the cargo is chemically bound. An example is poly(ethylene glycol)-*b*-poly(β -benzyl-

L-aspartate) synthesised by Bae et al.⁶⁶ These micelles have Adriamycin covalently bound via a pH cleavable linker, allowing for release in the acidic environment of cancerous tissue. However, micelles are able to physically entrap hydrophobic molecules within the hydrophobic core, as shown by Yokoyama et al.⁶⁷ who compared the chemical conjugation and physical entrapment of Adriamycin in PEG-*b*-poly(aspartic acid).

Vesicles, which are formed in a similar way to above, are also useful for drug delivery as they can encapsulate drug within their lumen. Napoli et al. developed oxidation-responsive vesicles which can destabilise on oxidation. These ABA block copolymer micelles are based on PEG and poly(propylene sulfide) (PPS) as PEG-PPS-PEG.⁶⁸

Hydrogels and nanogels have been researched extensively over the last few years due to their unique properties. These are formed of highly crosslinked polymers networks. Hydrogels are physical gels whereas nanogels are gels in the nanoscale. They take in water and have the ability to swell and shrink to encapsulate drug molecules. Zhang et al. have developed an oxidation responsive selenium-containing polyphosphoester nanogel (PSeP).⁶⁹ This PEGylated system releases encapsulated doxorubicin (DOX) due to its swelling on oxidation with hydrogen peroxide.

Dendrimers are branched polymers with a lot of opportunity to tune the nanoscale properties, making them ideal candidates for drug delivery systems. Khandare et al. synthesised both dendrimer and linear polymer-drug conjugates to determine the effect this had on drug delivery of the anticancer drug paclitaxel.⁶⁶ The linear polymer was a bis(PEG) and the dendritic polymer was polyamidoamine (PAMAM). It was found that the dendritic polymer enhances the anticancer properties and showed cytoplasmic and nuclear delivery of drugs.

Finally, polymers themselves can have biological activity for certain diseases leading to research into polymeric drugs.⁷⁰ Therefore, unlike the DDS above, these are not inert.

Examples of these are mentioned in section 1.4 as sequestrants of potassium. There has been a lot of study into their use for anticancer therapy, with the earliest clinical trials taking place in the 1960s on a copolymer of divinyl ether and maleic anhydride (DIVEMA).^{62,70} From this many other systems have been studied and have reached pre-clinical and clinical trials, however none of them have been released onto the market due to fears of systemic toxicity.^{70,71}

1.6. Historical clinical trials of polymer therapeutics

Although there is a lot of potential for polymeric DDS in clinical situations, due to the stringent criteria and the length of clinical trials there are very few which make it onto the market. Out of those that do, the majority of these are protein or aptamer conjugates, despite the research into other systems showing promising results. Most of these DDS are either sequestrants, mainly for potassium binding, or protein/aptamer conjugates. Of the conjugate systems, over 85% of these are poly(ethylene) glycol (PEG)-based systems.

Despite the first US Food and Drug Administration (FDA) and European Medicines Agency (EMA) approved systems being available from the late 1950s, there are still fewer than 30 DDS commercially available. Many systems do not make it through the stringent regulations of clinical trials.

Table 1.3 - A summary of polymeric drug delivery systems currently on the market (FDA/EMA approved), the type of system and their intended use.^{23,59,62,72}

Product	Year available on market	Type of DDS	Polymer	Function
Sodium Polystyrene Sulfonate	1958	Sequestrant	Sodium polystyrene sulfonate	Potassium binder for people with hyperkalemia
Renagel (sevelamer hydrochloride)	2000	Sequestrant	polyallylamine that is crosslinked with epichlorohydrin	Potassium binder for people with hyperkalemia
Renvela (sevelamer carbonate)	2009	Sequestrant	Polyallylamine that is crosslinked with epichlorohydrin	Potassium binder for people with hyperkalemia
Welchol, Cholestagel, Lodalis.	2008	Sequestrant	Colesevelam hydrochloride	Glycaemic control in type 2 diabetes. Lowers blood cholesterol levels.
Veltassa	2017	Sequestrant	Cross-linked polymer of calcium 2-fluoroprop-2-enoate with diethenylbenzene and octa-1,7-diene, combination with D-glucitol	Potassium binder for people with Hyperkalemia
Adagen (Pegademase bovine)	1990	Protein conjugate	Bovine adenosine deaminase derived from bovine intestine that has been extensively pegylated	Severe combined immunodeficiency disease

SMANCS (Zinostatin stimalamer)	1993	Protein conjugate	Copolymer of styrene maleic acid and the protein anti-cancer agent neocarzinostatin	Anticancer agent
Oncaspar (Pegaspargase)	1994	Protein conjugate	Pegylated L-asparagine amidohydrolase from E. coli.	Anticancer agent
Pegintron	2001	Protein conjugate	PEG-Interferon alpha 2b	Treats chronic Hepatitis C
Pegasys	2002	Protein conjugate	PEG-Interferon alpha 2a	Treats chronic Hepatitis C
Neulasta (pegfilgrastim)	2002	Protein conjugate	PEG-hrGCSF	Used to stimulate the growth of "healthy" white blood cells in the bone marrow
Somavert (pegvisomant)	2003	Protein conjugate	Protein containing 191 amino acid residues covalently bound to PEG	Treat acromegaly by maintaining normal IGF-I level in the blood
Macugen (Pegaptanib)	2004	Aptamer conjugate	Pegylated anti-vascular endothelial growth factor (VEGF) aptamer	Age-related macular degeneration
Micera	2007	Protein conjugate	Methoxy polyethylene glycol-epoetin beta	Symptomatic anaemia

Cimzia (certolizumab pegol)	2008	Protein conjugate	PEG-anti-TNF Fab	prevent inflammation resulting from an overactive immune system
Krystexxa (Pegloticase)	2010	Aptamer conjugate	Tetrameric protein composed of four identical chains of about 300 amino acids each. Approx. third of lysine PEGylated	Relieve gout symptoms
Lonquex (cf Neulasta) (Lipegfilgrastim)	2012	Protein conjugate	Covalent conjugate of filgrastim with 1 methoxypolyethylene glycol (PEG) molecule	Used following chemotherapy to help fight infection
Plegridy	2014	Protein conjugate	PEG-interferon beta-1 α (PEG 20,000 Da)	Relapsing forms of multiple sclerosis
Adynovate	2015	Protein conjugate	PEG-recombinant factor VIII (PEG 20,000 Da)	Haemophilia
Copaxone - Glatiramer acetate	2015	Bioactive polymer	Glu, Ala, Tyr copolymer	Multiple sclerosis
Lymphoseek	2014	Imaging agent	Tc ^{99m} labelled dextran-mannose	Intraoperative lymph node mapping
Movantig	2014	Drug conjugate	PEG-naloxone (PEG oligomer, <500 Da)	Treatment of opioid-induced constipation

Although these show promising results for the future of polymeric drug delivery systems, over the last 30 years there has been only a small amount of success of these systems making it onto the market. There have also been cases of these systems being removed from the market after clinical trials due to safety fears. One of the most recent cases of this is Omontys, which was approved for commercial use in 2012 but withdrawn in 2013 due to concerns of serious allergic reactions. The drug was to be used for the treatment of symptomatic anaemia associated with chronic kidney disease.⁷²

Table 1.4 - A summary of polymeric drug delivery systems currently in clinical trials and their intended use.⁷³

Product	Stage of clinical trials	Type of DDS	Polymer	Function
Vivagel	Phase III	Dendrimer – polymeric drug	Lysine-based dendrimer	Prevention of transmission of genital herpes and HIV
ILY101/ AMG 223	Phase III	Sequestrant		Phosphate binding
ADI-PEG 20	Phase III	PEGylated protein	PEG-arginine deiminase	Cancer treatment
Hemospan	Phase III	Polymer-protein conjugate	PEG–haemoglobin	Delivery of CO and O ₂ in trauma patients prevents premature offloading
SuliXen	Phase I/II	Polymer-protein conjugate	Polysialylated insulin	Provides a protective microenvironment for insulin
CDP 791	Phase II	Polymer-protein conjugate	PEGylated di FAB conjugate	Non-small cell lung cancer
Fovista E10030	Phase III	PEGylated-aptamer	PEG-anti-PDGF aptamer	age-related Macular Degeneration
CT-2103; Xyotax; Opaxio	Phase II/III	Polymer–drug conjugate	Poly-glutamic acid (PGA)-paclitaxel	Treatment of some cancers (some terminated at phase II)
Prolindac	Phase II	Polymer–drug conjugate	HPMA–copolymer–DACH platinate	Ovarian cancer
PEG-SN38, EZN-	Phase II	Polymer–drug conjugate	Multiarm PEG-camptothecin derivative	Advanced cancer treatment

2208				
XMT-1001	Phase I	Polymer–drug conjugate	Polyacetal-camptothecin conjugate –prodrug	Solid tumours
PEG–irinotecan, NKTR-102	Phase III	Polymer–drug conjugate	Etirinotecan pegol	Colorectal, breast, ovarian and cervical cancers
SP1049C	Phase II	Block copolymer micelles	Doxorubicin and two nonionic pluronic block copolymers	Anticancer agent
NK-6004 Nanoplatin	Phase II/III	Block copolymer micelles	PEG-nanoparticles containing cisplatin derivatives	Cancer treatment
ONM-100	Phase II	pH activated micelle		Fluorescence Imaging Agent for the Detection of Cancer
DOSE	Phase II	Micelles	Docetaxel-polymeric micelles (PM) and Oxaliplatin	Oesophageal Carcinoma
eRAPA	Phase I		Sub-micron rapamycin particles incorporated into anionic copolymers based on methacrylic acid and methyl methacrylate (Eudragit L 100 / S 100).	Prostate Cancer
CA102N	Phase I		Hyaluronic acid nimesulide-NH ₂ bioconjugate Combined with Trifluridine/Tipiracil	Advanced Solid Tumours

APH-1501	Phase II		Cannabinoid nanoformulations	Opioid Addiction
CRLX101 combined with Enzalutamide	Phase II		Nanoparticle (cyclodextrin-based polymer) Camptothecin with Enzalutamide	Resistant Prostate Cancer
STP705	Phase II	A siRNA (small interfering RNA) therapeutic	Polypeptide nanoparticle (PNP)	Squamous Cell Carcinoma Nonmelanoma Skin Cancer
TRC101	Phase I/II			Chronic Kidney Disease in Subjects with Metabolic Acidosis
Cetuximab nanoparticles	Phase I		Polymeric ethyl cellulose nanoparticles Loaded with Cetuximab and Decorated with Somatostatin Analogue	Colon Cancer

There are still polymer DDS in the numerous phases of clinical trials however, which are summarised in Table 1.4. When comparing these with the drug delivery systems on the market currently, it is seen that there are a wider range of polymers and polymer structures in the clinical stage.

Another important thing to note from the DDS currently on the market and in clinical trials, is that many of these are PEG-based, and many are in the form of PEG-protein conjugates. A benefit of PEG-based polymers is that many products on the market contain this, making it more likely that other PEG-based products will be approved for use by the U.S. Food and Drug Administration (FDA) approved. Also, with many drugs and DDS already on the market, many research groups chose PEG for its properties over less well-known polymer systems. The architecture and molecular weight of PEG in systems on the market do vary, however. PEG is often referred to as the 'gold standard' for biomedical applications. It can be synthesised with very narrow molecular weight distributions and is monofunctional, avoiding common issues with polymer therapeutics. As a hydrophilic molecule, it has been shown in many studies that PEGylation of proteins and other DDS increases their solubility, reduces immunogenicity and prolongs circulation time by preventing rapid renal clearance.^{74,75,76} It is also non-toxic at a range of molecular weights. Although it is not biodegradable, it has been suggested that as long as the molecular weight is controlled and it can undergo renal excretion, it is safe for use in these applications.⁵⁹

Recently, there has been growing concerns regarding the safety of PEG in biomedical formulation, with particular worries regarding accumulation over time due to its lack of biodegradability.⁷² It has been seen in some studies of these DDS, that PEG can be taken up by cells after the release of the drug, therefore in depth pharmacokinetic studies must be undertaken.⁷⁷ If there is potential accumulation after administration of the drug, this could be harmful for other people, for example in transfer from mother to foetus as has been seen with PEG and other polymers,^{78,79} or when used in veterinary situations, as it may be consumed and therefore be part of the food chain.⁸⁰ There has also been concerns raised regarding the immunogenicity, the factor which makes PEG so attractive

in the field. This suggests that the presence of pre-existed PEG antibodies can elicit an immune response in patients. Due to the increasing amount of non-pharmaceutical products on the market, the exposure to PEG has increased. It is used in many cosmetic products, mainly skin creams, toothpastes and as anti-foaming agents in foods for examples. There has been clear evidence of PEG antibodies found in a number of studies, correlating with the age of the patient, linking to the increase in exposure as mentioned above.⁸¹ Although generally the presence of these antibodies may not be dangerous, with the increase in clinical trials of PEG based products, severe allergic reactions may become a large problem in future. An example of how it is already a problem is where the administration of pegnivacogin, a PEG-aptamer, caused anaphylaxis due to a severe allergic reaction, and therefore termination of the clinical trial.⁸² Proof that this was due to the PEG and not the aptamer was also discovered.⁸³ Long-term studies on the accumulation of PEG within the body are now being conducted with drugs which are already on the market.⁷² Although this sensitivity to PEG is not a huge issue at the minute, if many polymeric DDS are formed of mainly PEG this could have ramifications in the future.

Many researchers in the field are also worried about the amount of 'follow-on' therapeutics.⁷² This details DDS already on the market which are altered in small ways to create a 'better' or cheaper product. Common changes are the molecular weight or architecture of the polymer used, use of a different linker or change in the site of conjugation. Although these save time by bypassing patent laws etc, they may have a negative impact on the safety as they may not be as rationally designed as the initial product.

It is therefore important that new DDS are rationally designed, with both the chemical and clinical needs considered. New systems should be developed for each application with rational thought in the development. An open communication between clinicians and research scientists should take place to increase the number of appropriate DDS entering clinical trials.

1.7. Redox responsive polymers

Redox responsive polymers are synthesised to target reductive sites, oxidative sites and sometimes both simultaneously, by responding to a particular concentration of the redox molecules in the body, to initiate a chemical change. The chemical change releases the drug attached to the polymer or changes the polymer from hydrophobic to hydrophilic to cause drug release.⁸⁴ Not only does this mean that drugs are targeted to a specific site, it means that these drugs can circulate the body and respond when needed, which is of particular use in diseases such as rheumatoid arthritis, multiple sclerosis, and other chronic conditions prone to flare up of symptoms and periods of worsening.^{42,31} The polymer can then be renally excreted via the kidneys once the drug has been used.

1.7.1. Reduction responsive systems

Reduction-responsive systems have been studied in a large amount of detail, especially with regard to drug delivery for cancer treatment. It has been found that the redox couple, glutathione/glutathione disulfide, is the most abundant in animal cells, so targeting areas where these are found in high concentrations is beneficial.⁸⁵ Research through in vivo studies in mice has shown that glutathione (GSH) concentrations are four times higher in tumour cells than healthy cells, implying that reduction responsive DDS could be used for cancer treatment.⁸⁶ Drug release may also occur due to the acidic environment of the tumour, which from can have a pH as low as 5, compared to the pH of blood and healthy tissues (pH 7.4) to pH 5. Increased levels of GSH in cancer tissues, and the build-up of lactic acid due to poor lymphatic drainage and high metabolism, cause this decrease in pH.⁸⁶

There are many ways to synthesise these polymers and numerous different functional groups which are sensitive to elevated levels of GSH and can therefore be used to cause drug release. The main functional groups are discussed in more detail below.

1.7.1.1. Sulfur

Most of research into reduction-responsive polymers is centred around sulfur, in particular compounds with disulfide linkages, which can be reduced in the presence of cysteine and

glutathione (GSH).⁸⁶ These compounds can be transported in the blood without reduction of these bonds due to the low concentration of glutathione outside the cells.

One example of such system was synthesised by Cheng et al,⁸⁷ where reduction-responsive micelles were synthesised with a hydrophobic core crosslinked with bis(2-azidoethyl)disulfide (BADS), a disulfide-based crosslinker. The diblock polymers themselves were poly(ethylene glycol)-*b*-poly(γ -propargyl-L-glutamate) (PEG-PPLG). Crosslinking gave the structures greater stability than the diblocks alone, allowing drug release in the presence of GSH.

There are many more examples of reduction responsive polymers with potential applications for drug delivery which are not covered in this report.^{85,88-90} However, it is important to note, that much of this research is based on the treatment of cancer.

1.7.1.2. Other reduction responsive compounds

There are a few reports of other reductive responsive systems, however, none have been as extensively researched as sulfur-containing compounds.

Diselenide compounds have been studied due to their similar properties to disulfide compounds. Also, they have the advantage of weaker bonds between C-Se and Se-Se when compared to the corresponding C-S and S-S bonds (Table 1.5).⁹¹ This means that drug delivery systems are more sensitive and can therefore transport drugs to more specific sites within the body. However, there are issues surrounding the solubility of these complexes which need to be overcome before it can be used as a drug delivery system.⁸⁵

Table 1.5 - A table to compare bond dissociation energies of sulfur and selenium bonds.⁹¹

Sulfur	Bond dissociation energy ΔH^f kJ/mol	Selenium	Bond dissociation energy ΔH^f kJ/mol
C – S	713.3 \pm 1.2	C – Se	590.4 \pm 5.9
S – S	425.30	Se – Se	330.5

An example of a reduction responsive selenium-based polymer was synthesised by Zhang et al,⁹² as a triblock copolymer of PEG-PUSESe-PEG, where PUSESe is a polyurethane block containing a diselenide linkage. These self-assembled into micelles in water but in the presence of either H₂O₂ (an oxidising agent) or GSH (a reducing agent), the Se-Se bond was cleaved and there is no self-assembly of the remaining polymers.

Platinum (IV) – coordinate polymers have also been suggested for drug delivery systems, particularly in the case of cancer. This is due to the use of cis-platin as an effective cancer treatment.⁹³ This drug could be coordinated to a polymer chain, masking the drug until it reaches an area with a higher the usual concentration of reducing species in the body where it is released. Diaminedichlorodihydroxyplatinum (DHP) or its dicarboxyl derivative diamminedichlorodisuccinatoplatinum (DSP) were the two monomers formed from cisplatin and used in this study.⁸⁵ A benefit of this system is that the reduction of Pt(IV) to Pt(II) occurs more readily at an acidic pH, such as those found in tumour tissue.

The last reduction responsive group discussed here is a polymeric system containing trimethyl-locked benzoquinone (TMBQ).⁹⁴ Serinol and TMBQ-succinimidyl ester react in a coupling reaction to give a diol with pendent TMBQ groups, which is then polymerised by reaction with adipoyl chloride. In the presence of the reducing agent sodium dithionite, the TMBQ is cleaved and the encapsulated drug (paclitaxel) was released according in vivo studies.⁹⁴

1.7.2. Oxidation responsive systems

Most of the research carried out in the area of redox responsive polymers has been into reductive responsive polymers as previously mentioned. However, the principles are the same for oxidative responsive polymers, but these will allow treatment of different diseases which cause oxidative stress, for example. There is a wide range of functional groups which are oxidation responsive and are discussed in more detail below (Figure 1.6).

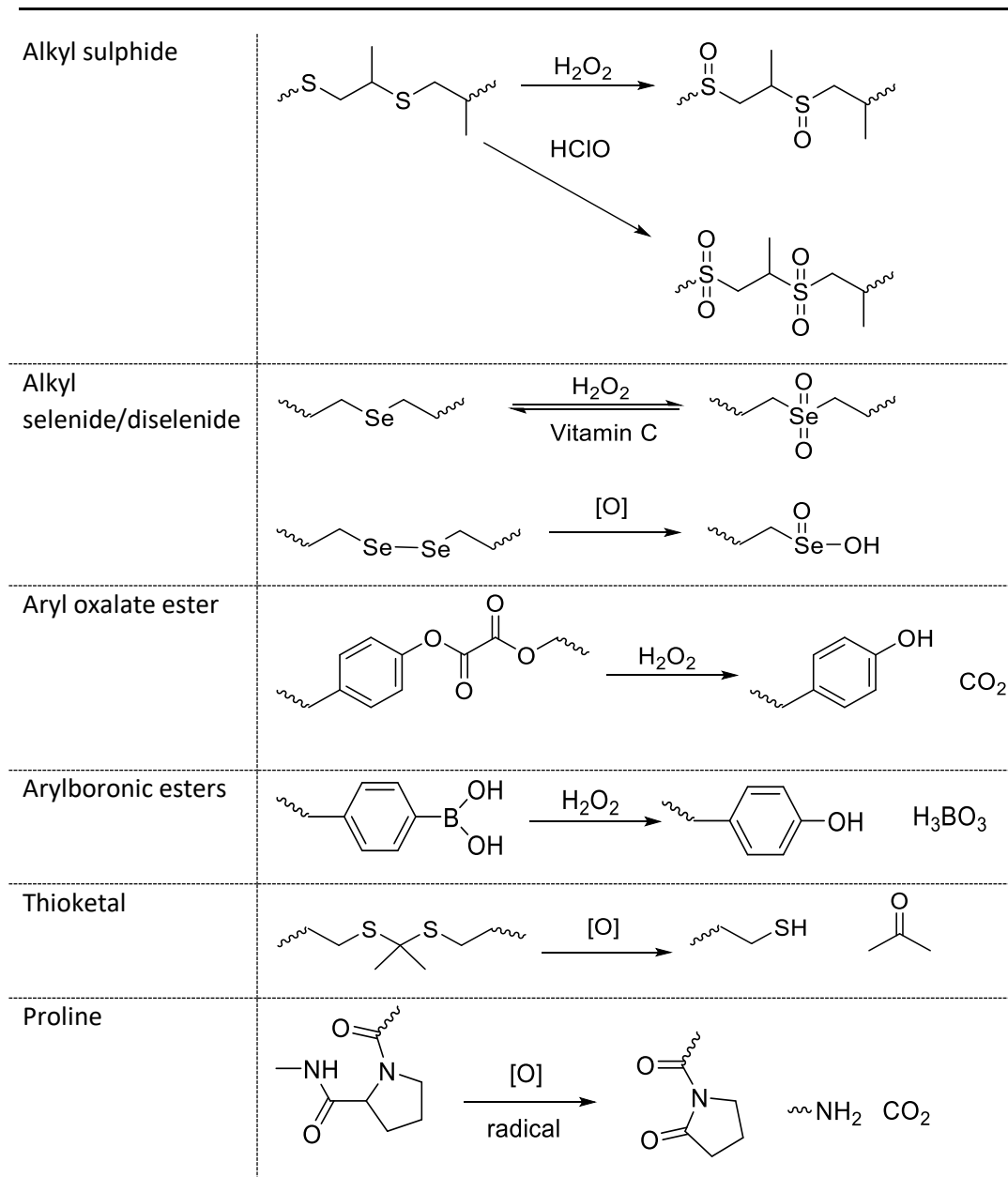


Figure 1.6 - A summary of the main oxidation-responsive functional groups and the products of oxidation (reproduced)⁹⁵

1.7.2.1. Alkyl sulfide/disulfide

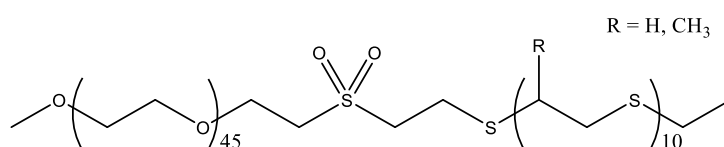
The first and most researched oxidative responsive system is one in which contains sulfur groups, in particular sulfur (II).⁶⁸ These are relatively hydrophobic and can be oxidised to sulfoxides or sulfones, which are more polar and hydrophilic.^{68,96} This means that once an oxidising species such as H_2O_2 is present, the polymer can release the drug and then the polymer carrier can be excreted, making it a great drug delivery system. One of the potential negative points of using a sulfur-based polymer as a DDS is that they can be responsive to both oxidation and reduction and therefore are not as specific.

Many of the examples of oxidation responsive sulfide-based delivery systems in the literature are created based on the response of poly(propylene sulfide). One example is crosslinked nanoparticles of poly(propylene sulfide) coated with the PEGylated emulsifier Pluronic F127, which have been found to exhibit an oxidation response with numerous oxidising agents.⁹⁷ Oxidation of these with H_2O_2 converts the sulfides to sulfoxides, increasing the polarity and causing the nanoparticles to swell in water, enabling the release of the emulsifier. However, when oxidised with ClO^- , a stronger oxidizing agent, the sulfides are oxidised to sulfones, which causes depolymerisation and solubilisation of the fragments. This product however causes higher toxicity. Both systems have potential to carry and release cargo. Allen et al. in a similar study of PPS nanoparticles with pluronic F-127 as the emulsifier found that encapsulated hydrophobic cargo can be released by concentrations of parts per million NaOCl and also oxidoreductase enzymes such as chloroperoxidase and myeloperoxidase in 200 mM NaCl and 500 μ M H_2O_2 .⁹⁸

PPS homopolymers have also been synthesised and show oxidation responsive behavior. As above, different products are obtained by oxidation depending on the ROS present which can influence the release response. Oxidation of these polymers in a THF/water environment with hydrogen peroxide produces water soluble products, with low toxicity, however, when hypochlorite is used the response is much faster and causes depolymerisation of the chain. This is better for an instant response such as an oxidative burst seen from immune response. It has also been found to have very low toxicity.⁹⁶

Many of these systems use PEGylation to afford stability and decrease attachment of proteins within the body and therefore phagocytic attack and toxicity. An example of this are ABA block copolymers which form stable vesicles in water. PEG is the hydrophilic block of the amphiphiles while the oxidation responsive PPS is the hydrophobic block. On oxidation, a change in the structure is seen and spherical micelles are observed with 0.03-10 vol% hydrogen peroxide.⁶⁸

As well as block copolymers incorporating PEG and PPS, linear, star and comb polymers with different numbers of arms can also form spherical micelles (Scheme 1.1). However, the greater the degree of branching i.e. the number of arms, the longer the lag time before the oxidation response is observed, for example there is a difference in lag time from 250-600 minutes as the number of arms increases from 1 to 20 arms (Figure 1.7). The presence of branching points is important as it increases stability against dilution and therefore premature release of cargo. These systems are still very sensitive to oxidation showing a response to 1 wt% H₂O₂.⁹⁹



Scheme 1.1 - The general structure of the PEG-polysulfide arms

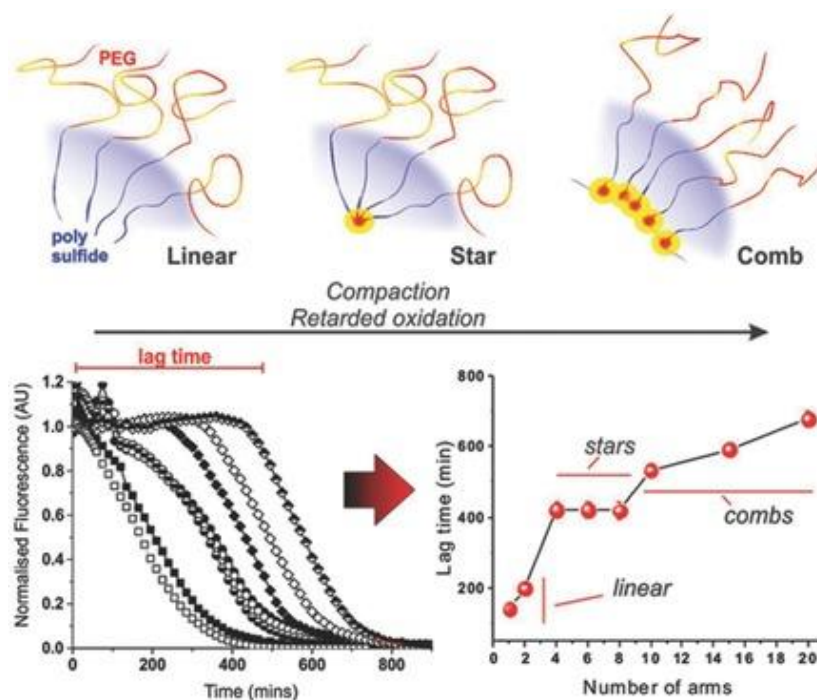


Figure 1.7 - A representation of the three types of self-assembled structures; linear, star and comb, and graphs comparing the lag time to oxidation dependant on the number of arms. Reproduced with permission from ref. 99. © 2016 WILEY-VCH Verlag GmbH & Co. KGaA, Weinheim.⁹⁹

Diblock copolymers containing PPS have also been synthesised. For example, PPS-*b*-PNIPAM polymers exhibit a dual response to both temperature and oxidation (see section 1.6.1 for more detail on the temperature responsive behavior of pNIPAM).¹⁰⁰ The self-assembly of these in H₂O

allowed the encapsulation of dye. Release studies were conducted at temperatures of 25, 37, 40 °C and with various concentrations of H₂O₂ (1, 2 and 5%). No release of the dye was observed with an increase in temperature alone, but faster release was observed at 37 °C with 1 wt% H₂O₂.

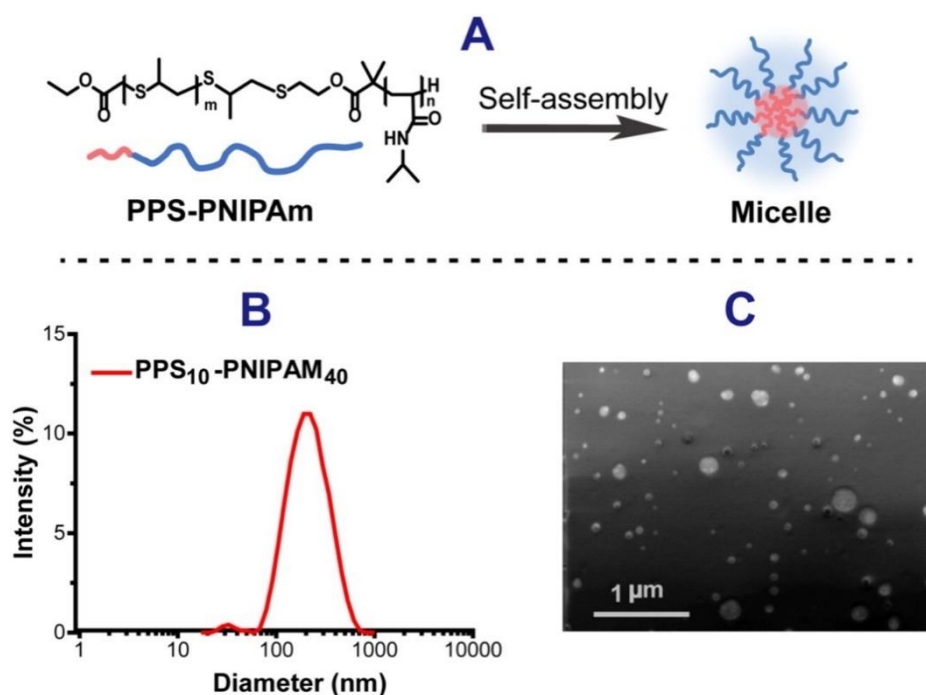


Figure 1.8 - A) Schematic illustration of the formation of PPS-PNIPAm micellar aggregation. B) DLS measurement of PPS₁₀-PNIPAM₄₀ particles in water. Polymer concentration: 1 mg/mL. C) SEM image of PPS₁₀-PNIPAM₄₀ particles. Polymer concentration: 0.5 mg/mL. Magnification: 30.0 kx. Reproduced with permission from ref.100. Copyright © 2016 Elsevier Ltd.¹⁰⁰

By conjugating a drug to a polymer, which is inactive in this state, a prodrug can be formed. Redox responsive prodrugs consisting of PEG bound to SN38 using a thioester linker containing a disulfide bond, PEG-2S-SN38, have been synthesized which assemble into nanocapsules.¹⁰¹ They have been showed to release SN38, an active metabolite of irinotecan which is used for the treatment of colorectal cancer, via thiolysis with GSH or by oxidation, with ROS, of the linker. It has shown high in vitro cytotoxicity and high in vivo anti-cancer activity. It has good potential as a DDS as it is a good size for the enhanced permeability and retention (EPR) effect to occur, has a high drug loading content of 35 wt% and is sensitive to very low concentrations of H₂O₂ (0.05 mM).¹⁰¹ The EPR effect is caused by angiogenesis in cancerous tissue, where the blood vessels are abnormal in architecture, which overall leads to abnormal molecules dynamics through tissues. Further enhancement of this

effect occurs due to other factors including, but not limited to, bradykinin, nitric oxide, prostaglandins, carbon monoxide, peroxynitrite and TNF- α . It makes tissues more permeable and molecules are retained in these.¹⁰²⁻¹⁰⁴

1.7.2.2. *Alkyl selenide/diselenide*

Selenium has properties similar to sulfur, and as such has been utilised in research regarding drug delivery systems. A benefit of selenium is that it is a more sensitive drug carrier as the bond energies are lower than that of sulfur.^{85,91} Like sulfur however, they are also sensitive to reduction.

Selenium groups can be incorporated into the main chain of polymers. An example is a polymeric system which has potential for combined chemotherapy and actinotherapy. The chains are formed of two PEG blocks and one poly-urethane block which contains the redox responsive selenium-selenium bond, PEG-PUse-Se-PEG. These self-assemble in water to form micelles and disassemble in the presence of either 0.01% H₂O₂ or glutathione (GSH).¹⁰⁵

A similar block copolymer has been synthesised and release studies have been carried out using DOX as the cargo (Figure 1.9). The self-assembled structures are relatively small measuring approximately 71 nm by DLS and 50-80 nm by TEM. As mentioned previously, these self-assemble in water. Disassembly is seen 5 h (Figure 1.10). after exposure to 0.1% H₂O₂ v/v. This structural dissociation is much quicker and therefore more sensitive than when a sulfur equivalent is used.¹⁰⁶

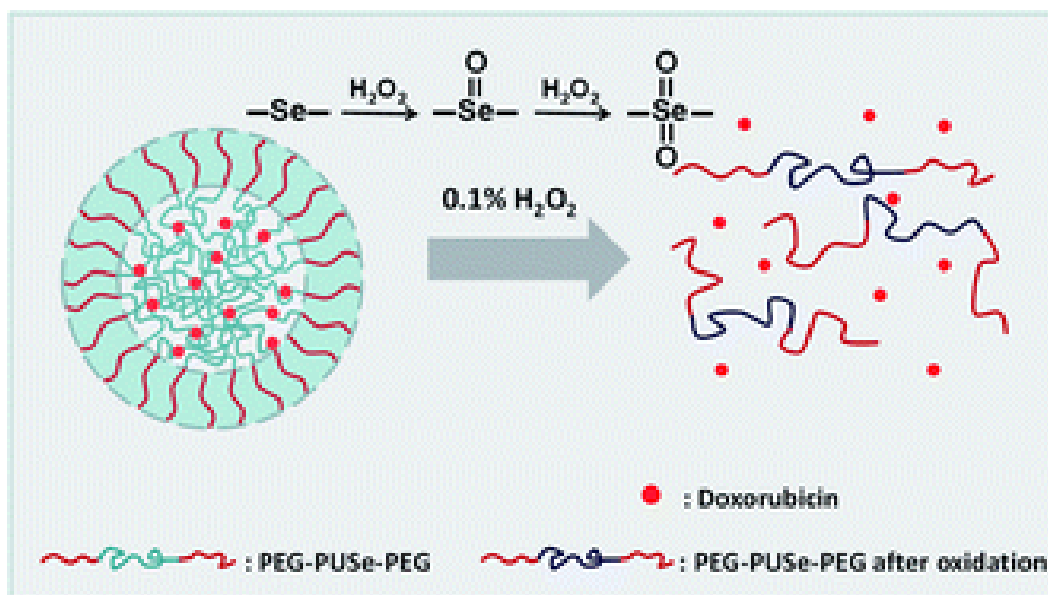


Figure 1.9 - A schematic of the oxidation and disassembly of selenium-containing block copolymer micelles with 0.1% v/v H_2O_2 , causing the release of DOX.¹⁰⁶ Reproduced by permission of The Royal Society of Chemistry

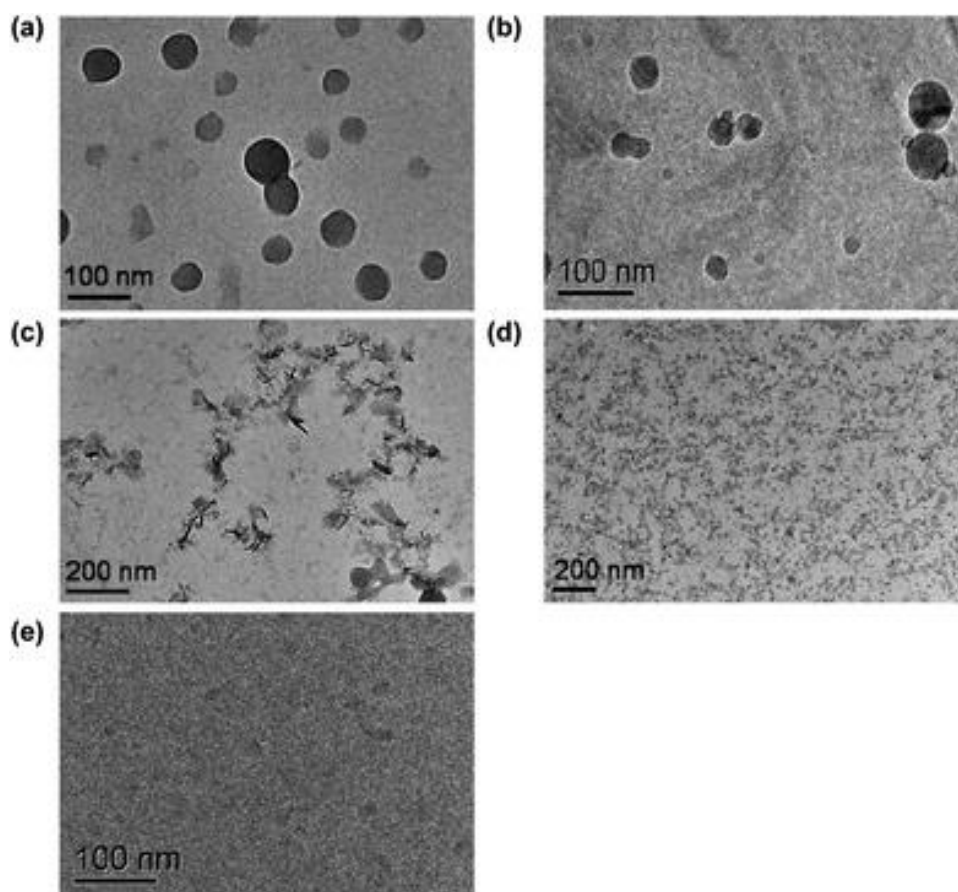


Figure 1.10 - TEM (a) and cryo-TEM (b) images of PEG-PUGe-PEG copolymer micelles; TEM images of the aggregates after 2 h (c) and 5 h (d) oxidation in 0.1% H_2O_2 solution; cryo-TEM image of the oxidized aggregates after 5 h (e). Reproduced from Ref. ¹⁰⁶ with permission from The Royal Society of Chemistry.¹⁰⁶

A selenium-based surfactant (SeQTA) that forms electrostatic interactions with PEG-PAA polymers to give micelles has also been developed. These have been found to disassemble in the presence of 0.1 v/v% H_2O_2 as oxidation of the surfactant causes it to become more hydrophobic and changes the strength of the electrostatic interactions. The potential for delivery was demonstrated by the loading the micelles with a fluorescent dye.¹⁰⁷

PEG-*b*-PAA polymer chains with $\text{O}(\text{CH}_2)_{11}\text{SeCH}_2\text{Ph}$ pendant groups grafted onto the carboxylic acid of the AA group can also form self-assembled spherical structures by nanoprecipitation. These disassemble in the presence of 0.1% H_2O_2 , however they are able to reassemble numerous times in the presence of vitamin C (Figure 1.11). Another benefit of these is that they are stable at ambient conditions for 1 month. This system shows potential as an antioxidant and drug delivery system.¹⁰⁸

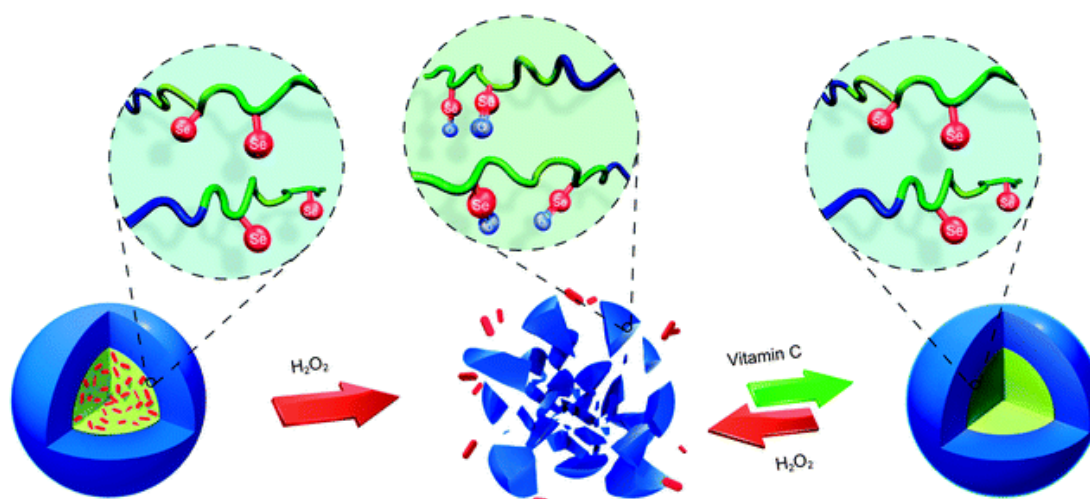


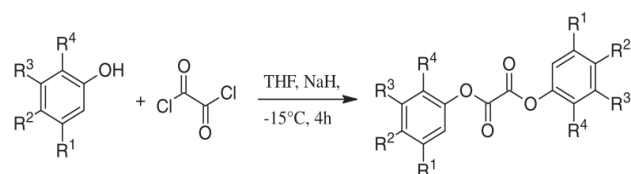
Figure 1.11 – The disassembly and reassembly of spherical PEG-*b*-PAA structures in the presence of H_2O_2 and vitamin C. Reproduced by permission of The Royal Society of Chemistry.¹⁰⁸

The final polymeric system to discuss is the formation of hyperbranched polymers which self-assemble into multi-core/shell micelles in water. These are formed of alternating hydrophobic selenide groups and hydrophilic phosphate groups. On oxidation the selenide groups are transformed to hydrophilic selenone groups and become completely water soluble. This has potential for a drug delivery system to cancer cells, especially due to the intrinsic anticancer effect that selenium compounds exhibit.¹⁰⁹

1.7.2.3. *Aryl oxalate esters*

There have only been a few publications where oxalates were used as an oxidation-responsive group, however they have the potential to be incorporated into a theranostic system. The oxidation of the oxalate group with hydrogen peroxide forms an excited state that can be used to excite a fluorophore and therefore cause chemiluminescence, combining drug delivery and imaging of the release site.

Czarnecki et al. have synthesised a range of bifunctional aryloxylate esters and determined their oxidation response.¹¹⁰ An important property of these oxalate groups is that they cleave entirely on oxidation with hydrogen peroxide and therefore have the potential to be used in the synthesis of nanogels with a crosslinked structure. On oxidation, the linker would break, causing release of any encapsulated materials. The six molecules synthesised varied using different positions of the functional groups bound to the aryl rings and their oxidation response was determined at room temperature at a concentration of 0.5 mg/ml, using 50 mmol/L H₂O₂ in acetonitrile, due to the molecules lack of solubility in water. The degradation was measured using HPLC and the rate was quantified using the half-lives of the oxalates. All the synthesised oxalates were cleavable by hydrogen peroxide and it was found that the sensitivity of this could be tuned by altering the position and nature of the substituents on the aryl rings (Figure 1.12). Therefore, these molecules show a large potential for drug delivery systems.



#	R ¹	R ²	R ³	R ⁴	Yield (%)	$\tau_{1/2}^a$	$\tau_{1/2}^b$
AOE1	H	Cl	H	Me	86	20	/
AOE2	H	Cl	Me	H	46	3	49
AOE3	Me	Br	Me	H	53	2	33
AOE4	H		H	H	60	6	56
AOE5	H		H	H	69	1	48
AOE6	H		H	-OMe	70	22	/

^a 50 mmol/L H₂O₂.

^b 5 mmol/L H₂O₂.

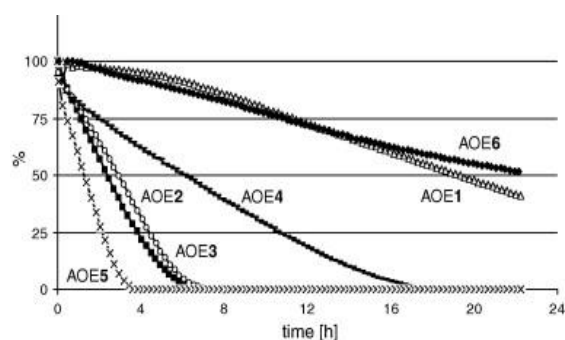


Figure 1.12 – Synthesis of the 6 different oxalates with their half-life on oxidation and the degradation of AOE1 Δ , AOE2 \circ , AOE3 \square , AOE4 $-$, AOE5 \times , AOE6 \blacklozenge . (0.5 mg/mL oxalates, 50 mmol/L H₂O₂), showing that the degradation rate depends on the position and nature of the substituents. Reproduced with permission from ref. ¹¹⁰. Copyright © 2011 Elsevier Ltd.

Other research groups have incorporated aryloxalates into polymeric systems. One research group synthesized a polymer of copolyoxalate and hydrobenzyl alcohol (HBA) referred to as HPOX, which form nanoparticles (Figure 1.13).¹¹¹ The copolyoxalate is responsive to hydrogen peroxide and HBA has both antioxidant and anti-inflammatory properties. On oxidation with H₂O₂, HPOX forms cyclohexanedimethanol which is an FDA approved food additive, so it should not be harmful to the body after oxidation, and the HBA can treat an affected area after its release from the polymer. As mentioned above, when combined with an appropriate fluorophore, aryl oxalates have combined imaging, therapeutics and drug delivery for diseased which produce a large amount of H₂O₂ (Figure 1.13).

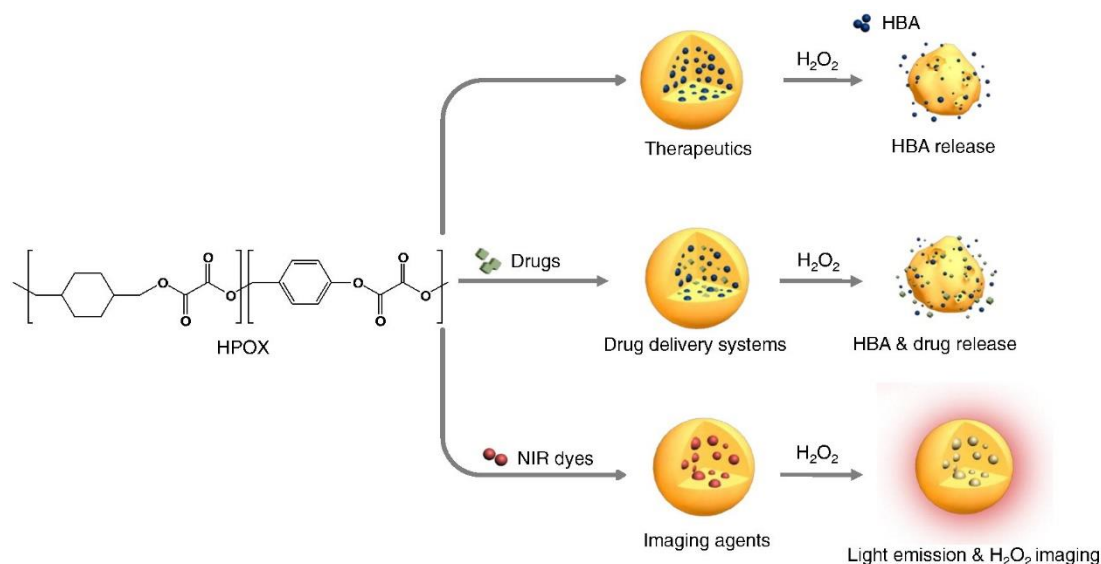


Figure 1.13 - Multifunctional H₂O₂-activatable nanoparticles as a novel strategy for bioimaging and therapy. HPOX nanoparticles can serve as H₂O₂ imaging agents, therapeutics and site-directed drug delivery systems. Reprinted from ref. ¹¹¹, Copyright (2013), with permission from Elsevier Ltd.

The other polymer system is a ferulic acid based poly(anhydride ester) (Figure 1.14).¹¹² As with the above system, it has been found that this incorporates an antioxidant (ferulic acid) which is released on oxidation of the oxalate linkages with hydrogen peroxide, enabling scavenging before and after release.

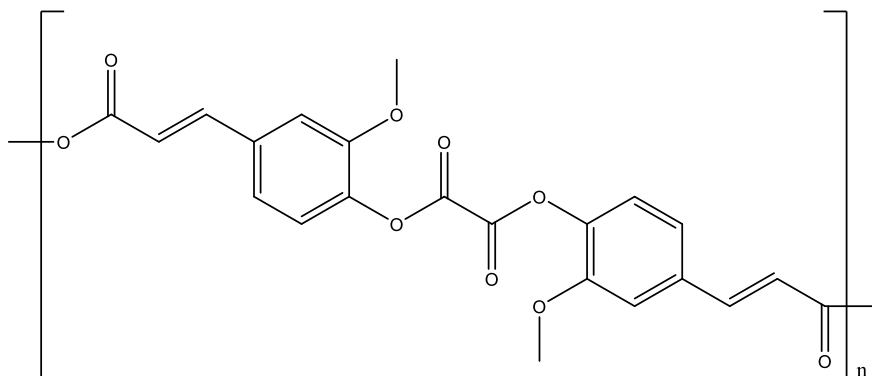


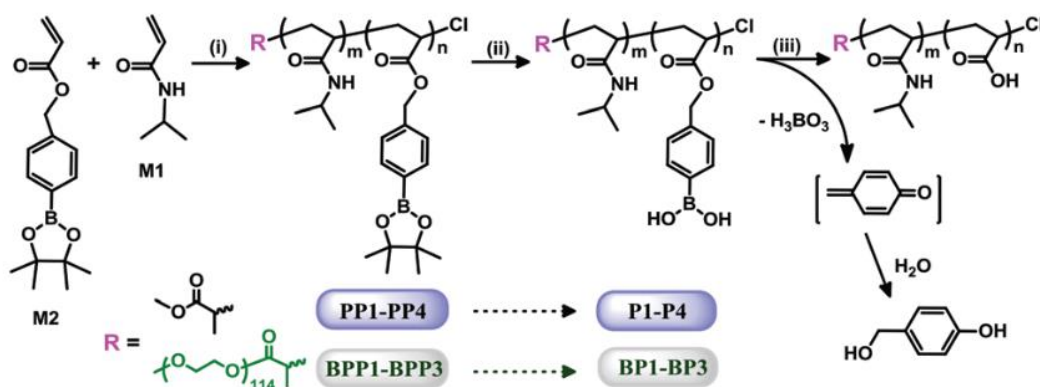
Figure 1.14 - The general structure of an oxalate-ester containing ferulic acid-based poly(anhydride ester).¹¹²

The use of polyaryloxalates with potential for drug delivery is not widely published as seen here, however it has a lot of potential for use in theranostics in the future.

1.7.2.4. Arylboronic esters

Arylboronic esters are excellent oxidation-responsive functional groups due to their high sensitivity to H_2O_2 over other ROS.¹¹³ Due to this, many polymer systems have been developed which contain these groups.

Many of these systems also incorporate PEG in some form to increase the stability in vivo. One system is formed of random copolymers of a boronic acid pinacol ester-based monomer and NIPAM (Scheme 1.2).¹¹⁴ These were synthesised by atom transfer radical polymerization (ATRP) with a PEG-Br initiator. When heated rapidly to 37 °C, these formed nanoparticles. They were found to have moderate encapsulation of DOX and be labile on exposure to concentrations of H_2O_2 as low as 0.4 mM, causing drug release.



Scheme 1.2 - Syntheses and H_2O_2 -induced decomposition of the dual responsive copolymers. (i) MCP, CuCl, Me_6TREN , DMF, 60 °C, 24 h; (ii) dialysis against H_2O , 4 °C; (iii) H_2O_2 , phosphate buffer solution (pH 7.4). Reproduced from Ref. ¹¹⁴ with permission from The Royal Society of Chemistry.¹¹⁴

Utilising the self-assembly behavior of amphiphilic diblock copolymers in water, a PEG macro chain transfer agent (macro-CTA) was used to form a polymer with a hydrophobic block containing arylboronate ester groups.¹¹⁵ These formed polymersomes which had the ability to target mitochondrion. On oxidation of primary amines, crosslinking occurs causing self-immolative cleavage and the formation of hydrophilic channels in the polymersome (Figure 1.15). This occurs at biological concentrations of H_2O_2 observed in cells (1 mM) and the permeable membrane will allow the release of any encapsulated cargo.

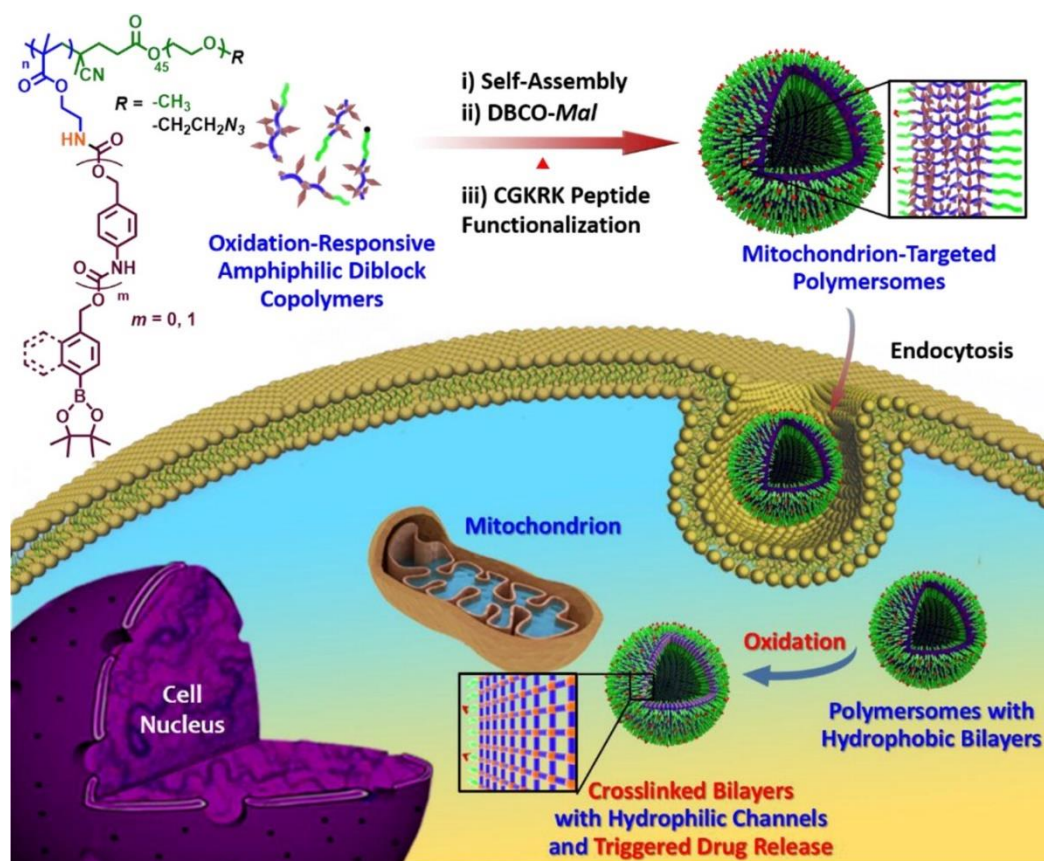


Figure 1.15 - Schematics for the Fabrication of Oxidation-Responsive Multifunctional Polymersomes Exhibiting Intracellular Milieu-Triggered Vesicle Bilayer Cross-Linking, Permeability Switching, and Enhanced Imaging/Drug Release Features. Reprinted with permission from Ref.¹¹⁵ Copyright 2019 American Chemical Society

An example where phenyl boronic acid pinacol ester is in the backbone of the polymer is formed through ROP of a cyclic carbonate.¹¹⁶ The resulting polymers were formulated into nanoparticles by an oil in water (o/w) emulsion method and can encapsulate hydrophobic molecules. These degraded on oxidation with H_2O_2 , releasing CO_2 and causing intramolecular cyclisation. This degradation method means that no acidic products are formed.

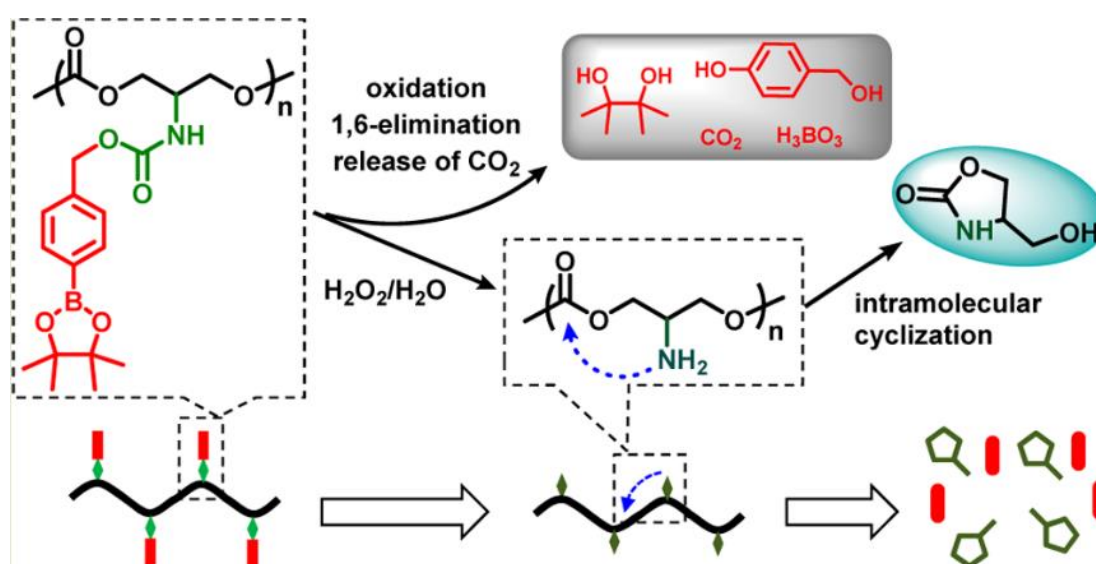


Figure 1.16 – Oxidation-promoted degradation of aliphatic Poly(carbonate)s via sequential 1,6-elimination and intramolecular cyclisation. Reprinted with permission from ref. ¹¹⁶. Copyright 2015 American Chemical Society.¹¹⁶

Instead of encapsulating an active drug, other groups have focused on research using prodrugs, where the drug is inactive until it is released from the carrier. A polymeric prodrug has also been synthesised which incorporates a drug (SN38), a fluorophore and a polymer with boronic acid pinacol ester moieties.¹¹⁷ On oxidation the drug is released and therefore becomes active, inhibiting tumour growth. The fluorophore enables this system to be used for imaging as well as delivery.

Another system formed nanoparticles by the oil in water (o/w) emulsion technique.¹¹⁸ They synthesised two types of polymers, one with boronic acid bound direct to the backbone and one connected via benzylic ether (boronic ester), to test the differences seen on response to a variety of H₂O₂ concentrations (250 mM, 100mM, 100 μM and 50 μM). These polymers were dissolved in dichloromethane, added to a solution of 1% polyvinyl alcohol (PVA) solution and stirred to achieve emulsification. Further emulsification occurred in a high-pressure homogenizer, forming spherical nanoparticles once the DCM had evaporated. These particles were spherical before oxidation, but oxidation caused the particles to look crumpled and ripped, as observed by transmission electron microscopy (TEM) (Figure 1.17). Full degradation was seen after 24 h., with the lowest concentration of oxidant.

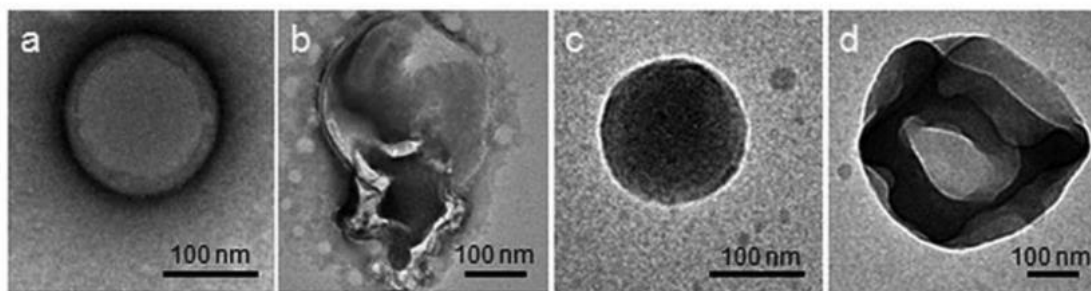


Figure 1.17 -TEM images of nanoparticles. (a, c) After 72 h of incubation in PBS; (b, d) after 72 h in PBS containing 1 mM H₂O₂. Reprinted with permission from reference ¹¹⁸. Copyright 2012 American Chemical Society.¹¹⁸

Upon stimulation via H₂O₂, some phenylboronic ester-containing polymers produce quinone methide intermediates. These are reactive electrophiles and can mediate the cytotoxicity of some anticancer drugs.^{119,120} This occurs as they react with biomolecules due to their high electrophilicity.¹²¹ Quinone methide intermediates can be quenched by water, however there are still concerns about how harmful these may be if the polymers are used as DDS.¹²² These intermediates are quenched by primary and secondary amino groups upon oxidation by H₂O₂. Therefore, phenyl-boronic pinacol ester-containing poly(amino ester) can be synthesised as they are able to reduce how harmful the above polymers are, but still enable an oxidative response behaviour.¹²¹ If these polymers include secondary or tertiary amino groups, they can also be pH responsive, creating a potential dual responsive drug delivery system.

Some research has also been carried out to look at the influence of numerous factors on the stability of polymer DDS, such as concentration of H₂O₂, degree of PEGylation and also pH.¹²¹ Polyaminoesters were formed by Michael-type addition polymerization of a phenyl boronic pinacol ester containing diacrylate and *N*-aminoethylpiperazine. The mPEG5K-succinimide ester was added by post-polymerization modification. On oxidation, with concentrations as low as 200 μM H₂O₂, self-immolation degrades the polymer chain. The amino groups on chain trap quinone methides in situ, minimising the production of toxic side products.

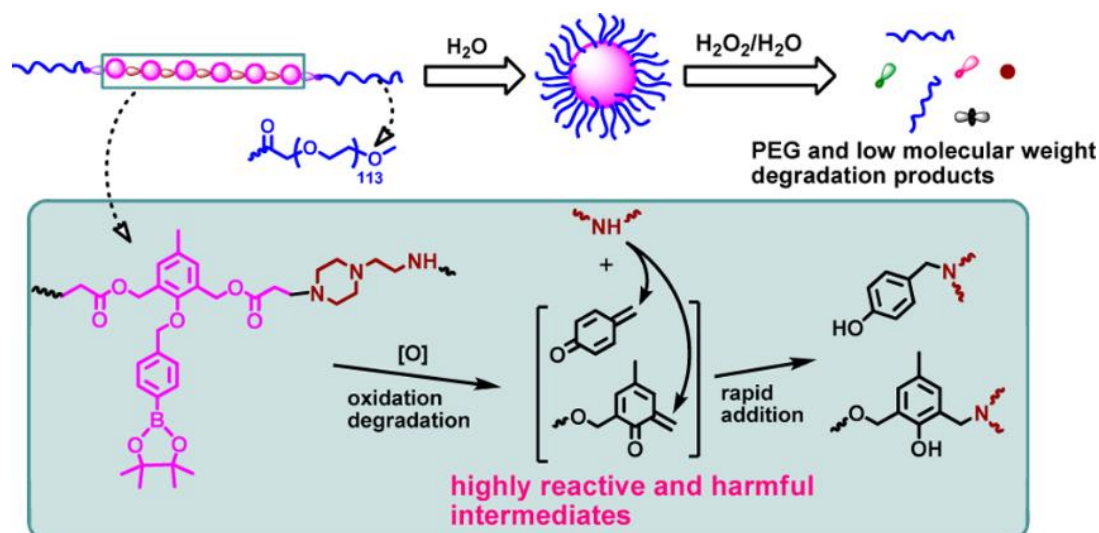


Figure 1.18 - Synthesis of oxidation responsive amphiphilic poly(amino ester)s which can be completely degraded in aqueous media via H_2O_2 oxidation. Reprinted with permission from reference ¹²¹. Copyright 2013 American Chemical Society.¹²¹

1.7.2.5. Thioketal

On oxidation with superoxide and some other reactive oxygen species, thioketal groups can be transformed to ketones and thiol groups. As with the other functional groups discussed in this section, there are many ways in which they can be incorporated into a potential drug delivery system. One way is to synthesise a polythioketal, where the thioketal groups are in the backbone. These polymers have shown promise for tissue engineering and drug and gene delivery applications. Martin et al. synthesized poly(thioketal) urethane scaffolds which were stable for nearly 6 months in aqueous conditions but gradually degraded when exposed to reactive oxygen species.¹²³ These are produced through normal cell functions which means that the scaffold will only begin to degrade after cell infiltration.

Another study into the oxidative sensitivity of polythioketals uses poly(1,4-phenyleneacetone dimethylene thioketal) nanoparticles as a vehicle for drug delivery of anti-cancer therapeutics.¹²⁴ When the vehicle reaches sites with elevated levels of ROS, the polymer backbone degrades through attack of the thioketal with hydroxyl radicals. This disrupts the assembled structure and releases drug at the targeted site. Another paper, using the same polymer as above, has shown that these nanoparticles are able to be orally delivered, transporting siRNA to the inflamed intestine of mice.¹²⁵

Upon reaching the site of inflammation, the polymer backbone was degraded by ROS and the siRNA was released. This was shown to decrease the levels of tumour necrosis factor α (TNF- α) in the colon, protecting from ulcerative colitis. A benefit of thioketal groups, especially for oral administration, is that they are stable to degradation by acid, base and protease-catalysis.

Poly(aminothioketals) have the addition benefit that the amine groups can bind to DNA and encapsulate it in order to deliver this to cancer cells. The DNA can be released on oxidation of the polymer backbone by H₂O₂.¹²⁶

1.7.2.6. *Proline*

Proline residues have been observed to be oxidised by radicals. There are a few literature examples where this chemistry has been employed as an oxidation responsive trigger. Sung et al. have synthesized oligoproline crosslinked polymeric bioscaffolds for prolonged drug release in conditions which cause chronic inflammation.¹²⁷ Diblock copolymers of PEG-*b*-poly(caprolactone) were crosslinked with biaminated PEG-Pro_n-PEG chains, where the proline block length varied in length. They found that the presence of H₂O₂ degraded the proline linkages causing controlled release. One of the important points to note from this study is that the scaffolds degraded under the macrophage-mediated oxidative degradation which mimics the concentrations of ROS present due to inflammation. Degradation occurs much more slowly when the macrophages are not activated by proinflammatory mediators. The same research group have further studied this system to create a porous stimuli-sensitive scaffold for tissue engineering applications.¹²⁸

Sung et al have also developed oligo-proline-derived nanoparticles for use in gene delivery.¹²⁹ Here they use a mixture of bioconjugation and reversible-addition chain-transfer (RAFT) polymerisation to create their nanocarriers. They synthesise a macro-initiator for RAFT polymerisation by conjugating the proline peptide chain with a maleimide functionalised methoxy-PEG polymer before coupling this with the RAFT agent NHS-ECT. This was used to form the diblock copolymer incorporating 2-(dimethylamino)ethyl methacrylate (DMAEMA), acrylic acid (AA) and butyl methacrylate (BMA);

pDMAEMA-*b*-p(DMAEMA-*stat*-BMA-*stat*-PAA). These polymers self-assembled in aqueous media and formed polyplexes with DNA. De-PEGylation of the nanocarriers was observed on oxidation which increased the cellular uptake of the polyplexes and therefore enhanced gene delivery and transfection of DNA into cells.

Overall, this seems like a very promising DDS, however there is a lot of scope to expand these ideas further. This group has been incorporated as both a macro-CTA and a crosslinking group but in a minimal amount of systems.

1.7.2.7. *Other oxidation responsive groups*

There are other oxidation responsive groups which have been studied, but to a lesser extent than those mentioned above.

One of these is the incorporation of a tetrafluoromethyl ketone moiety into a polymer system. Zhang et al found that it was possible to form a self-assembled amphiphilic copolymer in water which was sensitive to oxidation by peroxy nitrite, poly(ethylene oxide)-*b*-poly(trifluoro-3-ox-butyl phenyl methacrylate (PEO-*b*-PMATFK).¹³⁰ The oxidation occurs only in the presence of peroxy nitrite (ONOO⁻) making it a very sensitive and specific response, converting the polymer to poly(ethylene oxide)-*b*-poly(methacrylic acid) (PEO-*b*-PMAA). The oxidation of the tetrafluoromethyl ketone moiety causes the polymer to become water soluble and therefore disassemble. This therefore has the potential to release an encapsulated payload (Figure 1.19).

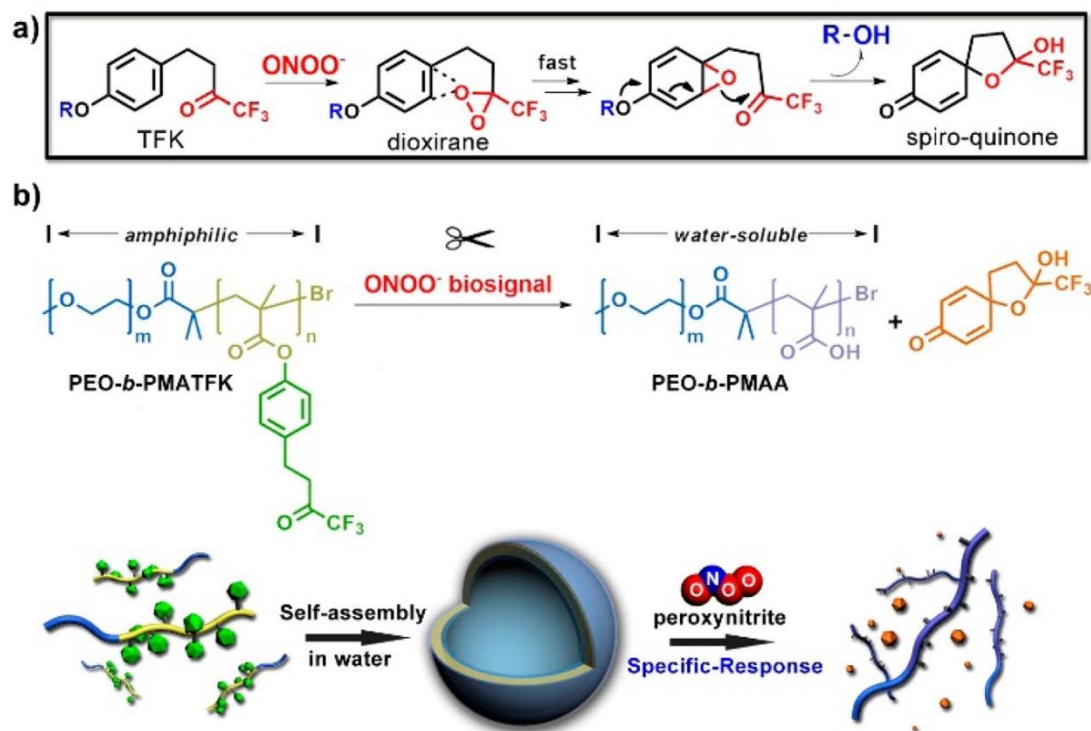
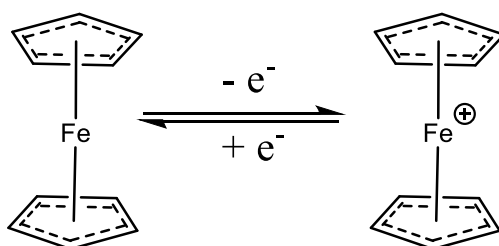


Figure 1.19 - Schematic Illustration of (a) ONOO^- -induced oxidation-elimination reaction, (b) ONOO^- signalling molecule responsive block copolymer (PEO-*b*-PMATFK), and their controllable self-assembly and disassembly. Reprinted with permission from Ref.¹³⁰ Copyright 2019 American Chemical Society

Ferrocene is another oxidation responsive group which has been incorporated into polymer systems (Scheme 1.3). This is studied much more with regards to cancer treatment as the toxicity of the ferrocenium group can be beneficial in the treatment. The toxicity is due to the ability of ferrocene derivatives to induce oxidative DNA damage.¹³¹



Scheme 1.3 - The oxidation of ferrocene to ferrocenium

One example of a potential ferrocene-based drug delivery system is supramolecular vesicles which are both thermal and oxidation responsive (Figure 1.20).¹³² These structures were formed through the host-guest interaction of two individually synthesised polymer chains, one a thermally responsive pNIPAM chain synthesised via RAFT polymerisation with a pillar[6]ene functionalised

RAFT agent, and the other a methoxy-PEG chain terminating with an oxidation responsive ferrocene group. When heated to body temperature, this supramolecular diblock copolymer is amphiphilic, rather than hydrophilic. On oxidation, the host-guest interaction no longer takes place and the structure disassembles meaning that encapsulated drugs could be released.

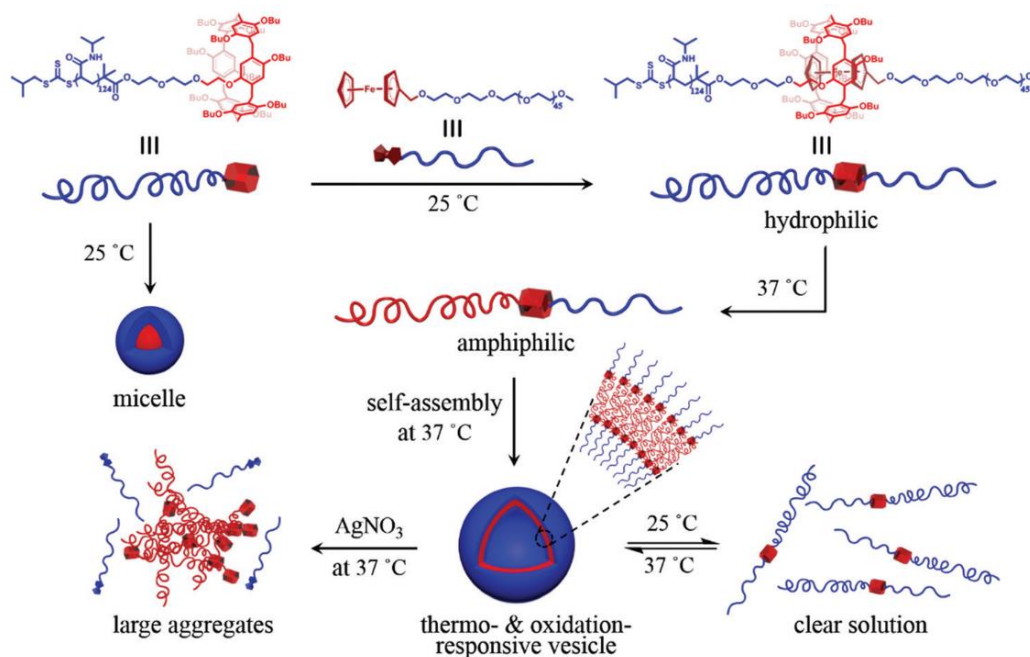


Figure 1.20 - Illustration of the assembly and disassembly of thermo- and oxidation-responsive supramolecular polymeric vesicles from PNIPAM-P[6] mPEG-Fc. Reproduced from Ref. ¹³² with permission from The Royal Society of Chemistry.¹³²

Another potential drug delivery system incorporating ferrocene was the preparation of 'patchy nanocapsules' with a poly(vinylferrocene)-*b*-p(methylmethacrylate) shell.¹³³ The poly(vinylferrocene) patches could be oxidised selectively which would give a hydrophobic object with hydrophilic patches in contrast to the totally hydrophobic object prior to oxidation. These swollen patches should allow the release of encapsulated hydrophobic drugs.

1.7.3. Summary of responsive systems

There are many functional groups which can be exploited within redox responsive DDS. This means the scope of molecules and therefore polymers which can be developed into these systems is very large. Research suggests that there is potential in the future for a polymeric, stimuli-responsive DDS to be developed which can be taken from a lab environment and into a clinic.

1.8. Temperature Responsive Polymers

There are many examples of temperature responsive polymers in the literature, which fall into two main categories: those with a lower critical solution temperature (LCST) and those with an upper critical solution temperature (UCST), however it is possible for a polymer to exhibit both. An LCST is the critical temperature of a polymer solution when it undergoes a phase transition, below this temperature the polymer is miscible with the solvent and above this temperature show phase separation (Figure 1.21). A UCST is the opposite of this behaviour.

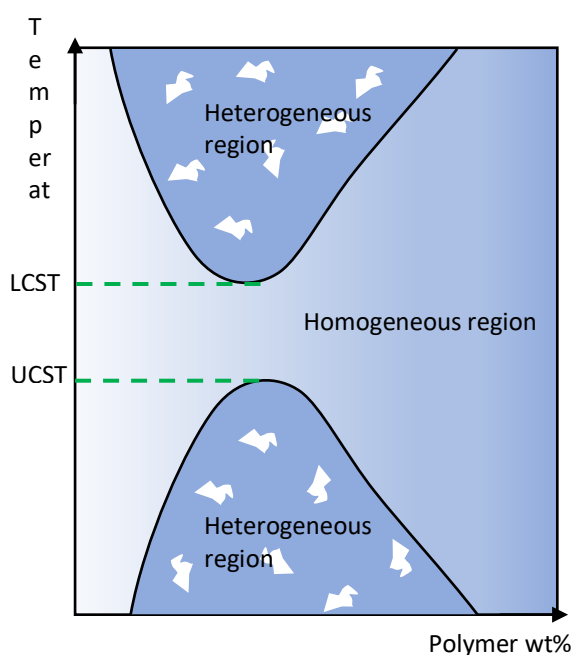
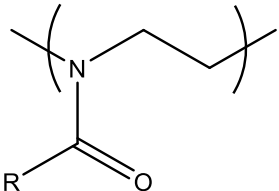
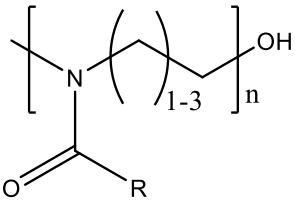
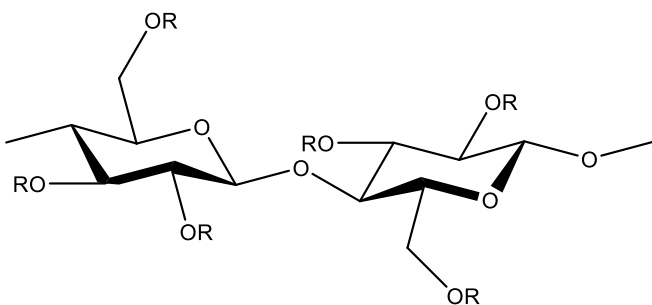
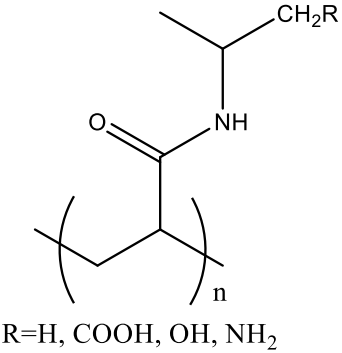
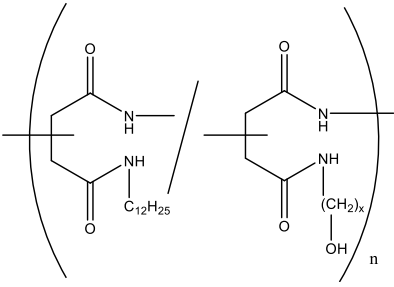
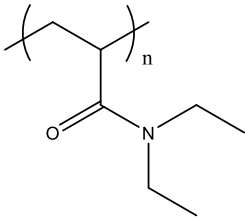
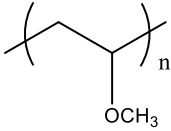
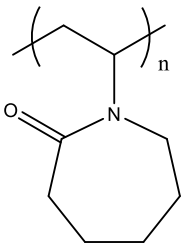


Figure 1.21 - An example figure showing polymer phase transitions including LCST and UCST.

For the purpose of this research, only polymers which exhibit an LCST which can be tuned were of interest. This is because it will need to be hydrophobic in the body to prolong circulation time and prevent premature excretion. Therefore, the LCST of the polymer needs to be below 37 °C in its native state. However, we do not want to have this polymer circulating around the body indefinitely, leaching into and getting trapped within the tissue, so the LCST of the polymer needs to be raised in response to a stimulus, i.e. oxidation, to cause a hydrophobic to hydrophilic transition and therefore safe renal excretion of the polymeric DDS.

Table 1.6 - A list of temperature responsive polymers alongside their LCST values in water.¹³⁴

Polymer	Abbreviation	LCST (°C)
Derivatives of 2-oxazoline ^{135,136,137,138} –  Poly(2-methyl-2-oxazoline) Poly(2-ethyl-2-oxazoline) Poly(2-cyclopropyl-2-oxazoline) Poly(2-n-propyl-2-oxazoline) Poly(2-isopropyl-2-oxazoline)	(Pox) (PMOx) (PEOx) (PcPOx) (PnPOx) (PiPOx)	No LCST 60 30 25 36
Poly(2-oxazine)s ¹³⁹ –  Poly(2-ethyl-2-oxazine) Poly(2-n-propyl-2-oxazine)	(POZIs) (PEOZI) (PnPropOZI)	56 11
Derivatives of cellulose –  Hydroxypropyl cellulose Methyl cellulose Hydroxypropyl methyl cellulose		45 40 69
Poly(N-isopropylacrylamide) and derivatives ^{140,141,142,143} –	NIPAM CIPAAM AIPAAM	32 LCST is dependent on the quantity

 <p>R=H, COOH, OH, NH₂</p> <p>Poly(N-isopropylacrylamide) Poly(2-carboxyl-isopropylacrylamide) Poly(2-amino-isopropylacrylamide) Poly(2-hydroxy-isopropylacrylamide)¹⁴⁴</p>	<p>HIPAAAM</p>	<p>incorporated.</p>
<p>Amphiphilic poly(asparagine)^{145,146}</p> 		<p>Dependent on composition ratio and side chains</p> <p>28-78</p>
<p>Poly(N,N'-diethylacrylamide)¹⁴⁷</p> 		<p>33</p>
<p>Poly(methyl vinyl ether)</p> 		<p>37</p>
<p>Poly(N-vinyl caprolactam)^{148,149,142}</p> 		<p>32</p>
<p>Polyethylene glycol -based copolymers^{150,151}</p>	<p>PEG</p>	<p>20-85</p>



Examples of polymers which exhibit an LCST can be seen in Table 1.6. Through this research, the polymers of most interest to us were polymers based on *N*-isopropylacrylamide (NIPAM), as the LCST of these in water are very close to body temperature.

1.8.1. *Poly(N-isopropylacrylamide)*

The main monomer used for the following study is *N*-isopropylacrylamide. The polymer of this is commonly used in lab-based development of drug delivery studies due to its biocompatibility, however no polymers of NIPAM have succeeded in clinical trials. Polymers of NIPAM display a temperature-response. Specifically, in water pNIPAM has an LCST of 32 °C, which is close to the temperature of the human body. Polymers can therefore be altered to make them suitable for biomedical applications, which is why it was the polymer chosen in this thesis. This behaviour can be explained by the thermodynamics of the polymer solution. Enthalpy is determined by the balance of intra- and intermolecular forces, with the main contributors in this case being hydrogen bonding between H₂O and amide groups, and hydrophobic interactions. Entropic effects are due to the ordering of water molecules to form hydrogen bonds and the disorder of breaking these. This behaviour causes a coil to globule transition in pNIPAM (Figure 1.22). When the temperature is lower than the LCST, the hydrated coil form is preferred. In this case, ΔH is negative so dominates the free energy. At higher temperatures however, the entropic component increases, causing the release of water and a dehydrated globule to form.^{152,153}

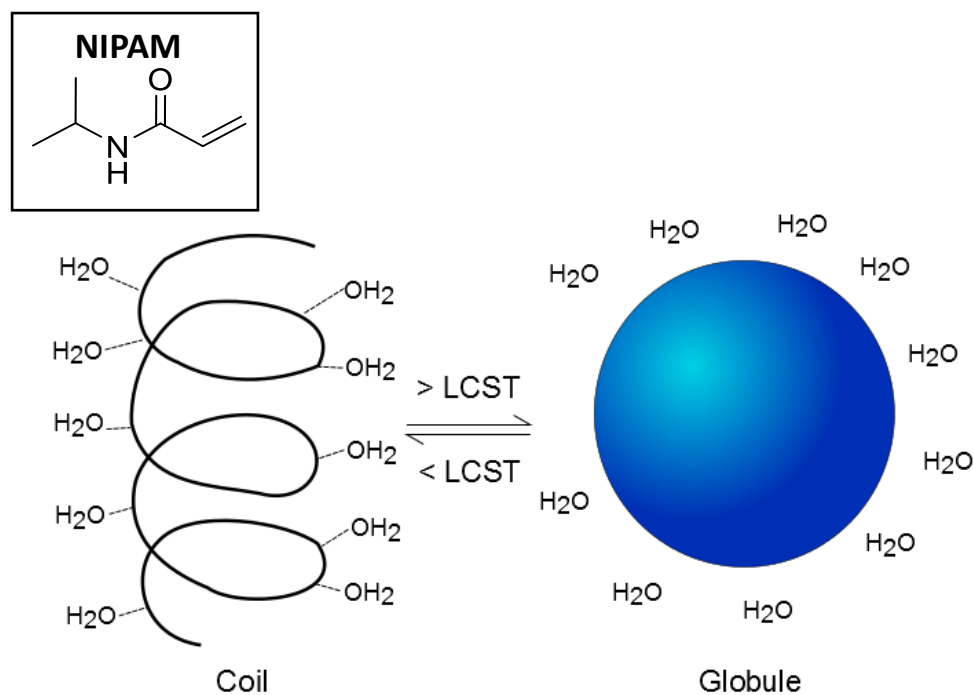


Figure 1.22 - The effect of temperature on pNIPAM showing the coil to globule transition when heated to temperatures above the LCST.

To determine the LCST of a polymer accurately a complete phase diagram for pNIPAM would be needed. However, it can be estimated using cloud point analysis which is a measurement of the turbidity of the polymer solution with temperature. There are many limitations to this technique however as it is sensitive to both the concentration of the polymer solution and the rate at which it is heated. The wavelength of light used is also important.

One of the disadvantages of using pNIPAM, is that the polymer backbone only contains carbon atoms, which are difficult for the body to break down. Therefore, polymer chain lengths must be kept short to allow safe excretion from the body.

1.9. Synthesis of polymers

1.9.1. Free radical polymerisation

Free-radical polymerisation is a type of chain-growth polymerisation that is characterised by the 4 steps: initiation, propagation, chain transfer and termination. It is a versatile polymerisation method, allowing polymer synthesis for a wide range of vinyl monomers, with processing conditions which

are not too stringent, which is why it is used in around 50% of industrial polymer synthesis processes.¹⁵⁴

It does however have many disadvantages. There is little control over the polymerisation which means it is difficult to accurately target a molecular weight, and therefore a broad molecular weight distribution is observed. Due to this, it is not possible to create polymers of a strict known composition and architecture, so it is difficult to incorporate functionalities into a specific position within the structure.¹⁵⁴

1.9.2. Controlled/Living radical polymerisation

Reversible deactivation radical polymerisations (RDRP), previously referred to as controlled/living radical polymerisations were developed to overcome the many disadvantages of free-radical polymerisation.¹⁵⁵ These are categorised as “Chain polymerisation, propagated by radicals that are deactivated reversibly, bringing them into active- dormant equilibria of which there might be more than one.”¹⁵⁵ To expand the scope of polymer chemistry, more control was needed over the synthesis so that they had specific functionalities. Control over molecular weight of the polymer is important to achieve this and can also cause the dispersity of the polymer chains to be narrow. In an ideal controlled/living polymerisation, all the initiator present would create polymer chains, and these would continue to propagate until all of the monomer stock in the reaction is exhausted, and no termination mechanism exists.¹⁵⁶ The living aspect of the polymerisation is that the dormant chains formed are capable of reactivation so functionalisation and chain extension with other monomers is possible.

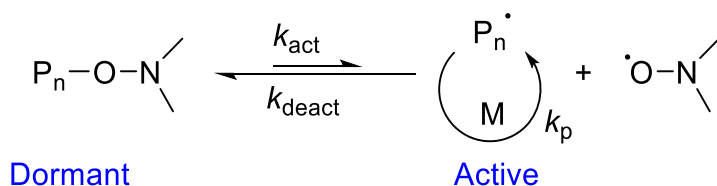
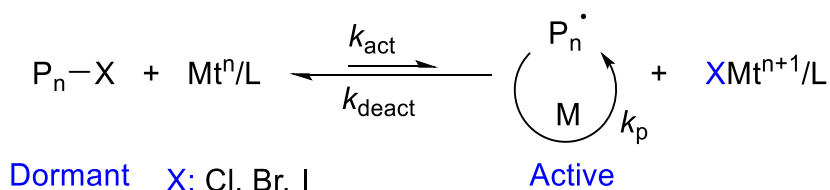
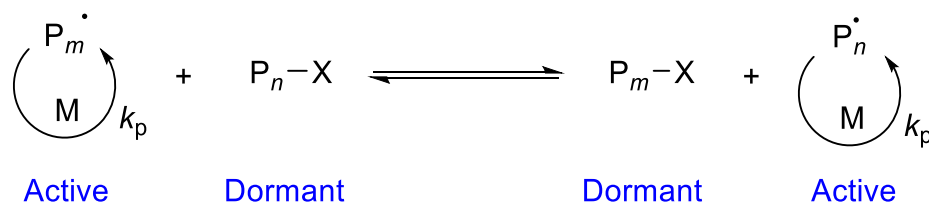
Another criterion for living/controlled polymerisation is that initiation should occur early in the polymerisation i.e. at low monomer conversion. This means that the dispersity will be low ($M_w/M_n < 1.2$) as the chains initiate at the same time and extend at the same rate.

There are three main RDRP techniques which have been developed to overcome this: stable free-radical polymerisation such as nitroxide mediated polymerisation (NMP), transition metal catalysed

atom transfer polymerisation (ATRP) and reversible addition-fragmentation chain transfer (RAFT) polymerisation.¹⁵⁶ These are usually termed as pseudo-living polymerisations, as although termination is minimised, it does occur, unlike in a true living polymerisation.

The controlled nature of these polymerisation methods relies on the dynamic equilibrium which is established between growing free radicals and various dormant species (Figure 1.23). Most of the chains are dormant chains which are unable to propagate or terminate, with only a small number of propagating chains, extending the lifetime of these. However fast exchange between dormant species and growing radicals is important to ensure that all chains grow at the same rate.¹⁵⁵

In both NMP and ATRP, the equilibrium is shifted towards the dormant, non-propagating species, whereas in RAFT polymerisation the equilibrium does not favour either product, having an equilibrium constant of $K=1$. In RAFT polymerisation, the polymeric starting materials and their products have very similar reactivities, only differing by molecular weight, whereas in ATRP and NMP the properties between the species are different. This can therefore be referred to as degenerative chain transfer process, as the only difference between the species at either side of the equilibrium is the relative molecular mass.^{155,157}

Nitroxide-mediated Polymerisation (NMP)Atom Transfer Radical Polymerisation (ATRP)Reversible Addition-Fragmentation Chain-Transfer (RAFT) PolymerisationFigure 1.23 - The equilibrium steps of the three common types of RDRP.^{158–160}

Even though standard free radical polymerisation has many advantages, there is a lack of control over molecular weights, giving a large polydispersity, and it is difficult to form particular architectures and compositions.

Although many polymerisation techniques have been discussed here, the details of these go beyond the nature of this work. The polymerisation technique used extensively throughout this research is RAFT polymerisation which is discussed in detail below.

1.9.2.1. Reversible addition-fragmentation chain transfer polymerisation – RAFT

RAFT polymerisation has all the benefits of a FRP, but it allows for the precise control of molecular weight, as all chains are initiated at the beginning of the reaction and grow at similar rates.¹⁶¹ RAFT polymerisation was developed at the Commonwealth Scientific and Industrial Research Organisation (CSIRO), with the first paper being published in 1998.¹⁶² These polymerisations occur with the same

monomers, initiators and solvents as free radical polymerisations, however a chain transfer agent (CTA) is used. Since then there has been a lot more research on this polymerisation technique.

A schematic of the species observed throughout a RAFT polymerisation process can be seen below (Figure 1.24).¹⁵⁸ Many of these are dormant, with only a few active chains at one time. Radical-radical termination can still occur, resulting in loss of the ZCS_2 RAFT chain end group, however this occurs to a much lower extent than in FRP. When this occurs, these chains are no longer able to take part in further polymerisation and are referred to as 'dead chains.' The process occurs due to a radical initiator being used, therefore some polymers have initiator-based end groups, however without this the polymerisation cannot proceed.

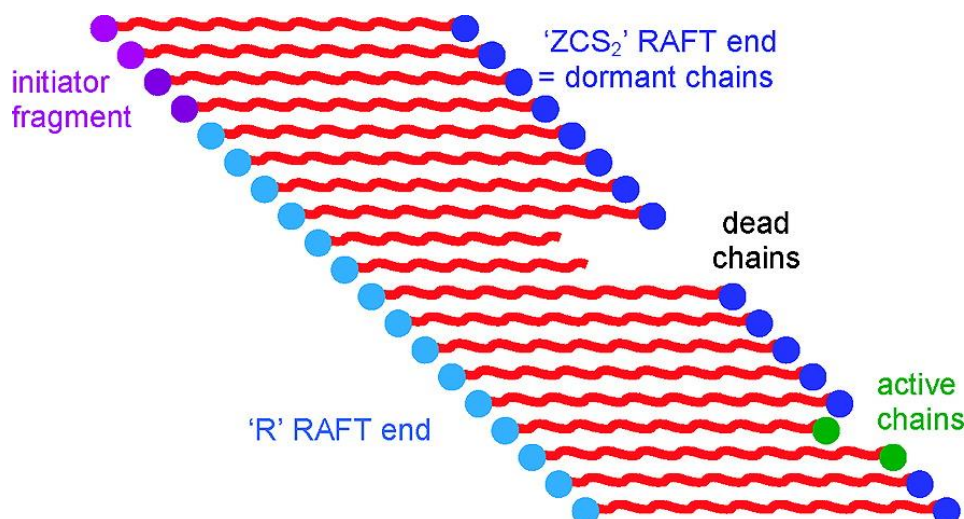
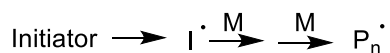
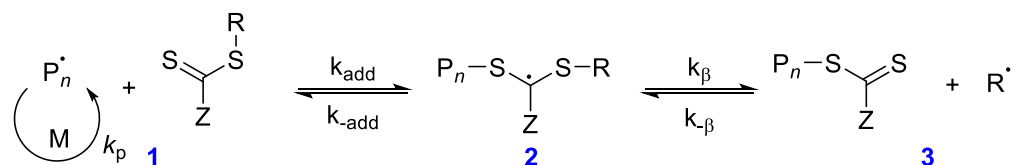


Figure 1.24 – A schematic of a RAFT polymerisation denoting many of the species present during a polymerisation of this kind. It must be noted however, that the concentration of initiator fragments is ideally not this high, and that the proportion of dormant chains is much higher than shown. Reprinted with permission from Ref. ¹⁵⁸. Copyright 2006 American Chemical Society.

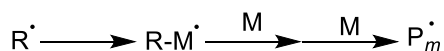
Initiation



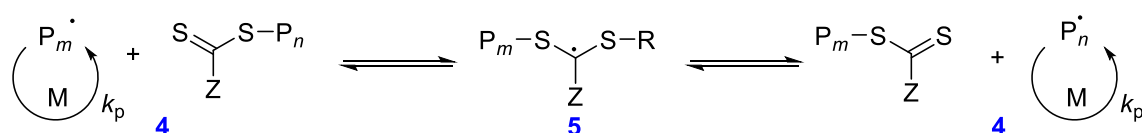
Reversible chain transfer



Reinitiation



Chain equilibrium



Termination

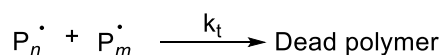


Figure 1.25 – The mechanism of RAFT polymerisation.^{157,163}

The mechanism of RAFT polymerisation can be seen above (Figure 1.25).^{158,164} The initiation and termination steps occur as in conventional FRP, it is the equilibrium steps which set RAFT apart. A decomposing radical initiator is used to initiate the polymerisation by reaction of the radical with a monomer unit. This yields $\text{P}_n \cdot$, a propagating polymeric unit, which reacts with more monomer units causing chain growth. These polymeric radicals can react reversibly with the CTA (1) in an equilibrium, producing $\text{R} \cdot$ and a polymeric RAFT chain transfer agent (3). The radical produced can form another polymer chain in the same way that the initial initiator works. Propagating polymer radicals form a chain equilibrium on the CTA, with the dormant species (4) having an equal opportunity to grow, which allows for the polymer chains to have a low PDI.

As mentioned previously, the nature of the narrow molecular weight of polymers synthesised using RAFT, is due to the rapid and reversible equilibrium between dormant and active chains, and therefore the rate constant for chain transfer (k_{tr}) is important:

$$k_{tr} = k_{add} \frac{k_{\beta}}{k_{-add} + k_{\beta}} = k_{add} \Phi \quad (1)$$

$$\Phi = \frac{k_{\beta}}{k_{-add} + k_{\beta}} \quad (2)$$

Where k_{add} is the rate constant for addition, k_{β} is the rate of β -scission and Φ is the partition coefficient, the ratio of solute concentrations.¹⁵⁸

Once all monomer has been used to make the polymer, termination of radical-radical species begins. Any other polymer chains will undergo bi-radical termination to form dead polymer chains i.e. chains that cannot react further. The CTA-polymer is now stable. Polymer growth can be initiated again for those chains still containing RAFT chain end groups, and polymerisation can continue with a different monomer. Block copolymers, combs, stars and more complex structures can be formed this way.¹⁶³

The CTA for RAFT can have one of four general structures; xanthates, trithiocarbonates, dithioesters and dithiocarbamates (Figure 1.26).¹⁶⁵⁻¹⁶⁷ In order for the polymerisation to occur, an appropriate CTA agent must be chosen for the monomer class i.e. acrylates, acrylamides etc. This is dependent of the Z and R groups of the CTA as the R group is a free radical leaving group and the Z group controls the reactivity of the C=S bond (Figure 1.27). These groups affect the speed and control of the polymerisation. There are only a few disadvantages of RAFT polymerisation but the main one is that CTAs are only suitable for a limited number of monomers, although others include the cost as well as the colour of the polymers produced. However, the advantages mentioned above far outweigh these.

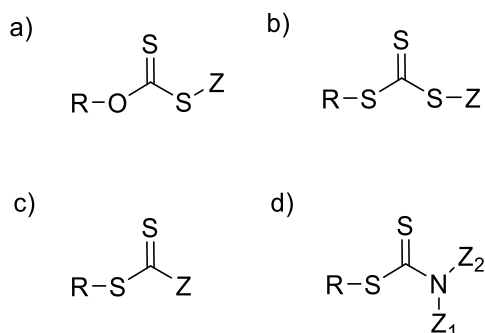


Figure 1.26 - Typical types of RAFT chain transfer agents: a) xanthates, b) trithiocarbonates, c) dithioesters and d) dithiocarbamates.^{164,165,167,168}

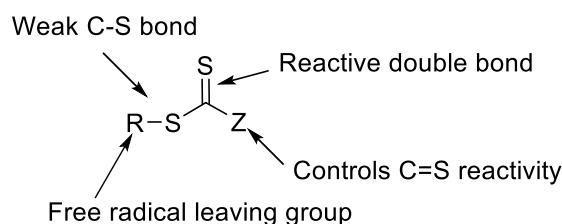


Figure 1.27- The general structure of a chain transfer agent.¹⁶³

As mentioned above, with RAFT polymerisation it is possible to control the degree of polymerisation (DP). This is done by varying the ratio of monomer to CTA agent concentrations:

$$DP = \frac{[M]}{[mCTA]} \quad (3)$$

This can allow you to predict the degree of polymerisation before you start the reaction, and determine the actual value afterwards using the percentage conversion of monomer, or by comparing the integrals of the CTA agent to the polymer peaks via 1H NMR spectroscopy.

1.10. Thesis Outline

The overall aim of this project was to develop an isothermally responsive polymeric drug delivery systems with an oxidative trigger. It should be non-toxic, having minimal interactions with proteins and not undergo phagocytic attack after administration into the body. This system should have a high drug loading efficiency of hydrophobic drug which remains encapsulated with minimal leakage until the drug reaches the target site. It should respond to levels of H_2O_2 produced in the body due to

various autoimmune diseases. Upon oxidation, the drug should be released to the desired area of the body, with the delivery system polymer becoming hydrophilic so it can be excreted safely.

In chapter 2, the synthesis and analysis of pNIPAM of various chain lengths and with different RAFT chain end groups will be discussed. The influence of oxidation on the RAFT chain end groups and how this effects the temperature responsive behaviour of the polymer is described.

In chapter 3, the synthesis and analysis of diblock copolymers with temperature and oxidation responsive groups are discussed in terms of their self-assembly and oxidation response.

In chapter 4, a variety of different NG systems are analysed to determine how the amount of crosslinker, NIPAM and oxidation responsive group can affect the size and morphology of the formed nanogels.

1.11. References

- 1 B. J. Crielaard, T. Lammers, R. M. Schiffelers and G. Storm, *J. Control. Release*, 2012, **161**, 225–234.
- 2 J. H. Lin and A. Y. H. Lu, *Pharmacol. Rev.*, 1997, **49**, 403–449.
- 3 S. C. Vikrant K. Bhosle, Gabriel Altit, Julie Autmizguine, Elsevier, 5th edn., 2017, pp. 187–201.
- 4 A. R. Khan, X. Yang, M. Fu and G. Zhai, *J. Control. Release*, 2018, **291**, 37–64.
- 5 S. M. Stamatovic, R. F. Keep and A. V Andjelkovic, *Curr. Neuropharmacol.*, 2008, **6**, 179–192.
- 6 G. Kroemer and J. C. Reed, *Nat Med*, 2000, **6**, 513–519.
- 7 M. Mittal, M. R. Siddiqui, K. Tran, S. P. Reddy and A. B. Malik, *Antioxid. Redox Signal.*, 2014, **20**, 1126–1167.
- 8 J. T. Hancock, R. Desikan and S. J. Neill, *Biochem. Soc. Trans.*, 2001, **29**, 345–50.
- 9 B. Halliwell, *Lancet*, 1994, **344**, 721–724.
- 10 B. Uttara, A. V Singh, P. Zamboni and R. T. Mahajan, *Curr. Neuropharmacol.*, 2009, **7**, 65–74.
- 11 C. A. Hitchon and H. S. El-Gabalawy, *Arthritis Res. Ther.*, 2004, **6**, 265–78.
- 12 I. Fridovich, *Ann. N. Y. Acad. Sci.*, 1999, **893**, 13–18.
- 13 R. T. Dean, S. Fu, R. Stocker and M. J. Davies, *Biochem. J.*, 1997, **324**, 1–18.
- 14 H. Wiseman and B. Halliwell, *Biochem. J.*, 1996, **313**, 17–29.
- 15 F. Schafer and G. Buettner, *Free Radic. Biol. Med.*, 2001, **30**, 1191–1212.
- 16 S. Papa and V. P. Skulachev, *Mol. Cell. Biochem.*, 1997, **174**, 305–19.
- 17 R. M. Touyz and E. L. Schiffrin, *Histochem. Cell Biol.*, 2004, **122**, 339–352.
- 18 S. Nie, Y. Xing, G. J. Kim and J. W. Simons, *Annu. Rev. Biomed. Eng.*, 2007, **9**, 257–288.
- 19 N. Li, L. Zhao, L. Qi, Z. Li and Y. Luan, *Prog. Polym. Sci.*, 2016, **58**, 1–26.
- 20 X. Guo, L. Wang, X. Wei and S. Zhou, *J. Polym. Sci. Part A Polym. Chem.*, 2016, **54**, 3525–3550.
- 21 V. M. Vijayan and J. Muthu, *Polym. Adv. Technol.*, 2017, **28**, 1572–1582.
- 22 T. Lammers, W. E. Hennink and G. Storm, *Br. J. Cancer*, 2008, **99**, 392–397.
- 23 R. Duncan, *Nat. Rev. Cancer*, 2006, **6**, 688–701.
- 24 C. Lahtz and G. P. Pfeifer, *J. Mol. Cell Biol.*, 2011, **3**, 51–58.
- 25 H. Lodish, A. Berk, P. M. S Lawrence Zipursky, D. Baltimore and J. Darnell., *Molecular cell biology*, W.H. Freeman, New York, 4th Ed., 2000.
- 26 L. M. Coussens and Z. Werb, *Nature*, 2002, **420**, 860–867.
- 27 A. Mantovani, P. Allavena, A. Sica and F. Balkwill, *Nature*, 2008, **454**, 436–44.
- 28 S. Khadraoui, F. Harrou, H. N. Nounou, M. N. Nounou, A. Datta and S. P. Bhattacharyya, *Inf. Sci. (Ny)*, 2016, **333**, 108–125.

- 29 N. J. Wheate, S. Walker, G. E. Craig and R. Oun, *Dalton Trans.*, 2010, **39**, 8113–8127.
- 30 D. J. Slamon, *N. Engl. J. Med.*, 2001, **344**, 783–792.
- 31 A. Gibofsky, *Am. J. Manag. Care*, 2012, **18**, 295–302.
- 32 P. L. van Lent, A. E. Holthuysen, L. van den Bersselaar, N. van Rooijen, L. B. van de Putte and W. B. van den Berg, *Scand J Rheumatol Suppl*, 1995, **101**, 83–89.
- 33 W. Hofkens, R. Schelbergen, G. Storm, W. B. van den Berg and P. L. van Lent, *PLoS One*, 2013, **8**, e54016.
- 34 S. Umar, J. Zargan, K. Umar, S. Ahmad, C. K. Katiyar and H. A. Khan, *Chem. Biol. Interact.*, 2012, **197**, 40–6.
- 35 A. Haghikia, R. Hohlfeld, R. Gold and L. Fugger, *Trends Mol. Med.*, 2013, **19**, 309–319.
- 36 M. E. Weinblatt, B. N. Weissman, D. E. Holdsworth, P. A. Fraser, A. L. Maier, K. R. Falchuk and J. S. Cobly, *Arthritis Rheum.*, 1992, **35**, 129–137.
- 37 M. E. Weinblatt, H. Kaplan, B. F. Germain, S. Block, S. D. Solomon, R. C. Merriman, F. Wolfe, B. Wall, L. Anderson, E. Gall, D. Torretti and B. Weissman, *Arthritis Rheum.*, 1994, **37**, 1492–1498.
- 38 S. Palmer and M. Sculpher, *NICE Technol. Apprais. Guid.*, 2007, 1–30.
- 39 J. R. O’ Dell, C. E. Haire, N. Erikson, W. Drymalski, W. Palmer, P. J. Eckhoff, V. Garwood, P. Maloley, L. W. Klassen, S. Wees, H. Klein and G. F. Moore, *N Engl J Med*, 1996, **334**, 1287–1291.
- 40 G. M. Bartelds, C. A. Wijbrandts, M. T. Nurmohamed, S. Stapel, W. F. Lems, L. Aarden, B. A. C. Dijkmans, P. P. Tak and G. J. Wolbink, *Ann. Rheum. Dis.*, 2007, **66**, 921–6.
- 41 B. G. Arnason, *Annu. Rev. Med.*, 1999, **50**, 291–302.
- 42 A. Compston and A. Coles, *Lancet*, 2008, **372**, 1502–1517.
- 43 J. Bennett, J. Basivireddy, A. Kollar, K. E. Biron, P. Reickmann, W. A. Jefferies and S. McQuaid, *J. Neuroimmunol.*, 2010, **229**, 180–91.
- 44 A. Minagar, *Yearb. Neurol. Neurosurg.*, 2012, **2012**, 85–86.
- 45 P. Patrikios, C. Stadelmann, A. Kutzelnigg, H. Rauschka, M. Schmidbauer, H. Laursen, P. S. Sorensen, W. Brück, C. Lucchinetti and H. Lassmann, *Brain*, 2006, **129**, 3165–3172.
- 46 NICE, *NICE*, 2002, 1–32.
- 47 Nice, *NICE Technol. Apprais. Guid. 127*, 2007, 21.
- 48 A. W. A. I. Polman, Chris H. O’Connor, Paul W. Havrdova, Eva. Hutchinson, Michael. Kappos, Ludwig. Miller, David H. Phillips, J Theodore. Lublin, Fred D. Giovannoni, Gavin. Wajgt, Andrzej. Toal, Martin. Lynn, Frances. Panzara, Michael A. Sandrock, *NEJM*, 2006, **354**, 899–910.
- 49 A. J. Coles, D. A. S. Compston, K. W. Selmaj, S. L. Lake, S. Moran, D. H. Margolin, K. Norris and P. K. Tandon, *NEJM*, 2008, **17**, 1786–1801.
- 50 S. Grund, M. Bauer and D. Fischer, *Adv. Eng. Mater.*, 2011, **13**, B61–B67.
- 51 D. F. Williams, *J. Biomed. Eng.*, 1989, **11**, 185–191.

- 52 D. F. Williams, *Biomaterials*, 2014, **35**, 10009–10014.
- 53 C. de Las Heras Alarcon, S. Pennadam and C. Alexander, *Chem. Soc. Rev.*, 2005, **34**, 276–285.
- 54 P. K. Dhal, S. C. Polomoscanik, L. Z. Avila, S. R. Holmes-Farley and R. J. Miller, *Adv. Drug Deliv. Rev.*, 2009, **61**, 1121–1130.
- 55 K. Miyata, R. J. Christie and K. Kataoka, *React. Funct. Polym.*, 2011, **71**, 227–234.
- 56 R. D’Arcy and N. Tirelli, *Polym. Adv. Technol.*, 2014, **25**, 478–498.
- 57 C. Dhand, M. P. Prabhakaran, R. W. Beuerman, R. Lakshminarayanan, N. Dwivedi and S. Ramakrishna, *RSC Adv.*, 2014, **4**, 32673–32689.
- 58 D. L. Elbert and J. A. Hubbell, *Annu. Rev. Mater. Sci.*, 1996, **26**, 365–294.
- 59 R. Gaspar and R. Duncan, *Adv. Drug Deliv. Rev.*, 2009, **61**, 1220–1231.
- 60 N. Angelova and D. Hunkeler, *Trends Biotechnol.*, 1999, **17**, 409–421.
- 61 A. Göpferich, *Biomaterials*, 1996, **17**, 103–114.
- 62 R. Duncan, *Nat. Rev. Drug Discov.*, 2003, **2**, 347–60.
- 63 I. Ekladios, Y. L. Colson and M. W. Grinstaff, *Nat. Rev. Drug Discov.*, 2019, **18**, 273–294.
- 64 E. M. Pelegri-Oday, E. W. Lin and H. D. Maynard, *J. Am. Chem. Soc.*, 2014, **136**, 14323–14332.
- 65 F. Greco and M. J. Vicent, *Adv. Drug Deliv. Rev.*, 2009, **61**, 1203–1213.
- 66 E. Chiessi and G. Paradossi, *J. Phys. Chem. B*, 2016, **120**, 3765–3776.
- 67 M. Yokoyama, S. Fukushima, R. Uehara, K. Okamoto, K. Kataoka, Y. Sakurai and T. Okano, *J. Control. Release*, 1998, **50**, 79–92.
- 68 A. Napoli, M. Valentini, N. Tirelli, M. Müller and J. A. Hubbell, *Nat. Mater.*, 2004, **3**, 183–189.
- 69 Y. Zhang, C. Ma, S. Zhang, C. Wei, Y. Xu and W. Lu, *Mater. Today Chem.*, 2018, **9**, 34–42.
- 70 J. Li, F. Yu, Y. Chen and D. Oupický, *J. Control. Release*, 2015, **219**, 369–382.
- 71 L. Seymour, *J. Bioact. Compat. Polym.*, 1991, **6**, 178–216.
- 72 R. Duncan, *J. Drug Target.*, 2017, **25**, 759–780.
- 73 clinicaltrials.gov, <https://www.clinicaltrials.gov/>.
- 74 F. F. Davis, *Adv. Drug Deliv. Rev.*, 2002, **54**, 457–458.
- 75 F. M. Veronese and A. Mero, *Biodrugs*, 2008, **22**, 315–329.
- 76 J. Israelachvili, *Proc. Natl. Acad. Sci.*, 1997, **94**, 8378–8379.
- 77 F. Zhang, M. Liu and H. Wan, *Biol. Pharm. Bull.*, 2013, **37**, 335–339.
- 78 A. R. Menjoge, A. L. Rinderknecht, R. S. Navath, M. Faridnia, C. J. Kim, R. Romero, R. K. Miller and R. M. Kannan, *J. Control. Release*, 2011, **150**, 326–338.
- 79 U. Mahadevan, D. C. Wolf, M. Dubinsky, A. Cortot, S. D. Lee, C. A. Siegel, T. Ullman, S. Glover, J. F. Valentine, D. T. Rubin, J. Miller and M. T. Abreu, *Clin. Gastroenterol. Hepatol.*, 2013, **11**, 286–292.
- 80 R. L. Hassfurth, T. N. Terhune and P. C. Canning, *Am. J. Vet. Res.*, 2015, **76**, 231–238.

- 81 Q. Yang, T. M. Jacobs, J. D. McCallen, D. T. Moore, J. T. Huckaby, J. N. Edelstein and S. K. Lai, *Anal. Chem.*, 2016, **88**, 11804–11812.
- 82 K. E. Maier and M. Levy, *Mol. Ther. - Methods Clin. Dev.*, 2016, **3**, 16014.
- 83 N. J. Ganson, T. J. Povsic, B. A. Sullenger, J. H. Alexander, S. L. Zelenkofske, J. M. Sailstad, C. P. Rusconi and M. S. Hershfield, *J. Allergy Clin. Immunol.*, 2016, **137**, 1610-1613.e7.
- 84 E. Lallana and N. Tirelli, *Macromol. Chem. Phys.*, 2013, **214**, 143–158.
- 85 M. Huo, J. Yuan, L. Tao and Y. Wei, *Polym. Chem.*, 2014, **5**, 1519.
- 86 C. Alvarez-Lorenzo and A. Concheiro, *Chem. Commun.*, 2014, **50**, 7743.
- 87 Y. Cheng, C. He, C. Xiao, J. Ding, K. Ren, S. Yu, X. Zhuang and X. Chen, *Polym. Chem.*, 2013, **4**, 3851.
- 88 A. Raza, U. Hayat, T. Rasheed, M. Bilal and H. M. N. Iqbal, *Eur. J. Med. Chem.*, 2018, **157**, 705–715.
- 89 S. Hajebi, N. Rabiee, M. Bagherzadeh, S. Ahmadi, M. Rabiee, H. Roghani-Mamaqani, M. Tahriri, L. Tayebi and M. R. Hamblin, *Acta Biomater.*, 2019, **92**, 1–18.
- 90 C. Ding, L. Tong, J. Feng and J. Fu, *Molecules*, 2016, **21**, 1715.
- 91 Y.-R. Luo, *Comprehensive Handbook of Chemical Bond Energies*, CRC Press, 2007, vol. 58.
- 92 Y. Li, Z. Wang, N. Ma, X. Zhang and H. Xu, *J. Am. Chem. Soc.*, 2009, **132**, 442–443.
- 93 D. Shaloam and P. B. Tchounwou, *Eur. J. Pharmacol.*, 2014, **740**, 364–378.
- 94 H. Cho, J. Bae, V. K. Garripelli, J. M. Anderson, H.-W. W. Jun and S. Jo, *Chem. Commun.*, 2012, **48**, 6043.
- 95 C.-C. Song, F.-S. Du and Z.-C. Li, *J. Mater. Chem. B*, 2014, **2**, 3413.
- 96 P. Carampin, E. Lallana, J. Laliturai, S. C. Carroccio, C. Puglisi and N. Tirelli, *Macromol. Chem. Phys.*, 2012, **213**, 2052–2061.
- 97 D. Jeanmaire, J. Laliturai, A. Almalik, P. Carampin, Richard d’Arcy, E. Lallana, R. Evans, R. E. P. Winpenny and N. Tirelli, *Polym. Chem.*, 2014, **5**, 1393.
- 98 B. L. Allen, J. D. Johnson and J. P. Walker, *ACS Nano*, 2011, **5**, 5263–5272.
- 99 R. d’Arcy, A. Gennari, R. Donno and N. Tirelli, *Macromol. Rapid Commun.*, 2016, **37**, 1918–1925.
- 100 M. Tang, Q. Zheng, N. Tirelli, P. Hu, Q. Tang, J. Gu and Y. He, *React. Funct. Polym.*, 2017, **110**, 55–61.
- 101 J. Wang, X. Sun, W. Mao, W. Sun, J. Tang, M. Sui, Y. Shen and Z. Gu, *Adv. Mater.*, 2013, **25**, 3670–3676.
- 102 H. Maeda, *J. Control. Release*, 2012, **164**, 138–144.
- 103 H. Maeda, J. Wu, T. Sawa, Y. Matsumura and K. Hori, *J. Control. Release*, 2000, **65**, 271–284.
- 104 J. Fang, H. Nakamura and H. Maeda, *Adv. Drug Deliv. Rev.*, 2011, **63**, 136–151.
- 105 H. Xu, W. Cao and X. Zhang, *Acc. Chem. Res.*, 2013, **46**, 1647–1658.
- 106 N. Ma, Y. Li, H. Ren, H. Xu, Z. Li and X. Zhang, *Polym. Chem.*, 2010, **1**, 1609.

- 107 P. Han, N. Ma, H. Ren, H. Xu, Z. Li, Z. Wang and X. Zhang, *Langmuir*, 2010, **26**, 14414–14418.
- 108 H. Ren, Y. Wu, N. Ma, H. Xu and X. Zhang, *Soft Matter*, 2012, **8**, 1460–1466.
- 109 J. Liu, Y. Pang, Z. Zhu, D. Wang, C. Li, W. Huang, X. Zhu and D. Yan, *Biomacromolecules*, 2013, **14**, 1627–1636.
- 110 P. V. Czarnecki, A. Kampert, S. Barbe and J. C. Tiller, *Tetrahedron Lett.*, 2011, **52**, 3551–3554.
- 111 D. Lee, S. Bae, Q. Ke, J. Lee, B. Song, S. Ananth, G. Khang, H. S. Choi and P. M. Kang, *J. Control. Release*, 2015, **172**, 1102–1110.
- 112 J. J. Faig, S. Klein, M. A. Ouimet, W. Yu and K. E. Uhrich, *Macromol. Chem. Phys.*, 2016, **217**, 108–114.
- 113 F. El-Mohtadi, R. d’Arcy and N. Tirelli, *Macromol. Rapid Commun.*, 2019, **40**, 1–24.
- 114 M. Zhang, C.-C. Song, R. Ji, Z.-Y. Qiao, C. Yang, F.-Y. Qiu, D.-H. Liang, F.-S. Du and Z.-C. Li, *Polym. Chem.*, 2016, **7**, 1494–1504.
- 115 Z. Deng, Y. Qian, Y. Yu, G. Liu, J. Hu, G. Zhang and S. Liu, *J. Am. Chem. Soc.*, 2016, **138**, 10452–10466.
- 116 F.-Y. Qiu, C.-C. Song, M. Zhang, F.-S. Du and Z.-C. Li, *ACS Macro Lett.*, 2015, **4**, 1220–1224.
- 117 E.-J. Kim, S. Bhuniya, H. Lee, H. M. Kim, C. Cheong, S. Maiti, K. S. Hong and J. S. Kim, *J. Am. Chem. Soc.*, 2014, **136**, 13888–94.
- 118 C. De Gracia Lux, S. Joshi-Barr, T. Nguyen, E. Mahmoud, E. Schopf, N. Fomina and A. Almutairi, *J. Am. Chem. Soc.*, 2012, **134**, 15758–15764.
- 119 E. Modica, R. Zanaletti, M. Freccero and M. Mella, *J. Org. Chem.*, 2001, **66**, 41–52.
- 120 P. Pande, J. Shearer, J. Yang, W. a. Greenberg and S. E. Rokita, *J. Am. Chem. Soc.*, 1999, **121**, 6773–6779.
- 121 C. C. Song, R. Ji, F. S. Du and Z. C. Li, *Macromolecules*, 2013, **46**, 8416–8425.
- 122 C. C. Song, R. Ji, F. S. Du, D. H. Liang and Z. C. Li, *ACS Macro Lett.*, 2013, **2**, 273–277.
- 123 J. R. Martin, M. K. Gupta, J. M. Page, F. Yu, J. M. Davidson, S. A. Guelcher and C. L. Duvall, *Biomaterials*, 2014, **35**, 3766–3776.
- 124 J. S. Kim, S. D. Jo, G. L. Seah, I. Kim and Y. S. Nam, *J. Ind. Eng. Chem.*, 2015, **21**, 1137–1142.
- 125 D. S. Wilson, G. Dalmaso, L. Wang, S. V. Sitaraman, D. Merlin and N. Murthy, *Nat. Mater.*, 2010, **9**, 923–928.
- 126 M. S. Shim and Y. Xia, *Angew. Chemie - Int. Ed.*, 2013, **52**, 6926–6929.
- 127 S. S. Yu, R. L. Koblin, A. L. Zachman, D. S. Perrien, L. H. Hofmeister, T. D. Giorgio and H. J. Sung, *Biomacromolecules*, 2011, **12**, 4357–4366.
- 128 S. H. Lee, T. C. Boire, J. B. Lee, M. K. Gupta, A. L. Zachman, R. Rath and H.-J. J. Sung, *J. Mater. Chem. B*, 2014, **2**, 7109–7113.
- 129 M. K. Gupta, S. H. Lee, S. W. Crowder, X. Wang, L. H. Hofmeister, C. E. Nelson, L. M. Bellan, C. L. Duvall and H.-J. J. Sung, *J. Mater. Chem. B*, 2015, **3**, 7271–7280.
- 130 J. Zhang, J. Hu, W. Sang, J. Wang and Q. Yan, *ACS Macro Lett.*, 2016, **5**, 919–924.

- 131 D. Osella, M. Ferrali, P. Zanello, F. Laschi, M. Fontani, C. Nervi and G. Cavigliolo, *Inorganica Chim. Acta*, 2000, **306**, 42–48.
- 132 S. Wang, C. Yao, M. Ni, Z. Xu, M. Cheng, X.-Y. Hu, Y.-Z. Shen, C. Lin, L. Wang and D. Jia, *Polym. Chem.*, 2017, **8**, 682–688.
- 133 and D. C. Roland H. Staff, Markus Gallei, Markus Mazurowski, Matthias Rehahn, Rüdiger Berger, Katharina Landfester, *ACS Nano*, 2012, **6**, 9042–9049.
- 134 Y. J. Kim and Y. T. Matsunaga, *J. Mater. Chem. B*, 2017, **5**, 4307–4321.
- 135 R. Hoogenboom and H. Schlaad, *Polym. Chem.*, 2017, **8**, 24–40.
- 136 R. Hoogenboom, *Angew. Chemie - Int. Ed.*, 2009, **48**, 7978–7994.
- 137 R. Luxenhofer, Y. Han, A. Schulz, J. Tong, Z. He, A. V. Kabanov and R. Jordan, *Macromol. Rapid Commun.*, 2012, **33**, 1613–1631.
- 138 O. Sedlacek, B. D. Monnery, S. K. Filippov, R. Hoogenboom and M. Hruby, *Macromol. Rapid Commun.*, 2012, **33**, 1648–1662.
- 139 M. M. Bloksma, R. M. Paulus, H. P. C. Van Kuringen, F. Van Der Woerdt, H. M. L. Lambermont-Thijs, U. S. Schubert and R. Hoogenboom, *Macromol. Rapid Commun.*, 2012, **33**, 92–96.
- 140 T. Yoshida, T. Aoyagi, E. Kokufuta and T. Okano, *J. Polym. Sci. Part A Polym. Chem.*, 2003, **41**, 779–787.
- 141 A. M. Dave, K. S. Soppimath, T. M. Aminabhavi, W. E. Rudzinski and S. G. Kumbar, *Drug Dev. Ind. Pharm.*, 2002, **28**, 957–974.
- 142 J. Ramos, A. Imaz and J. Forcada, *Polym. Chem.*, 2012, **3**, 852–856.
- 143 T. Aoyagi, M. Ebara, K. Sakai, Y. Sakurai and T. Okano, *J. Biomater. Sci. Polym. Ed.*, 2000, **11**, 101–110.
- 144 T. Maeda, K. Yamamoto and T. Aoyagi, *J. Colloid Interface Sci.*, 2006, **302**, 467–474.
- 145 E. Watanabe, N. Tomoshige and H. Uyama, *Macromol. Symp.*, 2007, **249–250**, 509–514.
- 146 Y. Takeuchi, T. Tsujimoto and H. Uyama, *Polym. Adv. Technol.*, 2011, **22**, 620–626.
- 147 X. André, M. Zhang and A. H. E. Müller, *Macromol. Rapid Commun.*, 2005, **26**, 558–563.
- 148 N. A. Cortez-Lemus and A. Licea-Claverie, *Prog. Polym. Sci.*, 2016, **53**, 1–51.
- 149 M. Webster, J. Miao, B. Lynch, D. Green, R. Jones-Sawyer, R. J. Linhardt and J. Mendenhall, *Macromol. Mater. Eng.*, 2013, **298**, 447–453.
- 150 L. Yu and J. Ding, *Chem. Soc. Rev.*, 2008, **37**, 1473–1481.
- 151 B. Jeong, S. Wan and Y. Han, *Adv. Drug Deliv. Rev.*, 2002, **54**, 37–51.
- 152 D. Schmaljohann, *Adv. Drug Deliv. Rev.*, 2006, **58**, 1655–1670.
- 153 C. Wu and X. Wang, *Phys. Rev. Lett.*, 1998, **80**, 4092–4094.
- 154 K. Matyjaszewski, *Symp. A Q. J. Mod. Foreign Lit.*, 2000, **40**, 2–26.
- 155 A. D. Jenkins, R. G. Jones and G. Moad, *Pure Appl. Chem.*, 2009, **82**, 483–491.
- 156 W. A. Braunecker and K. Matyjaszewski, *Prog. Polym. Sci.*, 2007, **32**, 93–146.

- 157 D. J. Keddie, G. Moad, E. Rizzardo and S. H. Thang, *Macromolecules*, 2012, **45**, 5321–5342.
- 158 G. Moad, E. Rizzardo and S. H. Thang, *Acc. Chem. Res.*, 2008, **41**, 1133–1142.
- 159 F. Chauvin, P. E. Dufils, D. Gigmes, Y. Guillaneuf, S. R. A. Marque, P. Tordo and D. Bertin, *Macromolecules*, 2006, **39**, 5238–5250.
- 160 M. Kamigaito, K. Satoh and M. Uchiyama, *J. Polym. Sci. Part A Polym. Chem.*, 2019, **57**, 243–254.
- 161 G. Moad, E. Rizzardo and S. H. Thang, *Polymer (Guildf.)*, 2008, **49**, 1079–1131.
- 162 J. Chiefari, Y. K. B. Chong, F. Ercole, J. Krstina, J. Jeffery, T. P. T. Le, R. T. A. Mayadunne, G. F. Meijs, C. L. Moad, G. Moad, E. Rizzardo, S. H. Thang and C. South, *Macromolecules*, 1998, **31**, 5559–5562.
- 163 G. Moad, E. Rizzardo and S. H. Thang, *Aust. J. Chem.*, 2005, **58**, 379–410.
- 164 G. Moad, J. Chiefari, Y. K. Chong, J. Krstina, R. T. a Mayadunne, a Postma, E. Rizzardo and S. H. Thang, *Polym. Int.*, 2000, **49**, 993–1001.
- 165 R. T. a Mayadunne, E. Rizzardo, J. Chiefari, Y. K. Chong, G. Moad and S. H. Thang, *Macromolecules*, 1999, **32**, 6977–6980.
- 166 S. H. Thang, B. Y. K. Chong, R. T. A. Mayadunne, G. Moad and E. Rizzardo, *Tetrahedron Lett.*, 1999, **40**, 2435–2438.
- 167 R. T. A. Mayadunne, E. Rizzardo, J. Chiefari, J. Krstina, G. Moad, A. Postma and S. H. Thang, *Macromolecules*, 2000, **33**, 243–245.
- 168 J. Chiefari, Y. K. Chong, F. Ercole, J. Krstina, J. Jeffery, T. P. T. Le, R. T. A. Mayadunne, G. F. Meijs, C. L. Moad, G. Moad, E. Rizzardo and S. H. Thang, *Macromolecules*, 1998, **31**, 5559–5562.

Chapter Two

2. Experimental

4.

2.1. General materials

N-Isopropylacrylamide (NIPAM, Fluorochem) was recrystallized from hexane and *N*-(2-hydroxyethyl) acrylamide (HEA, Sigma Aldrich, 97%) had the inhibitor removed by filtering through aluminium oxide. [2-ethyl sulfanyl thiocarbonylthio] 2-methyl propionic acid (EMP) was synthesised previously by Dr. S. G. Spain to a literature procedure.¹⁴ Ethanethiol (Alfa Aesar, 97%), propanethiol (Alfa Aesar, 98%), butanethiol (Acros Organics, 98%), dodecanethiol (Alfa Aesar, 98%), carbon disulphide (Sigma Aldrich, >99.9%), potassium phosphate tribasic (Alfa Aesar, 97%), methyl 2-bromopropionate (Sigma Aldrich, 98%), 2-bromopropionic acid (Fluorochem), dried magnesium sulfate (Fisher), 4-dimethylaminopyridine (DMAP, Fluka analytical), *N,N'*-dicyclohexylcarbodiimide (DCC, Alfa Aesar, 99%), Triethylamine (Sigma Aldrich, \geq 99%), glacial acetic acid (Fisher, 100%), sodium hydroxide pellets (Fisher), silica gel 40-63 μ m (VWR), hydrochloric acid (VWR, 35%), sodium hydrogen carbonate (Fisher), acryloyl chloride (Aldrich, 97%), 4-(hydroxymethyl) benzene boronic acid pinacol ester (Alfa Aesar), sodium sulfate anhydrous (VWR), hydrochloric acid (VWR, 35%), 4,4'-Azobis(4-cyanovaleric acid) (ACVA, Aldrich), phosphotungstic acid hydrate (Acros Organics), H₂O₂ (30%, VWR), FeCl₂ (Alfa Aesar, 99.99%, ultra-dry), L-Glutathione reduced (Sigma Aldrich, 98%) and 3-morpholinopyrrolidine hydrochloride (SIN-1 chloride, Fluorochem) were all used without further purification. 2,2'-azobisisobutyronitrile (AIBN, Sigma Aldrich) was purified by recrystallization from hexane and dried before use. Purification of the synthesised polymers was performed by dialysis against deionised water using 3500 Da MWCO SnakeSkin™ membrane (ThermoFisher). Methylene bisacrylamide was purified by recrystallization from methanol and dried before use. For variable temperature UV/vis measurements, the polymers were dissolved in Dulbecco's phosphate buffer solution (DPBS, Sigma Aldrich). Gel permeation chromatography (GPC) samples were run using dimethylformamide (DMF) with 0.1% LiBr for sample preparation and as the eluent. Solvents used were purchased from Sigma Aldrich or VWR, including deuterated solvents for NMR; deuterated dimethyl sulfoxide (DMSO-d₆) 99.9 atom% D, deuterated chloroform (CDCl₃) 99.8 atom% D.

Dichloromethane (DCM) was purchased from VWR and dried using a Grubbs system to give anhydrous DCM.

2.2. Instrumentation

2.2.1. NMR Spectroscopy. All ^1H NMR spectra were recorded using a Bruker Avance spectrometer at 400 MHz, with 64 scans per spectrum. All ^{13}C NMR spectra were recorded using a Bruker Avance 400 spectrometer at 100 MHz with 2048 scans per spectrum. All NMR spectra were recorded at ambient conditions. For both ^1H and ^{13}C NMR analysis, CDCl_3 (VWR) and D_2O (Sigma Aldrich) were used, where the signals for reference were the protonated solvent.

2.2.2. Gel Permeation Chromatography (GPC). Molecular weights and polydispersities were recorded using an Agilent 1260 infinity LC system fitted with two PLgel 5 μm mixed-C columns, which are heated to 50 $^\circ\text{C}$. The refractive index detector records the response against a series of near monodisperse poly(methyl methacrylate) standards which are used for calibration. 100 μL of sample is injected with 0.1% toluene, which is used as a flow rate marker. These samples are filtered through a 0.45 μm PTFE filter to remove any undissolved material before injection. Samples are run through the columns using HPLC grade DMF eluent at a flow rate of 1 mL min^{-1} .

2.2.3. Infrared (IR) Spectroscopy. IR spectra of liquid samples were recorded as thin films on polished sodium chloride plates on a Perkin Elmer FTIR spectrometer Spectrum Two recording %transmission between 4000 and 400 cm^{-1} with a 0.5 cm^{-1} resolution and 4 scans per sample. IR spectra of solid samples were recorded on a Thermo Scientific Nicolet iS10 ATR spectrometer. The % transmission was recorded between 4000 and 600 cm^{-1} .

2.2.4. Cloud point determination. Cloud points were estimated using the point of inflexion of a curve indicating the change in absorbance of a sample. Spectra were recorded using a Varian Cary 3 bio, a Varian Cary 300 bio spectrophotometer with temperature control or Stuart SMP50 automatic melting point apparatus. Polymer solutions were prepared in DPBS or water, dependant on the sample, at a concentration of 1 mg mL^{-1} . All samples were run twice, and an average determined. The wavelength was set at 550 nm and the temperature was increased by 0.3 $^\circ\text{C min}^{-1}$ on the UV/vis

spectrometers and $1\text{ }^{\circ}\text{C min}^{-1}$ on the automatic melting point and the temperature range altered depending on the sample.

2.2.5. Mass spectrometry. For small molecules, the mass spectra were recorded on a Micromass LCT classic using ESI positive mode. The samples were dissolved in MeOH/formic acid and directly infused into the MS at $20\text{ }\mu\text{L min}^{-1}$.

Polymers ran in ESI positive and ESI negative mode were dissolved in acetonitrile:H₂O in a 3:1 mixture with NaCl added.

Polymers with spectra recorded via MALDI-ToF were analysed on a Bruker Reflex III using a Reflectron positive ion. The polymer sample was dissolved in DCM at a concentration of 5 mg mL^{-1} using a matrix DCTB in DCM at a concentration of 20 mg mL^{-1} .

2.2.6. Elemental analysis. The percentages of C, H, N and S in relevant samples were analysed using an Elementar vario microcube analyser.

2.2.7. Gravimetric Analysis

Solids contents for each timepoint and final products were measured using a Kern DAB 100-3 moisture analyzer. A minimum of 1 g of polymer solution was heated in an aluminium pan to $150\text{ }^{\circ}\text{C}$ until a constant mass was attained.

2.2.8. Dynamic Light Scattering (DLS). Measurements were conducted using a Malvern Instruments Zetasizer Nano ZS series instrument with a laser wavelength of 633 nm and power of 4 mW or a Brookhaven Nanobrook Omni instrument with a laser wavelength of 640 nm and power of 40 mW. Samples were prepared at 1 mg/mL in water or DPBS, dependent upon the sample, in disposable plastic cuvettes. For all temperature responsive polymers, the temperature was varied so that measurements were run at temperatures above and below the LCST, as well as physiological temperature. The hydrodynamic diameters were determined from backscattering measurements (173°) averaged over approximately thirty runs using the Stokes-Einstein equation:

$$D_t = \frac{k_B T}{6\pi\eta R_H} \quad (2.1)$$

Where D_t is the translational diffusion coefficient, k_B is the Boltzmann constant, η is absolute viscosity and R_H is hydrodynamic radius.

2.2.9. Transmission Electron Microscopy (TEM). Diblock and nanogel solutions were purified by dialysis and diluted to give 0.1 wt% solutions. Polymer samples (10 μ L) were adsorbed onto copper 400 mesh grids coated with carbon film for 60 seconds before blotting with filter paper. The samples were stained with phosphotungstic acid (1.5 % w/v, pH 7, 10 μ L) for 30 seconds before blotting and drying under vacuum. The grids were imaged using a FEI Tecnai T12 Spirit TEM instrument at 120 kV.

2.2.10. Small-Angle X-ray Scattering (SAXS) measurements. SAXS patterns were collected using a Xenocs Xuess 2.0 laboratory beamline equipped with a Dectris Pilatus 1M detector and an Excillum liquid gallium MetalJet X-ray source ($\lambda = 1.34 \text{ \AA}$). The patterns were collected over a scattering vector length range of $0.0035 \text{ \AA}^{-1} < q < 0.28 \text{ \AA}^{-1}$, where $q = \frac{4\pi}{\lambda} \sin \theta$ and θ is a half of the scattering angle. One-dimensional (1D) scattering curves were obtained by an azimuthal binning and averaging of corresponding two-dimensional scattering patterns using software packages supplied with the SAXS instruments. Normalization, background subtraction, and further analysis of the 1D data was performed using Irena SAS macros for Igor Pro.²⁷

2.2.11. Asymmetric Flow Field-Flow Fractionation (AF4). AF4 experiments were performed on an MT2000 with RI and UV-Vis detectors. A multi-angle light scattering detector (MALS) PN3621; with a 21 angle (from 7° to 164°) detector operating at 532 nm power wavelength was coupled online to the AF4. The above and the autosampler (PN5300) were provided by Postnova Analytics, Landsberg/Germany. The hydrodynamic radius of the samples were obtained by dynamic light scattering (DLS) using a Malvern Zetasizer Nano ZS (running Malvern Zetasizer software V7.12) with a 633 nm He–Ne laser and the detector positioned at 173°. The DLS measurements were obtained using flow cell ZEN0023 with flow rate 0.5 mL/min at 28 °C, coupled online to the MT2000. A 350 μ m spacer and 10 kDa regenerative cellulose (RC) membrane were installed in the separation channel.

The conditions used for the separations was based on a method existing in the literature.^{28,29} Briefly, the mobile phase was 0.1 M NaNO₃ in Milli-Q H₂O. Type I distilled water was obtained from a water purification system had a resistivity of > 18 MΩ cm⁻¹ (PURELAB option R, Veolia). The solutions were filtered using a Corning bottle top vacuum filter system with cellulose acetate membrane with pore size 0.22 μm. The injected volume was 20 μL of a 1 mg/mL sample using the autosampler. Each sample was analysed three times to check good reproducibility. A blank was measured between injections of new sample to ensure that system was clean. The UV-Vis detector measured at a wavelength of 280 nm. The conditions used for the separations was as follows: The injection/focusing time was 3 min using a cross flow from 2 to 0.5 mL min⁻¹. The chosen cross flow rate (initial values of 2 mL/min to 0.5 mL/min were tested) was kept constant for the first 0.2 minutes ($t_0-t_{0.2}$), and thereafter, the cross flow was decreased in a power manner (exponent 0.2) from its initial value to 0.1 over a period of 40 minutes. Following the complete reduction in cross flow, the tip-flow 0.1 mL min⁻¹ continued for an additional 40 minutes. The optimised method for fractionation conditions of the nanogels is shown in Figure 2.1.

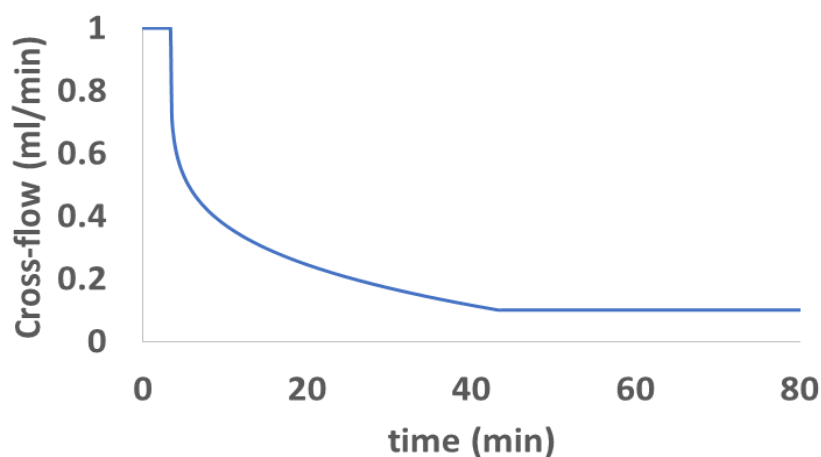


Figure 2.1 - Optimised method for fractionation conditions of the nanogels looking at the cross-flow over time.

2.3. Synthetic methods

2.3.1. General synthesis of RAFT chain transfer agents

A typical synthesis for the chain transfer agents used is as follows using methyl 2-(propylthiocarbonothioylthio)propanoate (MPP) as the example. Propanethiol (6 mL, 66.3 mmol) and K_3PO_4 (12.7 g, 59.8 mmol) were stirred in acetone (100 mL, 1.72 mol) under N_2 . CS_2 (8 mL, 0.132 mol) was added and the reaction was stirred for a further 30 min. Methyl 2-bromopropionate (7.5 mL, 67.2 mmol) was added and the mixture was left to react overnight. Salts formed were removed by vacuum filtration and the solvent was removed under reduced pressure. The crude product was purified via column chromatography, using hexane as the eluent to yield MPP (11.74 g, 74%) as a yellow oil.

Elemental analysis found: C, 40.45; H, 5.84, $C_8H_{14}O_2S_3$ requires, C, 40.37; H, 5.93%. FTIR: ν_{max}/cm^{-1} (thin film, NaCl plates) 2964 (COCH₃), 2931 (COCH₃), 2872 (COCH₃), 1740 (C=O), 1451 (CH₂-S), 1434 (CH₂-S), 1312, 1256, 1161 (C=S), 1066, 1048, 865, 816. δ_H (400 MHz; $CDCl_3$) 1.02 (3H, t, CH₃, *J* 7.4 Hz), 1.60 (3H, d, CH₃, *J* 7.4 Hz), 1.74 (2H, m, CH₂), 3.34 (2H, t, CH₂, *J* 7.3 Hz), 3.74 (3H, s, OCH₃), 4.84 (1H, q, H, *J* 7.4 Hz). δ_C (100 MHz; $CDCl_3$) 13.5 (CH₃CH₂CH₂), 17.0 (CH₃), 21.5 (CH₃CH₂CH₂), 39.1 (CH₃CH₂CH₂), 47.7 (CO), 52.9 (OCH₃), 171.6 (C=O) and 222.0 (C=S); LR-MS (ES+) *m/z* 449.0 (8.7%), 277.0 (3.4), 261.0 (47.0), 239.0 (100), 163.0 (3.2) and 119.0 (7.8). $[M+H]^+$ requires 239.02, $[M+Na]^+$ requires 261.00, $[M+K]^+$ requires 276.98.

Methyl (2-butylthiocarbonothioylthio) propanoate (MBP) (6.89 g, 49%) was isolated as a yellow oil.

Elemental analysis found C, 43.4; H, 6.43, chemical formula $C_9H_{16}O_2S_3$ requires theoretical, C, 42.82; H, 6.39%. FTIR: ν_{max}/cm^{-1} (thin film, NaCl plates) 3458, 2957 (COCH₃), 2931 (COCH₃), 2872 (COCH₃), 1740 (C=O), 1450 (CH₂-S), 1434 (CH₂-S), 1311, 1256, 1230, 1161(C=S), 1062, 856, 817. δ_H (400 MHz; $CDCl_3$) 0.95 (3H, t, CH₃, *J* 7.4), 1.44 (2H, m, CH₂, *J* 7.6), 1.61 (3H, d, CH₃, *J* 7.4), 1.70 (2H, m, CH₂, *J* 7.5), 3.38 (2H, t, CH₂, *J* 7.4), 3.76 (3H, s, OCH₃), 4.85 (1H, q, CH, *J* 7.4). δ_C (100 MHz; $CDCl_3$) 13.6 (CH₃CH₂CH₂), 17.0 (CH₃), 22.0 (CH₃CH₂CH₂CH₂), 30.0 (CH₃CH₂CH₂CH₂), 37.0 (CH₃CH₂CH₂CH₂), 47.7

(CO), 52.8 (OCH₃), 171.7 (C=O) and 222.0 (C=S). LR-MS (ES+) m/z 527 (29.2%), 291 (5.1), 275 (38.2), 253 (100) and 133 (19.2). [M+H]⁺ requires 253.04, [M+Na]⁺ requires 275.02, [M+K]⁺ requires 290.99.

Methyl (2-ethylthiocarbonothioylthio) propanoate (EMEM) (16.12 g, 89%) was isolated as a yellow oil. Elemental analysis found: C, 37.66; H, 5.33, C₇H₁₂O₂S₃ requires, C, 37.48; H, 5.39%. FTIR: $\nu_{\max}/\text{cm}^{-1}$ (ATR) 2978, 2951 (COCH₃), 2930 (COCH₃), 2872 (COCH₃), 1738 (C=O), 1449 (CH₂-S), 1434 (CHO₂-S), 1312, 1256, 1162 (C=S), 1079, 1044, 1031, 856, 816. δ_{H} (400 MHz; CDCl₃) 1.36 (3H, t, Me), 1.60 (3H, d, Me), 3.37 (2H, q, CH₂), 3.75 (3H, s, COMe), 4.84 (1H, q, CH). δ_{C} (100 MHz; CDCl₃) 13.0 (CH₃CH₂), 17.0 (CH₃), 47.7 (CO), 52.9 (OCH₃), 171.6 (C=O) and 221.8 (C=S). LR-MS (ES+) m/z 470.9 (10.7%), 262.9 (3.1), 246.9 (45.9), 227.0 (10.2), 224.9 (100) and 163.0 (9.9). [M+H]⁺ requires 225.01, [M+Na]⁺ requires 246.99, [M+K]⁺ requires 262.96.

2.3.2. Synthesis of methyl (2-dodecanethiocarbonothioylthio) propanoate (MDDP) RAFT chain transfer agent

Dodecanethiol (5 g, 5.94 mL, 0.025 mol) and K₃PO₄ (11.95 g, 0.055 mol) were stirred in acetone (125 mL) under N₂. CS₂ (8.44 g, 6.7 mL, 0.11 mol) was added and the reaction mixture was stirred for a further 30 minutes. 2-bromopropionic acid (8.47 g, 5 mL, 0.055 mol) was added and the mixture was left to react overnight. Salts which were produced were filtered and then the solvent was removed under reduced pressure and the residue was extracted with ethyl acetate and 1M HCl was added until the solid dissolved. The organic layer was dried with MgSO₄ and the product was purified by recrystallisation in hot hexane to yield MDDP acid (5.25 g, 67%), as a yellow solid.

Melting point: 79.3-79.6 °C. Elemental analysis found: C, 54.52; H, 8.44, C₁₇H₃₂O₂S₃ requires, C, 54.82; H, 8.63%. FTIR: $\nu_{\max}/\text{cm}^{-1}$ (ATR) 3150 (OH), 2955 (CH₂), 2918 (CH₂), 2849 (CH₃), 1702 (HOC(CO)), 1421 (SCH₂) and 1068 (C=S). δ_{H} (400 MHz; CDCl₃) 0.85 (t, 3H, CH₃), 1.20-1.80 (m, 20H, CH₂), 3.35 (t, 2H, CH₂ and CCH₃) and 4.88 (q, 1H, CH). δ_{C} (100 MHz; CDCl₃) 14.14 (CH₃CH₂CH₂), 16.61 (CH₂), 22.71 (CH₂), 27.85 (CH₂), 28.91 (CH₂), 29.01 (CH₂), 29.35 (CH₂), 29.44 (CH₂), 29.56 (CH₂), 29.63 (CH₂), 31.93 (CH₂),

37.49 (CH₃), 47.40 (C-O), 176.43 (C=O) and 222.0 (C=S); LR-MS (ES-) m/z 349.3 (100%), 305.3 (6), 289.3 (3) and 201.3 (13). [M-H]⁻ requires 349.14.

MDDP acid was esterified to form the MDDP. MDDP acid (2.5 g, 7.85 mmol) was dissolved in methanol (50 mL) and cooled. DMAP (few crystals) was added to the cooled solution followed by DCC (1.63 g, 7.90 mmol). This was stirred at room temperature overnight. The reaction mixture was acidified with acetic acid (0.12 mL, 0.3 eq.). The solvent was removed under reduced pressure and ethyl acetate (volume) was added. The organic layer was extracted and washed with saturated sodium bicarbonate, saturated NaCl and water. This was dried with MgSO₄ and the solvent was removed under reduced pressure. The crude product was purified by silica gel column chromatography (9:1 hexane to ethyl acetate) to yield MDDP (2.01 g, 77%) as a yellow oil.

Elemental analysis found: C, 56.23; H, 8.65, C₁₆H₃₀O₂S₃ requires, C, 56.07; H, 8.86%. FTIR: $\nu_{\max}/\text{cm}^{-1}$ (thin film, NaCl plates) 2953 (CH₂), 2925 (CH₂), 2853 (CH₃), 1742 (CO(CO)), 1453 (SCH₂), 1435 (SCH₂), 1255 (C(CO)OC) and 1161 (C=S). δ_{H} (400 MHz; CDCl₃) 0.85 (t, 3H, CH₃), 1.20-1.80 (m, 20H, CH₂), 3.35 (t, 2H, CH₂ and CCH₃) 3.80 (s, 3H, CH₃) and 4.88 (q, 1H, CH). δ_{C} (100 MHz; CDCl₃) 14.13 (CH₃CH₂CH₂), 16.95 (CH₃), 22.70 (CH₂), 27.89 (CH₂), 28.91 (CH₂), 29.1 (CH₂), 29.35 (CH₂), 29.44 (CH₂), 29.56 (CH₂), 29.63 (CH₂), 31.92 (CH₂), 37.28 (CH₂), 47.40 (CO), 52.84 (OCH₃), 171.63 and 221.96; LR-MS (ES+) m/z 365.2 (100%), 277.2 (12) and 169.3 (14). [M+H]⁺ requires 365.16, [M+Na]⁺ requires 387.15, [M+K]⁺ requires 403.12.

2.3.3. General synthesis of pNIPAM by RAFT polymerisation

A typical procedure for the RAFT polymerisation of NIPAM is as follows, using a targeted DP of 10 and MPP CTA as an example. Polymerisation ratios of CTA to initiator are 5:1. MPP (0.676 g, 2.84 mmol), NIPAM (2.591 g, 22.9 mmol), AIBN (0.065 g, 0.411 mmol) and DMF (13 mL, to give a 20 wt% solid solution), were added to a 50 mL round bottom flask and purged with N₂ for 30 minutes. This flask was lowered into a pre-heated heating block at 70 °C for 5 h. The polymerisation was quenched by removal from the heat and opening to air. The final NIPAM conversion was 88% as determined by

^1H NMR spectroscopy. The polymer was purified by diluting the reaction solution with water and dialysing against H_2O for 24 h. The resulting solution was freeze dried to give a yellow powder (2.29 g, 71%); $\nu_{\text{max}}/\text{cm}^{-1}$ (ATR) 3290 (NH), 2970, 2930, 2870, 1730, 1640 (C=O ester), 1530 (C=O amide), 1480, 1380, 1370 and 1140 (C-O); δ_{H} (400 MHz; CDCl_3) 1.0 (CH_3 , t), 1.2 (CH_3 , s), 1.3-2.6 (br, CH_2 , CH, m), 3.4 (SCH_2), 3.7 (OCH_3), 4.0 (NHCH) and 5.6-6.7 (br, NH, m). The number-average degree of polymerisation was 8 as determined by ^1H NMR spectroscopy. The M_n and M_w/M_n were determined by GPC (DMF 0.1% LiBr, PMMA standards) to be 1590 g mol^{-1} and 1.12, respectively.

Note: For all polymers with DP >10, DMSO was used as the solvent and the reactions were performed at 70°C for 3 hours.

2.3.4. Oxidation of pNIPAM using hydrogen peroxide

All polymers were oxidised in a 15 mM H_2O_2 DPBS solution, at a concentration of 1 mg mL^{-1} . Oxidations were stirred for approximately 36 h. under ambient conditions then dialysed for 24 h and freeze dried as described above. In all cases this yielded a white powder. For MPP DP10, as described above, $\nu_{\text{max}}/\text{cm}^{-1}$ (ATR) 3430 (OH), 3290 (NH), 2970, 2930, 2870, 1730, 1640 (C=O ester), 1530 (C=O amide), 1480, 1380, 1370, 1140 (C-O) and 1090; δ_{H} (400 MHz; CDCl_3) 1.0 (CH_3 , t), 1.2 (CH_3 , s), 1.3-2.6 (br, CH_2 , CH, m), 3.4 (SCH_2), 3.7 (OCH_3), 4.0 (NHCH) and 5.6-6.7 (br, NH, m). The peaks at 1.0 and 3.4 ppm are smaller when compared to the native polymer but still indicate presence of the RAFT chain end group. The M_n and M_w/M_n were determined by GPC (DMF 0.1% LiBr, PMMA standards) to be 1590 g mol^{-1} and 1.12 respectively.

2.3.5. Synthesis of 2-(propylthiocarbonothioylthio)propanoic acid (PPA) RAFT agent

Propanethiol (4.88 g, 5.95 mL, 0.064 mol) and K_3PO_4 (17.08 g, 0.08 mol) were stirred in acetone (150 mL) under N_2 . CS_2 (12.6 g, 10 mL, 0.165 mol) was added and stirring continued for 30 min. 2-bromopropionic acid (19.89 g, 11.7 mL, 0.13 mol) was added and the mixture was left to react overnight. Salts which were produced were filtered and then the solvent was removed under reduced pressure and the residue was extracted with ethyl acetate and 1M HCl was added until the

solid dissolved. The organic layer was dried with MgSO_4 and the product was purified by recrystallisation in hot hexane to yield the desired product (7.73 g, 51 %), as a yellow solid.

Elemental analysis found: C, 37.57; H, 5.24; S, 43.75, $\text{C}_7\text{H}_{12}\text{O}_2\text{S}_3$ requires, C, 37.47; H, 5.39; S, 42.87 %.

FTIR: $\nu_{\text{max}}/\text{cm}^{-1}$ (ATR) 3150 (br, OH), 2963 (COCH_3), 2930 (COCH_3), 2871 (COCH_3), 1700 ($\text{C}=\text{O}$), 1449 ($\text{CH}_2\text{-S}$), 1418 ($\text{CH}_2\text{-S}$), 1312 ($\text{C}=\text{S}$), 1232 ($\text{C}=\text{S}$). δ_{H} (400 MHz; CDCl_3) 1.05 (t, 2H, CH_3CH_2), 1.65 (d, 3H, CH_3CH), 1.75 (m, 2H, $\text{CH}_3\text{CH}_2\text{CH}_2$), 3.40 (t, 2H, $\text{CH}_3\text{CH}_2\text{CH}_2$) and 4.89 (q, 1H, CH_3CH). δ_{C} (100 MHz; CDCl_3) 13.5 (CH_3), 16.6 (SCH-CH_3), 21.5 (CH_3CH_2), 39.2 ($\text{CH}_2\text{CH}_2\text{S}$), 47.5 (SCH-CH_3), 177.0 ($\text{C}=\text{O}$) and 221.9 ($\text{C}=\text{S}$); LR-MS (ES-) m/z 223.0 (100%). $[\text{M-H}]^-$ requires 223.00.

2.3.6. Synthesis of pHEA-mCTA by RAFT polymerisation

A typical procedure for the RAFT polymerisation of HEA is as follows, using a targeted DP 60 and MPP CTA as an example. Polymerisation ratios of CTA to initiator were 10:1. MPP (0.086 g, 0.36 mmol), HEA (2.49 g, 21.6 mmol), AIBN (5.7 mg, 0.035 mmol) and DMSO (9.6 mL, to give a 20 wt% solid solution), were added to a 50 mL round bottom flask and purged with N_2 for 30 minutes. The flask was lowered into a pre-heated heating block at 70 °C for 45 min. The polymerisation was quenched by removal from the heat and opening to air. The final HEA conversion was 76% as determined by ^1H NMR spectroscopy. The integrals of the two peaks, 3.04-3.72 and 3.45-3.65 ppm, from $\text{CH}_2\text{CH}_2\text{OH}$, which are present in both monomer and polymer were compared to the integral of the peak at 5.67 ppm, equivalent to 1H of the vinyl group.

The polymer was purified by diluting the reaction solution with methanol and precipitated from acetone. The polymer was collected by centrifugation, diluted in water and dialysed against H_2O for 24 h. It was then freeze dried to give a yellow powder.

δ_{H} (400 MHz; D_2O) 0.93 (t, 3H, CH_3 (MPP)), 0.97 (m, 3H), 1.22-2.45 (br, 140H, CH_2 , CH, m, (polymer backbone)), 3.10-3.40 (m, br, 93H, $\text{CH}_2\text{CH}_2\text{OH}$) and 3.42-3.64 (s, br, 93H, $\text{CH}_2\text{CH}_2\text{OH}$). The M_n and M_w/M_n were calculated via GPC to be 10290 g mol^{-1} and 1.09 respectively. The DP was calculated by NMR spectroscopy to be 46, through comparison of the integral of 0.93 ppm, the CH_3 from MPP, to

the integrals of the peaks at 3.10-3.40 and 3.42-3.62 ppm, which are equivalent to the CH₂CH₂OH of HEA.

2.3.7. Synthesis of pHEA-*b*-pNIPAM diblock copolymers

A typical procedure for the dispersion polymerisation of pHEA-*b*-pNIPAM is as follows, using a targeted DP 25 and pHEA₄₆-MPP-mCTA as an example. Polymerisation ratios of mCTA to initiator were 5:1. pHEA₄₆-mCTA (0.58 g, 0.105 mmol), NIPAM (0.30 g, 2.65 mmol), AIBN (5.6 g, 0.034 mmol) and DMSO (4.6 mL, to give a 10 wt% solid solution), were added to a 25 mL round bottom flask and purged with N₂ for 20 min. This flask was lowered into a pre-heated heating block at 70 °C for 1 h. The polymerisation was quenched by removal from the heat and opening to air. The final NIPAM conversion was 78% as determined by ¹H NMR spectroscopy by comparison of the integral from the peak at 3.67-3.95 ppm, for CHCH₃ which is present in both monomer and polymer to the integral of the peak at 5.62 ppm, equivalent to ¹H of the vinyl group.

The polymer was purified by diluting the reaction solution with water and dialysed against H₂O for 24 h. It was then freeze dried to give a yellow powder.

δ_H (400 MHz; D₂O) 0.87 (t, 3H, CH₃ (MPP)), 1.03-2.38 (m, br, 250H, CH₂, CH (polymer backbone)), 3.05-3.32 (m, br, 75H, SCH₂, CH₂CH₂OH) 3.52 (s, br, 75H, CH₂CH₂OH) and 3.75 (s, br, 16H, CH₃CH).

The M_n and M_w/M_n were determined via GPC to be 12180 g mol⁻¹ and 1.11, respectively. The DP of the NIPAM block was determined by NMR spectroscopy to be 16, by comparing the integrals from CH₂CH₂OH, 3.05-3.32 and 3.52 ppm which represents the previously determined DP of the mCTA, with the integral from the peak at 3.75 ppm from the (CH₃)₂CH of NIPAM.

2.3.8. Synthesis of pNIPAM-*b*-pHEA diblock copolymers

A typical procedure for the dispersion polymerisation HEA using pNIPAM as a mCTA is as follows, using a targeted DP 50 and pNIPAM₂₃-MPP mCTA as an example. Polymerisation ratios of mCTA to initiator are 5:1. pNIPAM₂₃-mCTA (0.51 g, 0.173 mmol), HEA (1.03 g, 8.94 mmol), AIBN (5.5 mg, 0.034 mmol) and DMSO (5.5 mL, to give a 20 wt% solid solution), were added to a 25 mL round bottom

flask and purged with N₂ for 20 minutes. This flask was lowered into a pre-heated heating block at 70 °C for 1 h. The polymerisation was quenched by removal from the heat and opening to air. The final HEA conversion was 79% as determined by ¹H NMR spectroscopy, by comparing the integrals of the two peaks, 3.04-3.72 and 3.45-3.65 ppm, from CH₂CH₂OH, which are present in both monomer and polymer, with the integral of the peak at 5.67 ppm, equivalent to ¹H of the vinyl group.

The polymer was purified by diluting the reaction solution with water and dialysed against H₂O for 24 hours. It was then freeze dried to give a yellow powder.

δ_H(400 MHz; D₂O) 0.85 (t, 3H, CH₃ (MPP)), 0.91-2.17 (m, br, CH₂, CH (polymer backbone)), 3.04-3.35 (m, br, 61H, CH₂CH₂OH), 3.53 (s, br, 61H, CH₂CH₂OH) and 3.76 (s, br, 19H, CHCH₃). The *M_n* and *M_w*/*M_n* were calculated via GPC to be 12000 g mol⁻¹ and 1.1, respectively. The DP was calculated by NMR spectroscopy to be 32, by comparing the integrals of the peak at 3.71-3.94 ppm from the (CH₃)₂CH of NIPAM, which represents the previously determined DP of the mCTA, with the integrals from CH₂CH₂OH, at 3.04-3.35 and 3.53 ppm.

2.3.9. Synthesis of 4-(acryloyloxymethyl) phenylboronic acid pinacol ester (BAPE)

4-(hydroxymethyl)benzene boronic acid pinacol ester (1.51 g, 6.41 mmol) was dissolved in anhydrous DCM (10 mL). TEA (1 mL, 7.17 mmol) was added slowly and the solution was cooled to 0 °C. Acryloyl chloride (0.63 mL, 7.8 mmol) was dissolved in anhydrous DCM (1.5 mL) and added to the solution slowly dropwise. After addition, the mixture was left to react overnight. The salt was removed by filtration and the solvent from the filtrate was removed under reduced pressure. The residue was diluted with ethyl acetate and washed with brine 3 times. The organic layer was dried using MgSO₄ and the solvent was removed under reduced pressure. The yellow oil was purified by silica gel column chromatography (1:1 hexane to ethyl acetate), to give BAPE as a colourless oil (0.895 g, 49%).

Elemental analysis found: C, 66.51; H, 7.44, C₁₆H₂₁BO₄ requires, C, 66.69; H, 7.35%. FTIR: ν_{max}/cm⁻¹ (ATR) 2980 (CH₃), 1713 ((CO)O), 1681, 1614, 1516, 1465 (para-substituted benzene, (RHC=CH₂) and

1355 (B-O). δ_{H} (400 MHz; CDCl_3) 1.35 (s, 12H, 4 \times pinacol Me), 5.22 (s, 2H, CH_2), 5.87 (m, 1H, $\text{CH}=\text{CH}$, J 6.45), 6.20 (m, 1H, $\text{CH}=\text{CH}$), 6.45 (m, 1H, $\text{CH}=\text{CH}$), 7.40 (m, 2H, arom.) and 7.85 (m, 2H, arom.). δ_{C} (100 MHz; CDCl_3) 24.9 (CH_3), 66.2 (CH_2), 83.9 (CH_2), 126.0 (vinyl), 127.3 (vinyl), LR-MS (ES+) m/z 311.361 (22.86%), 307.2 (36.2), 229.1 (2.86), 217.1 (100) and 135.1 (8.57); $[\text{M}+\text{H}]^+$ requires 289.16, $[\text{M}+\text{Na}]^+$ requires 311.14, $[\text{M}+\text{K}]^+$ requires 327.12.

2.3.10. Synthesis of pHEA-*b*-pNIPAM diblock copolymers in cononsolvents

A typical procedure for the polymerisation of pHEA-*b*-pNIPAM is as follows, using a targeted NIPAM DP 311 and pHEA₄₅-MPP-mCTA as an example. The ratio of mCTA to initiator was 3:1. pHEA₄₅-mCTA (0.0311 g, 0.00707 mmol), NIPAM (0.20 g, 1.77 mmol), ACVA (0.66 mg, 0.0024 mmol, 0.13 mL added as a 5.11 mg/mL stock solution in ethanol) were dissolved in a 75:25 mixture by volume of water to ethanol (4.4 mL, to give a 5 wt% solid solution) and purged with N_2 for 20 minutes. The flask was lowered into a pre-heated heating block at 70 °C with stirring and left to react overnight (approximately 16 h.). The polymerisation was quenched by removal from the heat and opening to air. The final NIPAM conversion was 87% as determined by moisture analysis. The polymer was purified by dialysis against H_2O for 24 h. to give a translucent white liquid.

δ_{H} (400 MHz; D_2O) 0.75-2.20 (br, m), 3.01-3.32 (br, m, $\text{CH}_2\text{CH}_2\text{OH}$), 3.450-3.59 (br, s, $\text{CH}_2\text{CH}_2\text{OH}$) and 3.64-3.86 (br, s, CH_3CH), The M_n and M_w/M_n were calculated via GPC to be 27620 g mol^{-1} and 1.74, respectively. The DP of the NIPAM block was determined as described previously and found to be 292.

2.3.11. Synthesis of linear statistical copolymers of p(NIPAM-*stat*-BAPE)

A typical procedure for the RAFT polymerisation of NIPAM with BAPE is as follows, using 5 mol% BAPE and MPP as an example. Polymerisation ratios of CTA to initiator were 5:1. MPP (6.3 mg, 0.0265 mmol), NIPAM (0.3 g, 2.65 mmol), BAPE (0.0362 g, 0.133 mmol, 0.16 mL added as a 144.9 mg/mL stock solution in DMSO), AIBN (0.84 mg, 0.0053 mmol, 0.30 mL added as a 2.83 mg/mL stock solution in DMSO) and DMSO (0.66 mL, to give a 20 wt% solid solution), were added to a glass vial

and purged with N₂ for 30 min. This flask was lowered into a pre-heated water bath at 70 °C for 3 h. The polymerisation was quenched by removal from the heat and opening to air. The final NIPAM conversion was 94% as determined by ¹H NMR spectroscopy. This was calculated by comparing the integrals of the peak at 3.85 ppm (CH₃CH), which is present in both the monomer and polymer, with the integrals of the peak at 5.06 ppm which is equivalent to 1H of the vinyl group present in the monomer, NIPAM.

The polymer was purified by diluting the reaction solution with water and dialysing against H₂O for 24 h. It was then freeze dried to give a yellow powder.

δ_H (400 MHz; DMSO-d₆) 0.73-2.28 (m, br), 3.35 (s, br), 3.69 (s, br), 4.02 (s, br), 6.91-7.68 (s, br), 7.99 (s, br) and 8.07 (s, br). The *M_n* and *M_w*/*M_n* were calculated via GPC to be 6360 g mol⁻¹ and 1.71, respectively. The DP was calculated from ¹H NMR to be 96 where 93 units are NIPAM and 3 are BAPE. This is calculated by comparing the peak at 3.57 ppm, which is equivalent to 3H of the RAFT agent, with the integral of the peak at 3.85 ppm for ¹H (CH₃CH) on NIPAM and 7.79 and 8.10 ppm which are equivalent to 4H bound to the aromatic ring in BAPE.

2.3.12. Synthesis of pHEA-*b*-p(NIPAM-*stat*-BAPE) diblock copolymers in cononsolvents

A typical procedure for the polymerisation of pHEA-*b*-p(NIPAM-*stat*-BAPE) is as follows, using a targeted NIPAM DP 320 and pHEA₄₅-MPP-mCTA as an example. The ratio of mCTA to initiator was 3:1 and the percentage of the second block which is BAPE was 2 mol%. pHEA₄₅-mCTA (0.029 g, 0.00685 mmol), NIPAM (0.19 g, 1.68 mmol), BAPE (0.01 g, 0.0347 mmol), ACVA (0.64 mg, 0.00228 mmol, 0.13 ml added as a 4.58 mg/ml stock solution in ethanol) were dissolved in a 75:25 mixture by volume of water to ethanol (4.4 mL, to give a 5 wt% solid solution) and purged with N₂ for 20 minutes. The flask was heated to 70 °C with stirring and left to react overnight (approximately 16 h.). The polymerisation was quenched by removal from the heat and opening to air. The final NIPAM conversion was 91% as determined by moisture analysis. The polymer was purified by dialysis against H₂O for 24 h. to give a translucent white liquid.

δ_{H} (400 MHz; D₂O) 0.70-2.26 (br, m), 3.09-3.39 (br, m, CH₂CH₂OH), 3.50-3.67 (br, s, CH₂CH₂OH), 3.71-3.94 (br, s, CH₃CH), 7.28 (s, aromatic CH) and 7.74 (s, aromatic CH). The M_n and M_w/M_n were calculated via GPC to be 31030 g mol⁻¹ and 1.72, respectively. The DP was calculated from ¹H NMR to be 301, where 297 units are NIPAM and 4 are BAPE by comparing the integrals from CH₂CH₂OH, knowing the DP, with the integral from the peak at 3.71-3.94 ppm from the CH₃CH of NIPAM and the 4H aromatic proton integrals at 7.28 and 7.74 ppm from BAPE.

2.3.13. General synthesis of core-crosslinked nanogels by PISA of pHEA-*b*-pNIPAM in cononsolvents

A typical procedure for the polymerisation of pHEA-*b*-pNIPAM nanogels with a crosslinked pNIPAM core is as follows, using a targeted NIPAM DP 313 and pHEA₄₅-MPP-mCTA as an example. The ratio of mCTA to initiator was approximately 3:1 and the ratio of crosslinker to mCTA was approximately 7:2. pHEA₄₅-mCTA (0.030 g, 0.00707 mmol), NIPAM (0.2 g, 1.77 mmol), ACVA (0.00066 g, 0.00236 mmol, 0.13 ml added as a 5.11 mg/ml stock solution in ethanol) and *N,N'*-methylenebisacrylamide (0.0327 g, 0.0212 mmol, 0.37 ml added as a 8.68 mg/ml stock solution in water) were dissolved in a 3:1 mixture by volume of water to ethanol (4.45 mL, to give a 5 wt% solid solution) and purged with N₂ for 20 minutes. The flask was heated to 70 °C with stirring and left to react overnight (approximately 16 hours). The polymerisation was quenched by removal from the heat and opening to air. The final NIPAM conversion was 86% as determined by moisture analysis. The polymer was purified by dialysis against H₂O for 24 hours to give a translucent white liquid. The DP was calculated from the conversion to be 269.

2.3.14. General synthesis of core-crosslinked nanogels by PISA of pHEA-*b*-p(NIPAM-*stat*-BAPE) in cononsolvents

A typical procedure for the polymerisation of pHEA-*b*-p(NIPAM-*stat*-BAPE) nanogels with a crosslinked p(NIPAM-*stat*-BAPE) core is as follows, using a targeted NIPAM DP 304 and pHEA₄₅-MPP-mCTA as an example. The ratio of mCTA to initiator was approximately 3:1, the ratio of the

crosslinker methylene bisacrylamide to mCTA was approximately 7:2 and proportion of BAPE to NIPAM was 2 mol%. pHEA₄₅-mCTA (0.029 g, 0.00685 mmol), NIPAM (0.19 g, 1.68 mmol), BAPE (0.01 g, 0.0347 mol), ACVA (0.0055 g, 0.0196 mmol, 0.13 ml added as a 5.11 mg/mL stock solution in ethanol) and *N,N'*-methylenebisacrylamide (0.00317 g, 0.0206 mol, 0.69 ml added as a 7.89 mg/ml stock solution in water) were dissolved in a 3:1 mixture by volume of water to ethanol (4.42 mL, to give a 5 wt% solid solution) and purged with N₂ for 20 minutes. The flask was heated to 70 °C with stirring and left to react overnight (approximately 16 hours). The polymerisation was quenched by removal from the heat and opening to air. The final NIPAM conversion was 75% as seen by moisture analysis. The polymer was purified by dialysis against H₂O for 24 hours to give a translucent white liquid. The DP was calculated from the conversion to be 228.

2.3.15. Calculation of theoretical BAPE content in NGs

The theoretical BAPE content can be calculated from the mass of starting materials incorporated into the reaction. From this it is possible to approximate the minimum amount of H₂O₂ needed to fully oxidise the NG. Using the masses described in 4.2.2.2 for a nanogel with 2 mol% BAPE incorporated:

$$\text{ratio of BAPE in the NG} = \frac{\text{mass of BAPE}}{\text{Total mass of all NG components}} = \frac{0.01 \text{ g}}{0.2377 \text{ g}} = 0.0431 \quad (2.2)$$

In a 2 mL 0.1 wt% solution there is 0.002 g of NG and therefore 8.415×10^{-5} g of BAPE.

$$\text{Moles of BAPE} = \frac{\text{Mass of BAPE}}{M_r \text{ of BAPE}} = \frac{8.415 \times 10^{-5} \text{ g}}{288.151 \text{ g mol}^{-1}} = 2.91 \times 10^{-7} \text{ mol} \quad (2.3)$$

1 mole of H₂O₂ reacts with 1 mole of BAPE. Therefore, the concentration of hydrogen peroxide required to oxidise 2 mol% BAPE in a nanogel is:

$$\text{concentration} = \frac{\text{moles of H}_2\text{O}_2}{\text{volume}} = \frac{2.91 \times 10^{-7} \text{ mol}}{0.002 \text{ L}} = 1.46 \times 10^{-4} \text{ M} = 0.146 \text{ mM} \quad (2.4)$$

The concentration of hydrogen peroxide needed for the BAPE concentrations in the NGs discussed in this chapter are:

$$2 \text{ mol\%} = 0.146 \text{ mM}$$

$$3 \text{ mol\%} = 0.217 \text{ mM}$$

5 mol% = 0.330 mM

Chapter Three

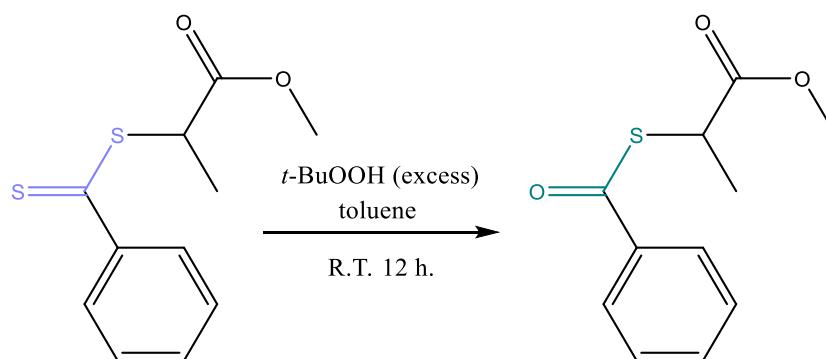
3. Utilisation of the RAFT chain end group as an oxidation sensitive trigger

3.1. Introduction

In this chapter, RAFT polymerisation was used to synthesise a range of polymers of NIPAM. RAFT polymerisation was used as it has many advantages where the size and dispersity of the sample is important. When using polymers inside the body, we must consider the passage of the polymer around the body to perform the intended task and ultimately the safe removal of the polymer after use. Safe removal requires the polymer to have a low molecular weight and small particle size to be excreted by the liver and kidneys rather than accumulate in the organs and tissues. It has been found that the molecular weight threshold for polymers to be excreted safely, i.e. the renal threshold is 45 kDa.¹ RAFT polymerisation affords polymers where the length can be targeted with a high degree of accuracy and the dispersity is narrow when compared to other polymerisation techniques.² Therefore, this should reduce the chance that blood vessels are blocked, build-up occurs and that an operation is ultimately needed to accumulated polymer.

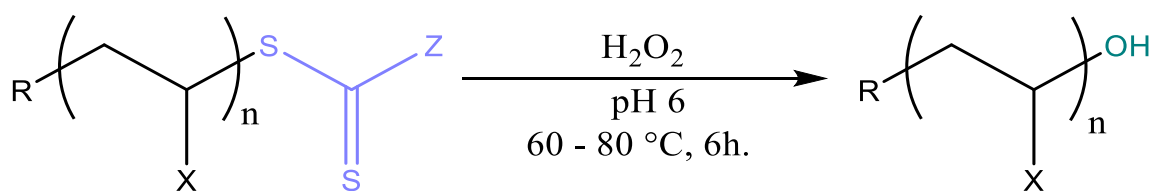
NIPAM was chosen as the monomer for this synthesis due to the temperature-responsive behaviour it exhibits after polymerisation.^{3,4} By tuning this temperature response, the LCST can be adjusted so that the polymer is hydrophobic before oxidation and on oxidation becomes soluble and can be safely excreted from the body.

It is widely reported in the literature that RAFT chain end groups can be cleaved after polymerisation.^{5,6,7} This has mainly been used to remove the colour and smell from the polymer, which are observed due to the thiocarbonylthio group of the RAFT agent, for applications such as paints and cosmetics, where these would affect the overall product. The literature states that the RAFT chain end group can be cleaved using oxidising agents, however, different products have been reported.⁵⁻⁷



Scheme 3.1 – The oxidation of a dithioester RAFT agent with *tert*-butyl hydroperoxide to give a thioester⁶

Vana et al. synthesised polymers of methyl acrylate via RAFT polymerisation using three dithiobenzoate compounds as the chain transfer agent: cumyl dithiobenzoate (CDB), cumyl *p*-fluorodithiobenzoate (CPFDB), and 1-phenylethyl dithiobenzoate (PEDB). It was found by mass spectrometry, that, on oxidation with *tert*-butyl hydroperoxide, the RAFT chain end group of these were converted from dithioesters to thioesters.⁶



Scheme 3.2 - The reaction of a RAFT chain end group with H_2O_2 at 60 °C to transform the dithioester group to a hydroxyl group⁵

Pfukwa et al. reported that the thiocarbonylthio group is removed on addition of an excess of H_2O_2 at elevated temperatures.⁵ The high temperatures cause the formation of hydroxyl radicals which add to the double bond of the $C=S$, causing the cleavage of the xanthate group. This means that the RAFT chain end group is replaced by a hydroxyl group which was indirectly confirmed by further crosslinking of this polymer to form a hydrogel.⁵ This method of RAFT chain end group removal is analogous to the method published by Perrier et al., where AIBN is used as the radical producing molecule rather than H_2O_2 .⁸ Jesson et al. have used hydrogen peroxide in similar conditions for end group removal from self-assembled block copolymer nano-objects in water. They did not characterise the precise nature of the end group removal, but UV-vis GPC confirms removal of the

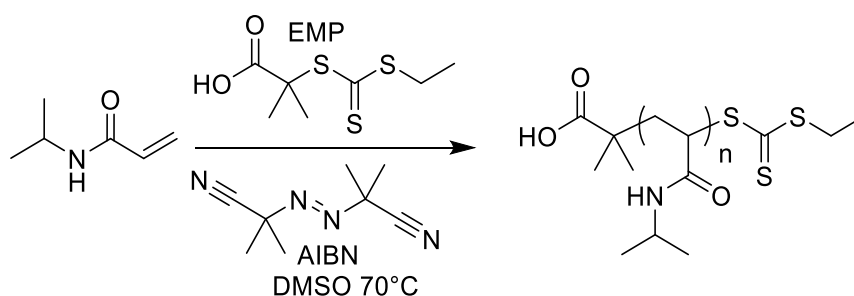
RAFT chain end group as does visual inspection of the polymers.⁷ They believe that this reaction however proceeds via an oxidation mechanism, rather than a radical mechanism as suggested above, as the speed of this cleavage is increased by the presence of oxygen. If this was a radical reaction, the rate would be expected to decrease as oxygen retards radical reactions.⁹

It was hypothesised that the oxidation of the RAFT chain end group of pNIPAM would affect its solubility in water, ultimately causing a change in the LCST of pNIPAM, as has been seen with other end group modifications.^{10,11,12,13} To test this hypothesis, a series of polymers of NIPAM with varying chain lengths and end groups were synthesised by RAFT polymerisation to determine how the end group changes and how this affects the temperature responsive behaviour of the polymer.

3.2. Results and Discussion

3.2.1. Synthesis of pNIPAM via RAFT solution polymerisation

To determine whether the RAFT end group can be utilised as an oxidation responsive trigger, a series of pNIPAM polymers were synthesised with different RAFT CTAs. RAFT polymerisation was chosen as the DP can be controlled easily using the RAFT agent to monomer ratio and it produces polymers with low dispersity, which is important for biomedical applications.



Scheme 3.3 - A reaction scheme for the polymerisation of NIPAM using the RAFT agent [2-ethyl sulfanyl thiocarbonyl] 2-methyl propionic acid (EMP)

Initially, the RAFT agent used to polymerise NIPAM was [2-ethyl sulfanyl thiocarbonylthio] 2-methyl propionic acid (EMP) (Scheme 3.3). It is important to select an appropriate RAFT agent for the monomer to be polymerised in order to have good control of the dispersity and retain end group fidelity. There are a variety of different groups of RAFT agents including dithioesters, dithiocarbamates, trithiocarbonates and xanthates.^{14,15} A trithiocarbonate was chosen as the appropriate RAFT agent for polymerisation of NIPAM. Although they are not the most active RAFT agent, they minimise side reactions while having adequate activity.

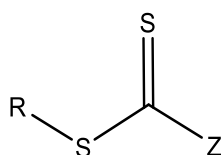


Figure 3.1 - The general structure of a RAFT agent indicating R and Z groups

As well as the main group of RAFT agents, it is important to choose an appropriate R group for the polymer (Figure 3.1).^{14,15} The R- group must be able to form a stable, initiating radical for the

monomer chosen. If the rate of the initiation period is lower than the rate of propagation however, an inhibition period is observed. Therefore, an R group which was not sterically hindered was chosen to avoid this. The Z group of the polymer controls the reactivity of the C=S double bond and influences the rate of radical addition. The R and Z group therefore have a large effect on the rate of polymerisation which controls the efficiency of the RAFT agent and controls retardation and inhibition of the polymerisation.

From previous work in the research group, it is known that the polymerisation of NIPAM reaches approximately 100% conversion after 3 h. in DMSO. Polymers with DPs of 50, 75 and 100 were targeted via the ratio of RAFT agent to monomer. The percentage conversion of monomer to polymer was calculated via NMR analysis of the reaction solution. The peaks remaining from the NIPAM monomer which are changed through polymerisation are the vinyl peaks at 5.25 and 5.9 ppm. These can be compared to the peak labelled 'h' on the NMR spectrum as this peak contains both monomer and polymer protons of this kind so can be set to 1 to indicate 100% of the NIPAM added (Figure 3.2).

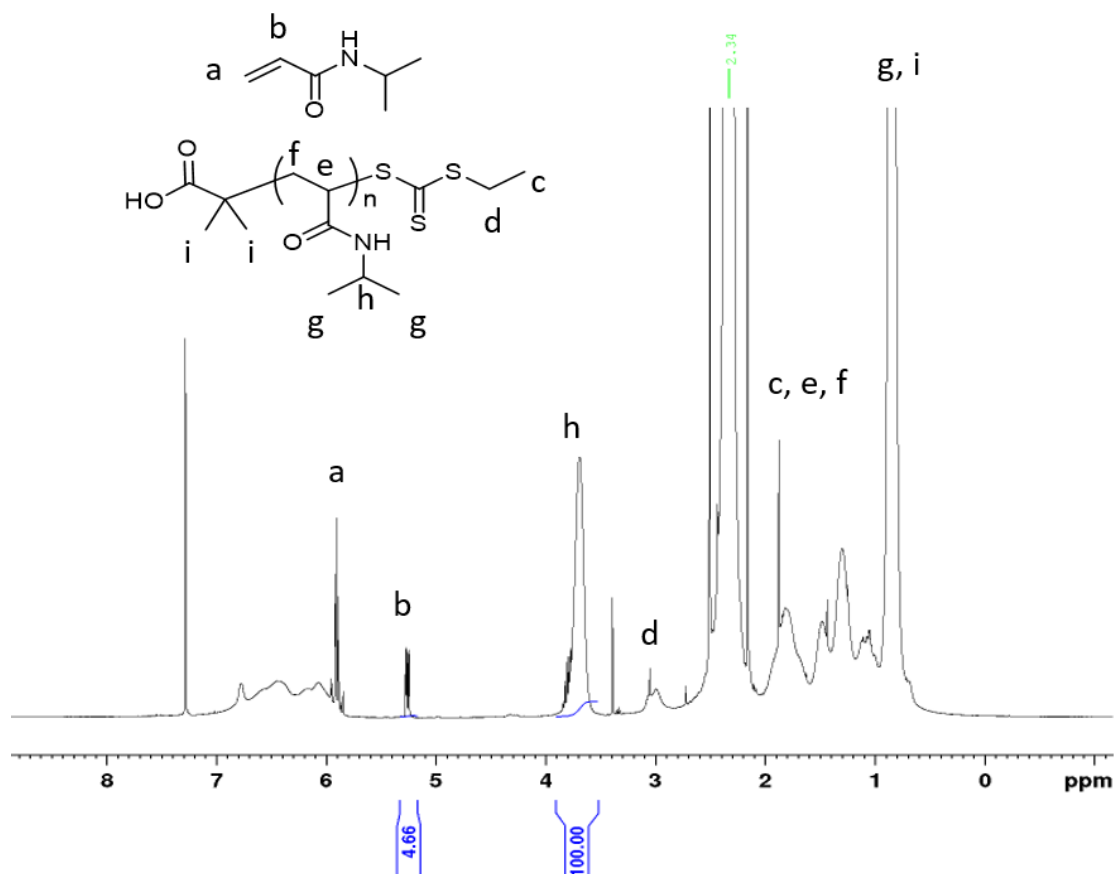


Figure 3.2 - ¹H NMR spectrum of pNIPAM₅₀ synthesised with EMP as the CTA in CDCl₃ before purification to determine the monomer to polymer conversion.

Polymers were analysed by GPC in DMF (0.1% LiBr) against pMMA standards. In all cases the polymers had narrow distributions and the GPC shows unimodal peaks (Table 3.1 and Figure 3.3). This shows that RAFT polymerisation gives good control of the chain length and polydispersity of the polymer.

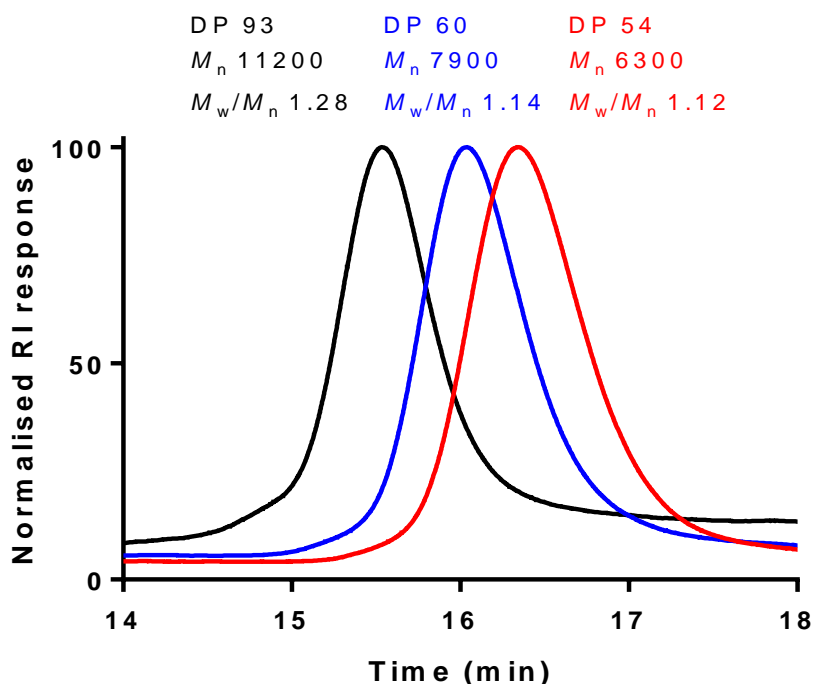


Figure 3.3 - GPC chromatograms (DMF 0.1% LiBr) of pNIPAM polymers with nominal targeted DP of 50, 75 and 100, where M_n refers to the number-average molecular weight and M_w/M_n refers to the dispersity calculated.

The M_n calculated by GPC is not as accurate as that calculated using NMR spectroscopy as the standards used for calibration are pMMA not pNIPAM. The ratio between the RAFT agent end groups and polymer peaks in the ^1H NMR spectra can be used to determine the DP. In this case, the CH_2 protons of the ethyl chain (peak c, Figure 3.4) of the RAFT agent at approximately 3.4 ppm can be compared to either the methine proton of the isopropyl group (peak d, Figure 3.4) at 4.0 ppm, or the protons labelled a and b. The DPs calculated by ^1H NMR spectroscopy were very similar to those determined from the conversion and the targeted degree of polymerisation.

Table 3.1 - Analytical data for pNIPAM synthesised by RAFT polymerisation using EMP as the CTA.

[M]/[RAFT agent]	Conversion / % ^a	Theoretical DP ^b	M_n / Da ^c	DP _n ^a	M_n / Da ^d	M_w/M_n ^d
98	97	95	11200	93	10700	1.28
71	96	68	8400	60	7900	1.14
55	95	52	6100	54	6300	1.12

^a Determined by ^1H NMR spectroscopy in CDCl_3 . ^b $[\text{M}]/[\text{RAFT agent}] \cdot \text{conv.}$ ^c Theoretical M_n from ^1H NMR spectroscopy. ^d Determined by GPC in DMF (0.1% LiBr) with pMMA standards.

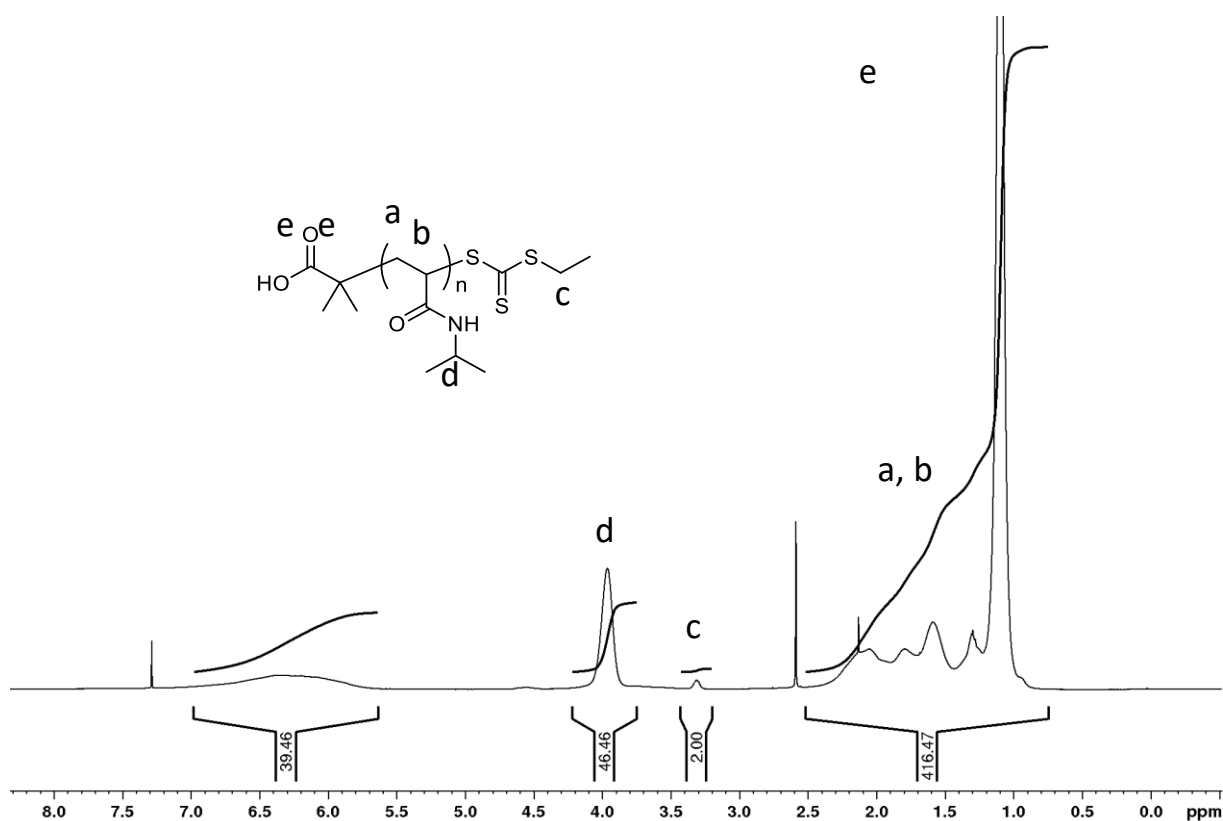


Figure 3.4 - ^1H NMR spectrum of pNIPAM synthesised with EMP as the CTA in CDCl_3 to determine the degree of polymerisation

3.2.2. Analysis of the effect of oxidation on the cloud point

Cloud points, as mentioned previously, are used to estimate the lower critical solution temperature (LCST). Samples were prepared in either Dulbecco's phosphate-buffered saline (DPBS) or water at a concentration of 1 mg mL^{-1} . DPBS was used here as it is a buffer solution which mimics physiological pH so is relevant when studying whether the oxidation would occur in the same way inside the human body. The cloud point was determined for polymers before and after oxidation to determine whether oxidation could cleave/modify the RAFT end group and if in turn this alters the LCST significantly. The polymers were oxidised in a 15 mM solution of H_2O_2 in both DPBS or water. This concentration of hydrogen peroxide was used initially as this is the concentration used in similar redox studies.^{16,17} These polymers were purified via dialysis against water for 24 h. to remove any

small molecules which may have formed due to the oxidation, as well as the removal of hydrogen peroxide. Cloud points were determined from the point of inflection of the absorbance curve.

Table 3.2 - Cloud point analysis of the three polymers synthesised using EMP RAFT agent

Target DP	CP before [O] DPBS / °C	CP after [O] DPBS / °C	Δ °C	CP before [O] H ₂ O / °C	CP after [O] H ₂ O °C	Δ °C
100	35.0	35.6	0.6	37.5	36.6	0.9
75	38.0	40.0	2	37.9	35.6	2.3
50	39.5	43.0	3.5	39.6	35.6	4.0

The most noticeable trend is that as the chain length decreases, the difference in the cloud point between oxidised and non-oxidised polymers increases, which is expected from reports in the literature.^{10,18,19} This implies that the shorter the polymer chain, the more influence modification of the RAFT end group by oxidation has. However, in DPBS the cloud point increases upon oxidation, whereas the opposite is true in H₂O, although the cloud points before oxidation are very similar. It is believed that this is due to the interaction of the carboxylic acid on the RAFT agent with water through hydrogen bonding (Figure 3.5, Figure 3.6). Deprotonation of the carboxylic acid in DPBS may also influence the position of cloud point. This deprotonation causes the end group to become more hydrophilic and therefore hydrogen bonding is stronger meaning that higher temperatures will be needed to cause precipitation.^{20,21}

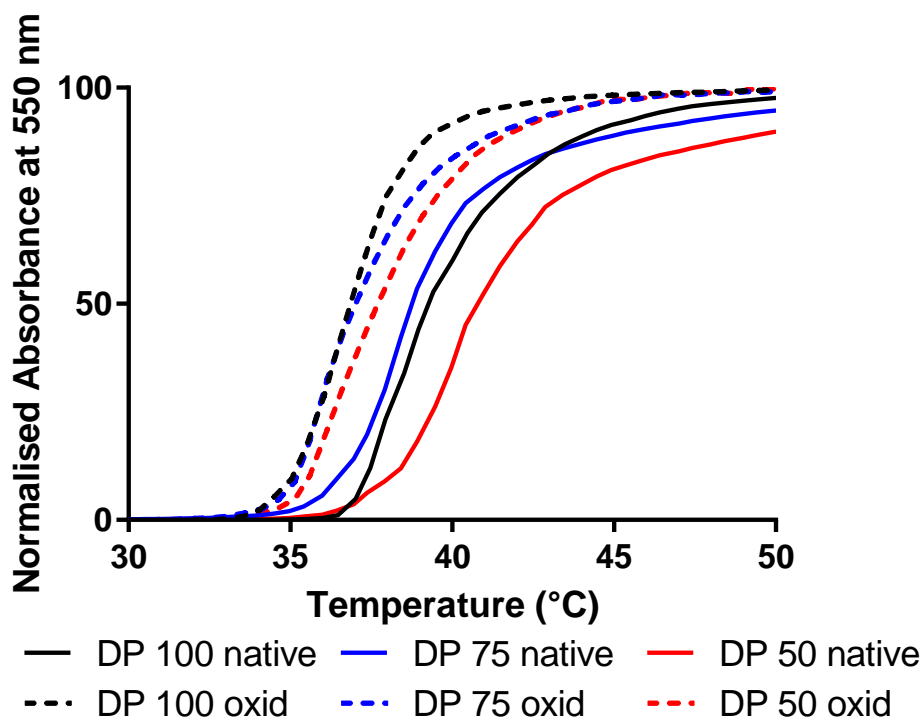


Figure 3.5 - UV/vis spectra monitoring change in absorbance over temperature at 550 nm of various pNIPAM-EMP samples before and after oxidation in water

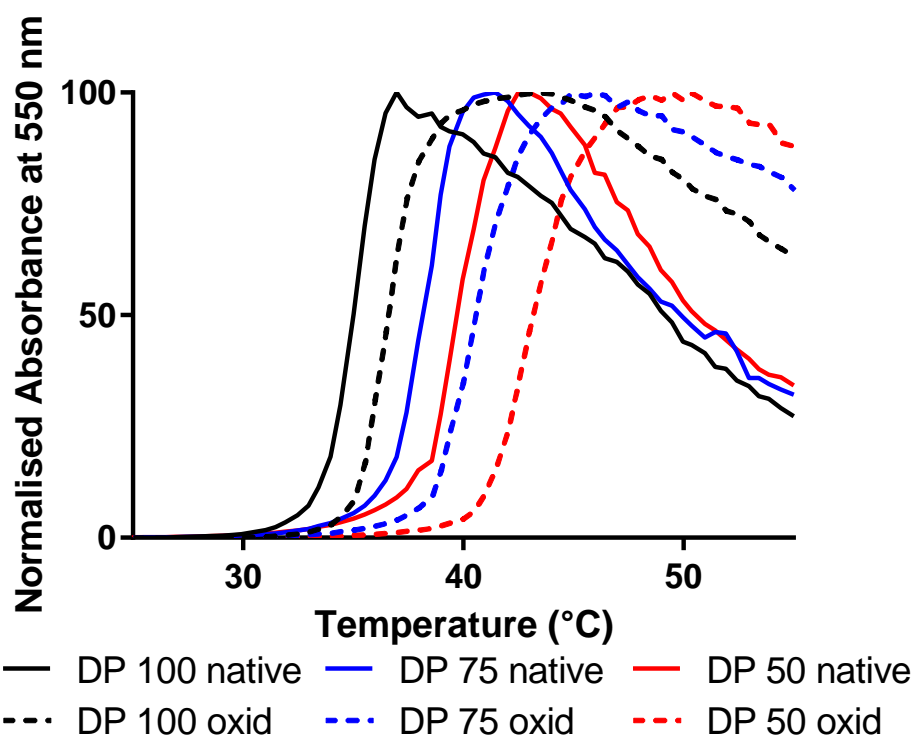
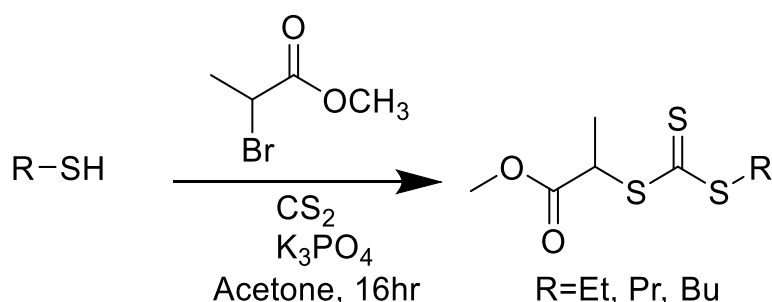


Figure 3.6 - UV/vis spectra monitoring change in absorbance over temperature at 550 nm of various pNIPAM-EMP samples before and after oxidation in DPBS

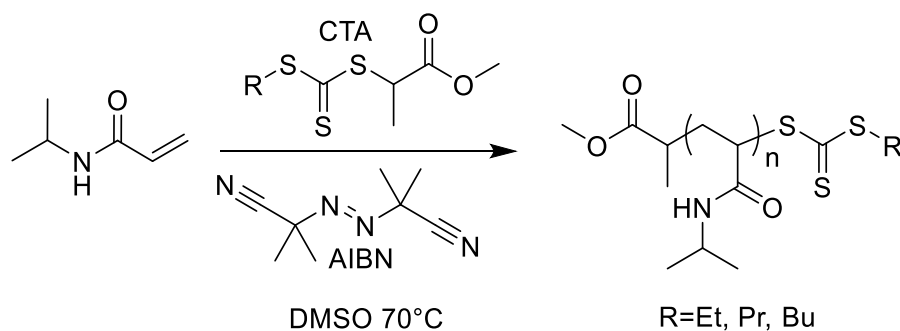
3.2.3. Synthesis of pNIPAM via RAFT solution polymerisation using non-ionisable RAFT agents

To minimise solvent and pH effects, three similar trithiocarbonate RAFT agents with ester end groups, rather than carboxylic acid end groups, were synthesised (Scheme 3.4). These RAFT agents differ from each by the length of the alkyl chain of the Z-group (ethyl, propyl or butyl). All CTAs were thoroughly characterised by ^1H and ^{13}C NMR and IR spectroscopies, mass spectrometry and elemental analysis (see section 2.2 and figures A1–6).



Scheme 3.4 - Synthesis of non-ionisable trithiocarbonate RAFT agents.

These RAFT agents were used to synthesise pNIPAM as before (Scheme 3.4). The targeted degree of polymerisation included some shorter chain lengths; 10, 25, 50 and 100, as it was noted that the shorter the polymer chain, the larger the difference in cloud point after oxidation. For the shortest polymers ($\text{DP}_n = 10$), DMF was used as the polymerisation solvent as literature reports suggested it would be possible to precipitate these polymers from DMF.²² However, due to their short chain length this was not possible so they were dialysed against water as before.



Scheme 3.1 - Reaction scheme for the polymerisation of NIPAM using the RAFT agents EMEM, MPP and MBP mentioned above

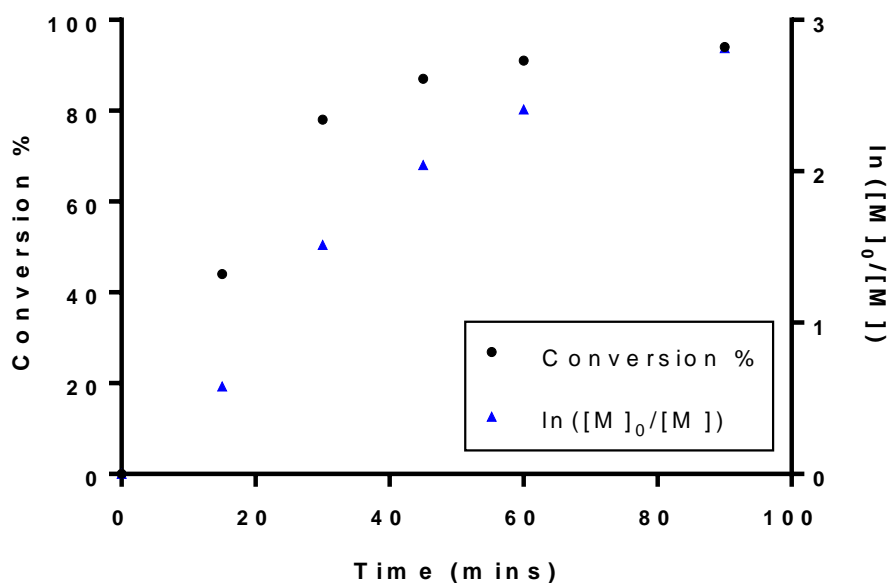


Figure 3.7 – Monomer conversion and pseudo-first order kinetic plot determined by ^1H NMR spectroscopy for the polymerisation of NIPAM (DP 22 as determined ^1H NMR spectroscopy) using MPP as the RAFT agent.

As has been found previously, the polymerisation is fast with approximately 90% monomer conversion after 3 h., as determined by ^1H NMR (Figure 3.7). Samples were also analysed by GPC (Figure 3.9) and molecular weights were found to increase linearly with conversion. This correlates with what was expected from the results from using EMP as the RAFT agents are very similar. The conversion, actual degree of polymerisation by NMR spectroscopy and GPC data can be found in Table 3.3.

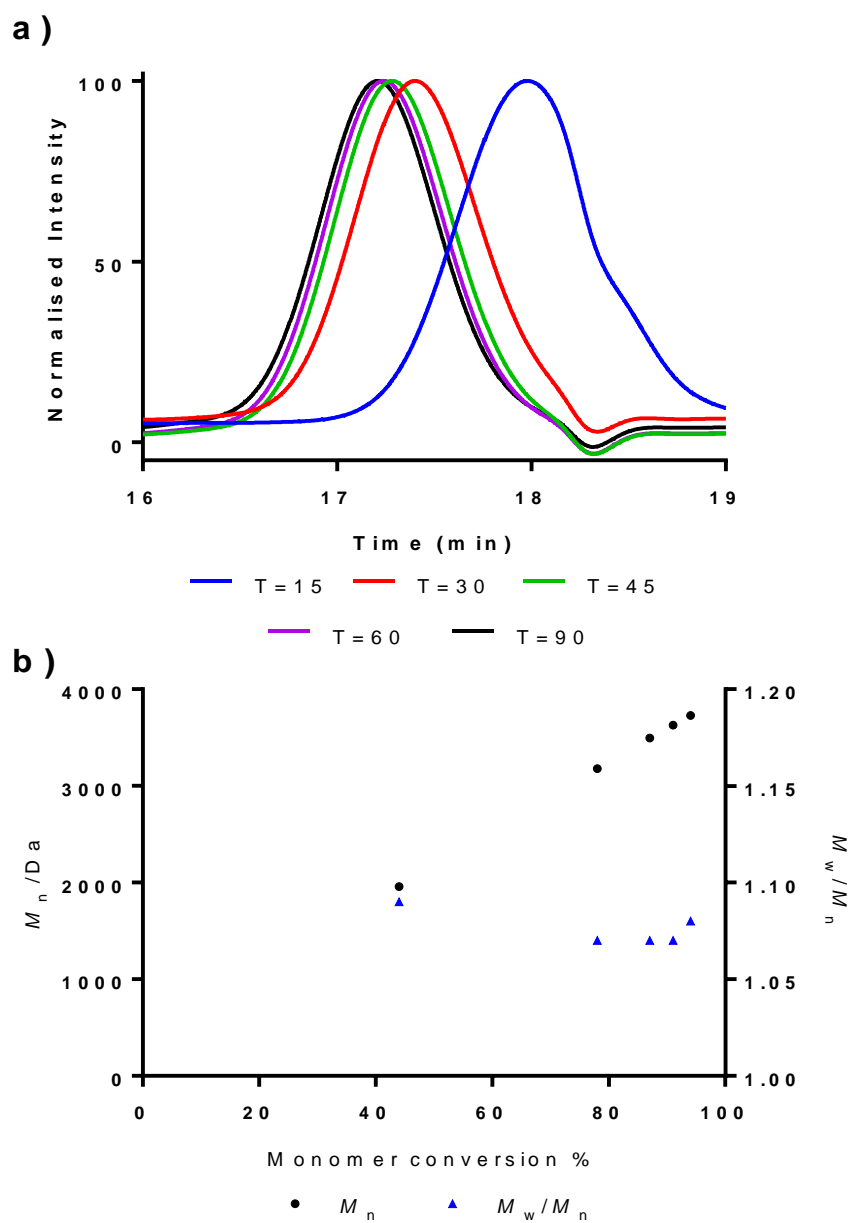


Figure 3.8 – a) GPC chromatograms (DMF 0.1% LiBr) of samples removed during the polymerisation of NIPAM (DP 22) using MPP as the RAFT agent. M_n and M_w/M_n were determined relative to pMMA standards and b) Evolution of M_n and M_w/M_n with monomer conversion.

Table 3.3 - Polymers synthesised using the RAFT agents EMEM, MPP and MBP giving their conversion, DP by NMR and GPC data

RAFT agent	[M]/[CTA]	Conv. / % ^a	Thr. DP ^b	M_n / Da ^c	DP _n ^a	M_n / Da ^d	M_w/M_n ^d
EMEM	10	96	10	1360	10	1700	1.09
EMEM	25	97	24	2940	27	3900	1.08
EMEM	50	96	48	5660	48	6700	1.08
EMEM	92	97	89	11540	100	13100	1.11
MPP	8	88	7	1140	8	1400	1.09
MPP	20	89	18	2390	19	3000	1.09
MPP	39	94	37	4430	37	5700	1.09
MPP	63	95	60	8050	69	8900	1.10
MPP	74	83	62	9060	78	10600	1.10
MBP	25	98	25	3310	27	4200	1.08
MBP	48	77	37	5000	42	6000	1.09
MBP	105	88	92	10440	90	13600	1.10

^a Determined by ¹H NMR spectroscopy in CDCl₃. ^b [M]/[RAFT agent] × conv. ^c Calculated M_n from ¹H NMR spectroscopy. ^d Determined by GPC in DMF (0.1% LiBr) with pMMA standards.

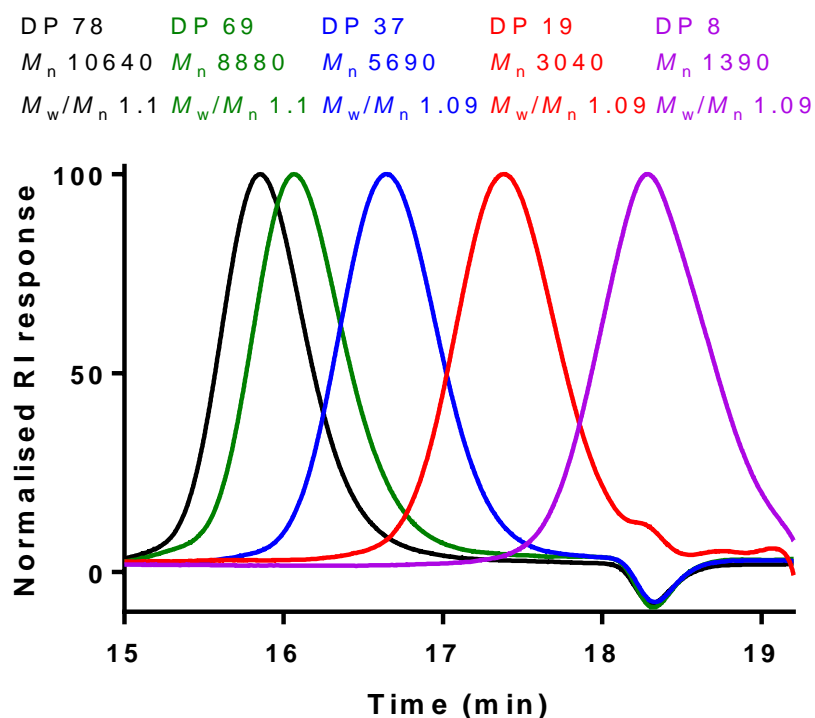


Figure 3.9 - GPC chromatograms (DMF 0.1% LiBr) of polymers of NIPAM synthesised using MPP RAFT agent with a DP of 8, 19, 37, 69 and 78, as determined by NMR spectroscopy.

In most cases, the DP_n determined using NMR spectroscopy was similar to the theoretical value determined from RAFT agent to monomer ratio and the monomer conversion. This was determined in the same way as with the EMP polymers, by using the RAFT end group.

The number-average molecular weight, M_n , determined by GPC increases with targeted DP however is not directly comparable to that determined from 1H NMR spectroscopy due to the use of pMMA standards. The dispersity is also low as expected for polymers formed by RAFT polymerisation (Figure 3.9, Figure A.7 and Figure A.8).

3.2.4. Effects of oxidation on the RAFT chain end group

These polymers were oxidised as before, purified, lyophilised and dissolved in DBPS as it a buffer which will maintain the solution in the physiological pH range. The average cloud point temperature before and after oxidation can be found in Table 3.4. UV/vis measurements were recorded twice under the same conditions to obtain an average. As predicted, the cloud point increased after oxidation. However, there was very little change in the cloud point when the DP was 50 or more.

This correlates with what was expected from our initial study of pNIPAM-EMP and reports of other pNIPAM systems in the literature^{18,19,10} and is consistent with it being an end group effect.

Table 3.4 - A table of the cloud point analysis before and after oxidation of the polymers synthesised using the RAFT agents EMEM, MPP and MBP. Analysis of cloud point was repeated twice for each sample.

RAFT agent	[M]/[RAFT agent]	DP _n ^a	Avg. CP before [O] °C	Avg. CP after [O] °C	Δ °C
EMEM	10	10	40.3 ± 0.4	45.0 ± 0.6	4.7 ± 1.0
EMEM	25	27	35.6 ± 0.8	37.1 ± 0.1	1.5 ± 0.9
EMEM	50	48	34.9 ± 0.5	35.6 ± 0.6	0.7 ± 1.1
EMEM	100	100	32.3 ± 1.0	32.8 ± 1.0	0.5 ± 2.0
MPP	8	8	31.9 ± 0.9	41.2 ± 0.7	9.3 ± 1.6
MPP	20	19	32.3 ± 0.2	37.9 ± 1.5	5.6 ± 1.8
MPP	39	37	32.4 ± 0.3	32.76 ± 0.2	0.4 ± 0.2
MPP	63	69	32.5 ± 0.5	32.4 ± 0.3	-0.1 ± 0.8
MPP	74	78	32.1 ± 0.6	32.0 ± 0.1	-0.1 ± 0.7
MBP	25	27	28.7 ± 0.8	32.7 ± 1.6	4.0 ± 2.4
MBP	48	42	32.1 ± 1.2	34.5 ± 2.2	2.4 ± 3.4
MBP	105	90	32.7 ± 1.0	32.1 ± 0.7	-0.6 ± 1.7

^a Determined by ¹H NMR spectroscopy in CDCl₃.

For clarity, only polymers synthesised using MPP as the RAFT agent will be discussed in detail as the results are similar for all RAFT agents. The data for the other RAFT agents has been included in the appendix. It is much easier to visualise the effect of chain length on cloud point when represented on a graph (Figure 3.10, Figure A.9 and Figure A.10).

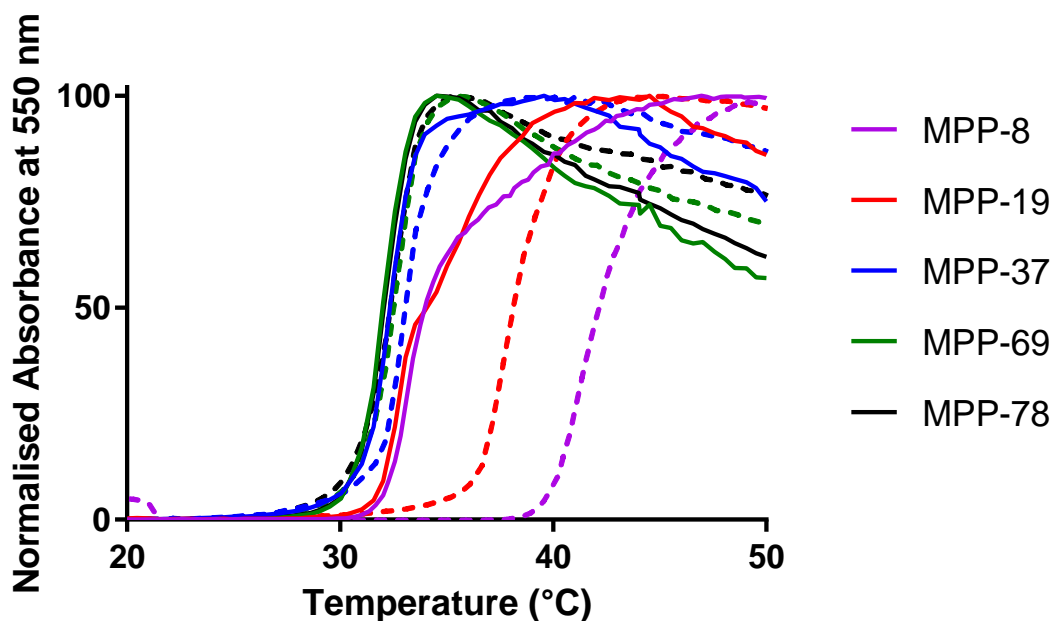


Figure 3.10 - Cloud point measurements of pNIPAM polymers synthesised using MPP before and after oxidation. Cloud point curves were recorded by monitoring the absorbance at 550 nm with increasing temperatures. The DP of the polymers refers to those calculated by ^1H NMR spectroscopy. The solid lines indicate polymers before oxidation and the dashed lines represent the polymers after oxidation.

For DP 41, 66 and 74 the differences are negligible and are due to experimental error as cloud point measurements vary slightly on differences in the concentration of the solution.^{23,24,25} However, the DP 8 and 20 polymers displayed a large change in cloud point with the shortest polymer showing the largest change (9.3 °C).

3.2.5. Determination of the chemical change in the end group of pNIPAM₈ by chemical analysis

As noted in the introduction, several species have been reported to form on oxidation of polymers synthesised by RAFT polymerisation. For example, it has been seen via MALDI-ToF that oxidation with H_2O_2 and elevated temperatures causes cleavage of the RAFT chain end group by hydroxyl radicals to give an OH end group.⁵ It has also been suggested that the C=S could become a C=O group.⁶

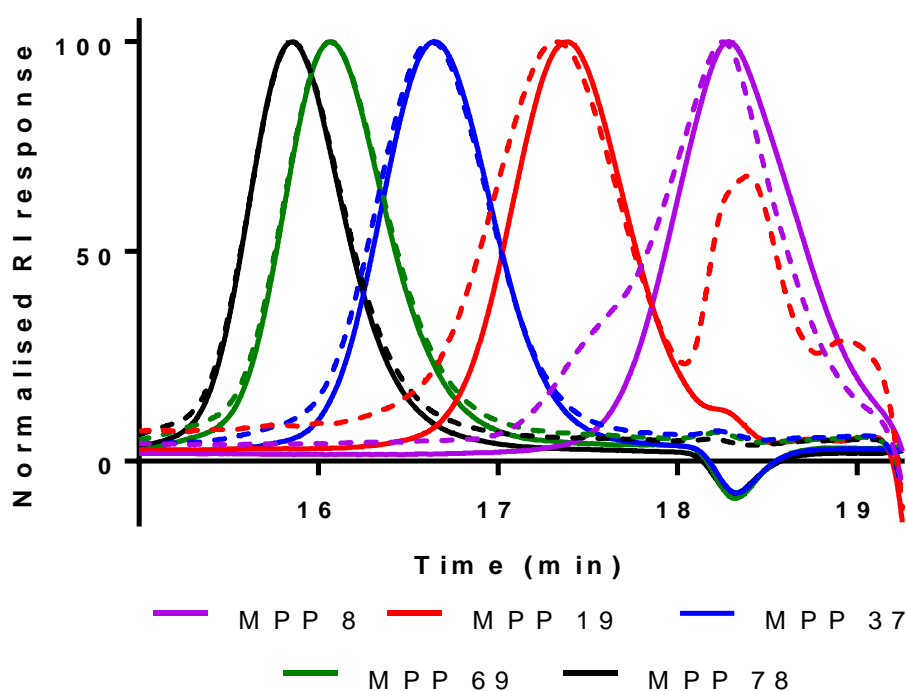


Figure 3.11 - GPC chromatograms (DMF 0.1% LiBr) of pNIPAM synthesised using MPP before and after oxidation with H_2O_2 . The solid lines indicate polymers before oxidation and the dashed lines represent the polymers after oxidation with 15 mM H_2O_2 .

To determine what causes the change in cloud point upon oxidation in this case, numerous analytical techniques were used. The GPC analysis of the polymers both before and after oxidation were very similar in terms of both molecular weight and their dispersity (Figure 3.11). The differences between these are very small which does not indicate that oxidation has had any effect on the overall length of the polymer chain and will not have affected the backbone of the polymer. It is likely that this indicates a change in the RAFT chain end group of the polymer. The only difference seen is that the polymer with a DP of 20 has an additional peak. This is also observed for some pNIPAM synthesised using the other RAFT agents (Figure A.11 and Figure A.12). This may be due to the purity of the compounds however, for all samples other than DP20, these peaks are not very intense. In the future, more analysis of any other fragments should be considered.

NMR analysis of the polymers after oxidation was performed, however there still appeared to be presence of many of the peaks seen in the NMR of the native polymer, although at a smaller ratio

(section 3.2.2 and 3.2.3). This does not give adequate evidence alone for a difference in structure after oxidation.

The shortest polymer synthesised was analysed in more depth to determine what chemical changes had occurred to cause a large difference in cloud point after oxidation. Infrared spectroscopy was used to determine whether a functional group was lost/gained through the oxidation. From the literature referenced above, it was predicted that oxidation would form a hydroxyl group or one of the sulfur groups in the trithiocarbonate could be transformed into an oxygen atom. Each of these functional groups would give a unique bond stretching frequency which would not be present in the initial polymer. It is important to note, however, that C-O and C=O stretches are already present due to the R group of the RAFT agent. Depending on the group formed on oxidation the following peaks could be observed: S-H ($2780-2700\text{ cm}^{-1}$, weak), S=O ($1350-1342\text{ cm}^{-1}$, strong), sulfonic acid hydrates ($2800-1650\text{ cm}^{-1}$, broad) and OH ($3550-3200\text{ cm}^{-1}$, broad).²⁶

In the infrared spectra of pNIPAM₈, there appears to be a broad peak in the spectrum of the oxidised polymer in the region between 3200 and 3600 cm^{-1} , which is not present in the polymer before oxidation (Figure 3.12). Broad peaks in this region indicate the presence of hydroxyl groups. Although there is a difference in the fingerprint region of the spectra, due to the large number of peaks in this region it is difficult to determine what the difference may be.

For an in-depth analysis of the structure of the end group, mass spectrometry can be used. By comparing the native polymer sample with the oxidised sample, the spectra can be overlaid and differences in them determined. Using this alongside other analytical techniques allowed the determination of the end group modification.

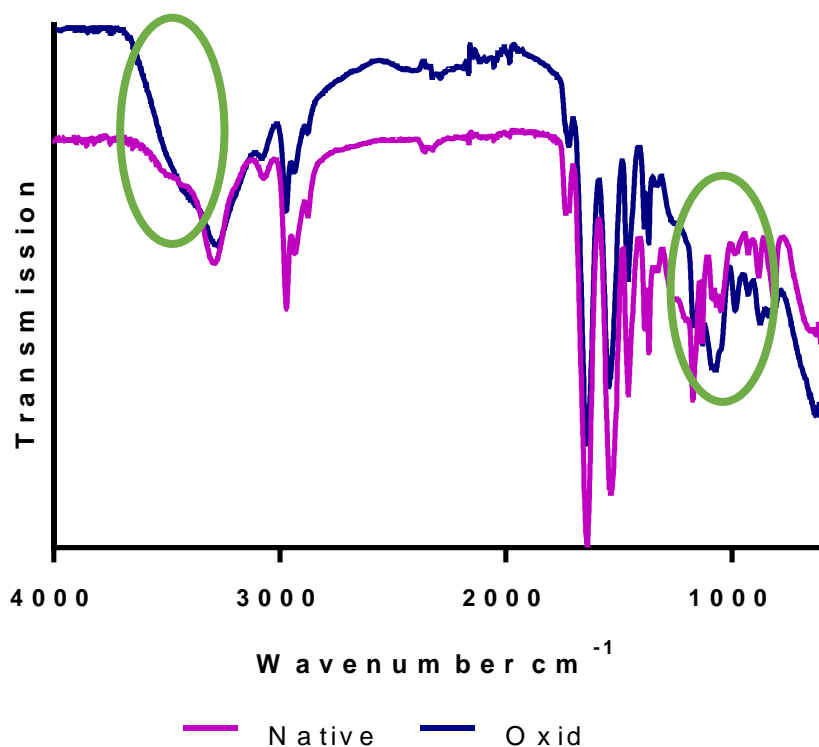


Figure 3.12 - A comparison of the IR spectra before and after oxidation of pNIPAM-MPP with a DP of 8. The green ovals highlight the main differences.

Mass spectrometry was performed on the DP 8 polymer before and after oxidation in electrospray ionisation positive and negative mode (Figure 3.13). The two different modes, and therefore with differing electric fields, were used as depending on the species formed after oxidation, it may not have been possible to observe the polymer in a single mode. It was found that the negative mode was better to observe the polymer after oxidation. The ES+ mode spectrum of the native polymer was compared with the ES- mode spectrum of the oxidised polymer. When these two spectra are overlaid, as expected, the gaps between the larger peaks have a value of 113 g mol^{-1} , which is the molecular mass of a single NIPAM unit. However, these peaks do not exactly overlay, they are shifted by approximately 85 g mol^{-1} . By looking at the data reported in literature surrounding what is predicted to happen upon oxidation of the RAFT agent, it was found that this shows that the trithiocarbonate is oxidised to a sulfonic acid group in this case (Scheme 3.5). It is also possible to see from the comparison of spectra that there is a minor product. This is a sulfur atom on the trithiocarbonate is replaced by an oxygen atom, as previously seen in literature.^{5,7}

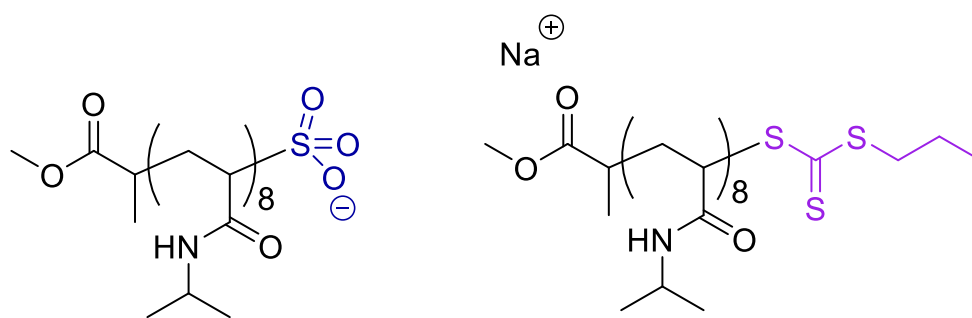
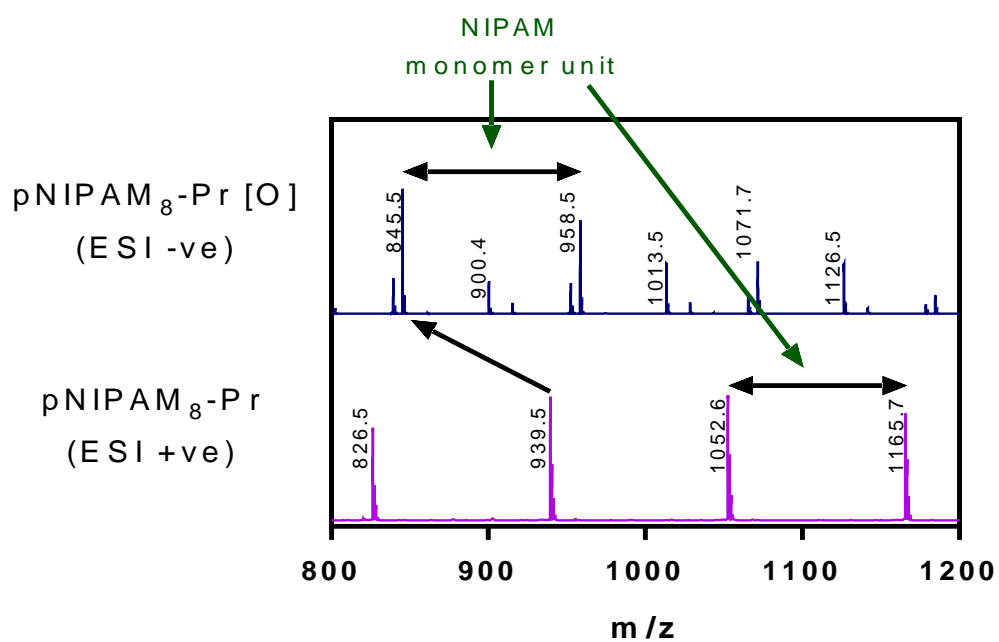
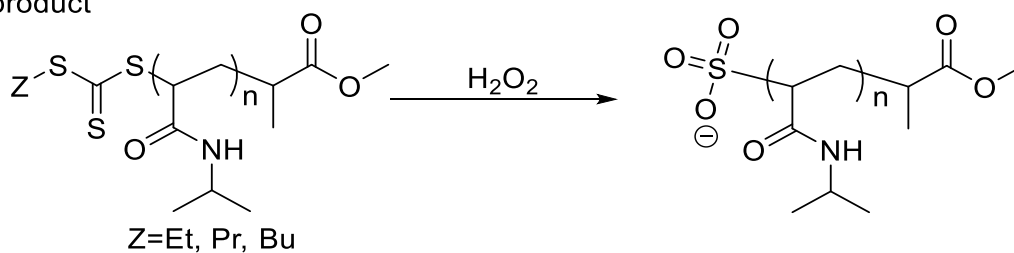
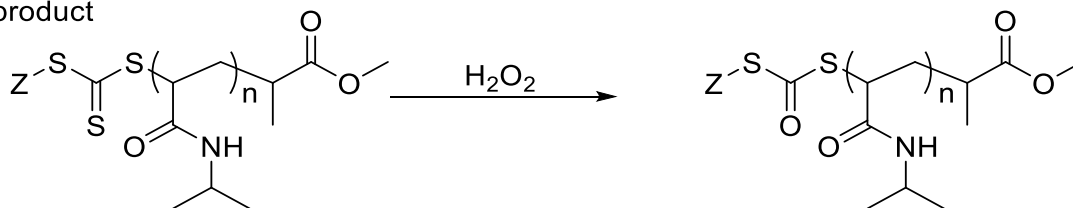


Figure 3.13 - Comparison of mass spectra data of pNIPAM8-MPP before and after oxidation in ES+ and ES- respectively.

Major product



Minor product



Scheme 3.5 - The major and minor oxidation products observed by mass spectrometry of pNIPAM₈-MPP when oxidised with 15 mM H₂O₂

3.2.6. The effect of oxidation of polymers with different RAFT chain transfer agents

Considering this information, it is expected that pNIPAM with the same DP would have the same cloud point after oxidation irrespective of which of the three synthesised RAFT chain transfer agents was used. This is because the only difference in the RAFT agents is the Z group, which is removed upon oxidation to form the sulfonic acid. To test this hypothesis, polymers needed to be synthesised with the same degree of polymerisation. Therefore, the above reactions were repeated with a target DP of 25.

Table 3.5 shows the NMR spectral data and GPC data for the targeted DP25 polymers. All these reactions went to over 95% conversion, so the actual degree of polymerisation is expected to be very close to the targeted value. From ^1H NMR spectroscopy, the DP and therefore molecular mass was found to be very similar to what was expected. This correlates with M_n produced on analysis of the GPC traces (Figure 3.14). The M_n values from GPC are within error of the pMMA standards and the polydispersity is low.

Table 3.5 - A table giving conversion, DP by NMR and GPC data of DP25 pNIPAM synthesised using the RAFT agents EMEM, MPP and MBP

RAFT agent	[M]/[RAFT agent]	Conversion / % ^a	Theoretical DP ^b	M_n / Da ^c	DP _n ^a	M_n / Da ^d	M_w/M_n ^d
EMEM	24	96	23	2950	22	3610	1.06
MPP	25	97	24	2960	25	3800	1.07
MBP	25	97	24	2970	26	3750	1.07

^a Determined by ^1H NMR spectroscopy in CDCl_3 . ^b calculated from $[\text{M}]/[\text{RAFT agent}] \times \text{conv.}$ ^c Theoretical M_n from ^1H NMR spectroscopy. ^d Determined by GPC in DMF (0.1% LiBr) with pMMA standards.

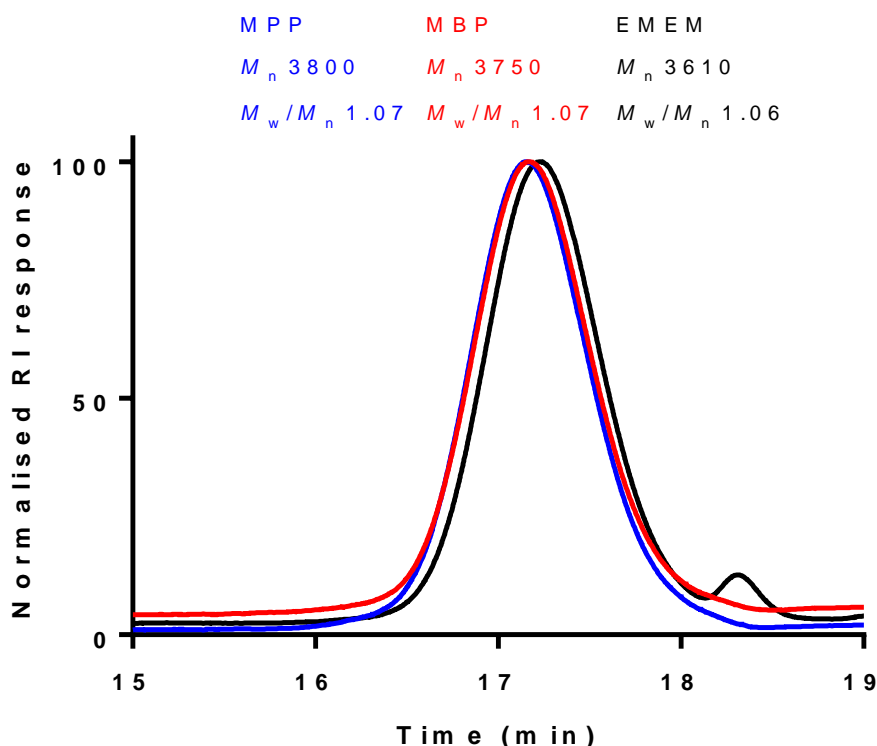


Figure 3.14 - GPC traces of pNIPAM with a DP of 25, synthesised using the RAFT agents EMEM, MPP and MBP

The cloud points of these polymers were measured before and after oxidation as before (Table 3.6). There is a large increase in the cloud point after oxidation. However, these do not rise to the same temperature as expected (Figure 3.15). This could be due to variations in the DP of the polymers, but more analysis needs to be conducted to state conclusively that the sulfonic acid group is produced and to what extent, especially to see if this is only the case when using MPP as the RAFT agent. It could suggest that the content of the minor non-sulfonic acid product observed in the MS may vary and causes the cloud points to differ.

Table 3.6 - A table giving the cloud point data for DP 25 pNIPAM synthesised using the RAFT agents EMEM, MPP and MBP. Analysis of cloud point was repeated twice for each sample.

RAFT agent	[M]/[RAFT agent]	DP _n ^a	Avg. CP before [O] °C	Avg. CP after [O] °C	Δ °C
EMEM	24	22	31.2 ± 0.3	37.7 ± 0.4	6.5 ± 0.7
MPP	25	25	33.7 ± 0.2	37.4 ± 0.56	3.7 ± 0.7
MBP	25	26	32.0 ± 0.3	35.7 ± 0.8	3.7 ± 1.1

^a Determined by ¹H NMR spectroscopy in CDCl₃.

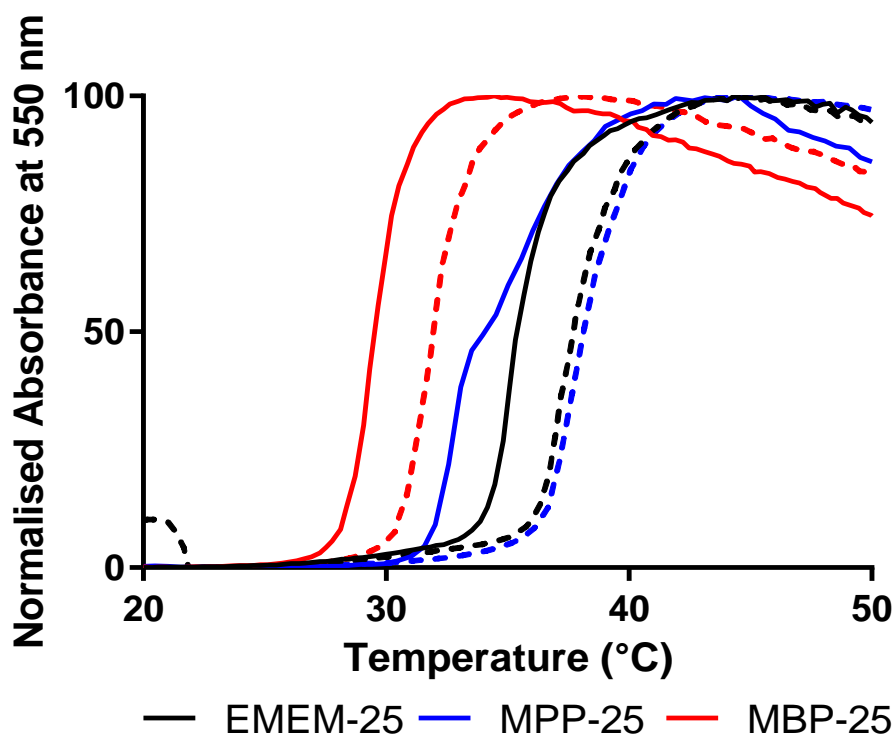


Figure 3.15 - Cloud point analysis at 550 nm of DP 25 pNIPAM synthesised using EMEM, MPP and MBP RAFT agents, before and after oxidation. The solid lines indicate polymers before oxidation and the dashed lines represent the polymers after oxidation.

The polymers synthesised using EMEM, MPP and MBP have very similar molecular weights, therefore the comparison of both IR and mass spectra in these cases are useful to determine whether there is any significant difference in the proportion of oxidation and the main product produced as the end group. For all pNIPAM₂₅ polymers, it is more difficult to determine whether the IR shows the presence of OH, as the spectra for the native and oxidised polymer look very similar (Figure 3.16). However, from mass spectra it is possible to see to that the major product after oxidation is the sulfonic acid polymer end group as observed above in section 2.3.5 (Figure A.13 and Figure A.14).

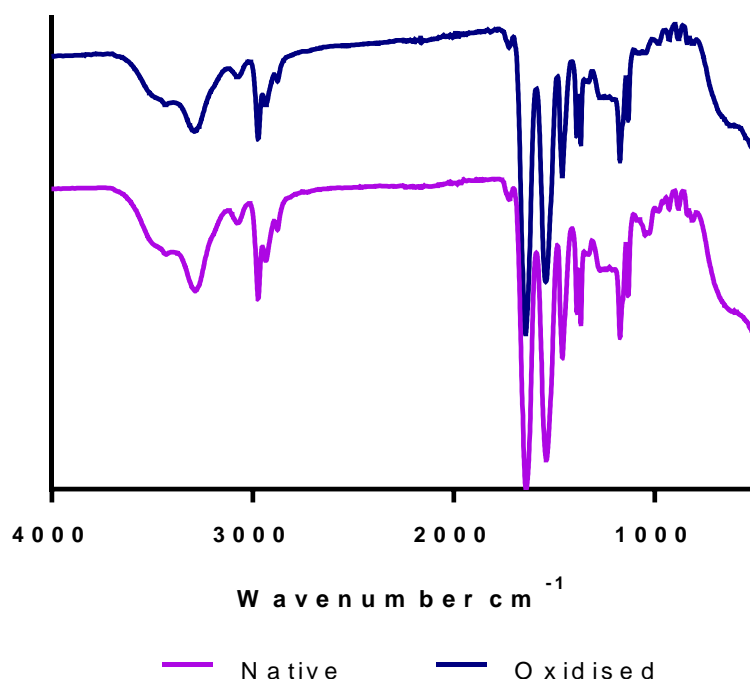


Figure 3.16 - A comparison of the IR spectra before and after oxidation with 15 mM H_2O_2 , of pNIPAM-MPP with a DP of 25. No obvious differences can be observed.

3.2.7. Oxidation using different concentrations of hydrogen peroxide

It was stated above that the concentrations of reactive oxygen species found in the body are much lower than 15 mM H_2O_2 that was tested here. Therefore, one of the polymers synthesised above, pNIPAM₂₅-MPP, was oxidised using various concentrations of H_2O_2 in DPBS. It was important to determine whether this RAFT chain end group effect was still as important under physiologically relevant conditions. It has been suggested in the literature that the concentration of H_2O_2 produced via an autoimmune response is approximately 50-100 μM .²⁷

Table 3.7 - A table giving the cloud point data for pNIPAM₂₅-MPP before and after oxidation with various concentrations of H_2O_2 . Analysis was repeated twice for each sample.

Conc. H_2O_2 mM	Avg. CP before [O] °C	Avg. CP after [O] °C	Δ °C
0.1	33.7 ± 0.2	32.3 ± 0.6	-1.4 ± 0.7
1	33.7 ± 0.2	32.5 ± 0.9	-1.2 ± 1.0
5	33.7 ± 0.2	33.0 ± 1.6	-0.7 ± 1.8
15	33.7 ± 0.2	37.4 ± 0.6	3.7 ± 0.7

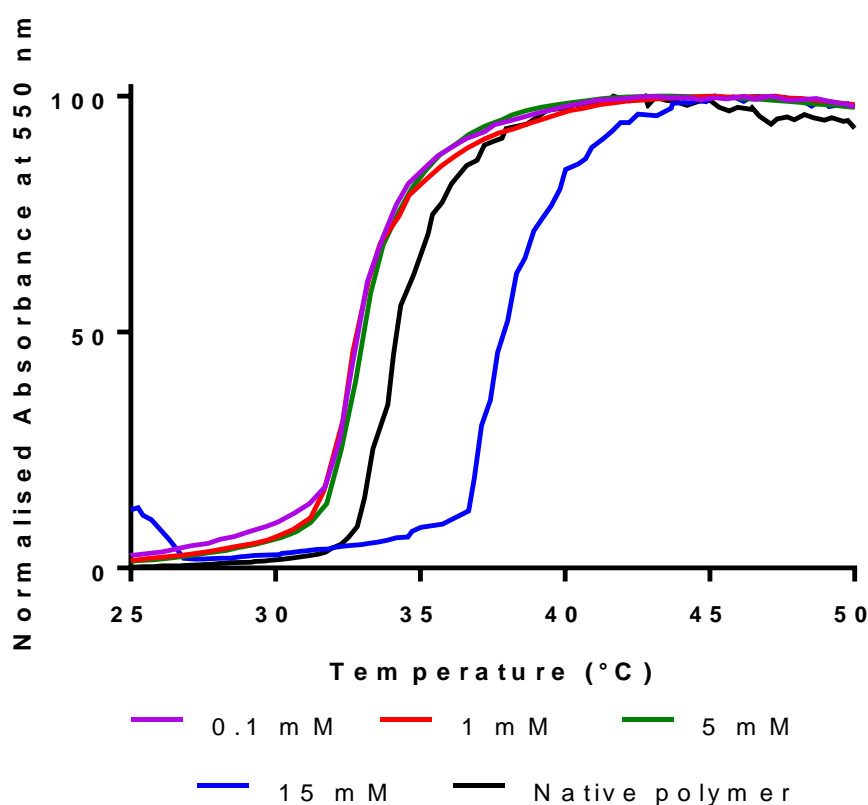


Figure 3.17 - Cloud point analysis at 550 nm of DP 25 pNIPAM-MPP before oxidation and after oxidation at a polymer concentration of 1 mg mL⁻¹, where the concentration of H₂O₂ has been varied.

The cloud point of the polymer was determined after oxidation with 0.1, 1 and 5 mM H₂O₂ (Figure 3.17). It can be seen from Table 3.7 that when the polymer is oxidised with 0.1, 1 and 5 mM there is little difference in the cloud point and that all cloud point measurements are very similar. These differ greatly when compared to the polymer oxidised with 15 mM H₂O₂, especially as the cloud point increases after oxidations whereas at lower concentration the cloud point decreases.

The mass spectrometry data before and after oxidation with 15 mM H₂O₂ of pNIPAM synthesised with the ethyl and butyl RAFT agents can be found in the appendices (Figure A.15, Figure A.16). Each oxidation product was run in both positive and negative mode and compared to the native polymer. These confirm that on oxidation with 15 mM H₂O₂, the major product is where the end group is transformed to a sulfonic acid end group. Also, the minor product is shown to be a change from a thiocarbonyl to a carbonyl.

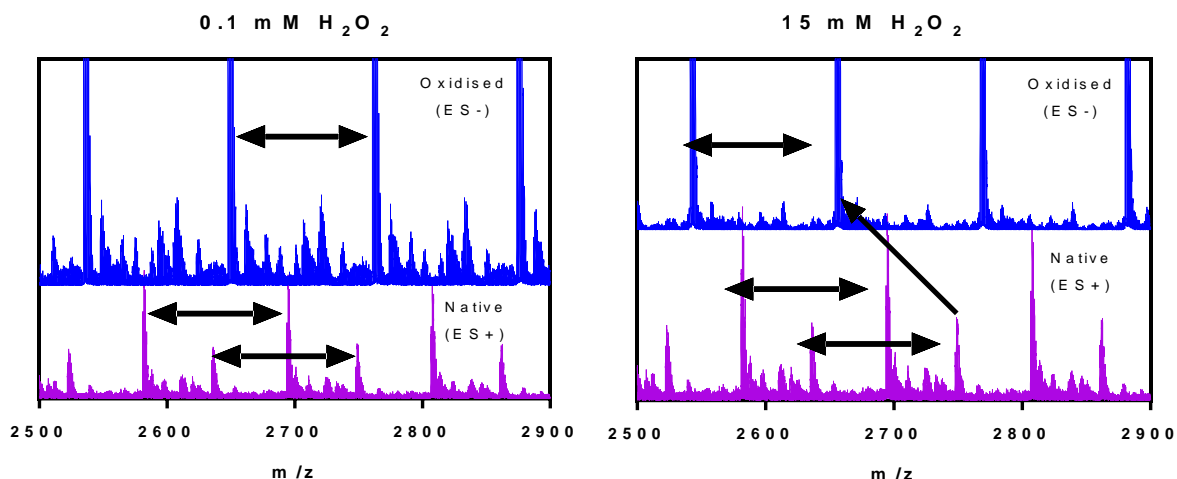


Figure 3.18 - Mass spectra of pNIPAM₂₅-MPP before and after oxidation with two different concentrations of H₂O₂, 0.1 and 15 mM. The double-headed arrow indicates NIPAM units and the single-headed arrow indicates the change from trithiocarbonate to a sulfonic acid end group.

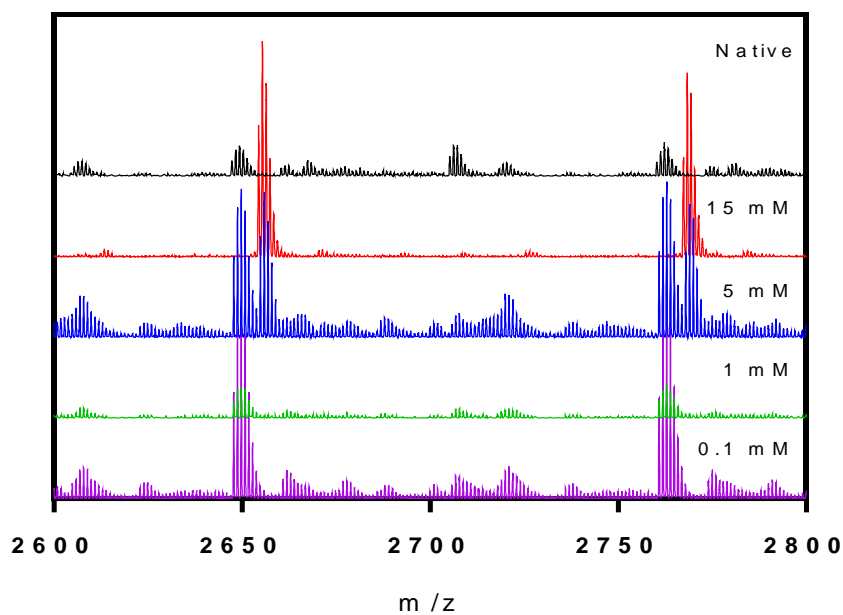


Figure 3.19 - Comparison of negative mode mass spectra of pNIPAM₂₅-MPP before and after oxidation with different concentrations of H₂O₂.

The different concentrations of H₂O₂ used could also affect the major product produced due to the oxidation. Therefore, MS was used again to compare the polymer before and after oxidation (Figure 3.18, Figure 3.19).

When comparing the MS of the highest concentration, 15 mM, with the lowest concentration, 0.1 mM, there is a large difference observed in the spectra (Figure 3.18). For the lower concentrations of hydrogen peroxide there are many peaks of low intensity, however it was not possible to determine with certainty what structures these result from. When compared to the native polymer there is a difference, however none of the peaks match any of the products which are expected from the literature. When higher concentrations of hydrogen peroxide were used, the peaks for the sulfonic acid end group are evident, as seen previously (Figure 3.18).

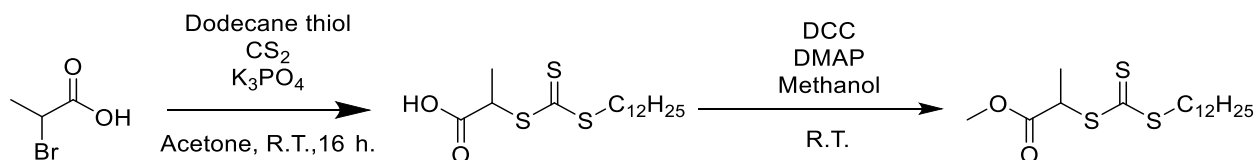
Figure 3.19 is a comparison of all the oxidised products in negative mode with the native polymer in negative mode. This ensures that the polymers can be directly compared in the same mode. From Figure 3.18, it is known where the peak for the sulfonic acid end group is observed, so by comparing all the spectra it is possible to determine which products have this peak. For concentrations of 0.1 and 1 mM, the spectra matches with the native polymer and therefore has little to no sulfonic acid end groups, whereas at a concentration of 15 mM, this appears to be the major product.

With a concentration of 5 mM hydrogen peroxide, although the sulfonic acid end group is apparent so is the peak seen for the native polymer. Although the intensities of these peaks look equivalent, their suitability for analysis in these conditions will vary so these cannot be directly compared. Unfortunately, due to the complexity of the mass spectra, it is not possible to analyse this with certainty.

Although an increase in cloud point is not seen as with the samples oxidised with 15 mM H₂O₂, this is not surprising as there have been reports in the literature that blends of different temperature responsive polymer do not necessarily change the cloud point.²⁸ Foralosso et al. used two different techniques to determine whether the aggregation temperatures of mixed and blended polymers could be controlled. The first was where two PLA-*b*-P(DEGMA)-*co*-(OEGMA)) polymers were blended together prior to the assembly of nanoparticles and one where preformed nanoparticles of different

polymers were mixed. They found in both cases there was no linear relationship between the ratios of polymers in the blended system and the critical aggregation temperature.²⁸

3.2.8. *Synthesis of pNIPAM via RAFT solution polymerisation using a more hydrophobic non-ionisable RAFT agent*



Scheme 3.2 - Synthesis of dodecyl based RAFT agent (MDDP) via the carboxylic acid

To further study the RAFT chain end group effect, pNIPAM synthesis was carried out using a more hydrophobic RAFT agent as the change to the hydrophilic nature of the end group should be more pronounced, causing a larger change in the cloud point. A dodecyl-based chain transfer agent, MDDP, was synthesised due to its similarity to the previously synthesised non-ionisable RAFT agents but it's much higher hydrophobicity (Scheme 3.2, Figures A.17-18).

MDDP was used to synthesise pNIPAM with three different targeted DPs; 25, 50 and 100, in the same way as above (Scheme 3.1). Although a DP 10 polymer was synthesised, it was not possible to determine the cloud point due to the increased hydrophobicity and therefore lack of water solubility. The kinetics of the polymerisation were monitored by ^1H NMR spectroscopy to determine the conversion of monomer to polymer with time. Controlled RAFT polymerisation using MDDP was shown to have similar reaction kinetics to that of the less hydrophobic RAFT agents using previously, reaching over 90% conversion after 90 minutes. GPC analysis of the kinetic samples show also show controlled polymerisation (Figure 3.20).

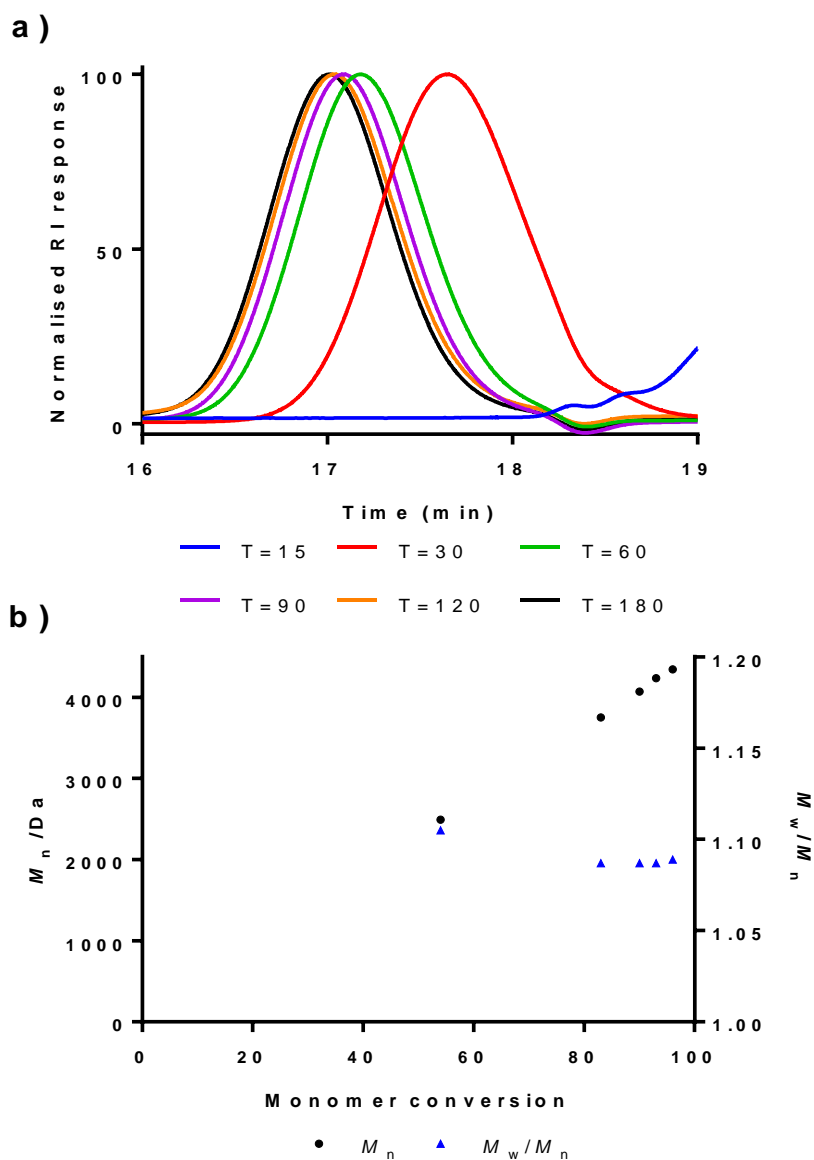


Figure 3.20 - a) GPC chromatograms (DMF 0.1% LiBr) of samples removed during the polymerisation of NIPAM (DP 21) using MDDP as the RAFT agent. M_n and M_w/M_n were determined relative to pMMA standards and b) Evolution of M_n and M_w/M_n with monomer conversion.

The polymers were purified by dialysis and analysed by NMR spectroscopy and GPC to determine the DP, M_n and dispersity of the polymer samples. The DP is very close to the targeted values and the GPC shows low dispersity as expected from RAFT polymerisation (Figure 3.21, Table 3.8).

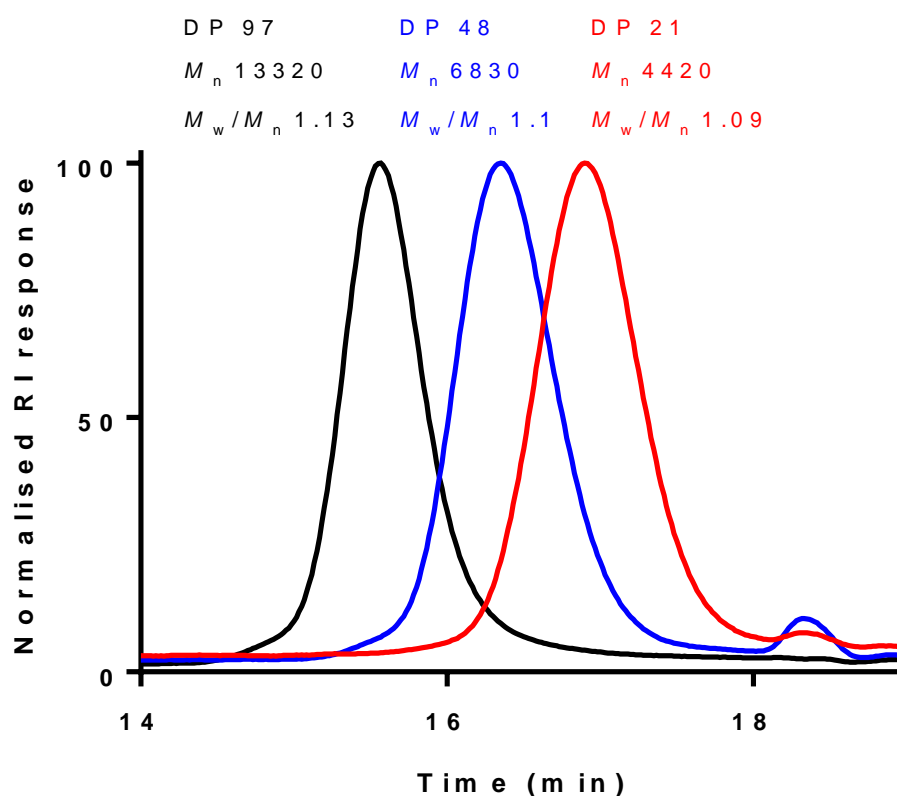


Figure 3.21 - GPC chromatograms (DMF 0.1% LiBr) for pNIPAM DP 21, 48 and 97 polymerised using MDDP as the RAFT agent

Table 3.8 - Conversion, DP and GPC data from the polymerisation of NIPAM using MDDP as the RAFT agent

[M]/[RAFT agent]	Conversion / X ^a	Theoretical DP ^b	M_n / Da ^c	DP _n ^a	M_n / Da ^d	M_w/M_n ^d
26	96	25	3080	21	4420	1.09
50	96	48	5800	48	6830	1.10
99	93	92	10890	97	13320	1.13

^a Determined by ¹H NMR spectroscopy in CDCl₃. ^b [M]/[RAFT agent]*conv. ^c Theoretical M_n from ¹H NMR spectroscopy. ^d Determined by GPC in DMF (0.1% LiBr) with pMMA standards.

It was expected that, due to the longer alkyl chain on the RAFT agent, the polymer would be more hydrophobic. On oxidation, from the above research, it was expected that the trithiocarbonate would become a sulfonic acid group, removing the long alkyl chain and cause a much larger difference in the cloud point. The polymers were oxidised as before with 15 mM H₂O₂ in DPBS, and cloud points were determined using an automatic melting point apparatus and temperature-controlled UV-vis spectroscopy (Figure 3.22a). There is very little change in the cloud point on

oxidation when compared to the native polymer. Although this was anticipated for the longer chain polymers, a large change was expected for the DP 25 polymer. To ensure that a large proportion of the RAFT chain end groups had been oxidised all three samples were oxidised again but using 100 mM H₂O₂ in DPBS and reanalysed (Figure 3.22b).

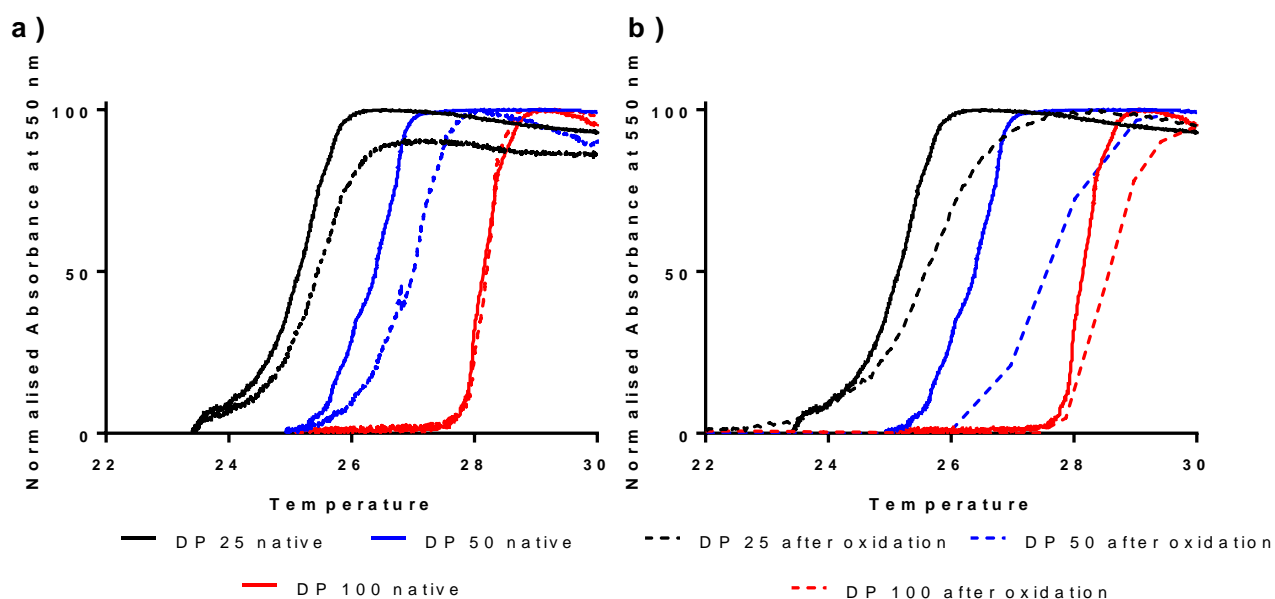


Figure 3.22 - Graphs showing the difference in cloud point between native pNIPAM and polymer oxidised with a) 15 mM H₂O₂ and b) 100 mM H₂O₂

Table 3.9 - Cloud point data from before and after the oxidation of pNIPAM with 15 mM and 100 mM H₂O₂. Analysis was repeated twice for each sample.

DP _n ^a	Avg. CP before [O] °C	Avg. CP after [O] °C	
		15 mM H ₂ O ₂	100 mM H ₂ O ₂
21	25.0 ± 0.7	25.2 ± 0.3	25.1 ± 0.6
48	26.3 ± 0.5	26.6 ± 0.2	27.0 ± 0.1
97	28.2 ± 0.2	28.1 ± 0.2	27.6 ± 0.5

^a Determined by ¹H NMR spectroscopy in CDCl₃.

Oxidation, even with a higher concentration of H₂O₂ had very little effect on the cloud point of the polymer. There are many instances in the literature where a polymer with a long alkyl chain and

therefore hydrophobic end group, self-assemble.^{29,30,31} This could explain the small change in cloud point on oxidation however DLS did not show any stable assembled structures at 15 °C (Figure 3.23).

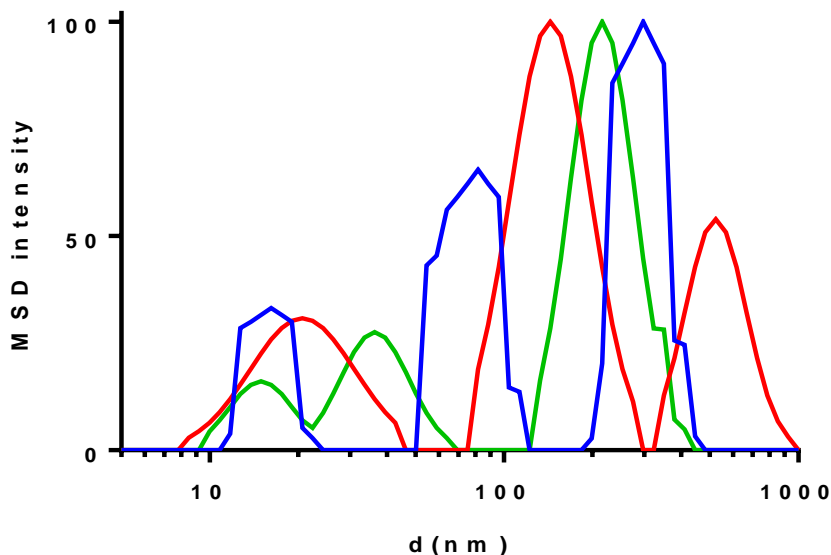


Figure 3.23 – DLS chromatograms (DMF 0.1% LiBr) of pNIPAM₂₅-MDDP at a concentration of 0.1 wt% in water at 15 °C. All 3 traces are different measurements at the same temperature of the same polymer to determine where self-assembly occurs. No stable self-assembly of these pseudo-amphiphilic polymers is observed with no overlap between traces.

Oxidation of the polymer did alter the colour of the dried solid sample from yellow to a white powder. This suggests that some chemical changes had taken place. To determine what this was, IR spectroscopy was used. If there was a change in functional groups in the RAFT chain end groups as anticipated by our previous work and other studies published in the literature, it may be possible to see by comparing IR spectroscopy of the native and oxidised samples. Using the DP 21 polymer of NIPAM, there is no obvious change in the IR spectrum after oxidation (Figure 3.24).

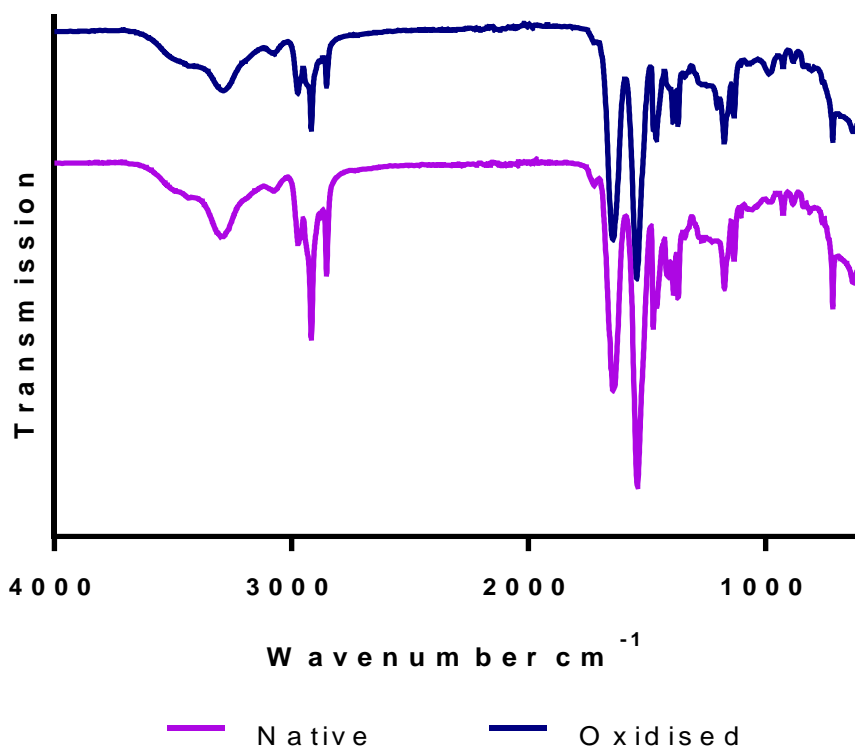


Figure 3.24 - A comparison of the IR spectra before and after oxidation of pNIPAM-MDDP with a DP of 21

The same polymer was analysed by MS before and after oxidation in both positive and negative mode to determine the effect of oxidation on the end group of the polymer. As was observed for the above polymers of NIPAM, the largest gaps between the peaks in the spectra are indicative of a unit of NIPAM (113.16 Da). Mass spectrometry data for the oxidised polymer was collected in both positive and negative mode to enable all potential oxidation products to be analysed (Figure 3.25). Due to the complex nature of this data, it was very difficult to determine all peaks with certainty, however a detailed table with all expected peaks was produced (Table 3.10).

The spectra of the oxidised polymer in positive mode is very similar to that of the native polymer. However, in the negative mode spectra, there are small peaks which are of interest. When comparing the spectra before oxidation (positive mode) to the spectra after oxidation (negative mode), the presence of a sulfonic acid group can be seen, however there are many other peaks of similar intensity which have not been determined. Therefore, on oxidation, the same product is seen

as above. Due to the complexity of the mass spectra, and the low intensity of many peaks, it is difficult to glean more information on what the product of oxidation might be.

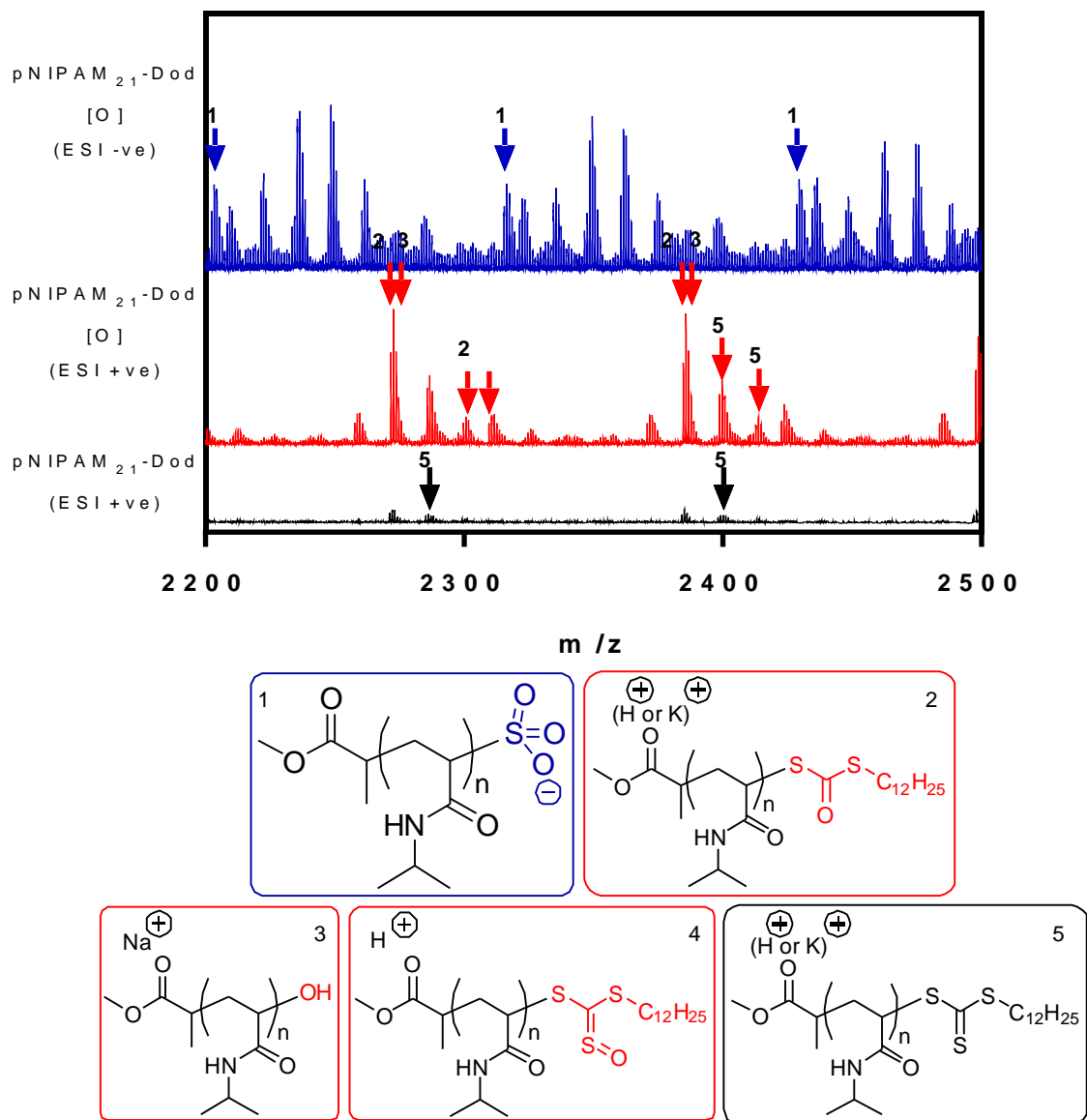
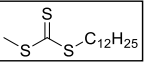
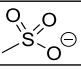
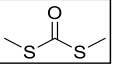
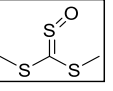
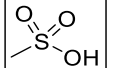
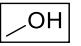


Figure 3.25 - Mass spectra of pNIPAM₂₁-MDDP before and after oxidation with 15 mM H₂O₂. The single-headed arrows indicate potential known products.^{5-7,32}

Table 3.10 -Detailed summary of expected mass spectrum peaks from oxidation of the RAFT chain end group of pNIPAM₂₁-MDDP and annotation with those seen in figure 2.25.

Native (+ mode)						Oxid (- mode)						Native +	
No charge	H	Na	K	No charge		No charge	Oxid -	Oxid +					
DP20	2625.84	2626.84	2648.83	2664.8	DP20	2428.68	DP20						
DP19	2512.76	2513.76	2535.75	2551.72	DP19	2315.6	DP19						
DP18	2399.68	2400.68	2422.67	2438.64	DP18	2202.52	DP18						
DP17	2286.6	2287.6	2309.59	2325.56									

Oxid (+ mode)						Oxid (+ mode)					
No charge	H	Na	K	No charge		H	Na	K			
DP20	2609.862	2610.87	2632.85	2648.82	DP20	2641.832	2642.84	2664.82	2680.8		
DP19	2496.782	2497.79	2519.77	2535.74	DP19	2528.752	2529.76	2551.74	2567.72		
DP18	2383.702	2384.71	2406.69	2422.66	DP18	2415.672	2416.68	2438.66	2454.64		
	2270.622	2271.63	2293.61	2309.58	DP17	2302.592	2303.6	2325.58	2341.56		

Oxid (+ mode)						Oxid (+ mode)					
No charge	H	Na	K	No charge		H	Na	K			
DP20	2429.69	2430.7	2452.68	2468.65	DP21	2478.81	2479.82	2501.8	2517.77		
DP19	2316.61	2317.62	2339.6	2355.57	DP20	2365.73	2366.74	2388.72	2404.69		
DP18	2203.53	2204.54	2226.52	2242.49	DP19	2252.65	2253.66	2275.64	2291.61		

It can be concluded that for the polymers of NIPAM synthesised using MDDP, a dodecyl-based RAFT agent, no change in cloud point is seen on oxidation, no self-assembly is observed by DLS due to the hydrophobic alkyl group and it is difficult to determine the oxidation products by IR spectroscopy and mass spectrometry. Therefore, the cleavage of the RAFT chain end group by oxidation may not be useful for the formation of oxidation responsive drug delivery systems.

3.3. Conclusion

Overall this chapter has shown that it is possible to alter the cloud point and therefore LCST of short chain polymers of NIPAM by oxidation of the RAFT chain end group. For example, a polymer of NIPAM synthesised with MPP and a DP of 8, has a difference in the cloud point of the native polymer and the oxidised polymer of 9.3 °C. The oxidation causes cleavage of the Z group of the RAFT agent converting the trithiocarbonate to a sulfonic acid group as the major product, changing the hydrophobicity of the polymer. As expected, this effect is greater for shorter chain polymers as the ratio of polymer to RAFT chain transfer agent is lower. When using RAFT chain transfer agents with a longer alkyl chain however, the same effects are not seen. The LCST changes but only minimally

which means it would not have the same properties on oxidation that some of the RAFT agents with shorter alkyl chains exhibit. Oxidation does have some effect on the chemical structure however, but it is difficult to determine what this change is and therefore the influence it has on the polymer.

Unfortunately, most linear homo-polymers are not useful for the encapsulation and delivery of drugs. They are unable to self-assemble in aqueous media as they do not exhibit an amphiphilic nature. Although there are reports in the literature of this behaviour being observed when the RAFT chain end group is hydrophobic in nature compared to the polymer chain, from the studies above it can be seen that this assembly is unstable.

Therefore, this work was utilised when designing diblock copolymers; using the short alkyl chain RAFT agents studied in this chapter, to form self-assembled copolymers capable of encapsulation. There is potential that if the second block is a short chain of pNIPAM, oxidation of the RAFT chain end group will be enough to increase the LCST. This will make the hydrophobic pNIPAM block hydrophilic, removing the amphiphilic nature needed for assembly, causing disassembly and release of any encapsulated materials.

3.4. References

- 1 S. Grund, M. Bauer and D. Fischer, *Adv. Eng. Mater.*, 2011, **13**, B61–B67.
- 2 J. Chiefari, Y. K. B. Chong, F. Ercole, J. Krstina, J. Jeffery, T. P. T. Le, R. T. A. Mayadunne, G. F. Meijs, C. L. Moad, G. Moad, E. Rizzardo, S. H. Thang and C. South, *Macromolecules*, 1998, **31**, 5559–5562.
- 3 J. Eliassaf, *J. Appl. Polym. Sci.*, 1978, **22**, 873–874.
- 4 H. G. Schild, *Prog. Polym. Sci.*, 1992, **17**, 163–249.
- 5 R. Pfukwa, G. Pound and B. Klumperman, *Polym. Prepr.*, 2008, **49**, 117–118.
- 6 P. Vana, L. Albertin, L. Barner, T. P. Davis and C. Barner-Kowollik, *J. Polym. Sci. Part A Polym. Chem.*, 2002, **40**, 4032–4037.
- 7 C. P. Jesson, C. M. Pearce, H. Simon, A. Werner, V. J. Cunningham, J. R. Lovett, M. J. Smallridge, N. J. Warren and S. P. Armes, *Macromolecules*, 2017, **50**, 182–191.
- 8 S. S. Perrier, P. Takolpuckdee and C. A. Mars, *Macromolecules*, 2005, **38**, 2033–2036.
- 9 V. A. Bhanu and K. Kishore, *Chem. Rev.*, 2005, **91**, 99–117.
- 10 S. Furyk, Y. Zhang, D. Ortiz-Acosta, P. S. Cremer and D. E. Bergbreiter, *J. Polym. Sci. Part A Polym. Chem.*, 2006, **44**, 1492–1501.
- 11 X. Qiu, T. Koga, F. Tanaka and F. M. Winnik, *Sci. China Chem.*, 2013, **56**, 56–64.
- 12 Z. Liu, Q. Liao, D. Yang, Y. Gao, X. Luo, Z. Lei and H. Li, *Des. Monomers Polym.*, 2013, **16**, 465–474.
- 13 Y. Xia, N. A. D. Burke and H. D. H. Stöver, *Macromolecules*, 2006, **39**, 2275–2283.
- 14 D. J. Keddie, G. Moad, E. Rizzardo and S. H. Thang, *Macromolecules*, 2012, **45**, 5321–5342.
- 15 G. Moad, *Polym. Chem.*, 2017, **8**, 177–219.
- 16 Y.-J. Pan, Y.-Y. Chen, D.-R. Wang, C. Wei, J. Guo, D.-R. Lu, C.-C. Chu and C.-C. Wang, *Biomaterials*, 2012, **33**, 6570–9.
- 17 Y. Wu, H. Kuang, Z. Xie, X. Chen, X. Jing and Y. Huang, *Polym. Chem.*, 2014, **5**, 4488–4498.
- 18 Q. Duan, Y. Miura, A. Narumi, X. Shen, S.-I. Sato, T. Satoh and T. Kakuchi, *J. Polym. Sci. Part A*

- Polym. Chem.*, 2006, **44**, 1117–1124.
- 19 Q. Wang, Y. Zhong, W. Liu, Z. Wang, L. Gu and X. Li, *Drug Deliv.*, 2019, **26**, 12–22.
- 20 H. Du, R. Wickramasinghe and X. Qian, *J. Phys. Chem. B*, 2010, **114**, 16594–16604.
- 21 R. Freitag and F. Garret-Flaudy, *Langmuir*, 2002, **18**, 3434–3440.
- 22 P. Liu, J. Liang, S. Chen and H. Zhang, *RSC Adv.*, 2014, **4**, 49028–49039.
- 23 I. Bischofberger and V. Trappe, *Sci. Rep.*, 2015, **5**, 1–10.
- 24 Y. Okada and F. Tanaka, *Macromolecules*, 2005, **38**, 4465–4471.
- 25 A. Milewska, J. Szydłowski and L. P. N. Rebelo, *J. Polym. Sci. Part B Polym. Phys.*, 2003, **41**, 1219–1233.
- 26 G. M. Lampman, D. L. Pavia, G. S. Kriz and J. R. Vyvyan, *Spectroscopy*, Brooks/Cole, Cengage Learning, Belmont, 4th edn., 2010.
- 27 C. De Gracia Lux, S. Joshi-Barr, T. Nguyen, E. Mahmoud, E. Schopf, N. Fomina and A. Almutairi, *J. Am. Chem. Soc.*, 2012, **134**, 15758–15764.
- 28 R. Foralosso, L. Moir, F. Mastrotto, L. Sasso, A. Tchoryk, A. Selo, A. Grabowska, M. B. Ashford, J. Aylott, P. R. Gellert, S. G. Spain and C. Alexander, *Soft Matter*, 2017, **13**, 7441–7452.
- 29 Y. Zhu, L. Liu and J. Du, *Macromolecules*, 2013, **46**, 194–203.
- 30 J. Du, H. Willcock, J. P. Patterson, I. Portman and R. K. O'Reilly, *Small*, 2011, **7**, 2070–2080.
- 31 J. Y. T. Chong, D. J. Keddie, A. Postma, X. Mulet, B. J. Boyd and C. J. Drummond, *Colloids Surfaces A Physicochem. Eng. Asp.*, 2015, **470**, 60–69.
- 32 T. J. Adley, A. K. M. Anisuzzaman and L. N. Owen, *J. Chem. Soc. C Org.*, 1967, 807.

Appendix A

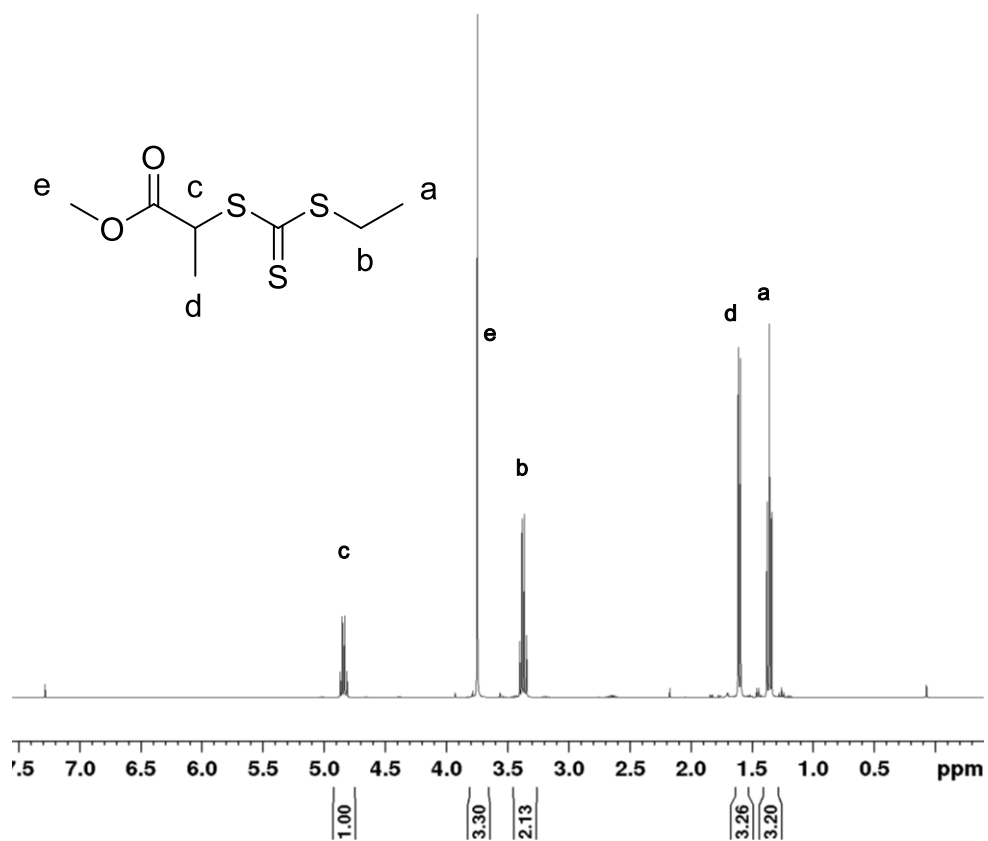


Figure A.1 - ^1H NMR spectrum of EMEM RAFT agent recorded in CDCl_3

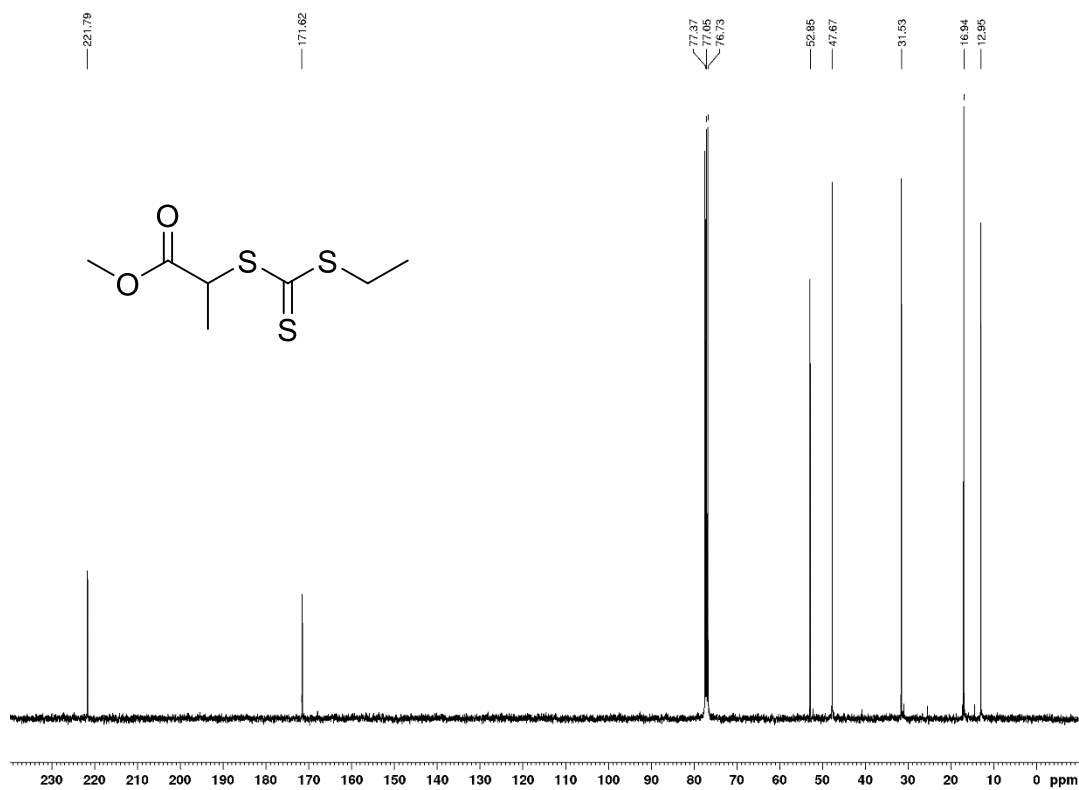


Figure A.2 - ^{13}C NMR spectrum of EMEM RAFT agent recorded in CDCl_3

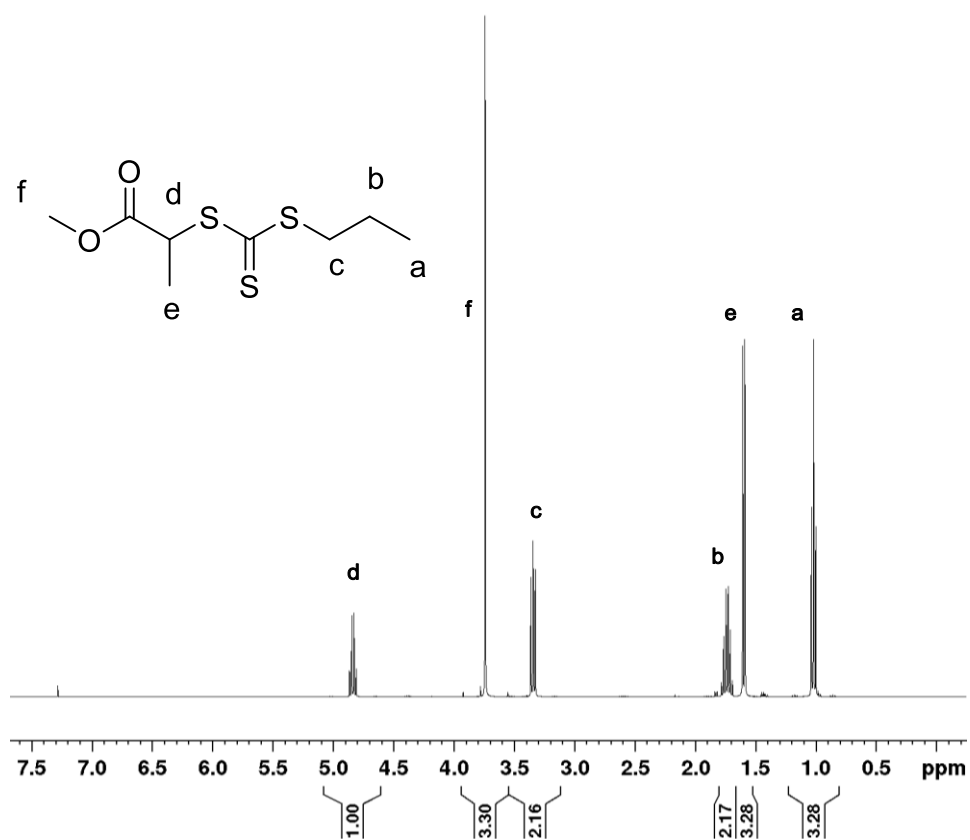


Figure A.3- ¹H NMR spectrum of MPP RAFT agent recorded in CDCl₃



Figure A.4 – ¹³C NMR spectrum of MPP RAFT agent recorded in CDCl₃

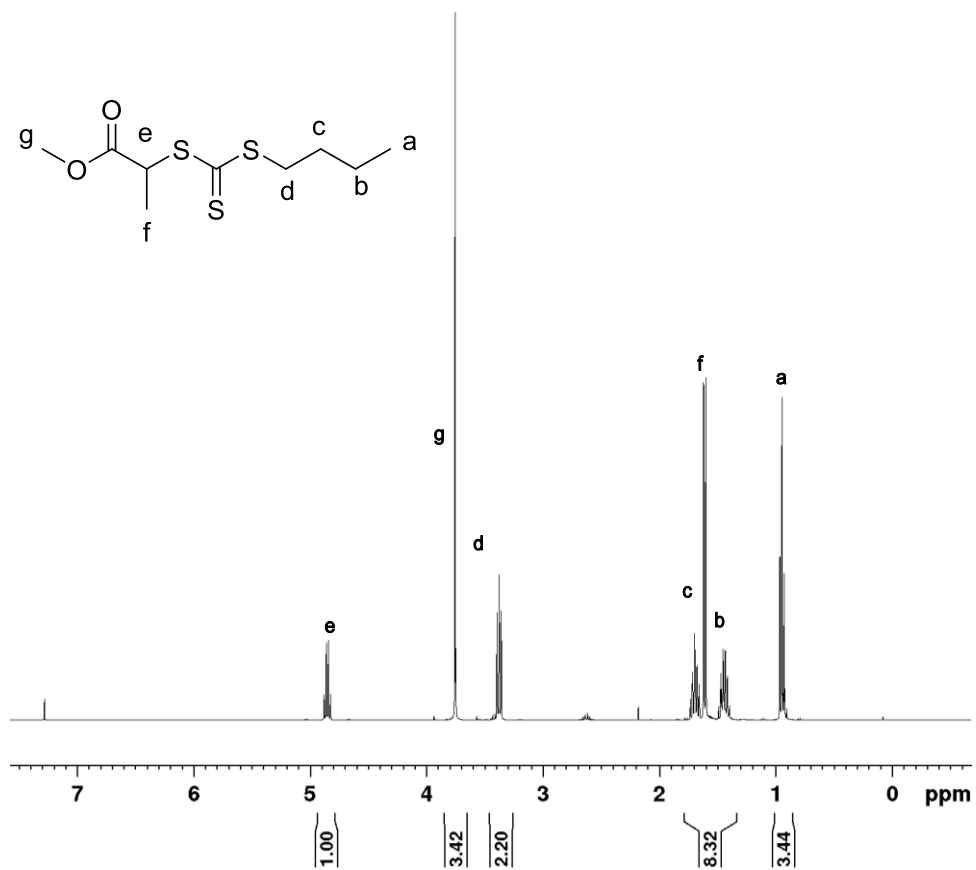


Figure A.5 - ^1H NMR spectrum of MBP RAFT agent recorded in

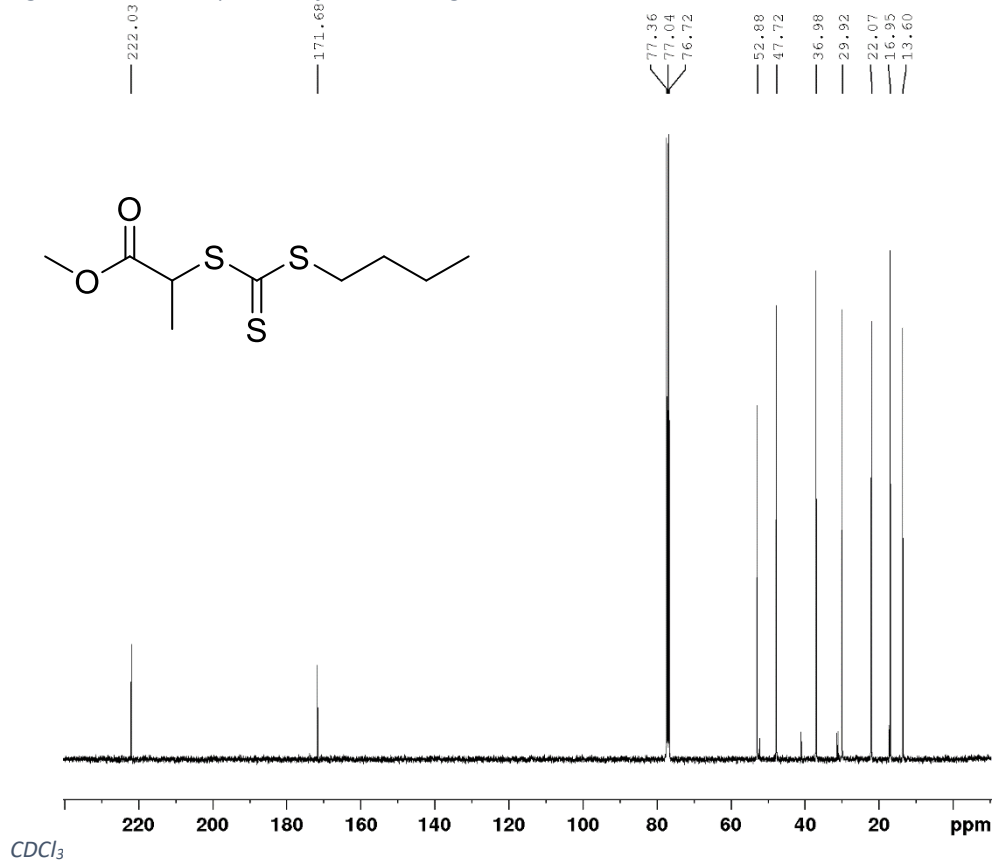


Figure A.6 - ^{13}C NMR spectrum of MBP RAFT agent recorded in CDCl_3

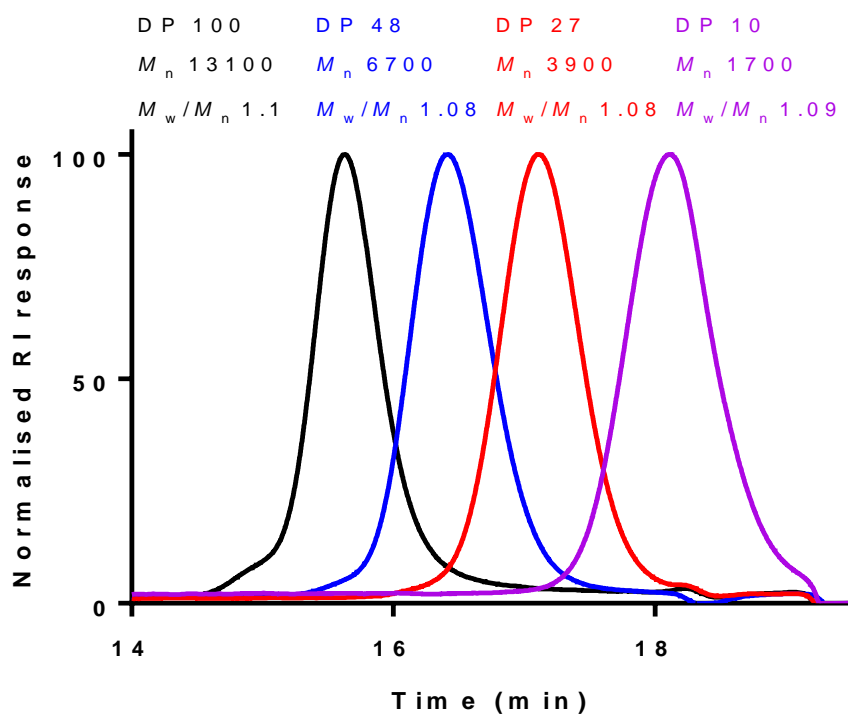


Figure A.7 - GPC trace of DP 10, 27, 48 and 100 pNIPAM synthesised using EMEM as the RAFT agent.

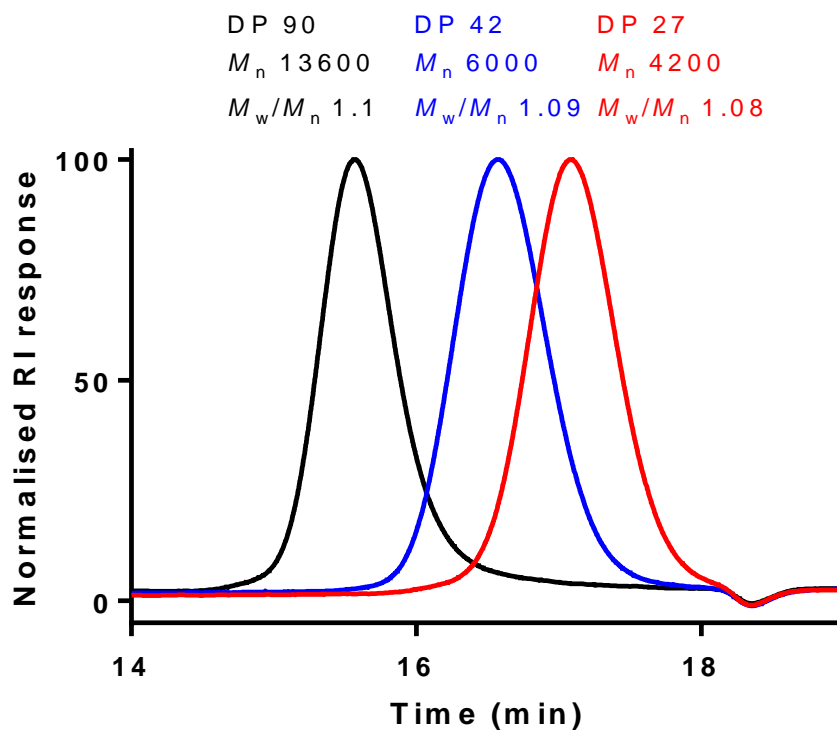


Figure A.8 - GPC trace of DP 27, 42 and 90 pNIPAM synthesised using MBP as the RAFT agent.

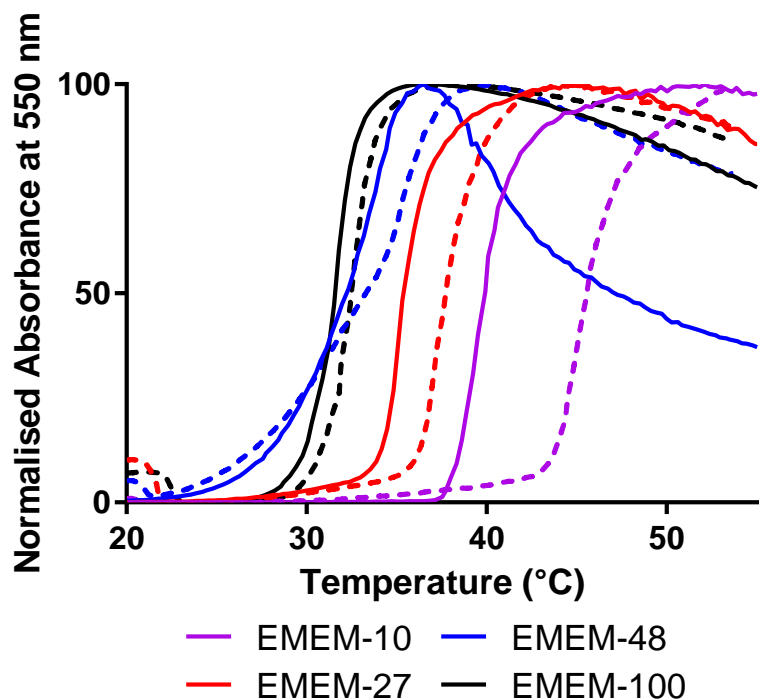


Figure A.9 - UV/vis traces giving the cloud point of pNIPAM polymers synthesised using the EMEM chain transfer agent before and after oxidation. The cloud point was determined with a polymer concentration of 1 mg mL^{-1} in water at a wavelength of 550 nm. The solid lines indicate polymers before oxidation and the dashed lines represent the polymers after oxidation.

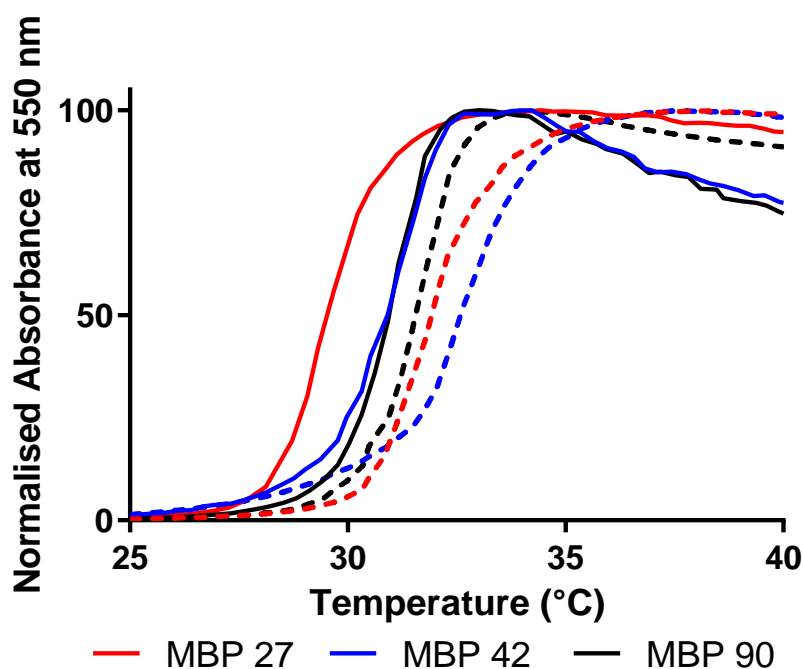


Figure A.10 - UV/vis traces giving the cloud point of pNIPAM polymers synthesised using the MBP chain transfer agent before and after oxidation. The cloud point was determined with a polymer concentration of 1 mg mL^{-1} in water at a wavelength of 550 nm. The solid lines indicate polymers before oxidation and the dashed lines represent the polymers after oxidation.

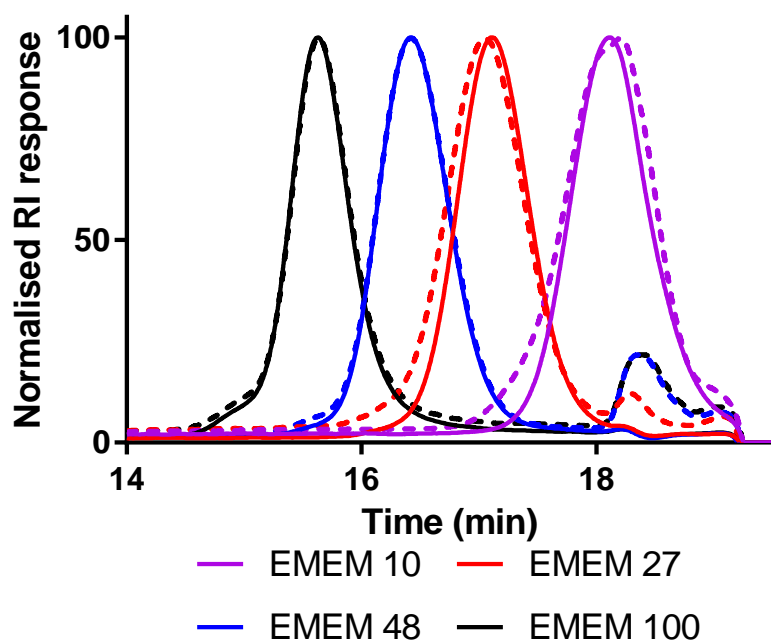


Figure A.11 - Comparison of the GPC traces before and after oxidation of pNIPAM-EMEM. The solid lines indicate polymers before oxidation and the dashed lines represent the polymers after oxidation.

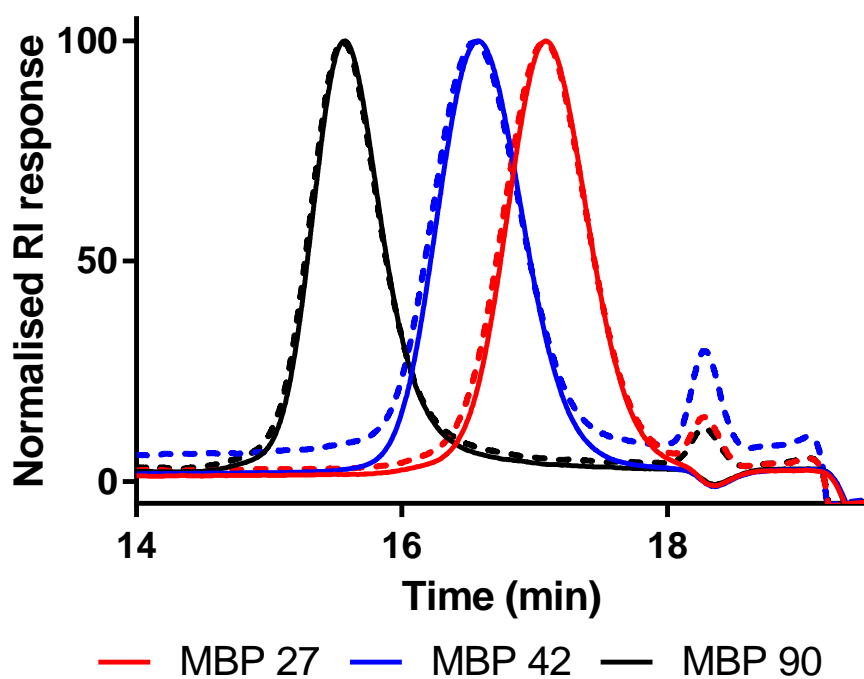


Figure A.12 - Comparison of the GPC traces before and after oxidation of pNIPAM-MBP. The solid lines indicate polymers before oxidation and the dashed lines represent the polymers after oxidation.

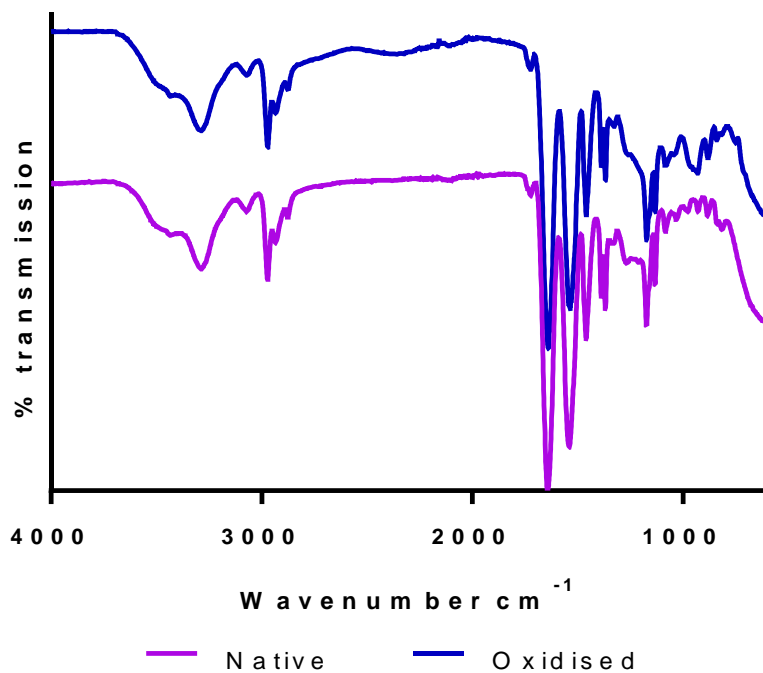


Figure A.13 - A comparison of the IR spectra before and after oxidation of pNIPAM-EMEM with a DP of 22

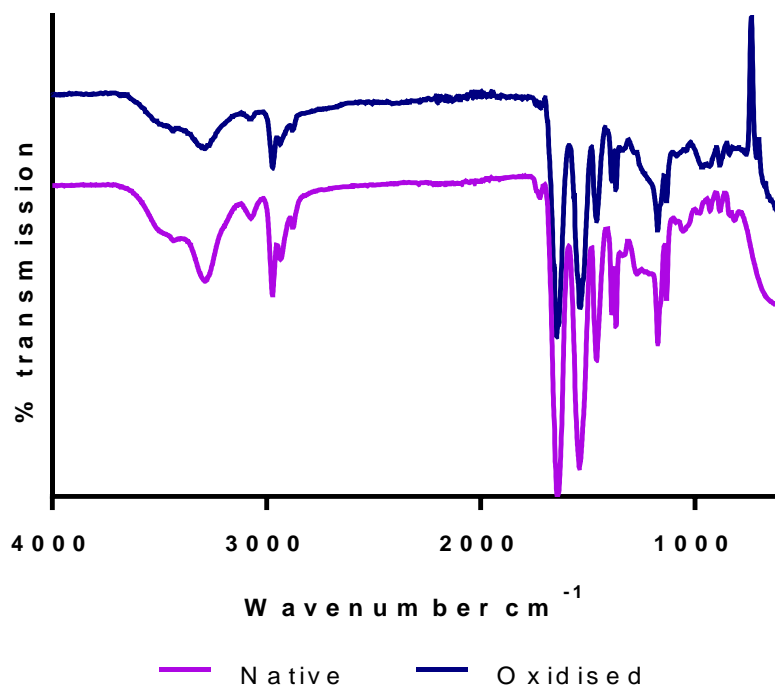


Figure A.14 - A comparison of the IR spectra before and after oxidation of pNIPAM-MBP with a DP of 26

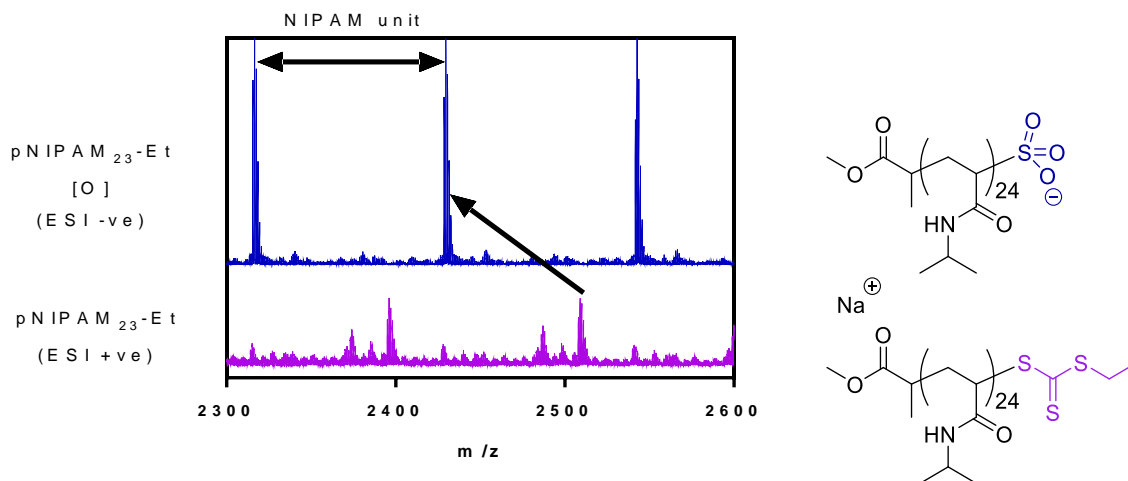


Figure A.15 - Comparison of mass spectra data of pNIPAM₂₃-EMEM before and after oxidation in ES+ and ES- respectively

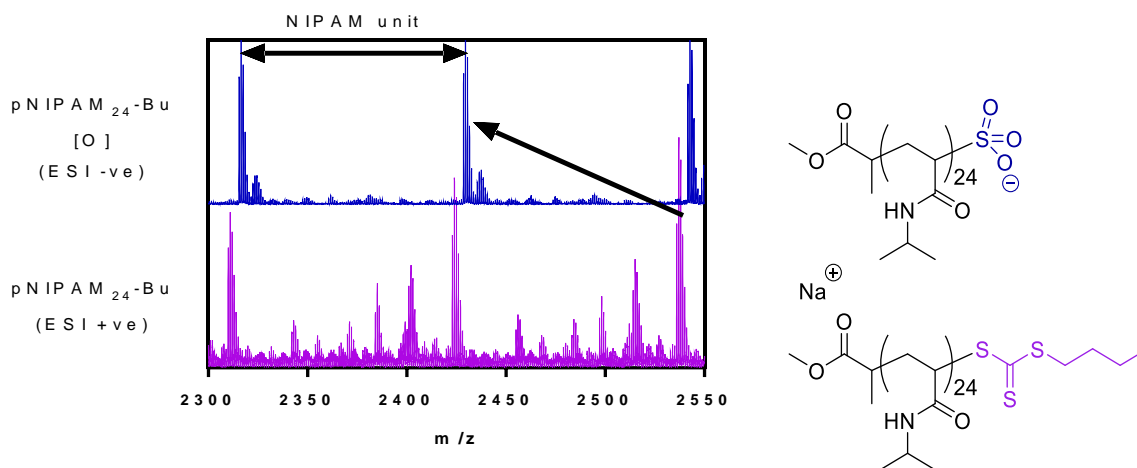


Figure A.16 - Comparison of mass spectra data of pNIPAM₂₄-MBP before and after oxidation in ES+ and ES- respectively.

Chapter 3: Utilisation of the RAFT chain end group as an oxidation sensitive trigger

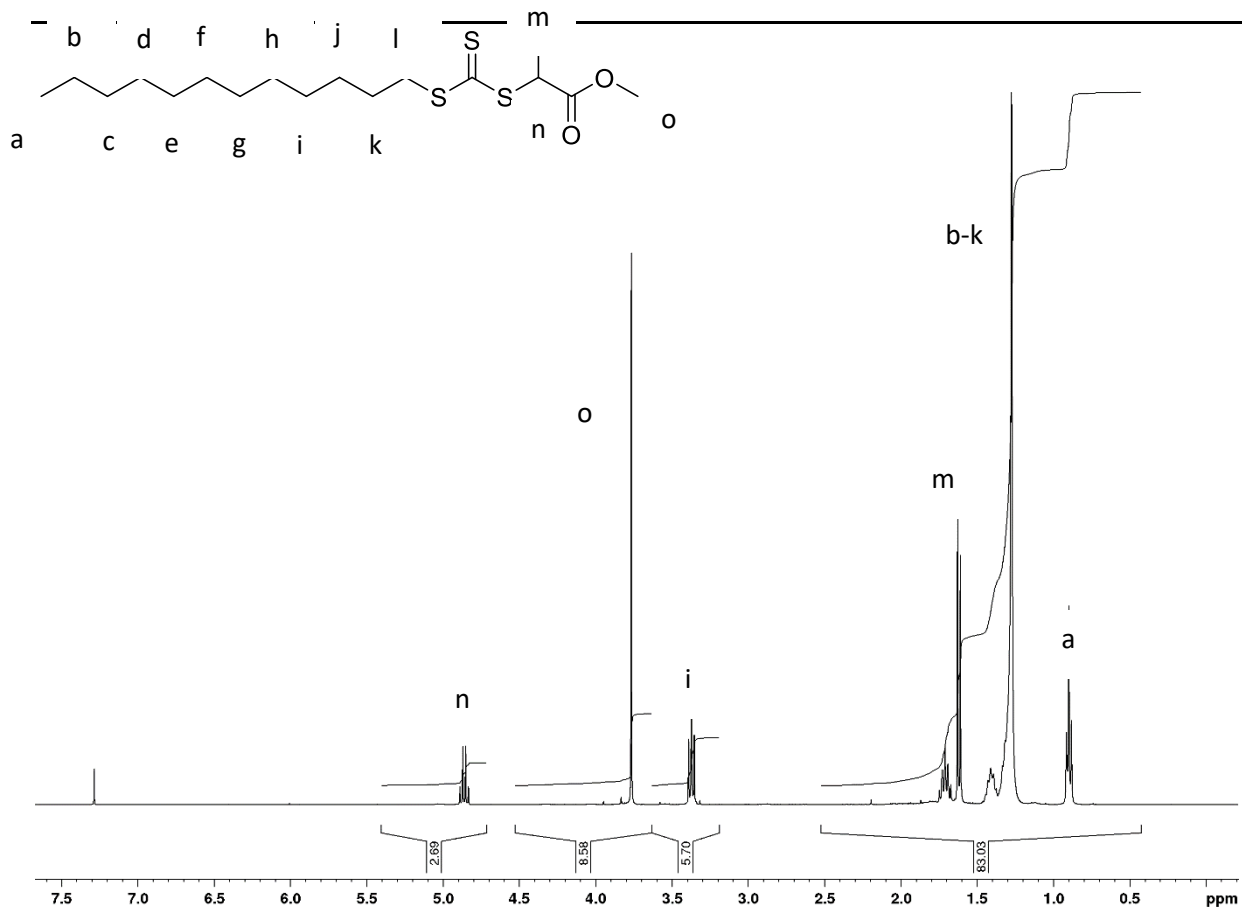


Figure A.17 - ¹H NMR spectrum of MDDP RAFT agent recorded in CDCl₃

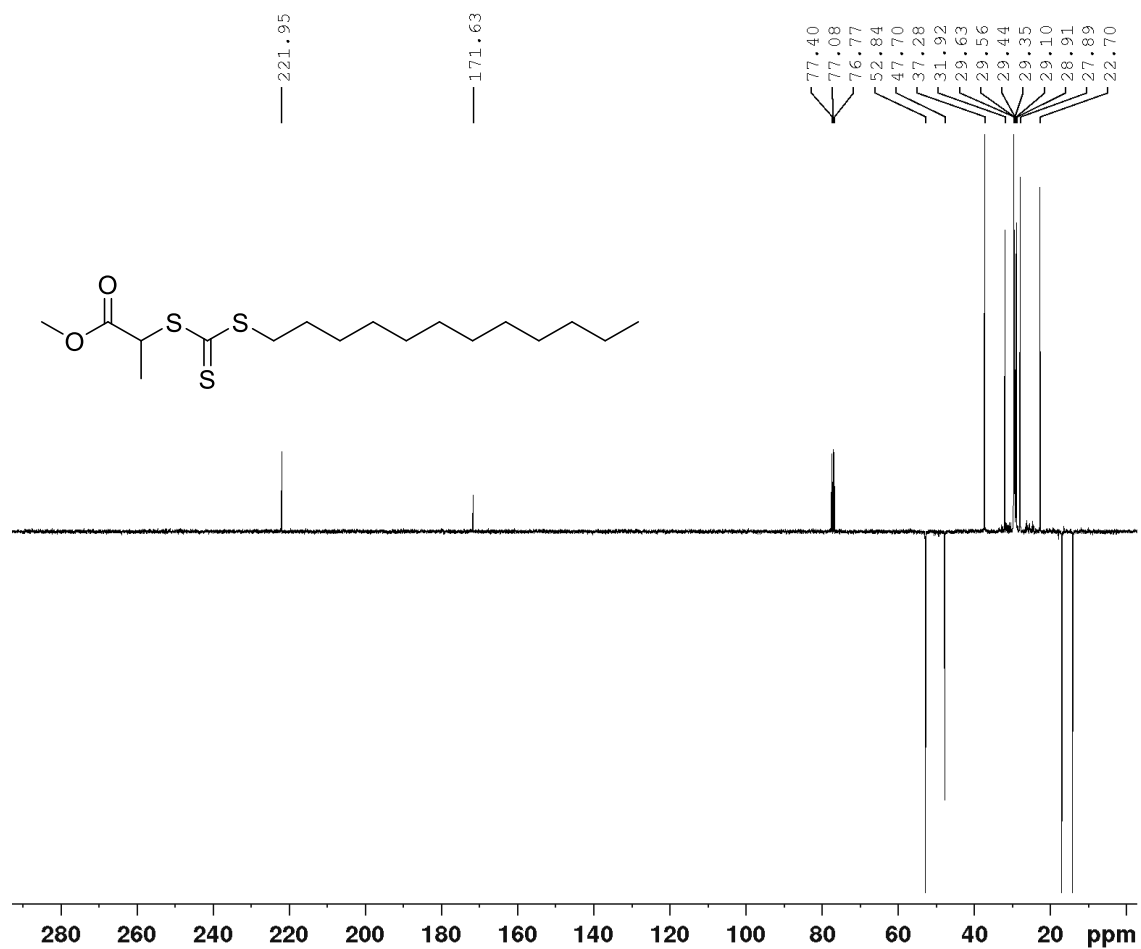


Figure A.18 – ^{13}C NMR spectrum of MDDP RAFT agent recorded in CDCl_3

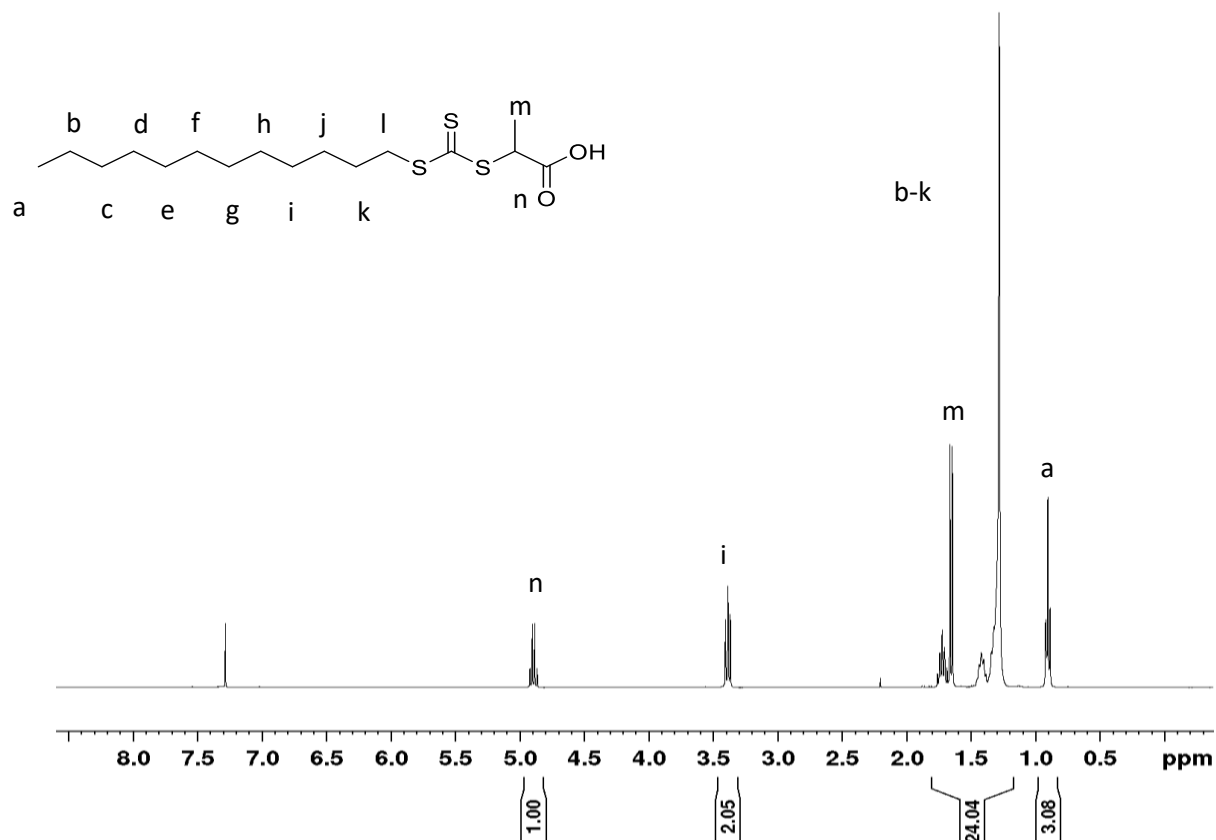


Figure A.19 – ^1H NMR spectrum of MDDP acid RAFT agent recorded in CDCl_3

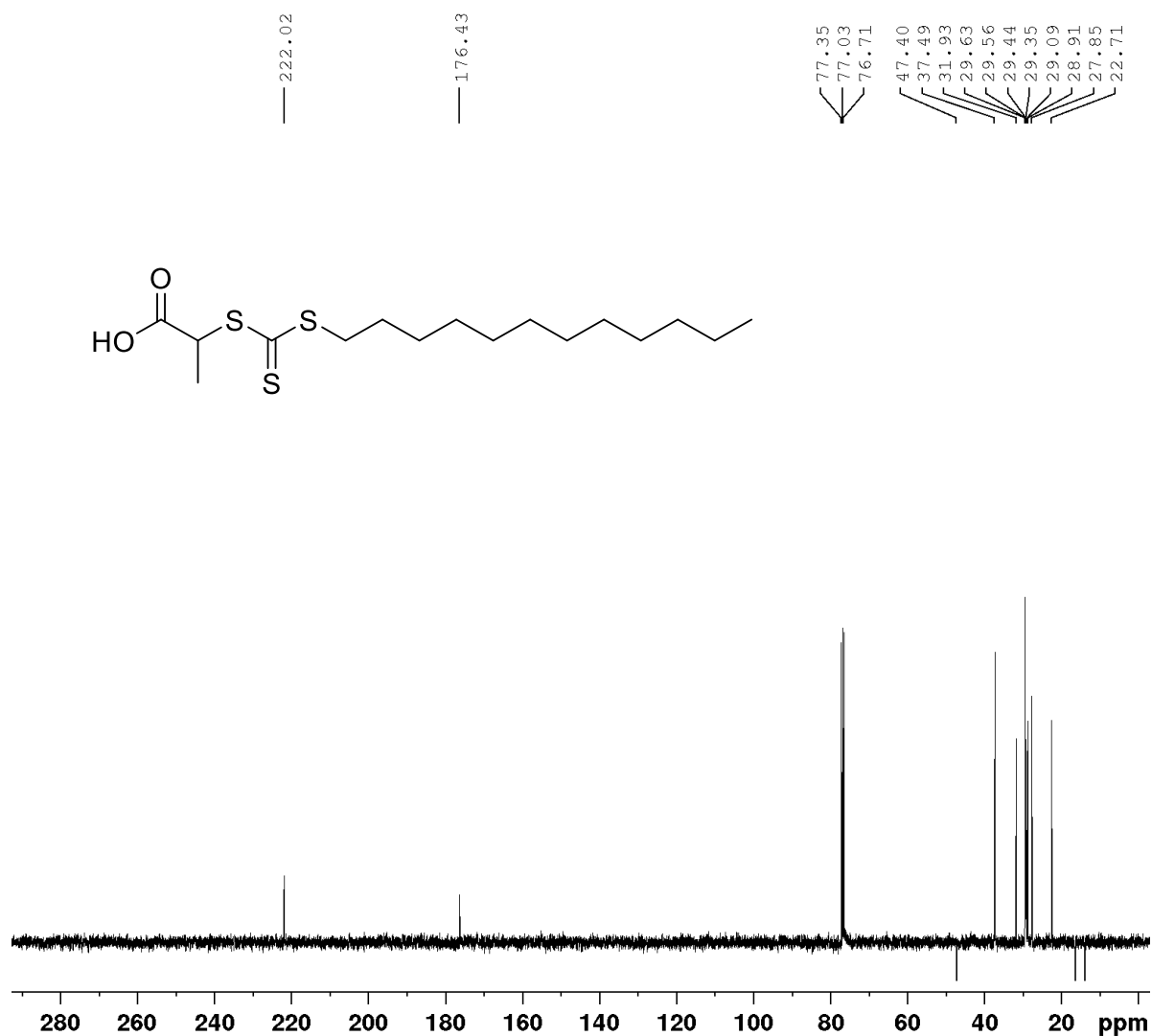


Figure A.20 - ^{13}C NMR spectrum of MDDP acid RAFT agent recorded in CDCl_3

Chapter Four

4 Oxidation-responsive block copolymer micelles of poly(*N*-(2-hydroxyethyl)acrylamide)-*b*-poly(*N*-isopropylacrylamide)

4.1. Introduction

For a successful polymeric drug delivery system (DDS) a drug must be conjugated to, or encapsulated within, a polymer system with minimal release before the drug reaches the target site. Polymers can be synthesised which have amphiphilic character, one block being hydrophilic and one hydrophobic. These self-assemble in an aqueous environment forming micelles. Free drugs generally are hydrophobic and have poor solubility.¹ Amphiphilic polymers have benefits when compared to these as the outer shell is hydrophilic, masking the hydrophobic nature of the core.

The characteristics of polymer micelles which make them suitable for drug delivery systems are their small size, usually 10-200 nm, the presence of the hydrophilic stabilising block which prevents phagocytic attack, high drug loading capacity, tuneable stability and morphology through block type and length, ease and reproducibility of the synthesis and the ability to incorporate stimuli response.²⁻⁴

In diblock copolymers, the hydrophobic block acts as the core and the hydrophilic block is the shell which provides stability to the structure. A drug can be encapsulated within the hydrophobic core of the polymer and transported around the body until it is stimulated to release the drug at the target site. The benefit of having a drug encapsulated within the core of the DDS is that the shell can protect the core from protein adsorption and other non-specific interactions, reduces immune response and minimises diffusion into tissues. It has also been suggested that the core can be stabilised by adding small hydrophobic molecules, such as drugs, as these can fill gaps between the chains causing a strengthening of the intermolecular associations.⁴ Due to all of the above features, alongside masking the polymer from hydration of the surface, the half-life in the blood is prolonged compared to the free drug.⁴

Making block copolymer systems via RAFT polymerisation has many advantages. The chain length and therefore molecular weight, can be controlled, which affects the morphology of the self-assembled structure and also the method of clearance from the body.⁵⁻⁸ By keeping the molecular

weight of the polymer chains at <45 kDa, it is possible to minimise accumulation of the DDS within the tissues and organs of the body, and also enables renal clearance, however it is important to note that accumulation due to non-biodegradable polymers, such as polyvinylpyrrolidone (PVP) has been seen for molecular weights between 25 and 40 kDa.⁹ The morphology of the particle also influences the clearance from the body, with spherical particles being cleared from the body much faster than rods or elongated structures, yet it is spherical particles which exhibit a larger stability due to their lowest surface energy.^{10,11}

There has been a lot of research published on micelles as drug delivery systems, especially those which respond to certain stimuli. Many have shown successful results from encapsulation and release studies, as well as showing minimal toxicity in both in vivo and in vitro studies. In one study, micelles of poly(propylene sulfide)-*b*-pNIPAM are formed. Poly(propylene sulfide) is oxidation-responsive, changing from a hydrophobic thioether group to a hydrophilic sulfoxide or sulfone (dependent on the oxidant), which affects the assembly of the micelles. It also exhibits a temperature response from the pNIPAM block, where the corona collapses at body temperature. These micelles showed promising results for the delivery and release of the drug doxorubicin (DOX) inside cells.¹² Another example of dual-responsive polymeric micelles is a temperature and pH responsive system described by Hiruta et al.¹³ This consisted of a temperature responsive corona of p(NIPAM-*stat*-*N,N*-dimethylacrylamide) and a pH responsive core segment of poly[2-(*N,N*-diisopropylamino)ethyl methacrylate], which can encapsulate DOX on assembly. The temperature responsive behaviour enables local-heating to be used to enhance cellular uptake due to collapse of the pNIPAM-based corona. Once inside tumour cells, the reduced pH of the endosome causes the core of the polymer to become protonated and this change in charge causes disassembly of the micelle and release of DOX.

The polymeric systems in this chapter draw on conclusions from the previous chapter to create a dual stimuli responsive system which responds to both temperature and oxidation. A water-soluble

poly(*N*-(2-hydroxyethyl)acrylamide) (pHEA) block is synthesised and then extended with NIPAM to form the hydrophobic block of the polymer. As pNIPAM exhibits an LCST, its solubility in water is temperature dependent. Therefore, this is an example of a pseudo-amphiphilic system as it will only self-assemble above the LCST of the pNIPAM block. There are some micellar systems which incorporate pNIPAM into a diblock copolymer with a hydrophobic block.¹⁴ In these systems the pNIPAM block acts as the shell as it is hydrophilic.

However, pNIPAM can also be the core-forming block of self-assembled structures. This is beneficial for drug loading capabilities as the polymer can be purified and added into an aqueous drug solution. On heating to temperatures above the LCST, micelles will form, encapsulating the drug within these.

To build from the research from Chapter 2, diblock copolymers with a short pNIPAM block were synthesised to study their assembly behaviour and how this changes on oxidation of the RAFT chain end group. As seen in Chapter 2, this change in end group caused an increase in the LCST, meaning that the oxidised polymer is more hydrophilic than the native polymer. If the pNIPAM block becomes more hydrophilic, disassembly will occur due to the solvation of both blocks. Polymers with longer pNIPAM block lengths were also synthesised, incorporating oxidation responsive moieties, to further tune the LCST behaviour to aid drug encapsulation and storage in a clinical situation.

4.2. Results and Discussion

4.2.1. Forming diblock copolymers with a short pNIPAM block to induce a change in cloud point large enough to disrupt self-assembly

From chapter 2, it is seen that the LCST of pNIPAM can be changed by oxidation of the RAFT chain end groups. As diblock copolymers require both a hydrophobic and hydrophilic block to self-assemble, they will only self-assemble above the LCST of the pNIPAM block. Oxidation must change the temperature of the LCST to a higher value, meaning that at body temperature (37 °C) self-assembly will no longer occur after oxidation. This can be adjusted if needed by the addition of other functional groups/monomers into the polymeric system. When making self-assembled structures the oxidation of the RAFT chain end group could have the ability to cause the hydrophobic block to become hydrophilic due to the change in LCST and solubilise the chains. This could in turn release any encapsulation material (Figure 4.1).

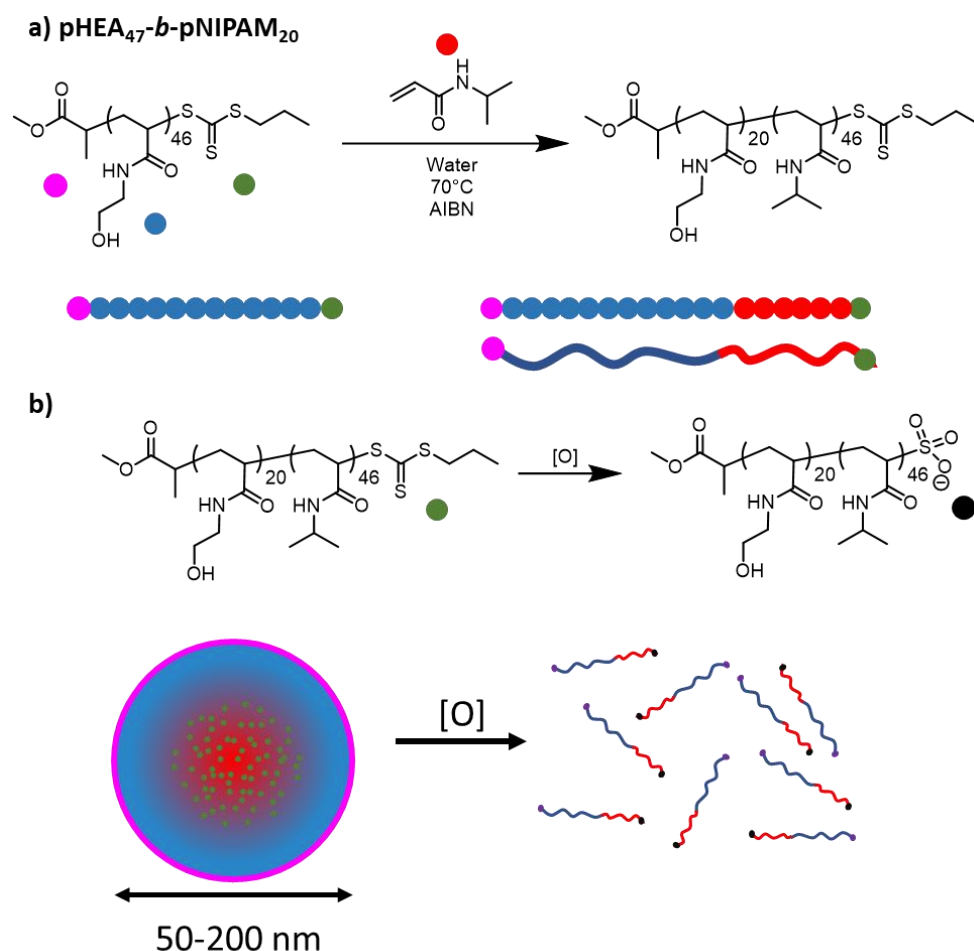


Figure 4.1 - a) The synthesis of pHEA-b-pNIPAM using the RAFT agent MPP as an example, defining where the RAFT chain end groups are bound to the polymer chains, b) The expected result on oxidation of the self-assembled polymer showing disassembly due to the chain in the RAFT chain end group bound to the pNIPAM block

4.2.1.1. Diblock copolymers using polymers of N-(2-hydroxyethyl)acrylamide as macro-chain transfer agents

To test the above hypothesis, three block copolymers were synthesised using the same RAFT agents as previous studies on linear polymers of NIPAM. The temperature responsive block had a target molecular weight of around 3000 Da, in order to maintain the temperature responsive behaviour observed in Chapter 2. First, a suitable macro-CTA to form the hydrophilic block of the polymer is needed. This is necessary as the block copolymer must be amphiphilic in nature to cause self-assembly in an aqueous environment, and at body temperature, pNIPAM is hydrophobic. N-(2-hydroxyethyl)acrylamide (HEA) was chosen as it polymerises with good control via RAFT solution

polymerisation, meaning that it is possible to target a specific degree of polymerisation with a high degree of accuracy.^{15,16,17}

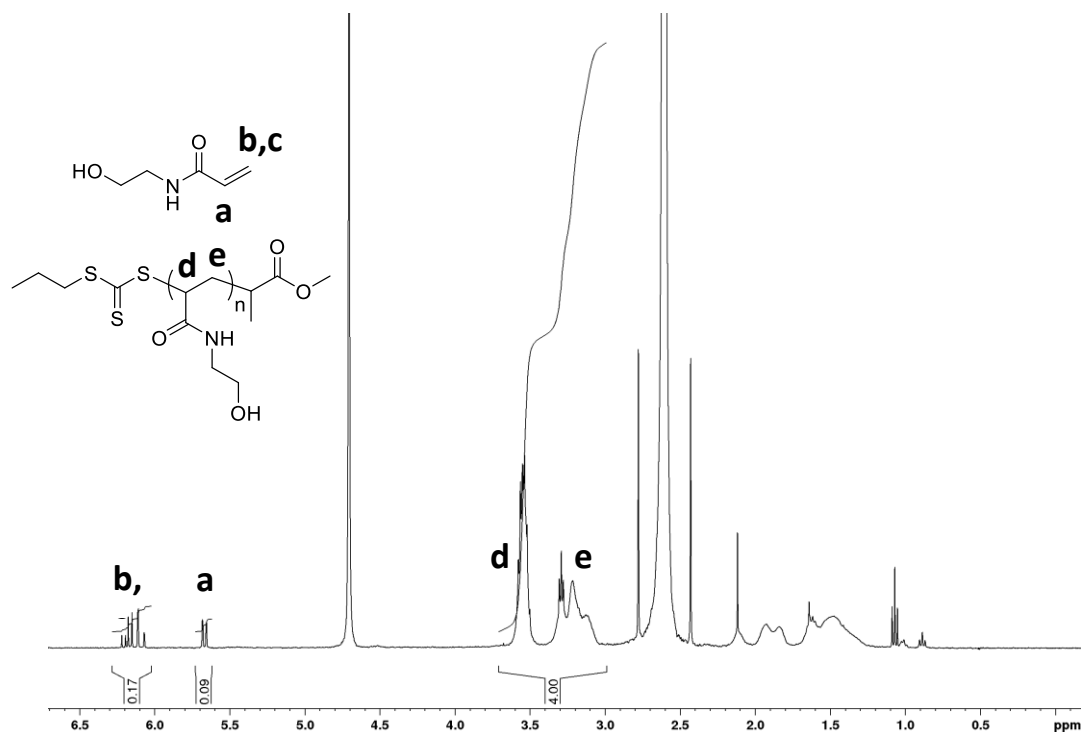


Figure 4.2 - A ^1H NMR spectrum of pHEA-MPP (target DP 50) in D_2O 90 minutes into the reaction to determine the monomer to polymer conversion. The ratio of total protons seen in both monomer and polymer (d and e) and those in the monomer only (a, b and c) can be used to determine the actual DP.

A kinetic study of the polymerisation of HEA was conducted so that the DP could be accurately targeted. Samples were taken from the polymerisation at various intervals and analysed by analysed by ^1H NMR spectroscopy and GPC until 300 minutes into the polymerisation. For the NMR spectra the conversion can be determined by comparing the remaining monomer vinyl peaks with peaks which are seen in both the monomer and polymer to determine the conversion (Figure 4.2). By comparing the peaks labelled d and e, which are present in both the polymer and monomer, to the peaks labelled a, b and c, which are the vinyl protons on the monomer, the conversion can be determined. The reaction behaves as pseudo-first order until 90 minutes where the conversion plateaus at 98%, which is expected as it will no longer follow the steady state approximation (Figure 4.3).

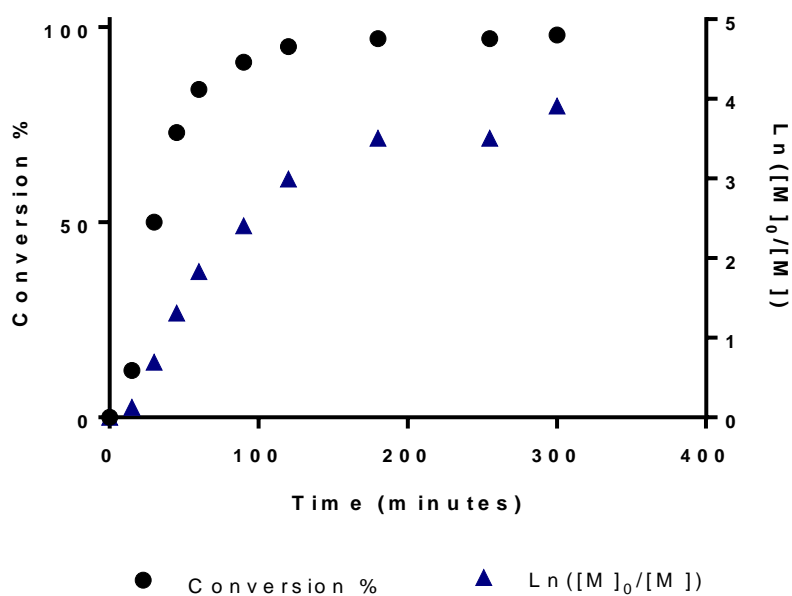


Figure 4.3 - Monomer conversion and pseudo-first order kinetic plot for the polymerisation of HEA (targeted DP 50) using MPP as the RAFT agent. Monomer conversion was determined by ^1H NMR spectroscopy.

Samples were also analysed by GPC and molecular weights were found to increase linearly and while the dispersity plateaus at 50% conversion with a final value of around 1.15 (Figure 4.4).

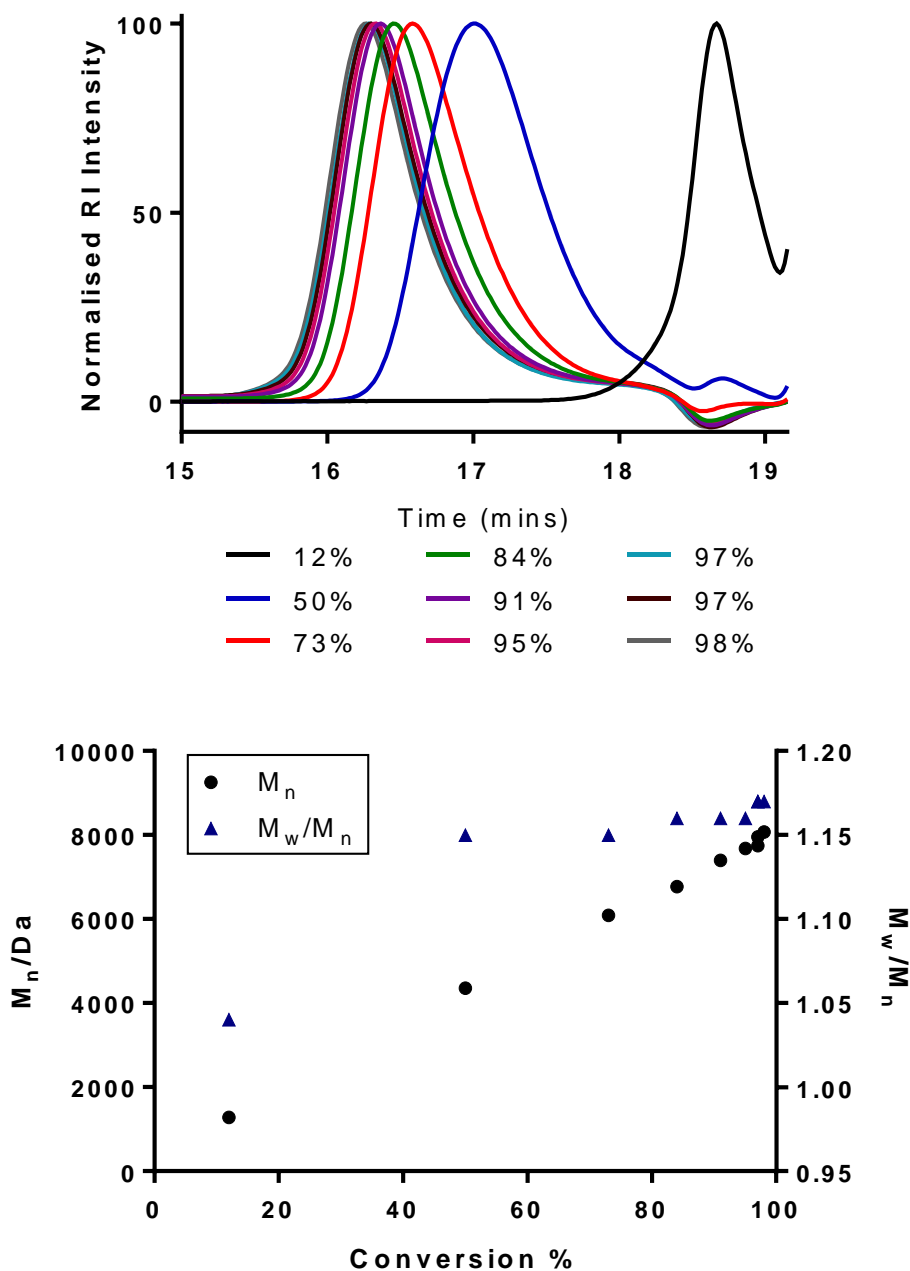
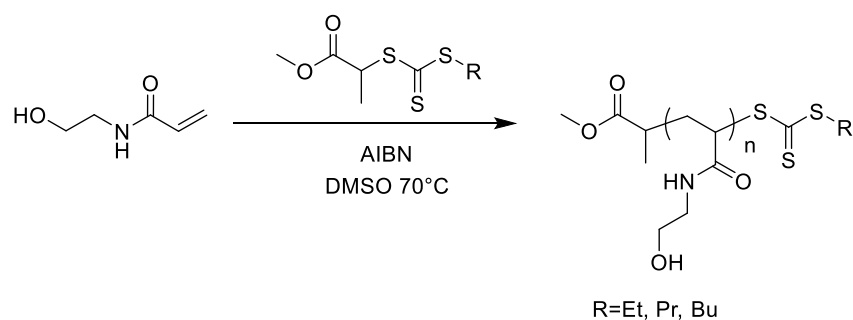


Figure 4.4 – a) GPC chromatograms (DMF 0.1% LiBr) of samples removed during the polymerisation of HEA (DP 50) using MPP as the RAFT agent. M_n and M_w/M_n were determined relative to pMMA standards and b) Comparison of the monomer conversion with M_n and M_w/M_n .

HEA was polymerised by RAFT polymerisation with EMEM, MPP and MBP RAFT agents to give an approximate DP of 60 (Scheme 4.1).



Scheme 4.1 - Synthesis of pHEA-mCTA via RAFT dispersion polymerisation

These were then used as macro-CTAs and chain extended with NIPAM to form a core block with approximately 25 NIPAM units. This length was chosen as with short pNIPAM chains, oxidation was seen to have a large effect on the LCST and, therefore, would hopefully cause disassembly of any self-assembled structures formed, ultimately leading to drug release if used as a drug delivery system (Table 4.1).

The pHEA macro-CTAs was purified by dilution with methanol and precipitation from acetone. The precipitate was collected by centrifugation and the polymer was dissolved in water before dialysis against distilled water and then freeze dried to give a yellow powder.

Table 4.1 – Analytical data for pHEA-mCTAs synthesised using EMEM, MPP and MBP RAFT agents

RAFT agent	[M]/[RAFT agent]	Conv. / % ^a	DP _{n, thr.} ^b	M _n / Da ^c	DP _n ^c	M _n / Da ^d	M _w /M _n ^d
EMEM	60	81	49	4980	42	11740	1.08
MPP	60	76	46	5560	47	10290	1.09
MBP	60	82	49	5910	50	11110	1.09

^a Determined by ¹H NMR spectroscopy in D₂O. ^b [M]/[RAFT agent] × conv. ^c M_n calculated from ¹H NMR spectroscopy. ^d Determined by GPC in DMF (0.1% LiBr) with pMMA standards.

The kinetic studies showed this to be a fast reaction, reaching over 80% conversion after 60 minutes. Using the above information, three pHEA-mCTAs were synthesised using three different RAFT agents; EMEM, MPP and MBP with a targeted DP of 50 assuming that after 45 minutes the monomer to polymer conversion is 80%, as seen during the reaction kinetics above. For all RAFT agents used,

the actual DP, as determined by ^1H NMR spectroscopy, was similar to this at 48, 46 and 49, respectively and the GPC data correlated with the expected DP (Table 4.1, Figure 4.5). In all cases, the M_w/M_n was less than 1.1 indicating good control of the polymerisation.

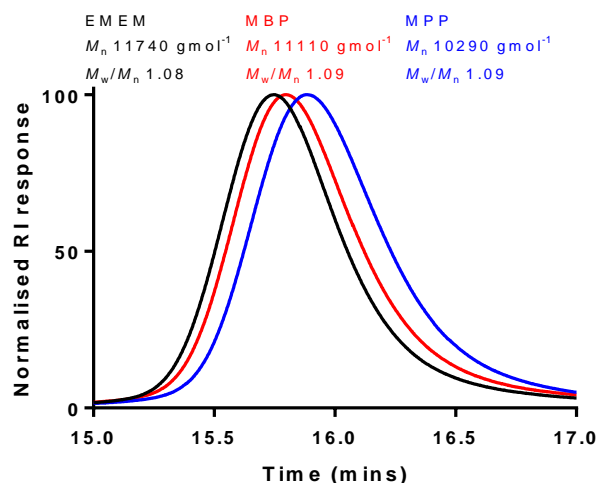
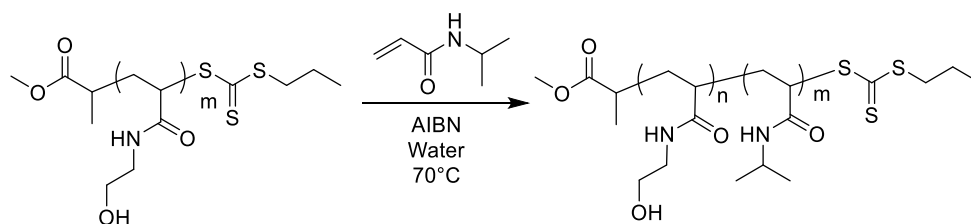


Figure 4.5 - GPC chromatograms (DMF 0.1% LiBr) of pHEA-mCTAs synthesised using 3 different RAFT agents.



Scheme 4.2 - Chain extension of pHEA-mCTA with NIPAM via aqueous RAFT dispersion polymerisation

pHEA-mCTAs were chain extended with NIPAM with a targeted DP of 25 to form diblock copolymers (Scheme 4.2). These polymers were analysed by NMR spectroscopy and GPC to determine the conversion, M_n and M_w/M_n . When the GPC chromatograms are compared to those of the appropriate macro-CTA, in all three polymers there is an increase in M_n equivalent to what is expected from the polymerisation with NIPAM (

Table 4.2, Figure 4.6). There is no peak in the block copolymer chromatograms at the same retention time as the mCTA, indicating a high level of blocking efficiency.

Table 4.2 - Analytical data for the 3 diblock copolymers: pHEA-b-pNIPAM with EMEM, MPP and MBP RAFT agents

mCTA	$[M]/[mCTA]$	Conv.	/	$DP_{n, thr.}^b$	M_n / Da^c	DP_n^a	M_n	/	M_w/M_n^d
------	--------------	-------	---	------------------	--------------	----------	-------	---	-------------

		% ^a				Da ^d	
pHEA-EMEM	25	71	18	7200	19	14120	1.1
pHEA-MPP	25	78	20	7910	20	12180	1.11
pHEA-MBP	25	74	19	8270	20	13150	1.11

^a Determined by ¹H NMR spectroscopy in D₂O. ^b [M]/[RAFT agent] × conv. ^c M_n calculated from ¹H NMR spectroscopy. ^d Determined by GPC in DMF (0.1% LiBr) with pMMA standards.

Although it is expected that all three of the diblock polymers would have very similar GPC traces, due to differences in the length of the macro-CTA and the mass of the RAFT agents these do not overlay (Figure 4.6). However, they all have a low dispersity and only a small shoulder indicative of bimolecular termination.

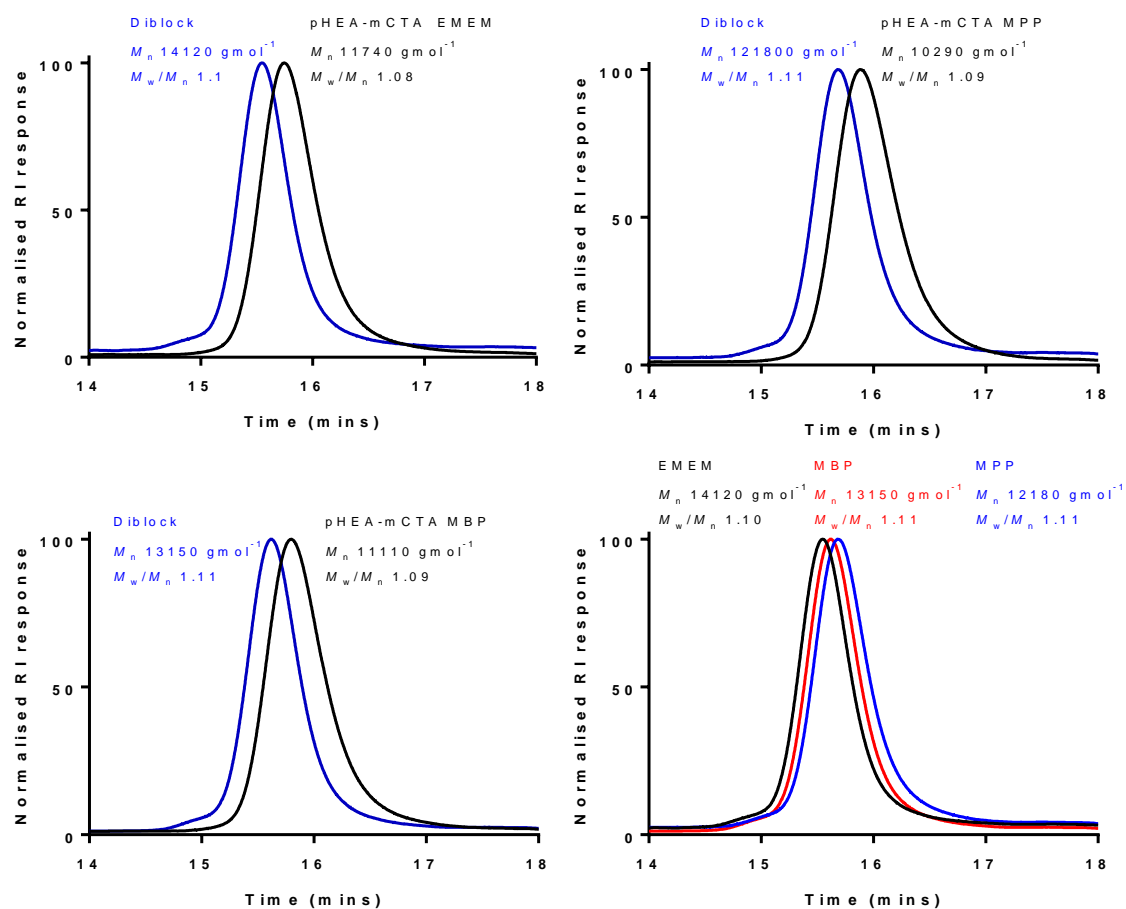
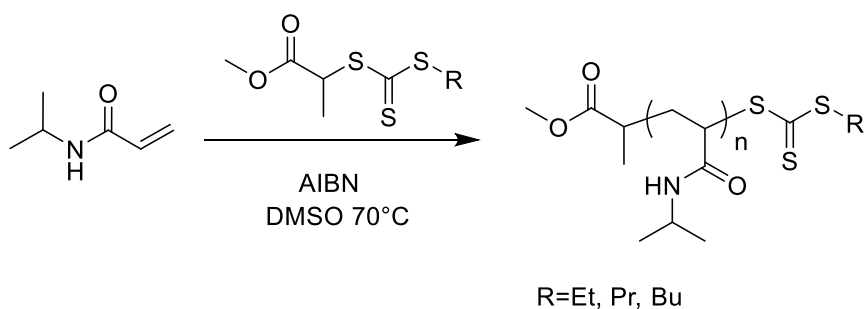


Figure 4.6 - GPC chromatograms (DMF 0.1% LiBr) of pHEA-mCTA and pHEA-b-pNIPAM, synthesised using 3 different RAFT agents: a) EMEM, b) MPP, c) MBP, and d) a comparison of the GPC chromatograms of the 3 diblock copolymers.

4.2.1.2. Diblock copolymers using polymers of N-isopropylacrylamide as macro-chain transfer agents



Scheme 4.3 - Synthesis of pNIPAM-mCTA via non-aqueous RAFT dispersion polymerisation using 3 different RAFT agents; EMEM, MPP and MBP.

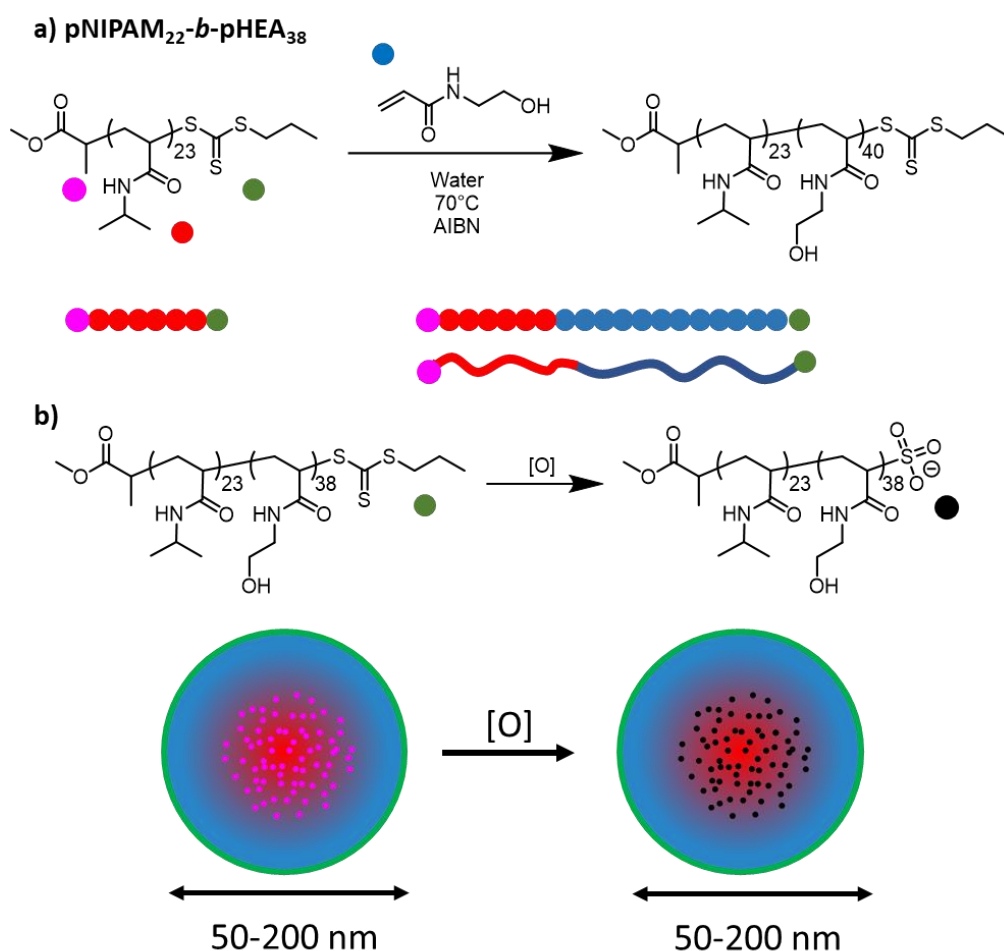


Figure 4.7 - a) The synthesis of pNIPAM-b-pHEA using the RAFT agent MPP as an example, defining where the RAFT chain end groups are bound to the polymer chains, b) The expected result on oxidation of the self-assembled polymer showing no disassembly as the resulting sulfonic acid group is not bound to the temperature responsive pNIPAM block

As well as the pHEA-mCTAs, pNIPAM-mCTAs were synthesised in the same way, using all three RAFT agents (Scheme 4.3). Although, above the LCST, this would self-assemble to form a diblock copolymer where the pNIPAM block is the core forming block, the position of the oxidation responsive RAFT chain end group would be different. The oxidation responsive trithiocarbonate group would now be covalently bound to the pHEA block of the polymer meaning a greater distance between this and the temperature responsive block (Figure 4.7). The LCST should therefore not be affected and disassembly on oxidation would not occur. This could therefore be used as a comparison to the self-assembled structures where the LCST will change on oxidation. It can be seen that the molecular weights of mCTAs are similar to the predicted values and therefore to each other, and that the GPC data shows low dispersities (Table 4.3, Figure 4.8).

Table 4.3 - A table giving NMR and GPC data from all three pNIPAM-mCTAs synthesised using EMEM, MPP and MBP RAFT agents

RAFT agent	[M]/[RAFT agent]	Conv. / % ^a	DP _{n, thr.} ^b	M _n /Da ^c	DP _n ^a	M _n /Da ^d	M _w /M _n ^d
EMEM	30	82	25	3050	24	4040	1.07
MPP	30	76	23	2730	22	3750	1.07
MBP	30	85	26	3300	23	3950	1.07

^a Determined by ¹H NMR spectroscopy in D₂O. ^b [M]/[RAFT agent] × conv. ^c M_n calculated using ¹H NMR spectroscopy. ^d Determined by GPC in DMF (0.1% LiBr) with pMMA standards.

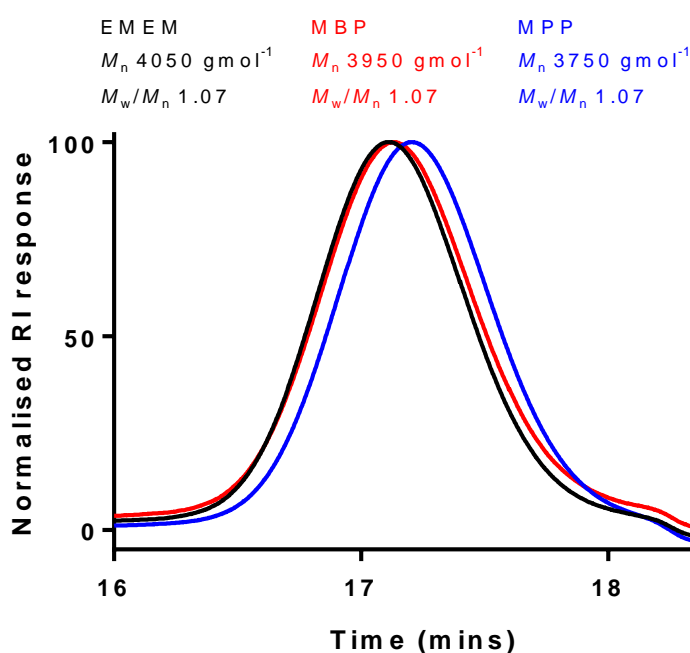


Figure 4.8 - The GPC chromatograms (DMF 0.1% LiBr) of three pNIPAM-mCTA synthesised using 3 different RAFT agents; EMEM, MPP and MBP, where M_n refers to the number average molecular weight and M_w/M_n refers to the dispersity.

These pNIPAM-mCTAs were chain extended with HEA to form pNIPAM-*b*-pHEA diblock copolymers.

There is no peak in the block copolymer chromatograms at the same retention time as the mCTA, indicating a high level of blocking efficiency, as seen above (Figure 4.8, Table 4.4). Also, when comparing the molecular weights of the three diblock copolymers, they are very similar, with narrow distributions, indicating good control (Figure 4.9, Table 4.4).

Table 4.4 – Analytical data for pNIPAM-b-pHEA diblock copolymers synthesised with EMEM, MPP and MBP RAFT agents

RAFT agent	[M]/[RAFT agent]	Conv. / % ^a	DP _{n, thr.} ^b	M _n / Da ^c	DP _n ^a	M _n / Da ^d	M _w /M _n ^d
pNIPAM-EMEM	50	85	43	7890	43	13640	1.09
pNIPAM-MPP	50	79	40	7100	38	12010	1.10
pNIPAM-MBP	50	60	30	6420	31	11700	1.11

^a Determined by ¹H NMR spectroscopy in D₂O. ^b [M]/[RAFT agent] × conv. ^c M_n calculated using ¹H NMR spectroscopy. ^d Determined by GPC in DMF (0.1% LiBr) with pMMA standards.

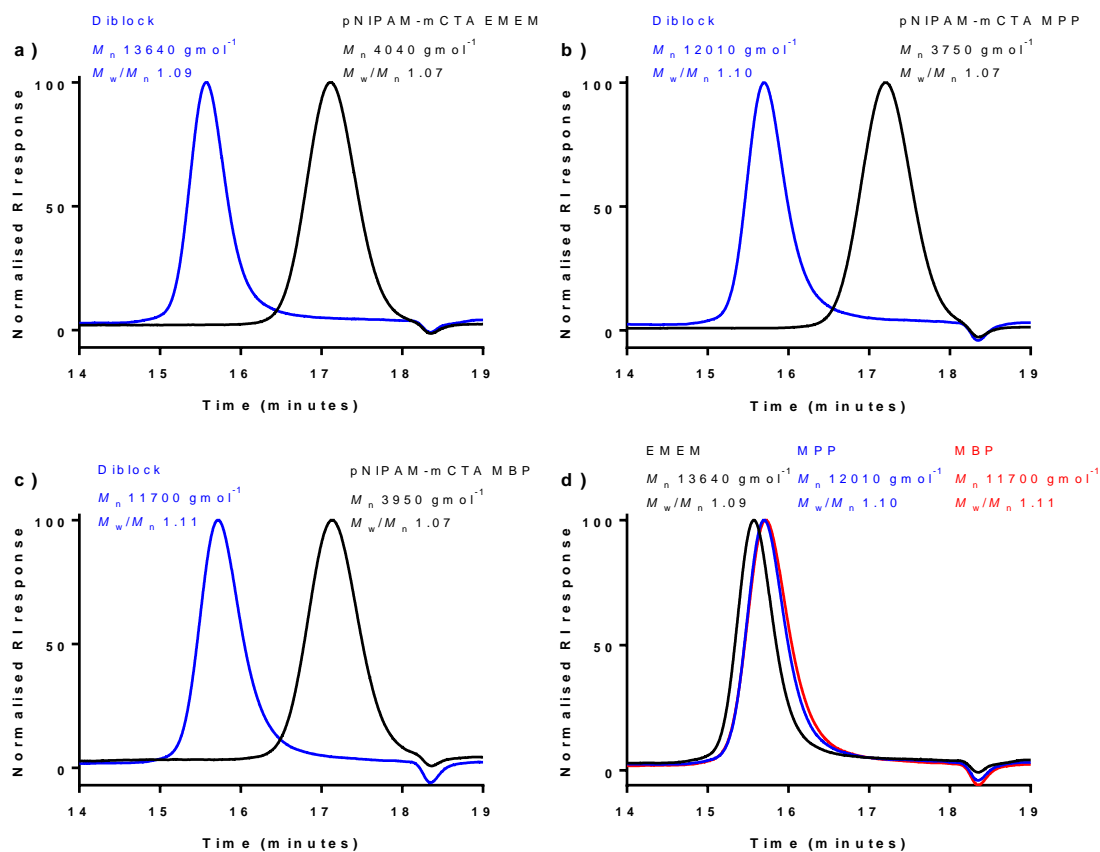


Figure 4.9 - GPC chromatograms (DMF 0.1% LiBr) of pNIPAM-mCTA and the chain extension of this with HEA, synthesised using 3 different RAFT agents: a) EMEM, b) MPP, c) MBP and d) a comparison of the GPC chromatograms of the 3 diblock copolymers.

4.2.1.3. Determination of the particle size of the self-assembled structures

For biomedical applications, it is important to characterise the size of the particle as well as the length and dispersity of the polymer chains.¹⁸ Particle size effects numerous processes which are necessary for the success of these as drug delivery systems, e.g. cellular uptake. Consequently, dynamic light scattering (DLS) was used to determine the hydrodynamic radius (R_H) of the nanoparticles formed. DLS uses the Stokes-Einstein equation to determine the hydrodynamic radius (Equation 2.2).

DLS is a very common technique used to determine the size of particles as the sample preparation is easy, it is non-invasive and does not destroy the sample, and the equipment does not require any calibration before use.¹⁹ As the size of the particles are much smaller than the wavelength of light used, light is scattered from these particles in all directions by Rayleigh scattering. The measurements recorded are the fluctuations in the intensity of the scattering of the incident light due to Brownian motion of the particles, which is proportional to the radii to the power of 6 and can therefore be related to particle diameter.

It is evident from DLS analysis that there is very little stable self-assembly for all the above diblock copolymers whether they are pHEA-*b*-pNIPAM or pNIPAM-*b*-pHEA, most likely due to constant disassembly and reassembly of the polymer chains (Figure 4.10, Figure 4.11). Oxidation of these polymer samples using 15 mM H₂O₂ seems to cause a change in the size of the structures however there is no apparent trend between whether these are bigger or smaller than that of the native polymer therefore it is not obvious what the effect of oxidation is.

To look at this behaviour in more detail, DLS measurements of the same sample were recorded at various temperatures. Using pHEA₄₆-*b*-pNIPAM₂₀-MPP as an example, even if the temperature is increased to 45 °C, well above the LCST of pNIPAM, there is still no evidence of stable assembly via DLS (Figure 4.11). When analysing the samples by DLS, at each temperature three traces were run consecutively. In a sample where the self-assembly of micelles is stable, it is expected that each of

these traces will overlap exactly. However, the particle size distributions for these polymers do not overlap exactly as expected, indicating that the assembly of the particles is not stable.

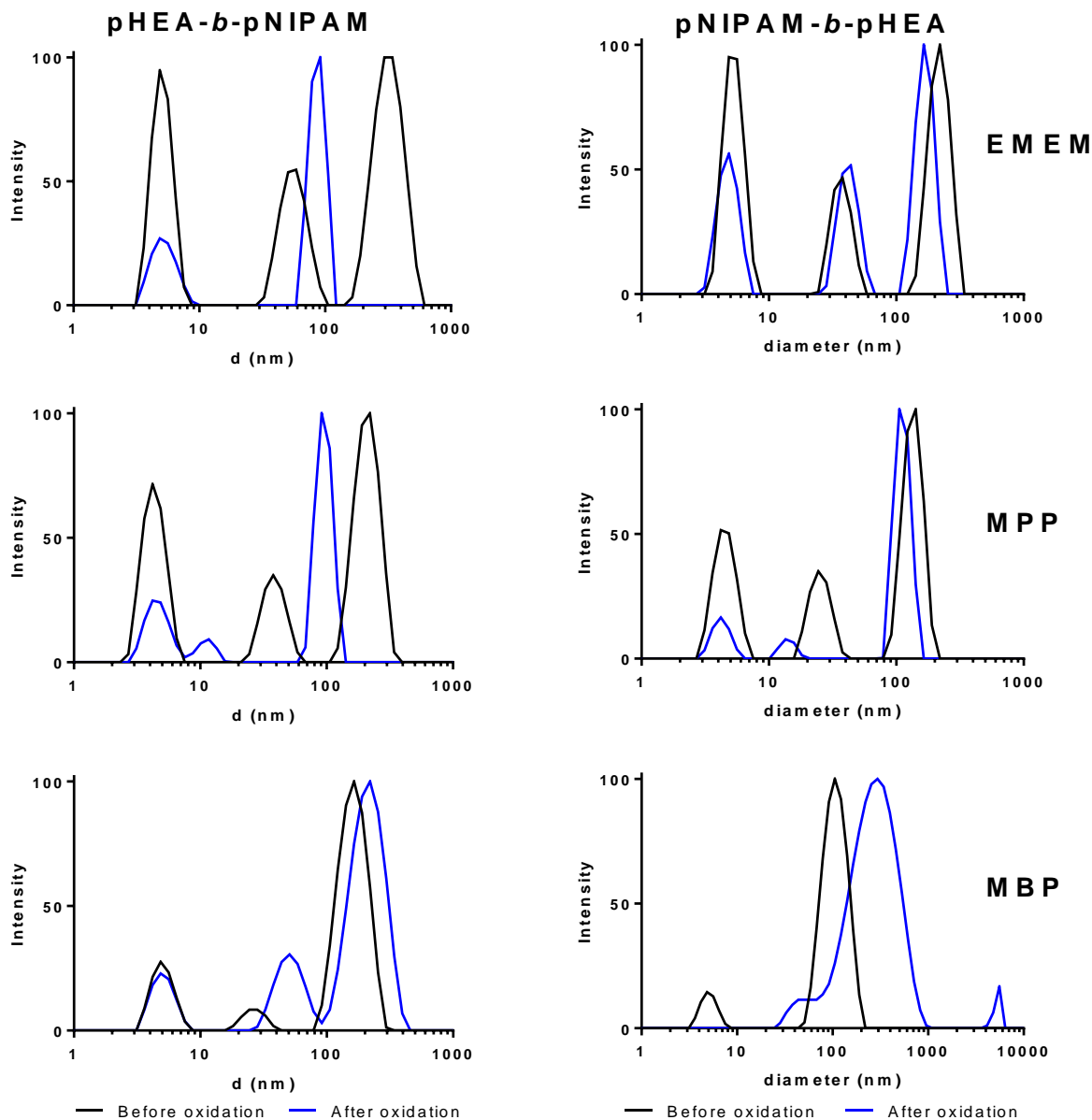


Figure 4.10 - DLS particle size distributions of a) pHEA-b-pNIPAM and b) pNIPAM-b-pHEA at a concentration of 1 mg/ml. These were recorded in water at 35 °C in water where the RAFT agent used initially to synthesise the macro-CTA is i) EMEM, ii) MPP and iii) MBP

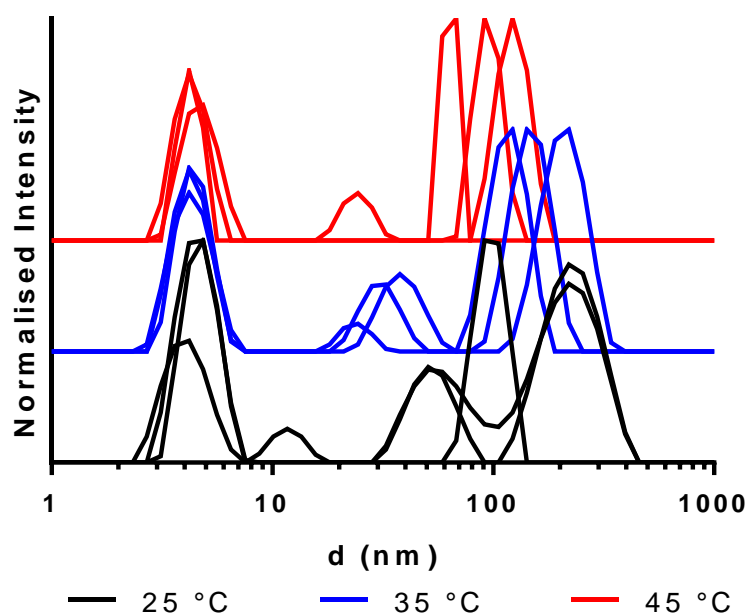
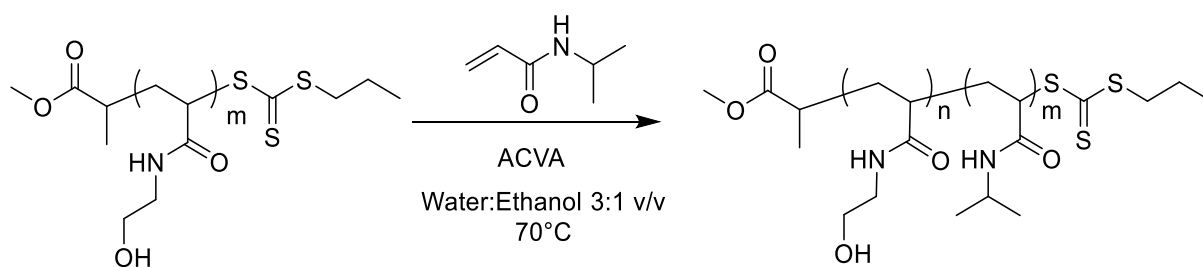


Figure 4.11 – Particle size distributions of pHEA₄₆-b-pNIPAM₂₀ MPP at 0.1 wt% in water at varying temperatures, 25, 35 and 45 °C

4.2.2. Synthesis of pHEA-*b*-pNIPAM diblock copolymers with longer pNIPAM block lengths in consolvents via RAFT dispersion polymerisation

4.2.2.1. Forming diblock copolymers which self-assemble in an aqueous environment at body temperature



Scheme 4.4 - Synthesis of pHEA-*b*-pNIPAM via RAFT solution polymerisation using a pHEA-*m*CTA synthesised with MPP as the RAFT agent

The lack of self-assembly of block copolymers is likely due to the short length of the pNIPAM block. An increase in length of the pNIPAM block would lower the critical micelle concentration due to an increase in the overall hydrophobicity of the block. The increase in entropy of the system due to release of water surrounding the hydrophobic segments means that micelles are more likely to

form.^{20,21} Therefore, block copolymers with a longer NIPAM block were synthesised to see if these would self-assemble and disassemble on oxidation. Although, oxidation may still change the RAFT chain end group, disassembly of any self-assembled structures is less likely as the end group is a much smaller percent of the polymer so the change in cloud point will be minimal. If this occurs another method must be employed to assist the removal of the polymeric drug delivery system from the body.

It has been widely reported in the literature that both the length of the hydrophobic block and the area of the head group of the hydrophilic block have a large influence on the morphology of self-assembled structures. It relates to the packing parameters and is defined in equation 1:²²

$$p = \frac{v}{a_0 l_c} \quad (1)$$

Where v refers to the volume of the hydrophobic chains, a_0 is the optimal area of the hydrophilic block and l_c is the length of the hydrophobic tail. The value of the packing parameter, in general, is a good indication of the morphology expected on self-assembly.²² Therefore, by changing the length of the hydrophobic block it may be possible to influence self-assembly as well as change the morphology of the formed nanoparticles.

To study this concept, another pHEA-mCTA was synthesised on a larger scale using MPP as the RAFT agent to conduct a thorough study into self-assembly and the use of diblock copolymers as drug delivery vehicles. This mCTA had a DP of 45 and was chain extended with NIPAM to give nominal block lengths of approximately 100, 150, 200, 250 and 300. Previous studies conducted to determine appropriate reaction conditions suggested that the reactions reach a conversion of between 80-90%. Therefore, the targeted DP was higher than the nominal block length mentioned above. This means that a variety of polymers can be synthesised with masses up to the suggested limit for biomedical applications, while still examining a variety of potential different particle sizes and morphologies. The only differences between the synthesis in Scheme 4.2 and those discussed in this section are the

increased size of the pNIPAM block and the solvent system used (Scheme 4.4). For these studies a 3:1 v/v mixture of water and ethanol was used. The refers to a 0.1 mole fraction (x) of ethanol. This mixture of solvents was chosen as it has low toxicity and would also allow inclusion of monomers that are not soluble in water alone (see section 4.2.3.). Also, it has previously been demonstrated to be suitable for RAFT dispersion polymerisation of NIPAM²³ due to cononsolvency. This is where a mixture of two solvents that the polymer is usually soluble in causes insolubility depending on their composition. The LCST behaviour of pNIPAM in these solvent mixtures can be tuned by varying the solvent ratios. Cononsolvency of pNIPAM in various water:solvent mixtures, i.e. THF,^{24,25} alcohols (methanol, ethanol and propanol),^{24,23,26,27} dioxane,²⁴ acetone,²³ DMF²³ and DMSO.^{23,28,29} Although this has been shown to alter the LCST of pNIPAM compared to aqueous solutions, when mixed with certain solvents, an UCST has also been observed. This large change in LCST could allow for self-assembly to be forced in these structures.^{30,31}

Monomer conversion was determined via gravimetric analysis, as the cononsolvency in this system made NMR analysis difficult, and the actual DP of the polymers was determined by ¹H NMR spectroscopy after purification (Table 4.5). GPC analyses of the pHEA-mCTA and the diblock copolymers were compared and show that all samples have been efficiently chain extended (Figure 4.12). There is presence of both tailing and shouldering of the GPC peaks giving a broader dispersity of the polymer. The tail indicates that some chains of pHEA homopolymer may still be present, likely due to loss of the RAFT chain end group in the synthesis, and that there is presence of bimolecular termination. These make up a very small proportion of the sample so should not have a large effect on self-assembly but could be avoided in future by minimising reaction times. All polymer samples were purified by dialysis against deionised water to remove any unreacted monomer and ethanol in the sample.

Table 4.5 - A table showing the conversion of monomer to polymer by gravimetric analysis and the actual DP of pHEA₄₅-b-pNIPAM_n

[M]/[pHEA-mCTA]	Conv. / % ^a	DP _{n,thr.} ^b	DP _n ^d	M _n / Da ^d	M _n / Da ^e	M _w /M _n ^e
126	91	114	132	20360	21250	1.32
189	83	156	194	27370	22960	1.53
250	85	212	250	33710	26650	1.63
311	87	270	292	38460	27620	1.74
376	85	319	370	47290	28930	1.81

^a Determined by gravimetric analysis against predicted solids content ^b [M]/[RAFT agent] × conv. ^c M_n from solids content. ^d Determined by ¹H NMR spectroscopy in D₂O ^e Determined by GPC in DMF (0.1% LiBr) with pMMA standards.

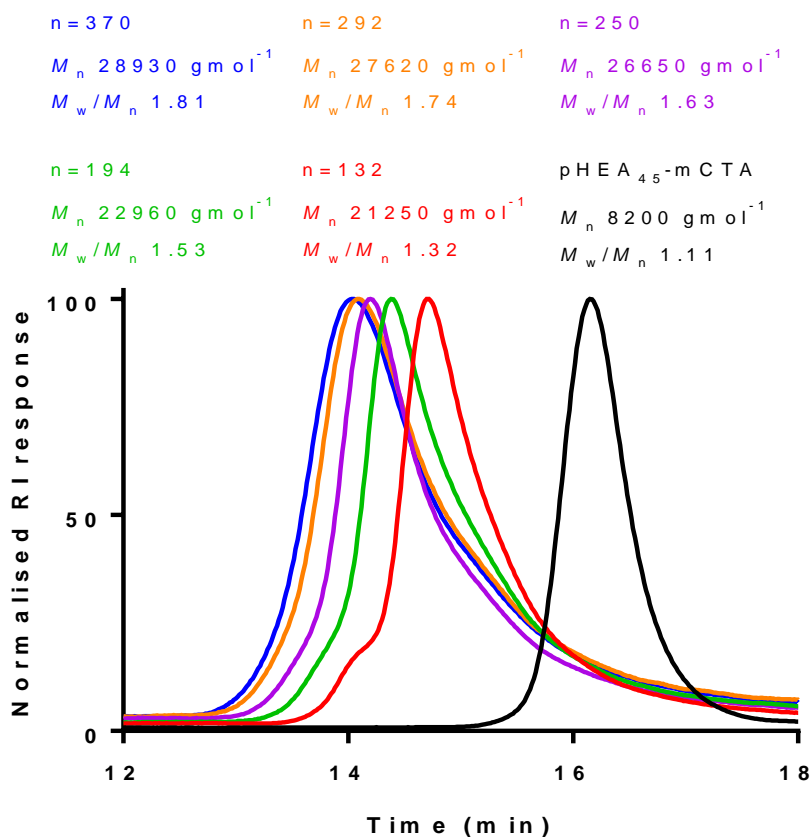


Figure 4.12 - GPC chromatograms (DMF 0.1% LiBr) of pHEA₄₅-mCTA compared with the chain extended diblock copolymers of pHEA₄₅-b-p(NIPAM-stat-BAPE)_n, where n=132, 194, 250, 292 and 370

4.2.2.2. Determination of the particle size of the self-assembled structures

There is a large difference in the reaction solutions after polymerisation, with these varying in colour from a blue hue to white, dependent on the length of the pNIPAM block. After purification by

dialysis to remove ethanol and unreacted starting material this was still seen (Figure 4.12). This occurs due to Mie scattering which causes the blue hue appearance of the solution initially, which becomes whiter in colour as the particle size increases. Mie scattering is seen when the diameters of the particles scattering light is similar to, or larger than the wavelength of the incident light.^{32,33,34} This is characteristic of nanoparticle formation and could be seen due to the aggregation of particles.^{35,36,37} It is different to Rayleigh scattering of light used in DLS analysis, where the particle sizes are much smaller than the wavelength of light used. It is important to note however, that Mie scattering is much stronger than Rayleigh scattering, which means that solutions must be dilute to be analysed by DLS.³⁸



Figure 4.13 – Photograph above the LCST of diblock polymer samples of $pHEA_{45}\text{-}b\text{-}pNIPAM_n$, with n being 132, 194, 250, 292 and 370 from left to right.

These polymers were oxidised with 15 mM H_2O_2 for 48 h., however they were not purified after oxidation. All the samples were diluted to 0.1 wt% and analysed by DLS before and after oxidation at 37 °C to determine whether if there was any stable self-assembly (Figure 4.14). This is possible by comparing DLS analysis of the size by intensity with the correlation curve. For the DP 100 polymer, a peak at around 10 nm is observed, which is approximately the size of the diblock copolymer when it is not assembled into a micelle, indicating that not all the polymer chains are self-assembled. Due to the dynamic nature of self-assembly in micelles, it could be that this self-assembly is not as stable as that seen for the longer length polymers. For all the other diblock copolymers, numerous peaks are

seen, however, the peaks at approximately 1 nm are most likely an artefact. 1 nm would be smaller than expected for a free chain mCTA, without any chain extension. Also, the correlation curves confirm this as an abnormal break in the curve is seen at a corresponding size. All of these do show self-assembly at 37 °C however, with particle sizes ranging between 65 and 121 nm depending on the length of the NIPAM block.

As stated previously, the particles were also sized by DLS after oxidation. The sizes seem to remain almost the same as they were before oxidation (Figure 4.14). Although there are slight deviations in size, these are minimal and would not indicate disassembly of the micelles. This could be due to the oxidation of the RAFT chain end group causing a change as seen in Chapter 3, however long pNIPAM chains do not exhibit a change in the LCST, so again this is unlikely to cause disassembly.

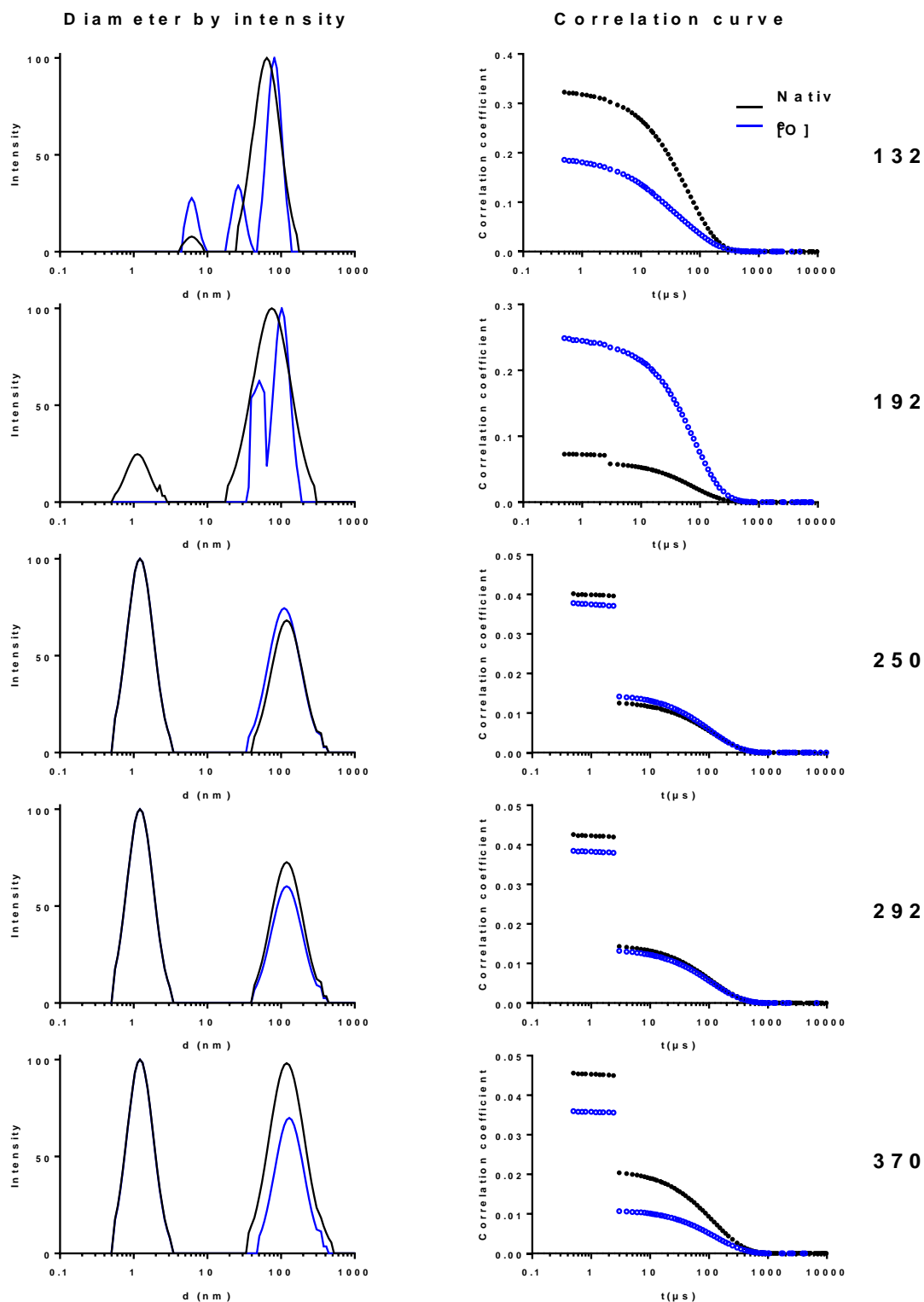


Figure 4.14 - DLS chromatograms and corresponding correlation curves (DMF 0.1% LiBr) of diblock copolymers of pHEA₄₅-b-pNIPAM_n at a concentration of 1 mg/ml. These were recorded in water held at 37 °C, before and after oxidation where a) n=132, b) n=194, c) n=250, d) n=292 and e) n=370.

By increasing the temperature from 25 °C to 45 °C, which are temperatures below and above the LCST of pNIPAM, respectively, it is possible to determine whether assembly occurs. At 25 °C, weak assembly is seen, giving particles of less than 100 nm, however there are particles seen at 10 nm, which are indicative of free polymer chains. As the temperature is increased to 35 and 45 °C, a peak at 1 nm is seen again as with the samples above, but there is indication of self-assembly giving particles of approximately 100 nm. The dispersity of these peaks appears to widen however as the temperature increases and therefore more assembly occurs. This could be due to a mixture of micelle sizes or could be due to these particles deviating from a spherical morphology.

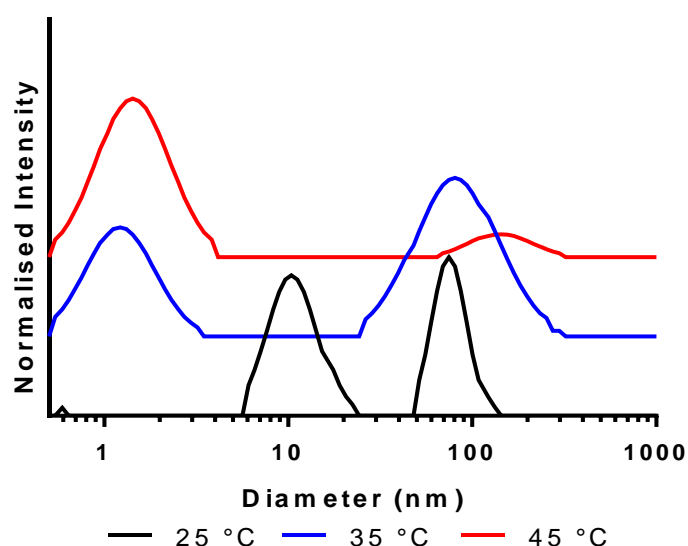
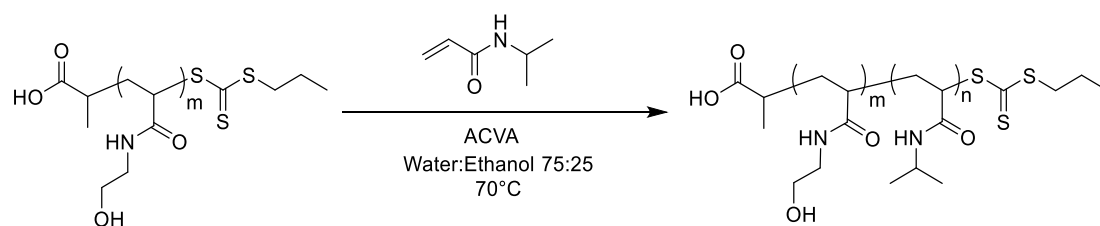


Figure 4.15 - A comparison of DLS of pHEA₄₅-b-pNIPAM₂₉₂ at a concentration of 1 mg/ml. These were recorded in water at temperatures above and below the LCST of the polymer to determine self-whether self-assembly occurs as the pNIPAM block becomes hydrophobic

4.2.2.3. Using a more hydrophilic RAFT agent (PPA) to promote self-assembly

To form a more stable assembled structure, other parts of the molecule which could influence this were altered. Literature has shown that when the end group is ionisable, the charge formed can influence the self-assembly. It has also been found that ionisable RAFT agents can have an effect on the self-assembly properties of polymers.^{39,40,41,42} Therefore, the RAFT agent was changed from MPP to PPA, where the ester group is replaced with a carboxylic acid group, which has the ability to be ionised.



Scheme 4.5 - Synthesis of pHEA-b-pNIPAM via RAFT solution polymerisation using a pHEA-mCTA synthesised with PPA as the RAFT agent

Table 4.6 – Characterisation data for the synthesis of pHEA₃₇-b-pNIPAM_n diblock copolymers synthesised with PPA as the RAFT agent

[M]/[pHEA-mCTA]	Conv. / % ^a	Thr. /DP ^b	DP _n ^d	M _n / Da ^d	M _n / Da ^e	M _w /M _n ^e
100	82	82	89	14560	16150	1.24
150	87	131	146	21010	17310	1.53
200	88	176	202	27340	26360	1.39
250	80	200	199	27230	26610	1.38
300	89	267	274	35490	32140	1.46

^a Determined by gravimetric analysis against predicted solids content ^b [M]/[RAFT agent] × conv. ^c M_n from solids content. ^d Determined by ¹H NMR spectroscopy in D₂O ^eDetermined by GPC in DMF (0.1% LiBr) with pMMA standards.

Therefore, the above procedure was repeated by synthesising a pHEA-mCTA where PPA was the RAFT agent (Scheme 4.5). The targeted length of the mCTA was the same as above and after purification and NMR analysis it was determined to have a DP of 37. Although the target DP was the same, the DP after polymerisation is shorter so these are not directly comparable to when MPP was used as the RAFT agent. This was then chain extended, keeping the conditions the same as before. The monomer conversion of each reaction was determined via gravimetric analysis and the actual DP inferred from this before comparing with ¹H NMR analysis of the pure polymer (Table 4.6).

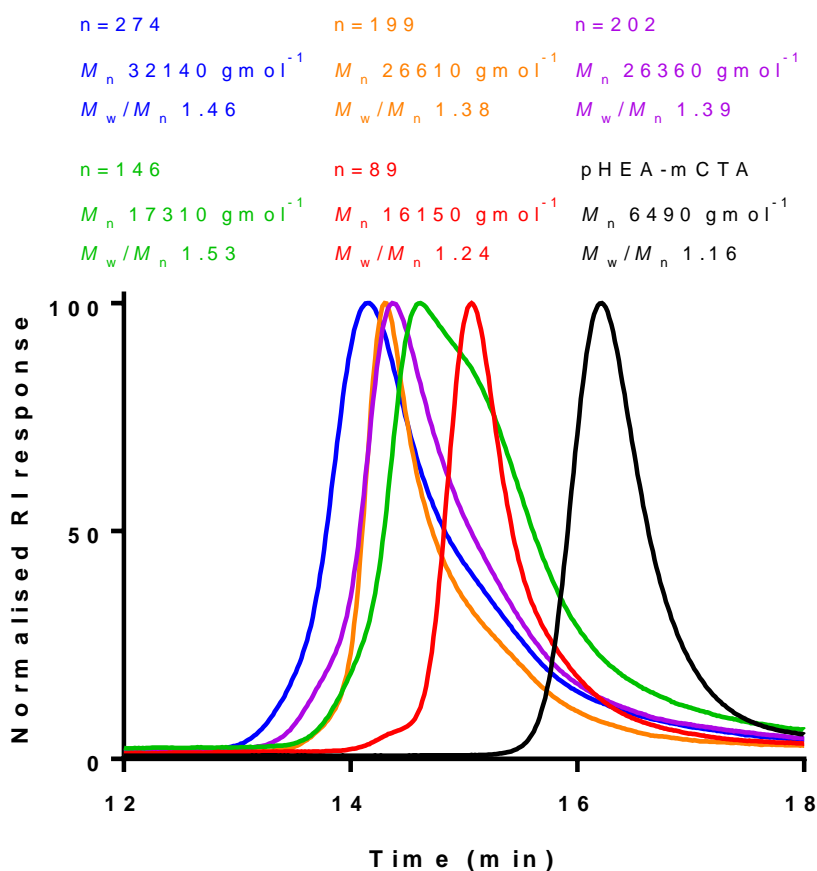


Figure 4.16 - GPC chromatograms (DMF 0.1% LiBr) of pHEA₃₇-mCTA compared with the chain extended diblock copolymers of pHEA₃₇-b-pNIPAM_n, where n=89, 146, 202, 199, 274.

Again, there is presence of both tailing and shouldering of the GPC peaks giving a broader dispersity of the polymer. The tail indicates that some chains of pHEA homopolymer may still be present, likely due to loss of the RAFT chain end group in the synthesis, and that there is presence of bimolecular termination, however not to as large an extent as with pHEA₄₅-MPP-mCTA (Figure 4.16). The analysis of the GPC traces shows high dispersity which is concurrent with the slight tailing observed and the M_n values agree with the DP found from the monomer to polymer conversion calculations. The trace where n=146 is broader than the others, however any differences in assembly will be apparent during DLS analysis.

4.2.2.4. Determination of the particle size of the self-assembled structures

DLS was employed again to determine the R_H of these particles. Polymers with varying length hydrophobic blocks were measured before and after oxidation at 37 °C to determine whether self-assembly could be seen and if oxidation affected this (Figure 4.17).

The results seen from DLS analysis correlate with those found when MPP is used as the RAFT agent. For polymers with a pNIPAM chain length of DP 150 and higher, self-assembly is observed, with particles sizes of around 100 nm. The peak at 1 nm is still observed but as mentioned previously, this does not represent the polymers due to the extremely small size and is therefore an artefact, as can be seen in the correlation curve. One difference that is seen by using this RAFT agent is that the previously poorly assembled DP100 block length of NIPAM lack any self-assembly when PPA is used as the RAFT chain end group. When the oxidised polymers were analysed very little change in size is seen, as observed for the MPP polymers.

The DLS data shows self-assembly for some of the diblock copolymer when the temperature is raised above the LCST (45 °C) (Figure 4.17). At 25 °C, there is a peak 10 nm, which is indicative of free polymer chains, not micelles. However, at 35 and 45 °C, there is clear evidence of self-assembly, with particles of approximately 100 nm. At the higher temperature range many polymers gave bimodal traces but there is no indication of free polymer chains, unlike the previously mentioned short pNIPAM block copolymers.

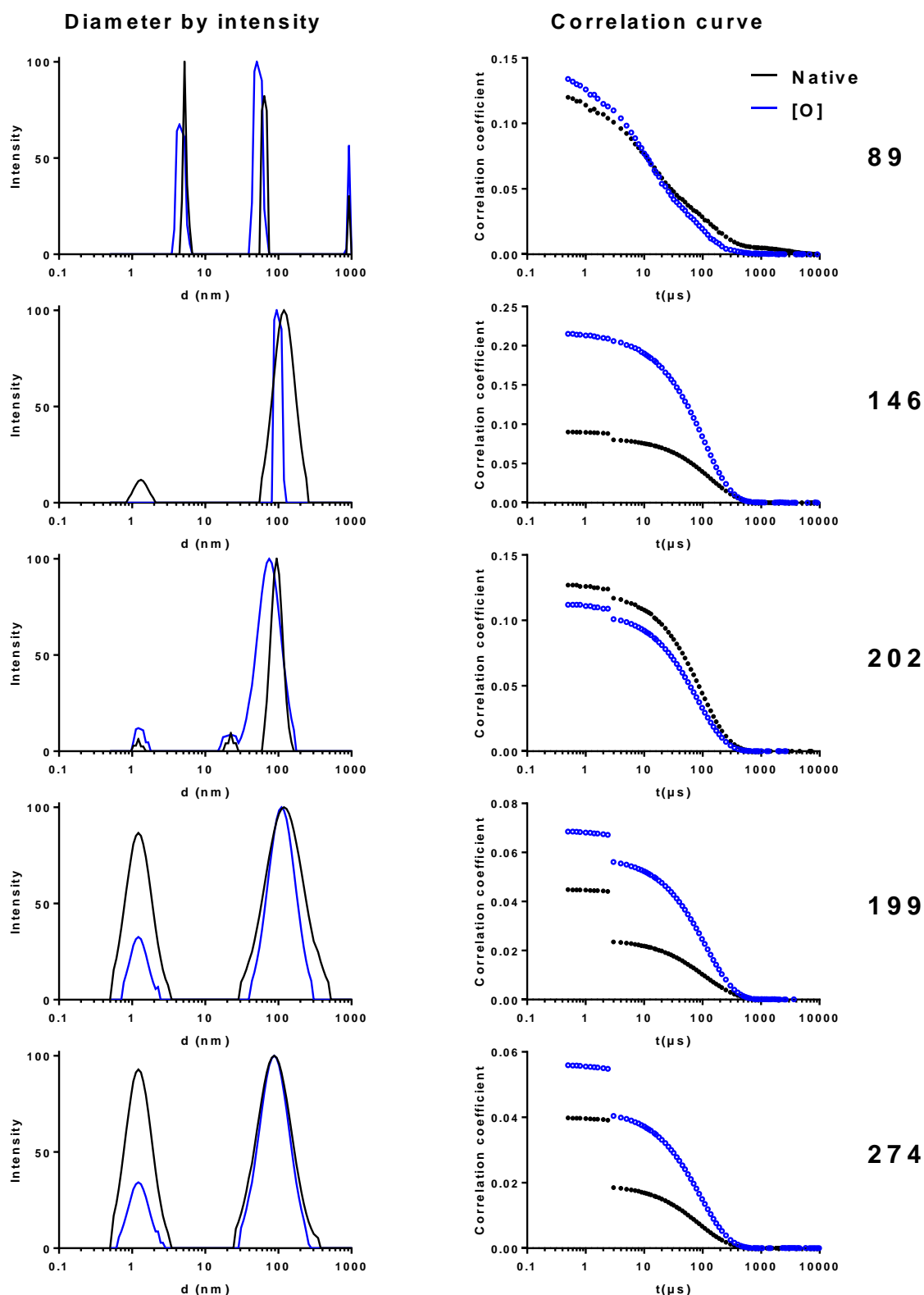


Figure 4.17 - DLS particle size distributions and the corresponding correlation curves of diblock copolymers of pHEA₃₇-b-pNIPAM_n at a concentration of 1 mg/ml. These were recorded in water held at 37 °C, before and after oxidation where a) n=89, b) n=146, c) n=202, d) n=199 and e) n=274.

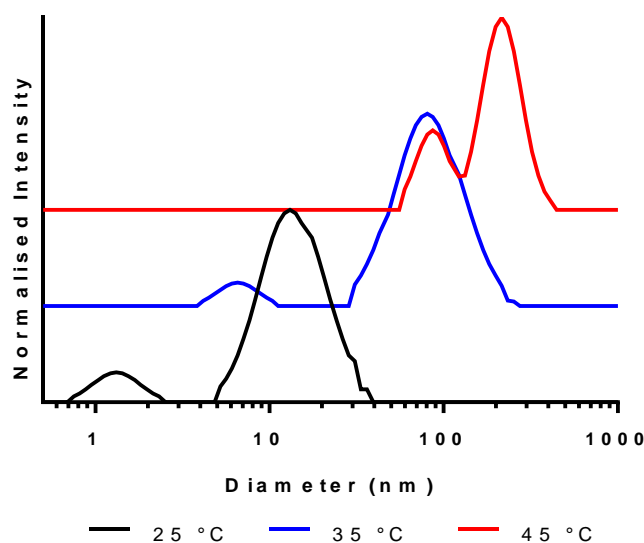
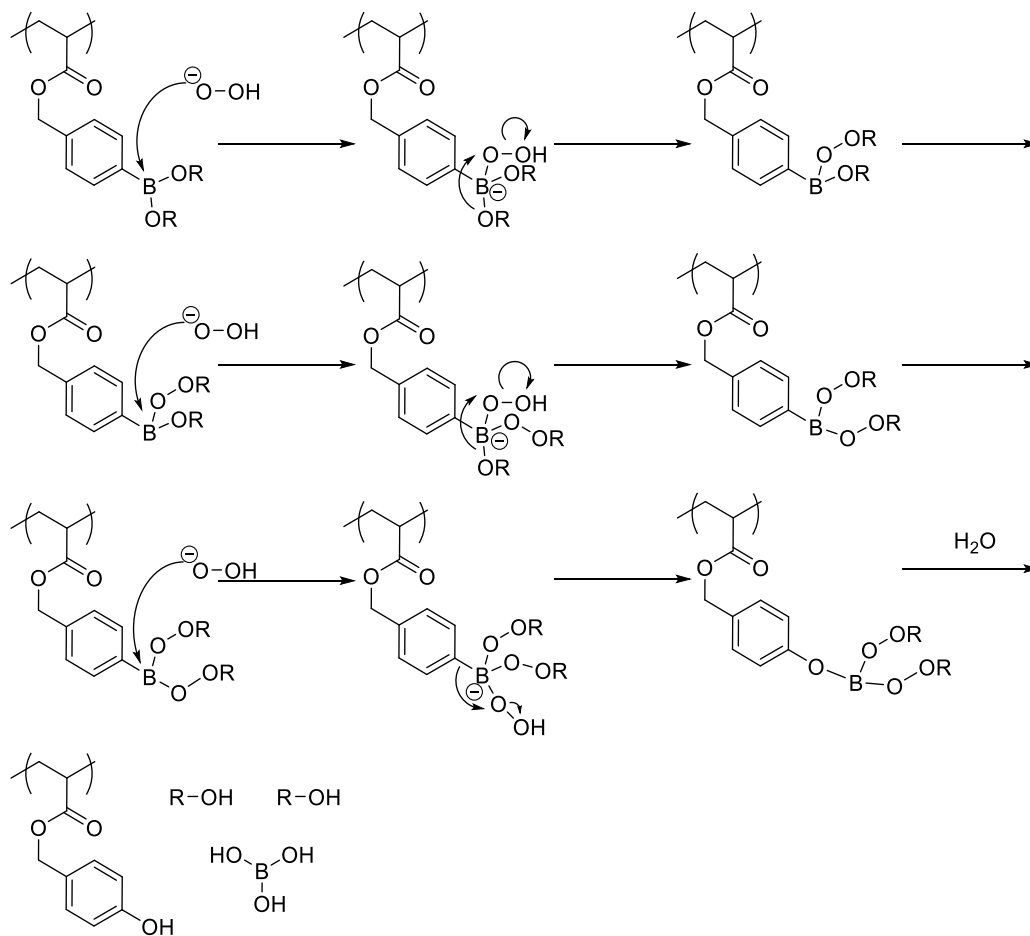


Figure 4.18 – A comparison of DLS of pHEA₃₇-b-pNIPAM₁₉₉ at a concentration of 1 mg/ml. These were recorded in water at temperatures above and below the LCST of the polymer to determine self-whether self-assembly occurs as the pNIPAM block becomes hydrophobic

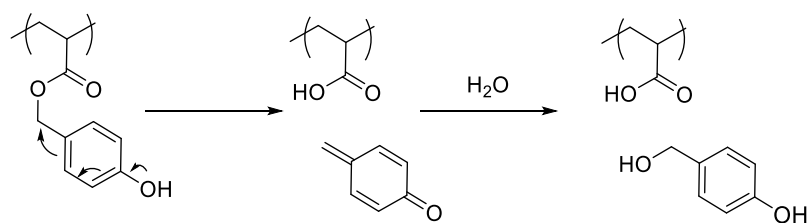
4.2.3. Synthesis of an oxidation responsive monomer and analysis of its impact on size and LCST of pNIPAM polymers

In order to form monomodal self-assembled diblock copolymers, an aryl boronic acid pinacol ester-based monomer, 4-(acryloyloxymethyl)phenylboronic acid pinacol ester (BAPE), was synthesised to be incorporated into the NIPAM block. Boronic acids and their pinacol esters are susceptible to oxidation by H₂O₂ but are not as sensitive to by other reactive oxygen species present in the body, meaning it is easier to develop a targeted release that is concentration dependant. It can be seen from the literature that aryl boronic acids and their pinacol esters are sensitive to H₂O₂ even at concentrations as low as 50 μM.^{43–48} Although it can be oxidised to a certain extent with higher concentrations of other ROS, they are not as sensitive to oxidation at biologically relevant concentration, unlike H₂O₂.^{49–52} They are highly sensitive to concentrations of peroxynitrite as low as 10 μM and react more quickly with this, however these are very reactive molecules making it difficult to use them as target molecules.^{53–56}

i) Nucleophilic addition



ii) 1,6-elimination



Scheme 4.6 - Oxidation of a boronic acid pinacol esters using hydrogen peroxide

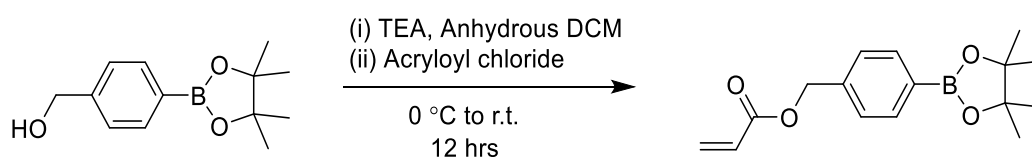
H_2O_2 reacts via the nucleophilic addition to the boron atom forming a phenol. The linker used to connect the arylboronic acid/ester to the polymer backbone has a large influence on the extent of the reaction.⁵⁷ If a carbamate or ester linkage is used, this can then undergo a 1,6-elimination to leave a carboxylic acid in the form of an acrylic acid unit in the polymer chain. For example, when an

ester linkage is used this leaves a carboxylic acid group attached to the polymer chain (Scheme 4.6).

It is therefore very important to correctly design these oxidation responsive molecules.

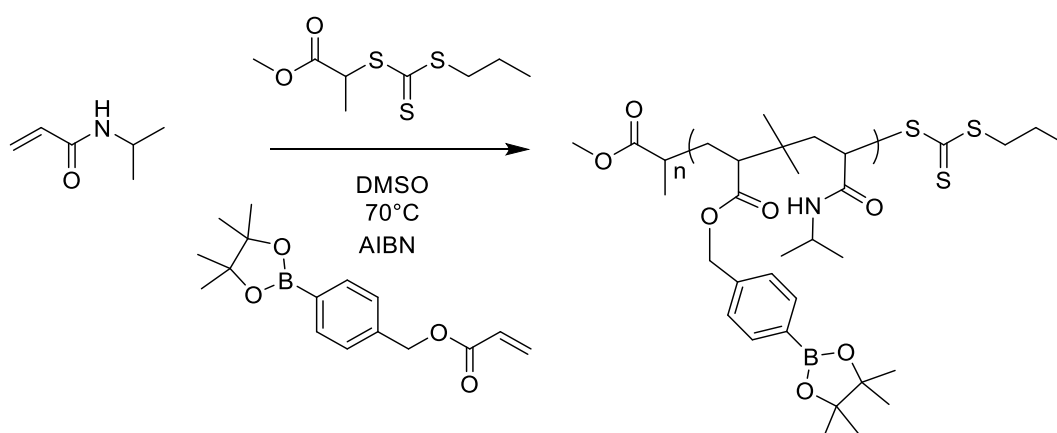
A number of small molecule side products are formed on oxidation, including quinone methides which have been suggested to be highly reactive and harmful in some studies.^{58,59} This toxicity would need to be assessed in future studies.

This monomer was chosen as it has previously been shown to have a large effect on the cloud point before and after on oxidation when copolymerised with NIPAM.⁶⁰ Consequently, it should enable the disruption of self-assembled structures which is needed in drug delivery systems. The additional hydrophobicity could also encourage self-assembly before oxidation, as has been seen in other thermoresponsive systems.⁶¹



Scheme 4.7 - Synthesis of the oxidisable monomer 4-(acryloyloxymethyl)phenylboronic acid pinacol ester (BAPE)

The oxidation-responsive monomer 4-(acryloyloxymethyl)phenylboronic acid pinacol ester (BAPE) was synthesised by reaction of acryloyl chloride with 4-(hydroxymethyl)benzene boronic acid pinacol ester under basic conditions (Scheme 4.7) as has been previously described.⁶²



Scheme 4.8 - Synthesis of statistical copolymers of NIPAM and BAPE via RAFT polymerisation

Initially, it was necessary to determine what molar ratio of BAPE should be incorporated into the NIPAM block of the polymer to achieve the desired changes in LCST. After consulting previous literature,⁶⁰ linear polymers of NIPAM were synthesised incorporating 3, 5 and 10 mol% BAPE (Scheme 4.8) as these were deemed likely to have an LCST close to 20 °C, much lower than body temperature, before oxidation.

The cloud point of each polymer was determined before and after oxidation. The ideal ratio of BAPE to NIPAM would give an LCST which is below body temperature, preferably below room temperature so that it doesn't need to be stored at an elevated temperature, before oxidation. On oxidation, the LCST should be higher than body temperature, which will cause the pNIPAM block to become soluble, releasing the drug and aiding excretion of the empty polymer.

Table 4.7 - Analytical data for p(NIPAM-*stat*-BAPE)₁₀₀ statistical copolymers with 3, 5 and 10 mol% BAPE

Feed BAPE mol%	[M]/[RAFT agent]	Conv. / % ^a	DP _{n, thr} ^b	M _n / Da ^c	Mole ratio of BAPE / % ^a	M _n / Da ^d	M _w /M _n ^d
2	100	94	94	11390	6.8	6930	1.61
3	100	96	96	11630	3.1	6180	1.56
5	100	96	96	9360	3.9	5670	1.41
10	100	94	94	11020	6.9	4200	1.73

^a Determined by ¹H NMR spectroscopy in D₂O. ^b [M]/[RAFT agent] × conv. ^c M_n calculated from ¹H NMR spectroscopy. ^d Determined by GPC in DMF (0.1% LiBr) with pMMA standards.

p(NIPAM-*stat*-BAPE) copolymers were synthesised by RAFT polymerisation using MPP as before and characterised by ¹H NMR spectroscopy and GPC to determine the degree of polymerisation, M_n and M_w/M_n (Table 4.7). From NMR, the mole percent BAPE in the final polymer can be calculated. It must be noted that there appears to be a larger than predicted amount of BAPE in the final polymer where a BAPE feed ratio of 2 mol% was used. As there is such a small amount of BAPE present it is difficult to determine accurately from NMR analysis, leading to a large error in the calculation. The data also suggests that once there is a lot of BAPE incorporated into the chains, NIPAM will

polymerise preferentially, which may be due to steric interactions. The GPC data shows that, as more BAPE is incorporated into the statistical copolymer, the measured molecular weight is reduced despite the theoretical molecular weights being higher. This is likely due to differences in polymer solubility in DMF when the amount of BAPE incorporated into the chain increases. Also, GPC analysis compares against a set of standards, in this case PMMA. As these polymers are composed of different concentrations of BAPE, they cannot be directly compared to each other or the standards. The dispersity of the polymers by GPC is higher than the homopolymers of NIPAM synthesised with MPP as the RAFT agent which could be caused by solubility difference as mentioned previously or by the amount of bimolecular termination observed with an increased mole percent of BAPE.

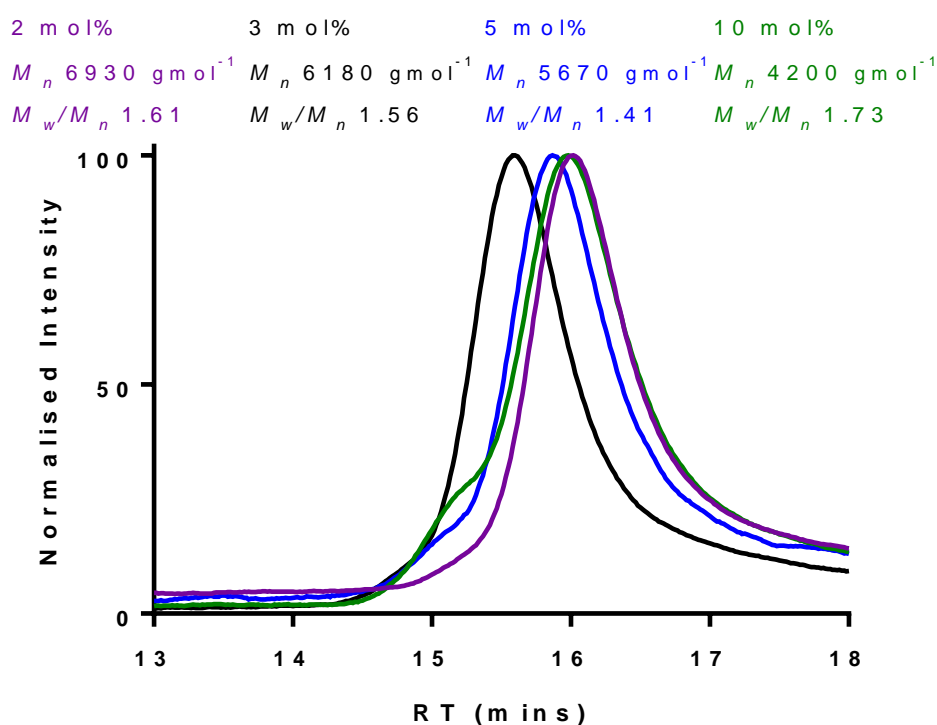


Figure 4.19 - GPC chromatograms (DMF 0.1% LiBr) for linear statistical polymers of pNIPAM-stat-BAPE with 2, 3, 5 and 10 mol% BAPE

The cloud point of these polymers was determined via temperature-controlled UV-vis spectroscopy. The polymers with 2, 3, 5 and 10 mol% of BAPE have LCSTs of 23.7, 22.7, 18.0 and 14.3 °C, respectively (Table 4.8). After oxidation with a 15 mM H₂O₂ DPBS solution, the cloud point of the

polymers containing 2, 3 and 5 mol% BAPE increased significantly to 36.5, 39.7 and 35.1 respectively, approximately an 18 °C increase in cloud point after oxidation (Figure 4.20). The mole ratios of BAPE in these differ to the feed ratios, which implies that the error associated with the calculation of BAPE mole percent may mean that the amount of BAPE between samples is more similar than expected, which explains the lack of trend in the cloud point data. After oxidation, the polymer with 10 mol% BAPE incorporated no longer exhibits a cloud point. As each BAPE unit is converted to an acrylic acid (AA) unit, it was possible to compare with literature cloud point values with p(NIPAM-*stat*-AA) polymers, which correlated with the cloud point data seen here.⁶³⁻⁶⁶ Yoo et al. for example, synthesised a number of statistical copolymers of NIPAM and AA, with an acrylic acid content ranging from 0 – 50 mol% AA, at 10 mol% intervals.^{64,65} At low pH, these polymers all exhibit an LCST, however as the mole % of AA increases so does the charge from the ionised groups causing the chains to repel and become soluble. This means that at higher pH values a LCST is not observed for polymers with a large amount of AA. Stile et al. however found that hydrogels with 4 mol% AA content do exhibit an LCST of around 38 °C.⁶⁶ It must therefore be noted that these values found only correlate and do not match exactly with literature values due to the concentration dependent nature of cloud points, the synthetic method and the pH responsivity of acrylic acid.

Table 4.8 - Cloud point analysis of the three statistical copolymers p(NIPAM-*stat*-BAPE) synthesised using various mol% of BAPE. Analysis was repeated twice for each sample.

Mol % BAPE	CP before [O] DPBS / °C	CP after [O] DPBS / °C	Δ °C
2	23.7 ± 0.8	36.5 ± 0.1	12.8 ± 0.9
3	22.7 ± 0.8	39.7 ± 1.2	17.0 ± 1.9
5	18.0 ± 1.0	35.1 ± 1.6	17.1 ± 2.5
10	14.3 ± 0.2	-	-

After initial studies of the linear polymers, the optimum ratio of the oxidisable monomer to NIPAM was shown to be 3 mol% as the cloud point of the polymer is 23.4 °C before oxidation and 41.4 °C

after oxidation. However, due to the presence of HEA in the diblock copolymers the cloud point will be affected. Therefore, the above diblock syntheses could be repeated with a ratio of 2 mol% boronate monomer incorporated into the second pNIPAM block. It is important to note that the cloud point could vary with the differing RAFT agent (PPA) and the presence of the HEA block.

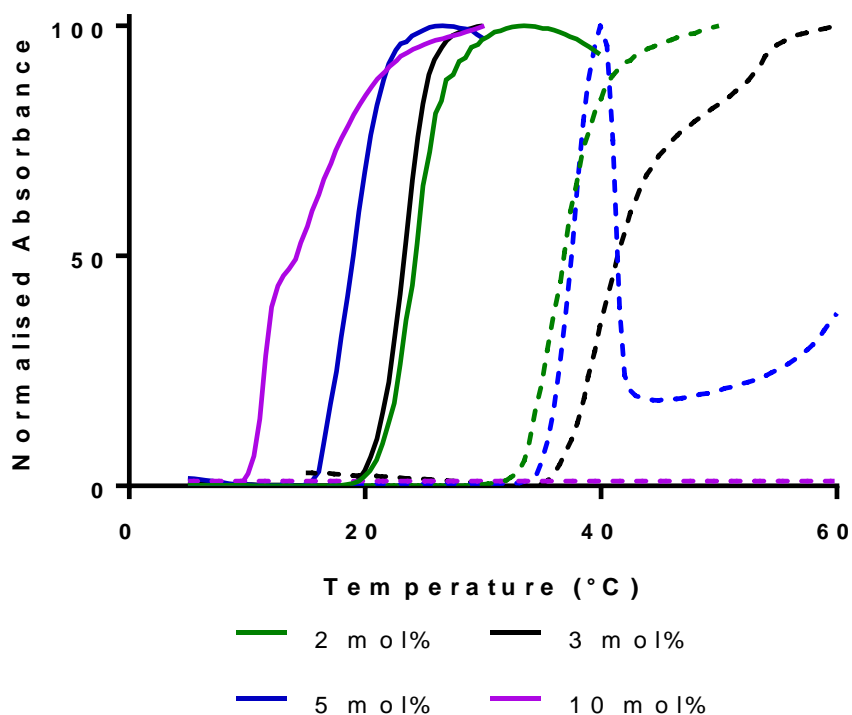
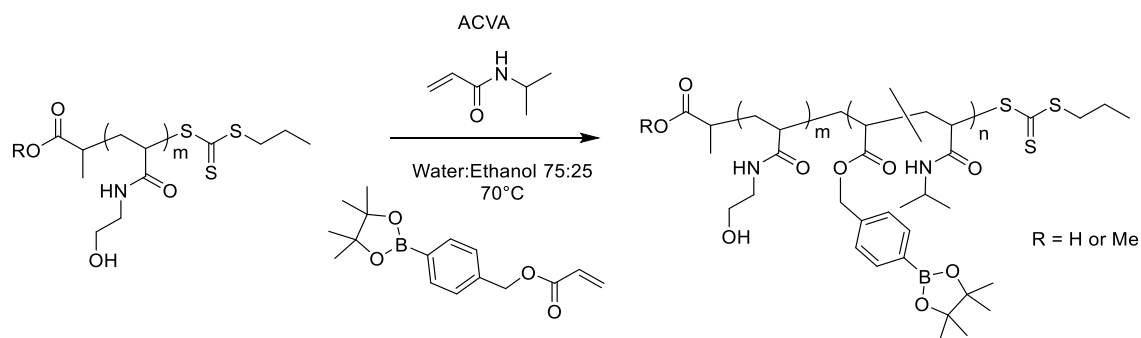


Figure 4.20 - UV-vis traces of the absorbance of $p(\text{NIPAM-stat-BAPE})_{100}$ at a concentration of 0.1 wt%, with a range of different mole percent of BAPE. This occurred over a range of temperatures, giving cloud point values before and after oxidation. Solid lines indicate native polymers and dashed lines indicate the oxidised polymer.

4.2.4. Synthesis of oxidation responsive diblock copolymers of pHEA-b-p(NIPAM-stat-BAPE) in consovents via RAFT dispersion polymerisation

Another series of diblock copolymers was synthesised using both the MPP and PPA-based pHEA-mCTA with 2 mol% BAPE incorporated into the NIPAM block (Scheme 4.9).



Scheme 4.9 - Synthesis of pHEA-b-p(NIPAM-stat-BAPE) diblock copolymers using pHEA-PPA and pHEA-MPP as the macro-CTAs

In total, 10 diblock copolymers were synthesised with BAPE incorporated into the pNIPAM block. The conversion of monomer to polymer was determined by gravimetric analysis and was found to be 80% or higher in all cases (Table 4.9). After purification by dialysis against water, the actual DP of the polymers was determined by ^1H NMR spectroscopy.

Table 4.9 - A table showing the conversion of monomer to polymer by gravimetric analysis and the actual DP of pHEA_{45/37}-b-p(NIPAM-stat-BAPE)_n

RAFT agent	[M]/[mCTA]	Conv. / % ^a	Thr. DP ^b	Avg. no. of BAPE		DP _{n,tot.} ^d	M _n / Da ^c	M _{n, GPC} / Da ^e	M _w / M _n ^e
				Thr.	NMR ^d				
MPP	126	96	121	2	2	127	20140	19060	1.39
MPP	192	90	172	3	3	193	27780	22540	1.59
MPP	259	83	215	4	4	244	33730	25730	1.67
MPP	320	91	291	6	4	301	40180	31030	1.72
MPP	363	99	315	6	4	330	43460	33520	1.67
PPA	100	96	96	2	7	101	17140	14950	1.38
PPA	150	90	135	3	3	147	21640	21280	1.34
PPA	200	93	186	4	3	193	26850	28260	1.33
PPA	250	87	218	4	4	262	34830	30590	1.38
PPA	300	90	270	5	4	318	41170	24430	1.76

^a Determined by gravimetric analysis against predicted solids content ^b [M]/[RAFT agent] × conv. ^c M_n from solids content. ^d Determined by ^1H NMR spectroscopy in D₂O ^e Determined by GPC in DMF (0.1% LiBr) with pMMA standards.

GPC analysis of these diblock copolymers showed that they are blocking efficiently, with minimal mCTA polymer chains remaining and only a small amount of bimolecular termination. However, as seen on previous polymers discussed in this chapter, there are both shoulders and tails present on all the traces (Figure 4.21, Figure 4.22). This is indicative of some pHEA which is unable to polymerise due to the loss of the RAFT agent from the ends of the polymer and that there is presence of self-termination which is likely due to the long reaction times (overnight).

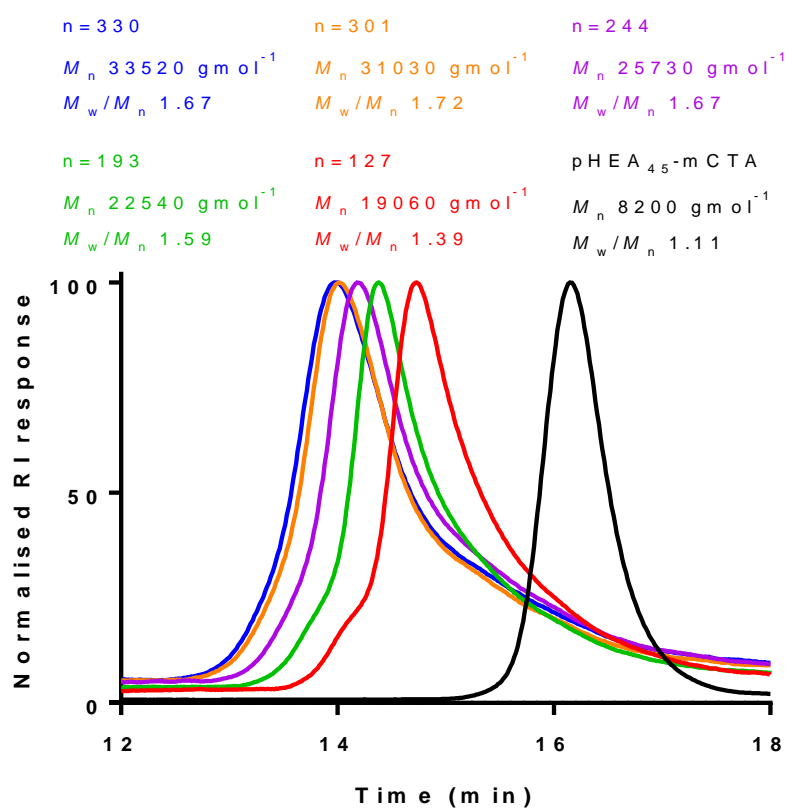


Figure 4.21 - GPC chromatograms (DMF 0.1% LiBr) of pHEA₃₇-mCTA compared with the chain extended diblock copolymers of pHEA₄₅-b-p(NIPAM-stat-BAPE)_n, where n=127, 193, 244, 301 and 330.

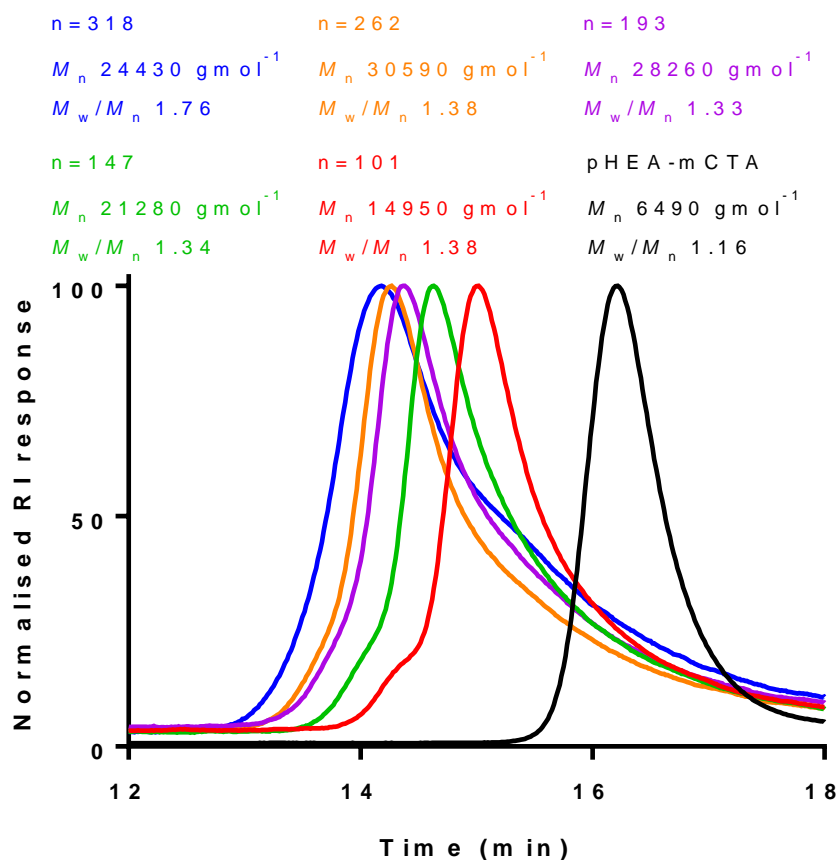


Figure 4.22 - GPC chromatograms (DMF 0.1% LiBr) of pHEA₃₇-mCTA compared with the chain extended diblock copolymers of pHEA₃₇-b-p(NIPAM-stat-BAPE)_n, where n=101, 147, 193, 262, 318.

4.2.4.1. Determination of the particle size of the self-assembled structures

As above, the initial sizing technique used to determine whether self-assembly had occurred was DLS. The temperature was increased from 15 °C to 45 °C and sizing measurements were recorded every 10 °C. Focusing on two samples, synthesised with MPP and PPA and with targeted core-forming blocks of DP 218/290 respectively, it was possible to determine whether self-assembly occurs (Figure 4.23). It can be seen clearly that at temperatures of 15 and 25 °C, minimal self-assembly is observed, seen by the peak at approximately 100 nm, however free polymer chains are seen, indicated by the peak seen at 10 nm. However, at both 35 and 45 °C, distinct particle sizes are observed but with varying particle size dispersities. The differences in dispersities is likely due to the dynamic nature of self-assembly. The structures are not fixed into their self-assembled formation and are able to move

and interchange between micelles. Another reason for the broadening of the dispersity could be due to the morphology of the particles formed. DLS uses the Stokes-Einstein equation which assumes that the particles are solid and spherical, and the rate of diffusion of these is what is correlated with the sample studied using DLS. However, it is well documented in the literature that the morphology of samples varies depending on the block length of both the hydrophilic and hydrophobic blocks, therefore the particles could deviate from a spherical morphology. Solvation of these particles also implies that these may not act as hard sphere. This could explain why the dispersity varies between samples.

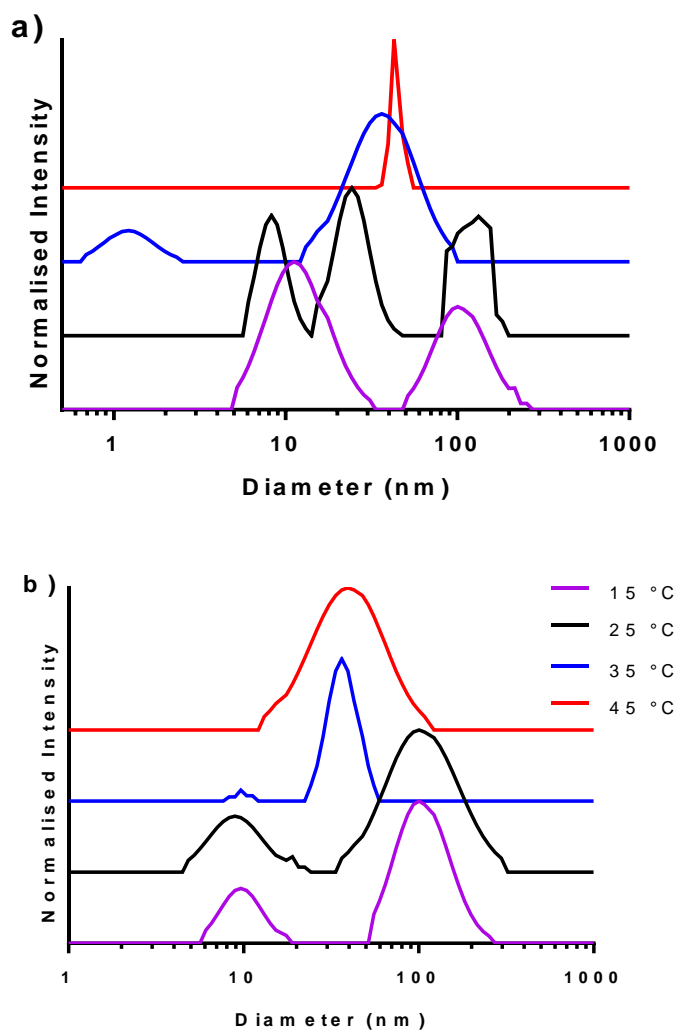


Figure 4.23 - A comparison of DLS of $pHEA_{45/37}\text{-}b\text{-}p(NIPAM\text{-}stat\text{-}BAPE)_{301/262}$, where a) MPP RAFT agent and b) PPA RAFT agent, at temperatures above and below the LCST of the polymer to determine whether self-assembly occurs as the $p(NIPAM\text{-}stat\text{-}BAPE)$ block becomes hydrophobic

DLS measurements of all 10 samples were also taken at physiological temperature (37 °C) before and after oxidation (Figure 4.25, Figure 4.26). When focusing on the influence of the two RAFT agents, MPP and PPA, and their effect on the cloud point of the BAPE containing polymers, a large difference can be seen. When the more hydrophilic RAFT agent, PPA, is used a lack of self-assembly is seen for the shortest second block length, as seen where this is a pure pNIPAM block (Figure 4.26). Whereas when MPP is the RAFT agent, this sample shows slightly weaker assembly (Figure 4.25).

When BAPE is incorporated into the second block, the size of these self-assembled structures are smaller, with all samples having a hydrodynamic diameter of less than 100 nm, indicating that BAPE must influence this (Figure 4.24). Again, peaks at 1 nm are seen in the majority of the DLS, but these are confirmed to be an artefact by the correlation curve and due to the size being smaller than the mCTA used. Although the length of the hydrophobic block varied between approximately 100 and 300, there is very little change in size on increasing the block length and the dispersities of the peaks alter but do not have an obvious correlation with the length of the hydrophobic block. It is difficult to determine accurately the dispersity of each sample as the presence of multiple peaks, in particular those at 1 nm, skew the value.

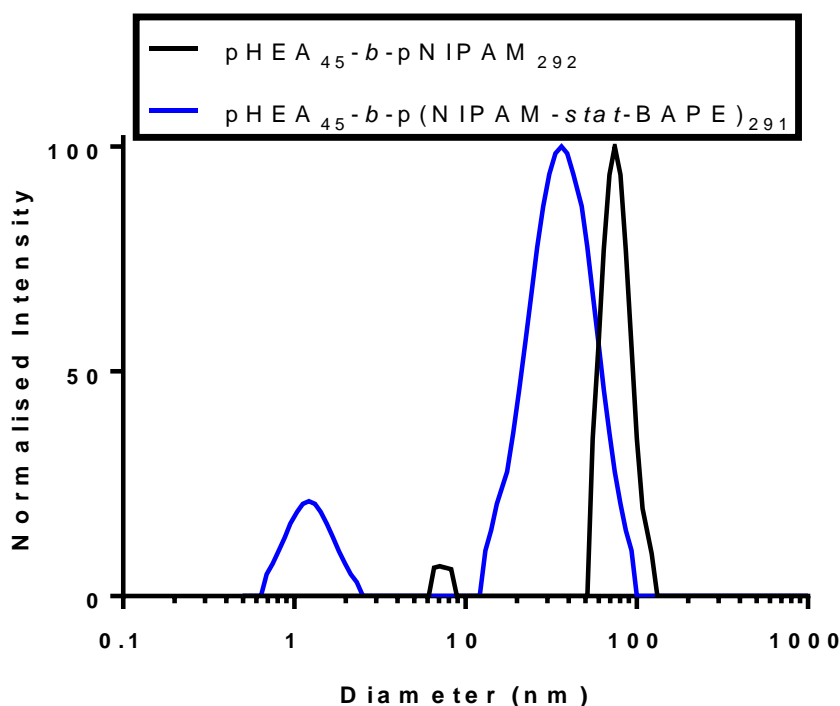


Figure 4.24 – DLS size comparison of two similar diblock copolymers, one with a pNIPAM hydrophobic core at temperatures above the LCST and the other with a NIPAM and BAPE core, at a concentration of 1 mg/ml. These were recorded in water and show that when BAPE is incorporated into the core the self-assembled structure is smaller at 35 °C.

Unlike the samples above where the second block consisted of only pNIPAM, the BAPE-containing polymers show a large change in size on oxidation when compared to the native polymer. The size of these particles increases to over 100 nm at every polymer length. This suggests that oxidation is changing the cloud point, as predicted from the results of the linear pNIPAM-*stat*-BAPE oxidation. The oxidised polymers are larger than the native polymers at the same temperature, which implies that there is a change in particle size when the LCST of the polymers are raised.^{30,67,68} However, these do not disassemble after oxidation which could indicate that the LCST value has not increased enough after oxidation to cause the pNIPAM block of the polymer to become soluble at body temperature.

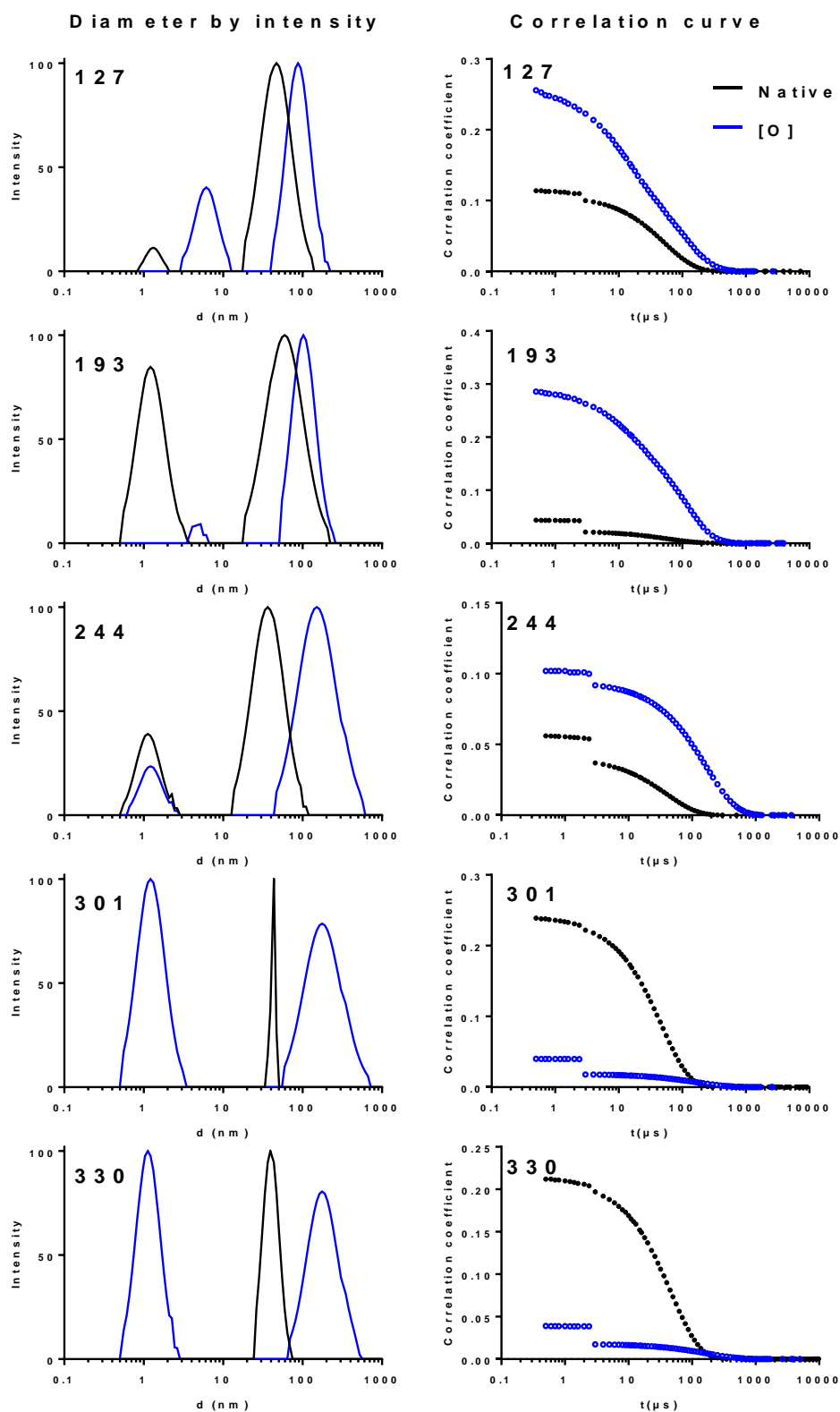


Figure 4.25 - DLS particle size distributions and corresponding correlation curves of diblock copolymers of $pHEA_{45}\text{-}b\text{-}p(NIPAM\text{-}stat\text{-}BAPE)_n$, with MPP as the RAFT agent and 2 mol% BAPE, at a concentration of 1 mg/ml. These were recorded in water and held at 37 °C, before and after oxidation where a) $n=127$, b) $n=193$, c) $n=244$, d) $n=301$ and e) $n=330$.

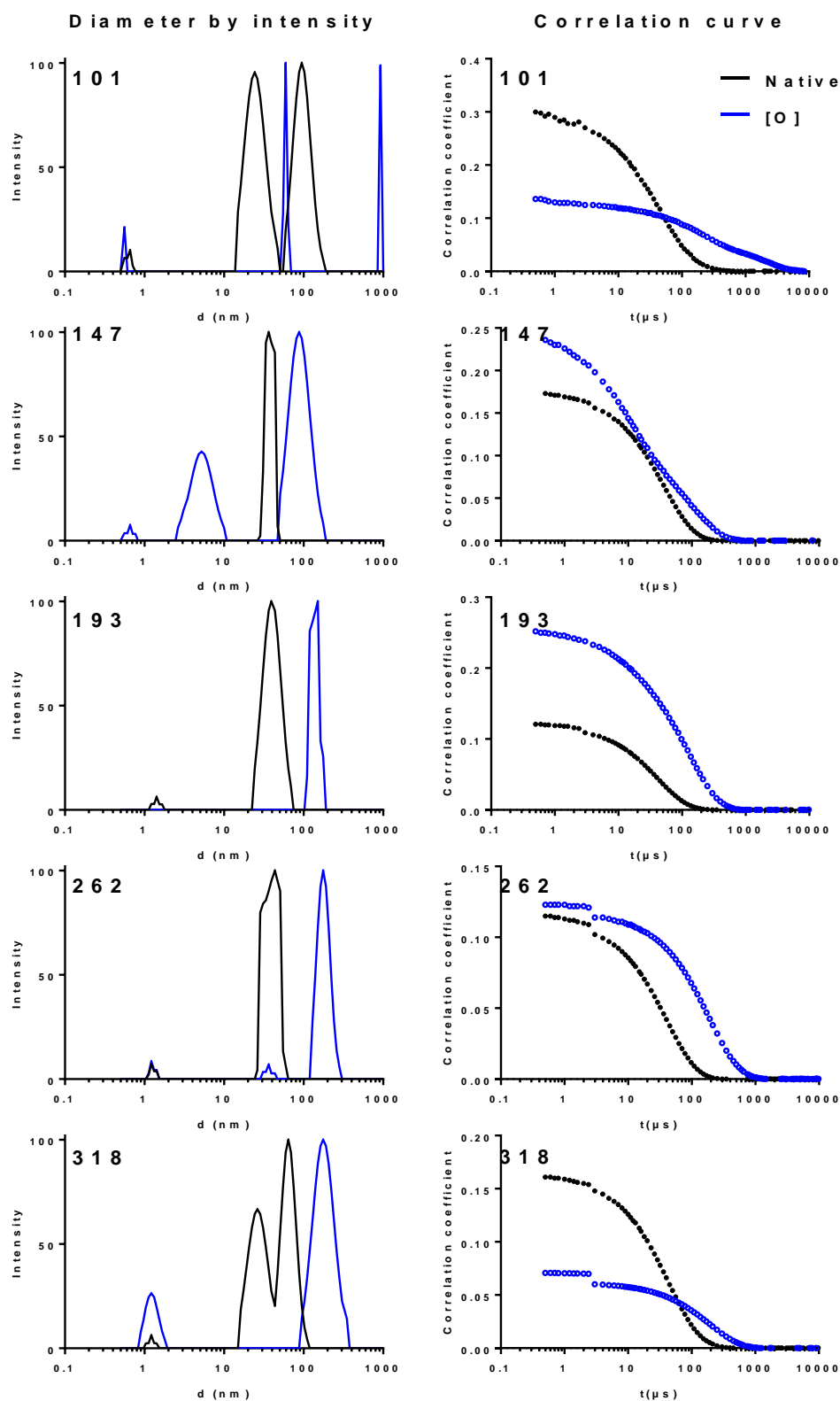


Figure 4.26 - DLS particle size distributions and corresponding correlation curves (DMF 0.1% LiBr) of diblock copolymers of $pHEA_{37}\text{-}b\text{-}p(NIPAM\text{-}stat\text{-}BAPE)_n$ with PPA as the RAFT agent and 2 mol% BAPE, at a concentration of 1 mg/ml. These were recorded in water and held at 37 °C, before and after oxidation where a) $n=101$, b) $n=147$, c) $n=193$, d) $n=262$ and e) $n=318$.

4.3. Conclusions

In conclusion, a range of temperature and oxidation-responsive block copolymers have been synthesised and show potential, with further work, for oxidation responsive drug delivery systems. The assembled size of the particles formed at temperatures above the LCST are below 100 nm, which is ideal for drug delivery. This enables safe movement around the body before drug release. Also, the lengths of the polymer chains have been targeted so that the final mass of these is <45 kDa, which has been stated in the literature as the limit for safe renal excretion.¹⁸

For the block copolymers with a short chain hydrophobic block, no self-assembly is observed by DLS. For the polymers with the longer chain hydrophobic group however, self-assembly is evident with particle sizes of approximately 100 nm. The incorporation of an oxidation responsive group into the hydrophobic block of the polymer caused an increase in size of the particles in all cases, for example, pHEA₄₅-*b*-pNIPAM₂₉₂ has a diameter of 36 nm by DLS, but a similar diblock copolymer, pHEA₄₅-*b*-p(NIPAM-*stat*-BAPE)₂₉₁, has a diameter of 74 nm, due to the change in LCST on oxidation. This could potentially cause faster release of any encapsulated material.

Although this system has many positive points, the self-assembly is unlikely to be stable enough to transport a payload without leakage. It is widely reported in the literature that disassembly of micelles can be caused by many different chemical and physical changes including heat, salt concentration, pH, polymer concentration and more, which could cause premature drug release.

This has provided a firm base for further work on these systems. A suitable oxidation responsive monomer which can be copolymerised with NIPAM has been found which can elicit an oxidation response with high sensitivity to H₂O₂. Problems with this system can be alleviated using the same procedures and reagents used here but incorporating a crosslinking molecule as the core forming block polymerises to form crosslinked particles. Crosslinked particles retain the self-assembled structure formed even when the temperature is much lower than the LCST. These nanogels could have an oxidation response incorporated through either the crosslinker, causing disassembly of the

structure on oxidation, or by incorporation of BAPE into the core to change the LCST and therefore change the size of the core due to swelling on oxidation.

4.4. References

- 1 K. T. Savjani, A. K. Gajjar and J. K. Savjani, *ISRN Pharm.*, 2012, **2012**, 1–10.
- 2 C. Deng, Y. Jiang, R. Cheng, F. Meng and Z. Zhong, *Nano Today*, 2012, **7**, 467–480.
- 3 K. Kataoka, A. Harada and Y. Nagasaki, *Adv. Drug Deliv. Rev.*, 2001, **47**, 113–131.
- 4 H. Cabral, K. Miyata, K. Osada and K. Kataoka, *Chem. Rev.*, 2018, **118**, 6844–6892.
- 5 J. A. Champion, A. Walker and S. Mitragotri, *Pharm. Res.*, 2008, **25**, 1815–1821.
- 6 A. Blanz, A. J. Ryan and S. P. Armes, *Macromolecules*, 2012, **45**, 5099–5107.
- 7 T. Yamaoka, Y. Tabata and Y. Ikada, *J. Pharm. Sci.*, 1994, **83**, 601–606.
- 8 T. Yamaoka, Y. Tabata and Y. Ikada, *J. Pharm. Pharmacol.*, 1995, **47**, 479–486.
- 9 L. W. Seymour, R. Duncan, J. Strohalm and J. Kopecek, *J. Biomed. Mater. Res.*, 1987, **21**, 1341–1358.
- 10 K. S. Soni, S. S. Desale and T. K. Bronich, *J. Control. Release*, 2016, **240**, 109–126.
- 11 Y. Geng, P. Dalhaimer, S. Cai, R. Tsai, M. Tewari, T. Minko and D. E. Discher, *Nat. Nanotechnol.*, 2007, **2**, 249–255.
- 12 M. Tang, P. Hu, Q. Zheng, N. Tirelli, X. Yang, Z. Wang, Y. Wang, Q. Tang and Y. He, *J. Nanobiotechnology*, 2017, **15**, 1–11.
- 13 Y. Hiruta, Y. Kanda, N. Katsuyama and H. Kanazawa, *RSC Adv.*, 2017, **7**, 29540–29549.
- 14 M. Nuopponen, J. Ojala and H. Tenhu, *Polymer (Guildf.)*, 2004, **45**, 3643–3650.
- 15 S. Kasmi, B. Louage, L. Nuhn, G. Verstraete, S. Van Herck, M. J. Van Steenberghe, C. Vervaeke, W. E. Hennink and B. G. De Geest, *Polym. Chem.*, 2017, **8**, 6544–6557.
- 16 D. D. Lane, D. Y. Chiu, F. Y. Su, S. Srinivasan, H. B. Kern, O. W. Press, P. S. Stayton and A. J. Convertine, *Polym. Chem.*, 2015, **6**, 1286–1299.
- 17 B. Louage, Q. Zhang, N. Vanparijs, L. Voorhaar, S. Vande Casteele, Y. Shi, W. E. Hennink, J. Van Bocxlaer, R. Hoogenboom and B. G. De Geest, *Biomacromolecules*, 2015, **16**, 336–350.
- 18 S. Grund, M. Bauer and D. Fischer, *Adv. Eng. Mater.*, 2011, **13**, B61–B67.

- 19 J. Yue, R. Wang, S. Liu, S. Wu, Z. Xie, Y. Huang and X. Jing, *Soft Matter*, 2012, **8**, 7426.
- 20 A. Nikoubashman and A. Z. Panagiotopoulos, *J. Chem. Phys.*, 2014, **141**, 1–5.
- 21 Z. Gao and A. Eisenberg, *Macromolecules*, 1993, **26**, 7353–7360.
- 22 A. Blanazs, S. P. Armes and A. J. Ryan, *Macromol. Rapid Commun.*, 2009, **30**, 267–277.
- 23 R. O. . Costa and R. F. . Freitas, *Polymer (Guildf).*, 2002, **43**, 5879–5885.
- 24 H. G. Schild, M. Muthukumar and D. A. Tirrell, *Macromolecules*, 1991, **24**, 948–952.
- 25 F. M. Winnik, M. F. Ottaviani, S. H. Boßmann, W. Pan, M. Garcia-Garibay and N. J. Turro, *Macromolecules*, 1993, **26**, 4577–4585.
- 26 M. J. A. Hore, B. Hammouda, Y. Li and H. Cheng, *Macromolecules*, 2013, **46**, 7894–7901.
- 27 S. Backes, P. Krause, W. Tabaka, M. U. Witt, D. Mukherji, K. Kremer and R. Von Klitzing, *ACS Macro Lett.*, 2017, **6**, 1042–1046.
- 28 H. Yamauchi and Y. Maeda, *J. Phys. Chem. B*, 2007, **111**, 12964–12968.
- 29 N. Osaka and M. Shibayama, *Macromolecules*, 2012, **45**, 2171–2174.
- 30 Y. Xu, Y. Li, X. Cao, Q. Chen and Z. An, *Polym. Chem.*, 2014, **5**, 6244–6255.
- 31 C. S. Biswas, K. Mitra, S. Singh and B. Ray, *J. Chem. Sci.*, 2016, **128**, 415–420.
- 32 R. B. Penndorf, *J. Phys. Chem.*, 2005, **62**, 1537–1542.
- 33 I. M. Krieger and F. M. O’Neill, *J. Am. Chem. Soc.*, 1968, **90**, 3114–3120.
- 34 H. Horvath, *J. Quant. Spectrosc. Radiat. Transf.*, 2009, **110**, 787–799.
- 35 Y. Zhang, S. Luo and S. Liu, *Macromolecules*, 2005, **38**, 9813–9820.
- 36 R. Zhang, R. Yao, B. Ding, Y. Shen, S. Shui, L. Wang, Y. Li, X. Yang and W. Tao, *Adv. Mater. Sci. Eng.*, 2014, **2014**, 1–9.
- 37 Y. Zhou, K. Jiang, Y. Chen and S. Liu, *J. Polym. Sci. Part A Polym. Chem.*, 2008, **46**, 6518–6531.
- 38 S. Bhattacharjee, *J. Control. Release*, 2016, **235**, 337–351.
- 39 J. R. Lovett, N. J. Warren, L. P. D. Ratcliffe, M. K. Kocik and S. P. Armes, *Angew. Chemie - Int. Ed.*, 2015, **54**, 1279–1283.

- 40 A. O. Moughton and R. K. O'Reilly, *Chem. Commun.*, 2010, **46**, 1091–1093.
- 41 P. A. Fitzgerald, S. Gupta, K. Wood, S. Perrier and G. G. Warr, *Langmuir*, 2014, **30**, 7986–7992.
- 42 M. J. Summers, D. J. Phillips and M. I. Gibson, *Chem. Commun.*, 2013, **49**, 4223–4225.
- 43 C. De Gracia Lux, S. Joshi-Barr, T. Nguyen, E. Mahmoud, E. Schopf, N. Fomina and A. Almutairi, *J. Am. Chem. Soc.*, 2012, **134**, 15758–15764.
- 44 K. Sato, M. Takahashi, M. Ito, E. Abe and J. I. Anzai, *Langmuir*, 2014, **30**, 9247–9250.
- 45 C. Li, J. Hu, T. Liu and S. Liu, *Macromolecules*, 2011, **44**, 429–431.
- 46 K. E. Broaders, S. Grandhe and J. M. J. J. Fréchet, *J. Am. Chem. Soc.*, 2011, **133**, 756–758.
- 47 A. Iturmendi, U. Monkowius and I. Teasdale, *ACS Macro Lett.*, 2017, **6**, 150–154.
- 48 T. Zhang, X. X. Chen, C. Xiao, X. Zhuang and X. X. Chen, *Polym. Chem.*, 2017, **8**, 6209–6216.
- 49 Y. Kuang, K. Balakrishnan, V. Gandhi and X. Peng, *J. Am. Chem. Soc.*, 2011, **133**, 19278–19281.
- 50 E. W. Miller, A. E. Albers, A. Pralle, E. Y. Isacoff and C. J. Chang, *J. Am. Chem. Soc.*, 2005, **127**, 16652–16659.
- 51 L. Wang, S. Xie, L. Ma, Y. Chen and W. Lu, *Eur. J. Med. Chem.*, 2016, **116**, 84–89.
- 52 G. C. Van de Bittner, E. A. Dubikovskaya, C. R. Bertozzi and C. J. Chang, *Proc. Natl. Acad. Sci.*, 2010, **107**, 21316–21321.
- 53 A. C. Sedgwick, X. Sun, G. Kim, J. Yoon, S. D. Bull and T. D. James, *Chem. Commun.*, 2016, **52**, 12350–12352.
- 54 A. C. Sedgwick, H. H. Han, J. E. Gardiner, S. D. Bull, X. P. He and T. D. James, *Chem. Sci.*, 2018, **9**, 3672–3676.
- 55 M. Reverte, A. Vaissiere, P. Boisguerin, J. J. Vasseur and M. Smietana, *ACS Sensors*, 2016, **1**, 970–974.
- 56 S. Palanisamy, P. Y. Wu, S. C. Wu, Y. J. Chen, S. C. Tzou, C. H. Wang, C. Y. Chen and Y. M. Wang, *Biosens. Bioelectron.*, 2017, **91**, 849–856.
- 57 J. L. M. Jourden, K. B. Daniel and S. M. Cohen, *Chem. Commun.*, 2011, **47**, 7968–7970.
- 58 C.-C. Song, F.-S. Du and Z.-C. Li, *J. Mater. Chem. B*, 2014, **2**, 3413.

- 59 I. Klopčič and M. S. Dolenc, *Chem. Res. Toxicol.*, 2019, **32**, 1–34.
- 60 M. Zhang, C.-C. Song, R. Ji, Z.-Y. Qiao, C. Yang, F.-Y. Qiu, D.-H. Liang, F.-S. Du and Z.-C. Li, *Polym. Chem.*, 2016, **7**, 1494–1504.
- 61 Y. Okamoto, K. Morishita, Y. Fuchi, S. Kobayashi and S. Karasawa, *Appl. Sci.*, 2018, **8**, 1080.
- 62 C. C. Song, R. Ji, F. S. Du, D. H. Liang and Z. C. Li, *ACS Macro Lett.*, 2013, **2**, 273–277.
- 63 X. Gao, Y. Cao, X. Song, Z. Zhang, C. Xiao, C. He and X. Chen, *J. Mater. Chem. B*, 2013, **1**, 5578–5587.
- 64 Mi Kyong Yoo, Yong Kiel Sung, S. C. Chong and M. L. Young, *Polymer (Guildf.)*, 1997, **38**, 2759–2765.
- 65 M. Kyong Yoo, Y. Kiel Sung, Y. Moo Lee and C. Su Cho, *Polymer (Guildf.)*, 1998, **39**, 3703–3708.
- 66 R. A. Stile, W. R. Burghardt and K. E. Healy, *Macromolecules*, 1999, **32**, 7370–7379.
- 67 E. Parrish, S. C. Seeger and R. J. Composto, *Macromolecules*, 2018, **51**, acs.macromol.8b00335.
- 68 M. Pruettiphap, G. L. Rempel, Q. Pan and S. Kiatkamjornwong, *Iran. Polym. J.*, 2017, **26**, 957–969.

Appendix B

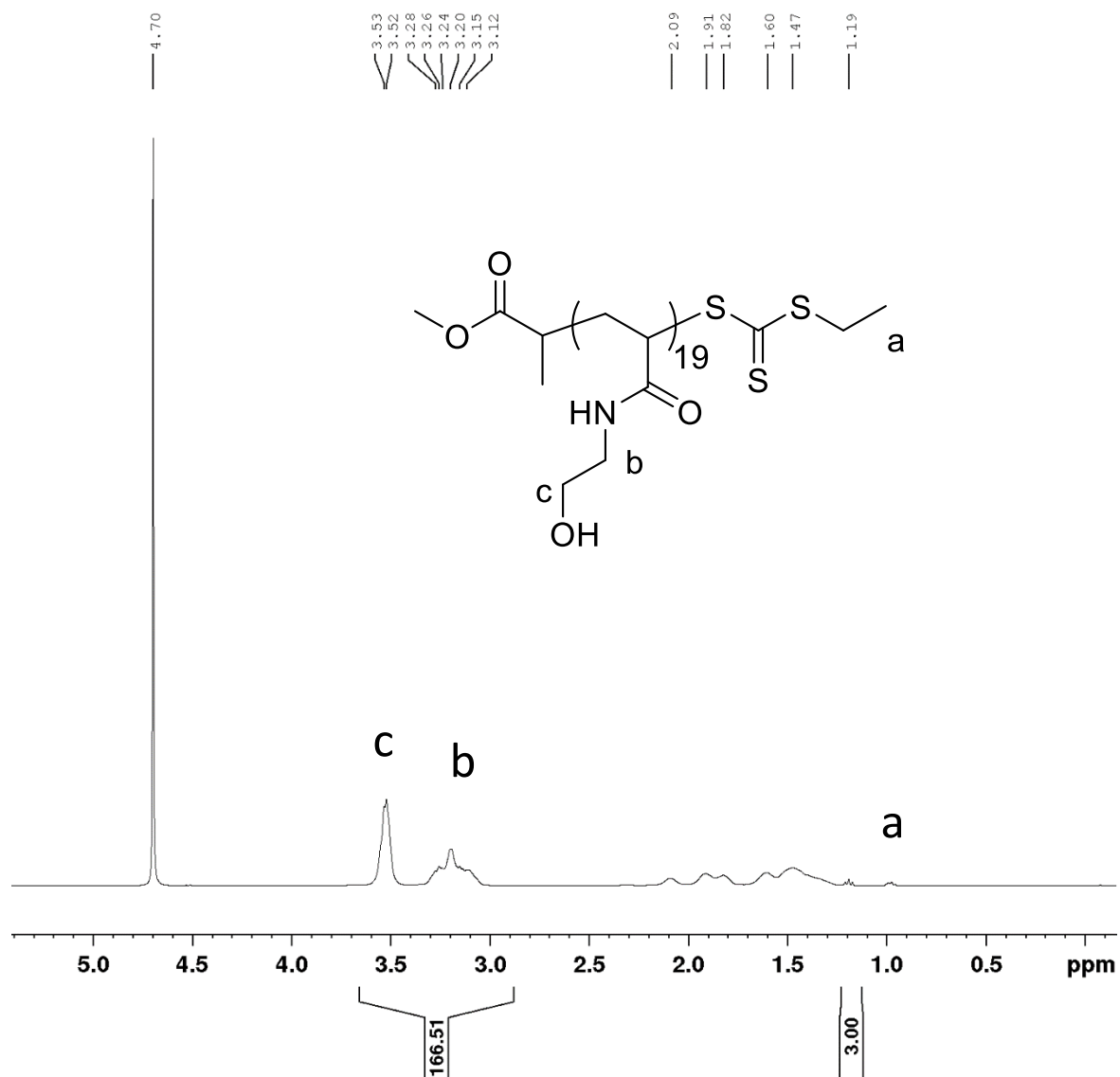


Figure B.1 - ^1H NMR spectrum of $\text{pHEA}_{19}\text{-EMEM}$ in D_2O . Degree of polymerisation was determined from the ratio of the integrals for methyl group of RAFT end group (1.20 ppm) and side chains on HEA (3.00-3.65 ppm).

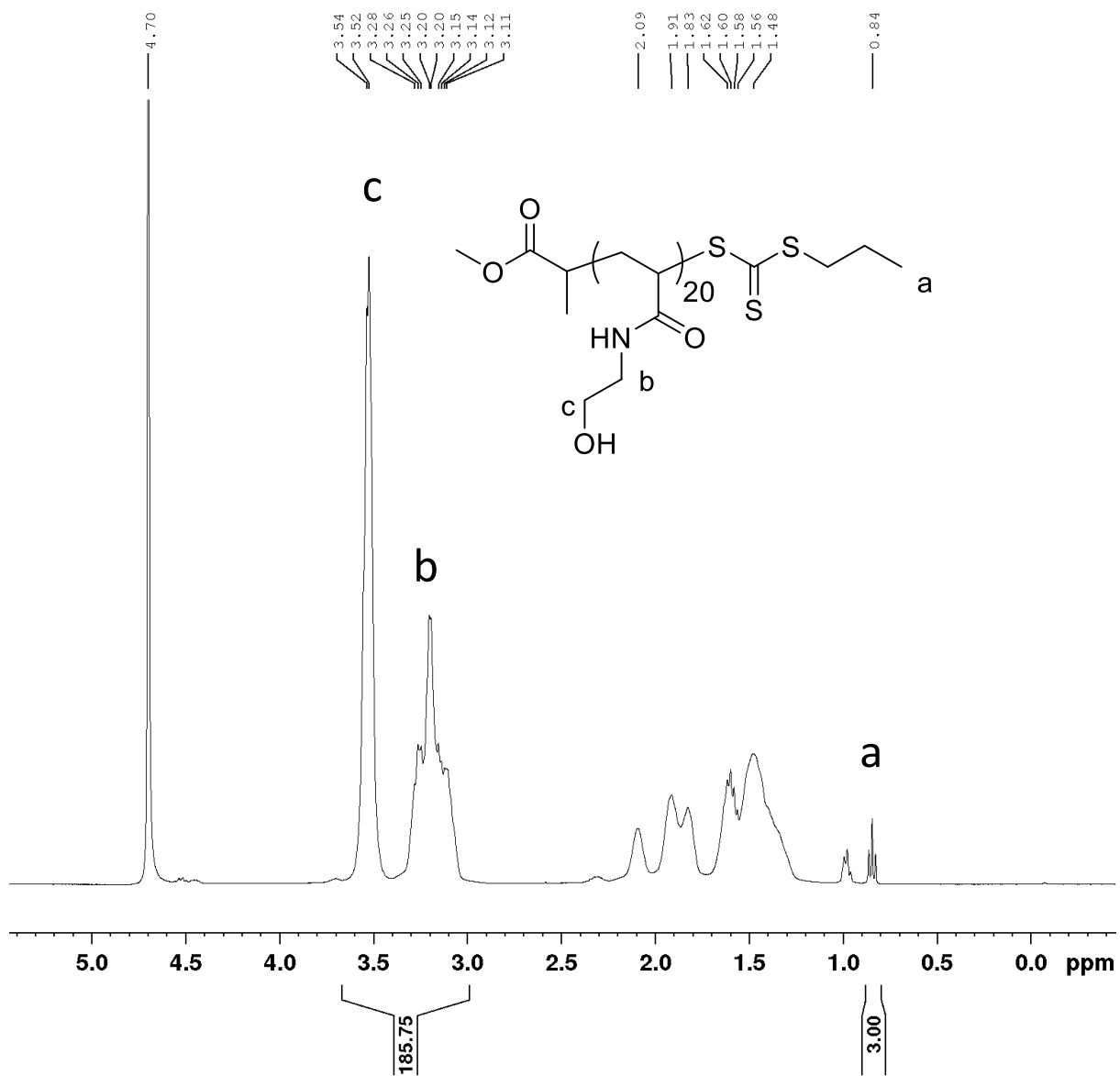


Figure B.2 - ^1H NMR spectrum of pHEA₂₀-MPP in D₂O. Degree of polymerisation was determined from the ratio of the integrals for methyl group of RAFT end group (0.85 ppm) and side chains on HEA (3.00-3.65 ppm).

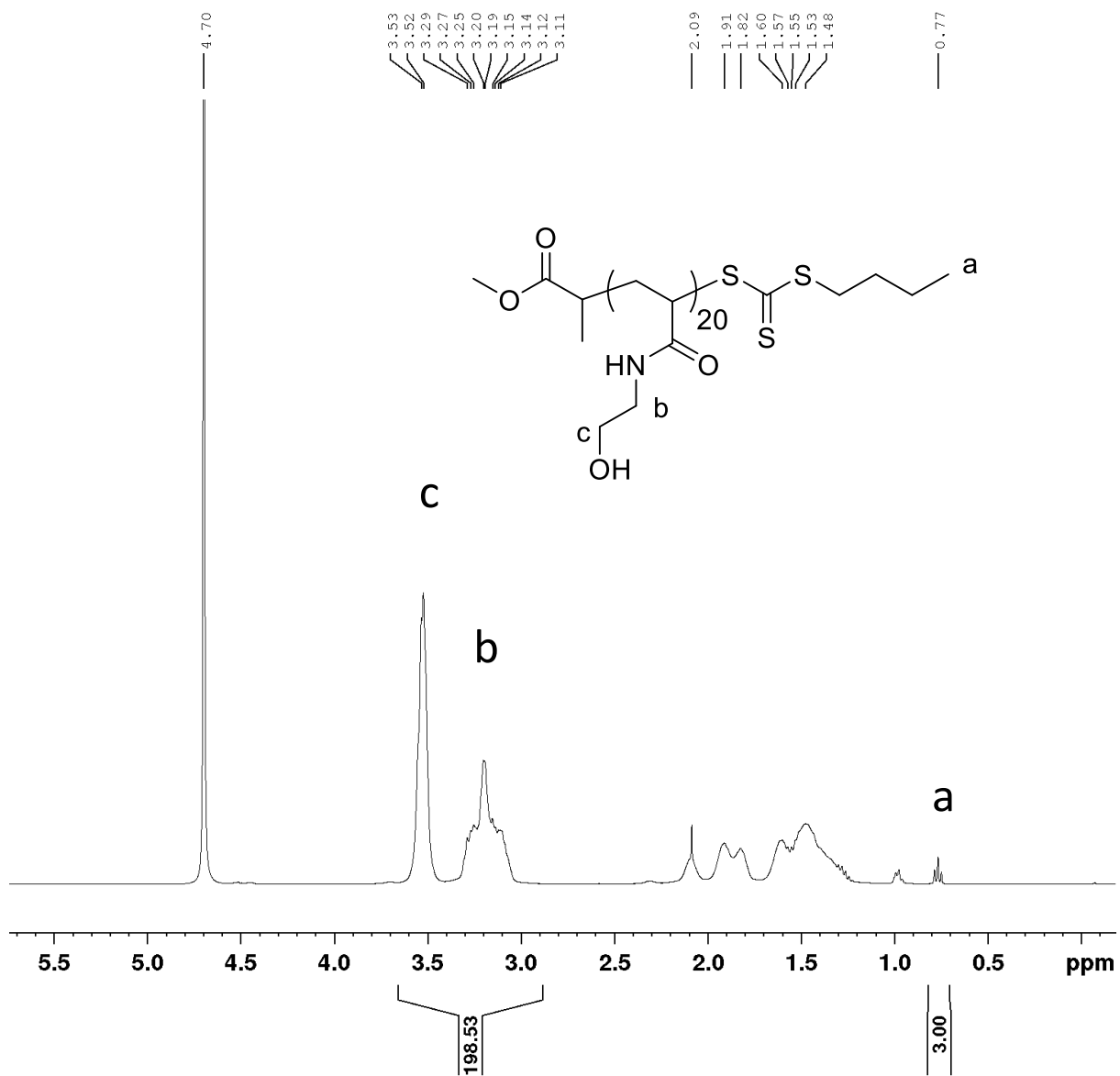


Figure B.3 ^1H NMR spectrum of $\text{pHEA}_{20}\text{-MBP}$ in D_2O . Degree of polymerisation was determined from the ratio of the integrals for methyl group of RAFT end group (0.75 ppm) and side chains on HEA (3.00-3.65 ppm).

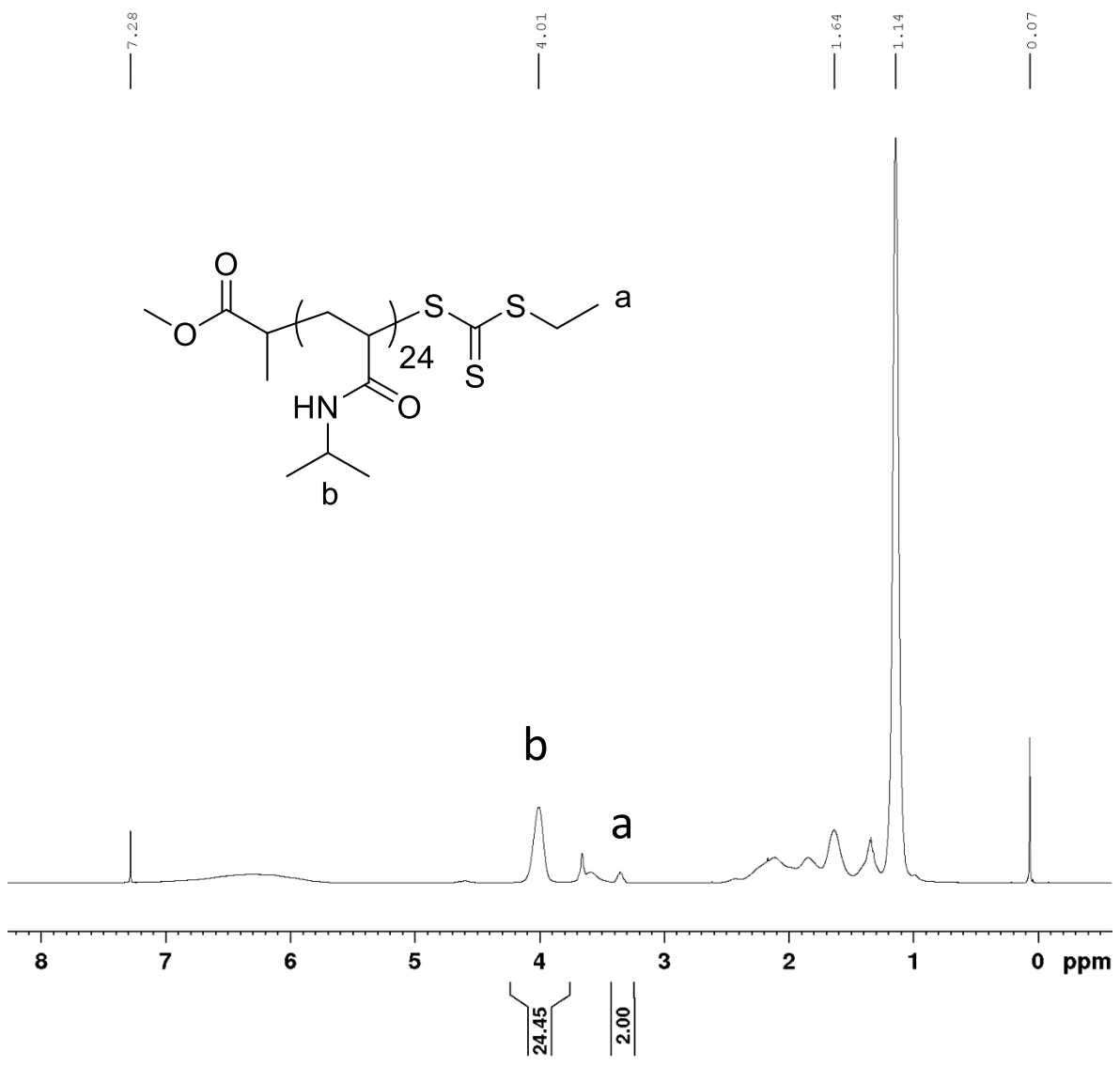


Figure B.4 - ¹H NMR spectrum of pNIPAM₂₄-EMEM in CDCl₃. Degree of polymerisation was determined from the ratio of the integrals for methylene group of RAFT end group (3.35 ppm) and the CH₃CH group on NIPAM (4.05 ppm).

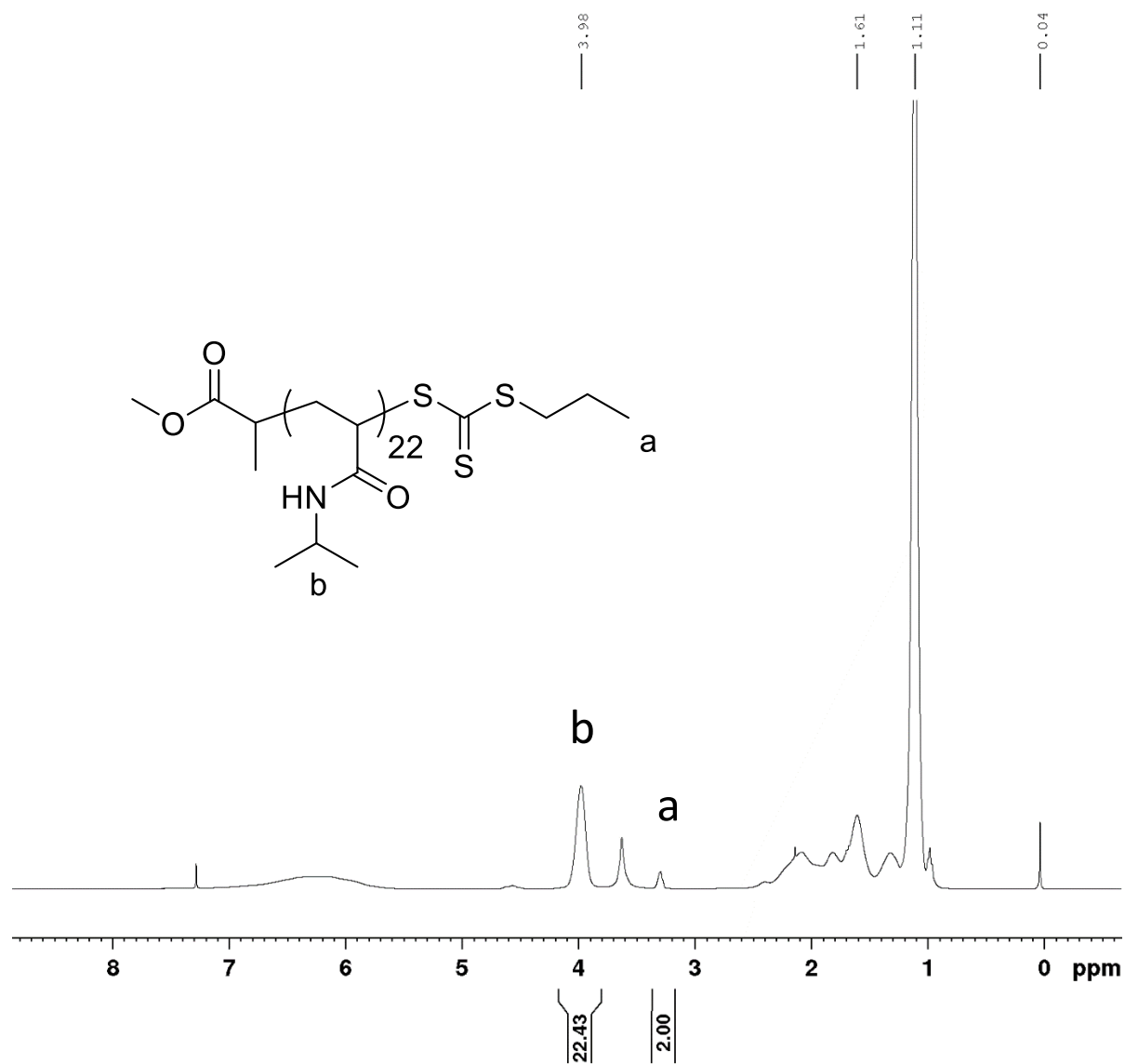


Figure B.5 - ¹H NMR spectrum of pNIPAM₂₂-MPP in CDCl₃. Degree of polymerisation was determined from the ratio of the integrals for methylene group of RAFT end group (3.35 ppm) and the CH₂CH group on NIPAM (4.05 ppm).

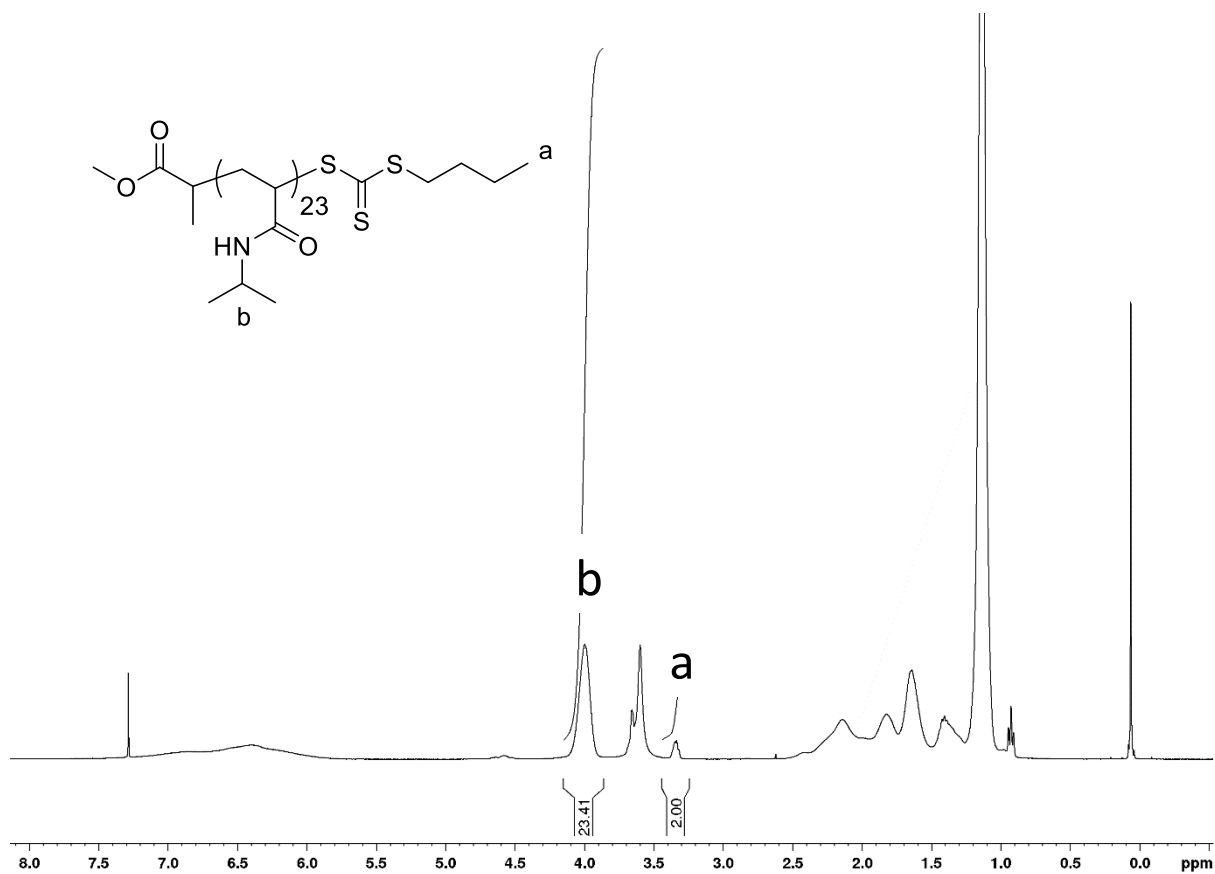


Figure B.6 - ¹H NMR spectrum of pNIPAM₂₃-MBP in CDCl₃. Degree of polymerisation was determined from the ratio of the integrals for methylene group of RAFT end group (3.35 ppm) and the CH₃CH group on NIPAM (4.05 ppm).

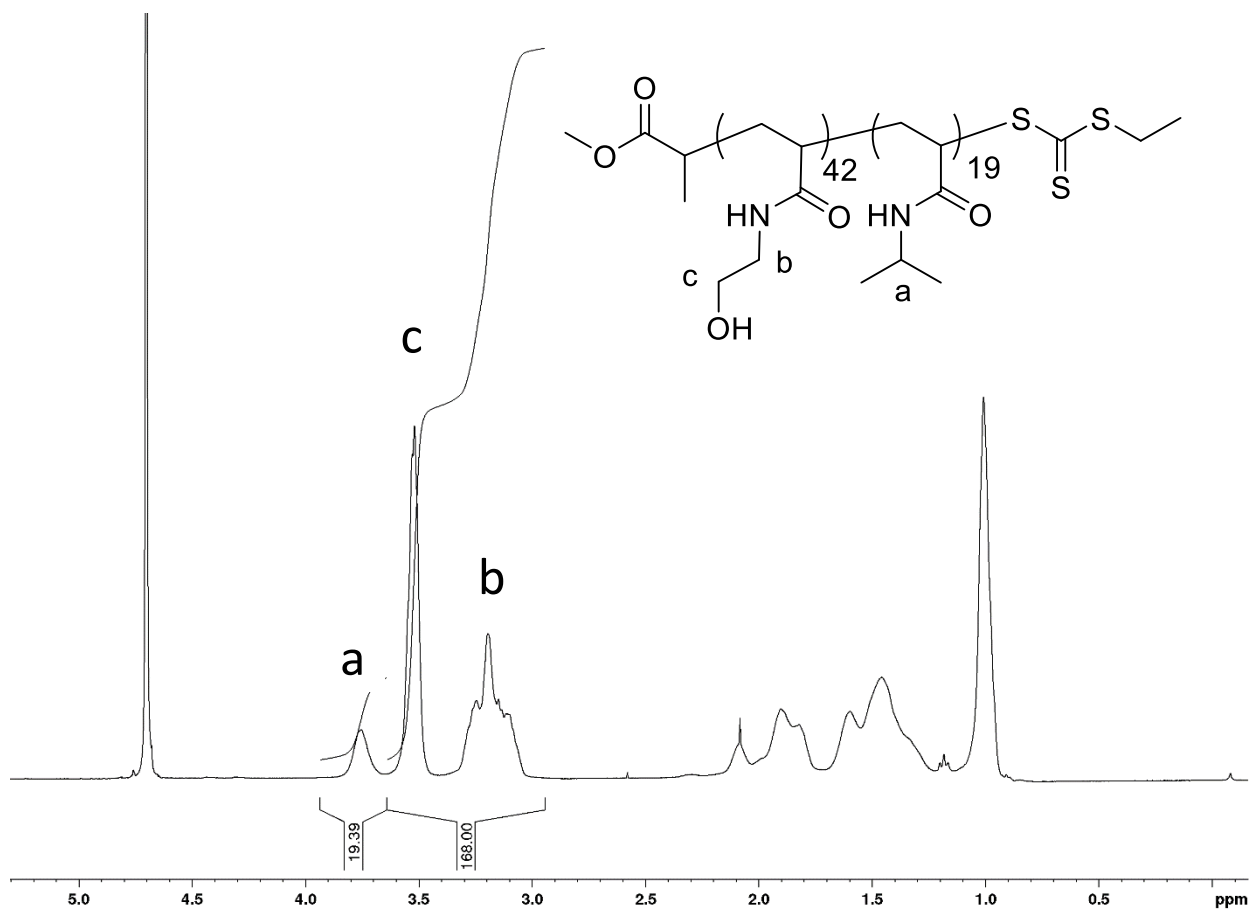


Figure B.7 - ^1H NMR spectrum of pHEA₄₂-b-pNIPAM₁₉-EMEM in D_2O . Degree of polymerisation was determined from the ratio of the integrals for the CH_3CH group on NIPAM (3.75 ppm) and the side chains on HEA (3.00-3.65 ppm), knowing the DP of the pHEA-mCTA.

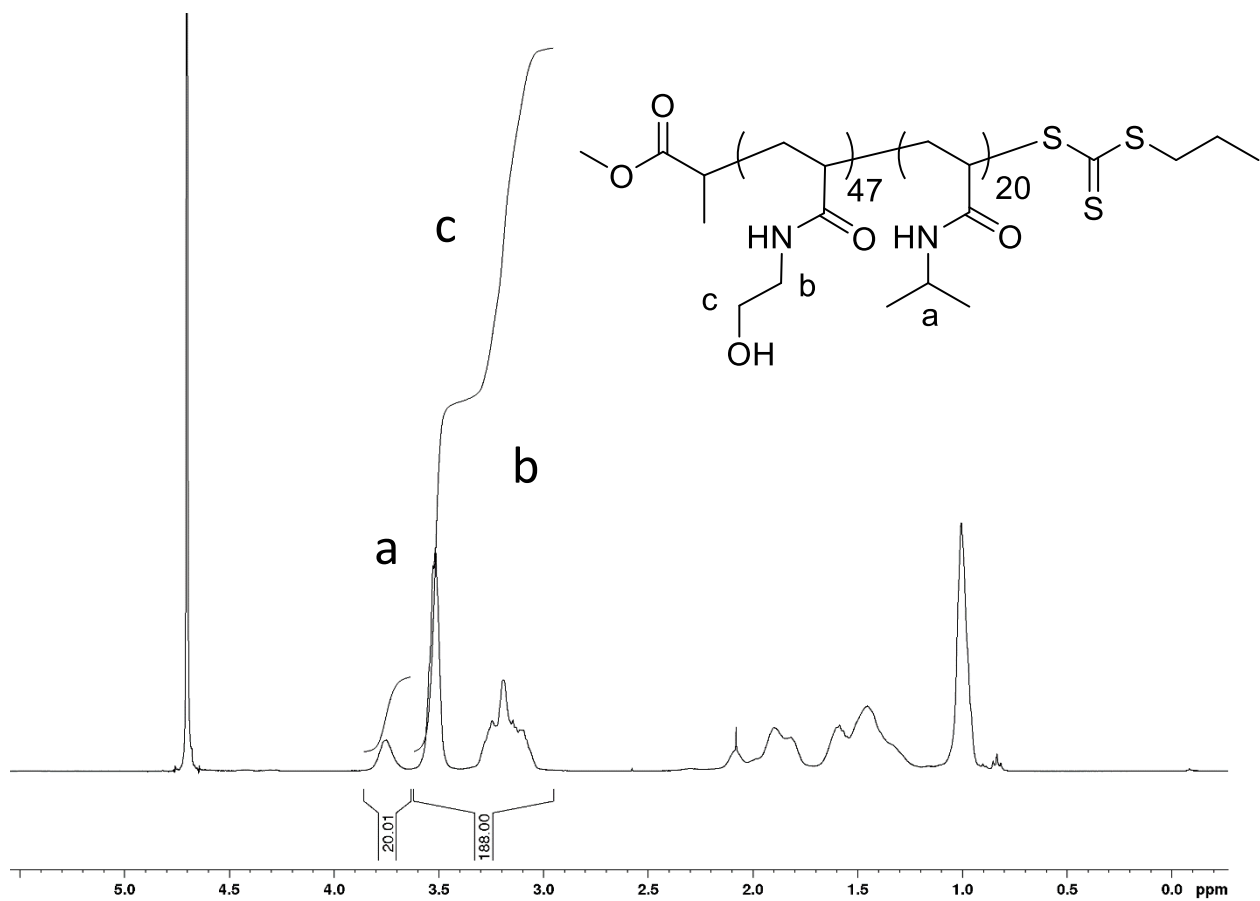


Figure B.8 - ^1H NMR spectrum of pHEA₄₇-b-pNIPAM₂₀-MPP in D_2O . Degree of polymerisation was determined from the ratio of the integrals for the CH_3CH group on NIPAM (3.75 ppm) and the side chains on HEA (3.00-3.65 ppm), knowing the DP of the pHEA-mCTA.

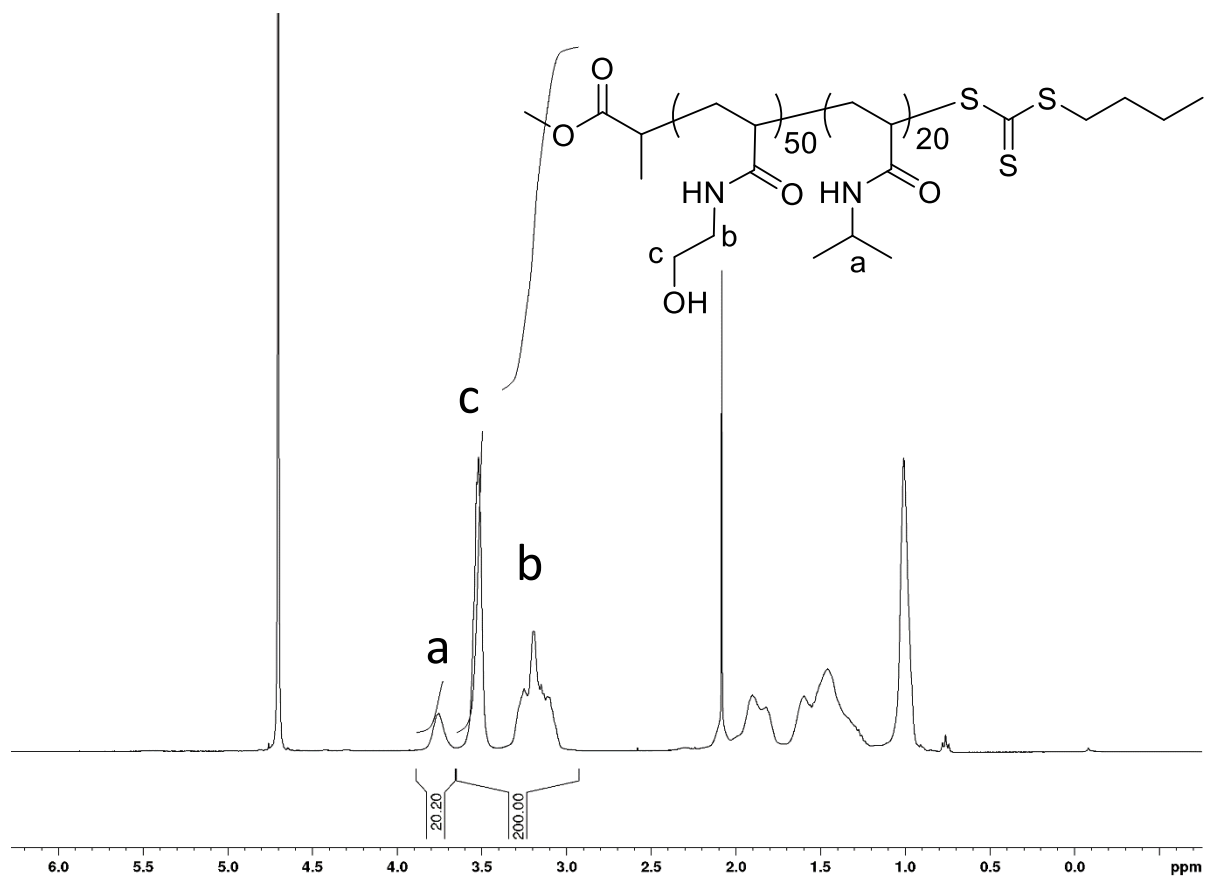


Figure B.9 - ^1H NMR spectrum of $\text{pHEA}_{50}\text{-b-pNIPAM}_{20}\text{-MBP}$ in D_2O . Degree of polymerisation was determined from the ratio of the integrals of the CH_3CH group on NIPAM (3.75 ppm) and the side chains on HEA (3.00-3.65 ppm), knowing the DP of the pHEA-mCTA.

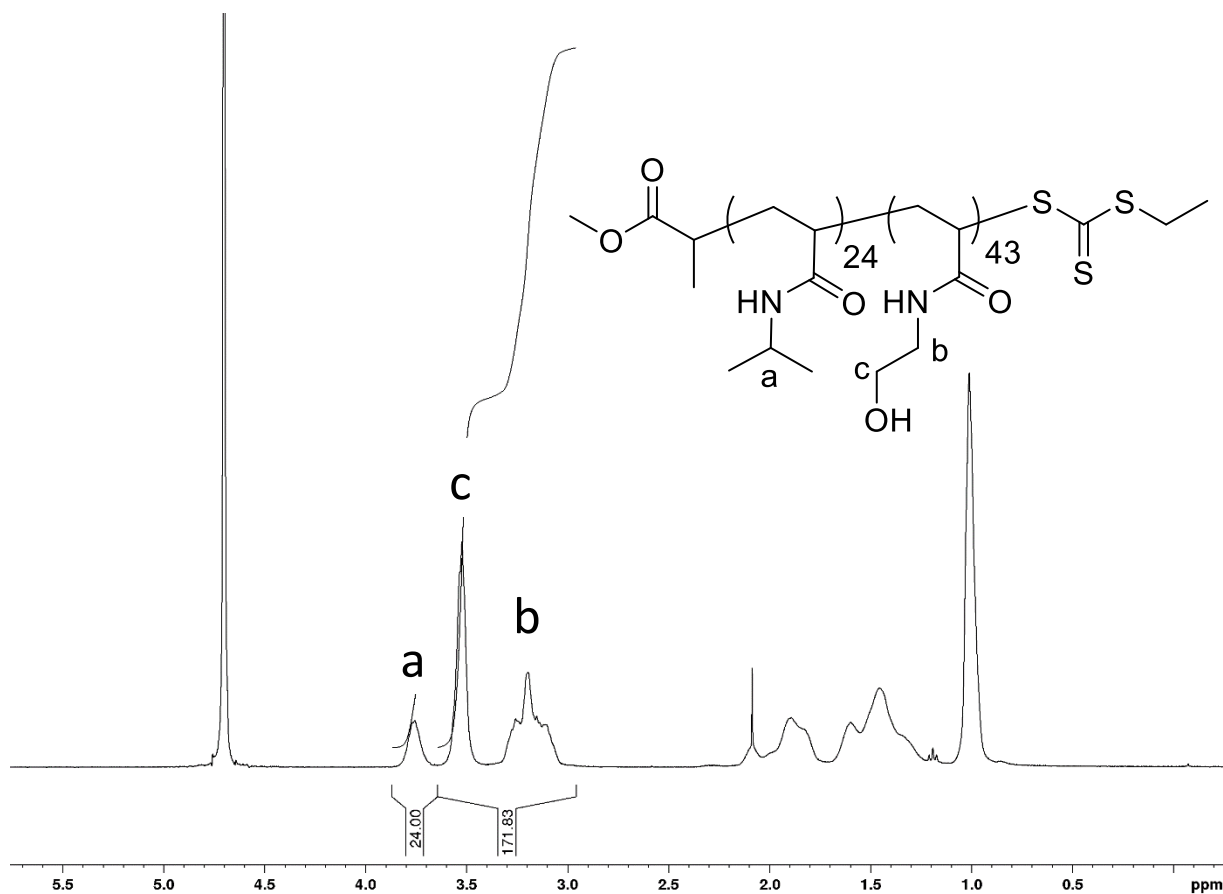


Figure B.10 - ^1H NMR spectrum of $p\text{NIPAM}_{24}\text{-}b\text{-}p\text{HEA}_{43}\text{-EMEM}$ in D_2O . Degree of polymerisation was determined from the ratio of the integrals of the CH_3CH group on NIPAM (3.75 ppm) and the side chains on HEA (3.00-3.65 ppm), knowing the DP of the $p\text{NIPAM-mCTA}$.

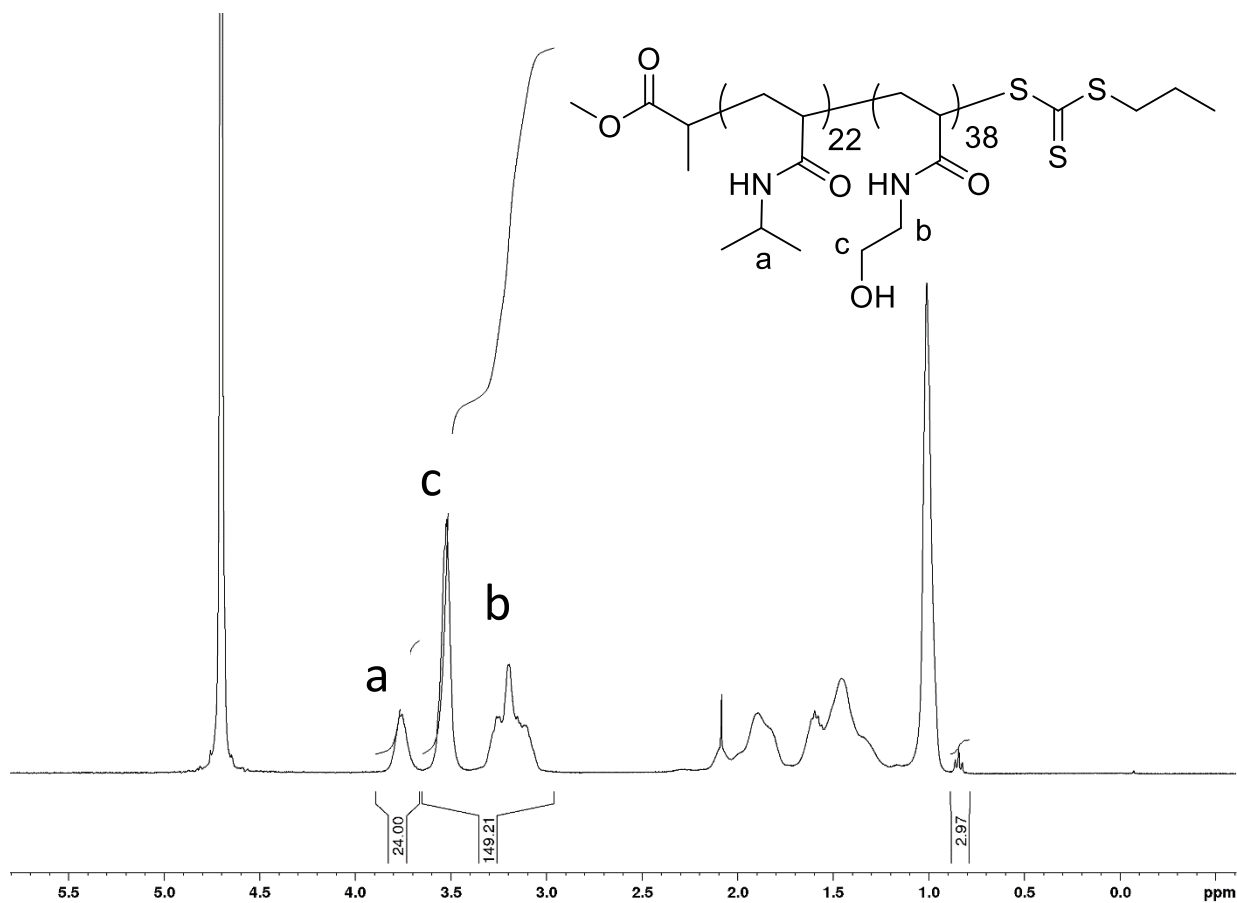


Figure B.11 - ^1H NMR spectrum of $p\text{NIPAM}_{22}\text{-}b\text{-}p\text{HEA}_{38}\text{-MPP}$ in D_2O . Degree of polymerisation was determined from the ratio of the integrals of the CH_3CH group on NIPAM (3.75 ppm) and the side chains on HEA (3.00-3.65 ppm), knowing the DP of the $p\text{NIPAM-mCTA}$.

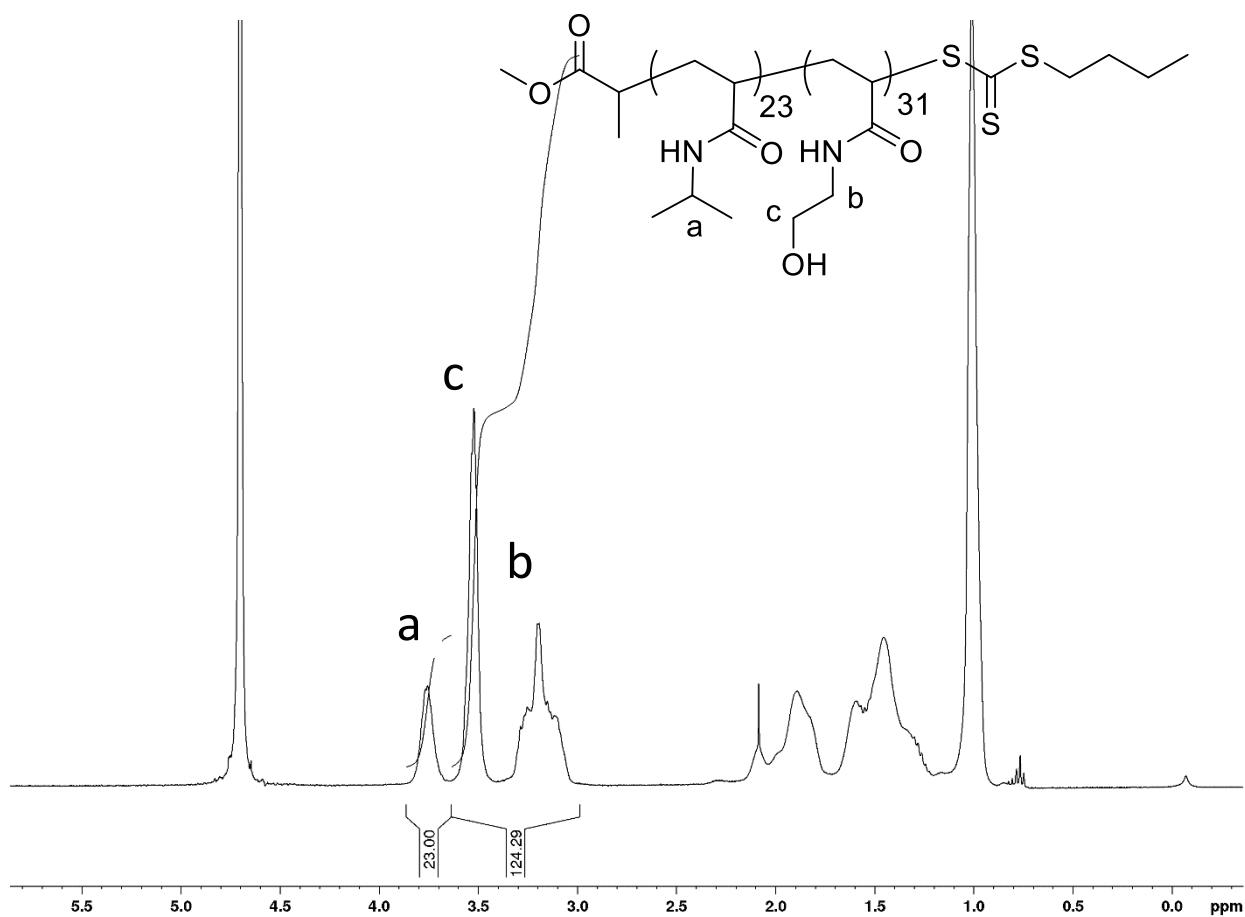


Figure B.12 - ^1H NMR spectrum of $p\text{NIPAM}_{23}\text{-}b\text{-}p\text{HEA}_{31}\text{-MBP}$ in D_2O . Degree of polymerisation was determined from the ratio of the for the CH_3CH group on NIPAM (3.75 ppm) and the side chains on HEA (3.00-3.65 ppm), knowing the DP of the $p\text{NIPAM-mCTA}$.

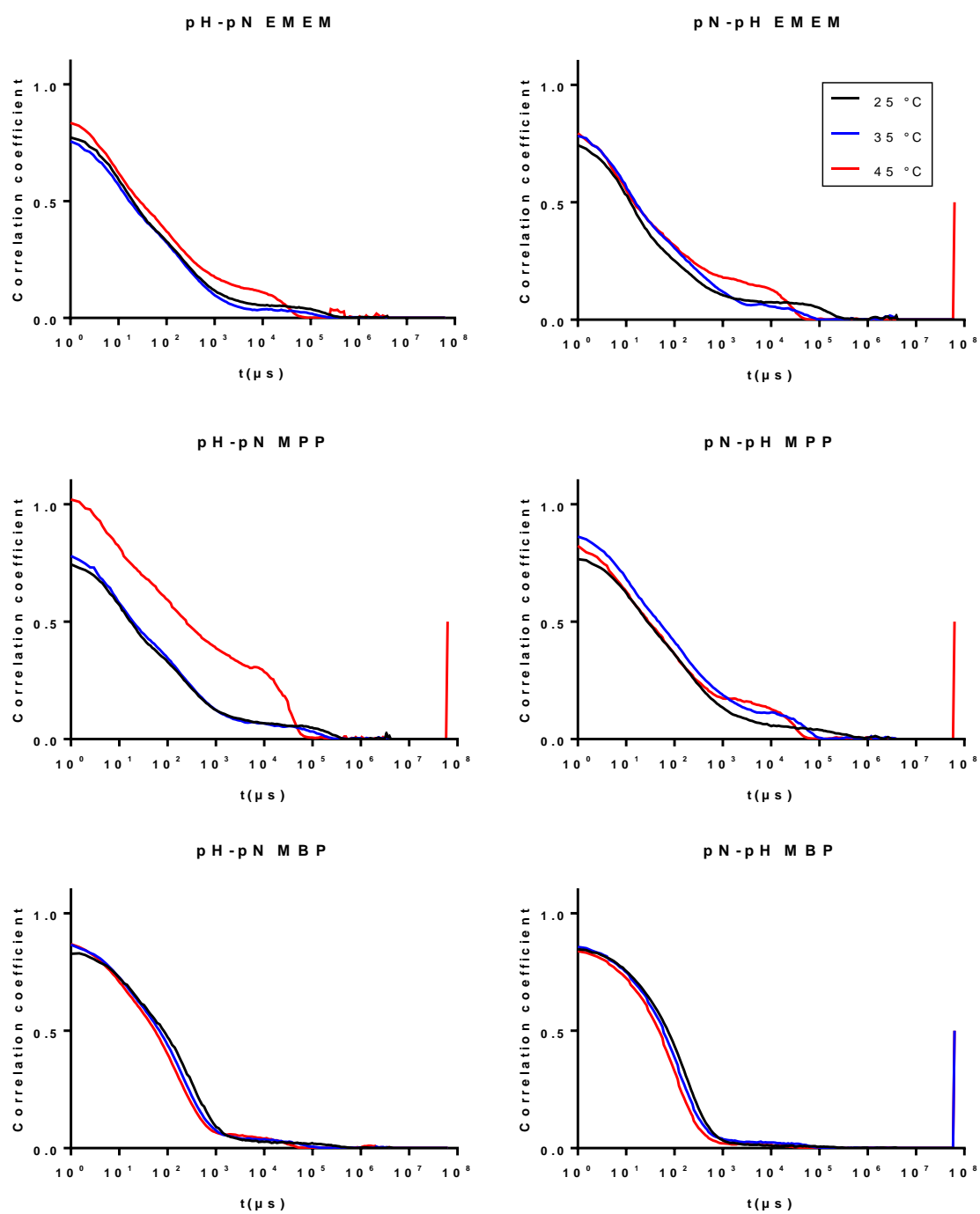


Figure B.13 - DLS correlation curves for all short chain pHEA-*b*-pNIPAM and pNIPAM-*b*-pHEA with EMEM, MPP and MBP RAFT agents at temperatures above and below the LCST, showing lack of self-assembly for these polymers as expected from the corresponding DLS chromatograms.

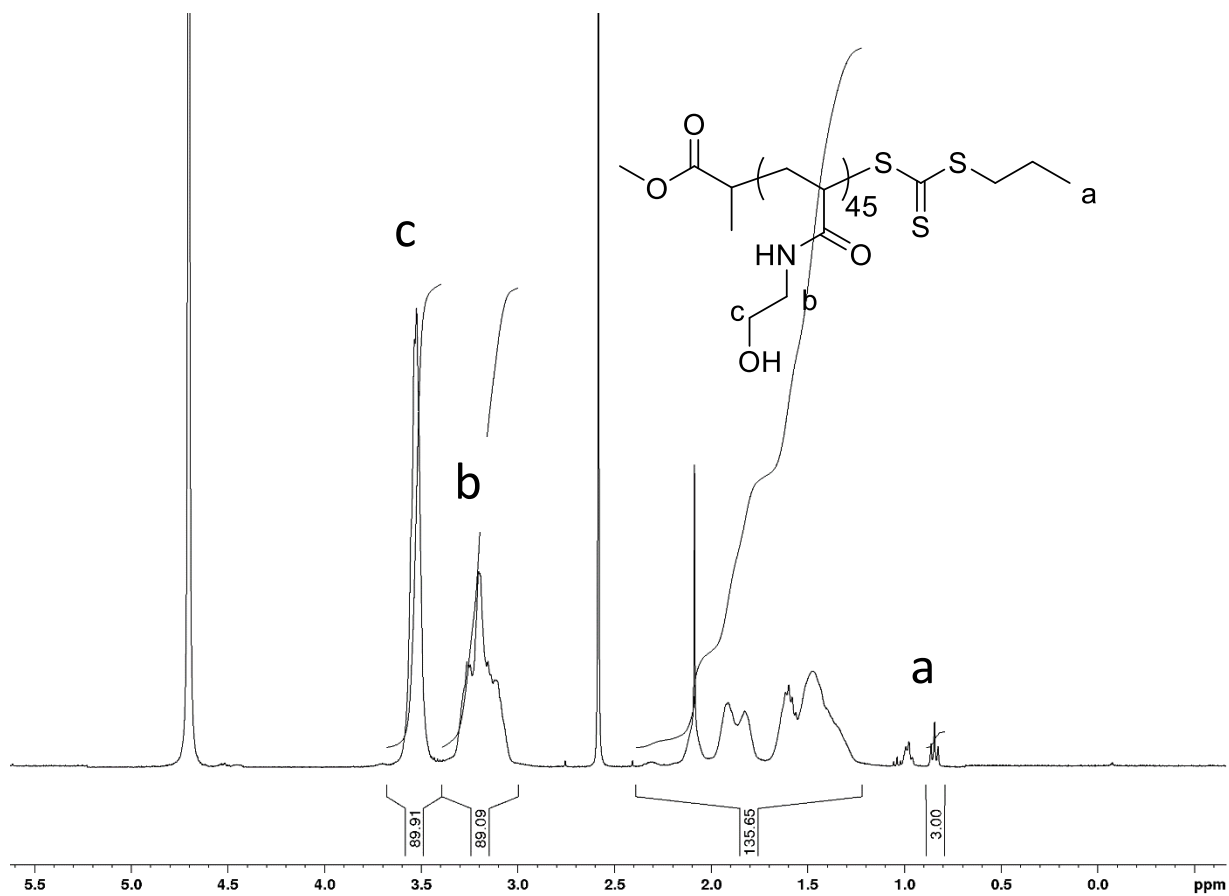


Figure B.14 - ^1H NMR spectrum of $p\text{HEA}_{45}\text{-MPP}$ in D_2O . Degree of polymerisation was determined from the ratio of the integrals for methyl group of RAFT end group (0.85 ppm) and side chains on HEA (3.00-3.65 ppm).

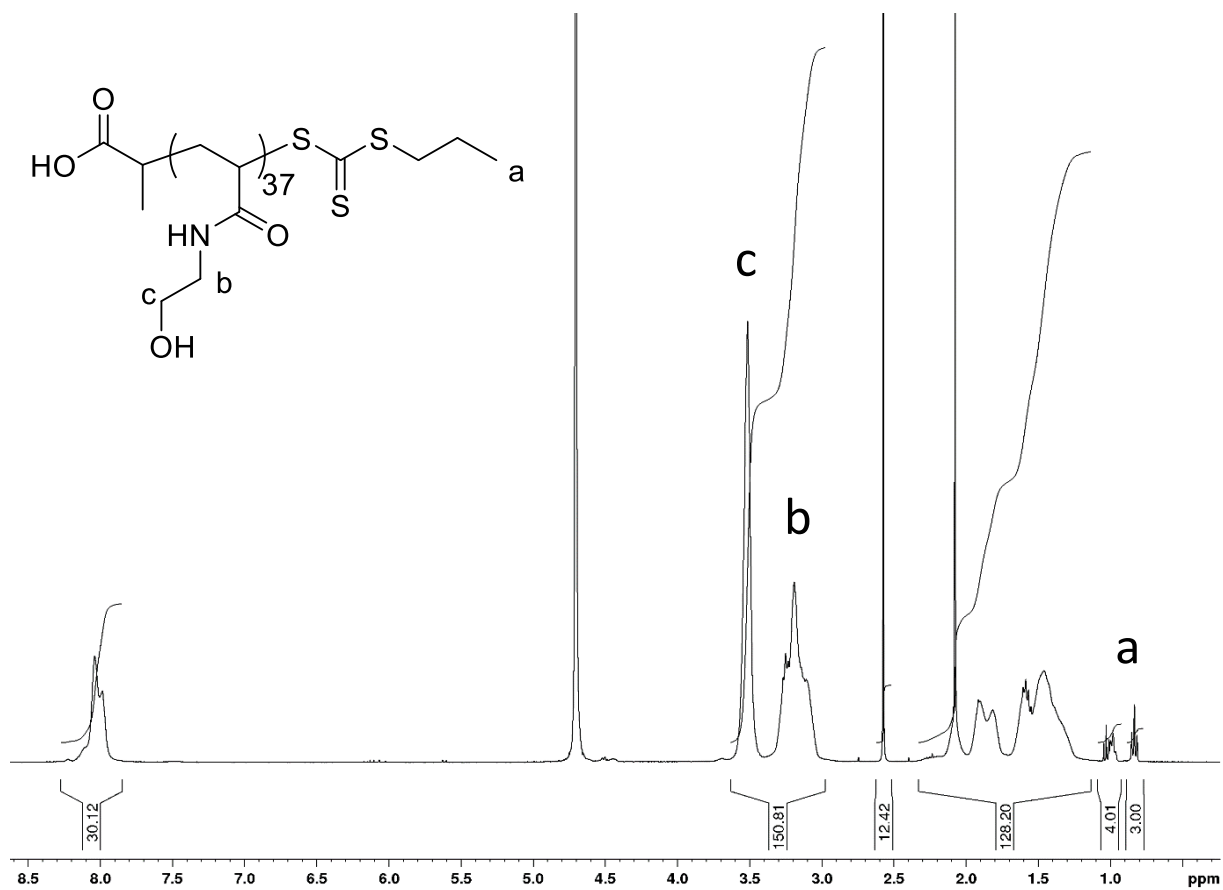


Figure B.15 - ¹H NMR spectrum of pHEA₃₇-PPA in D₂O. Degree of polymerisation was determined from the ratio of the integrals for methyl group of RAFT end group (0.85 ppm) and side chains on HEA (3.00-3.65 ppm).

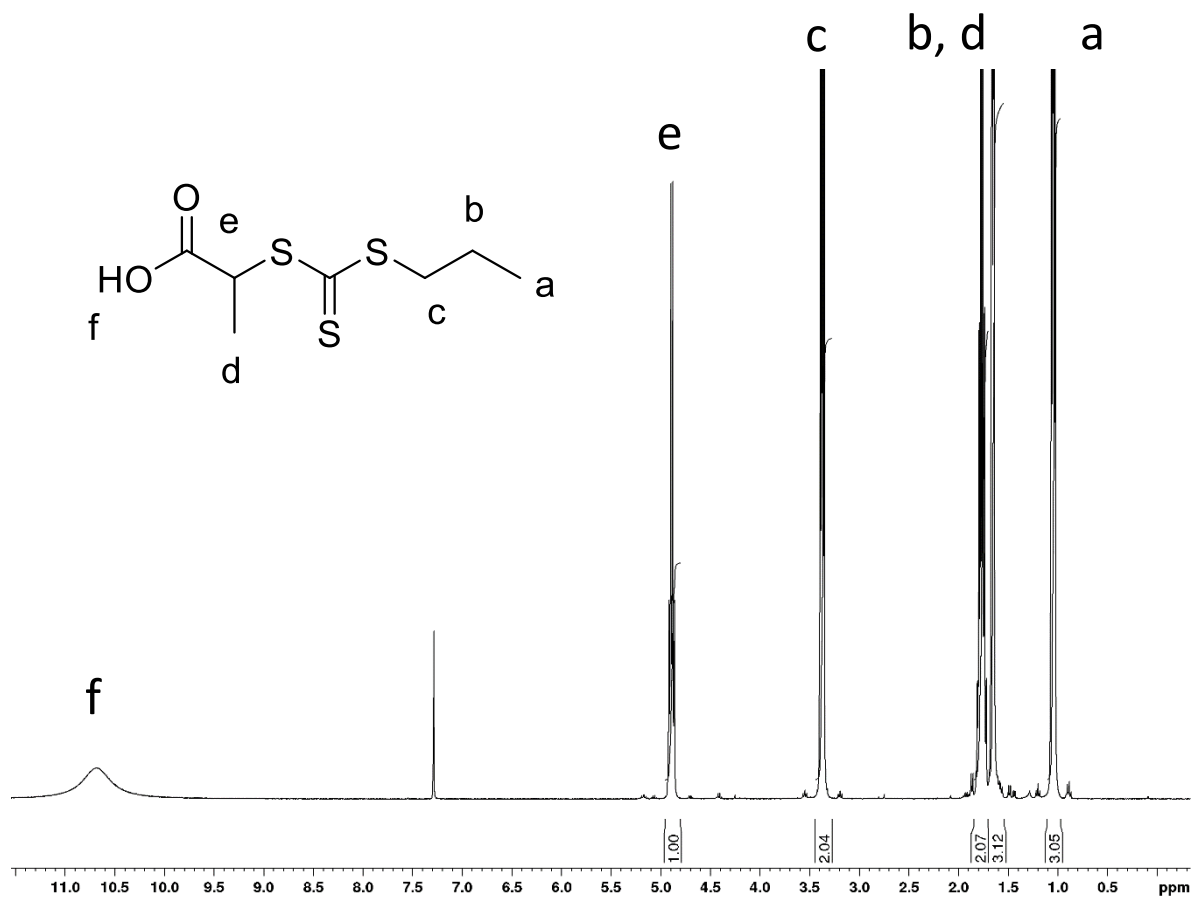


Figure B.16 ^1H NMR spectrum of PPA recorded in CDCl_3

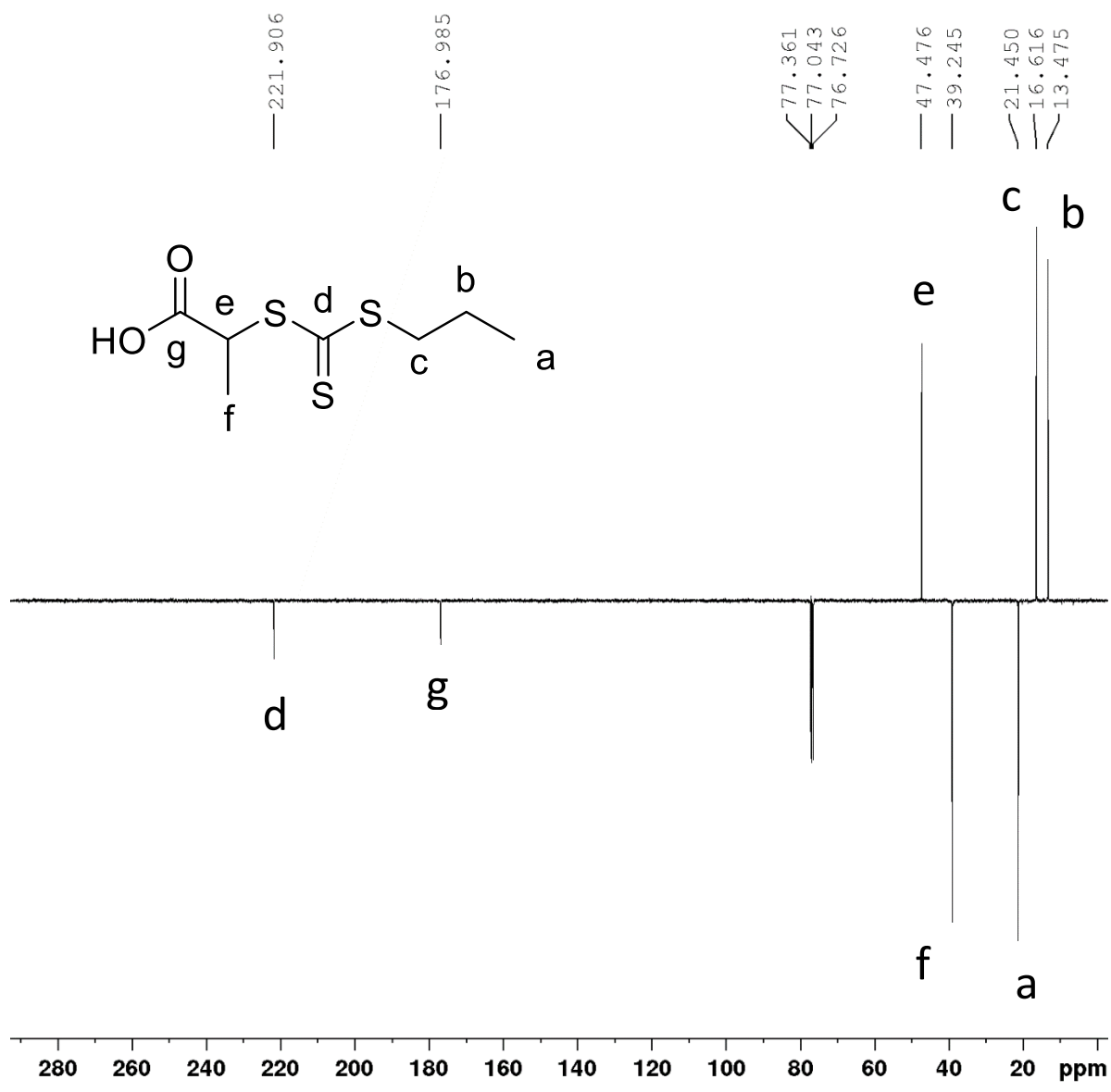


Figure B.17 - ¹³C NMR spectrum of PPA recorded in CDCl₃

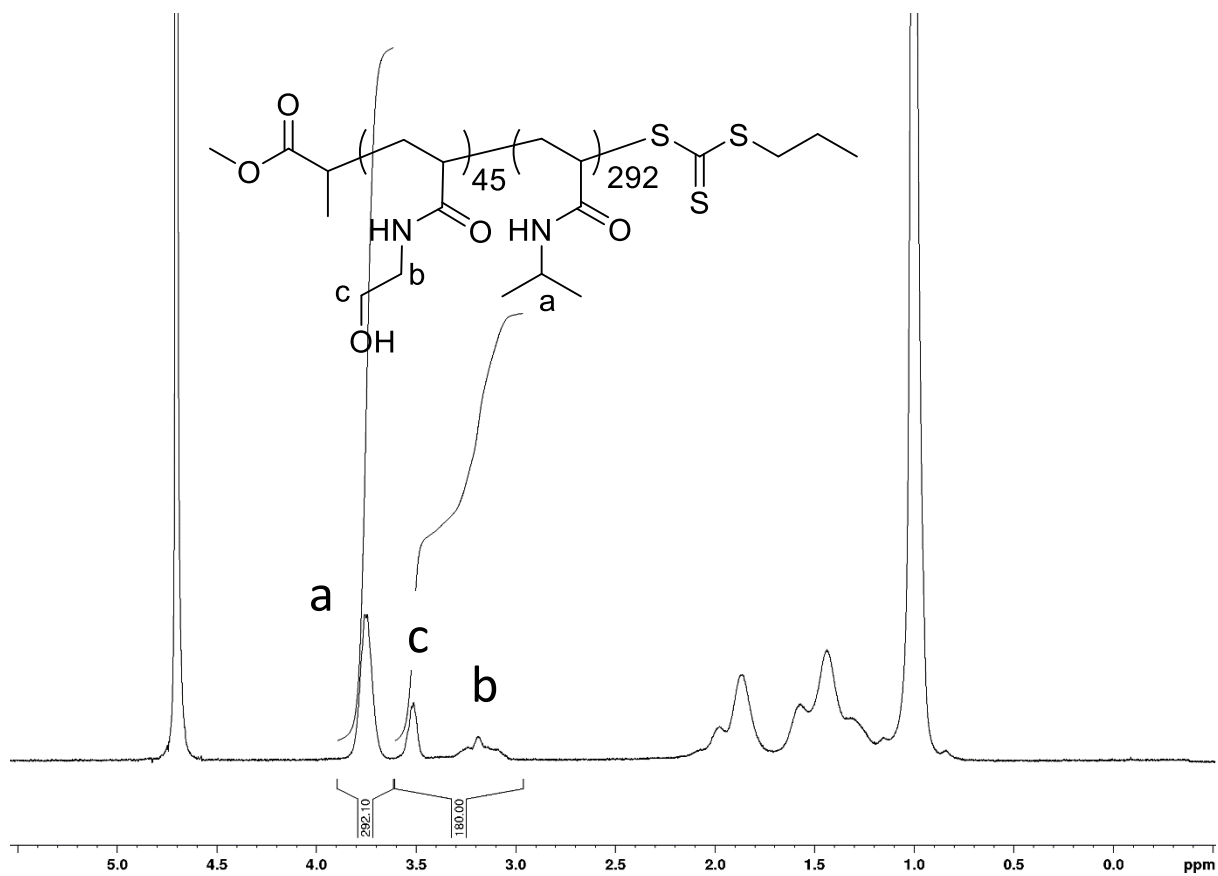


Figure B.18 - ^1H NMR spectrum of $p\text{HEA}_{45}\text{-}b\text{-}p\text{NIPAM}_{292}\text{-MPP}$ in D_2O . Degree of polymerisation was determined from the ratio of the integrals for the CH_3CH group on NIPAM (3.75 ppm) and the side chains on HEA (3.00-3.65 ppm), knowing the DP of the pHEA-mCTA.

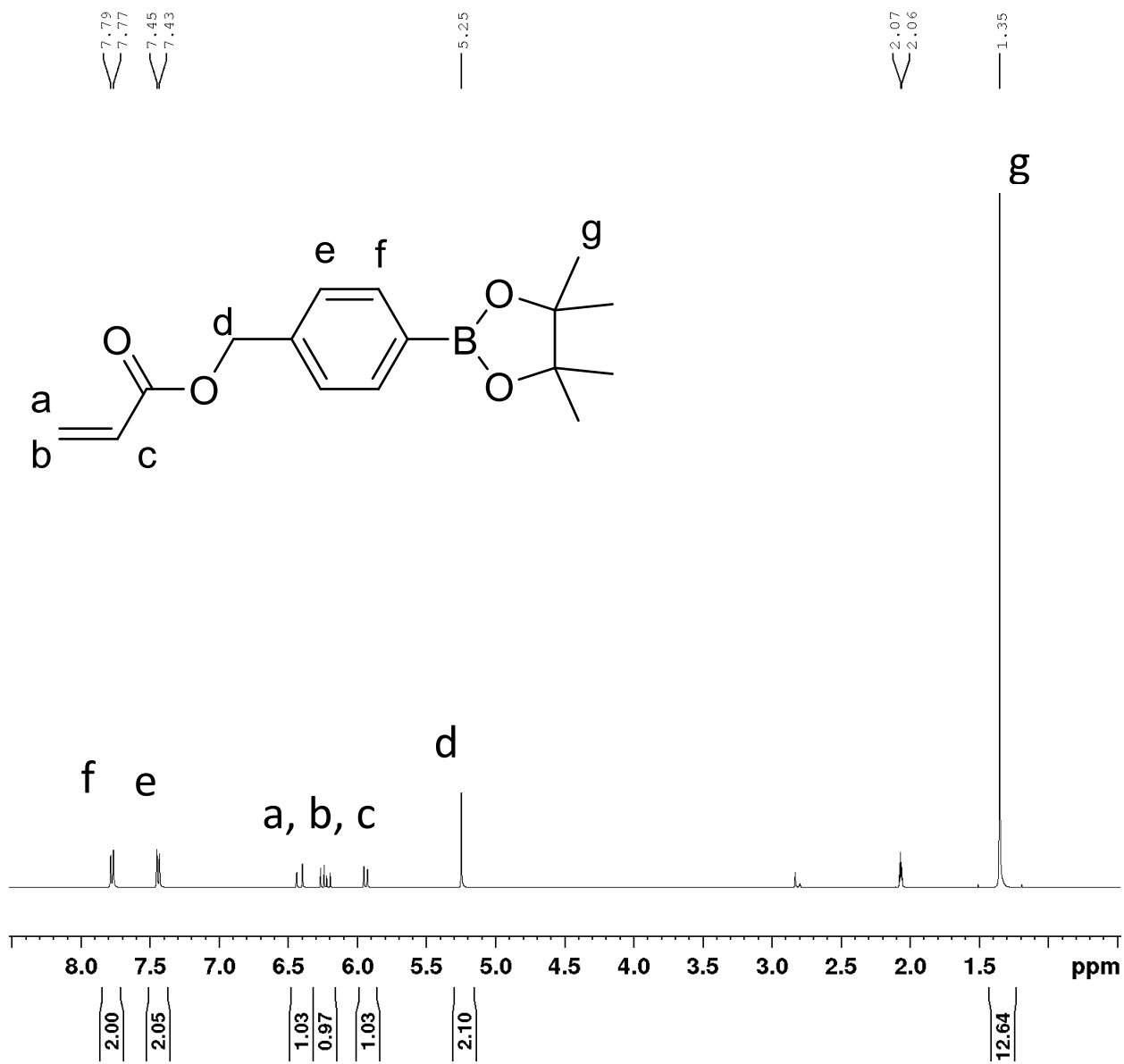


Figure B.19 - ¹H NMR spectrum of BAPE recorded in CDCl₃

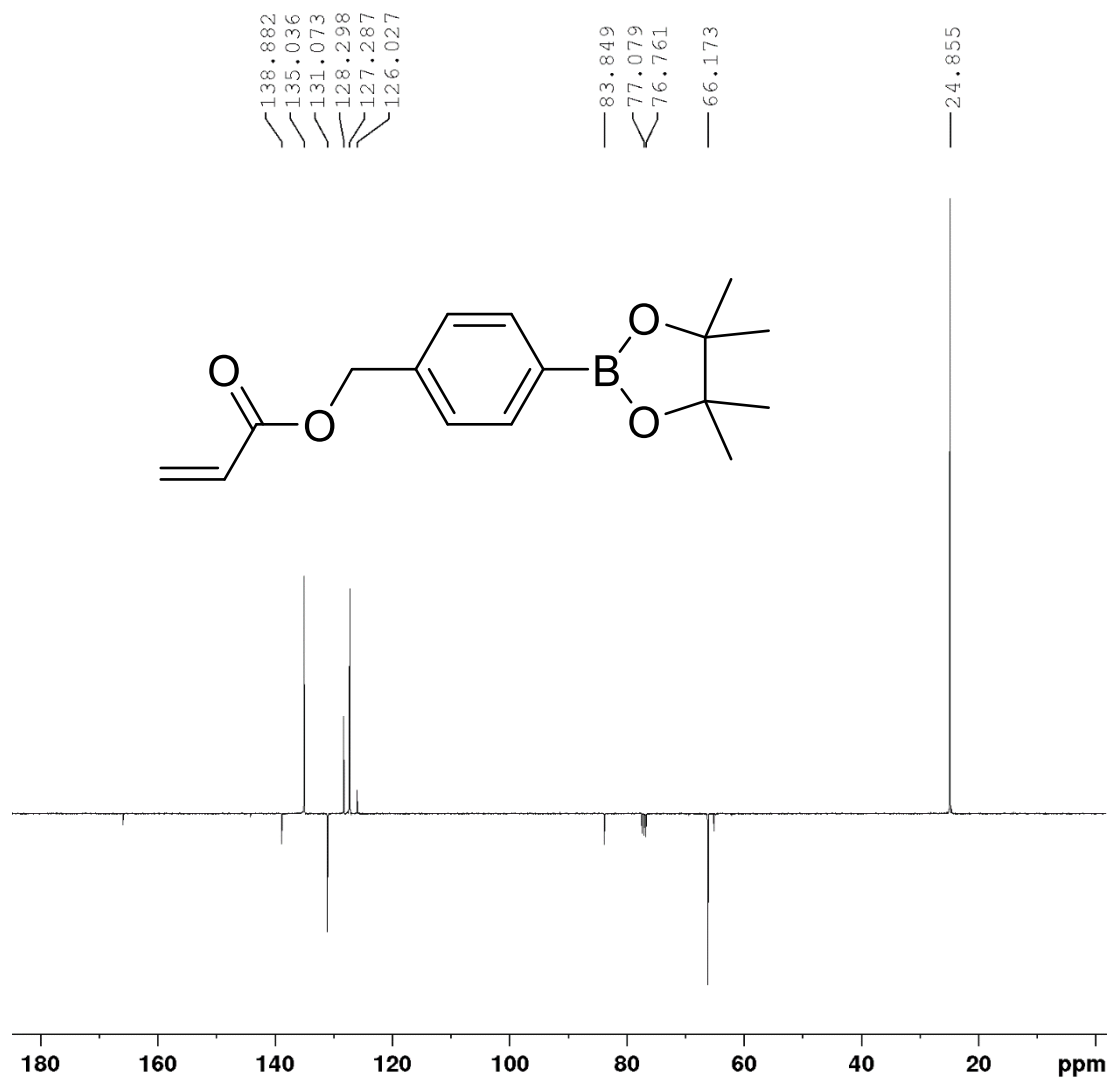


Figure B.20 - ¹³C NMR spectrum of BAPE recorded in CDCl₃

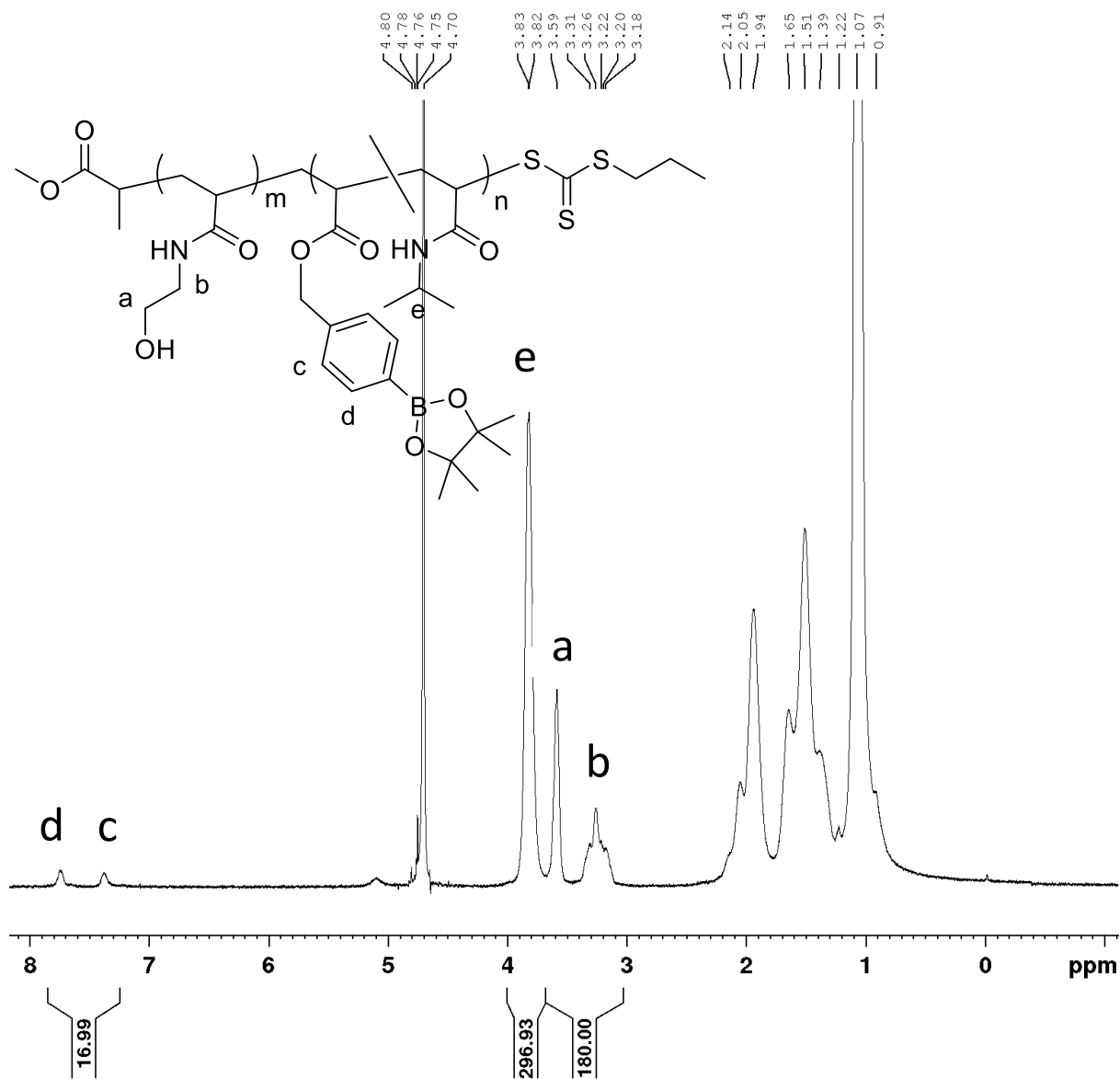


Figure B.21 - 1H NMR spectrum of $pHEA_{45}\text{-}b\text{-}p(NIPAM\text{-}stat\text{-}BAPE)_{301}\text{-}MPP$ in D_2O . Degree of polymerisation was determined from the ratio of the integrals for the CH_3CH group on NIPAM (3.75 ppm) and the aromatic ring in BAPE (7.35 and 7.75 ppm) with the side chains on HEA (3.00-3.65 ppm), knowing the DP of the pHEA-mCTA.

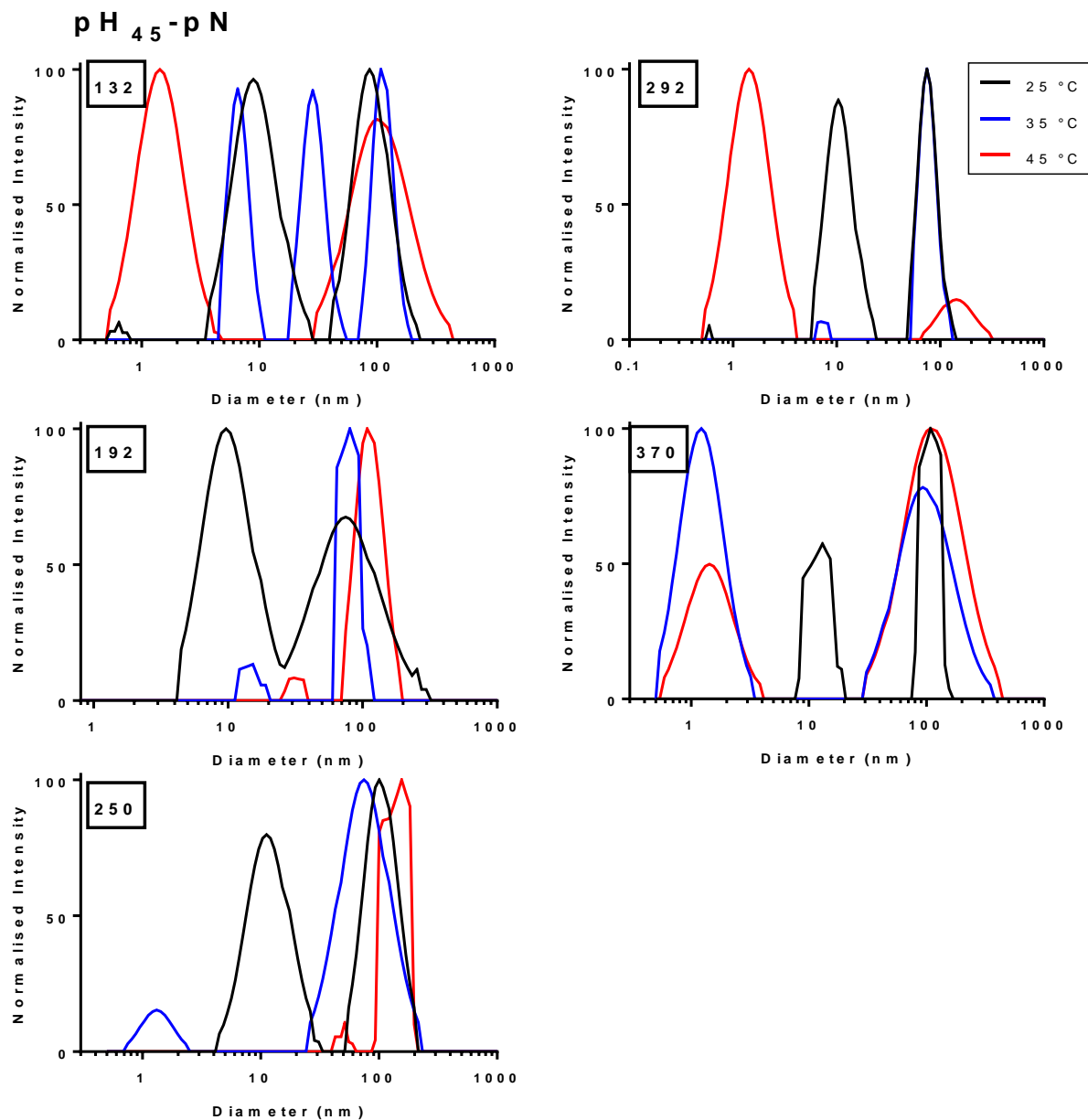


Figure B.22 - A comparison of DLS of pHEA₄₅-b-pNIPAM_n, where MPP is the RAFT agent, at temperatures above and below the LCST of the polymer to determine whether self-assembly occurs as the pNIPAM block becomes hydrophobic

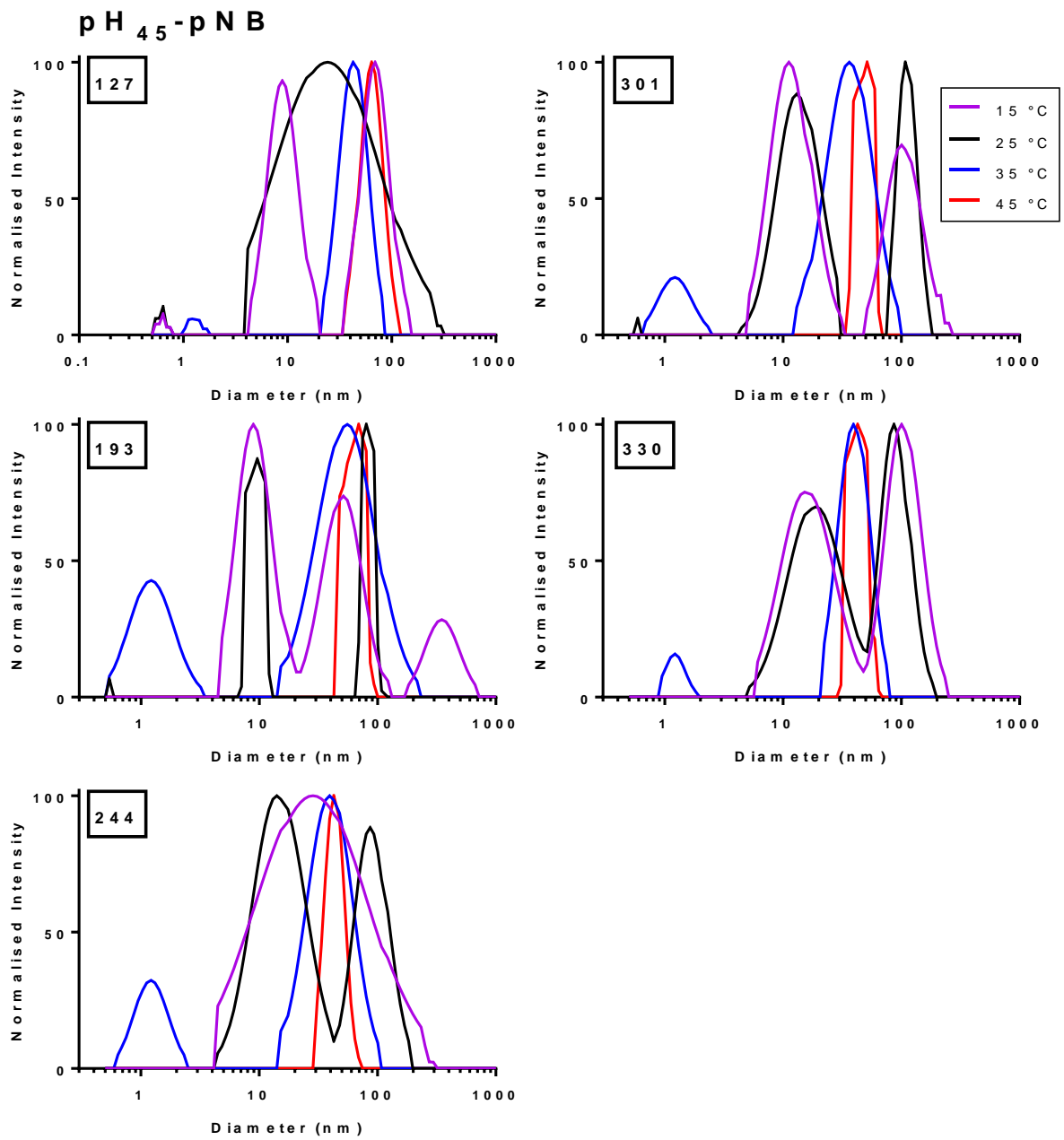


Figure B.23 - A comparison of DLS of $pHEA_{45}\text{-}b\text{-}p(NIPAM\text{-}stat\text{-}BAPE)_n$, where MPP is the RAFT agent, at temperatures above and below the LCST of the polymer to determine whether self-assembly occurs as the $p(NIPAM\text{-}stat\text{-}BAPE)$ block becomes hydrophobic

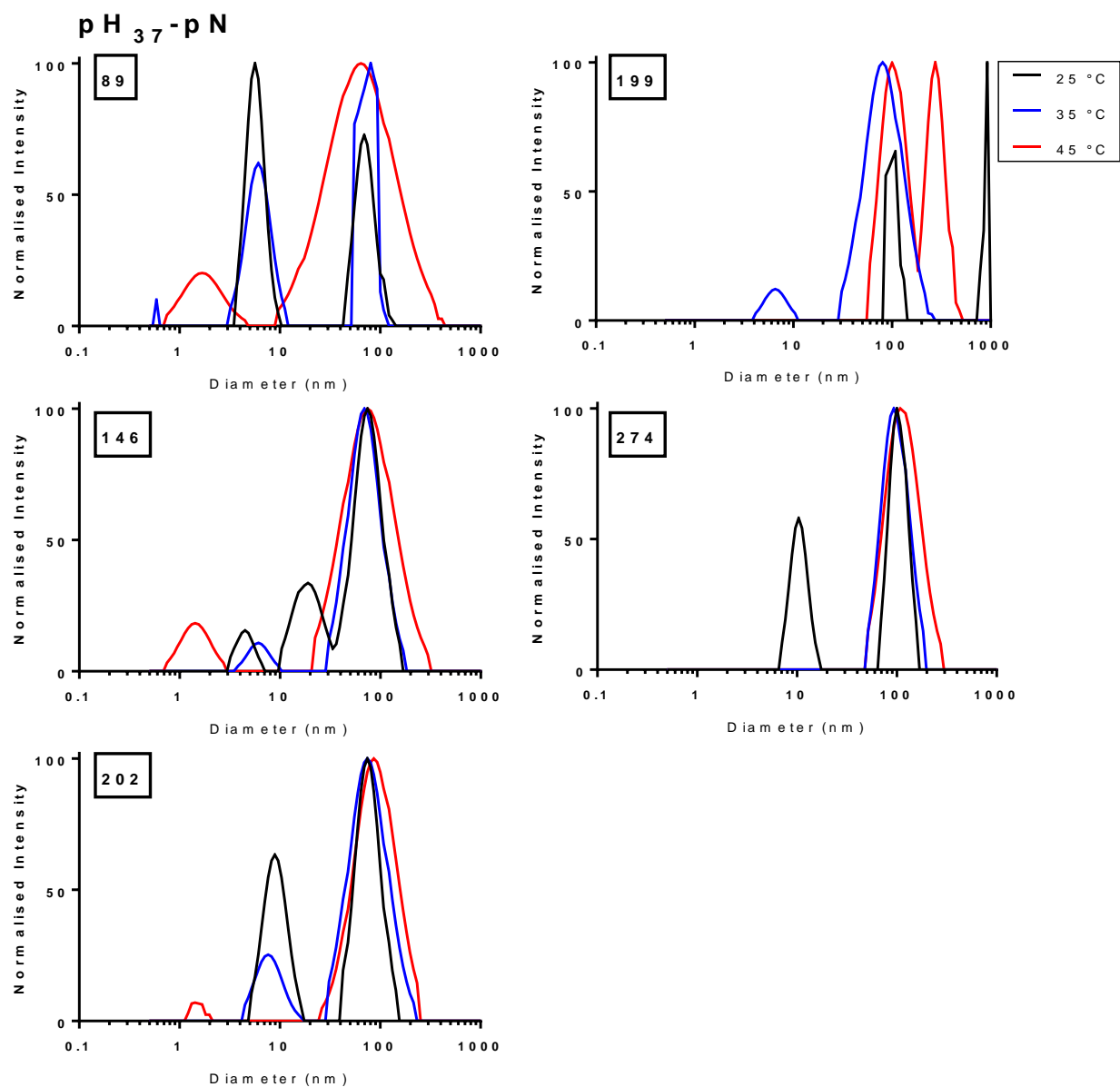


Figure B.24 - A comparison of DLS of $pHEA_{37}\text{-}b\text{-}pNIPAM_n$, where PPA is the RAFT agent RAFT agent, at temperatures above and below the LCST of the polymer to determine whether self-assembly occurs as the pNIPAM block becomes hydrophobic

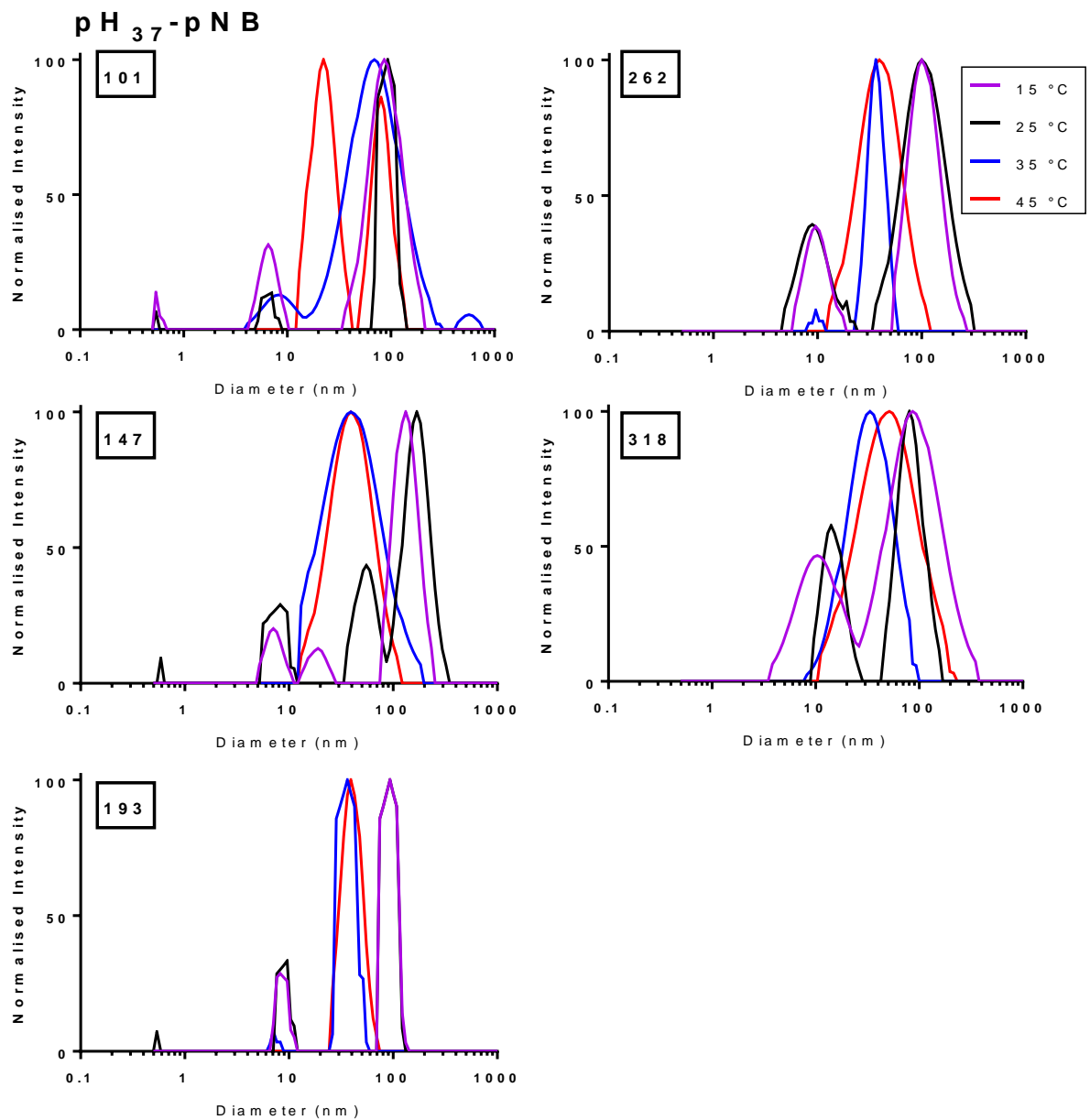


Figure B.25 - A comparison of DLS of $p\text{HEA}_{37}\text{-}b\text{-}p(\text{NIPAM}\text{-}\text{stat}\text{-}\text{BAPE})_n$, where PPA is the RAFT agent, at temperatures above and below the LCST of the polymer to determine whether self-assembly occurs as the $p(\text{NIPAM}\text{-}\text{stat}\text{-}\text{BAPE})$ block becomes hydrophobic

Chapter Five

5. Synthesis and characterisation of oxidation responsive nanogels

5.1. Introduction

Nanogels are of increasing interest in the field of polymer chemistry and in particular for use in drug delivery. Nanogels have all the unique properties of hydrogels, mainly the highly crosslinked nature of the polymer chains, but they are nanometer in size.¹ One of the unique properties of this system is the ability to swell and shrink in response to stimuli, whether this be temperature, redox, pH etc, allowing the release of encapsulated materials.²⁻⁶

There are many advantages of nanogels over typical drug delivery systems including inert behaviour in the blood stream. The inert behaviour occurs as nanogels have an internal aqueous environment, sometimes with a hydrophilic shell. This minimises the interaction with the blood and therefore prevents immune response.^{7,8} The tuneable small size of the nanogels (20-200 nm) is beneficial as it allows ease of movement in the body, including the potential to deliver drugs and other encapsulated material beyond the blood brain barrier, while avoiding rapid clearance from the body.^{7,9} The small size also allows quick response to external stimuli. The main benefit when compared to free drug is the increased drug loading ability, especially of poorly soluble drugs, as these can be effectively encapsulated in the hydrophobic core, shielding the hydrophobicity due to the hydrophilic corona. It allows increased cellular uptake than the free drug. Drugs can be loaded in three ways; physical entrapment, covalent attachment, and controlled self-assembly.^{8,10}

When compared to the micelle structure formed from amphiphilic block copolymers (discussed in depth in Chapter 4), nanogels are better suited for drug delivery. Their crosslinked structure can prevent the premature drug release which is seen in micelles through chemical and physical changes including heat, salt concentration, pH, polymer concentration and more.¹¹

Nanogels can be synthesised using a variety of different techniques including photolithography, emulsion, reverse microemulsion and inversion polymerisation, precipitation, free radical polymerisation and controlled/living radical polymerisations.^{12,13} In this chapter, the research is

focused on using only RAFT polymerisation, a controlled/living radical polymerisation process, therefore none of the above systems are discussed in more depth.¹⁴

Adaptations of the RAFT polymerisation technique used for the synthesis of diblock copolymers mentioned in chapter 3 were made to synthesise nanogels. The self-assembly of these copolymers occurs during the polymerisation and the added divinyl molecules cause crosslinking, forming stable nanogels. The monomers are soluble in water, however as the second block grows it becomes hydrophobic. In the case of the pNIPAM containing diblock copolymers, when the temperature is decreased and becomes lower than the LCST of pNIPAM, this block becomes hydrophilic causing the polymer to disassemble and form soluble polymer chains. When a soluble crosslinker is added during the polymerisation, it enables the self-assembled structure to become 'locked' in place. This prevents many of the issues seen with diblock copolymers disassembling due to changes in concentration, pH, temperature etc. Swelling/shrinking behaviour is observed in these nanogels on altering the temperature above or below the LCST but the polymer is now trapped in a self-assembled state.¹⁵ For nanogels and hydrogels, rather than referring to the LCST, the volume phase transition temperature (VPTT) is used instead to describe this swelling and shrinking behaviour. In this report, LCST will be used throughout, even to describe the VPTT, in order to remain consistent across chapters and to give comparable results.¹⁶

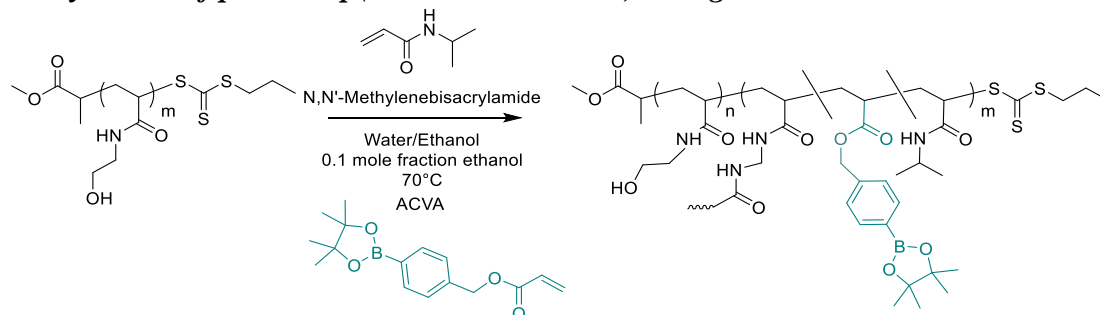
When synthesising these nanogels, certain criteria were chosen that the nanogel needed to exhibit in order to make a good drug delivery vehicle. Size is very important when administering anything into the body as some of the capillaries are very narrow, and the size can have implications on the excretion and therefore lack of accumulation in tissue. To avoid blockages and complications due to this, the nanogels were targeted to be between 50-100 nm in diameter.¹⁷ In addition, we wish to utilise the temperature responsive behaviour of the core to enable encapsulation of the drug. From previously published work, it was known that as the temperature of similar nanogels is increased above the LCST, the pNIPAM chains within the core collapse, causing shrinking of the nanogel, and

that the temperature of this transition can be easily tuned with the incorporation of other monomers.¹⁸⁻²³ Therefore, if the LCST is approximately room temperature, drugs can be trapped within the core by heating above this temperature and storage can be at relatively low temperatures. Upon oxidation with H₂O₂, ideally the LCST would now be higher than body temperature causing the nanogel to return to a swollen state and the drug to be released at the target site.

In this chapter, the synthesis of core-shell nanogels is reported. The core is comprised mainly of pNIPAM and small amounts of an oxidation responsive boronic acid pinacol ester-based monomer (BAPE). These are stimuli responsive, chemically crosslinked nanogels. The shell-forming block consists of a water-soluble polymer of hydroxyethyl acrylamide which was used as the macro-CTA. These were crosslinked with *N,N'*-methylenebisacrylamide (BIS), a non-oxidisable crosslinking molecule. The synthesis by RAFT dispersion polymerisation in a mixture of water and ethanol utilised the principles of cononsolvency, to allow the addition BAPE into the polymer.^{24,25} The benefit of synthesising via this method, rather than some of the techniques listed above, is that there is minimal non-aqueous solvent to remove and no surfactant which is notoriously difficult to remove.²⁶ We determined the size by DLS and TEM before and after oxidation with various H₂O₂ concentration to determine how oxidation affected the size and morphology of the nanogels.

5.2. Results and Discussion

5.2.1. Synthesis of pHEA-*b*-p(NIPAM-*stat*-BAPE) nanogels



Scheme 5.1 - A general synthetic scheme for the polymerisation of pHEA-*b*-pNIPAM crosslinked nanogels both with and without the incorporated of the oxidation responsive monomer BAPE into the core forming block.

Nanogels, as mentioned previously, are much better vehicles for drug delivery compared to diblock copolymers, where both chemical and physical changes including heat, salt concentration, pH, polymer concentration and more, can cause premature release of drug.¹¹ Nanogels are more stable due to crosslinking, where the extent of this is able to affect the rate of release. In an ideal stimuli-responsive nanogel, when drug is encapsulated, none should be released until the main response to stimuli. Whereas with diblock copolymers of the same system, the lack of crosslinking means the structures are more prone to disassembly on change in concentrations, pH amongst other factors.

To develop these nanogels, information found from the synthesis and analysis of diblock copolymers in chapter 4 was used. Combining this with nanogel behaviour should create an appropriate drug delivery vehicle. The same polymer of HEA synthesised using MPP as the RAFT agent was used, pHEA₄₅-mCTA, as this showed promise in the synthesis of diblock copolymers. The crosslinking molecule used in this synthesis is *N,N'*-methylene bisacrylamide (BIS), which is a symmetrical molecule with a vinyl group at both ends. The vinyl groups are expected to polymerise at a similar rate to NIPAM. It is important to note that BIS is not an oxidation responsive crosslinking molecule, so the crosslinks are expected to be stable to oxidation. This crosslinking molecule is added into the reaction at the beginning alongside the monomer, initiator and mCTA (Scheme 5.1).

As mentioned in the previous chapters, the temperature-responsive behaviour is important in the development of these oxidation responsive drug delivery systems. The phenomenon of consolvency is advantageous in this polymer system as it allows molecules which are not soluble in an entirely aqueous environment to be incorporated into the polymer, while also retaining the temperature responsive behaviour needed to cause self-assembly. There are many examples of consolvency of pNIPAM in water where varying mole fractions of the following solvents are incorporated; THF,^{24,30} alcohols (methanol, ethanol and propanol),^{24,31,32,33} dioxane,²⁴ acetone,³¹ DMF³¹ and DMSO.^{31,34,35} As BAPE, the oxidation response monomer, is insoluble in water, the consolvency behaviour that pNIPAM exhibits with water/ethanol mixes is exploited to ensure all reagents are soluble at the beginning of the reaction.

After 6 hours, the polymerisation was stopped by opening to air. Due to the complexity of ¹H NMR spectra in the two-solvent system, the monomer to polymer conversion was estimated using gravimetric analysis to give the final solids content of the reaction. On average these reactions reached approximately 80% conversion. From this analysis, it is possible to approximate the linear equivalent DP of the polymers synthesised. The full list of conversions and theoretical DPs for these polymerisations can be seen in the appendices.

A variety of polymers were synthesised to determine the effect of core-forming block length, crosslinker concentration and oxidation on the suitability of these nanogels as drug delivery systems. Polymers of pHEA₄₅-*b*-pNIPAM_{*n*} and pHEA₄₅-*b*-p(NIPAM-*stat*-BAPE)_{*n*}, both crosslinked with BIS, will be referred to as H₄₅-N_{*n*} and H₄₅-NB_{*n*} respectively, throughout the rest of the chapter for simplicity.

5.2.2. The effect of the length of the core-forming block on particle size

5.2.2.1. The block length effect on particle size with a pNIPAM core

Initially, the effect of the length of the core-forming block was studied. As stated in the introduction for this section, one of the criteria for these nanogel systems was that the size of the nanogel should be between 50 and 100 nm. The targeted length of the core forming blocks was between 100 and

400 NIPAM units long and the actual DP was determined by gravimetric analysis. Where the oxidation responsive monomer was incorporated into the second block, NIPAM units were replaced by a certain mole percent of BAPE.

Dynamic light scattering (DLS) was used to determine the hydrodynamic particle size (R_H) of the nanoparticles formed. For biomedical applications, it is important to characterise the size of the particle as well as the length and dispersity of the polymer chains.³⁶ Particle size effects numerous processes that are necessary when using these as delivery systems, i.e. cellular uptake, but also has an influence on the toxicity and dissolution after they have been administered.³⁷

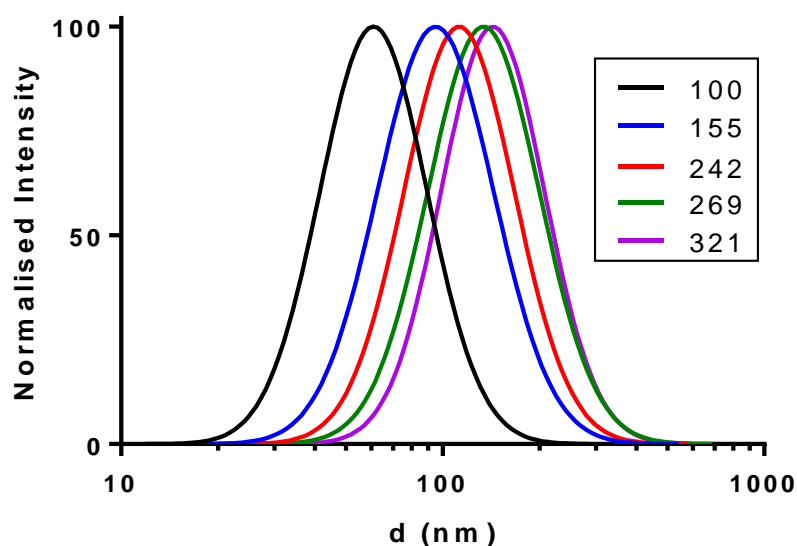


Figure 5.1 - DLS analysis at 37 °C showing particle size with increasing core block length of $H_{45}-N_n$ with a crosslinker to mCTA ratio of 5:1, at a NG concentration of 0.1wt%. The wavelength of the laser used is 640 nm and the backscattering was measured.

Using the group of polymers synthesised with only pNIPAM as the core-forming block and with a crosslinker to mCTA ratio of 5:1 as an example, DLS studies to determine particle size were carried out. Keeping the temperature constant at 37 °C, body temperature, the hydrodynamic radius of these nanogels were determined. It is possible to see that as the length of the core-forming block increases, so does the size of the nanogel, ranging from a z-average value of 59 nm for the shortest pNIPAM chain to 141 nm for the longest chain (Figure 5.1). Armes et al. found that when they

increased the length of the core forming block in diblock copolymers of pGMA-*b*-pHPMA, the size of the spheres increases with an increase in core forming block length.³⁸ It is important to note that when there is a change in morphology due to this increase, the trend is not observed.

The dispersities for these are broader than expected, ranging from 0.14 to 0.20, indicating that either there is a dispersity of particle sizes or that these are not entirely spherical particles.

DLS uses the Stokes-Einstein equation (Equation 2.2) to determine the hydrodynamic radius.

This equation assumes that the particles are solid and spherical. However, most samples analysed by DLS are solvated, in this case hydrated, which means that they can be soft particles, not hard spheres as the equation assumes. In addition, the morphology of samples could vary depending on the block length of both the hydrophilic and hydrophobic blocks. Consequently, it is difficult to use the hydrodynamic diameter from DLS to give meaningful data unless combined with other particle sizing techniques that provide more information about particle morphology.

Transmission electron microscopy (TEM) was used to compare the samples to DLS. To prepare the samples below, carbon coated copper grids were used, and the samples were negatively stained using a phosphotungstic acid stain. This stain was used to provide contrast between the particles and the background by staining the background but not the polymeric particles.

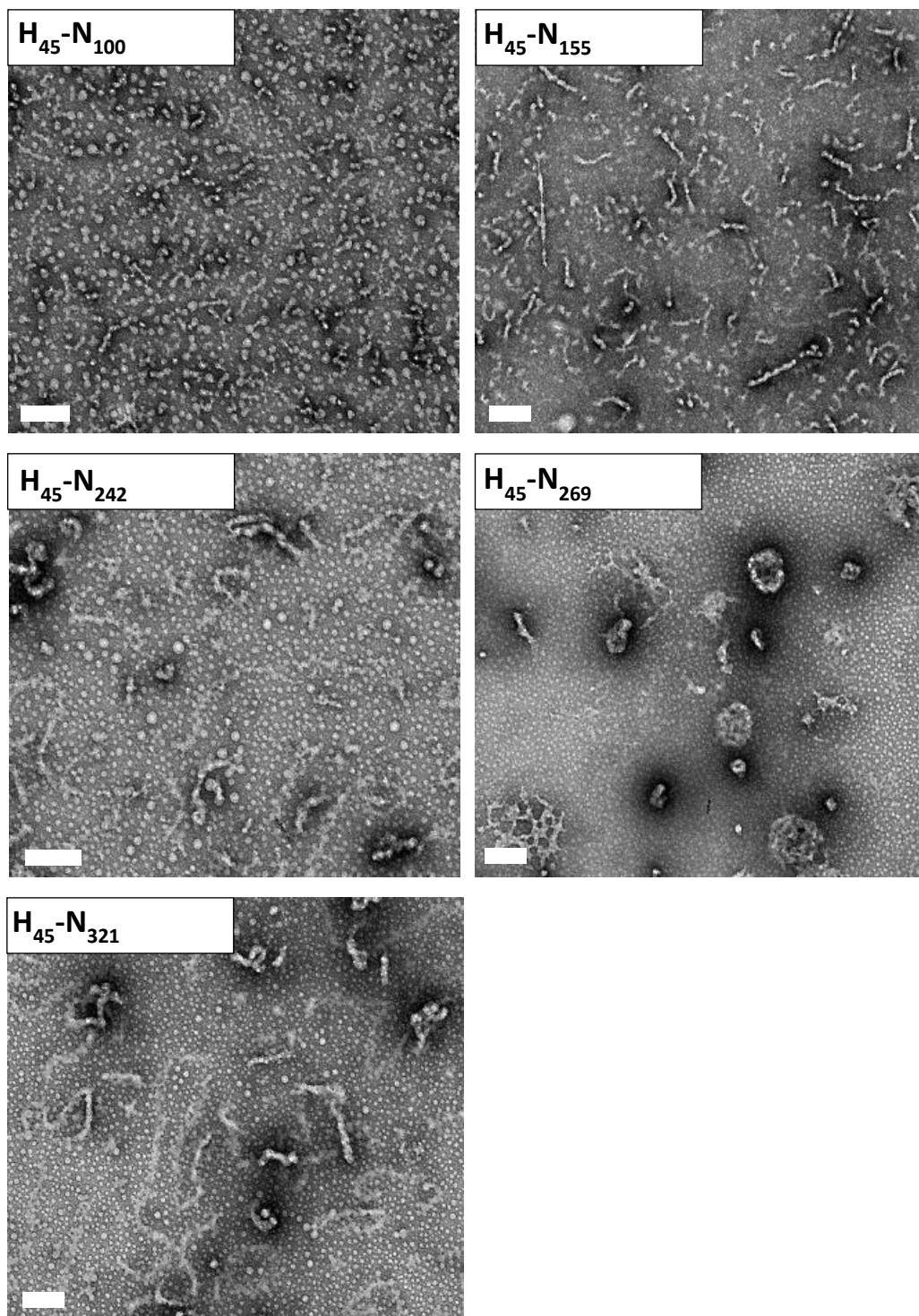


Figure 5.2 - TEM of particles of $H_{45}-N_n$, where n varies between 100 and 321, prepared at room temperature at a concentration of 0.05 wt% and stained with pH 7 phosphotungstic acid. The scale bars all represent 200 nm.

Particle sizes by TEM were smaller than seen in DLS. This is expected as in DLS the samples are in their hydrated form and the samples prepared for TEM are dry and under high vacuum. From the TEM images (Figure 5.2), it is possible to see a change in morphology on increasing the length of the

core-forming block. At the shorter pNIPAM length, small particles are seen which appear spherical, with some short worm-like structures forming. As the length of the block increases longer segmented worms are observed and some larger spheres. When the block length is 269, small spheres can still be seen but across the TEM grid, larger aggregated structures are seen with a few worm-like structures still present.

The morphology of self-assembled diblock copolymers is primarily determined by the packing parameter, defined in equation 5.1.^{39,40}

$$p = \frac{v}{a_0 l_c} \quad (5.1)$$

Where v refers to the volume of the hydrophobic chains, a_0 is the optimal area of the hydrophilic block and l_c is the length of the hydrophobic tail.

The value of the packing parameter, in general, is a good indication of the morphology expected on self-assembly.^{41,42} For spherical micelles $p \leq \frac{1}{3}$, an increase in the packing parameter to values between $\frac{1}{3} < p \leq \frac{1}{2}$ indicates a more elongated structure usually referred to as polymer worms, and a further increase in the packing parameter between $\frac{1}{2} < p \leq 1$ favours the formation of vesicles. Therefore, as the hydrophilic block is constant in this synthesis, the length of the hydrophobic block influences the morphology of the formed nanoparticles, as seen by TEM.

The very small spherical structures on the grid are most likely artefacts present due to the preparation of the grids (see section 5.2.7.3 for more details on the determination of this). These elongated structures explain the higher than expected dispersities observed from DLS. This is because the DLS data fits the scattering intensities to that of hard spheres, as mentioned above, which it is apparent the samples are not.

5.2.2.2. The incorporation of an oxidation sensitive monomer and the effect of chain length on particle size

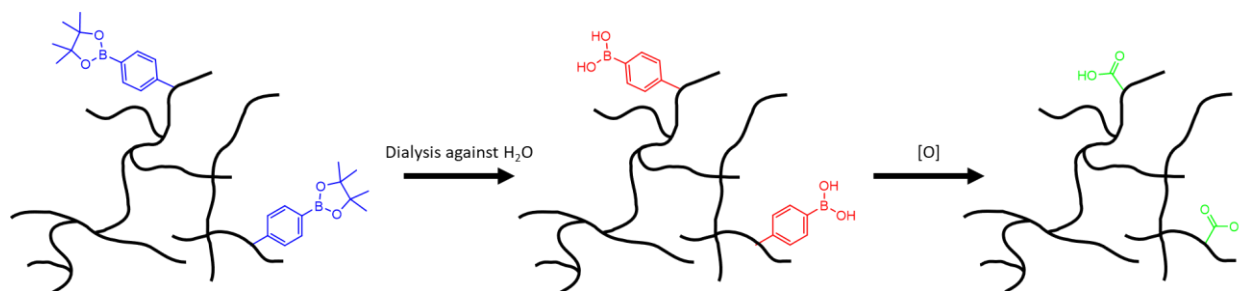


Figure 5.3 – A diagrammatical representation of BAPE incorporated into a crosslinked pNIPAM core, showing how BAPE is changed after dialysis and then the product of oxidation of the BAPE units.

The oxidation responsive group, BAPE, is added into the nanogels so that they are able to respond to oxidation. Boronic acid pinacol ester groups are converted to acrylic acid monomer units on oxidation with hydrogen peroxide (Figure 5.3). Through research done in Chapter 3, the concentration of BAPE incorporated into the nanogels remained the same as the diblock copolymers at 2 mol%. It was shown that this should cause a temperature response on oxidation, changing the LCST from room temperature to above body temperature.

The synthesis conditions remained the same, including the crosslinker to mCTA ratio, to afford comparability between the pNIPAM and pNIPAM-*stat*-BAPE cores, as the differing hydrophobicity is likely to affect the size and dispersity of the resulting nanogels.

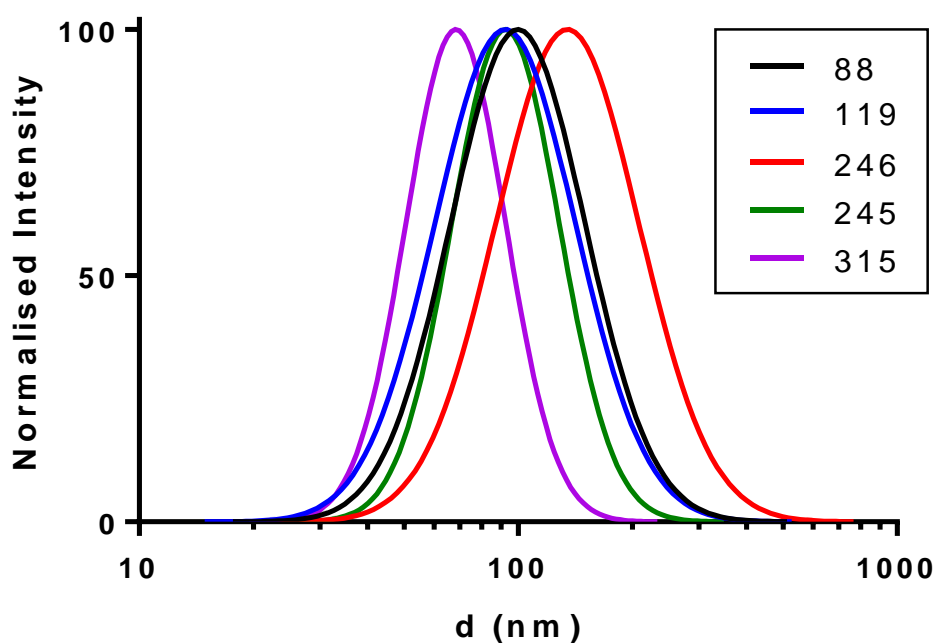


Figure 5.4 – DLS showing particle size with increasing core block length of $pHEA_{45}\text{-}b\text{-}p(NIPAM\text{-}stat\text{-}BAPE)_n$ with a crosslinker to $mCTA$ ratio of 5:1 at 37 °C, with a NG concentration of 0.1 wt%. The wavelength of the laser used is 640 nm and the backscattering was measured.

Unlike the nanogels with only NIPAM in the core, the hydrodynamic diameter of the BAPE containing nanogels does not increase with increasing length of the core-forming block (Figure 5.4). The z-average size of the particles by DLS varies from 78 nm to 135 nm with the dispersity having a larger difference between samples than above, 0.09-0.21. Also, the two polymers with core-forming block lengths of 245 and 246 (determined by gravimetric analysis) seem to have different particle sizes (135 nm and 91 nm) and the PDI of the polymer with block length of 246, 0.21 compared to 0.12 of the 245 sample, suggests that these deviate from a spherical morphology.

TEM was used to enable determination of the morphologies and to see whether these deviate from spherical particles as DLS implies (Figure 5.5). Segmented worm-like structures can be seen in most of the TEM images, with the lengths of these varying within one sample. When the TEM images of the two similar length polymers are compared, the sample with the larger PDI and therefore broader dispersity of sizes shows long worm-structures. Whereas the sample with the slightly shorter core forming block consists of smaller structures that appear to be similar to each other in size.

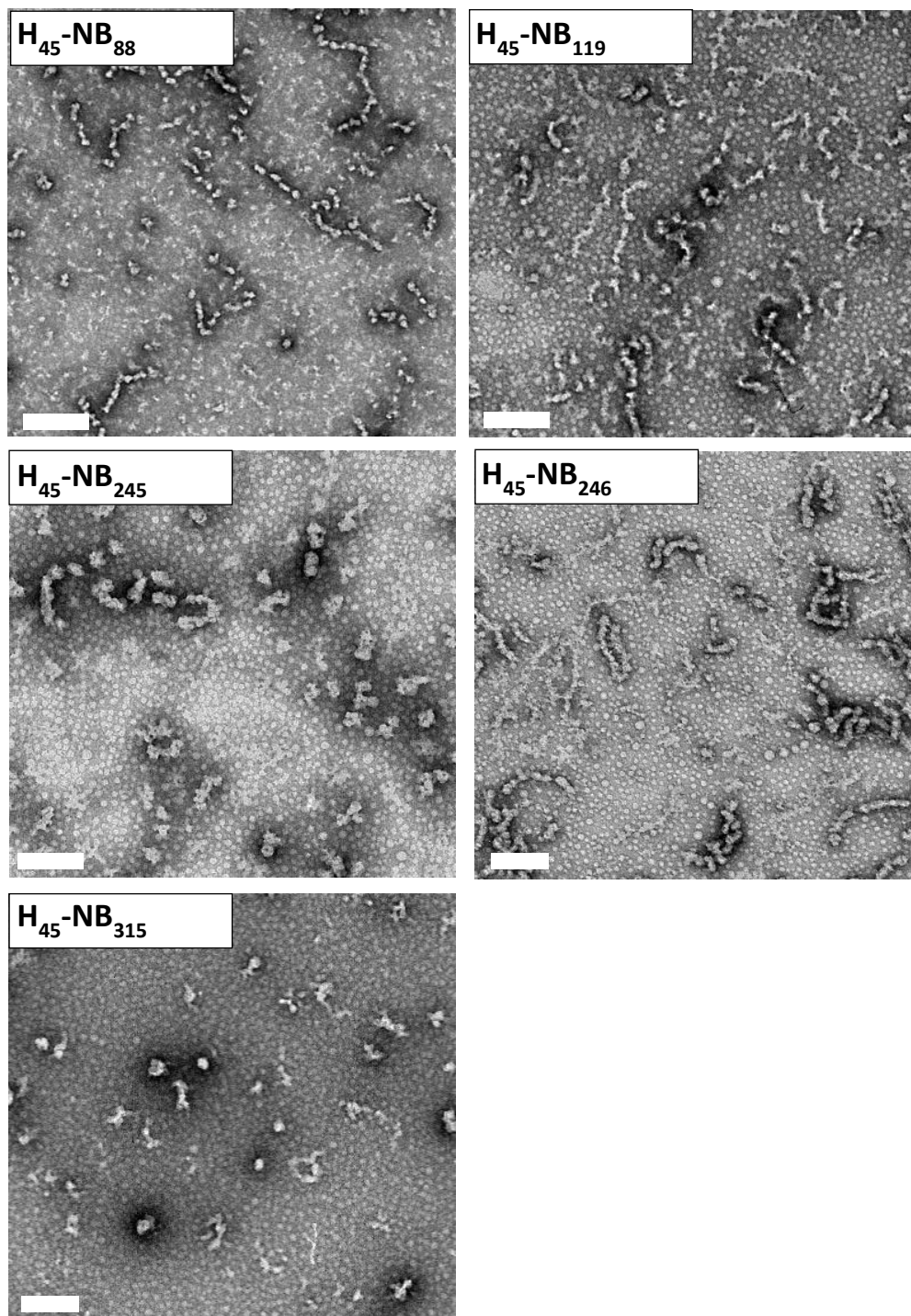
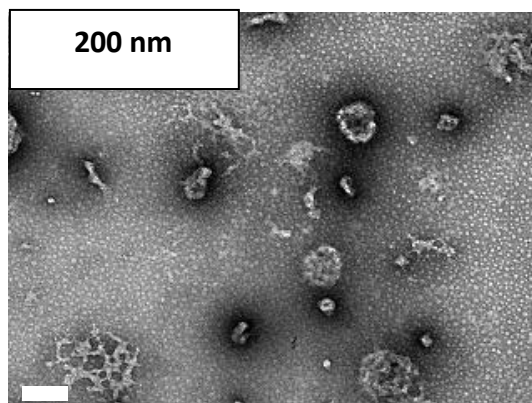
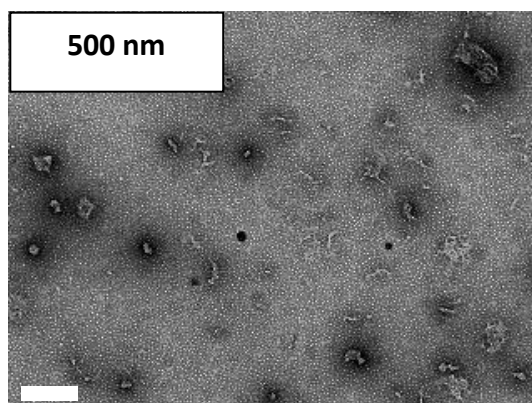
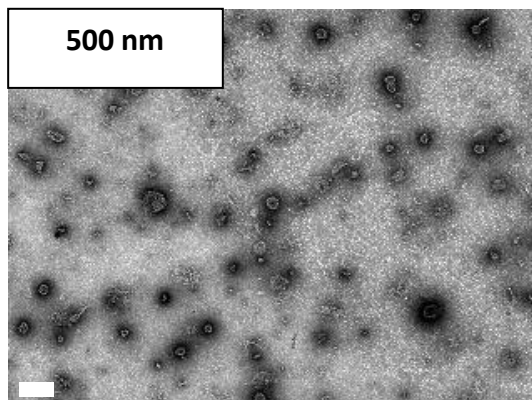


Figure 5.5 - TEM of particles of $pHEA_{45}-b-p(NIPAM-stat-BAPE)_n$, where n varies between 88 and 315, prepared at room temperature at a concentration of 0.05 wt% and stained with pH 7 phosphotungstic acid. The scale bars are all equal to 200 nm.

By comparing two similar core-forming block lengths of block pNIPAM and pNIPAM-*stat*-BAPE core forming blocks it is possible to see that there is a large difference in the morphology between the two samples (Figure 5.6). When BAPE is incorporated into the core, much smaller structures are seen, with none of the large structures with diameters over 100 nm. BAPE is a hydrophobic

monomer and therefore the incorporation of this will decrease the LCST of the pNIPAM block, meaning at the same temperature, the core will be smaller. The occurrence of elongated structures that appear to be composed of numerous spherical objects bound together is much more frequent.

pHEA₄₅-b-pNIPAM₂₆₉ 5:1



pHEA₄₅-b-p(NIPAM-*stat*-BAPE)₂₄₅ 5:1

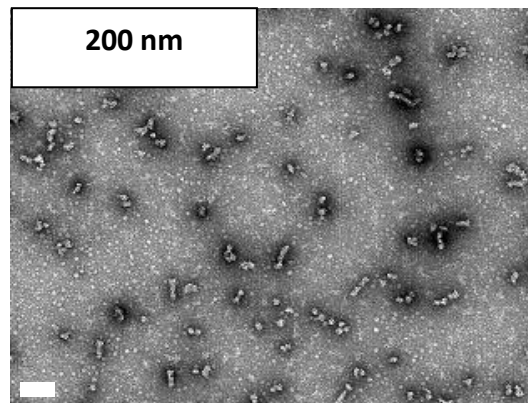
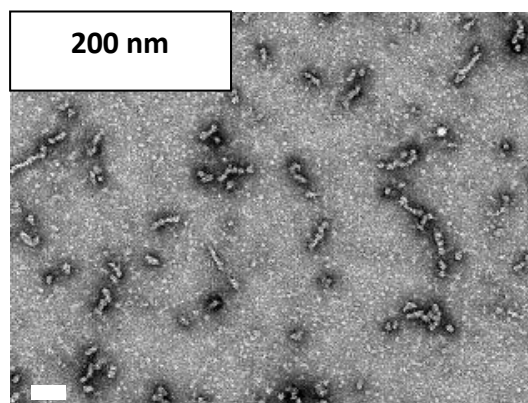
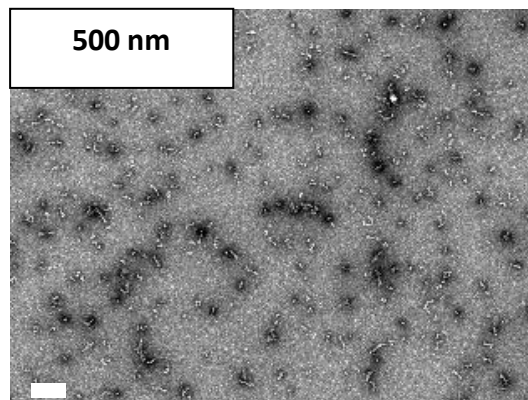


Figure 5.6 - TEM of particles of H₄₅-N₂₆₉ and H₄₅-NB₂₄₅ prepared at room temperature at a concentration of 0.05 wt% and stained with pH 7 phosphotungstic acid.

5.2.3. The temperature responsive behaviour of core-crosslinked nanogels

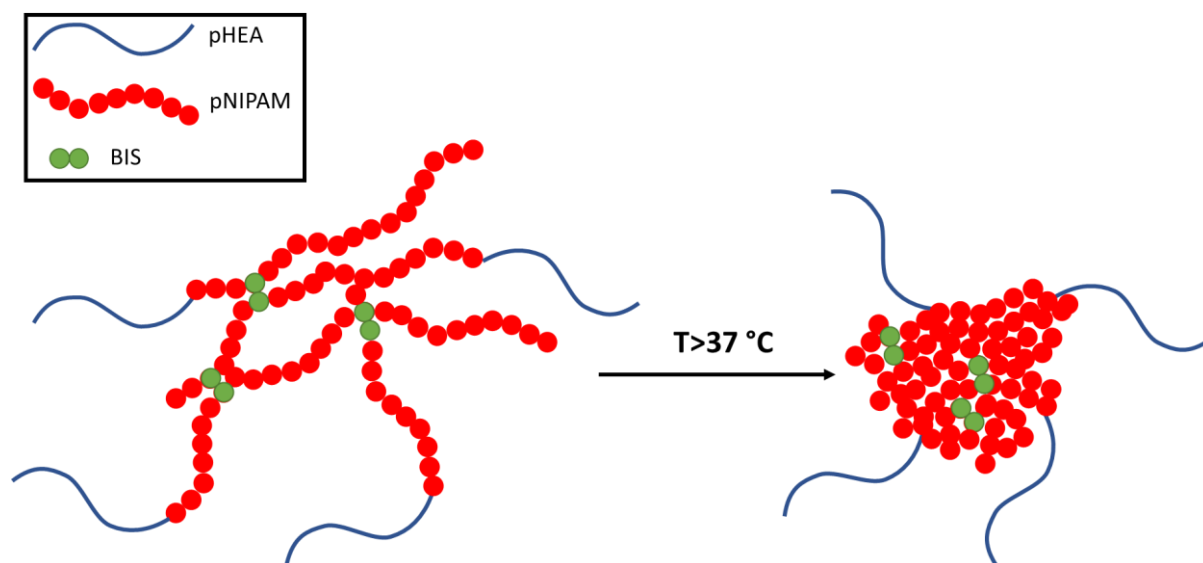


Figure 5.7 – A diagrammatical representation of the collapse of the crosslinked pNIPAM core on heating a nanogel solution to temperatures above its LCST. The hydrophilic chains remain the same but the core of the nanogel shrinks as the chains collapse from the coil form to a globule formation.

The temperature responsive behaviour of these nanogels is very important as this is what will be used to encapsulate and release a drug. It was predicted from the results observed with the diblock copolymers that the core would collapse when raising the temperature above the LCST of the polymer, giving a smaller overall nanogel size (Figure 5.7). It can be seen in the criteria in the introduction for this chapter that the ideal LCST of the nanogel before oxidation is below body temperature and ideally below room temperature. This will allow drug loading into the nanogels and will mean that when inside the body, the nanogels will not swell so there should be minimal leakage of drug.

To test the temperature responsive behaviour of these nanogels, DLS analysis was used over a range of temperatures below and above the LCST to estimate the size of the particles. For nanogels, both with and without BAPE in the core, shrinking is observed on heating above the LCST of the pNIPAM core (Figure 5.8). In the polymers where there is 2 mol% BAPE statistically incorporated into the pNIPAM core, the measurements were recorded at temperatures of 15, 25, 35 and 45 °C because BAPE has been shown, in Chapter 4, to reduce the LCST of the pNIPAM. Although the size of the NG changes by approximately 15 nm between 15 and 25 °C, the largest change in diameter occurs

between 25 and 35 °C. This change in size of approximately 36 nm suggests that the LCST of the BAPE containing nanogel is present between these temperatures. This is similar to the size difference observed in the nanogel with a NIPAM core at the same temperatures.

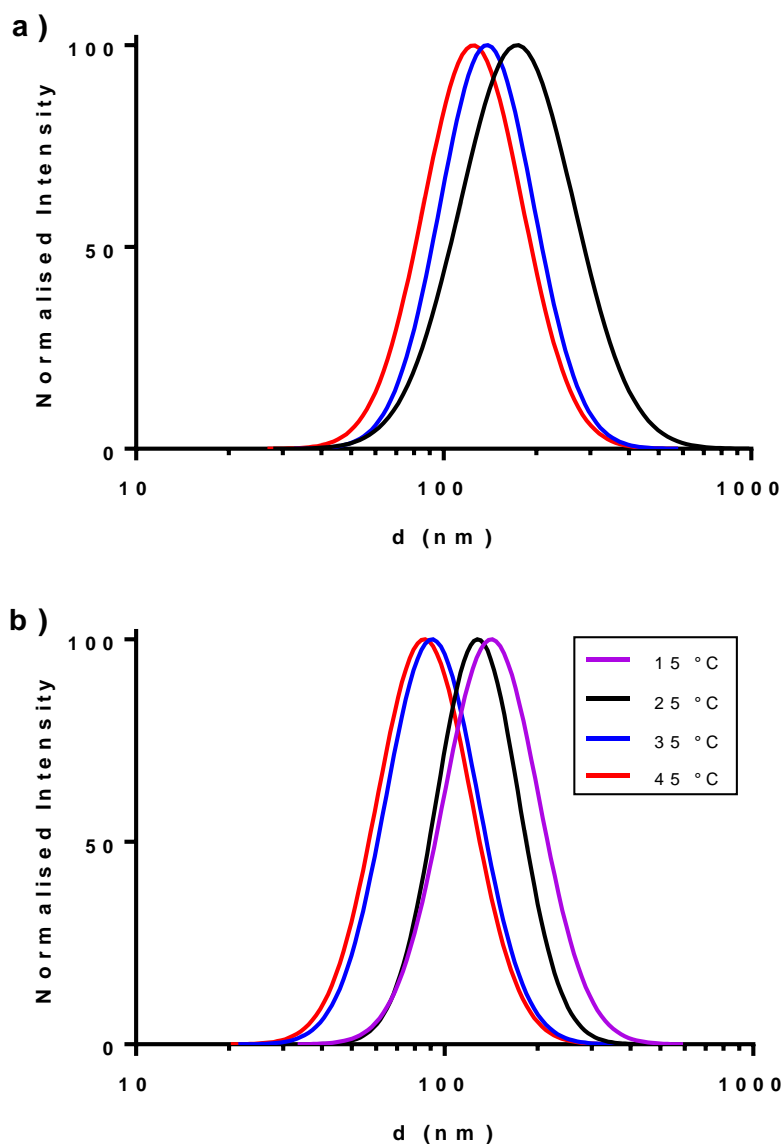


Figure 5.8 - The observable shrinking behaviour by DLS analysis of a) $H_{45}\text{-}N_{269}\text{ BIS}$ and b) $H_{45}\text{-}NB_{245}$ with crosslinker to mCTA ratios of 5:1, on heating to temperatures above the LCST of pNIPAM, with a NG concentration of 0.1 wt%. The wavelength of the laser used is 640 nm and the backscattering was measured.

The reproducibility of the swelling and shrinking behaviour is important to ensure that the behaviour remains constant throughout the use of the NGs, in particular that it stays constant in heating and cooling cycles. The diameter of particles of $H_{45}\text{-}NB_{291}$ with a crosslinker to mCTA ratio of 3:1 was

measured via DLS with increasing and decreasing temperature, in a cycle. It can be seen from Figure 5.9 that the size of the particles during this heating and cooling cycle overlap, showing good reproducibility of this behaviour and minimal hysteresis.

Another important thing to note from this figure, is that the change in size is gradual, over a temperature range, unlike the transition measured for the linear polymers in chapter 2 and 3. It is difficult to determine a specific temperature for the cloud point, but a range can be quoted from the beginning to the end of the transition. For $H_{45}\text{-NB}_{291}$ with a crosslinker to mCTA ratio of 3:1, shrinking begins at 20 °C but the size does not reach a minimum until heated to approximately 32 °C

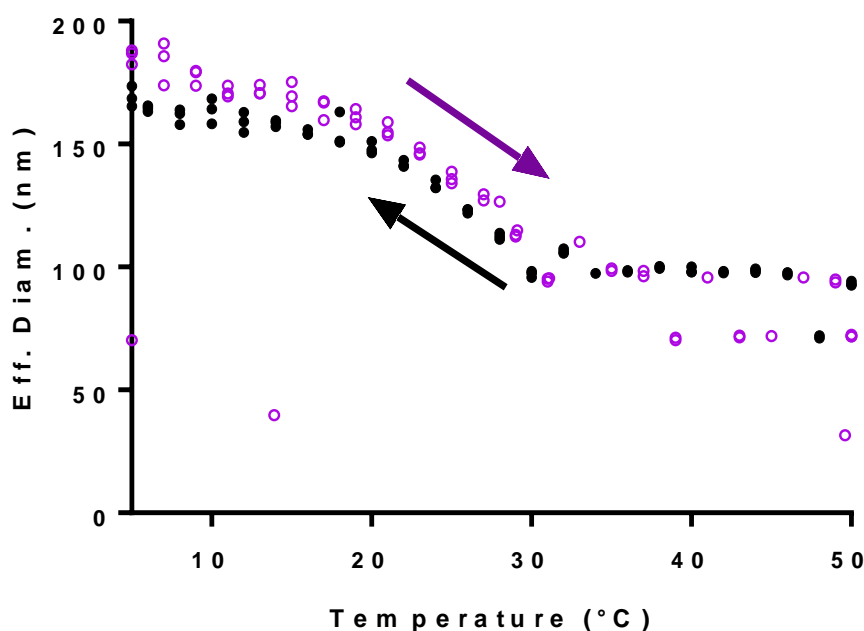


Figure 5.9 – Effective diameter of $H_{45}\text{-NB}_{291}$ 3:1 from DLS with increasing (purple) and decreasing (black) temperature, at a concentration of 0.1wt%. The wavelength of the laser used is 633 nm and the backscattering was measured.

5.2.4. Effect of crosslinker concentration on nanogel swelling

It is known that the crosslink density affects the swelling of hydrogels.⁴³⁻⁴⁵ Similarly, the amount of crosslinker incorporated into the core of a nanogel affects its ability to swell with more crosslinker in the core reducing the change in size in response to temperature. This is important when the

encapsulation and release of drug is related to the swelling behaviour. It is a balance between effective encapsulation with minimal drug leakage, but high loading efficiency and release.

Utilising DLS as a particle sizing method, it can be seen that on raising the temperature of nanogels, with similar length core forming blocks but different crosslinker to mCTA ratios, to above their LCST causes much more shrinkage when the ratio is 3:1 (Figure 5.10). On heating to temperatures above the LCST, the nanogels crosslinked with a 3:1 ratio of crosslinker to mCTA shrink in diameter by much more than the ones with a 5:1 ratio, as expected. For nanogels with a pNIPAM core, when a 3:1 ratio is observed, these shrink by 80 nm, whereas the nanogels crosslinked with a 5:1 ratio only shrink by 48 nm. The same behaviour is also seen in polymers with BAPE incorporated in the core, with 5:1 and 3:1 shrinking by 42 and 61 nm respectively at 45 °C when compared to the native nanogels at 25 °C.

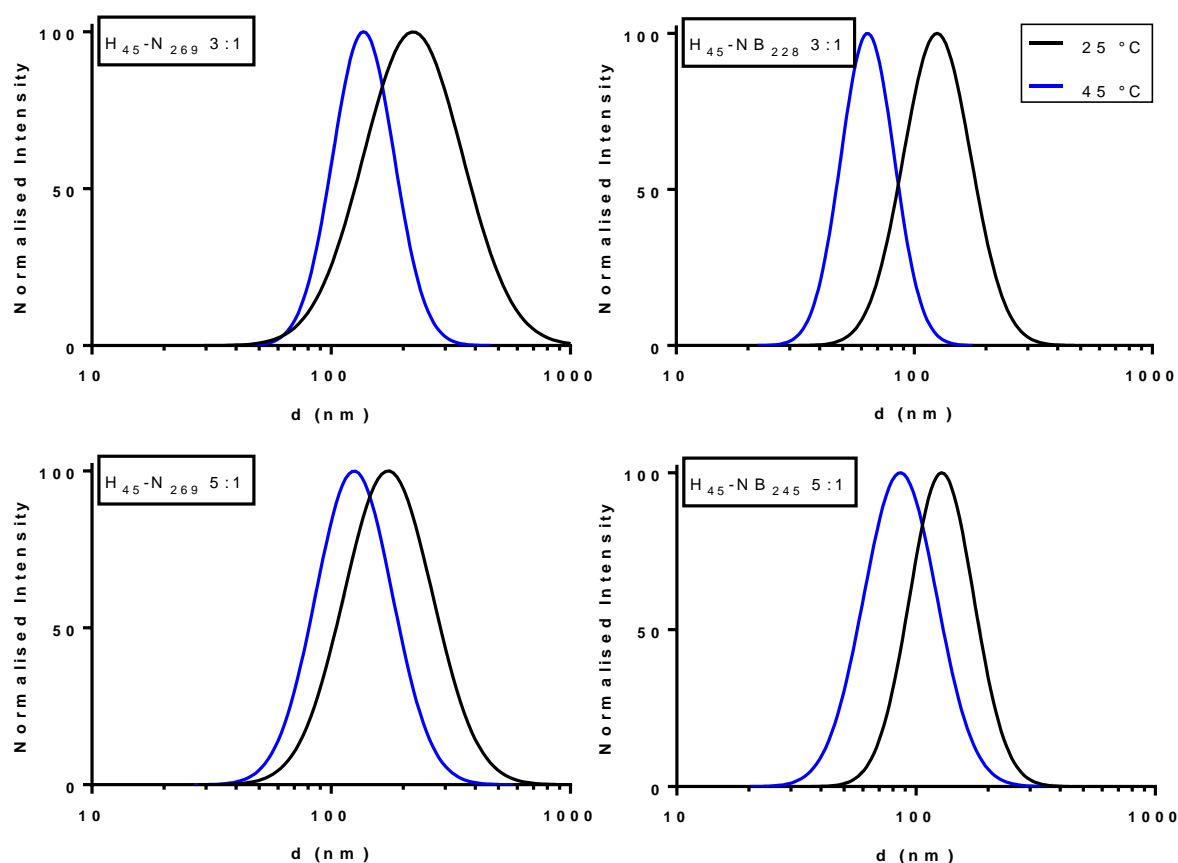
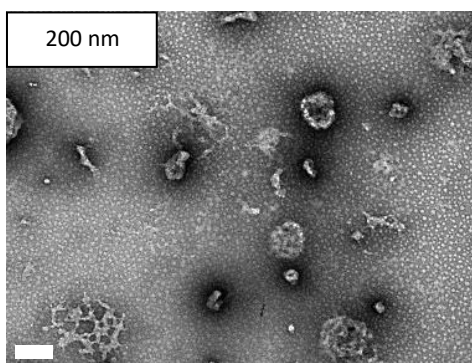
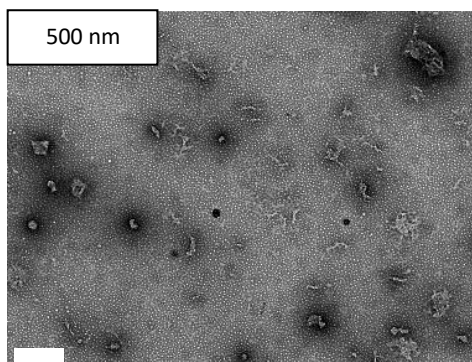
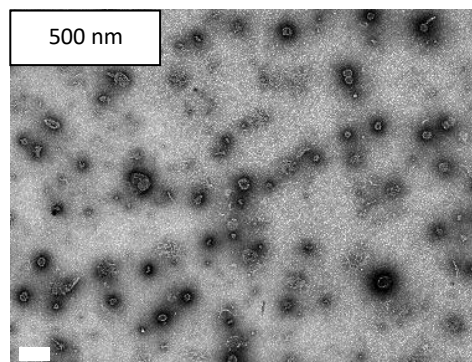


Figure 5.10 - DLS comparison of $H_{45}-N_{269/269}$ and $H_{45}-NB_{245/228}$ with crosslinker to mCTA ratio of 5:1 and 3:1 after polymerisation to observe the extent of shrinkage on heating the nanogels to temperatures above the LCST, with a NG concentration of 0.1wt%. The wavelength of the laser used is 640 nm and the backscattering was measured.

The differences caused by the incorporation of more crosslinker are also evident from analysis of TEM images (Figure 5.11 and Figure 5.12). When comparing samples with the same main block composition, samples with different crosslinker to mCTA ratios look similar with regards to the morphologies seen. The samples with a predominantly NIPAM core show some segmented worm-like structures, however many of the nanoparticles are spherical cage-like structures. This is most likely due to the crosslinking molecule being added at the beginning of the polymerisation. As the polymer chain grows and self-assembly occurs, if there are crosslinking molecules, it will begin to join these structures together, causing the morphologies seen here. The difference is the size of the larger structures. Although there vary in size in the same sample, overall, they are much larger with the lower crosslinker ratio.

Although there is a large difference seen between the BAPE containing samples and those without, the variation in crosslinking concentration is not as different. The samples with more crosslinker incorporated into the core appear to be more elongated and larger on average when compared to the samples with a lower amount of crosslinker.

pHEA₄₅-b-pNIPAM₂₆₉ 5:1



pHEA₄₅-b-pNIPAM₂₆₉ 3:1

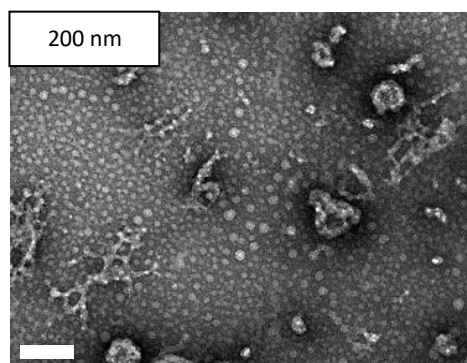
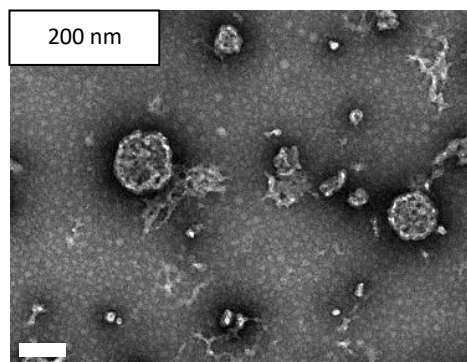
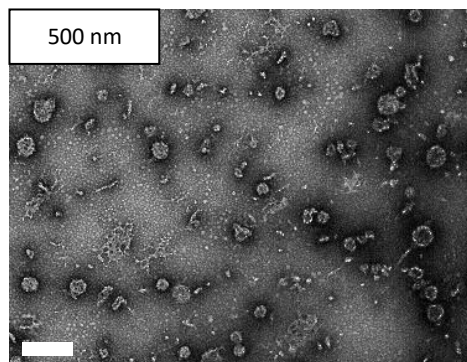
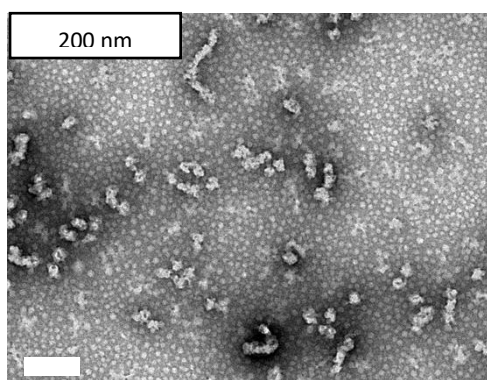
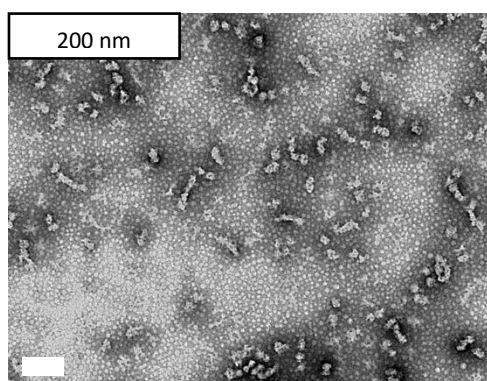
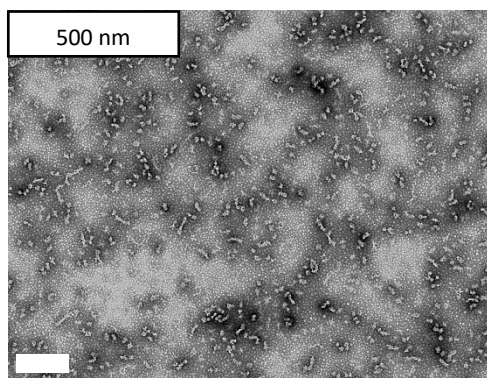


Figure 5.11 - TEM of particles of H₄₅-N_{269/269} with a crosslinker to mCTA ratio of 5:1 and 3:1 respectively, prepared at room temperature at a concentration of 0.05 wt% and stained with pH 7 phosphotungstic acid

pHEA₄₅-*b*-p(NIPAM-*stat*-BAPE)₁₉₈ 5:1



pHEA₄₅-*b*-p(NIPAM-*stat*-BAPE)₁₈₈ 3:1

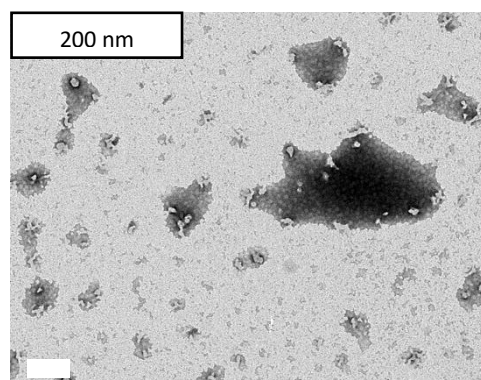
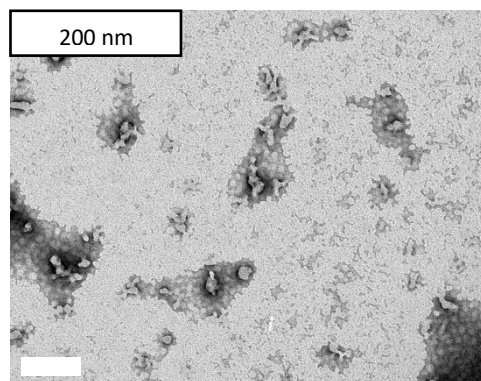
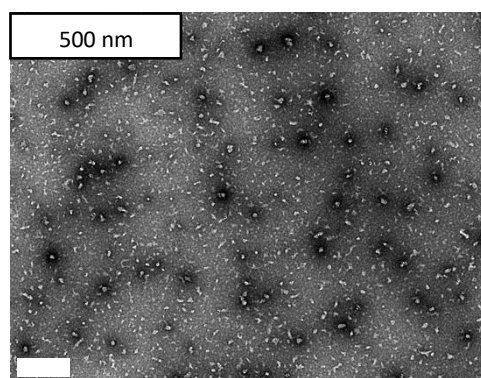


Figure 5.12 - TEM of particles of H₄₅-NB_{245/228} with a crosslinker to mCTA ratio of 5:1 and 3:1 respectively, prepared at room temperature at a concentration of 0.05 wt% and stained with pH 7 phosphotungstic acid.

5.2.5. The effect of BAPE concentration on particle size, morphology and oxidation response

To allow the delivery of drugs for autoimmune diseases, these nanogels must be stimuli responsive to hydrogen peroxide. In the case of these nanogels, the ideal behaviour would be that after oxidation the LCST of these nanogels is increased to above physiological temperature causing the nanogels to swell and release the encapsulated cargo. When comparing two nanogels with similar lengths of core forming block, it is expected that when the core contains only crosslinked pNIPAM

chains, there will be no change in size on oxidation. However, when BAPE is incorporated into this block, the boronic acid pinacol ester will be oxidised by H_2O_2 to form an acrylic acid unit in the polymer chain. This will cause a change in solubility of the core-forming block and therefore will alter the LCST, causing swelling of the nanogel core.

As described previously, incorporation of BAPE enables oxidation to affect the temperature-responsive behaviour of the nanogels. When BAPE is incorporated into the polymer it lowers the LCST but, after oxidation, the LCST is seen to be higher than body temperature ($37\text{ }^\circ\text{C}$) (See Chapter 3, section 3.3.4). NGs with BAPE in the core begin shrinking at much lower temperatures than those with mainly NIPAM cores, as can be seen via DLS analysis with increasing temperature (Figure 5.13).

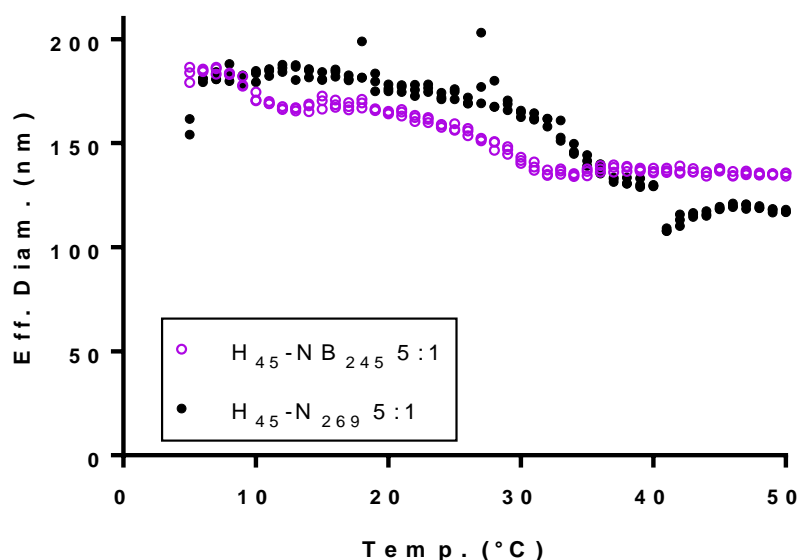


Figure 5.13 – Comparison DLS analysis at increasing temperatures of two samples with similar core forming block lengths to determine the effect of BAPE incorporation on LCST. The wavelength of the laser used is 640 nm and the backscattering was measured. Some very high eff. diam. Results were removed as anomalous values as these are continuous measurements therefore the large particles would be there at every measurement if they were real, and to make the data clearer. See zoomed out DLS in appendix (figure C.15).

DLS analysis was conducted on the native and oxidised polymer at $37\text{ }^\circ\text{C}$ and these size distributions were then compared. On oxidation of BAPE containing NGs, the BAPE would be oxidised, causing an increase in the LCST of the polymer, which correlates to an increase in size compared to the native NG at a given temperature. Therefore, this analysis determines whether the LCST has changed and

what degree of swelling would be expected. For nanogels without BAPE, the size distributions overlay almost exactly showing that there is no change in size after oxidation implying that the LCST of the polymer remains the same, as expected (Figure 5.14a). Conversely, when BAPE is incorporated into the core of the NG, a large increase in size from 90 nm to 165 nm is seen after oxidation (Figure 5.14b).

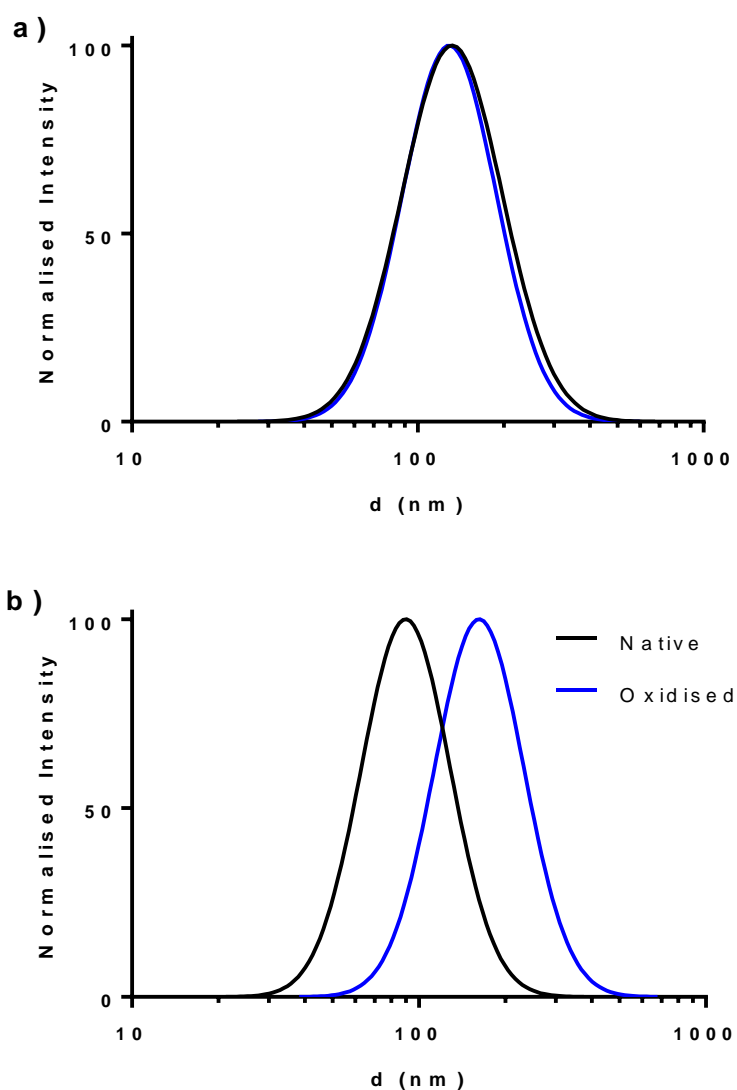


Figure 5.14 - DLS particle size distributions at 37 °C of a) $H_{45}\text{-}N_{269}$ and b) $H_{45}\text{-}NB_{245}$, both with a crosslinker to mCTA ratio of 5:1, before and after oxidation with 15 mM H_2O_2 , at a NG concentration of 0.1wt%,. The wavelength of the laser used is 640 nm and the backscattering was measured.

This nanogel increases in size by approximately 72 nm, which should be a large enough size difference to cause the release of any encapsulated material, especially as this is 21 nm larger than the native nanogel at 15 °C (Figure 5.15).

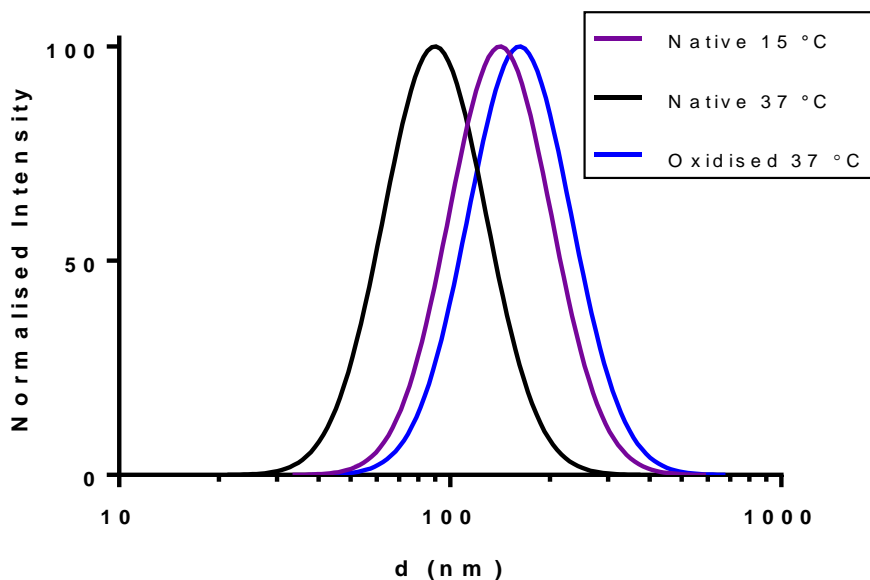


Figure 5.15 DLS analysis at 15°C and 37 °C before oxidation and 37 °C after oxidation of $H_{45}\text{-NB}_{245}$, 5:1, to show the extent of swelling, at a NG concentration of 0.1wt%. The wavelength of the laser used is 640 nm and the backscattering was measured.

Again, the LCST can be determined of the oxidised polymer and compared to the native polymer to demonstrate the change seen in size after oxidation (Figure 5.16). As mentioned above, the shrinking behaviour appears more gradual for the NGs with BAPE in the core, however, a shift in where this shrinkage is more pronounced is seen at higher temperatures in the oxidised polymer, when compared to the native polymer. There is a difference in size at 37 °C of approximately 41 nm.

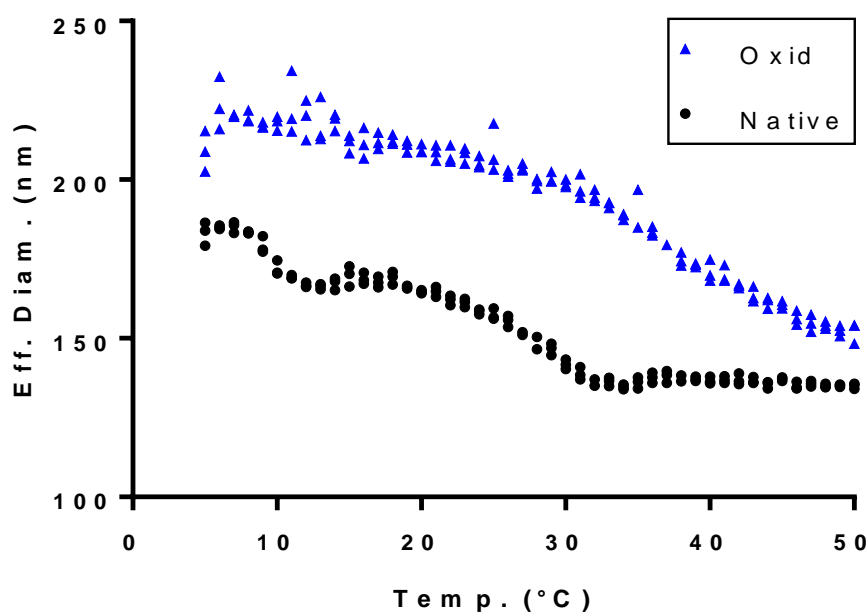


Figure 5.16 – Comparison of particle diameter by DLS analysis at increasing temperatures of H_{45} -NB $_{245}$ 5:1 to determine the effect of BAPE incorporation on LCST before and after oxidation, using a NG concentration of 0.1 wt%. The wavelength of the laser used is 640 nm and the backscattering was measured.

The above polymers were oxidised using 15 mM hydrogen peroxide. This is much higher than the concentrations found in the body with the estimation of hydrogen peroxide concentration due to autoimmune diseases at 50-100 μ M.⁴⁶ It is important to note here that a polymeric system that is too sensitive to low concentrations of hydrogen peroxide may also have drawbacks as hydrogen peroxide is produced during a normal immune response that protects the body from foreign objects. If the nanogels respond to a much lower concentration of H_2O_2 , the drug could be released prematurely causing negative effects.

To test the oxidation response, H_{45} -NB $_{291}$ with a 3:1 crosslinker to mCTA ratio was oxidised at 37 °C at a variety of H_2O_2 concentrations. The size of these nanogels was determined via DLS, with measurements taken after approximately 24 and 72 hours to determine whether the degree of swelling is based on the concentration of H_2O_2 , or the amount of time exposed to this concentration (Figure 5.17).

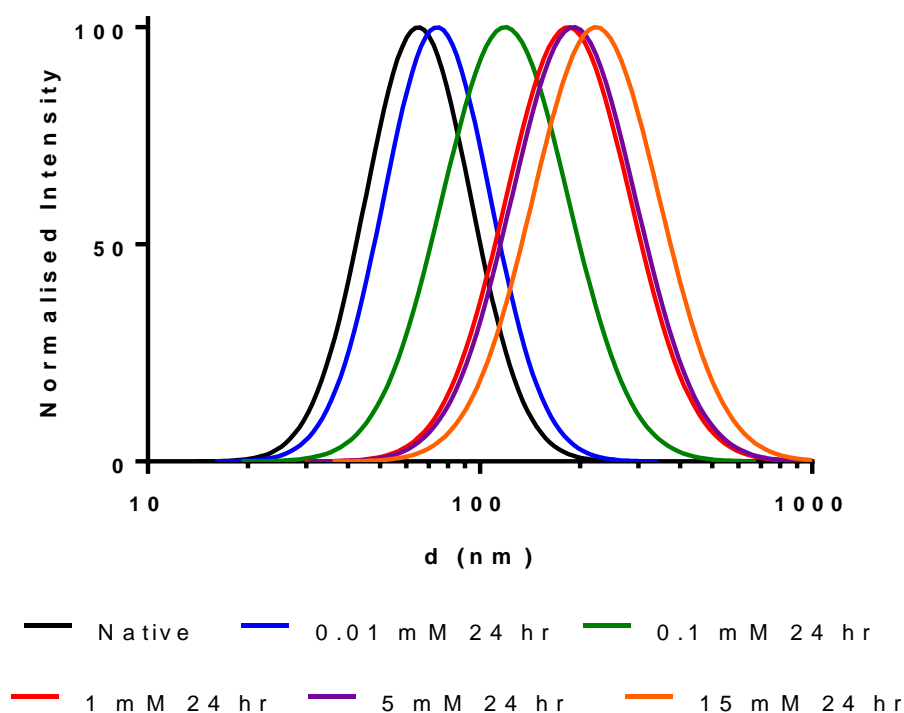


Figure 5.17 - DLS analysis at 37 °C of native H_{45} -NB $_{291}$ with a crosslinker to mCTA ratio of 3:1 and the oxidised nanogel using H_2O_2 at concentrations of 0.01, 0.1, 1, 5 and 15 mM, at a NG concentration of 0.1wt%. The wavelength of the laser used is 640 nm and the backscattering was measured.

At all H_2O_2 concentrations, nanogels are seen to swell after 24 hours. However, they do not swell to the same extent indicating that the rate of oxidation may be concentration dependent. It was important to test whether this was the full extent of oxidation, so these samples were left at 37 °C for a further 48 h. and analysed again by DLS. After 72 h., it is expected that all the available hydrogen peroxide will have been used in the reaction with the BAPE units in the polymer core and that the swelling of the NG is at the maximum for the concentration. Comparison of the samples that were oxidised at 0.1 and 5 mM H_2O_2 have average effective diameters of 118 and 196 nm respectively, compared to the native polymer which has a diameter of 65.5 nm. After 72 h the polymer oxidised with 5 mM H_2O_2 had not increased in size, indicating that is oxidised fully after 24 h. (Figure 5.18). However, even after 72 h, the NG oxidised with the lower concentration has not reached the same size, increasing from 118 nm to 180 nm.

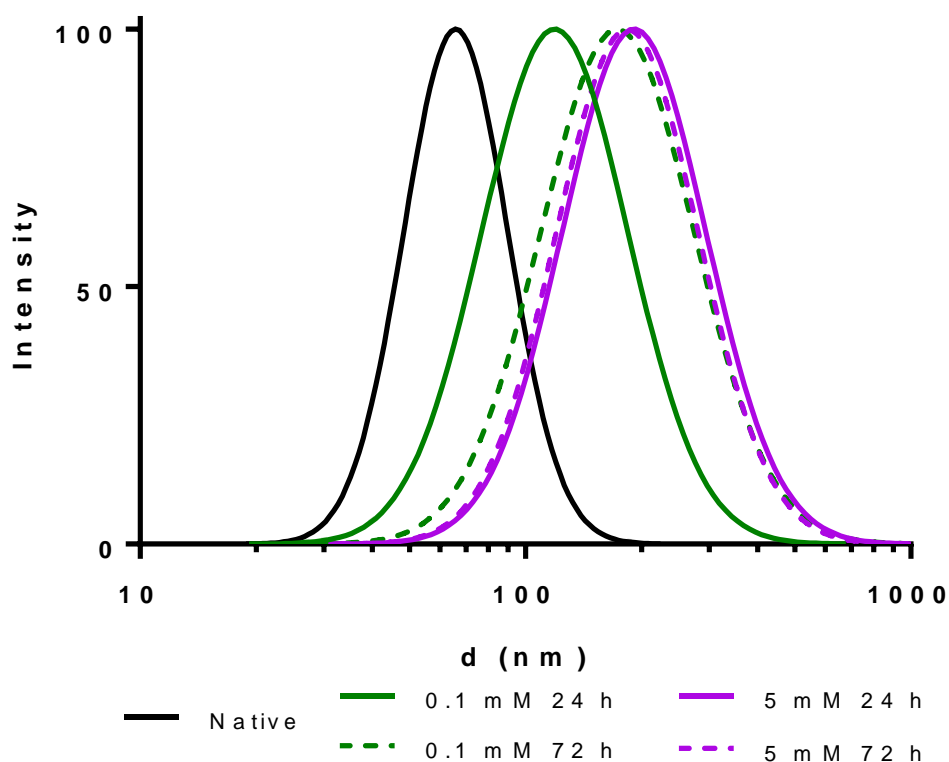


Figure 5.18 - DLS particle size distributions at 37 °C of native H_{45} -NB₂₉₁ with a crosslinker to mCTA ratio of 3:1 and the oxidised nanogel at 2 different time periods using H_2O_2 at concentrations of 0.1 and 5 mM, at a NG concentration of 0.1wt%. The wavelength of the laser used is 640 nm and the backscattering was measured.

These results indicate that the concentration of H_2O_2 is insufficient to oxidise all molecules of BAPE in the core of the nanogel, however the degree of swelling of the NG observed may be sufficient to release encapsulated drug. The amount of H_2O_2 required to oxidise all BAPE units in the NG can be approximated from the quantity of BAPE added into the reaction and a conversion the polymerisation (see equations 2.2-2.4 in section 2.3.15). The concentration of hydrogen peroxide needed to fully oxidise all BAPE in the sample, and therefore cause maximum swelling of the NG, was calculated to be 0.14 mM. 5 mM is much higher than this, so it is assumed that this sample is fully oxidised and has swollen to the maximum diameter. A concentration of 0.1 mM is less than the concentration needed to oxidise all BAPE units, which explains why that NG does not reach the same diameter, even after 72 h. This is the upper level of hydrogen peroxide concentration observed in the body due to autoimmune conditions so, although it does not cause maximum swelling, this may cause the NG to increase in size enough for release of encapsulated material.

To investigate the nature of oxidation further, the size of the nanogels was measured by DLS frequently throughout the oxidation. The same nanogel was used and oxidised with both 0.1 mM and 5 mM hydrogen peroxide. In doing so, a kinetics plot of nanogel diameter over time during oxidation at 37 °C could be developed (Figure 5.19). The gradient of the slope is much steeper when the nanogel is oxidised with a higher concentration of oxidising agent, which correlate to a faster rate of oxidation and therefore swelling. After 48 h. the slope for the lower concentration has not become flat as anticipated, suggesting that swelling of the nanogels is still occurring but at a much lower rate. After 24 h, the NG had swollen from 64 nm to 74 nm and 98 nm with 0.1 and 5 mM H₂O₂, respectively, and the diameter increased further to 103 nm and 153 nm after 48 h. When 5 mM H₂O₂ was used, the reaction was monitored for only 48 h as the above studies had shown very little difference in diameter between 24 and 72 h. Oxidation with the lowest concentration of H₂O₂ was left to react for 65 h. The diameter was still increasing after this giving a final diameter of 127 nm.

Another important thing to note is that the effective diameter increases with an almost constant gradient when the oxidant is a higher concentration, however with the lower concentration, the rate of swelling increases after around 30 minutes. This could be due to the increasing size of the core as more oxidation occurs and the LCST raises, meaning that some of the pendant BAPE groups are more easily accessible for the H₂O₂ to react.

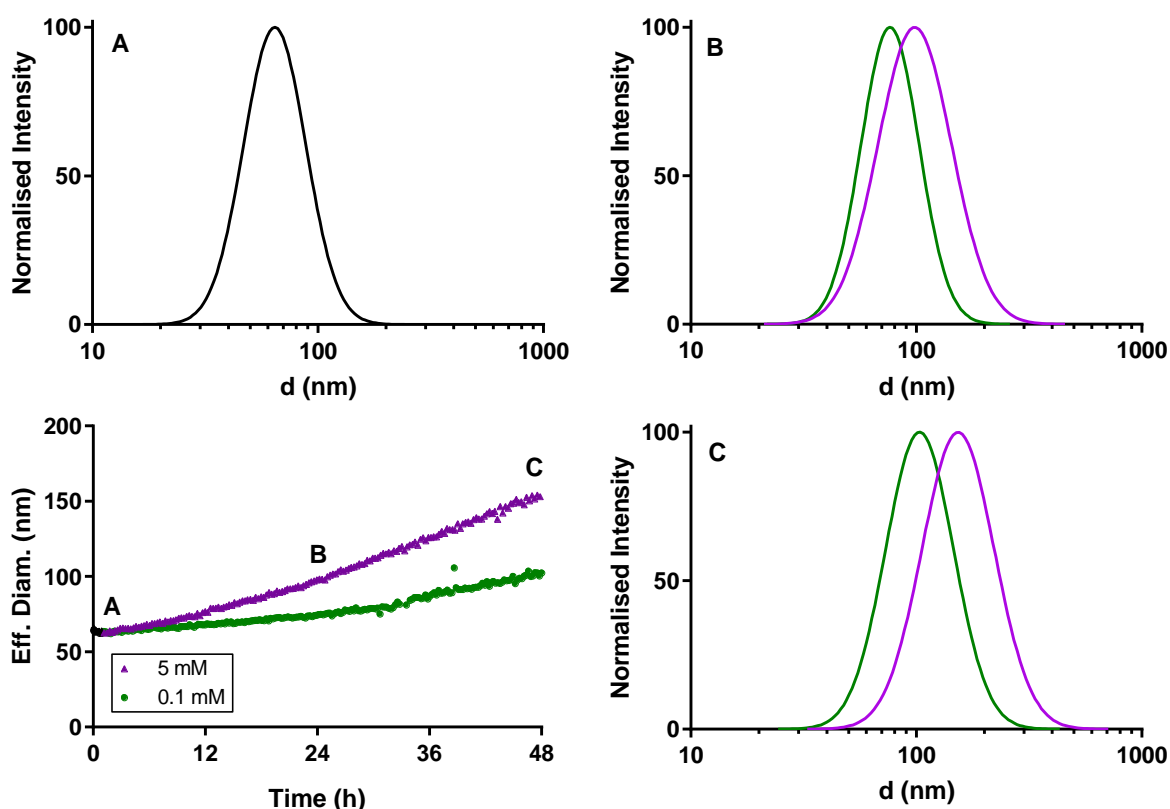


Figure 5.19 - Monitoring in situ oxidation by DLS at 37 °C at a NG concentration of 0.1wt%, H_{45} -NB $_{291}$ with a crosslinker to mCTA ratio of 3:1 was oxidised with concentrations of H_2O_2 of 0.1 mM and 5 mM over 48 h. The labelled size distributions relate to the labelled points on the kinetics plot. The wavelength of the laser used is 640 nm and the backscattering was measured.

5.2.6. The effect of increasing the amount of BAPE in the core forming block

Table 5.1 – Analytical data for nanogels synthesised with the same crosslinker to mCTA ratio but different concentrations of BAPE in the core forming block.

[M]/[pHEA-mCTA]	Mol % BAPE	Crosslinker/mCTA	Conv Crosslinker/mCTA	Conversion / X ^a	Approx. BAPE units per chain	Theoretical DP ^b
317	5	3.8	3	96	15	304
410	2	4.09	3	71	6	291

^a Determined by gravimetric analysis against predicted solids content ^b Theoretical DP. ^c Theoretical M_n from solids content.

From Chapter 3 it is known that the amount of BAPE incorporated into a statistical copolymer of NIPAM can affect the temperature responsive behaviour. In addition, with more BAPE units, it is expected that these polymers will be more sensitive to oxidation.

The difference between the linear copolymers and the nanogels, apart from the crosslinked chains, is the presence of a hydrophilic block. Therefore, before the oxidation behaviour of this nanogel is discussed it is important to determine the LCST of these. For nanogels, it is possible to use the size increase in the nanogel over a temperature range to estimate the LCST as the gels shrink as the temperature rises above the LCST. This can be done using DLS analysis of particle size with temperature ramping. Where there is less BAPE, 2 mol%, it is expected that the LCST is higher in the native nanogel than with 5 mol% BAPE, however this transition is not as sharp as seen with the NGs with a NIPAM core. These both seem to have a very similar LCST, with the NGs shrinking on increasing temperature over very similar temperature range (Figure 5.20). The LCST of the oxidised polymers was not recorded here as it has already been shown that the NGs are much more swollen than the native polymer in their oxidised state at 37 °C, which indicates a change in the LCST. Also, this transition is gradual, so it is likely that the ranges overlap as with the native polymers.

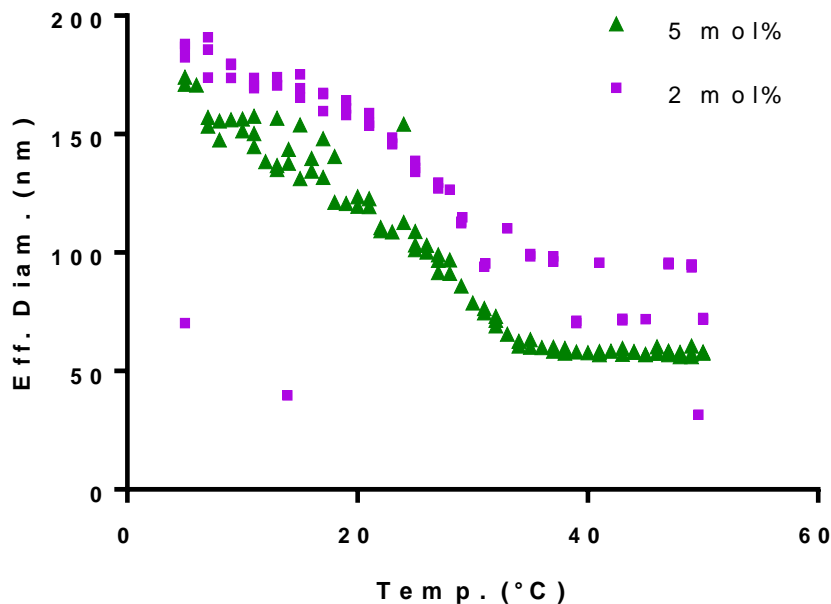


Figure 5.20 - LCST measurements using DLS to measure shrinking behaviour on increasing temperature of $H_{45}\text{-NB}_{291/304}$ 3:1 with 2 and 5 mol% BAPE respectively at a concentration of 0.1wt%. The wavelength of the laser used is 640 nm and the backscattering was measured. Some very high eff. diam. Results were removed as anomalous values as these are continuous measurements therefore the large particles would be there at every measurement if they were real, and to make the data clearer. See zoomed out DLS in appendix (figure C.16).

A larger amount of BAPE incorporated into the core-forming block may also affect the rate and degree of oxidation, as well as the LCST of the oxidised polymer and therefore its size. Initially these polymers were oxidised with 15 mM H_2O_2 to determine the size at 37 °C, where both polymers will be fully oxidised as predicted from results stated previously in this chapter. The native and oxidised polymers were compared by DLS, which shows that the 2 mol% NG increased in size by 128 nm, from 65 nm to 193 nm and the 5 mol% NG increased in size by 154 nm, from 52 nm and 206 nm (Figure 5.21). Although this shows that the nanogels have both increased in size by a large amount, it does not give much information about the kinetics of this.

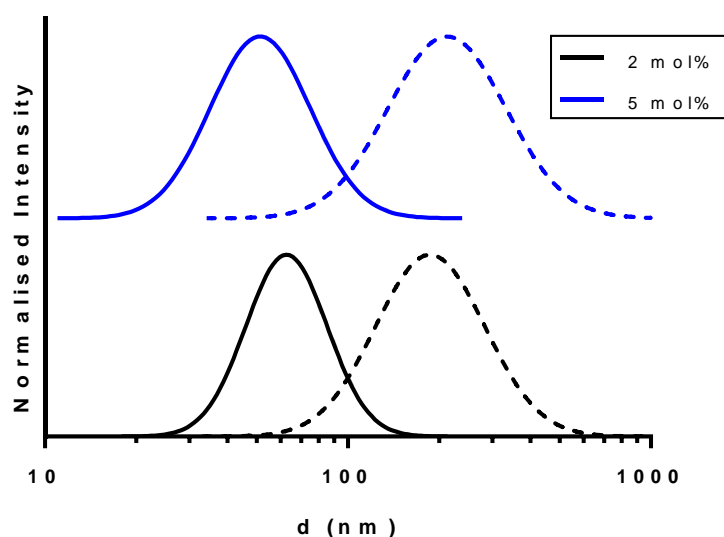


Figure 5.21 – Swelling behaviour of $H_{45}\text{-NB}_{291/304}$ 3:1 with 2 and 5 mol% BAPE respectively, at a concentration of 0.1wt%, when oxidised with 15 mM H_2O_2 . The solid lines represent the native polymers and the dashed lines represent the polymers after oxidation. The wavelength of the laser used is 640 nm and the backscattering was measured.

By monitoring the in situ oxidation of the two polymers with an oxidant concentration of 5 mM H_2O_2 , it is possible to determine the difference that the increased amount of BAPE has on the oxidation (Figure 5.22). Although both polymers have similar sizes after oxidation, the NG with a larger concentration of BAPE in the core is oxidised more quickly. Both polymers reach approximately the same size after 30 h and then the rate of reaction is the same for both polymers.

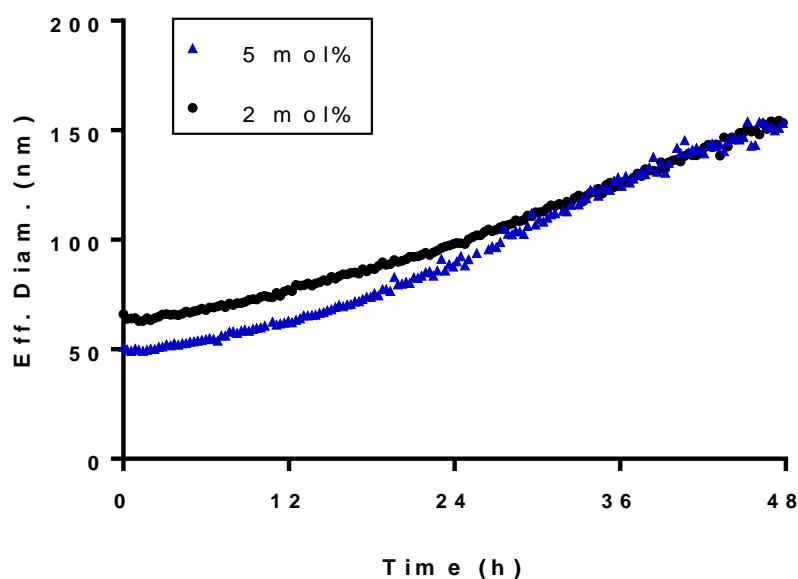


Figure 5.22 - In situ oxidation by DLS at 37 °C. H_{45} -NB_{291/304} with a crosslinker to mCTA ratio of 3:1 and 2 and 5 mol% BAPE respectively, at a concentration of 0.1wt%, oxidised with a H_2O_2 concentration of 5 mM over 48 h. The wavelength of the laser used is 640 nm and the backscattering was measured. Some very high eff. diam. Results were removed as anomalous values as these are continuous measurements therefore the large particles would be there at every measurement if they were real, and to make the data clearer. See zoomed out DLS in appendix (figure C.17).

As well as the rate at which the oxidation occurs, the larger the amount of BAPE incorporated, the more sensitive the NG should be to oxidation as more BAPE units will be available. It is important to note however that there must be an adequate concentration of H_2O_2 in order to oxidise all BAPE units (section 2.3.15), otherwise an increase in BAPE concentration is futile as it will not obtain the expected results.

When the NGs are compared by TEM, overall there is very little difference in size and morphology between the samples (Figure 5.23). The samples appear to be elongated spheres with an average diameter of approximately 100 nm. More BAPE incorporated into the sample has little effect on the morphology, especially when compared to the difference between H-N and H-NB samples.

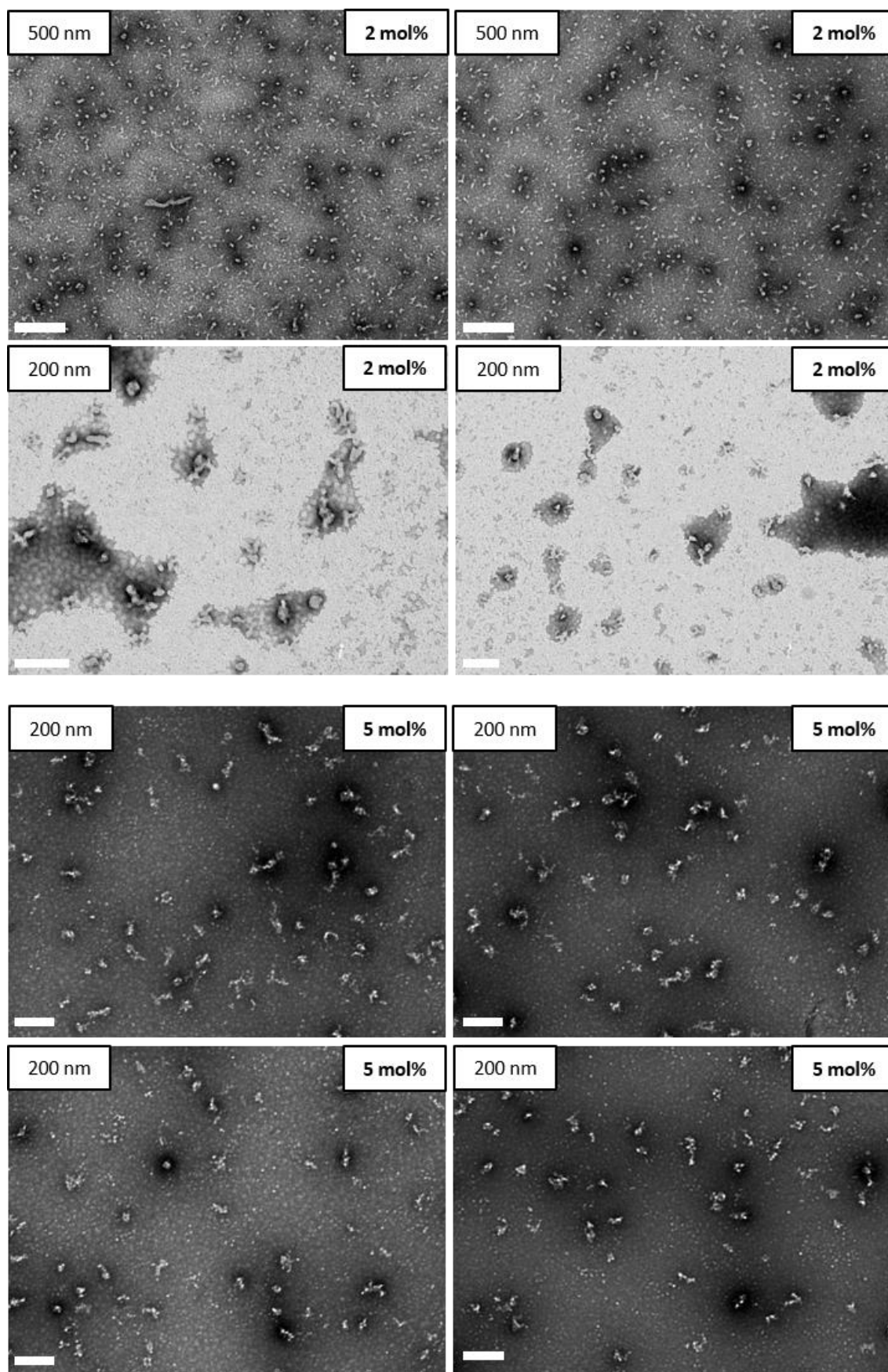


Figure 5.23 – TEM images of particles of $H_{45}\text{-NB}_{291/304}$ with BAPE concentrations of 2 and 5 mol% respectively, prepared at room temperature at a concentration of 0.05 wt% and stained with pH 7 phosphotungstic acid.

5.2.7. In depth analysis on the morphology and oxidation properties of the nanogels

5.2.7.1. Synthesis of comparable samples of nanogels to tune drug release behaviour

As mentioned in section 5.2.2, although two different particle sizing methods have been used to determine the size of the particles, there are discrepancies between the data of the same nanogels. DLS is a particle sizing method, which presumes that all scattering patterns can be fitted to that of hard sphere but in the case of hydrated, non-spherical nanogels, this will not give an exact value.^{47,48} In addition, as the morphologies deviate greatly from spherical particles; the DLS sizing data is difficult to interpret. Similarly, TEM also has disadvantages, for example, the way in which the carbon-coated TEM grids are prepared could influence the appearance of the sample. This could be the nature of the sample preparation using dried samples, the staining method used to image the samples, inadvertent selectivity due to the small sample size or the instability of the particles under the conditions of the microscopy i.e. electron beam.^{49,50} It is therefore important to discern whether these particles are spherical, segmented worms, large aggregates or a mixture of these.

To do this a few of the above polymers were re-synthesised with 3 mol% BAPE to allow for more analysis, with repetition of all the previous analyses to ensure direct comparisons. Also, studies of the oxidation behaviour with different oxidants was undertaken. The polymers focused on were those where the target DP of the second block is approximately 315. The mCTA remains the same and the crosslinker to mCTA ratio was either 5:1 or 3:1, assuming an approximate reaction conversion of 80%. Characterisation data for these polymers can be seen below (Table 5.2).

Table 5.2 – Analytical data for H_{45} -N and H_{45} -NB_n with a crosslinker:mCTA ratio of 5/3:1 after conversion.

[M]/[pHEA ₄₅ -mCTA]	BAPE mol%	Conversion / % ^a	[M]/[pHEA-mCTA]*conv. ^b	Approx. XL:mCTA ^c	Approx. BAPE units per chain
315	0	73	230	5:1	0
316	0	82	259	3:1	0
317	3	68	215	5:1	6
317	3	80	253	3:1	7

^a Determined by gravimetric analysis against predicted solids content ^b [M]/[pHEA-mCTA]*conv. ^c Theoretical XL:mCTA from solids content. ^dTheoretical M_n from solids content.

5.2.7.2. An in-depth study into the oxidation sensitivity of nanogels containing an arylboronic ester moiety

All NGs were analysed by DLS to determine their LCST before and after oxidation (Table 5.3, Figure 5.24). When the core is predominantly NIPAM, there is no change in LCST observed after oxidation, however, when BAPE is incorporated an increase in LCST is seen.

Table 5.3 – Approximate LCST of NGs with 3 mol% BAPE determined by DLS, comparing the effective diameter over a temperature range.

Nanogel	Native LCST (°C)	Oxidised LCST (°C)
H_{45} -N ₂₃₀ 5:1	30.1 – 37.2	30.1 – 37.2
H_{45} -N ₂₅₉ 3:1	33.3 – 36.3	33.3 – 36.3
H_{45} -NB ₂₁₅ 5:1	27.8 – 36.7	33.1 – 42.9
H_{45} -NB ₂₅₃ 3:1	26.1 – 34.6	36.8 – 45.1

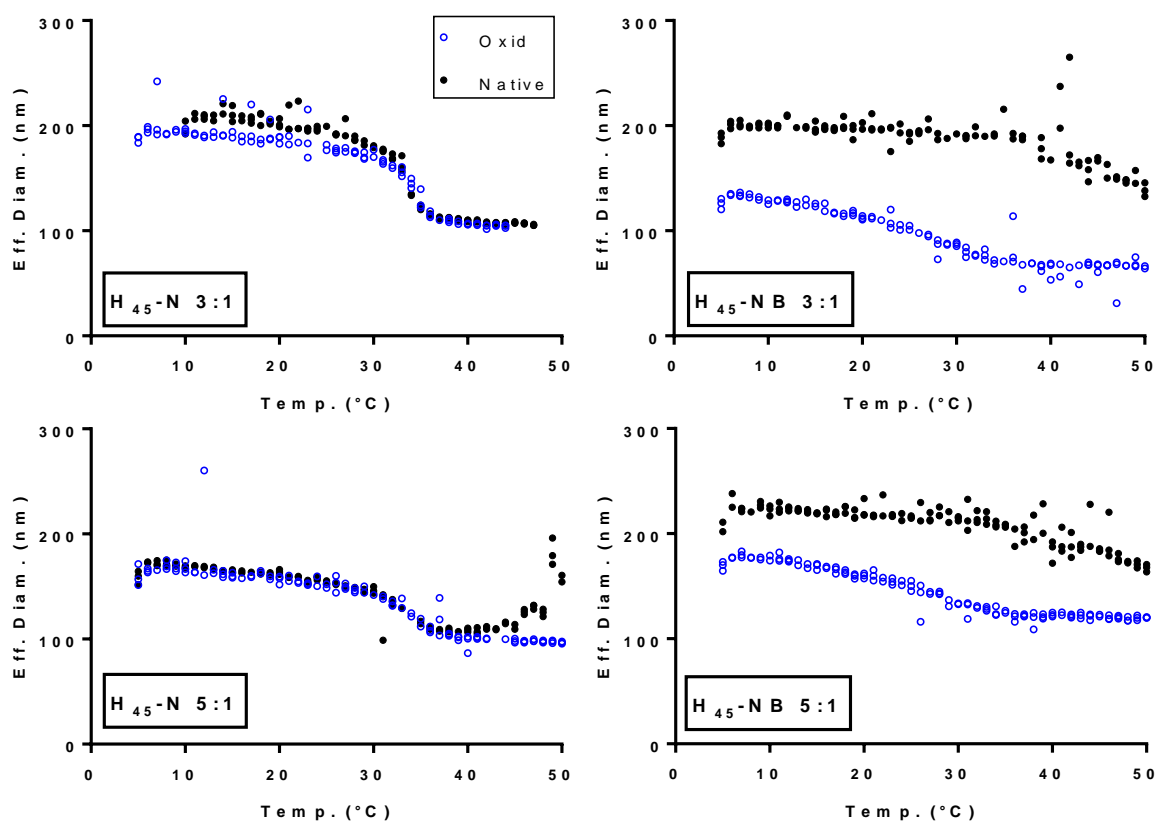


Figure 5.24 – Effective diameter measurements of four NGs, H-N and H-NB with crosslinker to mCTA ratios of 3:1 and 5:1, by DLS at a concentration of 0.1wt%, over a range of temperatures. The wavelength of the laser used is 640 nm and the backscattering was measured. Some very high eff. diam. Results were removed as anomalous values as these are continuous measurements therefore the large particles would be there at every measurement if they were real, and to make the data clearer. See zoomed out DLS in appendix (figure C.18).

This correlates with the data shown when these samples are analysed at 37 °C, the NIPAM core NGs remain the same size, whereas when the core is both NIPAM and BAPE, an increase in particle diameter is seen on oxidation. The change in LCST for these polymers alters the temperature at which they shrink so the higher the LCST, the larger the particles compared to the native polymer.

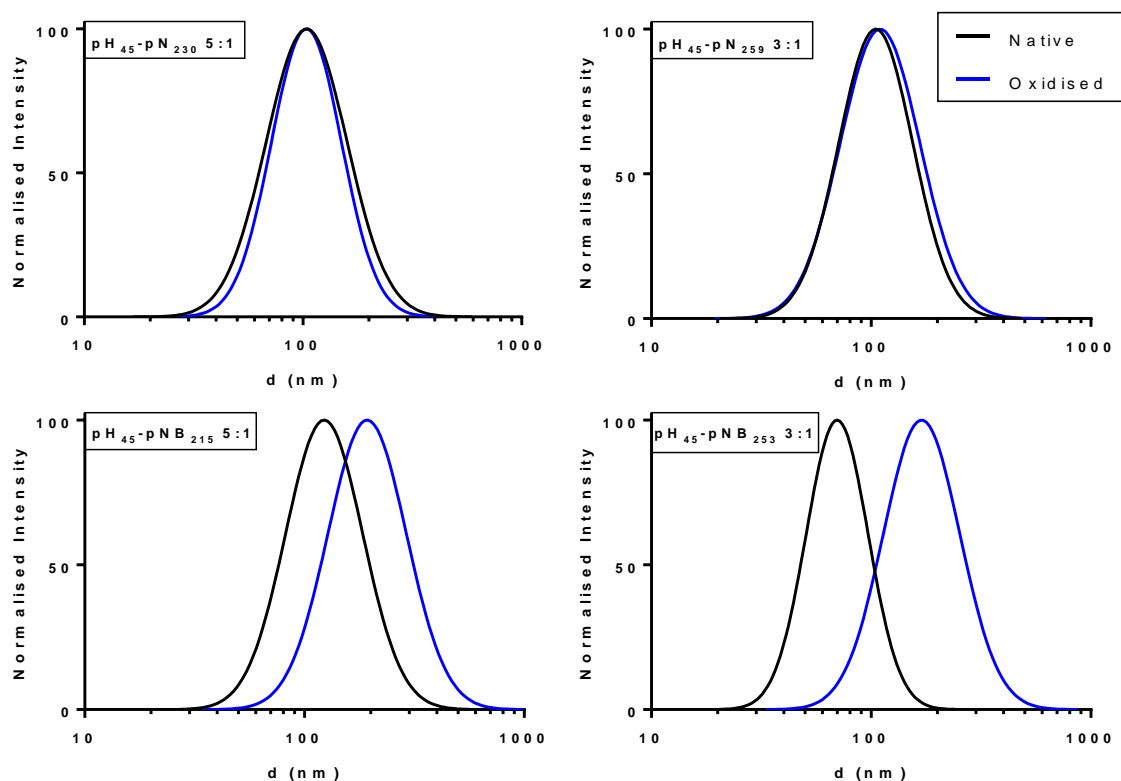


Figure 5.25 - DLS analysis at 37 °C of $H_{45}\text{-}N_n$ and $H_{45}\text{-}NB_n$ with 3:1 and 5:1 crosslinker to mCTA ratio, before and after oxidation with 15 mM H_2O_2 at a concentration of 0.1wt%. The wavelength of the laser used is 640 nm and the backscattering was measured.

Oxidation kinetics can be monitored in situ, as above, recording the change in diameter on oxidation over time. These reactions were carried out on all four NG samples, with and without BAPE in the core to confirm that the increasing size is due to the oxidation of BAPE, and not due to lack of stability at an elevated temperature over time (Figure 5.26). A concentration of 1 mM hydrogen peroxide was used here, which is closer to that produced due to inflammation in autoimmune diseases than used above.⁴⁶ When the core is not oxidation responsive there is minimal change in the diameter over 48 h. As expected, the oxidation-responsive NGs swell by 33 nm and 18 nm for 5:1 and 3:1 crosslinker to mCTA ratios, respectively.

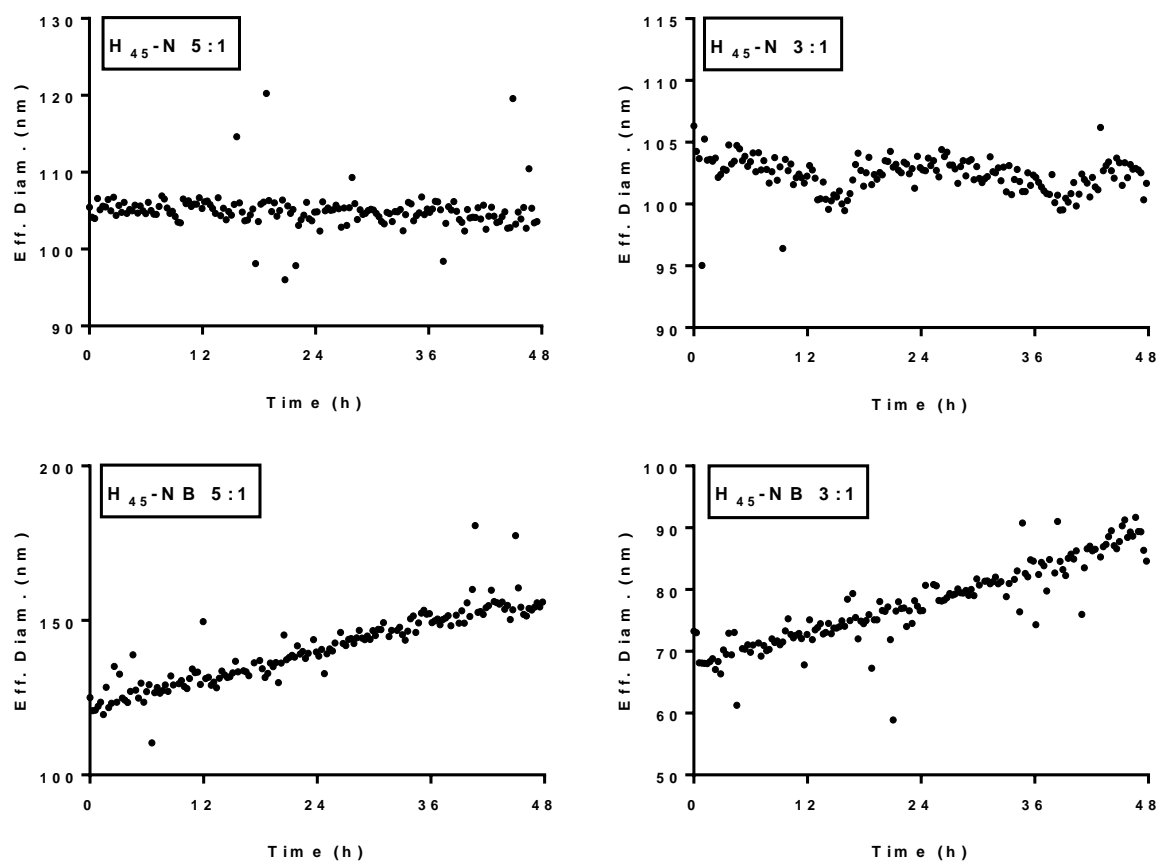


Figure 5.26 - Monitoring in situ oxidation by DLS at 37 °C of $H_{45}\text{-}N_n$ and $H_{45}\text{-}NB_n$ with crosslinker to mCTA ratio of 5:1 and 3:1, at a concentration of 0.1wt%, oxidised with a H_2O_2 concentration of 1 mM over 48 h. The wavelength of the laser used is 640 nm and the backscattering was measured. Some very high eff. diam. Results were removed as anomalous values as these are continuous measurements therefore the large particles would be there at every measurement if they were real, and to make the data clearer. See zoomed out DLS in appendix (figure C.19).

Concentrating only on the samples with BAPE incorporated, as DLS confirmed no change in size for the NIPAM only samples and therefore no oxidation effect. When compared directly, the sample with more crosslinker swells slightly faster on oxidation than the other NG (Figure 5.27).

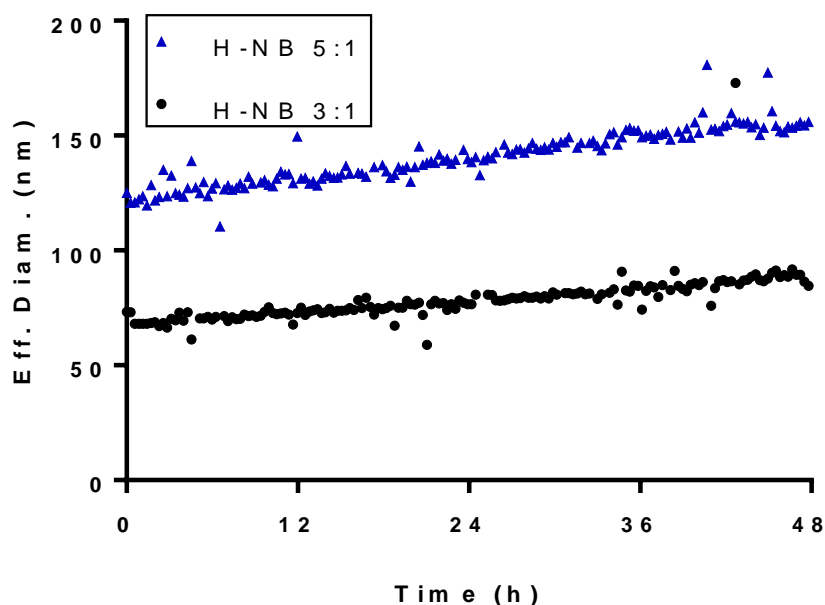


Figure 5.27 – Comparison of the *in situ* oxidation data from the two H-NB samples; $H_{45}\text{-NB}_{215}$ 5:1 and $H_{45}\text{-NB}_{253}$ 3:1, with different crosslinker to mCTA ratios, at a concentration of 0.1wt%. The wavelength of the laser used is 640 nm and the backscattering was measured. Some very high eff. diam. Results were removed as anomalous values as these are continuous measurements therefore the large particles would be there at every measurement if they were real, and to make the data clearer. See zoomed out DLS in appendix (figure C.20).

Again, TEM analysis of polymers before and after complete oxidation with 15 mM hydrogen peroxide was carried out (Figure 5.28, Figure 5.29). The samples look less aggregated after oxidation, implying that the change in LCST could be affecting the interactions between the NG particles at the temperature at which the grids are prepared. Oxidation will also see the formation of charged sulfonate groups from the oxidation of the RAFT chain end groups (see chapter 2), which could also explain the smaller amount of aggregation in the sample. This could however be due to the lack of purification after oxidation and therefore the presence of hydrogen peroxide in the sample. Although this may not affect the polymer further, the hydrogen peroxide could react with the phosphotungstic acid stain, meaning the staining is not comparable to the native polymers. These polymers should be purified after oxidation and analysis conducted again in future to remove this factor. In the sample with a 5:1 crosslinker to mCTA ratio, the polymer aggregates appear to be more worm-like structures after oxidation rather than spherical ‘bundles’ of polymer joined together.

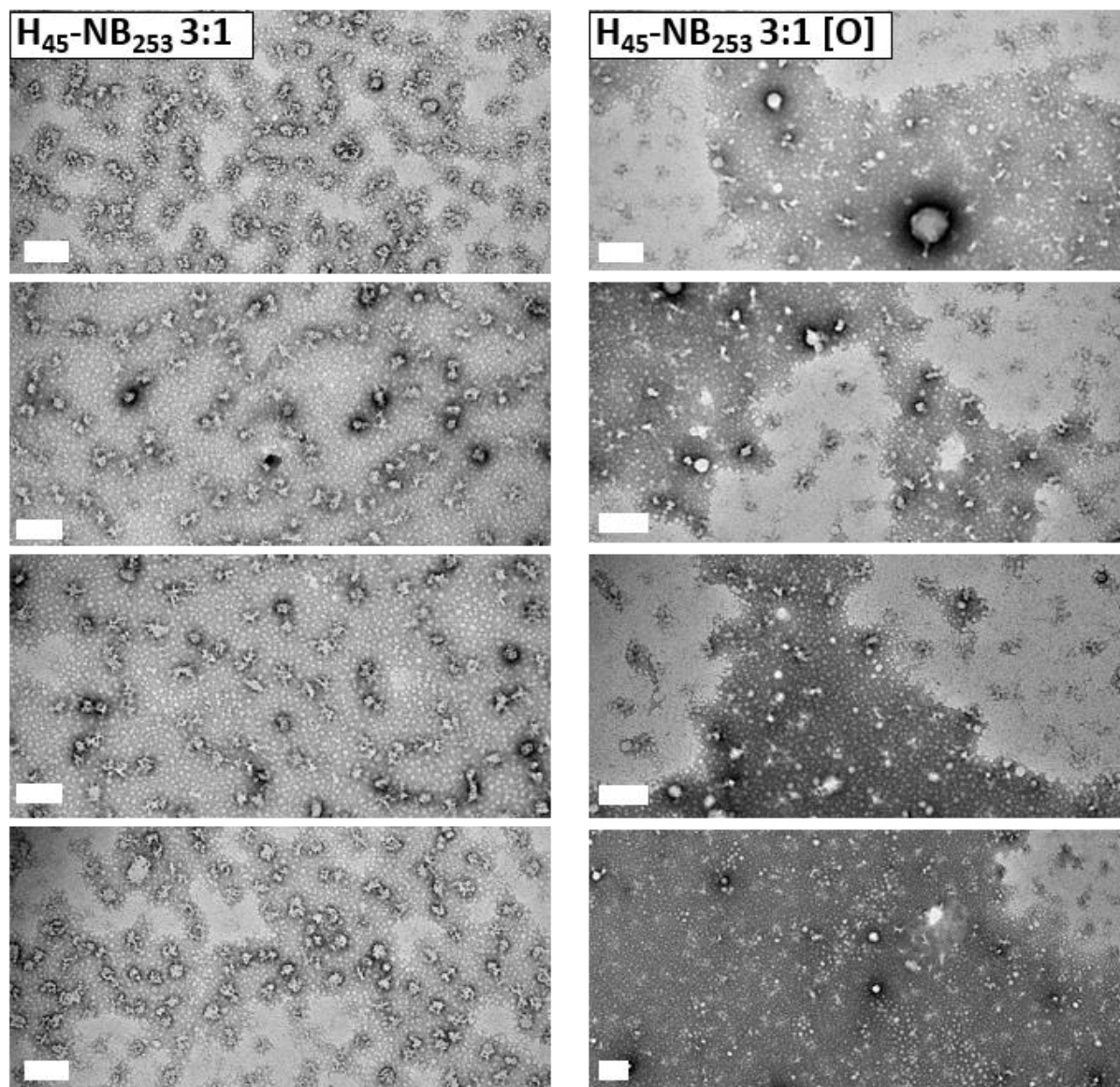


Figure 5.28 - TEM images of particles of H_{45} -NB₂₅₃ with a 3:1 ratio of crosslinker to mCTA before and after oxidation prepared at room temperature at a concentration of 0.05 wt% and stained with pH 7 phosphotungstic acid. The scale bars all represent 200 nm.

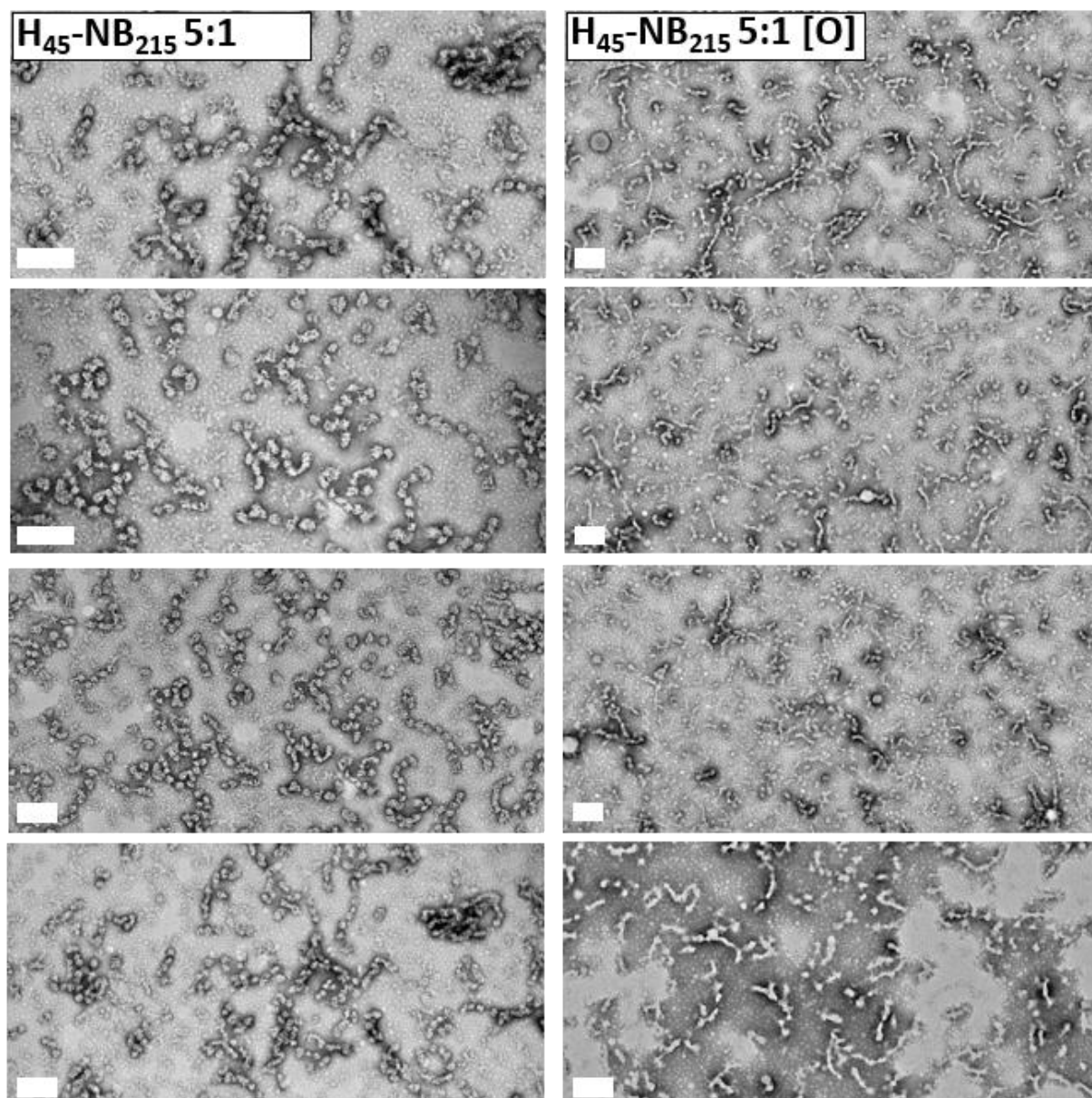


Figure 5.29 - TEM of particles of $H_{45}\text{-NB}_{215}$ with a 5:1 ratio of crosslinker to mCTA before and after oxidation prepared at room temperature at a concentration of 0.05 wt% and stained with pH 7 phosphotungstic acid. The scale bars all represent 200 nm.

It has been mentioned previously in this thesis that boronic acid pinacol esters are very sensitive to oxidation but with selectivity for hydrogen peroxide.⁵¹⁻⁵⁴ Therefore, in situ oxidation studies were carried out as before, to determine whether the NGs respond to hydroxyl radicals, SIN-1, glutathione and H_2O_2 . These chemicals were chosen as they are prevalent within the human body. SIN-1, otherwise known as 3-morpholinopyridone, rapidly decomposes at physiological conditions to give both nitric oxide, NO, and superoxide (O_2^-), which can then react with each other to form

peroxynitrite. These three chemicals are all present due to the oxidative stress produced due to immune response.^{55,56} The hydroxyl radicals (HO^\cdot) were produced in situ through the Fenton reaction between H_2O_2 and FeCl_2 .⁵⁷ This is a reaction that can occur in the body, causing significant damage to DNA and proteins. Glutathione is a reducing agent and is common to all cells in concentrations varying from 1-10 mM.⁵⁸ The main role of this chemical in the body is to remove any ROS which are harmful. The NG, $\text{pH}_{45}\text{-NB}_{253}$ with a 3:1 ratio of crosslinker was used in these oxidation studies and its size was monitored by DLS over 48 h in the presence of oxidants/reductants at concentrations of 1 and 5 mM. A concentration of 1 mM of H_2O_2 is higher than needed to oxidise all boronates in the core (as determined using equation 2.3). 5 mM was also tested for the other oxidants/reductants to determine boronate oxidation was truly selective for H_2O_2 or, instead, less sensitive to other reagents.

With concentrations up to 5 mM of glutathione, SIN-1 and HO^\cdot , no change in size is observed after oxidation for 48 h., suggesting that BAPE is not sensitive to these species (Figure 5.30 – In situ oxidation studies monitored by DLS of $\text{pH}_{45}\text{-pNB}_{253}$ with a crosslinker to mCTA ratio of 3:1 at a concentration of 0.1wt%, to determine the sensitivity of BAPE to other oxidants and reductants; H_2O_2 , hydroxyl radical, SIN-1 and glutathione. The wavelength of the laser used is 640 nm and the backscattering was measured. It must be noted that in the graph of the oxidation with HO^\cdot , the size is not constant initially in the reaction. These NG solutions were typically between a pH of 6.5 and 7.5 which could cause the FeCl_2 used for the Fenton reaction to precipitate out of solution slightly. Therefore the trace is not straight at the beginning of the reaction as expected. Hydrogen peroxide is sensitive to oxidation at concentrations as low as 0.1 mM, despite only a small amount of swelling, showing that BAPE is sensitive to H_2O_2 above other species in the body.

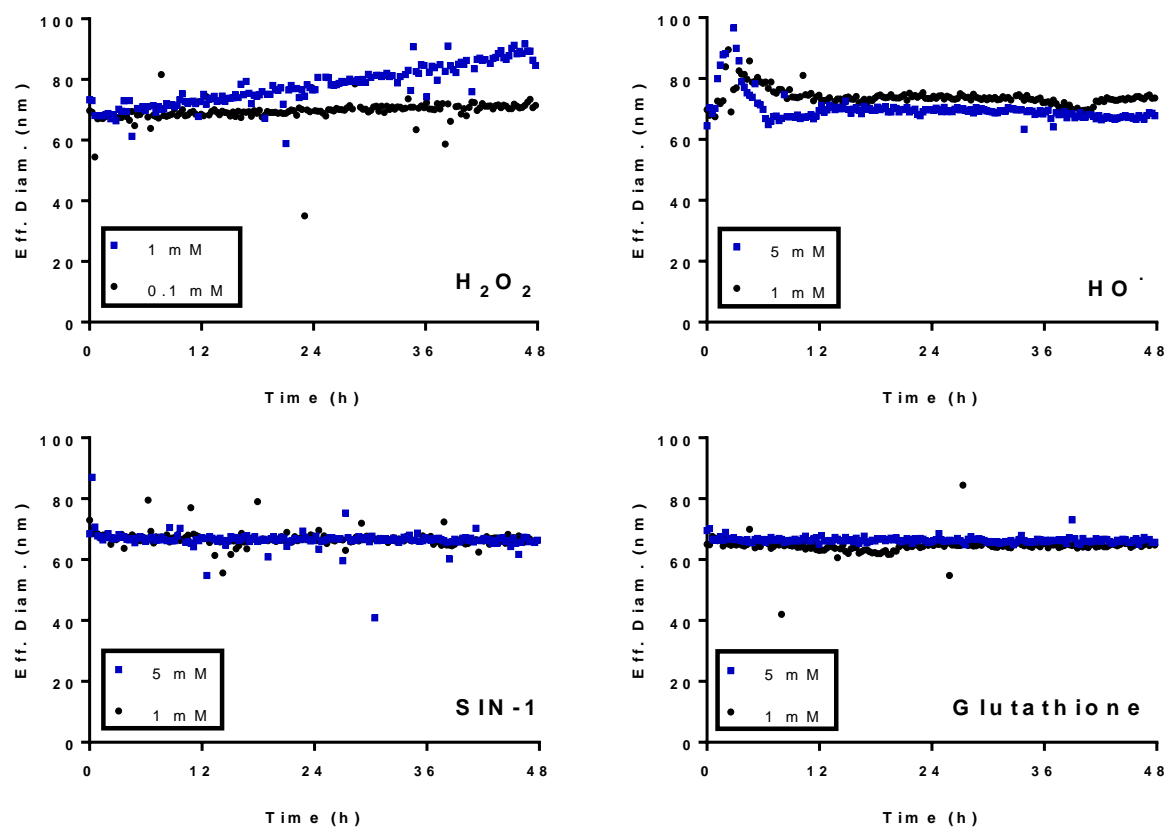


Figure 5.30 – *In situ* oxidation studies monitored by DLS of pH_{45} - pNB_{253} with a crosslinker to mCTA ratio of 3:1 at a concentration of 0.1wt%, to determine the sensitivity of BAPE to other oxidants and reductants; H_2O_2 , hydroxyl radical, SIN-1 and glutathione. The wavelength of the laser used is 640 nm and the backscattering was measured. Some very high eff. diam. Results were removed as anomalous values as these are continuous measurements therefore the large particles would be there at every measurement if they were real, and to make the data clearer. See zoomed out DLS in appendix (figure C.21).

5.2.7.3. Comparison of particle sizing techniques to determine particle morphology more accurately

Dynamic light scattering (DLS)

DLS can be utilised in many ways, as seen above, to characterise the properties of these nanogels. As stated previously, DLS is a technique which shines a laser of a set wavelength through a sample in a solvent. The particles in the solution scatter the light and the scattering is detected at an angle of 90° or 173° (backscattering).^{48,59} The Brownian motion of the particles is measured by the scattering of the light, and by using the Stokes-Einstein equation (Equation 2.2), the hydrodynamic radius (R_h), which is the average particle size, can be determined.^{48,60} This technique is able to analyse samples

as a whole at many concentrations as long as the solution is transparent and therefore is not biased in sampling like microscopy techniques.

To ensure that all analysis can be directly compared, DLS for these nanogels were conducted at 25 °C which is similar to the temperature that all other analysis was carried out (Figure 5.31).

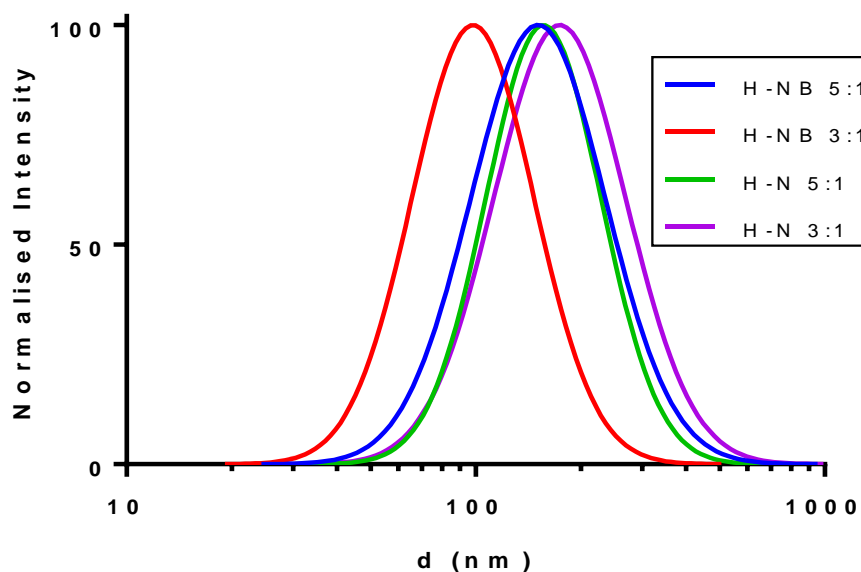


Figure 5.31 - DLS analysis at 25 °C of $H_{45}-N_n$ and $H_{45}-NB_n$ with 3:1 and 5:1 crosslinker to mCTA ratio. The wavelength of the laser used is 640 nm and the backscattering was measured.

This shows that the samples have broader dispersities than expected for monodisperse, spherical particles and that all the samples are between 98 and 171 nm in diameter by this technique (Table 5.4).

Table 5.4 – Effective diameter and PDI at 25 °C of all four nanogels with 3 mol% determined by DLS analysis at a concentration of 0.1wt% and averaged over three runs.

Nanogel	Effective diameter (nm)	PDI
$H_{45}-N_{230}$ 5:1	155	0.165
$H_{45}-N_{259}$ 3:1	170	0.218
$H_{45}-NB_{215}$ 5:1	151	0.200
$H_{45}-NB_{253}$ 3:1	99	0.160

There are a few disadvantages to this technique however, as the Stokes-Einstein equation assumes that the particles are solid and spherical as the rate of diffusion of these is what compared to the results by DLS.^{47,48,59} Therefore, for other morphologies, the hydrodynamic radius is not accurate. This can be seen with the larger PDI for the samples, which could indicate a broad distribution of sizes or could suggest elongated structures which do not fit the solid spherical particle model (Table 5.4). If the structures deviate from the spherical morphology, apart from the high PDI values there is no other morphology information available. Also, if there are multiple particle sizes present, as DLS is a batch measurement it takes an average and is unable to determine distinct particle sizes in solution.^{47,48,59} As the intensity is proportional to r^6 , it skews the radius results in favour of larger particles and in particular can produce significant errors if the size based on volume or number is used for polydisperse samples.^{47,48,59,61}

Transmission electron microscopy – TEM

Transmission electron microscopy (TEM) is another particle sizing technique used in for polymeric structures. This technique differs greatly to others discussed in this section as samples prepared for TEM are dry and under high vacuum, whereas in all other techniques discussed, they are in their hydrated state.^{50,62,63} TEM measures the size of the particles using an electron beam and creates an image based on the transmission of electrons through the sample.⁶² This is the only microscopy technique used to analyse these and therefore gives better morphological results than scattering methods, with structural features being observed in the nm scale.⁵⁰

As above, carbon coated copper grids were used, and the samples were negatively stained using a pH 7 phosphotungstic acid stain. This stain was used to provide contrast between the particles and the background by staining the background but leaving the particles untouched.⁶⁴

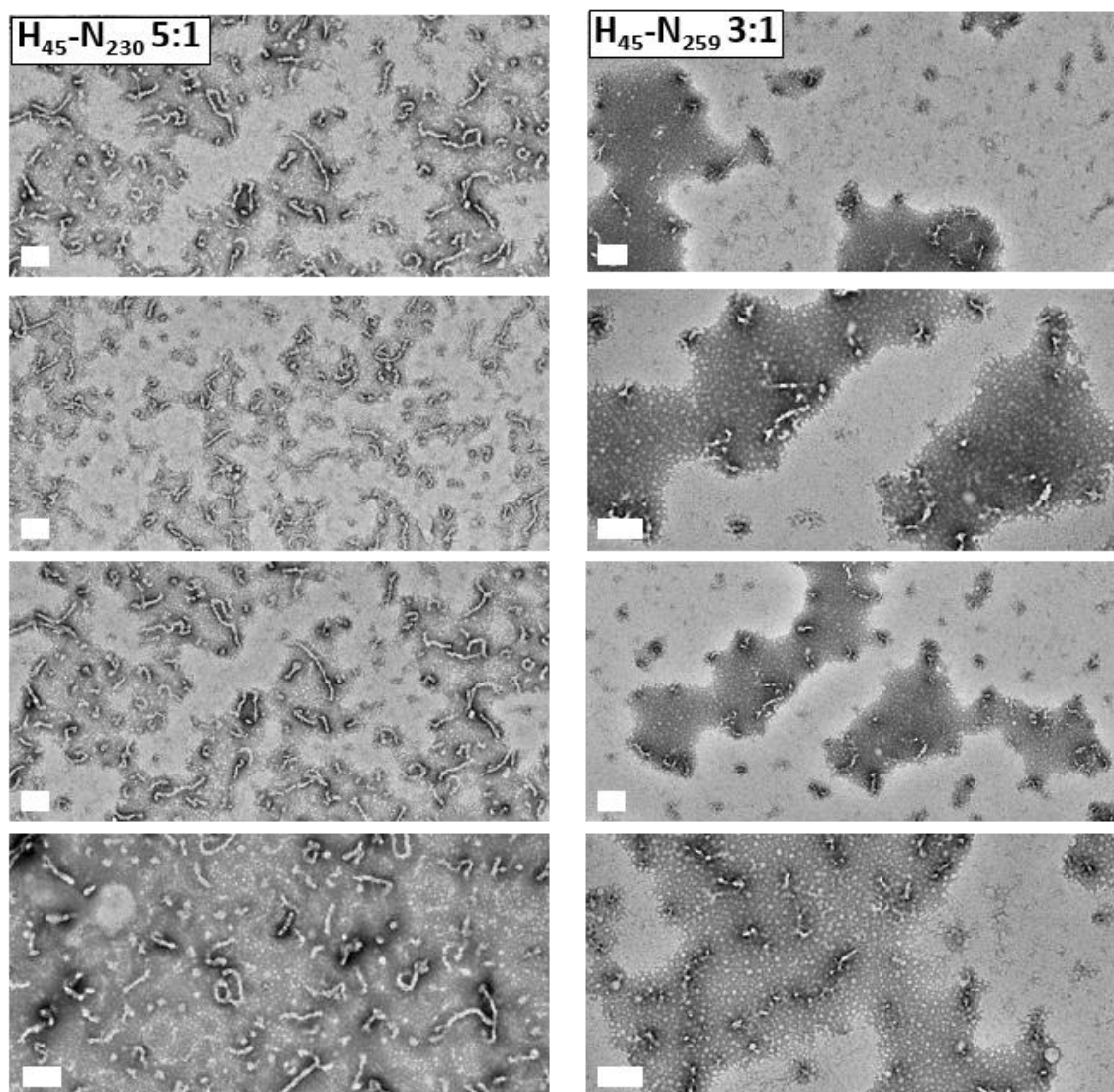


Figure 5.32 - TEM of particles of $H_{45}-N_n$ with crosslinker to mCTA ratios of 3:1 and 5:1 prepared at room temperature at a concentration of 0.05 wt% and stained with pH 7 phosphotungstic acid. The scale bars all represent 200 nm.

The sample with a lower crosslinker to mCTA ratio shows very few discernible structures, and those that can be seen range from spherical to elongated segmented worm-like structures. When a larger amount of crosslinker is added, more of the elongated structures are seen however. These structures correlate well with the broad PDI observed by DLS as this tends to indicate either a sample has multiple particle sizes, or that it deviates from the Stokes-Einstein equation used to analyse the movement of particles, as it characterises these as though they are hard spheres. Small spherical particles can be seen in both samples, however without further analysis it is difficult to determine where these are present in the sample or are merely staining artefacts.

The samples with the oxidation responsive monomer in the core look very different to those with a NIPAM core. These structures are more well defined, comprising of similar sized irregularly shaped structures. In the sample with less crosslinker, these polymer bundles are separate from and of similar size to each other, with an average diameter of 50 nm. However, when more crosslinker is incorporated into the core, these bundles appear to be joined together in a pearl necklace-like structure. The length of these aggregates varies significantly. Crosslinking molecules are added at the beginning of the polymerisation meaning that as the polymers are self-assembling, they are also crosslinking which could explain the connected structures.

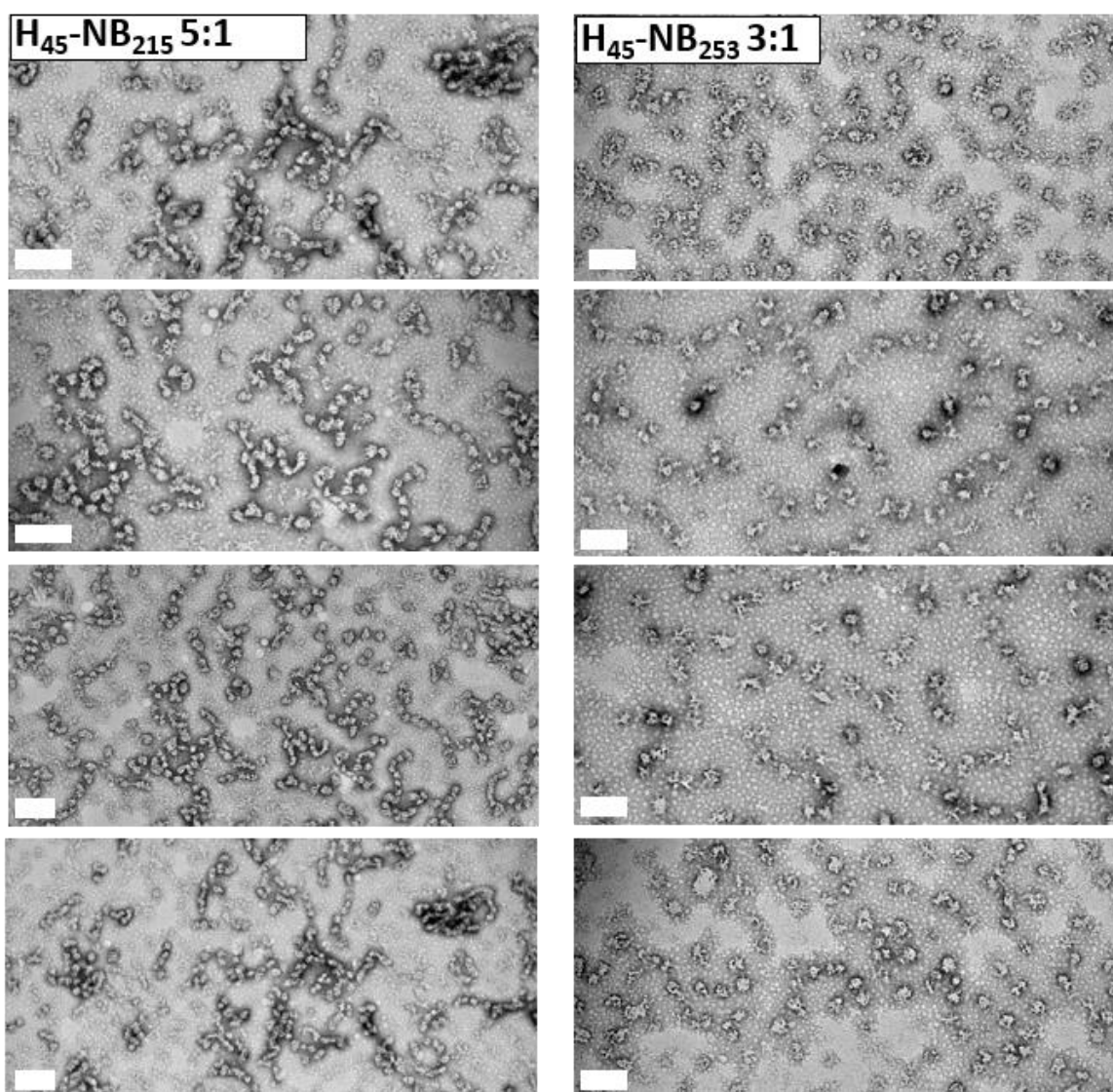


Figure 5.33 - TEM of particles of H₄₅-NB_n with crosslinker to mCTA ratios of 3:1 and 5:1 prepared at room temperature at a concentration of 0.05 wt% and stained with pH 7 phosphotungstic acid. The scale bars all represent 200 nm.

As with all the techniques discussed here, there are limitations. The main limitation for the use of microscopy is the limited sample size. Whereas with scattering techniques, a large proportion of the sample can be analysed easily, microscopy is very limited and also very subjective due to the number of particles analysed being many orders of magnitude smaller than the total number of particles which could be misleading to categorise the entire sample from this.⁶³⁻⁶⁵ Large aggregates may overshadow smaller nanoparticles, dependent on the magnification used. Also due to the longer processing time of microscopy it is impossible to look at all particles in depth.^{63,64}

One of the largest criticisms of TEM in particular is that the particles are imaged dry.⁴⁹ For most application of nanoparticles they are in their hydrated/solvated state so there is an issue whether this technique gives an accurate overview of the size and morphology or if what is seen is due to the method of drying. The staining process and interactions with the stain, alongside the high vacuum conditions used for TEM could affect the particle size and morphology too. Also, the type of stain and amount of stain used can limit the resolution and obscure any internal structures present.⁶⁶ Overall, alone this technique cannot give accurate results, however it provides a good model for scattering analysis to be compared to for complicated morphologies.

Small-angle X-ray scattering – SAXS

Note: SAXS analysis and modelling performed by Thomas Neal, University of Sheffield.

The other particle sizing technique utilised was small-angle X-ray scattering (SAXS) analysis. SAXS is able to determine an average particle size and shape from the scattering of X-rays from the particles.⁶⁷⁻⁶⁹ X-rays pass through a sample at a known wavelength and are scattered by the particles. The interference of scattering patterns holds information about the particle structure and the angle-dependant distribution of the intensity of this scattered radiation is useful to determine the average particle size. As the distances are measured relative to the wavelength of the applied radiation, scattering patterns are discussed in terms of the scattering vector, q , to be independent of this.

An average primary particle size can be estimated from SAXS, assuming that the particles are spherical, using equation 5.2, where r is the radius in angstrom \AA and q is the scattering vector.^{68,69}

$$r = \frac{4.49}{q} \quad (5.2)$$

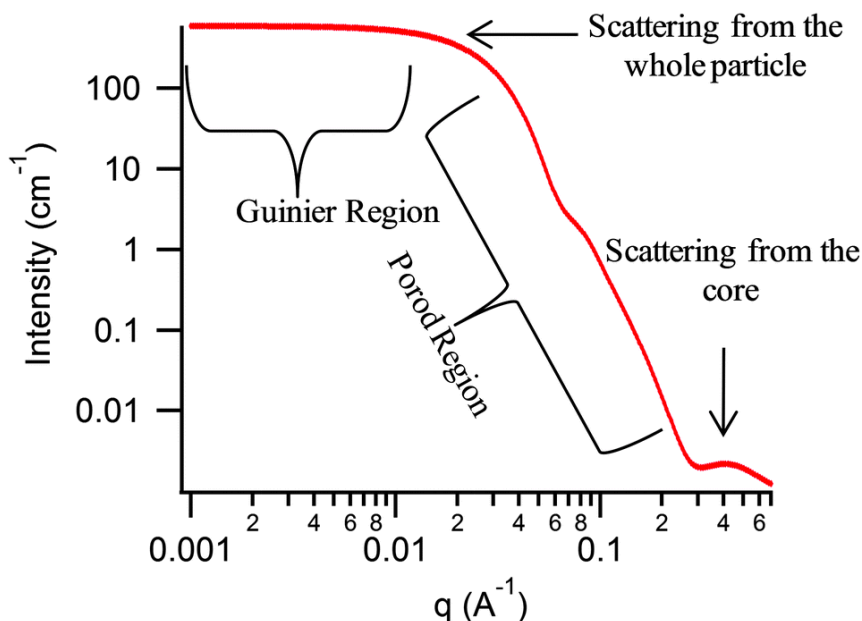


Figure 5.34 – An example SAXS pattern defining the Guinier region and the Porod region. Reproduced from Ref.⁶⁸ with permission from The Royal Society of Chemistry.⁶⁸

Comparing the two samples with a predominantly NIPAM core, the SAXS patterns seen are very similar. The Guinier region gives information about the overall size of the particle (Figure 5.34).^{68,69}

For the sample with a lower crosslinker to mCTA ratio, an upturn is seen at low q (0.003), which is indicative of ill-defined aggregates with a diameter greater than 300 nm. If these samples were small spheres, as seen by TEM, no slope would be seen at low q , a plateau would be observed instead.

From looking at the intensity minima in the form factor in the Porod region of the scattering pattern, it is possible to determine more about the primary particle size in the sample and the morphology (Figure 5.34).^{68,69} For the NG with the lower crosslinker to mCTA ratio, there is no well-defined minimum, which is indicative of a more disperse sample. The samples with more crosslinker incorporated has an intensity minima at a q -value 0.015, which gives a primary particle diameter of approximately 60 nm.

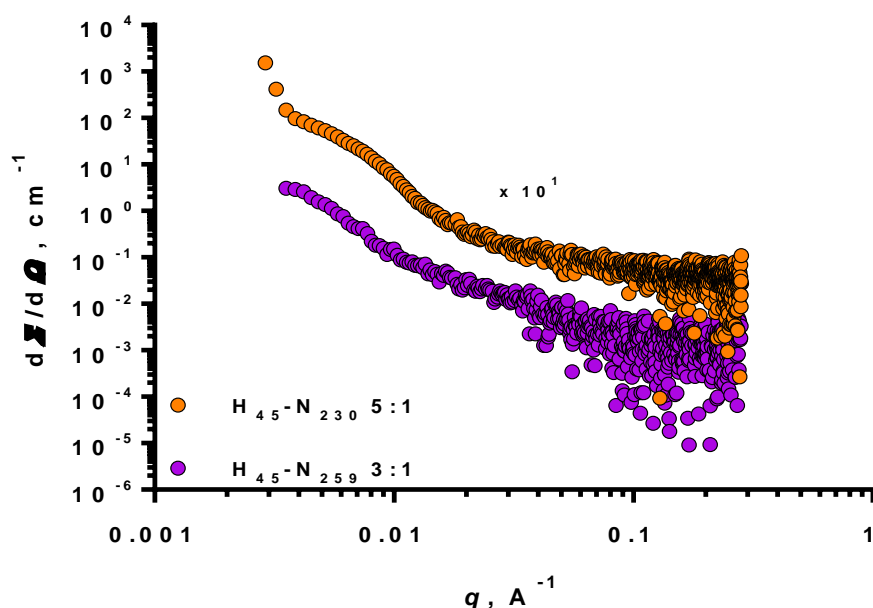


Figure 5.35 –SAXS patterns of pHEA₄₅-b-pNIPAM_{230/259} NGs synthesised with a crosslinker to mCTA ratios of 5:1 and 3:1. Patterns were recorded at 0.1 wt% in water.

The two samples with BAPE incorporated into the core have much more distinct particle sizes with minimal aggregation observed by SAXS analysis. Both samples have a slope of approximately -2 in the Guinier region (between 0.005-0.01), which is the region of the SAXS curve which describes the shape and morphology of particles.^{68,69} For diblock copolymers, a slope of -2 indicates that there may be vesicles present. It is also possible to estimate the membrane thickness of the vesicles using equation 5.3.^{67,70–72}

$$\text{membrane thickness} = \frac{2\pi}{q} \quad (5.3)$$

The sample with a larger ratio of crosslinker is more likely to be vesicles than the other BAPE sample due to the appearance of the rest of the SAXS pattern. Using equation 5.3 and the q value of the first minima, 0.02, the membrane thickness of these vesicles can be estimated, giving a value of approximately 31 nm. However, if this data is compared to the TEM images (Figure 5.33) for the same sample, there is no evidence for vesicles. These are more likely to be spheres, with a primary particle diameter of 49 nm, from equation 5.2. The sample with the lower crosslinker ratio is more likely to have two distinct particle sizes due to the broad spacing between the two minima. Again,

using equation 5.2, these particle diameters are 69 nm and 22 nm from the two minima with q values of 0.013 and 0.041, respectively.

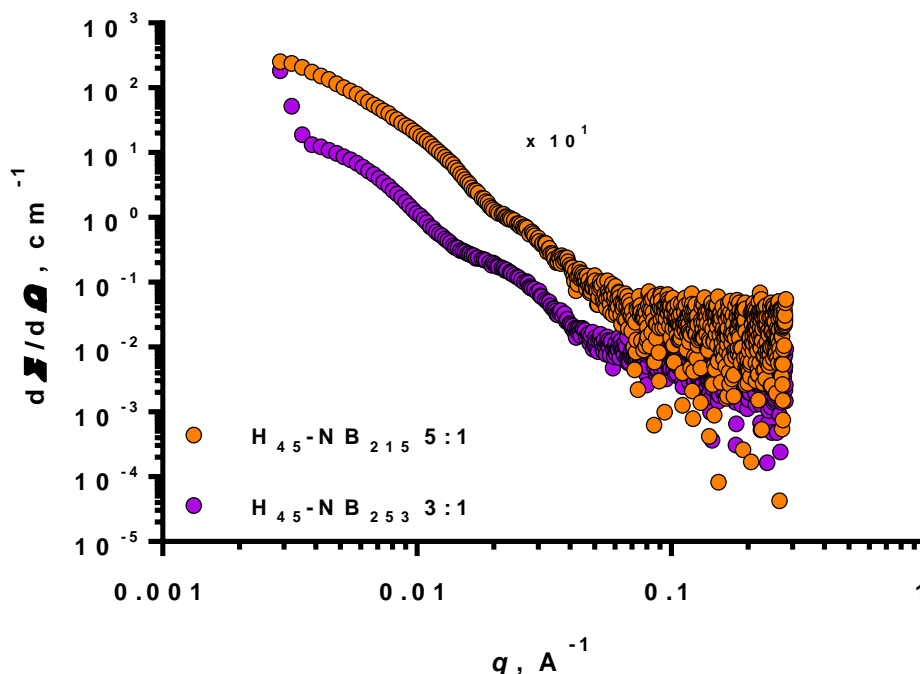


Figure 5.36 - Comparison of SAXS pattern recorded for 1.0 wt % nanogels in water where the NGs are pHEA₄₅-b-p(NIPAM-stat-BAPE)_{215/253} with a crosslinker to mCTA ratio of 5:1 and 3:1 respectively.

Overall, for these samples, SAXS data alone is inconclusive for determining the particle size and morphology. It is important to note that like all other techniques discussed in this section, there are limitations. One of the limitations of this technique is, like many other particle sizing techniques, it only gives an average particle size and therefore cannot accurately determine sizes and shapes of samples with a mixture of particle sizes. For example, in the presence of large particles, small particles are hardly visible. Although many models assume a solid spherical core with a corona of flexible chains, morphological information can be found.

Asymmetric flow field flow fractionation (AF4) – combined with multi-angle light scattering and dynamic light scattering

Note: AF4 measurements performed by Edyta Niezabitowska, University of Liverpool.

Apart from TEM, all the particle sizing methods above determine the average size of particles in batch measurements and are therefore not very useful when looking at a broad distribution of particle sizing in a single sample, which it is believed these samples are due to the above characterisation. Unlike other separation techniques, such as size exclusion chromatography (SEC), the sample will not irreversibly adsorb onto the stationary phases as one is not present, it should not degrade due to the gentle nature of separation and will not coelute.⁶¹

Field flow fractionation techniques were initially developed in 1966,^{73,74} and since then many different variations of the technique have been developed. This technique can be described simply as the separation of particles due to their translational diffusion and the friction coefficient provided by the cross-flow field force (Figure 5.37).⁶¹ The channel where the separation occurs is an open channel with two flows running perpendicular to each other; the carrier flow and the cross-flow which flows towards the porous membrane.⁶¹ Due to the interplay between the cross-flow, diffusion against this and the parabolic flow profile of the carrier flow, separation of different particle sizes occurs. The smaller the size of the particles, the higher their diffusion coefficient and therefore they diffuse further into the channel where the flow rate is higher thereby causing earlier elution. Conversely, the larger the particle, the lower their diffusion coefficient and therefore the later the elution.

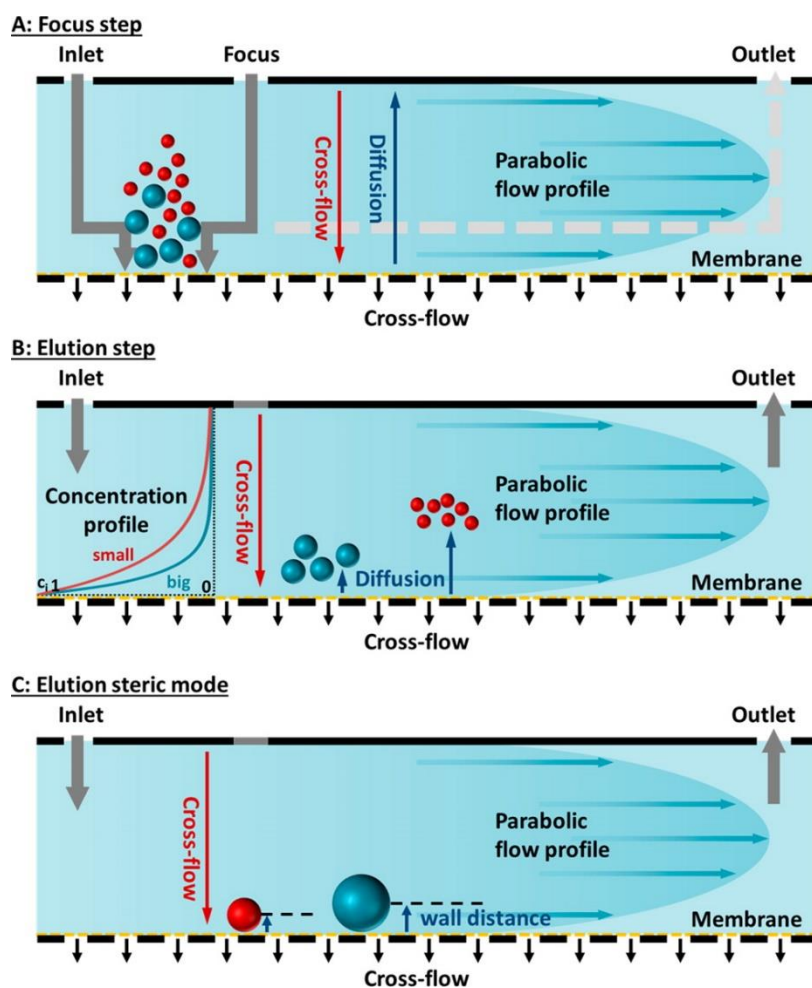


Figure 5.37 - Schematic representation of the AF4 principle. The eluent is pumped from the inlet to the outlet, and the cross-flow is applied perpendicular to the flow direction. The different steps are (A) the focusing process (stopped flow) and (B) the elution process under normal mode; part C shows elution under steric conditions. Reprinted with permission from reference.⁶¹ Copyright 2014 American Chemical Society.

Detectors of many types can be connected to an AF4 to analyse the particles after separation such as DLS,^{75,76} MALS,^{75,77} UV-vis,⁷⁵ inductively coupled plasma mass spectrometry (ICPMS),⁷⁸ viscometry.⁷⁹ IR detection,⁷⁹ SAXS⁷⁶ and many more.^{61,76,80–82} When analysing these NGs, a UV-vis detector, DLS and MALS detectors were used. From these results, the concentration can be determined by UV-vis. spectroscopy, the hydrodynamic radius (R_h) by DLS and the radius of gyration (R_g) by MALS.

The two NG samples with a predominately pNIPAM core had very similar results to one another and had much broader distributions than the BAPE containing samples (Figure 5.38). The R_h values determined from DLS after separation suggest particle size ranges from a radius of 50 – 83 nm for the NG with a 5:1 crosslinker to mCTA ratio and from 74 – 93 nm for the lower crosslinker

concentration. The average values of these correlate with those seen without particle size separation.

For the NGs incorporating BAPE, a much larger difference is seen between the samples. The sample with the lower crosslinker content has much smaller particles than the others with R_h values in the range of 38 – 62 nm. The size range for the sample with a larger crosslinker concentration is much broader, with R_h values ranging from 45 to 220 nm.

For the two samples sets, with and without BAPE, the same mCTA was used for synthesis so the shell thickness and properties should be the same for all four NGs. However, there is a difference between the R_h and R_g relationships, depending on whether BAPE is incorporated into the core. With a NIPAM only core, the R_g does not increase with the same gradient as R_h . The initial section shows the R_h and R_g being similar in size, however the final section shows the R_g being much higher than the R_h . An increase in R_g could be indicative of a change in particle properties for example morphological differences. For the NGs with BAPE in the core, the R_g and R_h increase in size together, For NG synthesised with a 5:1 BIS/mCTA ratio, these values are the same as each other throughout the measurement whereas with the lower crosslinker to mCTA ratio, the R_h value is higher throughout.

Initially, the increase in the R_g was believed to be due to some aggregation occurring due to the temperature being within error of the LCST or due to the mobile phase, 0.1 M NaNO₃. For example, the sample described as H₄₅-NB 5:1 shows a very large increase in R_g . However, DLS analysis under these conditions showed no sign of aggregation. This indicates the presence of more elongated structures.

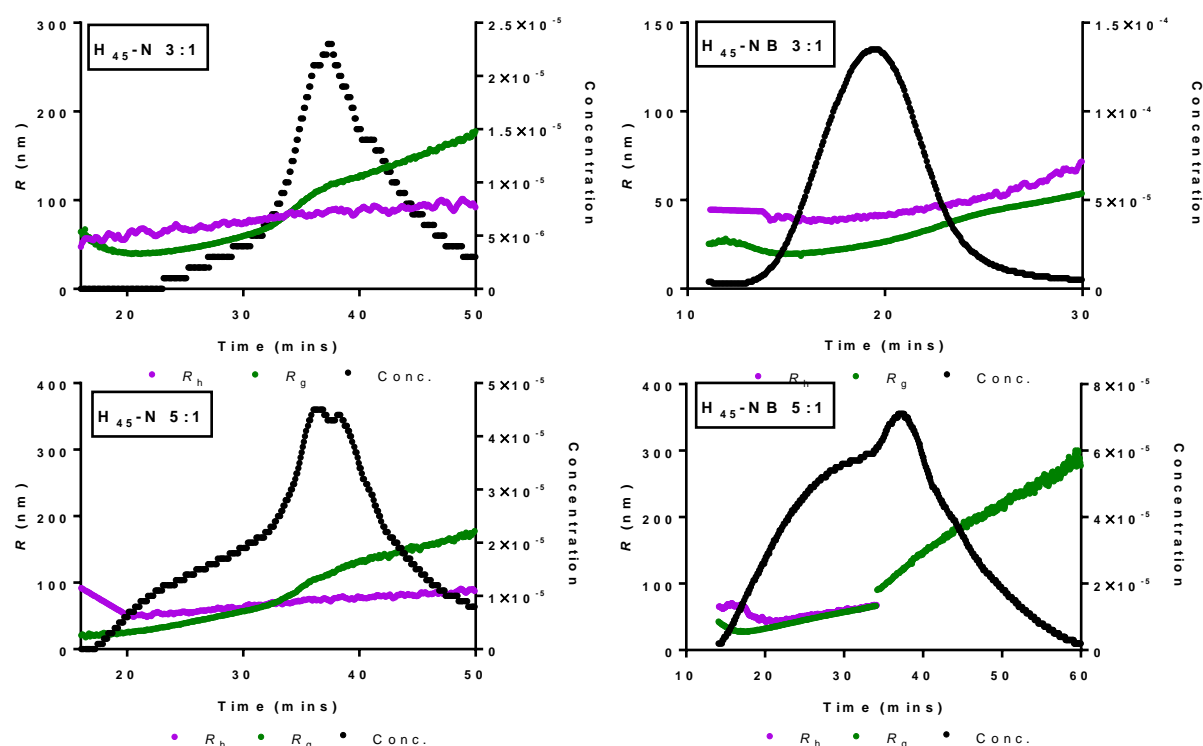


Figure 5.38 – AF4 data showing the concentration, R_g and R_h over time of 4 NGs with and without BAPE and at different crosslinker concentrations, as specified by the titles on each graph, showing the difference in size of the particles by DLS and MALS. The wavelength of the lasers used is 633 nm and 532 nm for DLS and MALS respectively.

Alongside the determination of the particle sizes of the NGs after separation, combination of the techniques allows an approximate determination of the morphology, which is probably the most important aspect of AF4 analysis in this way. The ratio of R_g/R_h provides a value known as the shape factor.^{83,84} This is important as if DLS analysis alone was conducted, two particles with same R_h may be wrongly characterised as being particles of the same shape as no information on the shape is determined. Whereas these may have different R_g values therefore the mass distribution and morphology will not be the same. The shape factor values found for all four samples indicate that they are all comprised of two different particle morphologies as each has two different R_g/R_h ratios.

For this analysis, only approximate values can be taken from this plot as there are a range of similar values. The values taken are from the midpoint of each 'step' in the graph. The 'steps' refer to a large change in the values for R_g/R_h and therefore a difference in the morphology of nanoparticles.

This analysis was conducted at 28 °C. Although this is lower than the anticipated LCST value, it has been shown in Figure 5.24 that particle shrinking due to temperature can happen over a wide temperature range. With a NIPAM core, this is between 30 and 35 °C, however with BAPE incorporated in the core, this can occur at temperature ranges of 15 °C. Therefore, at 28 °C, some of the NG particles could already be shrinking, giving a mix in particle size. As the particle size decreases due to this, the core becomes denser as the chains collapse reducing R_g more than R_h .

Focusing on the non-oxidation responsive samples, as these are quite similar, average R_g/R_h ratios of approximately 0.73 and 1.83 are seen for the samples with a larger crosslinker concentration, and 0.70 and 1.53 are seen for the samples with a smaller crosslinker concentration. The smaller value implies that there is more mass in the core and is indicative of core-shell particles where the core is more dense (0.778),⁸⁵ and the larger values are what is expected for more elongated structures such as prolate ellipsoids (1.36-2.24) or aggregated structures.^{68,83}

The oxidation-responsive NGs have very different shape factors from one another. The NG with the lower crosslinker concentration has average shape factors of 0.55 and 0.83 which indicate morphologies of core-shell particles (<0.7) and potentially a vesicle-like structure.^{86,87} The NG sample with more crosslinker in the core has two very different morphologies with shape factors of 0.93 and >2.55, which indicates soft spheres or vesicles (~1) and something very elongated, showing similar shape factors to fibres (1.89).^{85,86,88,89} As the R_g/R_h approaches 1, this could indicate that the core is less dense and that there is more mass on the outside i.e. a vesicle structure. Other analytical methods have also suggested that these may have some structures with a vesicle-like morphology. Analysis of other AF4 studies from the literature however give values of <1 for vesicles and suggest that anything larger than this suggests either elongation or aggregation.^{85,86}

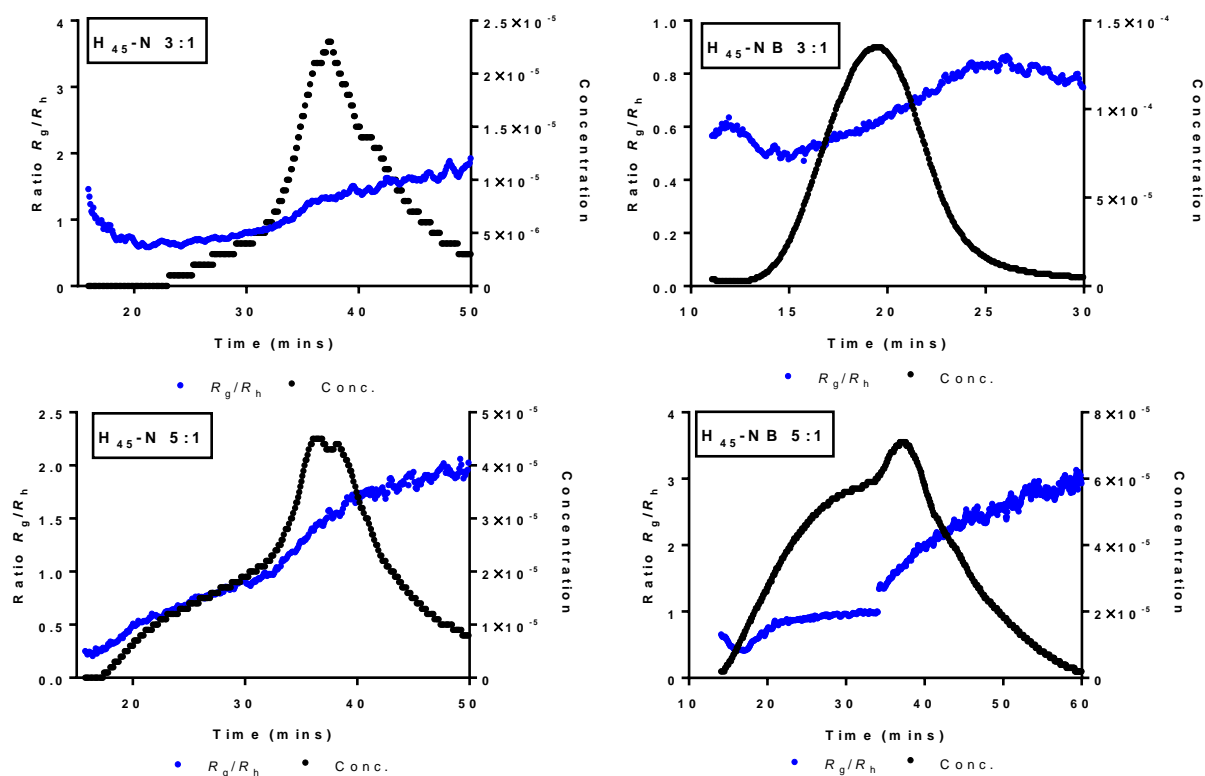


Figure 5.39 – Determination of the shape factor, R_g/R_h of 4 NGs with and without BAPE and at different crosslinker concentrations, as specified by the titles on each graph, showing the different morphologies observed by separation.

One thing to note about the use of AF4 for particle separation is that the separation is based on distance from the membrane due to the interaction of flows and the size of the particle. This will be accurate for spherical particles, however, as the morphology becomes more non-spherical, it approaches the membrane differently which could affect separation.

Like the other techniques mentioned, there are also limitations to AF4 combined with DLS and MALS. The main limitation is that choosing the condition can be a lengthy process as it is important to use an appropriate membrane and eluent.⁶¹ These must have minimal chemical interaction with the material you are trying to analyse, mainly to prevent absorption. The flow rates are also paramount to achieve good separation. The benefits of this outweigh the negatives as after separation, many different analytical instruments can be used which minimises errors seen in other bulk characterisation techniques. It is also important to note that the principle of separation relies

on the separation of spherical particles, however non-spherical particles may approach the membrane differently and therefore may be separated in a different manner.

Comparison of the analysis of particle sizing techniques

Table 5.5 – Particle size and morphological information from DLS, SAXS, TEM and AF4 combined with DLS and MALS.

Nanogel	DLS – eff. diam. (nm)	DLS – PDI	SAXS – diam. (nm)	TEM Avg. size range (nm)	AF4 – Approx. R_g/R_h Shape factor
H ₄₅ -N ₂₃₀ 5:1	155	0.165	60 nm >300 nm	Width – 32-60 Length – 30-450 Fibres	0.70 – Core-shell 1.53 - Elongated
H ₄₅ -N ₂₅₉ 3:1	170	0.218	>300 nm	45-250 Aggregates . Not well-defined	0.73 – Core-shell 1.83 - Elongated
H ₄₅ -NB ₂₁₅ 5:1	151	0.200	49 nm	44-56 diameter of 'balls' Differing length of joined polymer balls	0.55 – Core-shell 0.83 – Vesicles
H ₄₅ -NB ₂₅₃ 3:1	99	0.160	22 nm 68 nm	32-89 – Mainly spherical	0.93 – Soft spheres or Vesicles 2.55 - Fibres

The results for the above particle sizing techniques can be combined to give an overall view of the morphology of the NGs. Many different techniques must be used and cross-referenced with one another due to the differences and therefore strengths and weaknesses of the sizing methods individually.

SAXS, DLS and AF4 combined with MALS and DLS are all solution phase techniques. They therefore consider the interactions with solvents and are more representative of how the particles will look within the body. TEM is a technique which requires the sample to be dry and is likely to give very different results to the above. This is the only tool used here however which produces an image of the morphology of the particles.

Considering only the H₄₅-NB with crosslinker to mCTA ratios of 3:1 for simplicity, the techniques can be compared in detail. TEM suggests that these resemble balls of entwined polymer chains which are separate from and of similar size to each other. Small spherical structures are seen on the grid at <30 nm, yet it is believed that these are drying artefacts. This is corroborated by analysis SAXS which does not indicate the presence of something so small. From TEM, the larger structures on the grid appear to be separate spherical-like balls of polymer with diameters between 32 and 89 nm.

DLS of this sample indicates an effective diameter of 99 nm, which is larger than expected by TEM, however this is due to the hydration of the sample. The PDI is 0.16 which is higher than expected for a monomodal spherical particle system. This suggests either a deviation from a spherical morphology or a polydisperse sample with multiple particle sizes. Analyses of the SAXS pattern produced by this sample correlates with the DLS regarding the multiple particle sizes. It suggests that there may be two distinctly sized spherical particles with diameters of 68 and 22 nm. These are smaller than the size measured by DLS which is to be expected as these techniques measure different averages of distributions.

The most reliable particle scattering technique used is AF4 coupled to DLS and MALS, as this separates particles of different size before analysis by the connected instruments, therefore giving more accurate size information than DLS and SAXS which look at the bulk sample. From this it is possible to see a change in R_n from 38 to 62 nm, giving approximate particle diameters of 76 and 124 nm. Analysis by DLS before separation gives a value for a diameter which is in-between both of these. A benefit of AF4 is that by coupling this the DLS and MALS the shape factor can be determined

which gives morphology information which usually cannot be determined by DLS alone. For this sample two different values for the shape factor found; 0.55 and 0.83, which are indicative of core-shell particles and soft spheres/vesicles respectively. This corroborated what is seen by TEM as many of the particles seen look very similar with spherical like morphology.

For this sample, and that of the other oxidation-responsive nanogel, the results from all the above analyses fit together to give a good view on the size and morphology of the particles. The sample with more crosslinker incorporated has a more elongated structure, potentially formed of smaller particles aggregating together which is seen by a shape factor >2 and also the TEM images. As the crosslinker is added to the reaction at the beginning, it is likely that these structures are unable to fully form as the crosslinked nature constrains this. It could also cause two different self-assembled particles to bond together.

However, for the NIPAM core samples, as the structures are less well-defined by all techniques, it is difficult to gain a clear picture due to the limitations in each technique. Looking at the sample with a higher crosslinker content in the core initially, it can be seen that each technique alone does not give a clear picture. For example, DLS gives an average diameter of 70 nm however when we compare this to all other techniques, they indicate 2 separate particle sizes. SAXS shows small particles at around 60 nm which correlates well with the sizes of the particles seen via TEM. The lengths of these particles vary significantly from particles with lengths between 30 and 450 nm. Polydispersity values from the DLS are higher than expected which does indicate that these deviate from a spherical morphology. Analysis of the shape factor determined after separation by AF4 again shows two different particle morphologies, a core-shell and elongated structure. Although these correlate with one enough, it is not as clear as with the NGs with BAPE in the core.

The other NG with a smaller amount of crosslinker in the core is a lot less well defined. TEM and SAXS suggest large aggregates however some smaller particles are seen by TEM. Again, the polydispersity is high suggesting a wide range of particle sizes or a deviation from the spherical form

and the diameter by DLS is in-between the sizes seen from TEM. AF4, where the particles are separated by size before analysis, shows that there are two different particle morphologies, something more spherical with a core-shell structure and a more elongated structure.

Overall, this demonstrates the importance of utilising many different techniques when analysing nanoparticles, especially as it gives more confidence in the results found.^{68,90-93} AF4 analysis is better able to characterise samples due to the separation however it is very difficult to determine the morphology and size of ill-defined samples.

5.3. Conclusions

In this chapter, research has been presented showing the synthesis and analysis of dual responsive nanogels. The NG cores are both oxidation and temperature responsive, with the former affecting the latter. It has been shown that by increasing the length of the core forming block, the size and morphology of the nanoparticles can be altered, with the length of the core forming block increasing the size of the NGs with NIPAM cores from 59 to 141 nm, as seen by DLS, with a hydrophobic block lengths of 100 to 321 NIPAM units. Whereas when the oxidation-responsive monomer BAPE is incorporated, there is not a trend in size increase by DLS due to the morphological differences seen by TEM.

These NGs exhibit a temperature response, shrinking when they are heated to temperatures above their LCST due to the collapse of the pNIPAM chains in the core. For example, H₄₅-N₂₆₉ is 174 nm at 25 °C, but 124 nm at 45 °C. Also, when BAPE is incorporated, H₄₅-NB₂₄₅ is 127 nm at 25 °C, but 86 nm at 45 °C. An approximate LCST can be determined from this behaviour by observing the change in diameter of the NG over a temperature range. For NGs with a predominantly NIPAM core, the change in size happens at higher temperatures and over a narrower temperature range than those with a core consisting of NIPAM and BAPE. On oxidation, the LCST of the NGs with BAPE increasing to a temperature higher than body temperature, causing an increase in size.

The increase in size on oxidation is dependent on the amount of crosslinker incorporated into the temperature responsive core of the nanogel. When comparing two NGs of similar lengths but with different ratios of crosslinker, the one with more crosslinker shrinks by 42 nm when increasing the temperature from 25 to 45 °C, whereas the one with less crosslinker shrinks by 61 nm.

These NGs exhibit sensitivity to levels of hydrogen peroxide as low as 0.1 mM, which is similar to that observed in the body for autoimmune diseases. The amount needed for complete oxidation of all BAPE monomer units has been found to be 0.146 and 0.217 mM with 2 and 3 mol% BAPE respectively, which is in this region. As expected, the more H₂O₂ present, the faster the oxidation.

This does mean that incorporation of more BAPE may not improve the NGs significantly as the LCST does not appear to change much, and only the same number of BAPE units will be oxidised.

The sensitivity to other reactive oxygen species; SIN-1 and hydroxy radicals, and a common reducing agent found in the body, glutathione, was also determined using in situ DLS studies. It was found that none of these cause a size change in the NGs after leaving to react in situ at 37 °C, even at concentrations as high as 5 mM. This implies that at concentrations found within the body, it is likely that only hydrogen peroxide is able to cause swelling of the NGs and therefore drug release.

In depth analysis of the morphology of a few of these NGs was performed as the morphology can influence the rate of clearance from the body as well as the ability to encapsulate drugs. The combination of DLS, SAXS, TEM and AF4 combined with DLS and MALS allowed for successful determination of the size and shape of some of the NGs. This gave me a more accurate view of the particle morphologies, for example, the NG pH-NB with a crosslinker to mCTA ratio of 3:1, where DLS gave a size of approximately 99 nm but a PDI of 0.16 which is larger than expected for a hard sphere. Correlating with this, TEM, SAXS and AF4 imply that there are particles ranging between 22 and 89 nm which are mainly spherical and likely to be vesicles. Also, the presence of some elongated NGs are seen.

In order to determine the suitability of this as a DDS in-depth encapsulation and release studies would need to be carried out. These would assess the amount of drug which can be encapsulated, how leaky the nanogels are and the speed of drug release at biologically relevant levels of hydrogen peroxide. As well as encapsulation studies, the toxicity of the DDS and the toxicity of the oxidation products released must also be tested.

5.4. References

- 1 N. B. Graham and A. Cameron, *Pure Appl. Chem.*, 2007, **70**, 1271–1275.
- 2 M. Malmsten, *Soft Matter*, 2006, **2**, 760–769.
- 3 M. J. Murray and M. J. Snowden, *Adv. Colloid Interface Sci.*, 1995, **54**, 73–91.
- 4 S. K. Ahn, R. M. Kasi, S. C. Kim, N. Sharma and Y. Zhou, *Soft Matter*, 2008, **4**, 1151–1157.
- 5 M. A. C. Stuart, W. T. S. Huck, J. Genzer, M. Müller, C. Ober, M. Stamm, G. B. Sukhorukov, I. Szleifer, V. V Tsukruk, M. Urban, F. Winnik, S. Zauscher, I. Luzinov and S. Minko, *Nat. Mater.*, 2010, **9**, 101–13.
- 6 S. Mura, J. Nicolas and P. Couvreur, *Nat. Mater.*, 2013, **12**, 991–1003.
- 7 K. S. Soni, S. S. Desale and T. K. Bronich, *J. Control. Release*, 2016, **240**, 109–126.
- 8 V. P. Torchilin, *Adv. Drug Deliv. Rev.*, 2012, **64**, 302–315.
- 9 S. Vinogradov, *Curr. Pharm. Des.*, 2006, **12**, 4703–4712.
- 10 K. Raemdonck, J. Demeester and S. De Smedt, *Soft Matter*, 2009, **5**, 707–715.
- 11 M. Talelli, M. Barz, C. J. F. Rijcken, F. Kiessling, W. E. Hennink and T. Lammers, *Nano Today*, 2015, **10**, 93–117.
- 12 Y. Bin Hamzah, S. Hashim and W. A. W. A. Rahman, *J. Polym. Res.*, 2017, **24**, 134.
- 13 S. Khoee and H. Asadi, in *Encyclopedia of Biomedical Polymers and Polymeric Biomaterials*, Taylor & Francis, 2016, pp. 5266–5293.
- 14 Z. An, Q. Qiu and G. Liu, *Chem. Commun.*, 2011, **47**, 12424.
- 15 G. Moad, *Polym. Chem.*, 2017, **8**, 177–219.
- 16 M. Constantin, M. Cristea, P. Ascenzi and G. Fundueanu, *Express Polym. Lett.*, 2011, **5**, 839–

- 848.
- 17 S. T. Reddy, A. Rehor, H. G. Schmoekel, J. a. Hubbell and M. a. Swartz, *J. Control. Release*, 2006, **112**, 26–34.
- 18 Z. M. O. Rzaev, S. Dinçer and E. Pişkin, *Prog. Polym. Sci.*, 2007, **32**, 534–595.
- 19 V. C. Lopez, J. Hadgraft and M. J. Snowden, *Int. J. Pharm.*, 2005, **292**, 137–147.
- 20 D. Ruckling, C. D. Vo, H. J. P. Adler, A. Völkel and H. Cölfen, *Macromolecules*, 2006, **39**, 1585–1591.
- 21 J. D. Debord and L. A. Lyon, *Langmuir*, 2003, **19**, 7662–7664.
- 22 W. H. Blackburn and L. A. Lyon, *Colloid Polym. Sci.*, 2008, **286**, 563–569.
- 23 Y. Shin, J. H. Chang, J. Liu, R. Williford, Y. K. Shin and G. J. Exarhos, *J. Control. Release*, 2001, **73**, 1–6.
- 24 H. G. Schild, M. Muthukumar and D. A. Tirrell, *Macromolecules*, 1991, **24**, 948–952.
- 25 Y. Xu, Y. Li, X. Cao, Q. Chen and Z. An, *Polym. Chem.*, 2014, **5**, 6244–6255.
- 26 A. E. Ekkelenkamp, M. R. Elzes, J. F. J. Engbersen and J. M. J. Paulusse, *J. Mater. Chem. B*, 2018, **6**, 210–235.
- 27 J. Ilavsky and P. R. Jemian, *J. Appl. Crystallogr.*, 2009, **42**, 347–353.
- 28 K. Rebolj, D. Pahovnik and E. Žagar, *Anal. Chem.*, 2012, **84**, 7374–7383.
- 29 J. C. Gaulding, M. H. Smith, J. S. Hyatt, A. Fernandez-Nieves and L. A. Lyon, *Macromolecules*, 2012, **45**, 39–45.
- 30 F. M. Winnik, M. F. Ottaviani, S. H. Boßmann, W. Pan, M. Garcia-Garibay and N. J. Turro, *Macromolecules*, 1993, **26**, 4577–4585.
- 31 R. O. . Costa and R. F. . Freitas, *Polymer (Guildf)*, 2002, **43**, 5879–5885.

- 32 M. J. A. Hore, B. Hammouda, Y. Li and H. Cheng, *Macromolecules*, 2013, **46**, 7894–7901.
- 33 S. Backes, P. Krause, W. Tabaka, M. U. Witt, D. Mukherji, K. Kremer and R. Von Klitzing, *ACS Macro Lett.*, 2017, **6**, 1042–1046.
- 34 H. Yamauchi and Y. Maeda, *J. Phys. Chem. B*, 2007, **111**, 12964–12968.
- 35 N. Osaka and M. Shibayama, *Macromolecules*, 2012, **45**, 2171–2174.
- 36 S. Grund, M. Bauer and D. Fischer, *Adv. Eng. Mater.*, 2011, **13**, B61–B67.
- 37 C. de Las Heras Alarcon, S. Pennadam and C. Alexander, *Chem. Soc. Rev.*, 2005, **34**, 276–285.
- 38 A. Blanazs, A. J. Ryan and S. P. Armes, *Macromolecules*, 2012, **45**, 5099–5107.
- 39 N. J. Warren and S. P. Armes, *J. Am. Chem. Soc.*, 2014, **136**, 10174.
- 40 M. Antonietti and S. Förster, *Adv. Mater.*, 2003, **15**, 1323–1333.
- 41 A. Blanazs, S. P. Armes and A. J. Ryan, *Macromol. Rapid Commun.*, 2009, **30**, 267–277.
- 42 J. N. Israelachvili, D. J. Mitchell and B. W. Ninham, *J. Chem. Soc. Faraday Trans. 2 Mol. Chem. Phys.*, 1976, **72**, 1525–1568.
- 43 H. Inomata, N. Wada, Y. Yagi, S. Goto and S. Saito, *Polymer (Guildf.)*, 1995, **36**, 875–877.
- 44 Y. H. Bae, T. Okano and S. W. Kim, *J. Polym. Sci. Part B Polym. Phys.*, 1990, **28**, 923–936.
- 45 I. E. Pacios, M. J. Molina, M. R. Gómez-Antón and I. F. Piérola, *J. Appl. Polym. Sci.*, 2007, **103**, 263–269.
- 46 C. De Gracia Lux, S. Joshi-Barr, T. Nguyen, E. Mahmoud, E. Schopf, N. Fomina and A. Almutairi, *J. Am. Chem. Soc.*, 2012, **134**, 15758–15764.
- 47 B. B. Weiner, *Brookhaven Instruments*, 2010, 1–4.
- 48 S. Bhattacharjee, *J. Control. Release*, 2016, **235**, 337–351.

- 49 R. A. Sperling, T. Liedl, S. Duhr, S. Kudera, M. Zanella, C. A. J. Lin, W. H. Chang, D. Braun and W. J. Parak, *J. Phys. Chem. C*, 2007, **111**, 11552–11559.
- 50 K. Gnanasekaran, R. Snel, G. de With and H. Friedrich, *Ultramicroscopy*, 2016, **160**, 130–139.
- 51 Y. Kuang, K. Balakrishnan, V. Gandhi and X. Peng, *J. Am. Chem. Soc.*, 2011, **133**, 19278–19281.
- 52 E. W. Miller, A. E. Albers, A. Pralle, E. Y. Isacoff and C. J. Chang, *J. Am. Chem. Soc.*, 2005, **127**, 16652–16659.
- 53 L. Wang, S. Xie, L. Ma, Y. Chen and W. Lu, *Eur. J. Med. Chem.*, 2016, **116**, 84–89.
- 54 G. C. Van de Bittner, E. A. Dubikovskaya, C. R. Bertozzi and C. J. Chang, *Proc. Natl. Acad. Sci.*, 2010, **107**, 21316–21321.
- 55 R. J. Singh, N. Hogg, J. Joseph, E. Konorev and B. Kalyanaraman, *Arch. Biochem. Biophys.*, 1999, **361**, 331–339.
- 56 N. Hogg, V. M. Darley-Usmar, M. T. Wilson and S. Moncada, *Biochem. J.*, 2015, **281**, 419–424.
- 57 C. C. Winterbourn, *Toxicol. Lett.*, 1995, **82–83**, 969–974.
- 58 H. J. Forman, H. Zhang and A. Rinna, *Mol. Aspects Med.*, 2009, **30**, 1–12.
- 59 S. K. Brar and M. Verma, *TrAC - Trends Anal. Chem.*, 2011, **30**, 4–17.
- 60 C. M. Hoo, N. Starostin, P. West and M. L. Mecartney, *J. Nanoparticle Res.*, 2008, **10**, 89–96.
- 61 M. Wagner, S. Holzschuh, A. Traeger, A. Fahr and U. S. Schubert, *Anal. Chem.*, 2014, **86**, 5201–5210.
- 62 A. A. Sousa and R. D. Leapman, *Ultramicroscopy*, 2012, **123**, 38–49.
- 63 H. Friedrich, P. M. Frederik, G. De With and N. A. J. M. Sommerdijk, *Angew. Chemie - Int. Ed.*, 2010, **49**, 7850–7858.
- 64 M. R. Libera and R. F. Egerton, *Polym. Rev.*, 2010, **50**, 321–339.

- 65 R. D. Boyd, S. K. Pichaimuthu and A. Cuenat, *Colloids Surfaces A Physicochem. Eng. Asp.*, 2011, **387**, 35–42.
- 66 Y. Talmon, *J. Colloid Interface Sci.*, 1983, **93**, 366–382.
- 67 J. A. Bouwstra, G. S. Gooris, W. Bras and H. Talsma, *Chem. Phys. Lipids*, 1993, **64**, 83–98.
- 68 J. P. Patterson, M. P. Robin, C. Chassenieux, O. Colombani and R. K. O'Reilly, *Chem. Soc. Rev.*, 2014, **43**, 2412–2425.
- 69 H. Schnablegger and Y. Singh, *The SAXS Guide - Getting acquainted with the principles*, Anton Paar GmbH, Austria, 4th edn., 2017.
- 70 M. J. Derry, L. A. Fielding, N. J. Warren, C. J. Mable, A. J. Smith, O. O. Mykhaylyk and S. P. Armes, *Chem. Sci.*, 2016, **7**, 5078–5090.
- 71 C. J. Mable, L. A. Fielding, M. J. Derry, O. O. Mykhaylyk, P. Chambon and S. P. Armes, *Chem. Sci.*, 2018, **9**, 1454–1463.
- 72 A. Blanazs, N. J. Warren, A. L. Lewis, S. P. Armes and A. J. Ryan, *Soft Matter*, 2011, **7**, 6399–6403.
- 73 K. G. Wahlund and J. C. Giddings, *Anal. Chem.*, 1987, **59**, 1332–1339.
- 74 E. Grushka, K. D. Caldwell, M. N. Myers and J. C. Giddings, *Sep. Purif. Methods*, 1973, **2**, 127–151.
- 75 R. Mathaes, G. Winter, J. Engert and A. Besheer, *Int. J. Pharm.*, 2013, **453**, 620–629.
- 76 A. F. Thünemann, P. Knappe, R. Bienert and S. Weidner, *Anal. Methods*, 2009, **1**, 177–182.
- 77 S. Hupfeld, D. Ausbacher and M. Brandl, *J. Sep. Sci.*, 2009, **32**, 1465–1470.
- 78 S. Dubascoux, I. Le Hécho, M. Hassellöv, F. Von Der Kammer, M. Potin Gautier and G. Lespes, *J. Anal. At. Spectrom.*, 2010, **25**, 613–623.

- 79 E. P. C. Mes, H. de Jonge, T. Klein, R. R. Welz and D. T. Gillespie, *J. Chromatogr. A*, 2007, **1154**, 319–330.
- 80 N. M. Thang, R. Knopp, H. Geckeis, J. I. Kim and H. P. Beck, *Anal. Chem.*, 2000, **72**, 1–5.
- 81 F. V.D. Kammer, M. Baborowski and K. Friese, *J. Chromatogr. A*, 2005, **1100**, 81–89.
- 82 A. Exner, M. Theisen, U. Panne and R. Niessner, *Fresenius. J. Anal. Chem.*, 2000, **366**, 254–259.
- 83 A. K. Brewer and A. M. Striegel, *Analyst*, 2011, **136**, 515–519.
- 84 M. Baalousha, F. V.D. Kammer, M. Motelica-Heino, H. S. Hilal and P. Le Coustumer, *J. Chromatogr. A*, 2006, **1104**, 272–281.
- 85 Q. Yan and Y. Zhao, *Chem. Sci.*, 2015, **6**, 4343–4349.
- 86 T. A. Enoki, V. B. Henriques and M. T. Lamy, *Chem. Phys. Lipids*, 2012, **165**, 826–837.
- 87 L. Angeles and J. Vanzanten, *J. Colloid Interface Sci.*, 1991, **146**, 330–336.
- 88 B. M. Tande, N. J. Wagner, M. E. Mackay, C. J. Hawker and M. Jeong, *Macromolecules*, 2001, **34**, 8580–8585.
- 89 M. Dionzou, A. Morère, C. Roux, B. Lonetti, J. D. Marty, C. Mingotaud, P. Joseph, D. Goudounèche, B. Payré, M. Léonetti and A. F. Mingotaud, *Soft Matter*, 2016, **12**, 2166–2176.
- 90 E. G. Kelley, T. P. Smart, A. J. Jackson, M. O. Sullivan and T. H. Epps, *Soft Matter*, 2011, **7**, 7094–7102.
- 91 O. Colombani, M. Ruppel, M. Burkhardt, M. Drechsler, M. Schumacher, M. Gradzielski, R. Schweins and A. H. E. Müller, *Macromolecules*, 2007, **40**, 4351–4362.
- 92 J. P. Patterson, A. O. Moughton, M. P. Robin, A. Lu, D. Cheung, R. K. O’Reilly, E. G. Kelley, R. P. Murphy, M. O. Sullivan, T. H. Epps, O. Colombani and C. Chassenieux, *Macromolecules*, 2013,

46, 6319–6325.

- 93 D. J. Adams, C. Kitchen, S. Adams, S. Fuzeland, D. Atkins, P. Schuetz, C. M. Fernyhough, N. Tzokova, A. J. Ryan and M. F. Butler, *Soft Matter*, 2009, **5**, 3086–3096.

Appendix C

Table C.1 - A table showing the conversion of monomer to polymer by moisture analysis and the actual DP of nanogels synthesised.

[M]/[pHEA-mCTA]	Mol % BAPE	Crosslinker/mCTA	Conv Crosslinker/mCTA	Conversion / X ^a	Approx. BAPE units per chain	Theoretical DP ^b	M _n / Da ^c
125	0	6.3	5	80	0	100	17500
189	0	6.3	5	82	0	155	23730
255	0	6.3	6	95	0	242	33730
325	0	6.45	5	83	0	269	36630
387	0	6.43	5	83	0	321	42510
126	0	3.79	3	85	0	107	18000
190	0	3.81	3	82	0	156	23530
264	0	3.98	3	81	0	213	29980
313	0	3.71	3	86	0	269	36320
384	0	3.8	3	86	0	330	43220
128	2	6.41	4	69	2	88	16340
192	2	6.43	4	62	2	119	19850
251	2	6.25	6	98	5	246	35060
310	2	6.16	5	79	5	245	34790
363	2	5.92	5	87	6	315	43110
127	2	3.8	3	70	2	89	16300
190	2	3.78	3	88	3	167	25300
268	2	4.01	3	77	4	206	29890
304	2	3.64	3	75	4	228	32380
317	5	3.8	3	96	15	304	42910
410	2	4.09	3	71	6	291	39860

^aDetermined by moisture analysis against predicted solids content ^b [M]/[pHEA-mCTA]*conv. ^c Theoretical M_n from solids content.

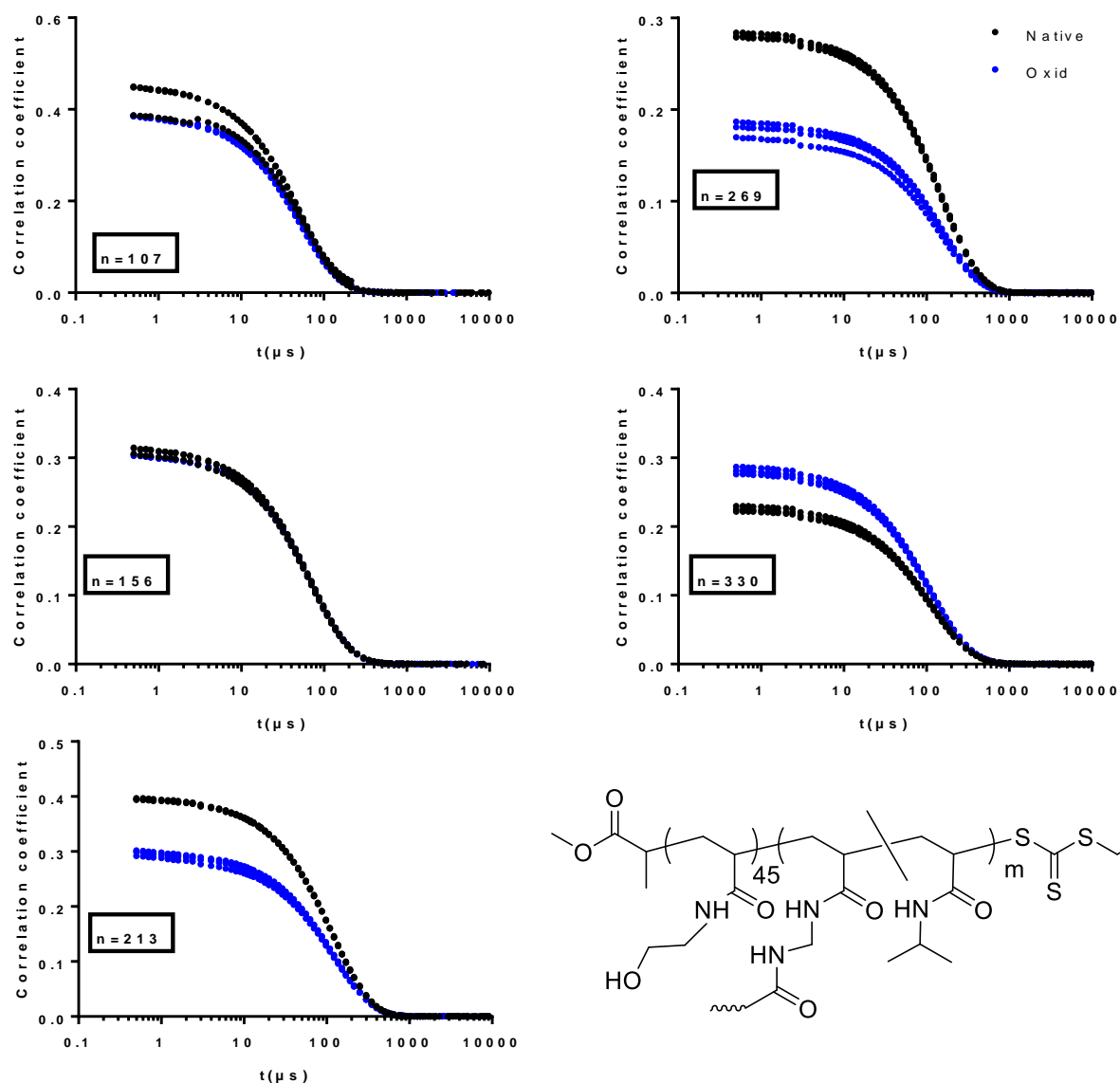


Figure C.1 – Correlation curves related to DLS analysis of $H_{45}-N_n$ 3:1 for the native and the oxidised polymer, at a NG concentration of 0.1wt%.

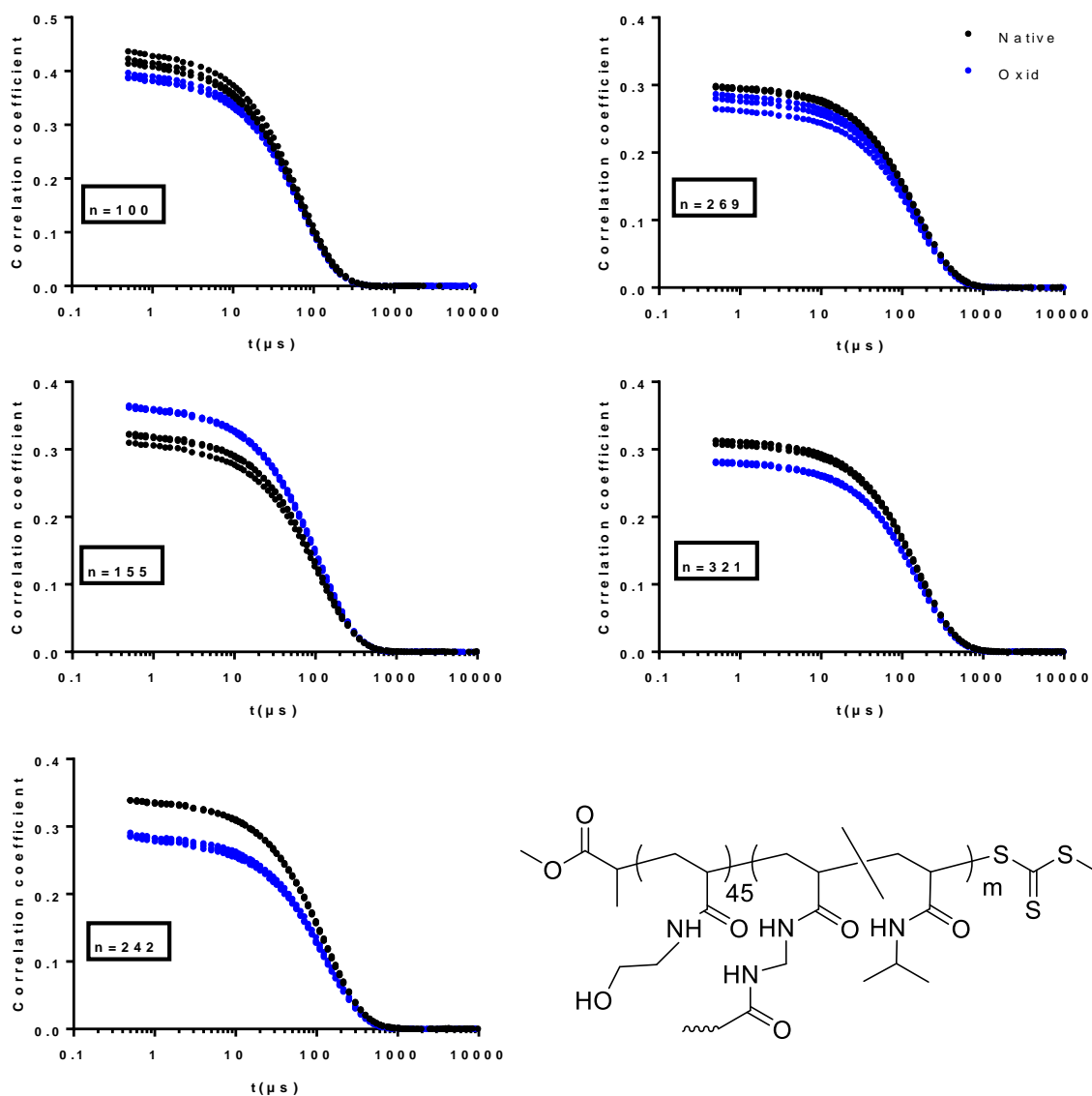


Figure C.2 - Correlation curves related to DLS analysis of $H_{45}\text{-}N_n$ 5:1 for the native and the oxidised polymer, at a NG concentration of 0.1wt%.

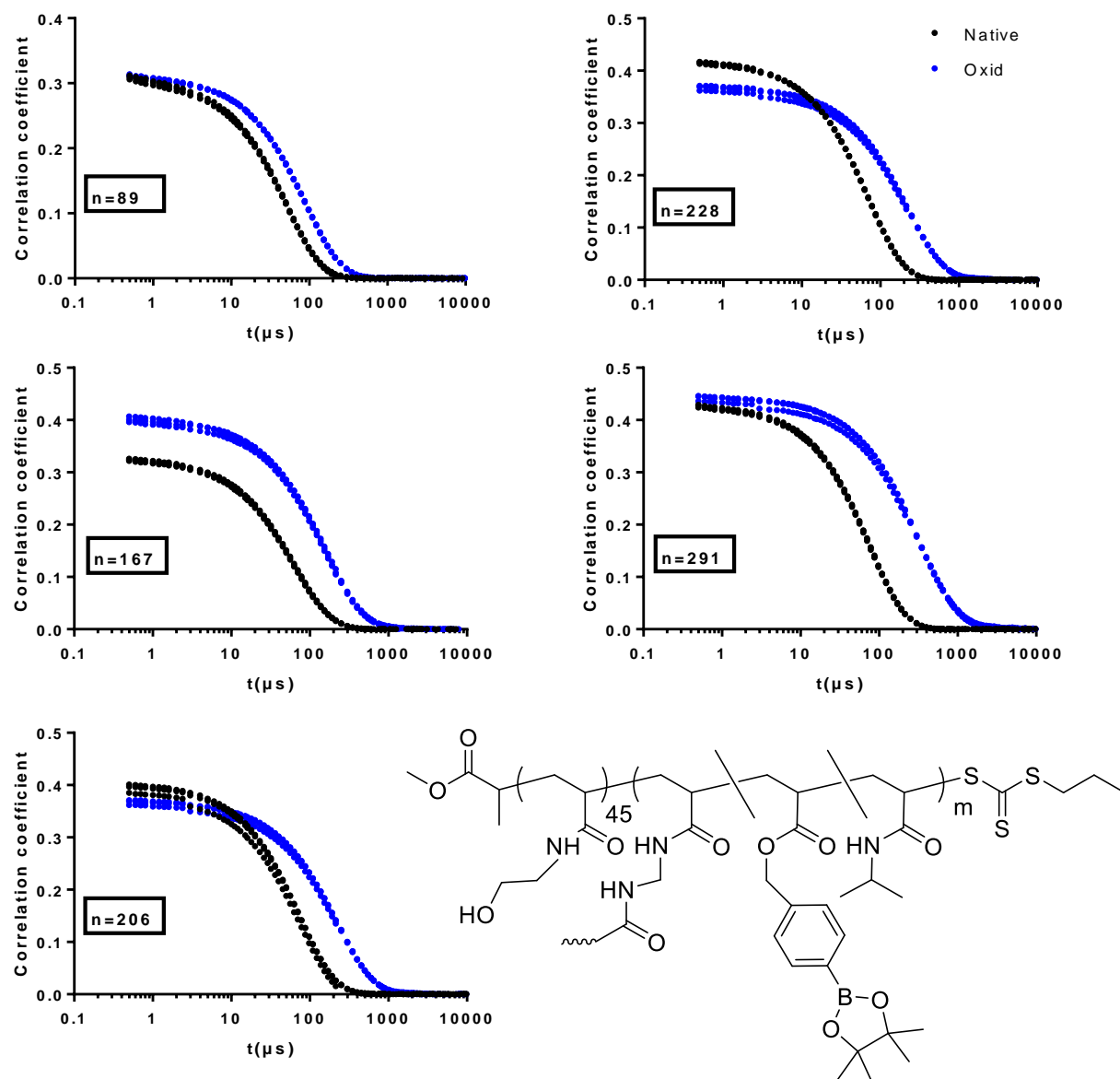


Figure C.3 - Correlation curves related to DLS analysis of $H_{45}-NB_n$ 3:1 for the native and the oxidised polymer, at a NG concentration of 0.1wt%.

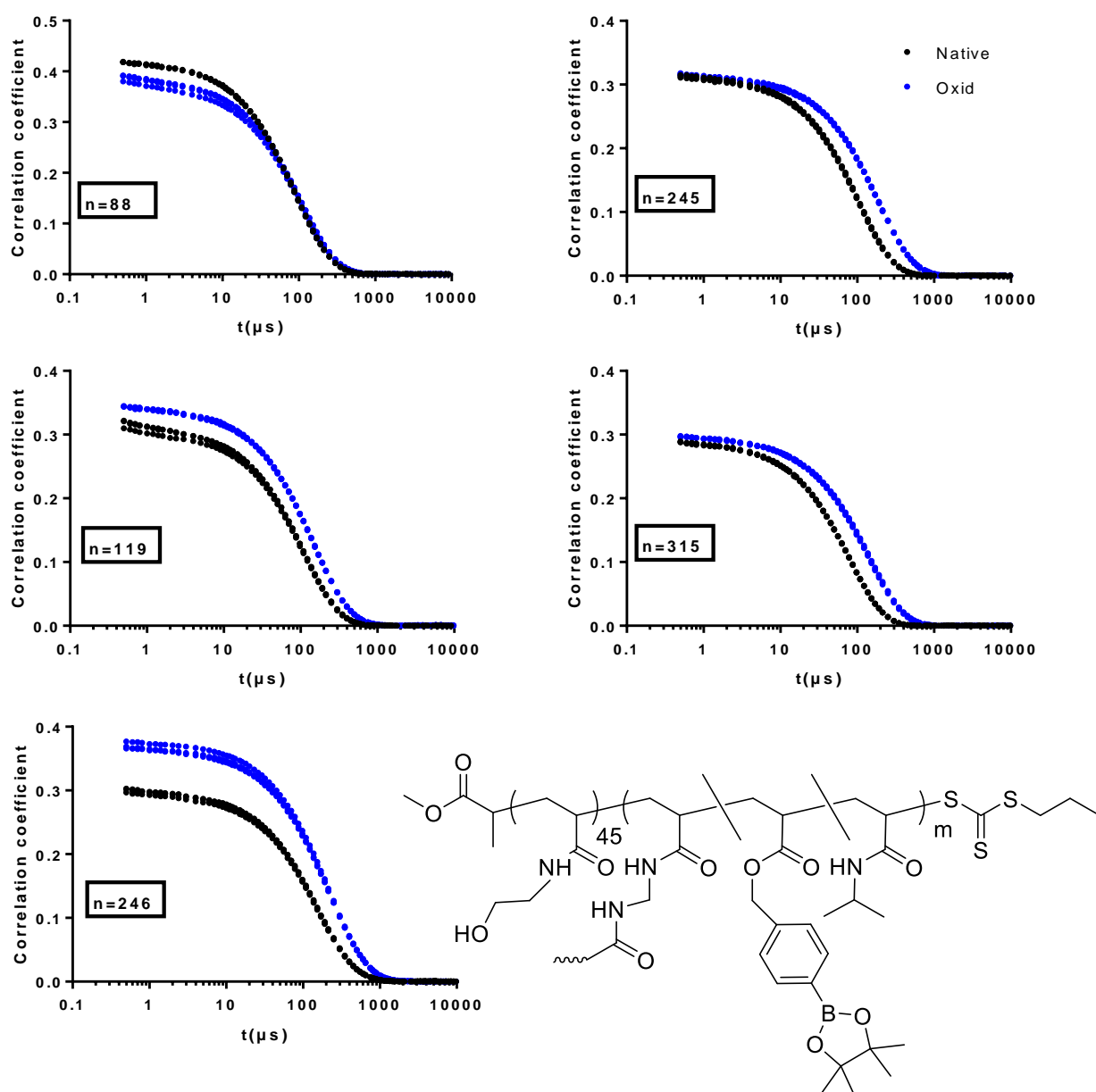


Figure C.4 - Correlation curves related to DLS analysis of $H_{45}\text{-NB}_n$ 5:1 for the native and the oxidised polymer, at a NG concentration of 0.1wt%.

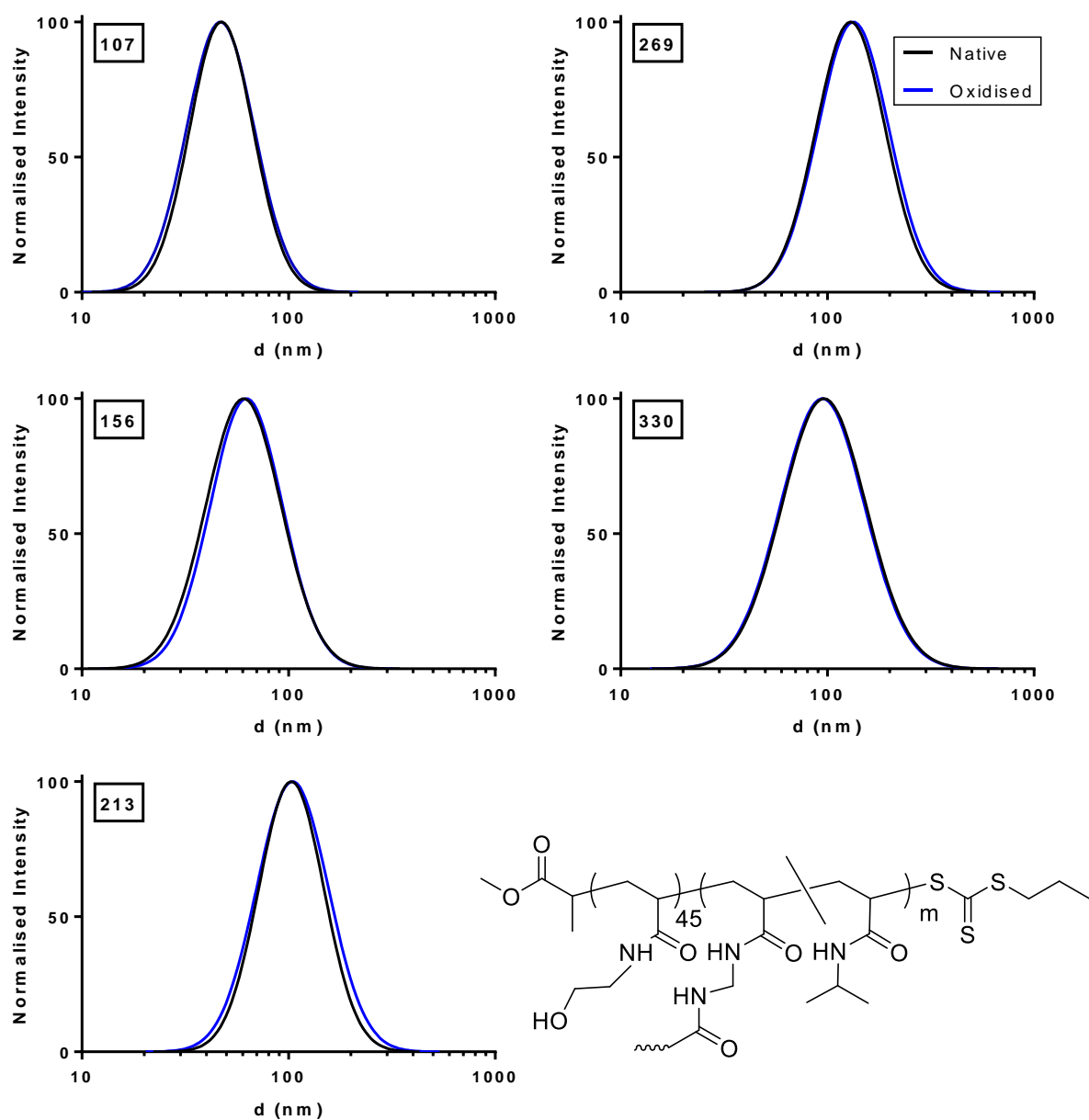


Figure C.5 - DLS analysis at 37 °C of $H_{45}-N_n$ with a crosslinker to mCTA ratio of 3:1 at a NG concentration of 0.1wt%, before and after oxidation with 15 mM H_2O_2 .

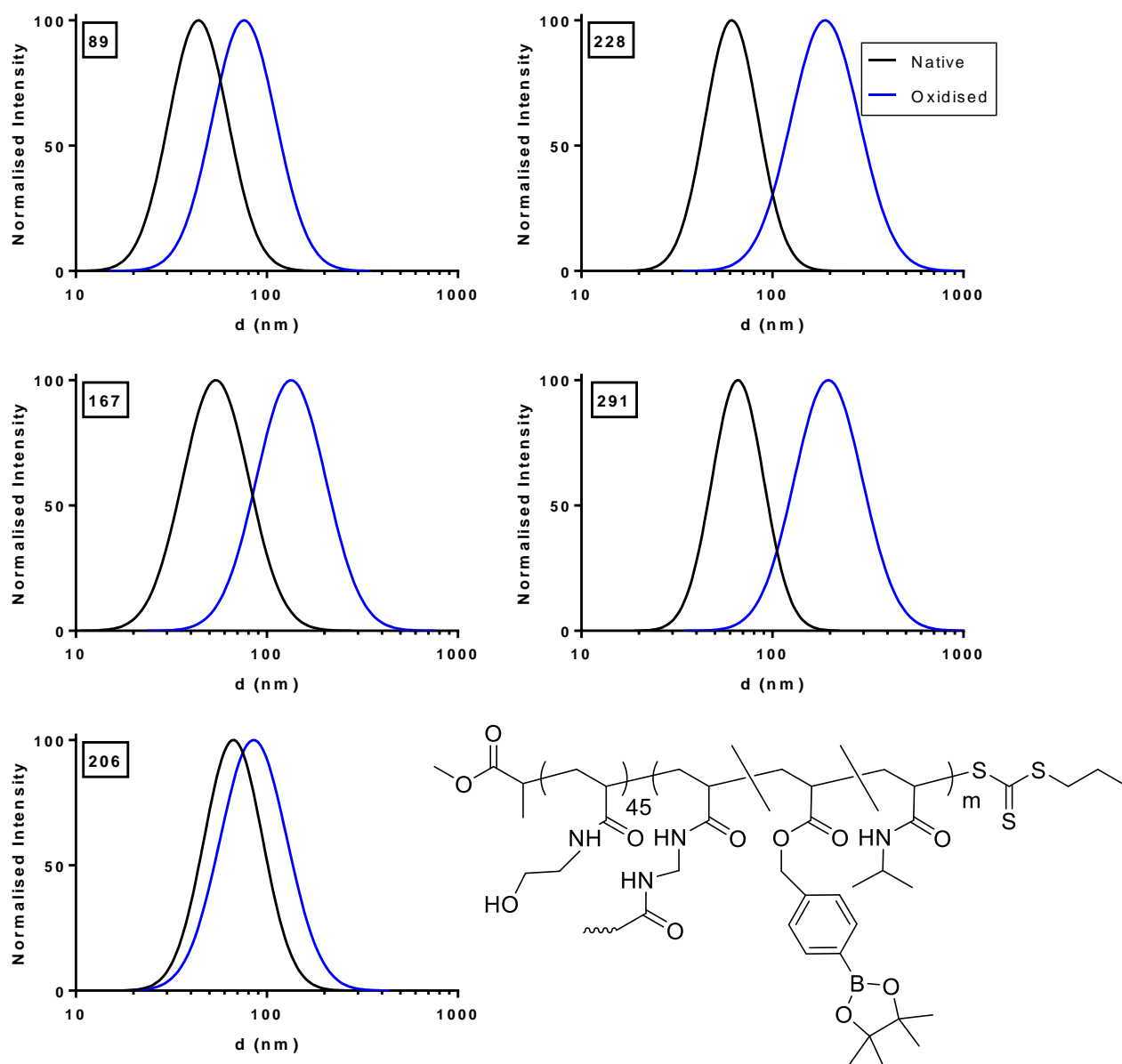


Figure C.6 - DLS analysis at 37 °C of H_{45} - NB_n with a crosslinker to mCTA ratio of 3:1 at a NG concentration of 0.1wt%, before and after oxidation with 15 mM H_2O_2 .

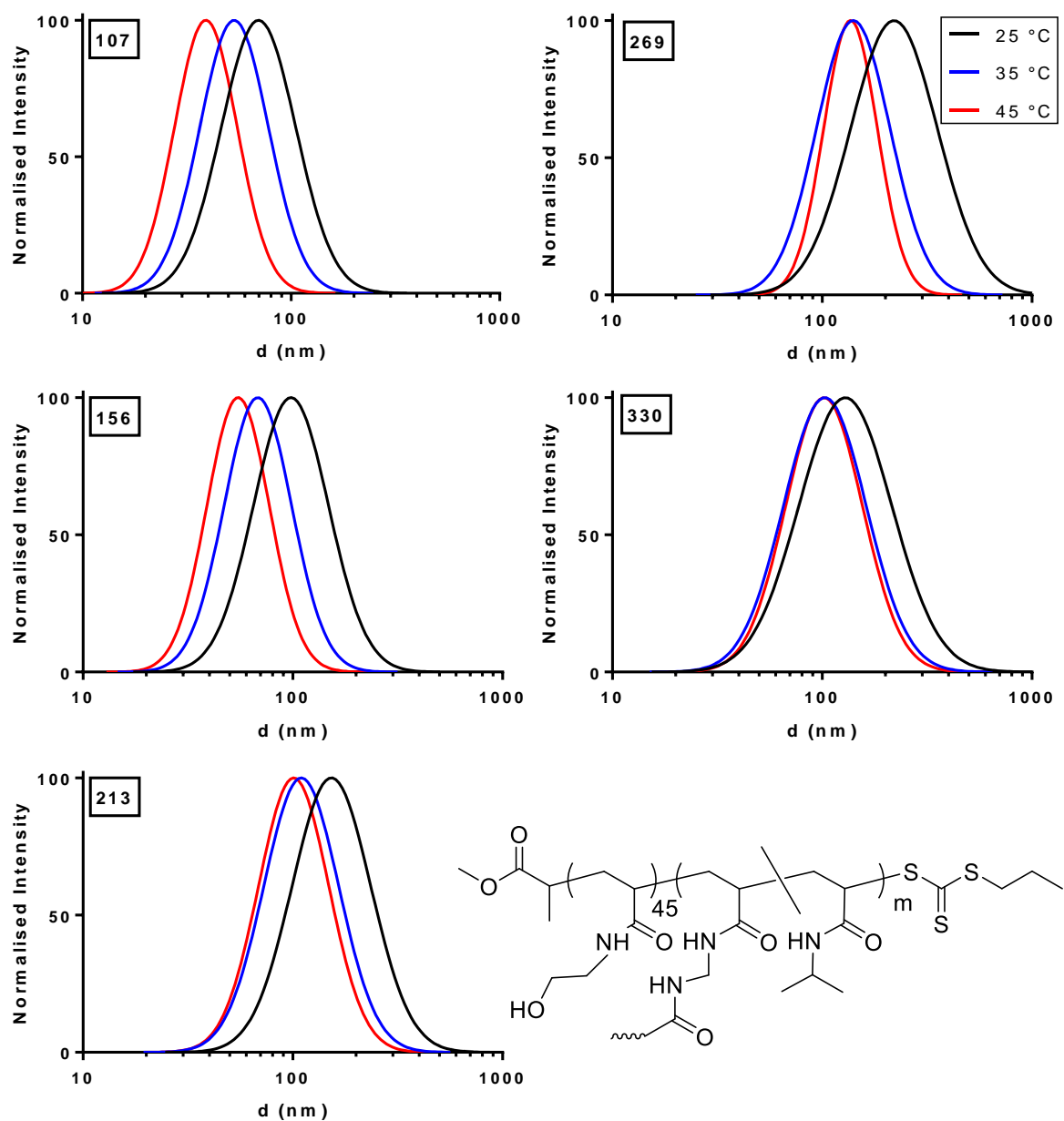


Figure C.7 - The observable shrinking behaviour by DLS analysis of $H_{45}-N_n$ with crosslinker to mCTA ratios of 3:1 at a NG concentration of 0.1wt%, on heating to temperatures above the LCST of pNIPAM.

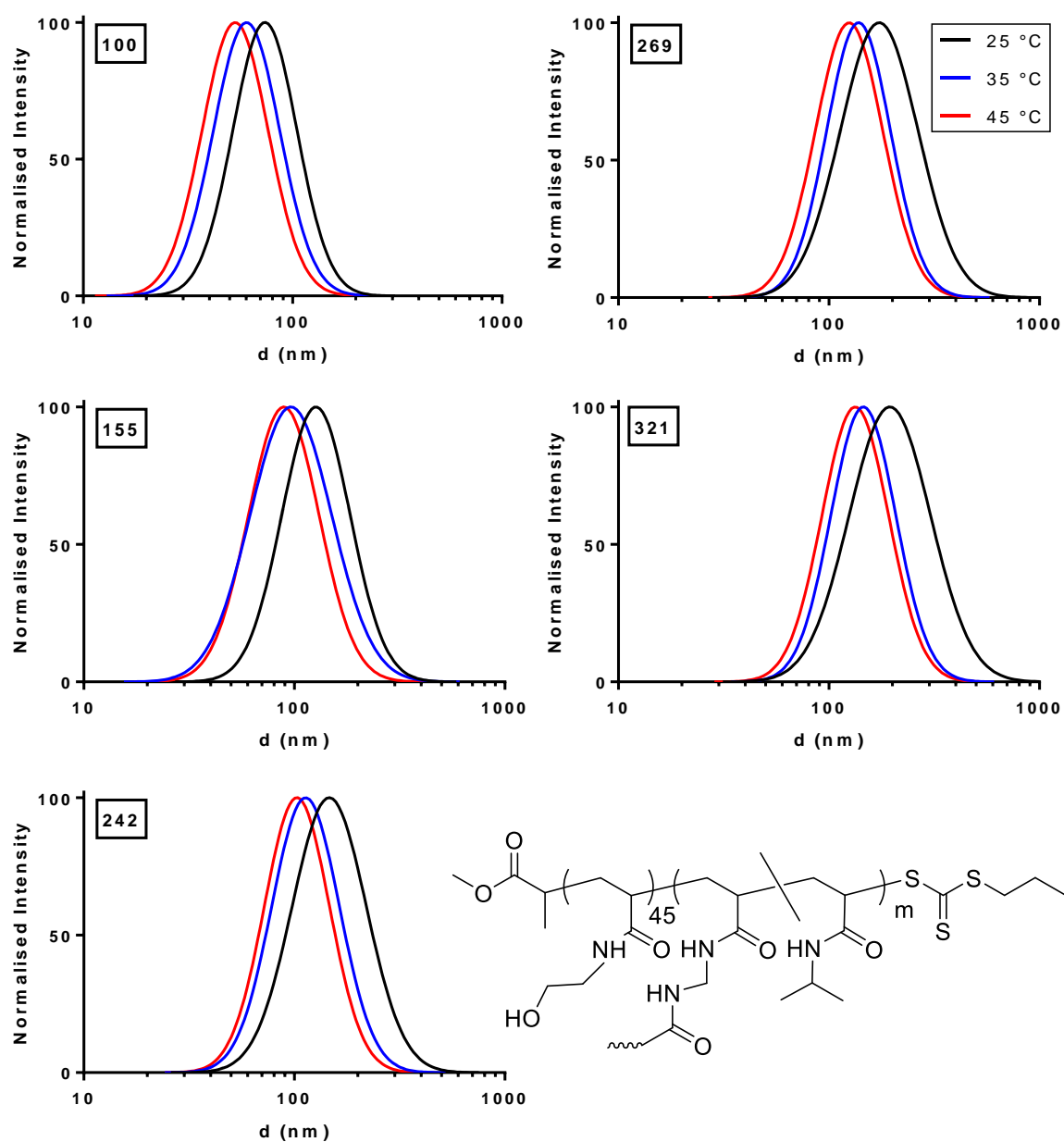


Figure C.8 - The observable shrinking behaviour by DLS analysis of $H_{45}-N_n$ with crosslinker to mCTA ratios of 5:1 at a NG concentration of 0.1wt%, on heating to temperatures above the LCST of pNIPAM.

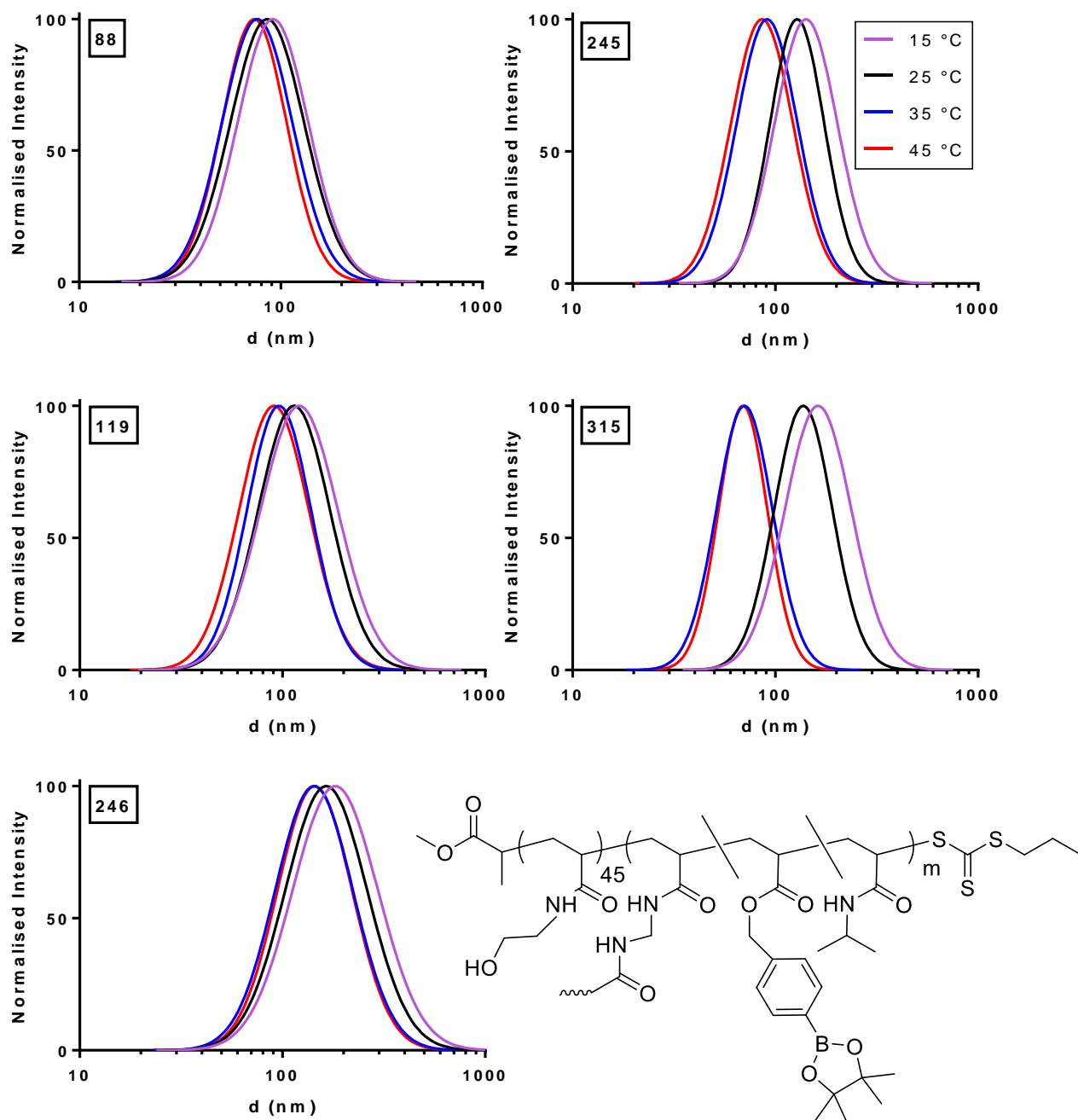


Figure C.9 - The observable shrinking behaviour by DLS analysis of $H_{45}\text{-NB}_n$ with crosslinker to mCTA ratios of 5:1 at a NG concentration of 0.1wt%, on heating to temperatures above the LCST of pNIPAM.

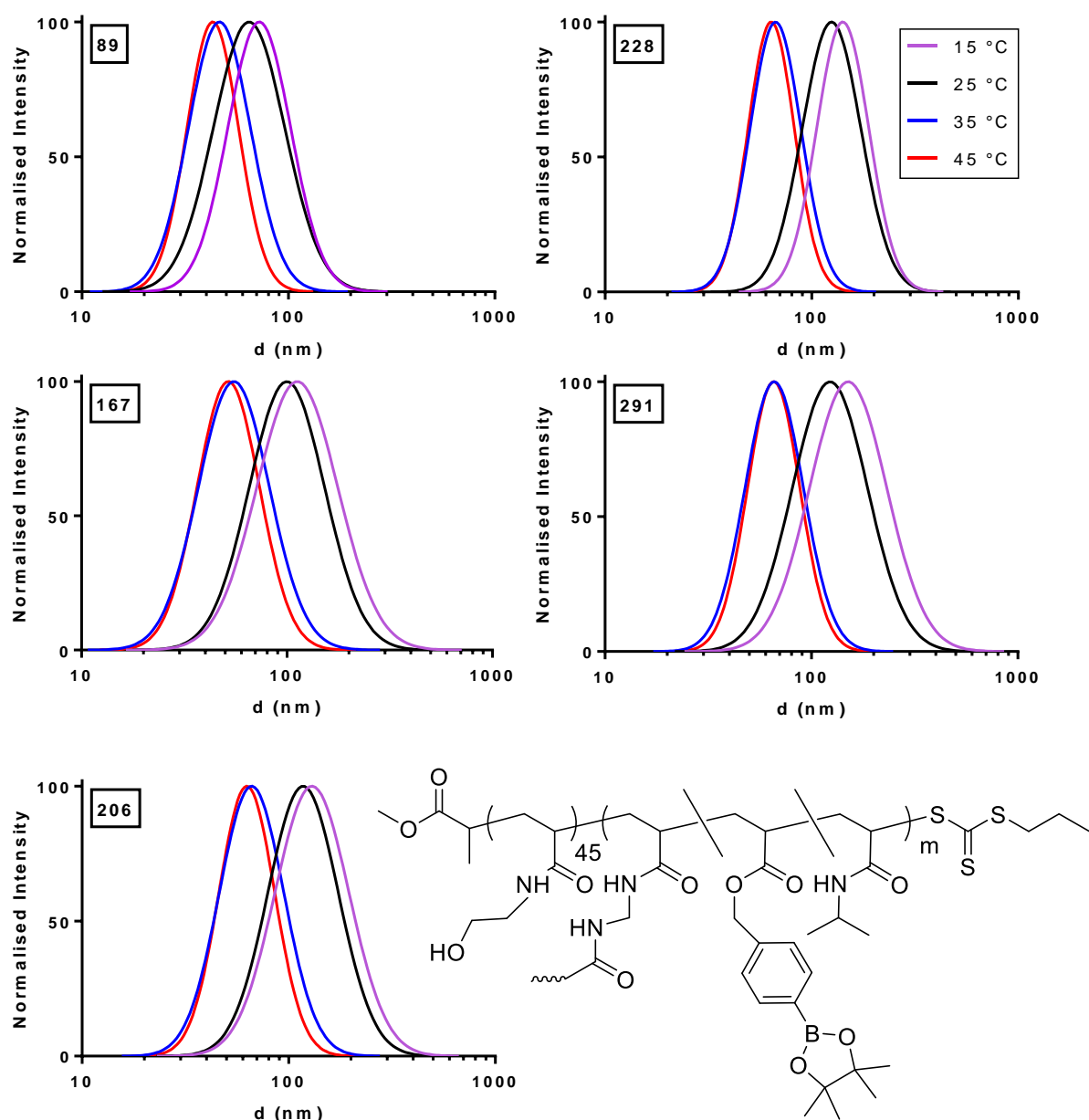


Figure C.10 - The observable shrinking behaviour by DLS analysis of $H_{45}\text{-NB}_n$ with crosslinker to mCTA ratios of 3:1 at a NG concentration of 0.1wt%, on heating to temperatures above the LCST of pNIPAM.

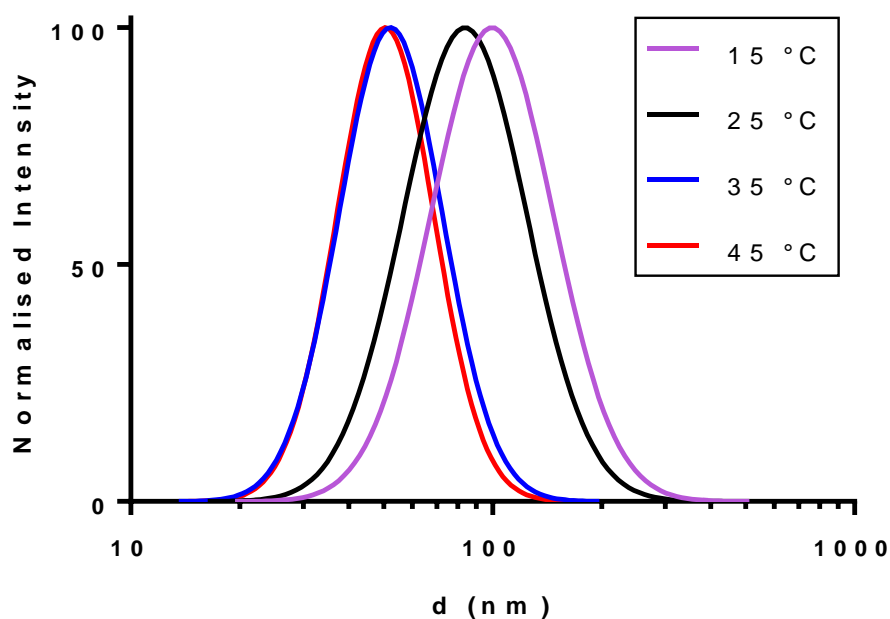


Figure C.11 - The observable shrinking behaviour by DLS analysis of $H_{45}\text{-NB}_{304}$ with crosslinker to mCTA ratios of 3:1 and 5 mol% BAPE incorporated into the core, at a NG concentration of 0.1wt%, on heating to temperatures above the LCST of pNIPAM.

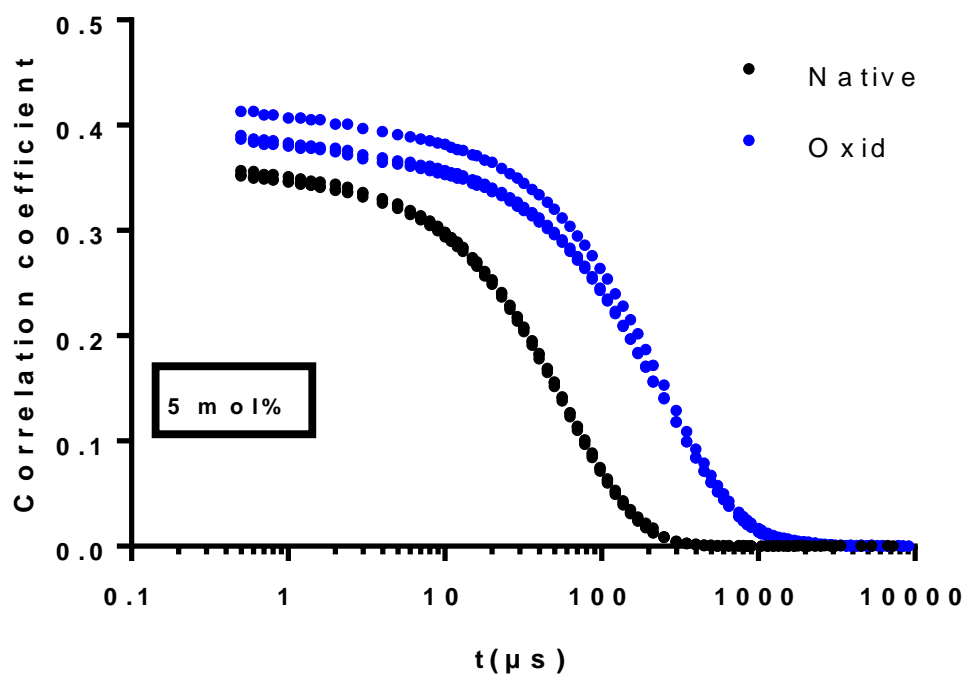


Figure C.12 - Correlation curves related to DLS analysis of $H_{45}\text{-NB}_{304}$ with a mCTA to crosslinker concentration of 3:1 and 5 mol% BAPE incorporated into the core, for the native and the oxidised polymer, at a NG concentration of 0.1wt%.

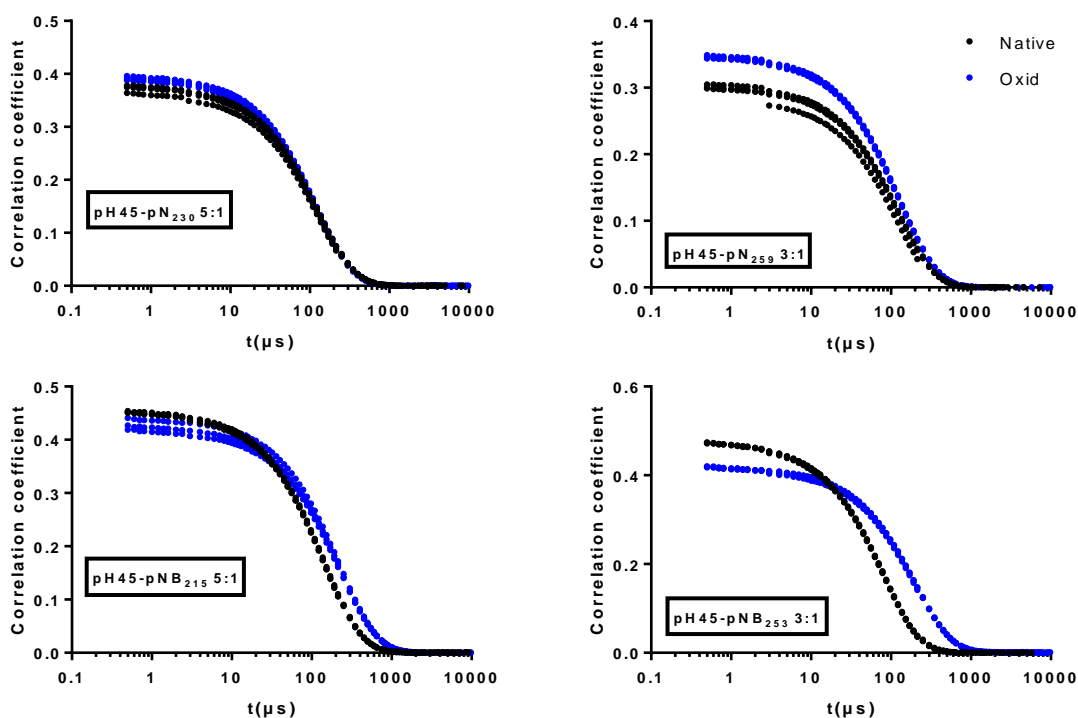


Figure C.13 - Correlation curves related to DLS analysis of $H_{45}\text{-}N_n$ and $H_{45}\text{-}NB_n$ at 37 °C with a mCTA to crosslinker concentration of 3:1 and 5:1, for the native and the oxidised polymer, at a NG concentration of 0.1wt%.

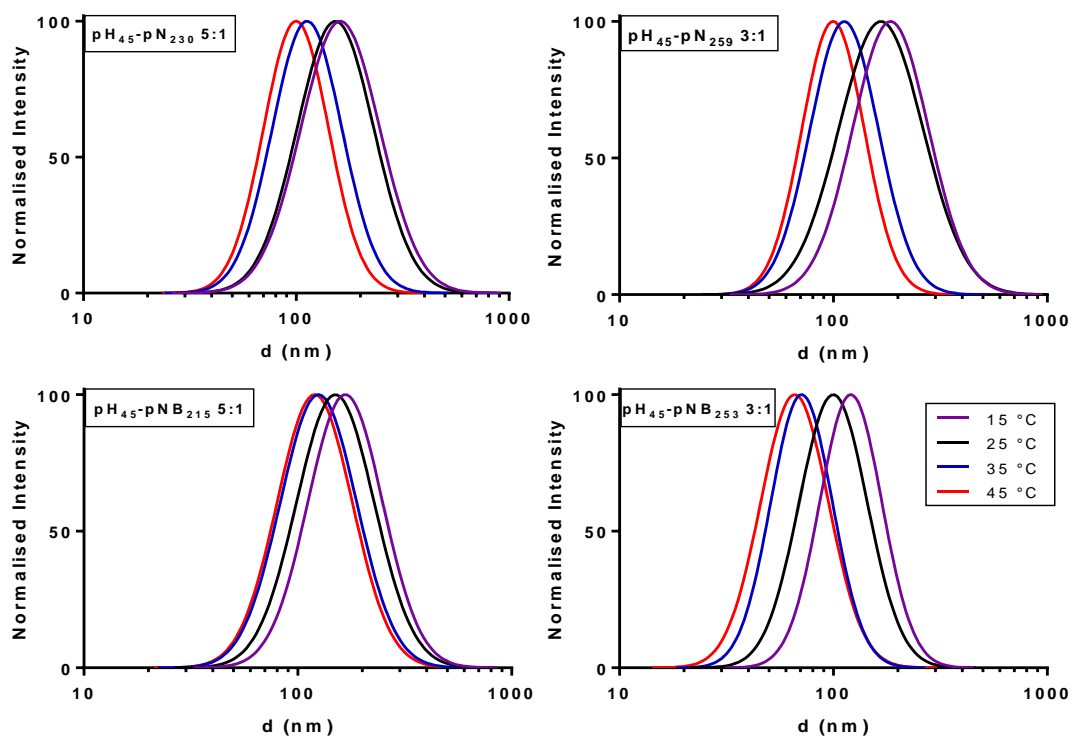


Figure C.14 - The observable shrinking behaviour by DLS analysis $H_{45}\text{-}N_n$ and $H_{45}\text{-}NB_n$ on heating to temperatures above the LCST of pNIPAM at a NG concentration of 0.1wt%.

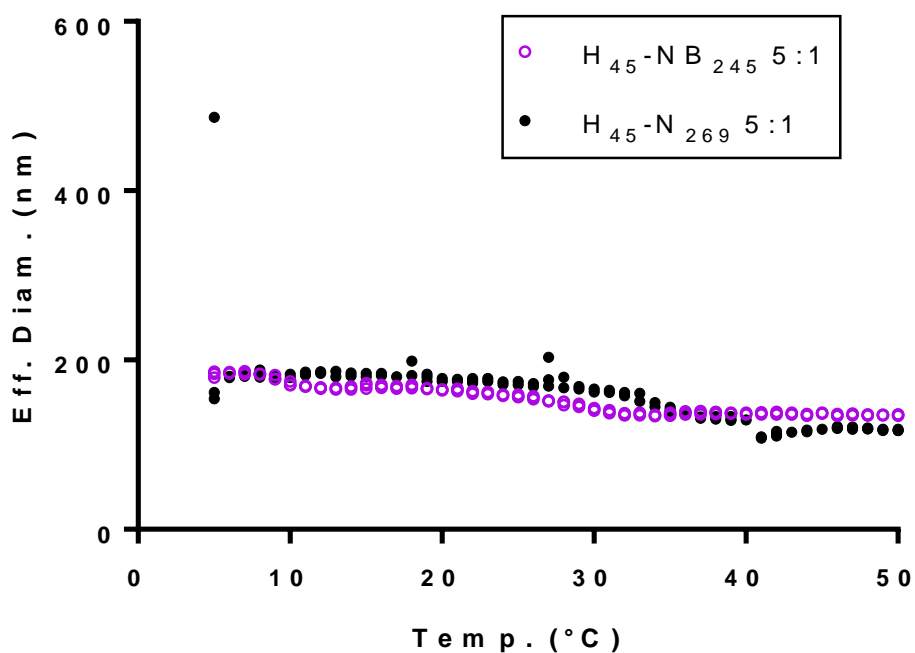


Figure C.15 - Comparison DLS analysis at increasing temperatures of two samples with similar core forming block lengths to determine the effect of BAPE incorporation on LCST. The wavelength of the laser used is 640 nm and the backscattering was measured.

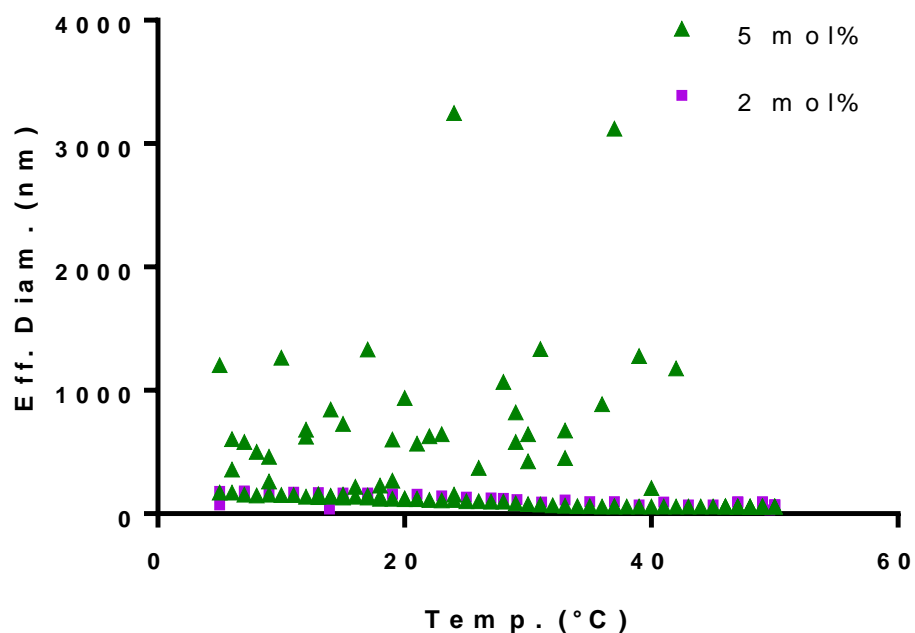


Figure C.16 -LCST measurements using DLS to measure shrinking behaviour on increasing temperature of H₄₅-NB_{291/304} 3:1 with 2 and 5 mol% BAPE respectively at a concentration of 0.1wt%. The wavelength of the laser used is 640 nm and the backscattering was measured.

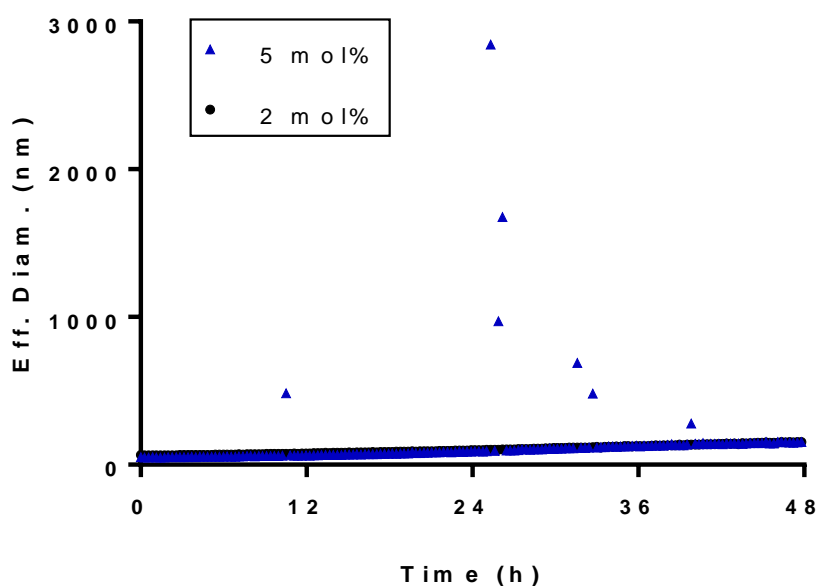


Figure C.17 - In situ oxidation by DLS at 37 °C. H_{45} -NB_{291/304} with a crosslinker to mCTA ratio of 3:1 and 2 and 5 mol% BAPE respectively, at a concentration of 0.1wt%, oxidised with a H_2O_2 concentration of 5 mM over 48 h. The wavelength of the laser used is 640 nm and the backscattering was measured.

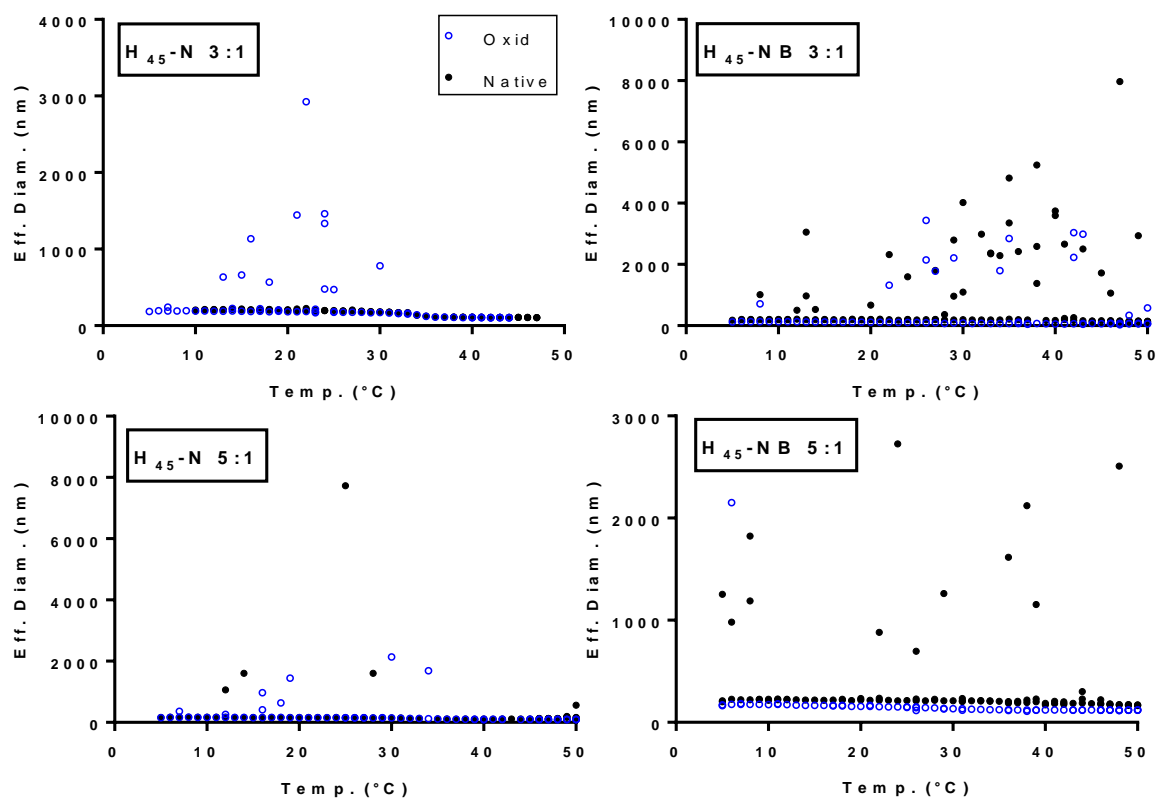


Figure C.18 - Effective diameter measurements of four NGs, H-N and H-NB with crosslinker to mCTA ratios of 3:1 and 5:1, by DLS at a concentration of 0.1wt%, over a range of temperatures. The wavelength of the laser used is 640 nm and the backscattering was measured. Some very high eff. diam.

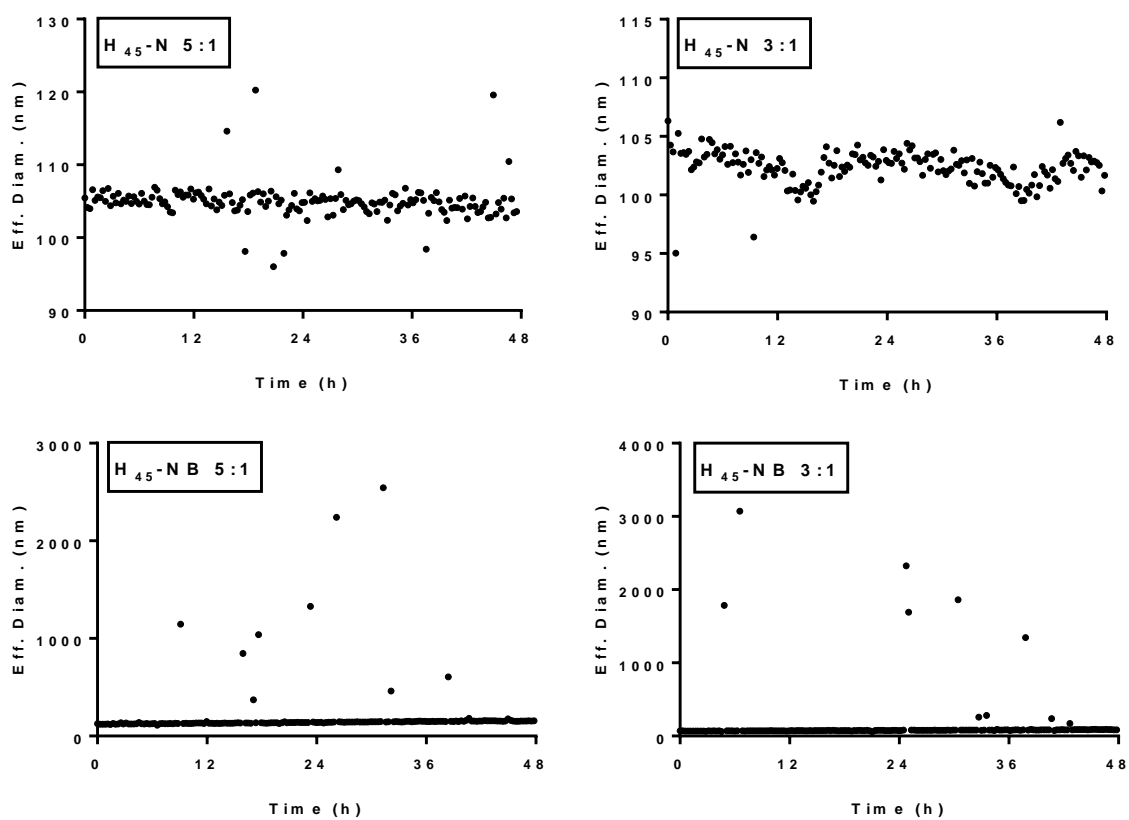


Figure C.19 - Monitoring in situ oxidation by DLS at 37 °C of H₄₅-N_n and H₄₅-NB_n with crosslinker to mCTA ratio of 5:1 and 3:1, at a concentration of 0.1wt%, oxidised with a H₂O₂ concentration of 1 mM over 48 h. The wavelength of the laser used is 640 nm and the backscattering was measured.

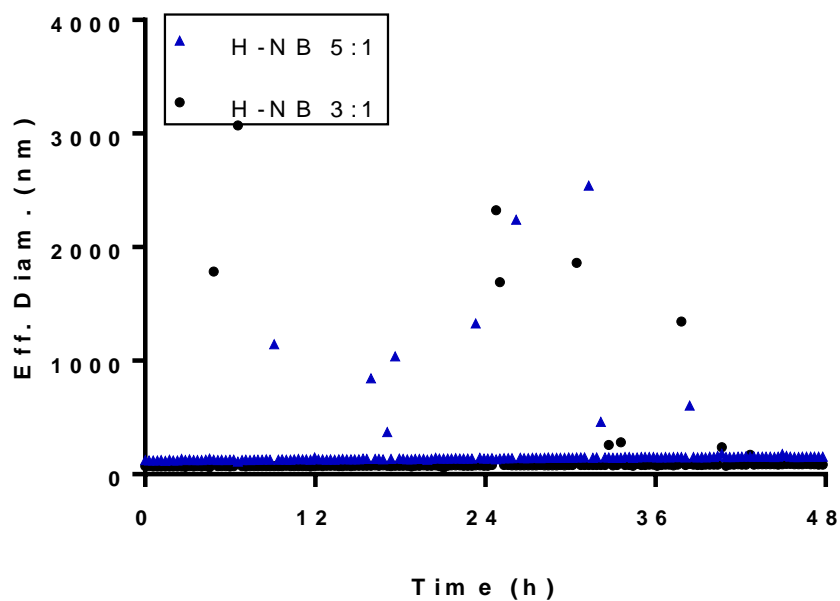


Figure C.20 - Comparison of the in situ oxidation data from the two H-NB samples; $H_{45}\text{-NB}_{215}$ 5:1 and $H_{45}\text{-NB}_{253}$ 3:1, with different crosslinker to mCTA ratios, at a concentration of 0.1wt%. The wavelength of the laser used is 640 nm and the backscattering was measured.

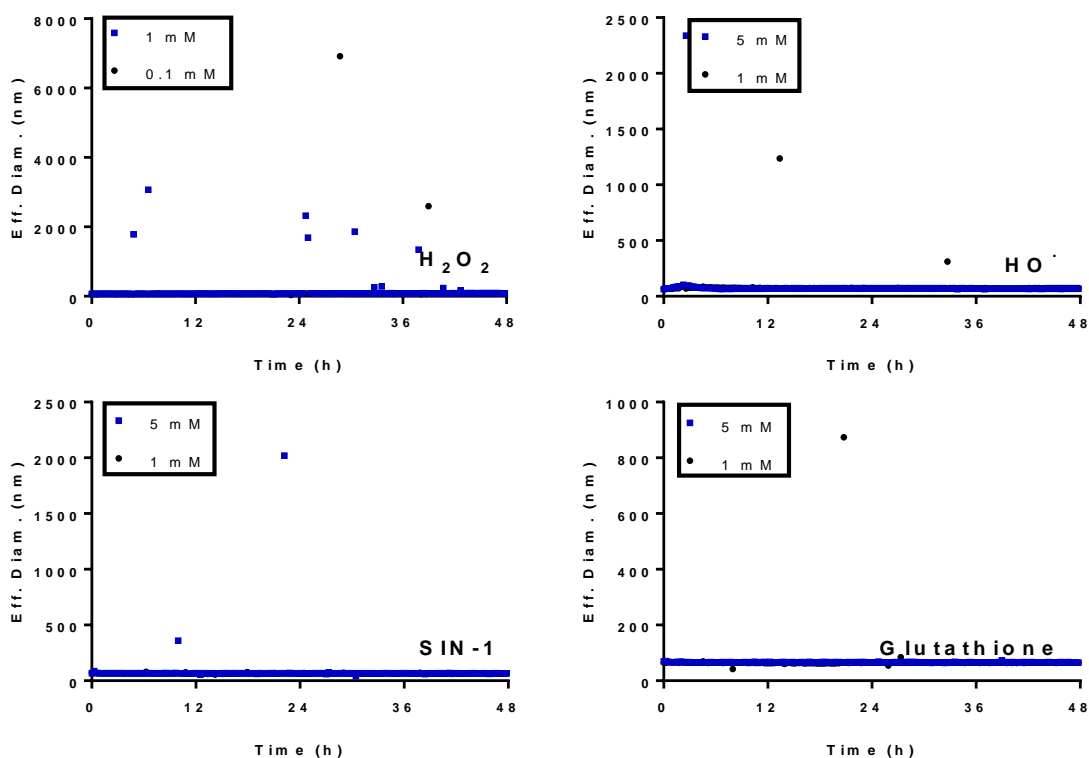


Figure C.21 - In situ oxidation studies monitored by DLS of $\text{pH}_{45}\text{-pNB}_{253}$ with a crosslinker to mCTA ratio of 3:1 at a concentration of 0.1wt%, to determine the sensitivity of BAPE to other oxidants and reductants; H_2O_2 , hydroxyl radical, SIN-1 and glutathione. The wavelength of the laser used is 640 nm and the backscattering was measured.

Chapter Six

6 Conclusions and Future work

6.1. Conclusions

The aim of the research in this thesis was to synthesise an oxidation responsive polymer which also exhibits a temperature response. This was to be sensitive to low concentrations of hydrogen peroxide, similar to those found within the body due to an autoimmune response. These polymers should change on oxidation in a way that any encapsulated material should be released.

In this thesis, a range of dual-responsive materials have been synthesised with varying degrees of success regarding their applications. All polymers synthesised respond to temperature and many to oxidation by hydrogen peroxide but to different extents.

Initially, in chapter 2, linear polymers of NIPAM were synthesised by RAFT polymerisation with a variety of different CTAs. On oxidation it was shown that the RAFT chain end group was changed from a trithiocarbonate to a sulfonic acid group, as a major product. The sulfonic acid end group increased the hydrophobicity of the polymer chains and therefore altered the cloud point of the polymers when compared to that of the native polymer.

In chapter 3, to follow on from this work, a series of diblock copolymers were successfully synthesised by RAFT polymerisation. Poly(*N*-(2-hydroxyethyl)acrylamide (pHEA) was chosen as the macro-CTA due to its hydrophilic nature and from this core-forming pNIPAM blocks of various lengths were grown. With a short pNIPAM block length of around 20 NIPAM units, these particles did not self-assemble in water, even at temperatures above the LCST of the polymer.

Those with a longer core forming block did self-assemble above the LCST, forming particles with a diameter below 100 nm, as seen by DLS. Incorporation of an oxidation responsive boronic acid pinacol ester monomer (BAPE) into the temperature responsive polymer lowered the LCST of these before oxidation and raised it above 37 °C after oxidation. This change in LCST on oxidation also caused an increase in size of the particles, which indicated that a suitable oxidation responsive moiety had been found.

To encapsulate and release polymers a system less prone to leakage, and with better release behaviour was needed to the above. Chapter 4 described the synthesis of oxidation-responsive nanogels. These were synthesised in the same way diblock copolymers in chapter 3, but an additional divinyl based molecule was added during the synthesis of the core forming block to enable crosslinking of the core. These NGs had cores which were both oxidation and temperature responsive, with former affecting the latter. It has been shown that by increasing the length of the core forming block, the size and morphology of the nanoparticles can be altered. When they are heated to temperatures above their LCST they shrink due to the collapse of the pNIPAM chains in the core. An approximation of the LCST was determined from DLS data by observing the change in diameter of the NG over a temperature range.

These NGs exhibited high sensitivity to hydrogen peroxide observed. Swelling of the NG after oxidation by 106 nm was observed at concentrations as low as 0.1 mM for the nanogel H₄₅-NB₂₉₁, with a crosslinker to mCTA ratio of 3:1. The more H₂O₂ present, the faster the oxidation as was predicted, however not all BAPE units are required to be oxidised for the nanogel to swell. The sensitivity to other reactive oxygen species, including peroxyxynitrite and hydroxy radicals, and a common reducing agent found in the body, glutathione, was also determined using in situ DLS studies, showing no change in the size of the polymer after 48 h. exposure to a concentration of 5 mM.

In depth analysis of the morphology of a few of these NGs was performed using a combination of DLS, SAXS, TEM and AF4 combined with DLS and MALS. This allowed for a more accurate view of the size and shape of some of the NGs synthesised, by minimising the limitations of individual techniques. For example, pH-NB 3:1 was found to have particles which were spherical and vesicle-like in nature with a dual particle size of around 20 nm for the smaller particles and 70 nm for the larger particles. For the equivalent sample without BAPE however, the results were still unclear on

the morphology, indicating that there was a wide size and morphological range throughout the sample, with it mainly containing ill-defined aggregates with sizes ranging between 45 and 200 nm.

6.2. Future work

Although in this thesis there are a lot of examples of oxidation responsive polymers, they have not been assessed for their suitability as a drug delivery system. There are many other factors which must be assessed alongside size, morphology and responsive behaviour to make these suitable as DDS. Two main examples of these are toxicology studies to assess how safe this material is inside the human body, and encapsulation and release studies to ensure these nanogels can encapsulate drug with minimal leakage.

Toxicology studies are very important for DDS. These would involve determining the toxicity of both the NGs before and after oxidation to ensure that polymer and/or side products of the oxidation of this are deemed safe in cell-based assays, as well as ensuring that there isn't a negative interaction between the drug and polymer. This is particularly important as there are disputes in the literature on the toxicity of the intermediates formed during the oxidation of BAPE with hydrogen peroxide.¹⁻³ In vitro studies are a priority for any further work on this topic as development will depend on toxicity.

Preliminary encapsulation studies have been carried out using the hydrophobic drug, prednisolone, and a hydrophilic fluorophore, rhodamine-B. These tests showed little difference in the speed of release from the dialysis tubing between samples which contain NG and drug/dye, and those which also contained an oxidising agent. It is believed that this is related to the LCST of the polymers and in particular, the shrinking and swelling behaviour occurring over a temperature range. Without any oxidising agent, the NGs should be in a shrunken state at 37 °C, however encapsulation began at room temperature and then the temperature was increased to 37 °C. It has been seen from the LCST studies performed by DLS that the shrinking of the NGs may begin at temperatures as low as 20 °C, which could indicate that encapsulation was not efficient as the core was not in its fully extended

state. It was difficult to determine if the measurements made from the contents of the dialysis water are of release of the drug from the nanogel, or merely release from the dialysis membrane when no encapsulation has taken place. Even though these samples were dialysed for 1 hour before changing the water and adding the oxidant, it is not possible to tell whether all material that was not encapsulated was removed after this time. Therefore, another release study would need to be conducted in future.

The scope for future work relating to this project is wide, especially as there are currently no NG-based DDS on the market, and although these have shown a lot of hope in the laboratory, many have failed throughout clinical trials.

The main aspects of future work would link with the statements above about the LCST and drug encapsulation. It is necessary to lower the LCST further so that the NG will not begin to shrink at room temperature. Although it was indicated that the presence of a larger BAPE concentration may be beneficial here from studies on linear polymers of p(NIPAM-*stat*-BAPE), when incorporated into a NG the change in LCST was not significant. This is likely due to the hydrophilic nature of the pHEA block and therefore it may be necessary to incorporate another temperature responsive monomer in the core which has a much lower LCST than NIPAM. In doing so, the oxidation responsive behaviour will be the same as these polymers, although the size will vary, but the lower LCST should aid encapsulation.

Another route forward with this study would be to change the crosslinking molecule to one which responds to oxidation. The incorporation of BAPE into the core block would still cause an increase in LCST on oxidation and therefore these structures would not be assembled as micelles after this, therefore breaking of the crosslinking molecule has the potential to disassemble the polymer on oxidation to give free polymer chains which are water soluble. Hydrophilicity of the remaining DDS after drug release will aid safe excretion from the body, especially when compared to excreting intact NG particles. Throughout this research, this work has already been started, with numerous

potential crosslinking molecules being synthesised. One of the main issues faced was due to the solubility of these. NGs are usually synthesised in water and, in this case, a mixed aqueous system due to the cononsolvency behaviour that pNIPAM exhibits and dialysed against water afterwards. A range of aqueous/organic solvent mixtures were studied with various synthesised crosslinkers, however with little success. Either the amount of organic solvent was too high for pNIPAM to exhibit an LCST and therefore no self-assembly was observed and no NGs were formed, or the crosslinker could be incorporated with a NIPAM core, but when BAPE was also added it caused both BAPE and the crosslinker to precipitate from the solution. These crosslinking molecules must have an oxidation sensitive group, be soluble in the solvent and have similar reactivity to NIPAM and BAPE. Some of the crosslinkers examined can be seen in Figure 6.1, however there is a strong possibility that molecules of this kind could play a large role in the field of oxidation responsive DDS. A boronic acid pinacol ester containing crosslinker could influence the LCST, while also causing disassembly of the NGs on oxidation as it has been shown clearly here that these molecules are very sensitive to oxidation with H_2O_2 .

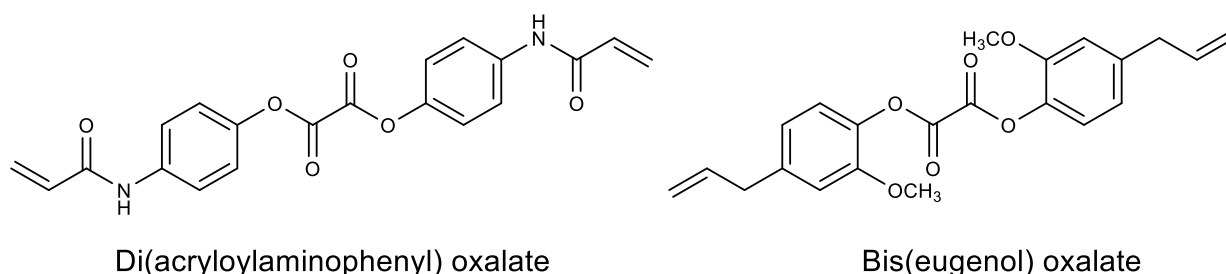


Figure 6.1 - Two oxidation responsive crosslinkers which were synthesised, with preliminary studies carried out testing their crosslinking ability in the nanogel system above.

It is important to note here that nanogels are not the only potential DDS currently showing success in the literature. From the initial encapsulation studies, these have been shown to be difficult to load effectively and are quite leaky. Therefore, the ideas studied here could be utilised in a completely different type of polymeric DDS.

By removing NIPAM as the comonomer, and therefore the temperature responsive behaviour it may be possible to form structures which are still oxidation responsive but easier to load. Achievement of this would involve using a different type of DDS however still using some form of a phenylboronic ester as this exhibit's sensitivity at low concentrations. An example of such system is by Deng et al. who have shown that polymersomes can be used as DDS. Oxidation of these causes the phenylboronic ester side chains to become crosslinked and form hydrophilic chains in the bilayer to allow the release of drugs.⁴ Due to the lack of a temperature responsive portion, self-assembly and subsequent drug encapsulation is easier. Ideally however, the polymersome itself would degrade.

Overall the research carried out in this thesis has increased our understanding of the responsiveness of polymers and has led to the identification of different potential future routes into the synthesis and applications of these.

6.3. References

- 1 E. Modica, R. Zanaletti, M. Freccero and M. Mella, *J. Org. Chem.*, 2001, **66**, 41–52.
- 2 P. Pande, J. Shearer, J. Yang, W. a. Greenberg and S. E. Rokita, *J. Am. Chem. Soc.*, 1999, **121**, 6773–6779.
- 3 C. C. Song, R. Ji, F. S. Du and Z. C. Li, *Macromolecules*, 2013, **46**, 8416–8425.
- 4 Z. Deng, Y. Qian, Y. Yu, G. Liu, J. Hu, G. Zhang and S. Liu, *J. Am. Chem. Soc.*, 2016, **138**, 10452–10466.